TESIS DE LA UNIVERSIDAD DE ZARAGOZA

2013

24

Belén Hernández Gascón

Mechanical modelling of the abdominal wall and biomaterials for hernia surgery

Departamento
Ingeniería Mecánica

Director/es
Calvo Calzada, Begoña
Peña Baquedano, Estefanía

ISSN 2254-7606

Prensas de la Universidad
Universidad Zaragoza

Universidad Zaragoza
1542

Tesis Doctoral

MECHANICAL MODELLING OF THE ABDOMINAL WALL AND BIOMATERIALS FOR HERNIA SURGERY

Autor

Belén Hernández Gascón

Director/es

Calvo Calzada, Begoña
Peña Baquedano, Estefanía

UNIVERSIDAD DE ZARAGOZA

Ingeniería Mecánica

Departamento de
Ingeniería Mecánica
Universidad Zaragoza

Escuela de
Ingeniería y Arquitectura
Universidad Zaragoza

Mechanical modelling of the abdominal wall and biomaterials for hernia surgery

by

BELÉN HERNÁNDEZ GASCÓN

Doctoral Degree in *Computational Mechanics*

Faculty Advisors

Begoña Calvo Calzada and Estefanía Peña Baquedano

Departamento de Ingeniería Mecánica. Escuela de Ingeniería y Arquitectura,
Universidad de Zaragoza
Zaragoza, Diciembre de 2012

Departamento de
Ingeniería Mecánica
Universidad Zaragoza

Doña Begoña Calvo Calzada, Catedrática del Departamento de Ingeniería Mecánica de la Escuela de Ingeniería y Arquitectura, de la Universidad de Zaragoza, y Doña Estefanía Peña Baquedano, Profesora Titular de Universidad del Departamento de Ingeniería Mecánica de la Escuela de Ingeniería y Arquitectura, de la Universidad de Zaragoza,

CERTIFICAN:

Que la memoria de Tesis Doctoral presentada por la ingeniera doña Belén Hernández Gascón con el título *"Mechanical modelling of the abdominal wall and biomaterials for hernia surgery"* ha sido realizada bajo nuestra dirección en el Departamento de Ingeniería Mecánica, de la Escuela de Ingeniería y Arquitectura, de la Universidad de Zaragoza, y se corresponde con el Proyecto de Tesis aprobado por la Comisión de Doctorado en 2012, por lo que autorizamos su presentación en la modalidad de compendio de publicaciones y con la Mención de "Doctor Internacional" cumpliendo por lo tanto las condiciones requeridas para que su autora pueda optar al grado de Doctora de la Universidad de Zaragoza.

Y para que conste así, firman las presentes en Zaragoza, a 10 de Diciembre de 2012.

Fdo.: Begoña Calvo Calzada

Fdo.: Estefanía Peña Baquedano

This thesis is presented as a compendium of articles published to obtain the title of Doctor at the University of Zaragoza, following the agreement of the 17th of December 2008 of the Governing Council of the University that approves the Regulations on Doctoral Thesis.

The articles that are part of the thesis and that have been published in journals indexed in the ISI are:

1. B. Hernández, E. Peña, G. Pascual, M. Rodríguez, B. Calvo, M. Doblaré, J. M. Bellón, 2011. Mechanical and histological characterization of the abdominal muscle. A previous step to modelling hernia surgery. *Journal of the mechanical behavior of biomedical materials*, 4(3): 392-404. (Journal Impact Factor: 2.814)

2. B. Hernández-Gascón, E. Peña, H. Melero, G. Pascual, M. Doblaré, M. P. Ginebra, J. M. Bellón, B. Calvo, 2011. Mechanical behaviour of synthetic surgical meshes: Finite element simulation of the herniated abdominal wall. *Acta Biomaterialia*, 7(11): 3905-3913. (Journal Impact Factor: 4.865)

3. B. Hernández-Gascón, E. Peña, G. Pascual, M. Rodríguez, J. M. Bellón, B. Calvo, 2012. Long-term anisotropic mechanical response of surgical meshes used to repair abdominal wall defects. *Journal of the mechanical behavior of biomedical materials*, 5(1): 257-271. (Journal Impact Factor: 2.814)

4. B. Hernández-Gascón, A. Mena, E. Peña, G. Pascual, J. M. Bellón, B. Calvo, 2012. Understanding the passive mechanical behavior of the human abdominal wall. *Annals of Biomedical Engineering*, In press, DOI: 10.1007/s10439-012-0672-7. (Journal Impact Factor: 2.368)

5. B. Hernández-Gascón, N. Espés, E. Peña, G. Pascual, J. M. Bellón, B. Calvo, 2012. Computational framework to model and design surgical meshes for hernia repair. *Computer Methods in Biomechanics and Biomedical Engineering*, In Press, DOI:10.1080/10255842.2012.736967. (Journal Impact Factor: 1.169)

6. J. Grasa, B. Hernández-Gascón, A. Ramírez, J. F. Rodríguez, B. Calvo, 2012. Numerical simulation of the behaviour of musculoskeletal tissue. *Revista Internacional de Métodos Numéricos para Cálculo y Diseño en Ingeniería*, 28(3), 177-186. (Journal Impact Factor: 0.167)

In addition to the articles previously listed and already published, two articles that are under review are part of this thesis:

7. B. Hernández-Gascón, E. Peña, J. Grasa, G. Pascual, J. M. Bellón, B. Calvo, 2012. Mechanical response of the herniated human abdomen to the placement of different prostheses. Submitted.

8. B. Hernández-Gascón, J. Grasa, B. Calvo, J. F. Rodríguez, 2012. A 3D continuum model for simulating skeletal muscle contraction. Submitted.

Besides, two published articles are included and, although they have been part of the work developed in the thesis, their main contribution correspond to the Translational Research Group in Biomaterials and Tissue Engineering at the University of Alcalá de Henares (Madrid, Spain):

9. G. Pascual, B. Hernández-Gascón, M. Rodríguez, S. Sotomayor, E. Peña, B. Calvo, J. M. Bellón, 2012. The long term behavior of lightweight and heavyweight meshes used to repair abdominal wall defects is determined by the host tissue repair process provoked by the mesh. *Surgery*, 152(5), 886-895. (Journal Impact Factor: 3.103).

10. G. Pascual, B. Hernández-Gascón, S. Sotomayor, E. Peña, B. Calvo, J. Buján, J. M. Bellón, 2012. Short-term behaviour of different polymer structure lightweight meshes used to repair abdominal wall defects. *Histology and Histopathology*, Accepted. (Journal Impact Factor: 2.480)

Esta tesis se presenta como un compendio de artículos publicados para optar al título de Doctor en la Universidad de Zaragoza, siguiendo el acuerdo de 17 de diciembre de 2008 del Consejo de Gobierno de la Universidad por el que se aprueba el Reglamento sobre Tesis Doctorales.

Los artículos que forman parte de la tesis y que han sido publicados en revistas indexadas en el ISI son:

1. B. Hernández, E. Peña, G. Pascual, M. Rodríguez, B. Calvo, M. Doblaré, J. M. Bellón, 2011. Mechanical and histological characterization of the abdominal muscle. A previous step to modelling hernia surgery. *Journal of the mechanical behavior of biomedical materials*, 4(3): 392-404. (Factor de Impacto: 2.814)

2. B. Hernández-Gascón, E. Peña, H. Melero, G. Pascual, M. Doblaré, M. P. Ginebra, J. M. Bellón, B. Calvo, 2011. Mechanical behaviour of synthetic surgical meshes: Finite element simulation of the herniated abdominal wall. *Acta Biomaterialia*, 7(11): 3905-3913. (Factor de Impacto: 4.865)

3. B. Hernández-Gascón, E. Peña, G. Pascual, M. Rodríguez, J. M. Bellón, B. Calvo, 2012. Long-term anisotropic mechanical response of surgical meshes used to repair abdominal wall defects. *Journal of the mechanical behavior of biomedical materials*, 5(1): 257-271. (Factor de Impacto: 2.814)

4. B. Hernández-Gascón, A. Mena, E. Peña, G. Pascual, J. M. Bellón, B. Calvo, 2012. Understanding the passive mechanical behavior of the human abdominal wall. *Annals of Biomedical Engineering*, In press, DOI: 10.1007/s10439-012-0672-7. (Factor de Impacto: 2.368)

5. B. Hernández-Gascón, N. Espés, E. Peña, G. Pascual, J. M. Bellón, B. Calvo, 2012. Computational framework to model and design surgical meshes for hernia repair. *Computer Methods in Biomechanics and Biomedical Engineering*, In Press, DOI:10.1080/10255842.2012.736967. (Factor de Impacto: 1.169)

6. J. Grasa, B. Hernández-Gascón, A. Ramírez, J. F. Rodríguez, B. Calvo, 2012. Modelado numérico del comportamiento del tejido músculo esquelético. *Revista Internacional de Métodos Numéricos para Cálculo y Diseño en Ingeniería*, 28(3), 177-186. (Factor de Impacto: 0.167)

Junto a los artículos previamente enumerados y ya publicados, forman parte del desarrrollo de esta tesis dos artículos que se encuentran en proceso de revisión:

7. B. Hernández-Gascón, E. Peña, J. Grasa, G. Pascual, J. M. Bellón, B. Calvo, 2012. Mechanical response of the herniated human abdomen to the placement of different prostheses. Submitted.

8. B. Hernández-Gascón, J. Grasa, B. Calvo, J. F. Rodríguez, 2012. A 3D continuum model for simulating skeletal muscle contraction. Submitted.

También se incluyen dos artículos publicados y, aunque han formado parte del trabajo desarrollado en la tesis, la aportación principal de los mismos ha correspondido al Grupo de Investigación Traslacional en Biomateriales e Ingeniería Tisular de la Universidad de Alcalá de Henares (Madrid, España):

9. G. Pascual, B. Hernández-Gascón, M. Rodríguez, S. Sotomayor, E. Peña, B. Calvo, J. M. Bellón, 2012. The long term behavior of lightweight and heavyweight meshes used to repair abdominal wall defects is determined by the host tissue repair process provoked by the mesh. *Surgery*, 152(5), 886-895. (Factor de Impacto: 3.103).

10. G. Pascual, B. Hernández-Gascón, S. Sotomayor, E. Peña, B. Calvo, J. Buján, J. M. Bellón, 2012. Short-term behaviour of different polymer structure lightweight meshes used to repair abdominal wall defects. *Histology and Histopathology*, Accepted. (Factor de Impacto: 2.480)

Abstract

Abdominal surgery for hernia repair is based on the implantation of a synthetic mesh in the defect area which aims at reinforcing the damaged wall. This clinical intervention is common in today's society and, in unfavorable cases such as obese patients or patients with large defects, can lead to a number of problems that reduce the quality of life of patients. The most common problems are the appearance of fibrosis, the hernia recurrence and occurrence of abdominal discomfort due to poor compliance between the host tissue and the prosthesis. Currently, surgeons have no definitive and universally accepted guidelines for the selection of the appropriate prosthesis for each patient and type of defect. Therefore, the choice of one or another mesh, and their placement in case of anisotropic meshes, is a decision to be taken by the surgeons according to their experience.

This thesis aims to study the abdominal hernia surgery from the continuum mechanics point of view. However, for the supply and validation of the generated models, it is necessary to perform an experimental study in an animal model. Since this is a multidisciplinary problem, the study approached was developed in collaboration with the Translational Research Group in Biomaterials and Tissue Engineering at the University of Alcalá de Henares (Madrid).

The final goal of hernia surgery is that the prosthesis ensures adequate tissular integration, being capable, among other things, to reproduce the mechanical behaviour of the healthy abdominal wall and to absorb the stresses due to the physiological loads to which the abdomen is subjected. Therefore, in addition to addressing the study in animal models to analyze the integration on the wall, the mechanical modelling of the abdominal wall and the biomaterials used in hernia repair is essential. For this, the construction of an *"in silico"* model of the human abdomen has been developed.

Due to the diversity of commercial products on the market, this thesis focusses on the study of three representative prostheses, specifically Surgipro®, Optilene® and Infinit®. These meshes are characterized by different geometric parameters and are made of different materials. In this work, the mechanical properties of the prostheses have been determined experimentally and different constitutive models, that reproduce the patterns of the mechanical behaviour observed in both, the abdominal muscle and implanted biomaterials, have been proposed. Specifically, the numerical modelling of the response of the abdominal muscle, including both active and passive responses, and prostheses have been approached within the framework of the nonlinear hyperelasticity

in large deformations.

The latter approach of this thesis aims to simulate computationally, using the finite element method, the response of the wall with the implanted mesh. A complete model of the human abdomen has been defined from nuclear magnetic resonance imaging. This complete model allows to differentiate the main anatomical units of the abdomen and it is used to simulate the passive and active responses. Furthermore, this model allows the study of the response of the healthy wall and the analysis of the final mechanical response of the herniated human abdomen to the placement of different prostheses.

In summary, this thesis establishes a methodology that opens doors to the automation of computational models that enable the simulation of personalized surgical procedures in order to select the most appropriate mesh for each patient as well as the appropriate placement on the defect in the case of anisotropic prostheses.

Keywords: Biomechanic, soft tissues, abdominal muscle, experimental characterization, constitutive model, anisotropy, hyperelasticity, collagen fibres, muscular fibres, finite elements, initial strains, hernia, reticular meshes, polypropylene, tissular integration.

Sinopsis

La cirugía abdominal de reparación de hernias está basada en la implantación de una malla sintética en la zona del defecto cuyo objetivo es reforzar la pared dañada. Esta intervención clínica es frecuente en la sociedad actual y, en casos desfavorables como son los pacientes obesos o con defectos de gran tamaño, puede dar lugar a una serie de problemas que disminuyen la calidad de vida del paciente. Los problemas más frecuentes son la aparición de fibrosis, la recidiva de la hernia y aparición de molestias abdominales debido a la deficiente adaptabilidad mecánica entre el tejido receptor y la prótesis. Actualmente los cirujanos no disponen de protocolos definitivos y universalmente aceptados para la selección de la prótesis más adecuada para cada paciente y tipo de defecto. Por tanto, la elección de una u otra malla, así como su colocación en casos de mallas anisótropas, es una decisión que debe tomar el cirujano en función de su experiencia.

Esta tesis tiene como finalidad el estudio de la cirugía herniaria abdominal desde el punto de vista de la mecánica de los medios continuos. Sin embargo, para la alimentación y validación de los modelos generados, se hace necesario realizar un estudio experimental en un modelo animal. Dado que se trata de un problema multidisciplinar, el estudio abordado se ha desarrollado en colaboración con el Grupo de Investigación Traslacional en Biomateriales e Ingeniería Tisular de la Universidad de Alcalá de Henares (Madrid).

El objetivo final de la cirugía herniaria es que la prótesis garantice una adecuada integración tisular, siendo capaz, entre otras cosas, de reproducir el comportamiento mecánico de la pared abdominal sana y absorber las tensiones provocadas a consecuencia de las cargas fisiológicas a las que está sometido el abdomen. Por tanto, además de abordar el estudio en modelos animales para analizar la integración en la pared, es fundamental el modelado mecánico de la pared abdominal y de los biomateriales utilizados en la reparación herniaria. Para ello, se ha abordado la construcción de un modelo *"in silico"* del abdomen humano.

Debido a la diversidad de productos comerciales existentes en el mercado, esta tesis se centra en el estudio de tres prótesis representativas; concretamente las mallas Surgipro®, Optilene® e Infinit®. Estas mallas están caracterizadas geométricamente por diferentes parámetros y fabricadas de diferentes materiales. En esta tesis se han determinado experimentalmente las propiedades mecánicas de las mismas y se han planteado diferentes modelos constitutivos que reproducen los patrones de compor-

tamiento mecánico observados tanto en el músculo abdominal como en los biomateriales implantados. Específicamente, el modelado numérico de la respuesta de las prótesis y del músculo abdominal, incorporando tanto la respuesta pasiva como la activa, se han abordado bajo el marco de la hiperelasticidad no lineal en grandes deformaciones.

El último abordaje de esta tesis tiene como objetivo la simulación computacional por elementos finitos de la respuesta de la pared con la malla implantada. Se ha definido un modelo completo de abdomen humano obtenido a partir de imágenes de resonancia magnética nuclear. Este modelo completo permite diferenciar las unidades anatómicas principales del abdomen utilizándose para la simulación de las respuestas pasiva y activa del mismo. Este modelo permite estudiar la respuesta de la pared sana y la influencia que tiene el uso y la orientación de diferentes biomateriales sobre la respuesta mecánica final.

Resumiendo, esta tesis establece una metodología de trabajo que abre las puertas a la automatización de modelos computacionales que permitan la simulación de intervenciones quirúrgicas personalizadas, con el fin de seleccionar el tipo de malla más adecuada para cada paciente así como la orientación idónea en el defecto en el caso de prótesis anisótropas.

Palabras clave: Biomecánica, tejidos blandos, músculo abdominal, caracterización experimental, modelo constitutivo, anisotropía, hiperelasticidad, fibras de colágeno, fibras musculares, elementos finitos, deformaciones iniciales, hernia, mallas reticulares, polipropileno, integración tisular.

Agradecimientos

A mi madre y a mi padre, a quienes nunca olvidaré, por ser el pilar fundamental en todo lo que soy, en toda mi educación, tanto académica, como de la vida, que me dan la fuerza necesaria para seguir adelante día a día.

A mis hermanos, Paquito, María Isabel y Alberto, por el ánimo infundido, el apoyo contínuo y la confianza depositada en mí. No me olvido de las dos pequeñas de la familia, María y Marta, que son las personas que consiguen sacarme una sonrisa hasta en el peor de los momentos. Aprovecho también para agradecer también el apoyo de José Antonio y de toda la familia.

Me gustaría que estas líneas sirvieran para expresar mi más profundo y sincero agradecimiento a Begoña Calvo y a Estefanía Peña, directoras de esta tesis, por aceptarme para realizar este trabajo bajo su dirección. Especial reconocimiento merece la orientación, el seguimiento y la supervisión contínua de la misma, pero sobre todo por la motivación, el apoyo recibido y la confianza depositada en mí a lo largo de estos años, no sólo en el ámbito científico sino también en el personal.

También quiero expresar mi agradecimiento a Juan M. Bellón, del Departamento de Cirugía, y a Gemma Pascual, del Departamento de Especialidades Médicas, de la Facultad de Medicina de la Universidad de Alcalá de Henares, que con su ayuda han colaborado en la realización del presente trabajo multidisciplinar. Debo destacar, por encima de todo, el buen trato recibido en mis horas de trabajo en sus instalaciones, su disponibilidad y paciencia a la hora de hacerme entender los conceptos de la medicina y la biología.

Quiero extender un sincero agradecimiento a Jorge Grasa y a José Félix Rodríguez, por su paciencia, disponibilidad y apoyo en los momentos difíciles de la tesis, ya que su colaboración ha sido fundamental. Les agradezco también por sus siempre atentas y rápidas repuestas a las diferentes inquietudes surgidas durante el desarrollo de este trabajo, lo cual se ha visto también reflejado en los buenos resultados obtenidos.

Especial agrademiento merece Philippe Young, que me dió la oportunidad de realizar una estancia doctoral en su empresa, *"Simpleware"* (Exeter, Reino Unido), por su colaboración y su apoyo, permitiéndome vivir una experiencia profesional y personal que nunca olvidaré.

Quisiera hacer extensiva mi gratitud a todos los que han sido y son compañeros del Departamento de Ingeniería Mecáncia de la Escuela de Ingeniería y Arquitectura de la Universidad de Zaragoza: profesores, técnicos de laboratorio y personal administrativo. Especial reconocimiento merece la ayuda y las sugerencias recibidas de Miguel Ángel Martínez, Victor Alastrué, Mauro Malve, Andrés Mena y Elena Lanchares.

Para mis compañeros de grupo con los que he compartido esta experiencia día a día, doctorandos/as y posdocs, para los que sólo tengo palabras de agradecimiento. Ha sido un camino largo y duro en el que, algunas veces, los agobios del trabajo hacen alejarse de trato personal, pero otros momentos han sido de diversión. Quiero expresar agradecimiento especial a Myriam, a la que no puedo considerar solamente como una compañera de trabajo, sino que es una gran amiga que me ha apoyado en todos los momentos, buenos y malos, de estos cuatro años. Especial mención merecen Carlos, Fares, Pablo, Sergio y Sara, y algunas personas que ya dejaron el Departamento, Diego y Juan, todos ellos compañeros y amigos siempre dispuestos a ayudar, con los que he compartido conomientos y experiencias no sólo profesionales sino también personales, que nunca olvidaré.

En último lugar, y no por ello menos importantes, agradecer a mis amigos que han compartido conmigo todos los momentos durante estos años, por su apoyo y confianza; A mis amigos de la Universidad y Zaragoza, con especial agradecimiento a Paola, Lupi y Martín. A la *"Peña el Atasco"* de Calamocha, los amigos de toda la vida, que son aquellos con los que el paso de tiempo no importa porque seguimos estando unidos. Y como no, a mis *"hermanas sevillanitas"*, Laura y Julia, para las que no tengo palabras que describan el agradecimiento de su apoyo a nivel personal.

A todos los que confían en mí.

Zaragoza, 10 de Diciembre de 2012.

Índice General - Contents

INTRODUCCIÓN GENERAL Y RESUMEN

Modelado mecánico de la pared abdominal y biomateriales para la cirugía herniaria

Capítulo I

Motivación y objetivos

Una de las enfermedades más comunes en el campo de la medicina es la aparición de hernias. Un hernia se define como la protusión de uno o varios órganos internos a través de una abertura en la cavidad que los contiene debido a un debilitamiento de la pared de la misma. Según datos estadísticos, se estima que anualmente se reparan más de 20 millones de hernias en todo el mundo (Kingsnorth and LeBlanc, 2003). Desde otra perspectiva, un 3% de la población sufre, a lo largo de la vida, algún tipo de hernia, siendo cinco veces más común esta patología en hombres que en mujeres (Park et al., 2006). Aunque es difícil estimar el coste total que esta patología supone para la sociedad, se estima que puede ascender a 2,5 billones de euros al año en los Estados Unidos.

Las hernias pueden surgir en cualquier lugar del cuerpo, pero son más frecuentes en el área abdominal o inguinal. La cavidad abdominal no está protegida por ninguna estructura oseocartilaginosa, por lo que la protección de esta región anatómica queda enteramente a cargo de la pared abdominal. Por tanto, la integridad de la pared abdominal permite su correcto funcionamiento, debido a que funciona como un sistema dinámico y está sometida a cambios agudos de presión (tos, vómito etc.) o mantenidos (obesidad, embarazo etc.) (Cobb et al., 2005; Song et al., 2006b). Los factores más comunes que provocan la aparición de las hernias son el incremento de la presión abdominal debido a tos crónica, estreñimiento, obstrucción urinaria, levantamiento de cargas pesadas, historial familiar y obesidad. Otra de las causas de aparición de hernias es el debilitamiento de los tejidos y, consecuentemente, la pérdida de rigidez de los mismos. Por otra parte, es muy frecuente el debilitamiento de la región frontal del abdomen a consecuencia de una incisión laparotómica a través de la línea alba para acceder al interior de la cavidad abdominal o en otras cirugías.

La cirugía abdominal por medio de la implantación de mallas sintéticas es la técnica más frecuentemente utilizada actualmente para la reparación de hernias. A lo largo del tiempo, las técnicas quirúrgicas destinadas a la reparación herniaria han ido evolucionando desde la autoplastia, empleando los propios tejidos del individuo, hasta el empleo de los materiales protésicos (Deysine, 1998). Concretamente, el panorama terapéutico de los defectos herniarios ubicados en la pared abdominal ha cambiado con los resultados aportados por el grupo de Lichtenstein relacionados con las prótesis (Lichtenstein and Shulman, 1986; Lichtenstein et al., 1989). El uso de biomateriales para la reparación de hernias ha demostrado gradualmente su eficacia, aunque la reparación de hernias incisionales de gran tamaño es más complicada y está asociada a complicaciones de alto riesgo en el post-operatorio (Sabbagh et al., 2011). El polipropileno (PP), en forma de prótesis reticular, es uno de los biomateriales más empleados para la reparación de defectos herniarios. A lo largo del tiempo, su utilización se ha ido generalizando y es uno de los mejores biomateriales para tratar defectos, incluso cuando existe infección (Alaedeen et al., 2007).

A pesar de que existen multitud de mallas comerciales utilizadas para la reparación herniaria, cada una de ellas puede provocar, en mayor o menor medida, una variedad de problemas que disminuyen la calidad de vida del paciente. Una de las ocurrencias más frecuentes es la aparición de fibrosis, definida como el crecimiento de tejido anormal en la zona del defecto, debido a la presencia de un cuerpo extraño, y que puede dar lugar a la encarcelación o estrangulación de las vísceras. La recidiva de la hernia se considera otro de los problemas más importantes en la cirugía herniaria y, generalmente, tiene lugar por la sutura entre la prótesis y el tejido. Además, la mala adaptabilidad mecánica entre el tejido receptor y la prótesis, debido a una diferencia significativa de la rigidez de ambos tejidos (Schimidbauer et al., 2005), puede provocar incomodidad, e incluso dolor, en los pacientes (Welty et al., 2001; Holste, 2005). Por otra parte, los cirujanos no disponen de protocolos definitivos y universalmente aceptados para la elección de la prótesis más adecuada para cada paciente y tipo de defecto. Por tanto, la elección de una u otra malla, así como su colocación, es una decisión a tomar por el cirujano en función de su experiencia.

Debido a que esta patología médica es muy común, numerosos científicos están centrados en su estudio tanto desde el punto de vista clínico como biomecánico. En particular, la biomecánica es una disciplina científica cuyo objetivo es el estudio de las estructuras biológicas que existen en los seres vivos desde el punto de vista mecánico. Esta área de conocimiento aglutina diferentes ciencias biomédicas, utilizando conocimientos de la mecánica, la ingeniería, la anatomía, la fisiología y otras disciplinas, con el fin de estudiar el comportamiento del cuerpo humano y resolver los problemas derivados a los que puede verse sometido.

Para un correcto modelado y análisis del problema se han de tener en cuenta una serie

de consideraciones que a continuación se describen. En primer lugar, las propiedades mecánicas de los tejidos musculares vienen dadas por la composición microestructural de los mismos. Concretamente, los tejidos musculares están formados por una red de fibras musculares, de colágeno y elastina que están embebidas en una matriz más o menos isótropa (Loocke et al., 2008; Ito et al., 2010) y están catalogados como tejidos blandos. La respuesta mecánica de estos tejidos blandos evidencia una respuesta no lineal y en grandes deformaciones puesto que para bajos niveles de carga se obtienen grandes desplazamientos y para altos niveles de carga los tejidos rigidizan notablemente (Calvo et al., 2010; Martins et al., 2012). A su vez, el alto contenido de agua presente en estos tejidos, cercano al 70%, les confiere un caracter incompresible. La orientación preferencial de las fibras musculares y de colágeno da lugar a una respuesta mecánica anisótropa. Las fibras de colágeno son las responsables de la respuesta pasiva (Calvo et al., 2009; Martins et al., 2012), mientras que las fibras musculares son las responsables de la respuesta activa del músculo (Linden, 1998; Arruda et al., 2006). La pared abdominal está sometida a una distribución de tensiones iniciales o residuales como resultado del proceso de crecimiento desde el estado embrionario hasta la edad adulta. Estas tensiones residuales se revelan al realizar una extracción del tejido, puesto que se produce una retracción del mismo, y la configuración de equilibrio se modifica a causa de la liberación de dichas tensiones residuales (Fung, 1993; Gardiner et al., 2001; Peña et al., 2006).

La caracterización mecánica de la respuesta pasiva del tejido abdominal se ha llevado a cabo principalmente a través de modelos de experimentación animal (Nilsson, 1982a,b; Hwang et al., 2005). También hay estudios que utilizan modelos de experimentación humanos (Arampatzis et al., 2005; Song et al., 2006a,b) a pesar de que, en este caso, la obtención de las muestras es complicada. La mayoría de los estudios incorporan ensayos de caracterización uniaxial de tracción (Nilsson, 1982a,b; Gajdosik, 2001) y compresión (Loocke et al., 2004) aunque también se utilizan ensayos biaxiales (Hwang et al., 2005) o de inflado (Song et al., 2006b), más próximos a la situación fisiológica. La respuesta mecánica del abdomen difiere en función de la zona del abdomen analizada (Nilsson, 1982a,b) y de la dirección del ensayo, por lo que la respuesta es anisótropa (Hwang et al., 2005; Song et al., 2006a,b; Martins et al., 2012). Concretamente, la respuesta mecánica es más rígida en el plano transversal que en el plano craneo-caudal (Song et al., 2006a,b). También hay estudios que indican que la respuesta mecánica depende de la edad y el sexo del sujeto (Junge et al., 2001) aunque otros estudios descartan tal evidencia (Rath et al., 1996).

Según el conocimiento de la autora, no existen estudios experimentales que caractericen la respuesta activa del músculo abdominal, aunque sí que hay estudios en la literatura de otros músculos, tanto de animales (Hill, 1938; Ramsey and Street, 1940; Abbot and Wilkle, 1953; Huxley and Hanson, 1954; Huxley and Niedergerke, 1954; Huijing, 1998) como humanos (Maganaris and Paul, 1999; Arampatzis et al., 2005).

La informacion obtenida mediante la caracterización experimental se ha utilizado para la definición de modelos constitutivos que reproducen la respuesta mecánica de los tejidos blandos (Bol and Reese, 2008; Odegard et al., 2008; Stålhand et al., 2008; Calvo et al., 2010; Morrow et al., 2010; Ramírez et al., 2010; Stålhand et al., 2010; Bol et al., 2011; Ehret et al., 2011; Grasa et al., 2011; Hodgson et al., 2012; Martins et al., 2012). El modelado numérico de los tejidos musculares se ha planteado tanto a nivel microscópico (Sharafi and Blemker, 2010) como macroscópico (Martins et al., 2012), a través de modelos lineales (Boriek et al., 2000) y no lineales (Martins et al., 2012) e incluso algunos modelos recogen la respuesta en grandes deformaciones de los tejidos (Calvo et al., 2009; Chi et al., 2010; Ito et al., 2010; Hodgson et al., 2012). Los modelos numéricos planteados dentro de la teoría de la hiperelasticidad exigen la definición de una función densidad energía de deformación (FDED) que suele expresarse en función de los invariantes cinemáticos (Spencer, 1971) y considera de forma aditiva las respuestas activa (capaz de generar fuerza) y pasiva (resistencia a deformación). A su vez, la componente pasiva de estas funciones suelen considerar las contribuciones de la respuesta isótropa (Yeoh, 1993; Ogden, 2001) y anisótropa del tejido (Demiray et al., 1988; Holzapfel et al., 2000; Calvo et al., 2009) de forma desacoplada.

Una vez caracterizado y seleccionado el modelo de comportamiento que reproduce el comportamiento de los tejidos, es posible abordar la simulación numérica con elementos finitos, pudiendo así reproducir estados de carga fisiológicos o no fisiológicos en una determinada geometría cuya solución analítica no es posible. La respuesta pasiva de las regiones abdominales e inguinales se ha simulado numéricamente en algunos estudios con geometrías o modelos simples (Song et al., 2006a,b; Szymczak et al., 2010; Förstemann et al., 2011; Smietanski et al., 2012; Szymczak et al., 2012). Por otra parte, Fortuny et al. (2009a) y Fortuny et al. (2009b) simularon la respuesta activa de la zona inguinal pero no se conocen estudios que modelen la respuesta activa del músculo abdominal según el conocimiento de la autora. Por el contrario, otros estudios de la literatura recogen la simulación computacional del comportamiento mecánico activo de otros tejidos musculares lisos (Stålhand et al., 2008, 2010) o esqueléticos (Blemker et al., 2005; Bol and Reese, 2008; Grasa et al., 2011).

La investigación y desarrollo en biomateriales destinados a reparar defectos de pared abdominal ha evolucionado y progresado en los últimos años, con el fin de encontrar la "prótesis ideal". En lo que respecta a las prótesis reticulares, uno de los objetivos de investigación ha sido valorar la cantidad de material implantado. También se han diseñado prótesis reticulares de tipo híbrido (Klosterhalfen et al., 2005), en las cuales hay componentes absorbibles y no absorbibles, facilitando el proceso de integración tisular. Los nuevos diseños también tienen en cuenta, como parámetro fundamental, el tamaño del poro, y otros aspectos como el diámetro de los filamentos, la distribución espacial de los mismos y el polímero con el cual han sido generados (Pandit and Henry, 2004; Rosch et al., 2004). En la actualidad, junto al polipropileno, se emplean otros

polímeros como el politetrafluoroetileno expandido (PTFE) para fabricar estas prótesis. Asímismo, la distribución espacial de los filamentos genera una respuesta mecánica isótropa o anisótropa del implante, de modo que la orientación de la malla sobre el tejido abdominal receptor, que a su vez tiene también un comportamiento anisótropo (Hwang et al., 2005), es fundamental.

De forma general, se han clasificado las prótesis reticulares en biomateriales de alto o bajo peso, dependiendo del parámetro de densidad g/m^2 que tengan las mismas (Klinge, 2007). Se consideran prótesis de alto peso o *"heavyweight"* (HW) aquellas que se sitúan por encima de 80 g/m^2, mediano peso o *"mediumweight"* (MW) entre $50 - 80$ g/m^2 (Cobb et al., 2006) y de bajo peso o *"lightweight"* (LW) las que se encuentran por debajo de 50 g/m^2. El proceso de integración tisular después del implante depende de la prótesis implantada (Schachtrupp et al., 2003). Concretamente, la fibrosis generada por las prótesis convencionales HW podría verse disminuida con el implante de prótesis tipo LW (Conze et al., 2005; O'Dwyer et al., 2005). Es decir, una de las finalidades de las prótesis LW es la de disminuir la cantidad de cuerpo extraño residual que permanece a nivel de los tejidos receptores. De esta forma puede obtenerse una menor reacción de cuerpo extraño y un proceso reparativo generador de menos fibrosis en los tejidos receptores (Klinge et al., 2002b).

Como se ha comentado previamente, la pared abdominal funciona como un sistema dinámico y está sometida a cambios agudos de presión o mantenidos en el tiempo (Cobb et al., 2005; Song et al., 2006b). Por todo ello, tras la colocación de un material protésico, debe quedar una cierta distensibilidad que permita una movilidad no restrictiva de la pared (Junge et al., 2001; Klinge et al., 2002a) sin que ello menoscabe la resistencia mecánica final de la misma.

La caracterización del comportamiento de diferentes prótesis se ha abordado en numerosos estudios experimentales encontrados en la literatura (Afonso et al., 2008; Hollinsky et al., 2008; Bellón, 2009; Saberski et al., 2010; Yoder and Elliott, 2010; Deeken et al., 2011). Otros trabajos se centran en el estudio y análisis del comportamiento de las suturas que permiten la unión de la prótesis al tejido (Kes et al., 2004; Schwab et al., 2008) y en el tamaño del solapamiento mínimo necesario para que prevenir la dislocación temprana de la prótesis (Binnebösel et al., 2007).

Respecto al modelado de su comportamiento, los modelos constitutivos han de reproducir los patrones de comportamientos observados en las prótesis ante diferentes cargas. En general, la respuesta mecánica de las prótesis se asocia a fenómenos que tienen lugar a diferentes escalas. Las evidencias experimentales indican una respuesta no lineal, cambios drásticos en la malla debido al colapso de los poros de la malla bajo condiciones de carga uniaxial y una fuerte componente anisótropa en algunas de las mallas comerciales. Dichos fenómenos se pueden estudiar a partir del análisis de

la celda unidad o patrón que define, por repetición en el espacio, el tejido de la malla (Röhrnbauer et al., 2011). Por otra parte, la fricción entre los hilos de la malla provocan fenómenos como histéresis, dependencia de la velocidad de deformación y procesos de deformación irreversibles que provocan cambios significantes en la geometría de la celda durante ciclos de carga. Algunos modelos computacionales reproducen la geometría de los filamentos (Kuwazuru and Yoshikawa, 2004) mientras que otros autores proponen modelos continuos (King et al., 2005; Röhrnbauer et al., 2011).

Después de la cirugía, las propiedades mecánicas del conjunto tejido-malla se modifican debido al proceso de integración tisular. Por esta razón, la caracterización mecánica experimental (Cobb et al., 2006; Bellón et al., 2007; Ozog et al., 2011) e histológica (Hilger et al., 2006; Pascual et al., 2008) del conjunto tejido-malla tiene como objetivo la determinación de las propiedades mecánicas del lugar del implante tras diferentes tiempos después de la operación. La rigidez del conjunto tejido-prótesis final debe ser mayor debiendo reproducir con el tiempo el comportamiento original del tejido abdominal sano (Cobb et al., 2006; Pascual et al., 2008; Bellón et al., 2009). En los casos con infección, el PP es de los pocos materiales con los que es posible el rescate parcial de la prótesis (Bellón-Caneiro et al., 2004; Jezupors and Mihelsons, 2006) y sus propiedades no se alteran con el paso del tiempo. Sin embargo, el PP presenta el inconveniente de que tiene mal comportamiento en la interfaz peritoneal y aparecen complicaciones como fistulizaciones al intestino (Chew et al., 2000) y migraciones a órganos cavitarios (Chuback et al., 2000). Como se ha introducido previamente, el tejido abdominal es anisótropo (Hwang et al., 2005) y algunas de las prótesis comerciales presentan también anisotropía (Yoder and Elliott, 2010). En estos casos, una vez que la malla se integra en el tejido receptor, el conjunto resultante tejido-malla sigue siendo anisótropo (Ozog et al., 2011). Por tanto, si bien la adaptación final de la malla sintética ha de ser tal que mimetice la respuesta original del tejido sano, su disposición y orientación en el abdomen es importante (Anurov et al., 2010; Ozog et al., 2011). Concretamente, la dirección más rígida de la malla ha de colocarse paralela a la dirección donde el esfuerzo muscular es mayor (Anurov et al., 2010) y a lo largo de la dirección donde están dispuestas las fibras en las aponeurosis (Anurov et al., 2012).

A pesar de los trabajos existentes que hay en la literatura acerca de la caracterización experimental del músculo abdominal, no existen datos acerca de las deformaciones iniciales en el abdomen y no existe ningún estudio completo que determine las propiedades mecánicas de todos los músculos en el mismo especimen. A su vez, no se han encontrado trabajos que describan numéricamente la respuesta pasiva del tejido abdominal desde el marco de la hiperelasticidad no lineal anisótropa, ni trabajos que modelen la respuesta activa del abdomen. Por otra parte, no se conocen trabajos que modelen experimental y numéricamente el comportamiento de prótesis simultáneamente y, a pesar de que el proceso de integración tisular ha sido ampliamente estudiado en la literatura, el análisis de la respuesta mecánica del conjunto tejido-malla ha sido abordado mayoritariamente

a corto plazo. Por tanto, a pesar de los trabajos existentes que hay en la literatura acerca de la caracterización experimental y computacional del abdomen y prótesis, no son suficientes para abordar nuestro estudio de forma completa. Dada la importancia de la problemática de la cirugía abdominal en la sociedad actual y las deficiencias de los estudios disponibles en la literatura, esta tesis está enfocada al modelado del comportamiento mecánico de la pared abdominal y de diferentes mallas sintéticas utilizadas en la reparación herniaria.

Dada la amplitud y complejidad del problema a abordar se necesita la formación de un grupo multidisciplinar de trabajo. En este caso particular, dicho equipo está formado por especialistas en la mecánica de medios continuos y el modelado de tejidos dentro de la Ingeniería (Grupo de Mecánica Aplicada y Bioingeniería de la Universidad de Zaragoza), biólogos y especialistas clínicos con experiencia a nivel de experimentación en modelos animales y con la inquietud innovadora de dar soluciones para las patologías herniarias (Grupo de Investigación Traslacional en Biomateriales e Ingeniería Tisular de la Universidad de Alcalá de Henares). La formación de este equipo nos ha permitido abordar el estudio de esta patología bajo dos escenarios diferentes: inicialmente, se ha realizado el estudio en un modelo animal, el conejo blanco de nueva Zelanda, que nos ha permitido llevar a cabo los ensayos experimentales de caracterización de los tejidos, así como la evaluación de la integración tisular con tres prótesis comunes. Por otro lado, en función de los resultados experimentales obtenidos se han podido proponer, definir y validar los modelos numéricos de comportamiento mecánico. Posteriormente, los resultados obtenidos sobre el modelo animal se han extendido al humano construyendo un modelo *"in silico"* de la pared abdominal partiendo de imágenes de resonancia magnética. Este modelo nos ha permitido estudiar la respuesta de la pared sana y tras la colocación de los tres tipos de mallas seleccionadas. La ventaja de la metodología propuesta es reducir los costes de experimentación y las pruebas clínicas, que en el caso de humanos son difíciles de abordar.

El desarrollo de esta tesis se enmarca dentro dos proyectos de investigación financiados primeramente por el CIBBER-BBN y, posteriormente, por el Ministerio de Economía y Competitividad: "Desarrollo y validación de un nuevo concepto de implante protésico para la reparación de defectos de la pared abdominal" (ABDOMESH) y "Modelado biomecánico del tejido músculo-esquelético abdominal" (DPI2011-27939-C02-01), respectivamente. Por otro lado, esta tesis se ha podido realizar gracias a la beca FPI BES-2009-021515, concedida por el Ministerio de Ciencia e Innovación.

I.1 Objetivos

El objetivo principal de la tesis es establecer una metodología de trabajo que permita analizar la respuesta de prótesis en la cirugía de hernias abdominales mediante técnicas experimentales y computacionales. Para obtener este objetivo principal es necesario alcanzar los siguientes objetivos parciales (ver Figura I.1):

- Caracterización experimental y modelado numérico del comportamiento mecánico pasivo del músculo abdominal de un modelo de experimentación animal.
- Caracterización experimental y modelado numérico del comportamiento mecánico de diferentes mallas sintéticas comerciales.
- Caracterización histológica y experimental a corto y largo plazo del comportamiento mecánico pasivo del conjunto músculo abdominal-malla sintética tras diferentes tiempos del implante (14, 90 y 180 días) y tipos de implante.
- Definición de una metodología de trabajo para diseñar y validar el comportamiento de prótesis.
- Definición de un modelo computacional de elementos finitos simplificado del animal de experimentación para la reproducción del comportamiento abdominal sin hernia y después de la cirugía.
- Definición de un modelo computacional de elementos finitos completo basado en la geometría del cuerpo humano, obtenida mediante imágenes de resonancia magnética nuclear, para la reproducción de la mecánica de la pared abdominal sana.
- Definición de un modelo computacional de elementos finitos completo del abdomen humano herniado y reparado, utilizando diferentes prótesis, y análisis de la respuesta del conjunto en función de la malla comercial y su orientación en el abdomen.
- Modelado numérico del comportamiento activo del tejido músculo esquelético.

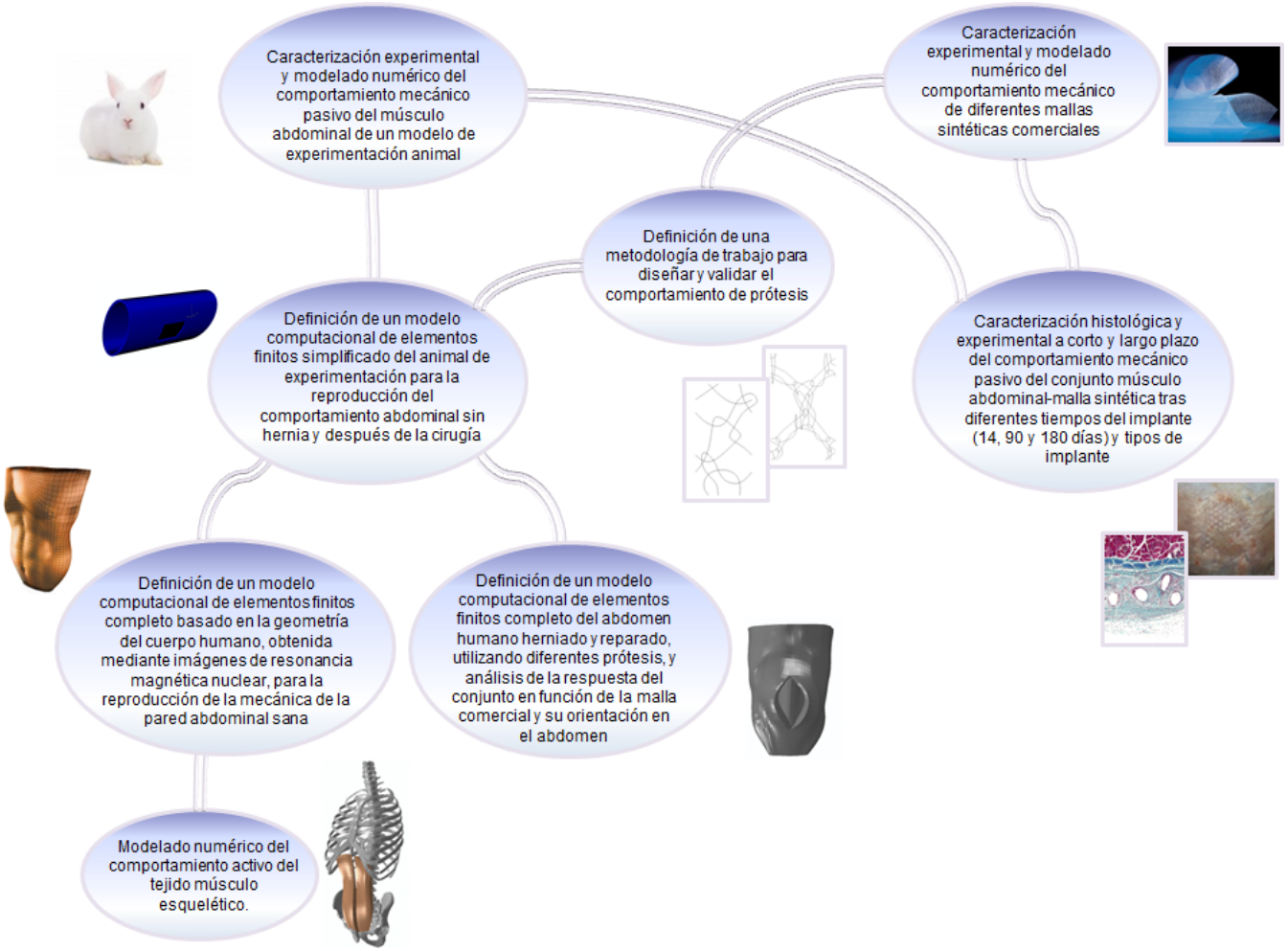

Figura I.1: Objetivos parciales de la tesis.

I.2 Estructura de la Tesis

La tesis se presenta como un compendio de publicaciones y el presente documento cumple con los requisitos establecidos por la Universidad de Zaragoza, siguiendo el acuerdo de 17 de diciembre de 2008 del Consejo de Gobierno de la Universidad por el que se aprueba el Reglamento sobre Tesis Doctorales y donde se contemplan las tesis elaboradas como compendio de publicaciones.

En la página inicial se ha especificado que la tesis es un compendio de trabajos y se han enumerado las referencias completas de cada uno de los artículos que constituyen el cuerpo de la tesis.

La presente tesis se compone de cinco partes que se describen a continuación. En primer lugar, en el Capítulo I, titulado ***Motivación y objetivos***, se presenta la motivación del estudio desarrollado en la tesis y los objetivos de la investigación.

En segundo lugar, el Capítulo II, titulado ***Pared abdominal y biomateriales para la cirugía herniaria***, presenta una revisión y el estado del arte de los principales temas relacionados con la mecánica, anatomía y fisiología de la pared abdominal y las prótesis utilizadas en el implante, así como del proceso de integración tisular. Estos conceptos son importantes para entender los resultados y el alcance de esta tesis. Asímismo, se incluye la descripción detallada de la problemática generada como consecuencia de la cirugía abdominal desde el punto de vista mecánico, así como considerando algunos aspectos clínicos relacionados en el tratamiento de hernias.

En tercer lugar, el Capítulo III, titulado ***Resultados, publicaciones y conclusiones de la tesis***, presenta los resultados principales obtenidos en la tesis, que se agrupan según la metodología seguida para el desarrollo de la misma, justificándose la unidad temática de los trabajos incluidos en el compendio de publicaciones. También se describen las contribuciones originales de la tesis y las conclusiones finales, así como las líneas futuras de trabajo.

A continuación se incluyen los artículos que forman el compendio de publicaciones y, finalmente, se incluyen tres apéndices. El primer apéndice describe las características de las revistas donde se han publicado los artículos, el segundo incluye la carta de aceptación del trabajo 10 y, en último lugar, se incluye la renuncia de los coautores no doctores a presentar los trabajos de los que son coautores como parte de otra tesis doctoral.

Capítulo II

Pared abdominal y biomateriales para la cirugía herniaria

II.1 Introducción

A pesar de que, normalmente, las hernias suelen ser pequeñas y relativamente asintomáticas, éstas pueden provocar dolor e incomodidad en los pacientes que las sufren afectando a su calidad de vida. Además, ocasionalmente algunas de las hernias llevan a la encarcelación y estrangulación de los intestinos y otras vísceras, convirtiéndose en una enfermedad muy grave. Si se considera a su vez el hecho de que uno de cada cinco pacientes que sufren una intervención por laparotomía desarrollan una hernia incisional, las hernias abdominales se han convertido en una patología habitual en el sistema de la salud. Aunque es difícil estimar el coste total que esta patología supone para la sociedad, se estima que puede ascender a 2,5 billones de euros al año en Estados Unidos. La gran relevancia médica que tiene esta patología ha llevado a numerosos grupos de investigación a estudiar dicha patología, entre otros campos, en el campo de la biomecánica.

En el presente capítulo se han incluido diferentes secciones que describen los conceptos fundamentales necesarios para la comprensión del contenido de la tesis. En las Secciones II.2 y II.3 se han descrito los términos más importantes relacionados con la cirugía herniaria así como la anatomía y fisiología de la pared abdominal. A continuación, las Secciones II.4, II.5, II.6 y II.7 hacen referencia al estudio de la pared abdominal y de las prótesis utilizadas en la reparación de hernias, al proceso de integración tisular tras la cirugía y al diseño de mallas sintéticas, respectivamente. Dichas

secciones describen los conceptos fundamentales incluyéndose una revisión bibliográfica de los trabajos existentes en la literatura relativos a cada tema.

II.2 Cirugía herniaria

Una hernia se produce cuando aparece un defecto en el tejido, provocando la protusión de los órganos internos al exterior de la cavidad que los contiene (ver Figura II.1). Las causas que provocan la aparición de hernias pueden ser diversas (Park et al., 2006). Un factor común es el incremento de la presión abdominal debido a tos crónica, estreñimiento, obstrucción urinaria, levantamiento de cargas pesadas, hidropesía del vientre (fluido en el abdomen), cirugía abdominal previa y obesidad, entre otros. Además, la pérdida de rigidez en el tejido, el daño de los nervios como consecuencia del debilitamiento de los músculos, la presencia de canales embriológicos en el caso de hernias congenitales (defectos de nacimiento) y el historial familiar son otras de las causas que pueden provocar la aparición de hernias. Por otra parte, la realización de incisiones laparotómicas a través de la línea alba para acceder a la cavidad peritoneal constituye uno de los abordajes más frecuentes en cirugía abdominal. Esta técnica provoca el debilitamiento de dicha región donde intersectan las fibras que envuelven a los músculos abdominales, convirtiéndose así en una zona susceptible de sufrir una hernia incisional (ver Figura II.2).

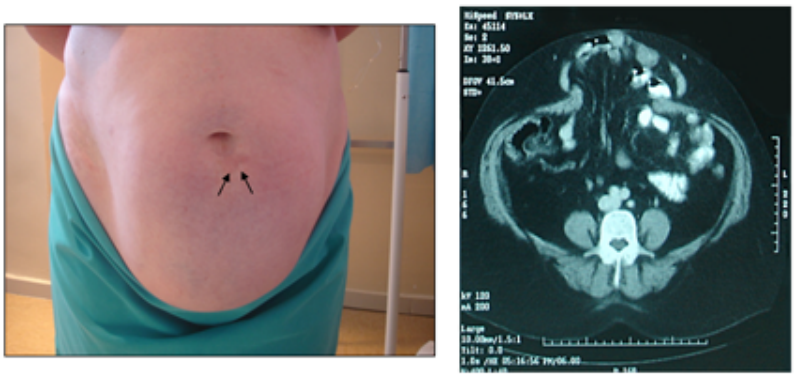

(a) (b)

Figura II.1: (a) Imagen macroscópica de una hernia abdominal. (b) Detección de la hernia en (a) mediante imagen de resonancia magnética (Bellón, 2012).

Existen varios tipos de hernias, según el lugar de la cavidad abdominal en el que aparecen (ver Figura II.3). Las más comunes se enumeran a continuación:

- Hernia inguinal: se produce cuando un defecto en la pared muscular de la región

(a)

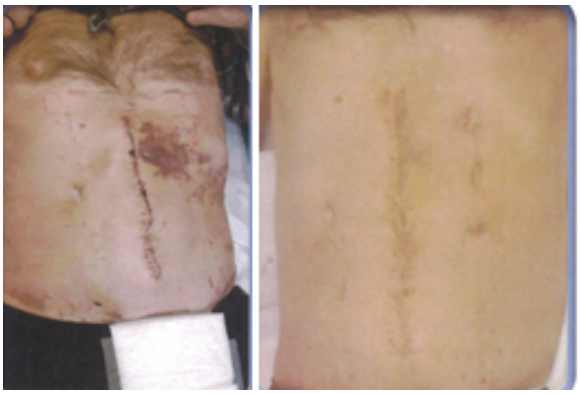

(b)

Figura II.2: (a) Hernia abdominal a lo largo de la línea alba. (b) Aspecto del abdomen tras la cirugía herniaria (Ramshaw, 2009).

inguinal permite que el contenido abdominal (normalmente intestino o vejiga urinaria) aparezca debajo de la piel recubierto por un saco de peritoneo. Existen hernias inguinales de dos tipos: directas e indirectas. En hernias inguinales directas, presentes normalmente en hombres de mediana y avanzada edad, el contenido abdominal, en concreto el intestino delgado, pasa a través de una debilidad de la musculatura y protruye en el área del triángulo de Hasselbach. Las hernias inguinales indirectas se producen cuando el contenido abdominal protruye a través del anillo inguinal interno o profundo, bajan a lo largo del cordón espermático y, con el tiempo, suelen llegar al escroto. Estas últimas se suelen presentar en hombres jóvenes y niños.

- Hernia femoral o crural: afecta principalmente a las mujeres de edad avanzada, pero puede darse también en mujeres jóvenes tras el embarazo y el parto. Aparece en las ingles, o justo bajo ellas. Una parte del intestino pasa por el conducto por donde discurre normalmente la arteria y vena femoral, bajo el ligamento inguinal. Se estrangulan muy fácilmente, y suelen ser pequeñas y poco dolorosas.

- Hernia incisional o eventración: se desarrollan en los lugares donde se ha practicado una operación quirúrgica (principalmente después de una abertura longitudinal de la línea media del vientre) ya que esas regiones de la pared abdominal se encuentran debilitadas por la misma: la cicatriz joven ofrece una resistencia menor, y el intestino puede crear una abertura e infiltrarse.

- Hernia umbilical: Se desarrollan cuando el anillo umbilical se debilita y el contenido abdominal sobresale. Esta parte suele estar debilitada por naturaleza, ya que tiene vasos sanguíneos del cordón umbilical. Suele estar presente, por tanto, desde el nacimiento debido a una debilidad congénita del anillo umbilical. Se suele cerrar espontáneamente en los primeros años de vida del niño, aunque puede aparecer a cualquier edad.

- Hernia epigástrica o ventral: se suele dar más en hombres de edades entre veinte y cincuenta años, y aparece en la línea media del abdomen, entre el esternón y el ombligo (aunque también puede aparecer bajo el ombligo, levemente hacia la izquierda o la derecha). Su causa es la relativa debilidad de la pared abdominal a lo largo de la línea alba.

- Hernia de Spiegel: la línea de Spiegel, corresponde al borde lateral externo de los músculos rectos del abdomen, donde a partir de la aponeurosis de los músculos anchos se forman las dos vainas de los músculos rectos. Es en el llamado arco de Douglas donde suelen aparecer, en la zona situada entre la espina iliaca anterior y el ombligo, a nivel del borde externo del músculo recto, donde la hoja posterior deja de serlo, convirtiéndose en una zona de menor consistencia, pudiéndose producir en este lugar hernias ventrales laterales.

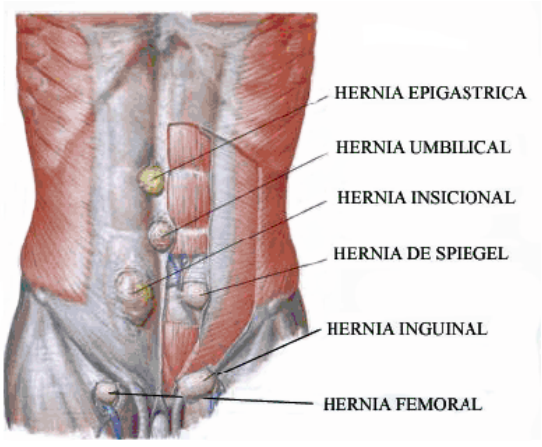

Figura II.3: Tipos de hernias (Pqax, 2011).

La reparación de una hernia o cirugía herniaria se conoce como herniorrafia. Este procedimiento quirúrgico se puede realizar mediante dos métodos:

- Método convencional: se realiza una incisión, o corte, sobre el área de la hernia, la porción sobresaliente se vuelve a colocar en la cavidad abdominal y el orificio o debilitamiento en la pared abdominal se repara cosiendo sobre el defecto los músculos resistentes que lo rodean.

- Técnica de malla sin tensión: se realiza una incisión sobre el área de la hernia, la porción sobresaliente se vuelve a colocar en la cavidad abdominal y se usa una porción de malla sintética para cubrir el debilitamiento en la pared abdominal, sin tener que coser los músculos que rodean el área. Ésta técnica puede llevarse a cabo mediante el método laparoscópico. Con esta técnica se realizan tres o cuatro incisiones pequeñas en el abdomen cerca del área de la hernia. En una de ellas se inserta una sonda metálica (llamada laparoscopio) con una luz y un visor. En las otras incisiones se insertan instrumentos para reparar la hernia. El visor del laparoscopio se conecta a una pantalla que permite al cirujano ver la hernia para repararla. La porción sobresaliente de tejido se vuelve a colocar en la cavidad abdominal y el orificio o debilitamiento en la pared abdominal se repara colocando una malla sobre el defecto. Debido a que el método convencional genera problemas como la reaparición de hernias, el principio de reconstrucción anatómica tendió a reemplazarse por la sustitución protésica donde la prótesis resistente cubre la discontinuidad y se convierte en una nueva pared. Cuatro emplazamientos distintos se pueden considerar a la hora de implantar las prótesis, clasificados de más profundo a más superficial: intraperitoneal, preperitoneal, retromuscular prefascial y premusculoaponeurótico (ver Figura II.4).

  - Implantación intraperitoneal: la prótesis se implanta en el lado más profundo de la pared tras la liberación de las vísceras. Este emplazamiento tiene la ventaja de no comportar disección parietal, de ser siempre utilizable esté donde esté la hernia y de beneficiarse de la presión abdominal. Para evitar la adherencia intestinal, se deben utilizar biomateriales *"composites"* o con una superficie visceral microporosa, ya que ésta provoca menos adherencias.
  - Implantación preperitoneal: consiste en colocar (por simple aposición, o con la ayuda de algún punto) una prótesis en el lado más profundo de la pared, justo delante del peritoneo, de manera que los bordes sobresalgan mucho de los límites de la abertura. Así, se refuerza el peritoneo y se crea una adherencia parieto-protésica tal que el conjunto equivalga a una nueva pared.
  - Implantación retromuscular prefascial: la prótesis se implanta entre el cuerpo muscular y la aponeurosis posterior, y se sutura. La reparación es eficaz, pero necesita disección parietal y pueden aparecer dolores residuales por interposición accidental de fibras nerviosas en los puntos de fijación.
  - Implantación premusculoaponeurótica: el principio es reforzar con una prótesis una reparación parietal por sutura y autoplastia. El inconveniente de este emplazamiento es su carácter superficial, sin otra contrapresión más que la

cutánea, causa de fragilidad cuando aumenta la presión abdominal. Toda infección superficial o necrosis cutánea expone la prótesis. Sin embargo, es el emplazamiento que favorece una mejor integración del tejido y una mayor vascularización (ver Figura II.5).

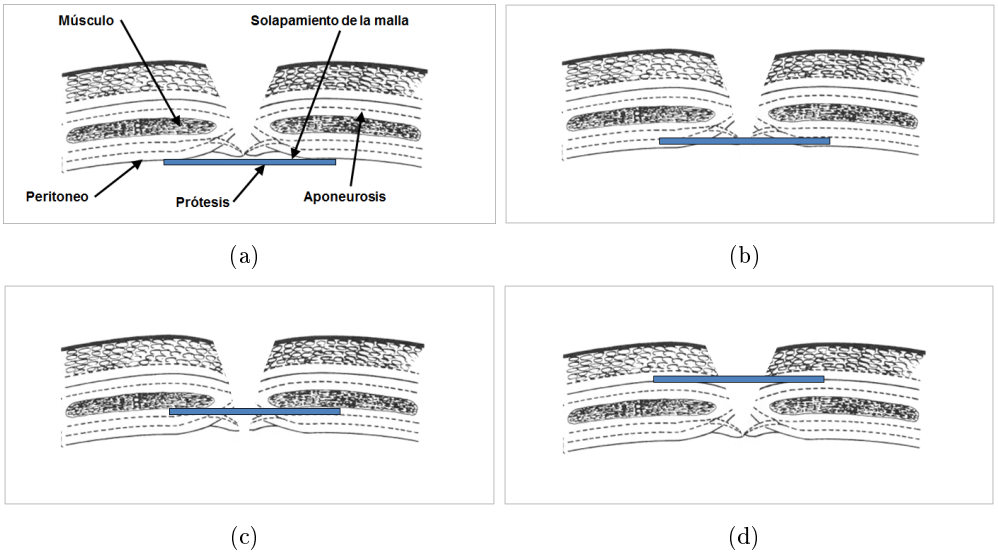

Figura II.4: Emplazamientos posibles de la prótesis, de más profundo a más superficial: (a) intraperitoneal, (b) preperitoneal, (c) retromuscular prefascial, (d) premusculoaponeurótico (Bellón, 2012).

II.3 Anatomía y fisiología de la pared abdominal anterior

El tronco es, en el caso de los mamíferos, una zona anatómica de vital importancia por contener la mayoría de los órganos vitales pertenecientes a los sistemas respiratorio, digestivo, excretor, cardiovascular y reproductor. Está constituido por las cavidades torácica y abdominopélvica, siendo ésta última el objeto del presente estudio.

Al contrario que la cavidad torácica, la cavidad abdominal no está protegida por ninguna estructura oseocartilaginosa, por lo que la protección de esta región anatómica queda enteramente a cargo de la pared abdominal. La integridad de la pared abdominal conlleva la realización de las actividades normales de manera automática. Cualquier lesión a este nivel interfiere en las funciones de la pared abdominal, como son la movilidad (flexión ventral, rotación y movimientos laterales, estar de pie, caminar, inclinarse, esfuerzos para levantar pesos, etc), la protección y contención del contenido abdominal, la respiración (junto a la cavidad torácica) y soportar la presión abdominal (micción, defecación, parto, tos, vómito, etc.).

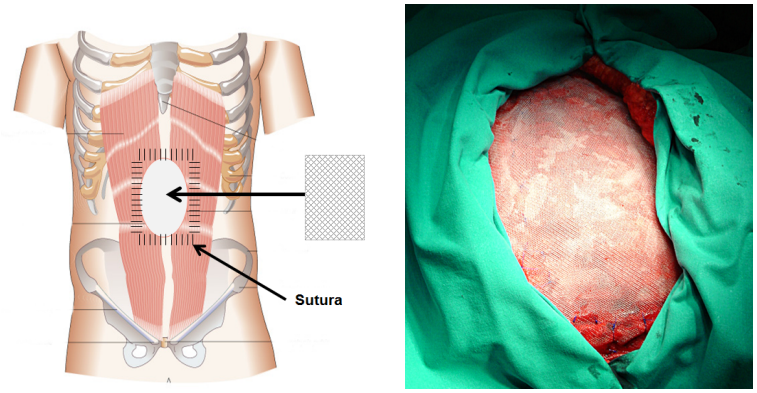

(a) (b)

Figura II.5: (a) Esquema de implantación premusculoaponeurótica de una prótesis en la cirugía herniaria. (b) Malla Surgipro® colocada en una hernia abdominal en un humano (Bellón, 2012).

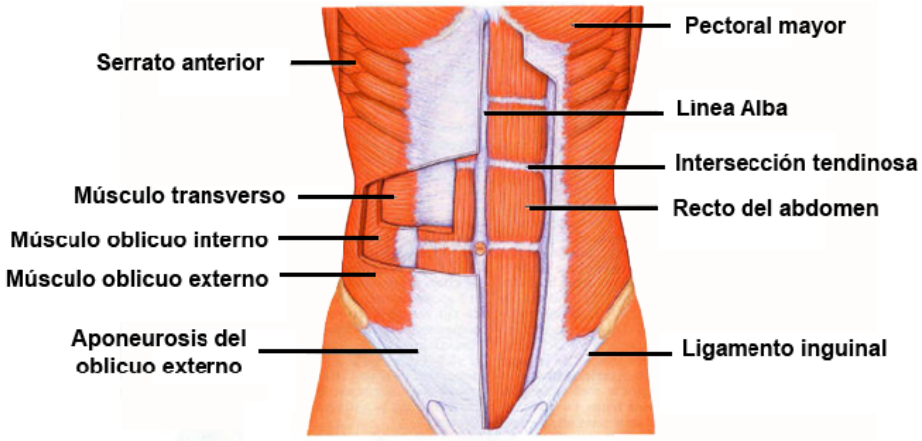

Figura II.6: Principales músculos abdominales (Murphy, 2010).

Los músculos abdominales tienen su fijación a su vez en las estructuras oseocartilaginosas que componen la caja torácica, incluyendo la columna vertebral, así como en la pelvis. Estas estructuras proporcionan las condiciones de fijación y anclaje de los músculos de la pared abdominal. La piel del abdomen es laxa y no esta adherida salvo a nivel de la línea alba y del ombligo. El desarrollo de este tejido en cada individuo se relaciona con sus hábitos alimenticios y con los antecedentes quirúrgicos.

La pared abdominal anterolateral está compuesta de cuatro pares de músculos principales y sus proyecciones aponeuróticas (Moore W., 2008) (ver Figura II.6). Los cuatro músculos principales son el músculo recto abdominal, el músculo oblicuo externo del abdomen, el músculo oblicuo interno del abdomen y el músculo transverso del abdomen. Otro músculo existente en la pared abdominal es el músculo piramidal del abdomen,

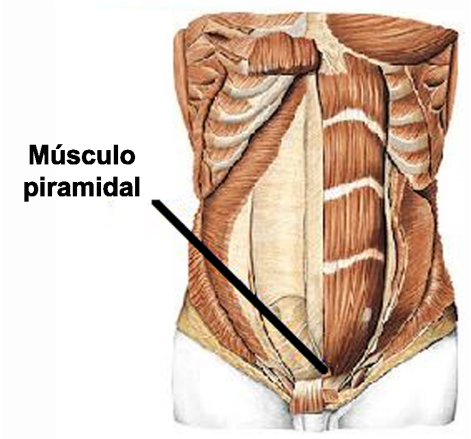

Figura II.7: Músculo piramidal del abdomen (Sistema-Muscular, 2012).

es de tamaño variable, normalmente pequeño y puede estar ausente (entre un 15-20% de la población carece de él) (ver Figura II.7). Tiene su origen en la cresta del pubis (sínfisis púbica), estando situado inmediatamente inferior y anterior al músculo recto del abdomen, yendo contenido en la vaina de este último y se inserta en la línea alba. Su función es la de tensor de la línea alba.

II.3.1 Músculo recto abdominal

El músculo recto abdominal es un músculo par (el músculo se divide en dos partes simétricas entre sí) con forma de cinta (ver Figuras II.6 y II.8) (Moore W., 2008). Sus fibras musculares están dispuestas en la dirección craneo caudal del cuerpo. El origen de este músculo se encuentra en la sínfisis y en la cresta del pubis y se inserta en los cartílagos costales V-VII y en el apéndice xifoides.

Cada miembro del par muscular está separado entre sí por la denominada línea alba, estando a su vez cada músculo dividido por tres o cuatro tendones o intersecciones aponeuróticas, llamadas metámeras. A su vez, éste par muscular se encuentra dentro de una vaina tendinosa (fascia o aponeurosis) que está formada por las aponeurosis de los tres pares de músculos anchos (transverso, oblicuo externo y oblicuo interno). Concretamente, la lámina anterior de la vaina se extiende sobre toda la superficie del músculo y se une al periostio de las inserciones óseas. La lámina anterior proviene de la aponeurosis del oblicuo externo y la lámina anterior de la aponeurosis del oblicuo interno (ver Figura II.8). Por otra parte, la lámina posterior de la vaina se extiende sobre los 2/3 superiores del músculo y está formada por la lámina posterior de la aponeurosis del oblicuo interno y la aponeurosis del músculo transverso del abdomen. En el tercio inferior, la lámina posterior pasa a la parte anterior del recto. En esta zona, el músculo

entra en contacto con la fascia transversal y el tejido conectivo extraperitoneal (ver Figura II.8). La línea arqueada se define como la línea donde se produce este paso de la vaina posterior a la parte anterior del recto y está situada en el límite entre los dos tercios superiores y el tercio inferior de los músculos rectos.

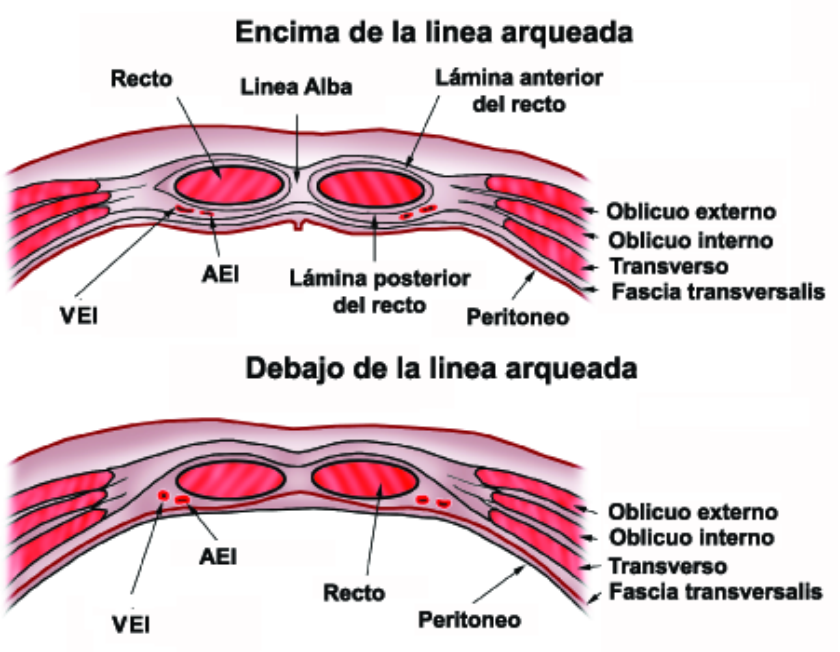

Figura II.8: Sección transversal del músculo recto abdominal. Disposición de las láminas anterior y posterior del músculo por encima (a) y por debajo (b) de la línea arqueada, situada en el límite entre los dos tercios superiores y el tercio inferior de los músculos rectos (AEI: Arteria epigástrica inferior. VEI: Vena epigástrica inferior) (WebMD-LLC, 1994).

Las funciones de este músculo abdominal son la flexión del tronco o elevación de la pelvis, la aproximación del tórax a la pelvis, la colaboración en la espiración y mantener el tono de la pared abdominal (ver Figura II.9.a). Además, colabora en la prensa abdominal, que es el proceso a través del cual se produce un aumento de presión en la cavidad abdominal con la finalidad de realizar un determinado esfuerzo (toser, expulsar la orina, las heces, etc.)

II.3.2 Músculo oblicuo externo

El oblicuo externo o mayor del abdomen constituye el más externo de los músculos anchos laterales del abdomen (Moore W., 2008). Sus fibras musculares van desde los pares costales V-XII hacia la cresta ilíaca y la zona del pubis, es decir, la dirección de

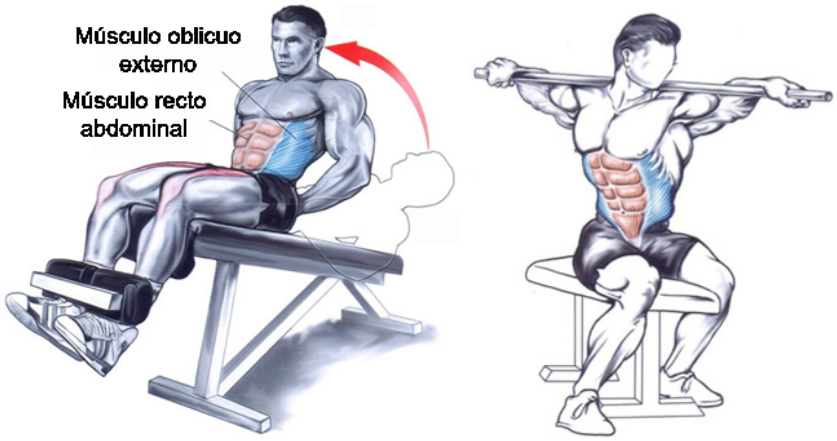

(a) (b)

Figura II.9: Músculos abdominales activados en los movimientos de flexión (a) y rotación (b) del tronco abdominal (WordPress, 2012).

las fibras musculares es oblicua hacia la parte inferior y medial (ver Figuras II.6, II.10 y II.11).

El origen de esta estructura anatómica se encuentra en la cara externa de los pares costales V-XII, donde se interdigita con los músculos de la pared torácica, serrato mayor y dorsal ancho (ver Figura II.11). La inserción de dicho músculo tiene lugar en el borde interior de la cresta ilíaca, en el ligamento inguinal mediante inserciones tendinosas y en el tubérculo del pubis. Además, este músculo se inserta mediante la aponeurosis del músculo oblicuo externo (proyección aponeurótica o fascia), que ayuda a formar la capa anterior de la vaina del músculo recto del abdomen y la línea alba.

La función unilateral del músculo oblicuo externo es la rotación del tronco hacia el lado contrario, la inclinación lateral del tronco y la elevación del borde pélvico lateral (ver Figura II.9.b). Sus acciones bilaterales son la inclinación del tronco hacia delante, la elevación de la pelvis y, a su vez, colabora en la prensa abdominal y en la espiración.

II.3.3 Músculo oblicuo interno

El músculo oblicuo interno o menor del abdomen está localizado en el lugar intermedio de los músculos anchos del abdomen (Moore W., 2008). La dirección de sus fibras musculares es aproximadamente perpendicular a la de las fibras del oblicuo externo (Figuras II.6, II.10 y II.12), yendo desde el reborde costal hacia las apófisis espinosas de la quinta vértebra lumbar, el ligamento inguinal, la cresta ilíaca y el hueso del pubis.

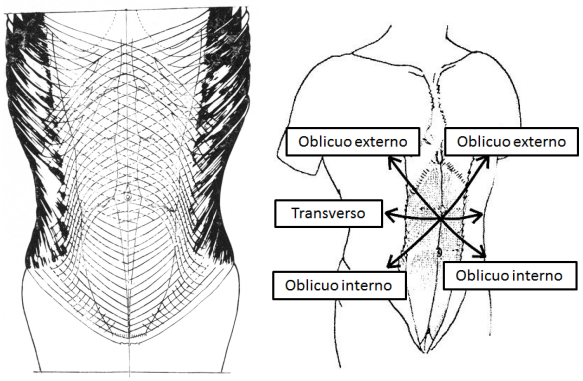

(a) (b)

Figura II.10: (a) Orientación de las fibras de colágeno en las aponeurosis de los músculos oblicuos externo e interno que recubren la lámina anterior del recto abdominal hasta la línea alba (Askar, 1977). (b) Dirección de las fibras musculares en los músculos oblicuo externo e interno (simetría con respecto a la línea alba) y músculo transverso (Axer et al., 2001a).

Su origen se encuentra en el arco crural (ligamento inguinal), espina ilíaca y fascia toracolumbar, la cual está anclada a su vez a las apófisis espinosas de la última vértebra lumbar y la primera sacra. Su inserción tiene lugar en la línea alba, el reborde costal de los pares X-XII mediante inserciones aponeuróticas y en la línea pectínea. Por encima de la línea arqueada, la proyección aponeurótica del oblicuo menor se divide en dos, formando parte tanto de la vaina posterior como de la anterior de la cobertura del músculo recto abdominal. Por debajo de la línea arqueada, la proyección aponeurótica del músculo oblicuo interno pasa a formar parte de la vaina anterior del recto abdominal.

El músculo oblicuo interno tiene la función de la contracción unilateral, mediante la rotación del tronco hacia el mismo lado y hacia delante. A su vez, la contracción bilateral se produce mediante la inclinación del tronco hacia delante y la elevación del borde anterior de la pelvis. Además, colabora en la prensa abdominal y en la espiración.

II.3.4 Músculo transverso

El músculo transverso del abdomen es el músculo más profundo de los pares de músculos abdominales antero-laterales (Moore W., 2008). Sus fibras musculares van desde la línea alba a las apófisis espinosas lumbares, es decir, su dirección es aproximadamente perpendicular a la dirección craneo caudal del cuerpo humano (ver Figuras II.6, II.10 y II.13).

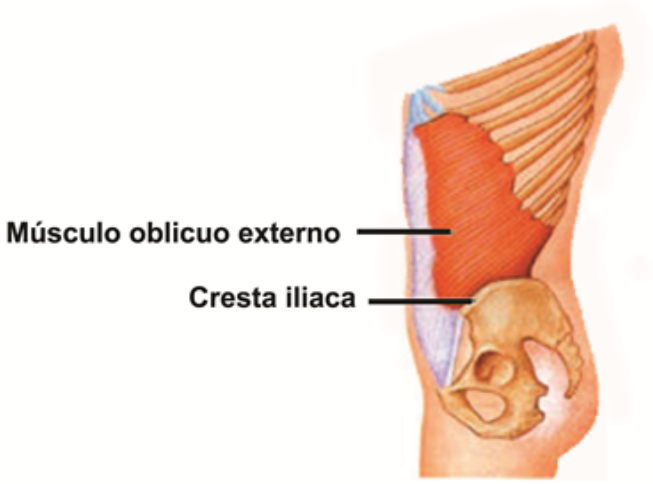

Figura II.11: Músculo oblicuo externo del abdomen (Automattic-Inc, 2005).

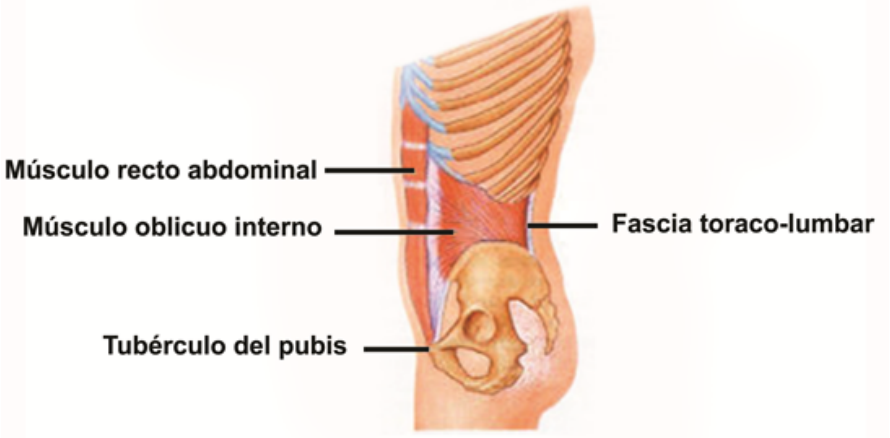

Figura II.12: Músculo oblicuo interno del abdomen (Automattic-Inc, 2005).

Su origen tiene lugar en la cara interna de las costillas de los pares XI y XII y de los cartílagos costales de los pares VII a X, donde por digitaciones se entrelaza con el diafragma, en la fascia toracolumbar, en los dos tercios anteriores de la parte interna de la cresta ilíaca y en el tercio lateral del ligamento inguinal mediante inserciones aponeuróticas. Con respecto a su inserción, ésta tiene lugar en la línea alba, en la línea pectínea y en la cresta del pubis. Por encima de la línea arqueada, la proyección aponeurótica del músculo transverso pertenece a la cara posterior de la cobertura fibrosa del par de músculos abdominales rectos. Por debajo de la línea arqueada, dicha proyección aponeurótica pasa a recubrir la cara anterior de los músculos rectos abdominales. Por otra parte, la cara posterior del músculo transverso del abdomen está adherida al tejido fibroso denominado fascia transversalis.

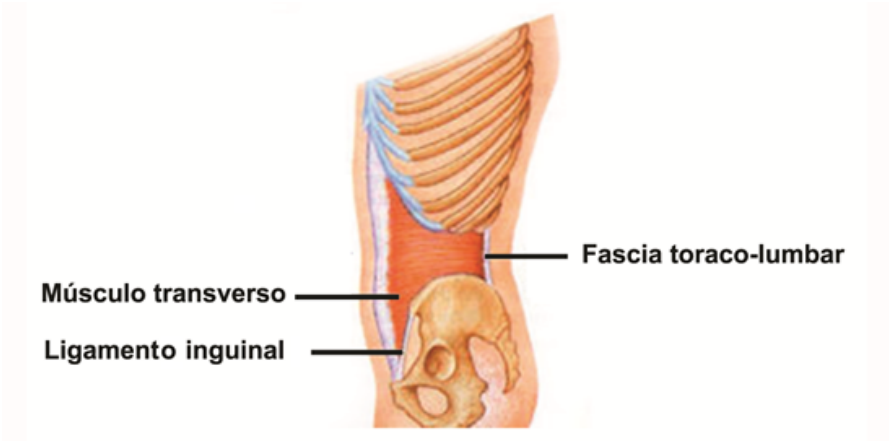

Figura II.13: Músculo transverso del abdomen (Automattic-Inc, 2005).

Sus funciones son, además de mantener la presión y el tono de la cavidad abdominal, la rotación del tronco hacia su mismo lado, la contracción y distensión de la pared abdominal, fundamentalmente en la contracción bilateral, y la colaboración en la prensa abdominal y en la espiración.

II.3.5 Línea alba

La línea alba se encuentra entre los bordes mediales de los rectos abdominales y se extiende desde el xifoides hasta la sínfisis del pubis (ver Figuras II.6 y II.8) (Moore W., 2008). Consiste en una banda de tejido fibroso y denso formado por la fusión de las aponeurosis de los oblicuos externos e internos y el músculo transverso. La línea alba se amplía conforme se acerca al xifoides llegando a veces entre 1,25 a 2,5 cm de ancho. En la porción supraumbilical de la línea alba las fibras entrelazadas de las aponeurosis dejan pequeños orificios elípticos a través de los cuales pasan los vasos y nervios.

II.3.6 Fascia transversalis

La fascia transversalis es una lámina aponeurótica que recubre interiormente la pared muscular abdominal completa, tapizando la cara profunda del músculo transverso (ver Figura II.8) (Moore W., 2008). Sus fibras de colágeno están principalemente orientadas en dirección perpendicular a la dirección craneo caudal del cuerpo humano. Esta estructura anatómica, en la mitad superior de la pared abdominal, es una lámina fina muy adherida a la fascia subperitoneal. Su estructura va siendo más firme, y en consecuencia más consistente en su mitad inferior.

La fascia transversalis cubre, por tanto, toda la extensión de la cara profunda del músculo transverso a excepción de la parte de la aponeurosis de este músculo que, por debajo del arco de Douglas, pasa por delante del recto mayor. En este nivel la fascia transversalis abandona la aponeurosis del transverso y pasa a cubrir por detrás al músculo recto mayor. Por tanto, en esta zona sólo la fascia transversalis y el peritoneo forman la hoja dorsal de la vaina del recto. En la parte superior del abdomen esta fascia está fusionada íntimamente con el diafragma.

II.3.7 Otras estructuras anatómicas

Junto con los músculos abdominales y fascias descritas, existen otras estructuras anatómicas en la pared abdominal que son necesarias definir para describir adecuadamente la cavidad abdominal (Moore W., 2008):

- Diafragma: esta estructura anatómica supone la separación entre las cavidades torácica y abdominopélvica, teniendo su principal función en el movimiento respiratorio. En su posición normal, relajada, el diafragma es convexo, permitiendo la expulsión del aire de los pulmones y la expansión de los órganos alejados en la cavidad abdominal, mientras que durante la inspiración, se aplana, permitiendo el paso del aire a los pulmones y ayudando al tránsito intestinal. Está constituido por fibras tendinosas, todas ellas confluyendo en su parte central y más elevada, denominada centro frénico. Su inserción se da en los bordes costales de la caja torácica, extremos de la XI y XII costilla, apófisis xifoides del esternón, vértebras lumbares y algunos ligamentos de la pared abdominal posterior.

- Línea arqueada o línea de Douglas: marca el límite entre los dos tercios superiores y el tercio inferior de los músculos rectos. Es a la altura de esta línea donde las aponeurosis del oblicuo menor perteneciente a la vaina posterior y del músculo transverso pasan de la vaina posterior a la vaina anterior de la cobertura del músculo recto.

- Línea semilunar o línea de Spiegel: es aquella que marca la transición entre los músculos rectos y los músculos laterales. Se encuentra a ambos lados de la anatomía humana y recorre desde el arco de las costillas a la espina púbica.

- Ligamento inguinal: se considera como el borde de la aponeurosis del músculo oblicuo mayor que va desde la espina ilíaca anterosuperior hasta la espina del pubis (ver Figura II.6).

- Suelo pélvico: es un sistema de músculos y ligamentos que cierran el suelo del abdomen manteniendo en posición correcta la vejiga, la vagina, el útero, etc.

II.4 Mecánica de los tejidos de la pared abdominal

El tejido abdominal es un músculo esquelético que está catalogado desde el punto de vista mecánico como tejido blando. Histológicamente, los músculos abdominales están constituidos por fibras musculares, de colágeno y elastina. Esta red entremezclada de fibras se encuentra rodeada de la llamada "sustancia fundamental" de tipo polisacárido (proteoglicanos), que actúa como adhesivo, lubricante y absorbedor de impactos (Kjaer, 2004; Loocke et al., 2008; Ito et al., 2010). Por otro lado, las estructuras aponeuróticas o fascias, que cubren los músculos, son unidades básicamente colagenosas con ausencia de fibras musculares.

Las fibras de colágeno son las responsables de la respuesta pasiva del material (Calvo et al., 2009; Martins et al., 2012), mientras que las fibras musculares son las responsables de la respuesta activa del músculo (Linden, 1998; Arruda et al., 2006). Concretamente, la componente pasiva es aquella que aparece en el tejido como respuesta a cargas bajo las cuales el músculo sólo ofrece resistencia y no se contrae. Sin embargo, cuando se estimula al músculo mediante un estímulo eléctrico (bien externo o interno), el músculo genera una contracción que produce una fuerza adicional. La tensión activa, consecuencia de la contracción muscular, es la diferencia de tensiones entre la total y la pasiva. Dado que, en términos generales, aparecen dos respuestas mecánicas diferentes en el músculo, ambas se han abordado de forma separada en esta tesis.

Dado que el objetivo final en la cirugía abdominal es que la prótesis implantada se integre en el tejido abdominal mimetizando el comportamiento original del tejido, es fundamental el estudio del comportamiento mecánico del mismo. Su respuesta mecánica dependerá de la naturaleza y proporción de los componentes que lo forman. Por tanto, en este trabajo se ha abordado el estudio de la mecánica de la pared abdominal experimentalmente tal que dichos resultados permitan seleccionar o definir los modelos de comportamiento necesarios para la simulación numérica.

Esta sección se estructura en dos apartados que describen los principales conceptos relativos al patrón de respuesta mecánica experimental y modelado numérico de los tejidos abdominales, respectivamente. También se incluye una revisión bibliográfica de los estudios descritos en la literatura.

II.4.1 Caracterización mecánica experimental

La realización de ensayos experimentales proporciona información acerca del comportamiento del tejido muscular (Nilsson, 1982a,b; Hwang et al., 2005; Calvo et al., 2010; Martins et al., 2010; Grasa et al., 2011; Martins et al., 2012). Concretamente, los

ensayos experimentales mecánicos permiten establecer la relación entre la carga aplicada y la respuesta del tejido. Además, a medida que se desarrollan modelos computacionales más sofisticados, se exigen nuevos ensayos experimentales que puedan sustentar y validar dichos modelos.

Para la caracterización mecánica pasiva del tejido músculo-esquelético a corto plazo, las pruebas experimentales más habituales son ensayos uniaxiales (Nilsson, 1982a), biaxiales (Hwang et al., 2005) o de inflado (Song et al., 2006b) mientras que los ensayos cíclicos (Kirilova et al., 2009) se utilizan para determinar la respuesta a largo plazo.

Dado que la aplicación clínica a estudiar es la cirugía abdominal en humanos, es el tejido humano el que se debería caracterizar para reproducir el comportamiento real de los tejidos del abdomen. Sin embargo, no siempre es posible la obtención de muestras de tejido humano, que además garanticen la repetibilidad deseada, al no ser posible el control de factores como el tipo de alimentación, la restricción de movimiento, el tipo y nivel de entrenamiento físico, etc. Para solventar esta problemática se suele recurrir a modelos animales. De esta forma, en la literatura existen estudios que utilizan diferentes modelos de experimentación animal como perros (Hwang et al., 2005), gatos (Sandercock, 2003), cerdos (Loocke et al., 2008), conejos (Davis et al., 2003), ratas (Grover et al., 2007), etc.

El patrón de comportamiento mecánico pasivo viene dado por una respuesta no lineal y en grandes deformaciones ante cargas fisiológicas (Calvo et al., 2010; Hodgson et al., 2012; Martins et al., 2012). Este comportamiento no lineal se ha atribuido al patrón ondulado de las fibrillas de colágeno y elastina; para bajos niveles de carga se obtienen grandes desplazamientos, ya que el arrollamiento de las fibras es fácil de deshacer, y para altos niveles de carga los tejidos se rigidizan notablemente, ya que las fibras ya alíneadas con la dirección de la carga se alargan elásticamente hasta la rotura. La orientación preferencial de las fibras musculares y de colágeno da lugar a una respuesta mecánica anisótropa (Hwang et al., 2005). Además, el elevado porcentaje de agua de los tejidos, cercano al 70%, les confiere un comporamiento prácticamente incompresible. Otra característica del tejido muscular, al igual que del resto de tejidos biológicos blandos, es que se encuentran sometidos a tensiones residuales, resultado del proceso de crecimiento desde el estado embrionario hasta la edad adulta (Fung, 1993; Peña et al., 2006; Lanchares et al., 2008). Dichas tensiones residuales se revelan al realizar un corte sobre un tejido libre de carga externa. Tras dicho corte, se produce una modificación de la configuración de equilibrio a causa de la liberación de dichas tensiones residuales. Esta distribución de deformaciones es tridimensional y su medida directa es compleja e imposible de realizar *"in vivo"*. El comportamiento no lineal de los tejidos biológicos blandos hace que la determinación de dichas deformaciones iniciales sea muy importante (Fung, 1993; Gardiner et al., 2001; Peña et al., 2006). Por otra parte, el tejido muscular muestra un comportamiento viscoelástico (relajación y/o

fluencia) el cual es atribuido a la interacción tangencial del colágeno y fibras musculares con la matriz de proteoglicanos (lubricante viscoso entre las fibras de colágeno) (Loocke et al., 2008, 2009). Este efecto se observa cuando el tejido se tensiona hasta un determinado nivel y a continuación se descarga, produciéndose una histéresis. Así mismo, si el tejido se deforma hasta un valor determinado de alargamiento y a continuación se mantiene constante, se observa que con el tiempo la tensión se relaja desde la tensión inicial hasta una tensión de equilibrio. La razón del precondicionamiento en los ensayos experimentales reside en el carácter viscoelástico de estos tejidos y en los cambios que tienen lugar en su estructura durante los primeros ciclos. Al cabo de un cierto número de ciclos se alcanza el equilibrio. En último lugar, el tejido muscular tiene la capacidad de modificar su estructura en función del ambiente y los estímulos mecánicos, biológicos o químicos que los rodean (Taber, 1995). El crecimiento tiene lugar cuando se producen cambios en la masa y/o volumen tanto de las células como de la matriz extracelular y la remodelación cuando se produce una modificación de la microestructura sin modificar su tamaño y forma.

En lo que concierne a la respuesta mecánica activa del tejido muscular, la fuerza activa se produce durante la activación o contracción del músculo (Bol and Reese, 2008; Stålhand et al., 2010; Ramírez-Martínez, 2011). El mecanismo de contracción muscular se inicia al llegar un impulso nervioso procedente del nervio motor a la unión neuromuscular o placa motora. A partir de este momento el potencial de acción despolariza toda la membrana de la fibra muscular y los túbulos T. Los túbulos T o túbulos transversales son estructuras presentes en las células del músculo esquelético y cardíaco. Concretamente, son invaginaciones membranosas que conectan el sarcolema de la fibra muscular, dando lugar al túbulo al exterior de la fibra. La despolarización provoca un aumento de la permeabilidad y la salida masiva de iones $Ca2+$ desde el retículo endoplasmático hacia el interior de la célula, uniéndose a la troponina C. Esta unión provoca un cambio en el resto de componentes del complejo de troponina, es decir en la troponina I y troponina T. El cambio en la troponina T provoca un desplazamiento de la tropomiosina que deja al descubierto los lugares de unión entre la actina y la miosina. La energía liberalizada produce el solapamiento de los filamentos de actina o filamentos finos y filamentos de miosina o filamentos gruesos, acortando el sarcómero y produciéndose la contracción. Experimentalmente en el laboratorio, la activación de los músculos se produce habitualmente mediante activación eléctrica directa del nervio o mediante la inmersión del tejido en baños de calcio a diferentes concentraciones (ver Figura II.14). Esta activación siempre tiende a provocar acortamiento pero, en función de la voluntad del sujeto o la relación que se establezca con las resistencias externas, se pueden encontrar tres tipos de acciones (ver Figura II.15): acortamiento o acción dinámica concéntrica cuando la fuerza ejercida es capaz de mover la carga externa, alargamiento o acción dinámica excéntrica cuando la carga es mayor que la fuerza ejercida y mantenimiento de la longitud o acción isométrica cuando la fuerza muscular es equivalente a la carga externa.

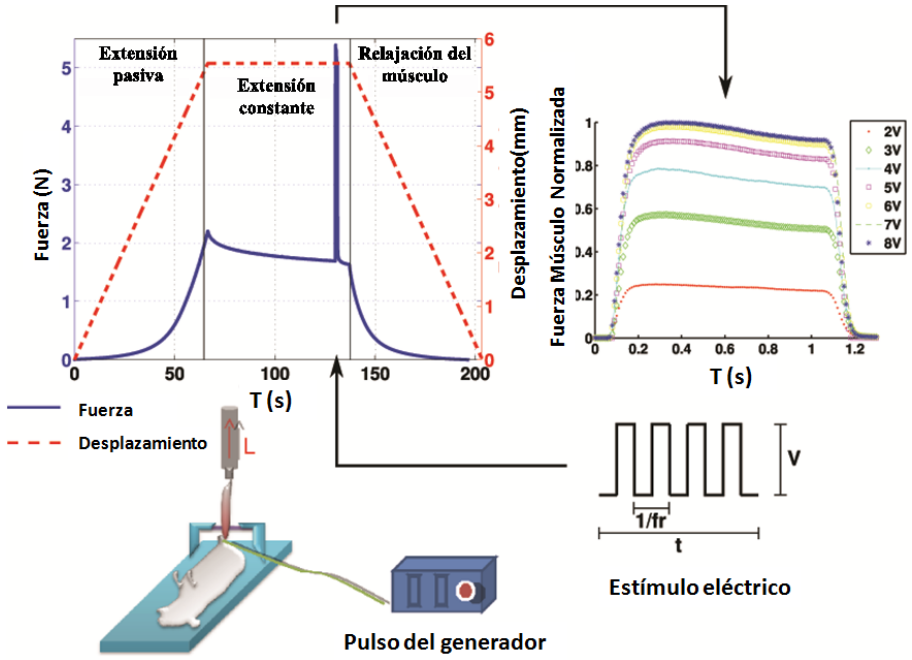

Figura II.14: Fuerza (N) activa y pasiva del músculo y desplazamiento (mm) provocado en función del estímulo eléctrico.

La fuerza activa que puede desaroolar el músculo depende de diferentes factores, de los cuales los más importantes son la longitud, la velocidad y la señal de excitación (Ramírez et al., 2010). A continuación se describen brevemente dichos factores:

(a) Relación fuerza-longitud.

La generación de fuerza activa se produce por el deslizamiento de los filamentos de actina sobre los filamentos de miosina, lo que permite el acercamiento de las líneas Z, que son las líneas que limitan la unidad funcional de la célula muscular, el sarcómero. La energía necesaria para este proceso se obtiene a partir del ciclo de los puentes cruzados, definidos como el número de puntos activos que están interactuando entre la actina y la miosina. Por tanto, el grado de fuerza ejercida por el músculo depende del número de puentes cruzados activos en un momento dado, de forma que a mayor número de puentes cruzados, mayor fuerza se ejerce. Si la longitud del sarcómero varía, también cambia el solapamiento de los filamentos de actina y miosina provocando cambios en el número de sitios activos de los filamentos de actina que pueden entrar en contacto con la miosina. Por tanto, la fuerza ejercida por el músculo está influenciada por la longitud del sarcómero dependiendo del número de puentes cruzados (Huxley, 1966; Enoka, 2002; González-Badillo and Ribas, 2002) (ver Figura II.16.a). De hecho, existe una longitud

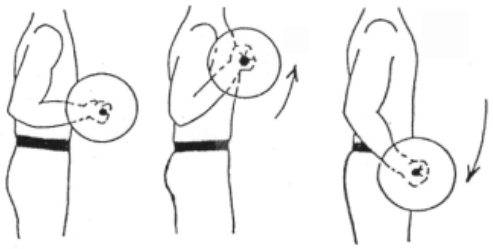

(a) (b) (c)

Figura II.15: Tipos de acción muscular: isométrica (a), concéntrica (b) y excéntrica (c).

óptima en la que el músculo ejerce la fuerza máxima.

(b) Relación fuerza-velocidad.

La fuerza activa ejercida por el músculo también depende de la velocidad de acción del músculo (ver Figura II.16.b). La velocidad con la que se acorta un músculo va a depender de la carga que tiene que mover. A mayor carga, la fuerza que hay que hacer es mayor y, por tanto, la velocidad a la que se acorta el músculo es menor. Durante los movimientos concéntricos, el desarrollo de la fuerza máxima decrece progresivamente a velocidades más altas (cuando se levanta un objeto muy pesado, se hace lentamente, maximizando la fuerza que se va a realizar).

(c) Relación fuerza-señal de excitación.

La activación del músculo puede realizarse voluntariamente, por medio de la señal neuronal, o artificialmente, por ejemplo, por medio de un electrodo en contacto con el nervio. La estimulación artificial ofrece la ventaja de que se conocen las características de la señal de entrada al sistema. Por lo tanto, será posible controlar la intensidad, el voltaje, la frecuencia y el tiempo del estímulo. Durante el estímulo, las motoneuronas se activarán dependiendo de si la señal que las estimula sobrepasa el umbral de reclutamiento característico de cada una de ellas. La fuerza activa que puede producir un músculo es mayor a medida que el voltaje de la señal aumenta (ver Figura II.16.c).

Una vez quedan descritos los principales conceptos relativos al patrón de respuesta mecánica experimental de los tejidos músculo-esqueléticos, se introduce a continuación

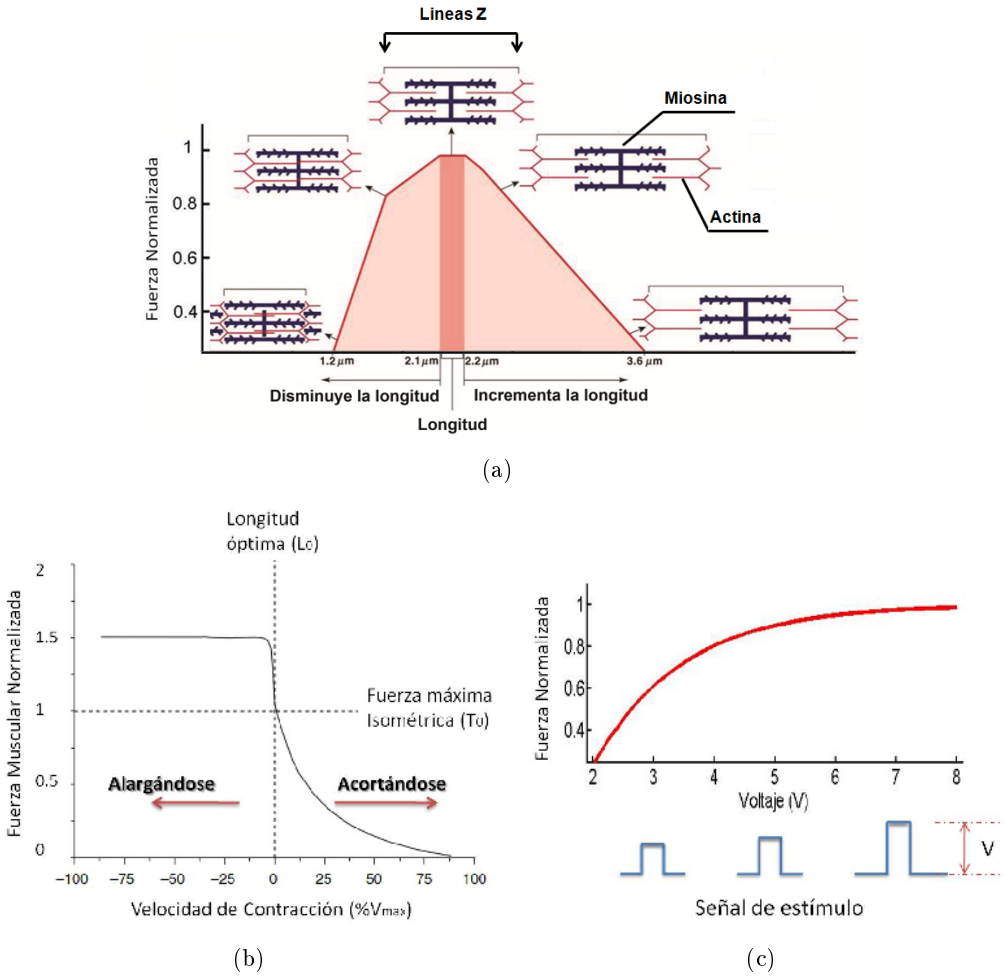

Figura II.16: Relación de la fuerza activa con la longitud (a), la velocidad (b) y la señal de excitación (c).

el estado del arte acerca de los trabajos existentes en la literatura relativos a la caracterización experimental pasiva (Sección II.4.1.1) y activa (Sección II.4.1.2) del tejido muscular abdominal.

II.4.1.1 Comportamiento pasivo. Estado del arte

En la literatura existen diversos trabajos que estudian la respuesta mecánica pasiva de la pared abdominal mediante experimentación animal o humana, centrándose en el estudio de diferentes músculos o fascias.

La mayor parte de los estudios en la literatura realizan ensayos uniaxiales de tracción (Nilsson, 1982a,b; Gajdosik, 2001; Hwang et al., 2005) y compresión (Loocke et al.,

2004). También hay estudios que muestran datos de ensayos biaxiales (Hwang et al., 2005), los cuales reproducen más fielmente el comportamiento real de las estructuras abdominales, así como ensayos de punzamiento (Junge et al., 2001; Podwojewski et al., 2012). Nilsson (1982a,b) comprobó, realizando ensayos en conejos, que el comportamiento mecánico pasivo del tejido abdominal es diferente en cada una de las zonas del abdomen. Este hecho es debido a que en cada zona de la pared abdominal están alojados diferentes músculos y estructuras aponeuróticas, cada uno de los cuales tiene su correspondiente disposición de fibras. Nilsson (1982b) evidenció que el tamaño de las muestras extraídas es influyente y atribuyó este fenómeno a que en muestras más pequeñas el número de fibras que están sujetas entre las mordazas del equipo de ensayo es superior que cuando la muestra es de mayor tamaño. Los resultados se presentan en medidas de fuerza y desplazamiento y debido a la falta de datos geométricos de las muestras no se pueden trasladar dichos resultados a tensiones, que son necesarias para nuestro problema. Hwang et al. (2005) desarrolló un estudio comparativo entre los músculos oblicuo interno y transverso mediante ensayos uniaxiales y biaxiales en tejido abdominal de perros. Su objetivo era ver qué diferencias había en el comportamiento pasivo de los músculos de forma conjunta y de forma individual, estudiándose las diferencias en la respuesta mecánica pasiva a lo largo de las fibras musculares y en dirección perpendicular a ellas. Sus principales conclusiones indican que la respuesta mecánica es anisótropa siendo más rígida en la dirección perpendicular a las fibras musculares que a lo largo de las mismas. Finalmente, Hwang et al. (2005) evidenció que la anisotropía es menos pronunciada al estudiar los músculos conjuntamente debido a la presencia del tejido conectivo extracelular (Huijing, 1997) que permite la transmisión de fuerzas de una capa muscular a otra.

A pesar de que es difícil la obtención de tejido humano para la caracterización experimental del mismo, también existen algunos estudios experimentales que caracterizan la respuesta de la pared abdominal humana mediane ensayos *"in vivo"* e *"in vitro"*. Song et al. (2006a,b) caracterizó la respuesta mecánica de la pared abdominal por medio de ensayos de inflado a través de cirugía laparoscópica *"in vivo"*. Este procedimiento quirúrgico se fundamenta en el inflado de la cavidad abdominal y ofrece una oportunidad para llevar a cabo la medición de las propiedades mecánicas de la pared abdominal. Estos autores llegaron a la conclusión de que el abdomen tiene una respuesta más rígida en el plano transversal que en el plano craneo-caudal. A su vez, Song et al. (2006b) justificó que esta diferencia de comportamientos entre las dos direcciones se debe a la disposición de las fibras musculares en el abdomen.

Recientemente se han aplicado métodos de análisis inverso que permiten la obtención de los desplazamientos de cada uno de los puntos de interés mediante la toma y procesado de imágenes. Szymczak et al. (2012) determinó las deformaciones que tienen lugar en el abdomen humano a partir de imágenes. Smietanski et al. (2012) examinó el comportamiento de la parte frontal de la pared abdominal con el objetivo de describir

su elasticidad *"in vivo"*. Determinaron la deformación del abdomen para correlacionarla con los alargamientos que pueden experimentar las prótesis, en caso de reparación herniaria, y que puede causar el fallo de la unión entre tejido y malla.

Estudios más recientes, enfocados al estudio de la elasticidad de la pared abdominal, detectan diferencias en la respuesta mecánica de los tejidos entre hombres y mujeres (Junge et al., 2001). Junge et al. (2001) llevó a cabo ensayos experimentales de punzamiento e indicó que el comportamiento de la pared abdominal en una sola dirección no puede ser extrapolado a la respuesta global de la pared abdominal.

Varios autores han propuesto modelos sobre la arquitectura de la línea alba (Rizk, 1980; Askar, 1977; Axer et al., 2001a,b). Específicamente, los modelos de Rizk (1980) y Askar (1977) definen seis capas aponeuróticas en la línea alba, dispuestas de forma oblicua y definen la línea alba como una línea de terminación de fibras. Axer et al. (2001a,b) llevó a cabo un estudio detallado de la distribución de fibras en la línea alba y en las aponeurosis del músculo recto abdominal. Su estudio propuso un nuevo modelo de la arquitectura de las fibras en la línea alba (Axer et al., 2001a) definiéndolas con una continuidad a través de ella, encontrándose que existen diferencias en la arquitectura de las fibras en función del género (Axer et al., 2001b). A la luz de estos estudios, Grassel et al. (2005) llevó a cabo un estudio para analizar las diferentes propuestas de disposición de fibras en la línea alba. Si bien sus resultados no son directamente extrapolables a la población jóven, sus resultados están de acuerdo con el modelo propuesto previamente por Axer et al. (2001a).

La bibliografía referente a la caracterización experimental del tejido abdominal incluye otros estudios que evidencian el patrón de respuesta mecánica de la línea alba. La línea alba, al igual que la mayoría de los tejidos blandos, muestra una respuesta elástica no lineal. Rath et al. (1996) realizó un estudio biomecánico de la línea alba para estudiar su morfología y los parámetros mecánicos de resistencia, deformación y elasticidad y observaron una respuesta más flexible en la zona subumbilical que en la supraumbilical. Konerding et al. (2011a) evaluó las tensiones que se generan en la parte supraumbilicar ante diferentes valores de presiones intraabdominales utilizando cadáveres de humanos. Para ello, Konerding et al. (2011a) realizó ensayos en los cuales insertaba un balón en el interior de la cavidad abdominal y, posteriormente, variaba la presión intraabdominal. Las tensiones longitudinales no se evaluaron en este estudio ya que otros estudios biomecánicos de la línea alba remarcan el papel predominante de la dirección transversal en la formación de hernias incisionales (Klinge et al., 1998; Junge et al., 2001; Grassel et al., 2005; Song et al., 2006a).

También hay estudios focalizados en el estudio de estructuras aponeuróticas. Kirilova et al. (2009) y (Kirilova et al., 2010) publicaron trabajos centrados en el estudio de las propiedades mecánicas viscoelásticas de la fascia abdominal de humano *"in vitro"*

mediante ensayos uniaxiales. Estos autores analizaron experimentalmente la influencia de la dirección y la localización de las muestras. Sus conclusiones indican que la localización de las muestras influye en la respuesta viscoelástica del tejido. Kureshi et al. (2008) correlacionó las propiedades de la fascia transversalis no herniada y herniada *"in vitro"* con muestras de humano mediante ensayos uniaxiales. Su metodología se basó en el análisis de la respuesta mecánica y de imágenes de colágeno en ambos tejidos. Con ello, comprobó que el proceso de daño herniario y de posterior remodelación del tejido no altera significantemente las propiedades de la fascia transversal. Finalmente, un estudio reciente caracteriza el comportamiento mecánico, mediante ensayos uniaxiales, y modela el proceso de daño que se produce en la aponeurosis anterior del recto en dos direcciones (Martins et al., 2012), donde los ensayos uniaxiales se realizaron a lo largo de las fibras de colágeno así como de forma perpendicular a las mismas.

Analizando los trabajos existentes sobre el tejido abdominal, ninguno de ellos proporciona información acerca de las deformaciones iniciales que se producen al extraer las muestras del modelo de experimentación ni se realiza una caracterización completa de todos los músculos en el mismo especimen. Además, algunos de los datos proporcionados no consideran el espesor a pesar de su importancia en el cálculo de tensiones. Puesto que los trabajos existentes en la literatura no proporcionan datos suficientes, esta tesis abordará la caracterización experimental de la respuesta pasiva de la pared abdominal en un modelo animal ampliamente utilizado en la literatura, como es el conejo blanco de Nueva Zelanda (Nilsson, 1982a,b; García-Moreno, 2001; LeBlanc et al., 2002; Johnson et al., 2004; Judge et al., 2007; Pascual et al., 2008).

II.4.1.2 Comportamiento activo. Estado del arte

Según el conocimiento de la autora, no existen estudios experimentales que caractericen la respuesta activa del tejido muscular abdominal. Sin embargo, la caracterización de la respuesta mecánica activa de otros tejidos musculares ha sido abordada en numerosos estudios de la literatura, en otros músculos esqueléticos de animales como ranas (Hill, 1938; Ramsey and Street, 1940; Abbot and Wilkle, 1953; Huxley and Niedergerke, 1954) o ratas (Ramírez et al., 2010) y también en humanos (Maganaris and Paul, 1999; Arampatzis et al., 2005).

Hill (1938) fue el primero en determinar experimentalmente la relación entre fuerza y velocidad para el acortamiento del músculo de rana. Sus estudios descubrieron que la velocidad a la que se acorta el músculo depende de la carga que se quiere mover. De esta forma, Hill (1938) obtuvo la curva fuerza-velocidad mediante la aplicación de diferentes cargas. Cuando se mantiene la carga constante, se denominan contracciones isotónicas mientras que cuando se mantiene constante la velocidad de contracción se

denominan contracciones isocinéticas. Cuando el músculo se alarga, también se ha descrito la relación fuerza-velocidad (Katz, 1939).

En lo que respecta a la dependencia entre la fuerza ejercida por el músculo y la longitud del mismo, diversos estudios han construido la curva fuerza-longitud a partir de datos obtenidos en ensayos experimentales de contracción, desarrollados para diferentes longitudes de músculos y bajo condiciones isométricas (Ramsey and Street, 1940; Abbot and Wilkle, 1953). Estos estudios demuestran que la fuerza isométrica del músculo de rana alcanza un valor máximo a una determinada longitud, denominada longitud óptima. Sin embargo, hay que tener en cuenta que las características de la relación fuerza-longitud no son constantes para todas las condiciones de ensayos (Huijing, 1998).

Años mas tarde, en 1954, se publicaron dos estudios que proponen que la contracción del músculo es debida a la interacción de los filamentos de actina y miosina cuando uno desliza sobre el otro (Huxley and Hanson, 1954; Huxley and Niedergerke, 1954). La fuerza generada por los puentes cruzados genera el deslizamiento de los filamentos (Huxley, 1957). Esta teoría es considerada la más importante en lo que respecta a la respuesta activa muscular y justifica las relaciones de la fuerza con la longitud y la velocidad. Concretamente, Gordon et al. (1966) evidenció experimentalmente que la relación fuerza-longitud en condiciones isométricas de un sarcómero totalmente activado esta relacionada con el solapamiento de los filamentos de actina y miosina. El número de puentes cruzados disponibles para generar fuerza depende del solapamiento. Por otra parte, la velocidad de contracción depende del ratio de formación y desaparición de puentes cruzados (Huxley, 1957).

En general, para cuantificar el comportamiento de la unidad músculo tendón se han desarrollado experimentos *"in vitro"* en el tendón (Colomo et al., 1997; Ciarletta et al., 2006), en el músculo completo (Davis et al., 2003; Grover et al., 2007; Ramírez et al., 2010; Grasa et al., 2011) y en fibras musculares (Konishi and Watanabe, 1998). Por otra parte, otros estudios de la literatura aportan la caracterización de la respuesta activa de modelos *"in vivo"* en el músculo (Grover et al., 2007; Ramírez et al., 2010).

Con el desarrollo de técnicas de observación ha sido posible cuantificar características mecánicas de la contracción muscular sobre humanos. Por ejemplo, la ultrasonografía es una técnica que se utiliza para visualizar tejidos ubicados superficialmente en el cuerpo, ricos en colágeno, tales como los músculos, tendones o ligamentos (Maganaris and Paul, 1999). Se usa dentro de un protocolo médico no invasivo que consiste en medir la deformación y la sección transversal del tejido en diferentes posiciones de flexión y extensión, mientras se cuantifica el momento articular por medio de un dinamómetro isocinético (Maganaris and Paul, 1999; Arampatzis et al., 2005).

Una técnica utilizada frecuentemente en laboratorio es la estimulación del nervio

mediante un impulso eléctrico que genera la contracción muscular (Ramírez et al., 2010). Esta metodología es posible cuando existe un nervio que se pueda aislar del resto del músculo para llevar a cabo la experimentación, como por ejemplo en los músculos fusiformes. Sin embargo, en otros músculos como es el caso del tejido abdominal, la activación ha de forzarse a través de la inmersión del tejido en un baño iónico. En lo que concierne al desarrollo de esta tesis, no se ha realizado la caracterización experimental de la respuesta activa de la pared abdominal, por quedar fuera del alcance de esta tesis. Sin embargo, a día de hoy, el protocolo de ensayo se está estableciendo en el marco de otra tesis doctoral, de modo que se han tomado datos de la literatura que obtienen la respuesta mecánica activa del músculo tibial anterior de rata (Ramírez et al., 2010). Dichos datos se han obtenido en función de la longitud del músculo, voltaje y frecuencia de excitación.

II.4.2 Modelado numérico

La simulación con elementos finitos, en el ámbito de la biomecánica, tiene como finalidad evaluar de forma aproximada el estado tensional y de deformación ante estados de carga fisiológicos o no fisiológicos de cualquier geometría cuya solución analítica no es posible obtener. Esta metodología ha sido ampliamente utilizada en la literatura para simular diferentes órganos y estructuras: tejido músculo esquelético (Lemos, 2001), músculos abdominales (Smietanski et al., 2012), cartílago (Palomar and Doblaré, 2006), vena cava (Alastrué et al., 2008), etc. Para ello, han de definirse la geometría de estudio, el modelo constitutivo, las propiedades mecánicas de cada uno de los materiales que intervienen en el modelo, las condiciones de contorno y las cargas.

La información procedente de la caracerización experimental de los tejidos se utiliza para el desarrollo y ajuste de modelos constitutivos tales que reproduzcan la respuesta mecánica del material (Fung, 1993; Weiss, 1994; Holzapfel, 2006; Calvo et al., 2010; Peña et al., 2010; Grasa et al., 2011). Los modelos constitutivos han de reproducir los patrones de comportamientos observados en los tejidos blandos, tales como el comportamiento no lineal en grandes deformaciones (Lemos, 2001; Holzapfel and Ogden, 2009; Calvo et al., 2010; Martins et al., 2010; Grasa et al., 2011; Martins et al., 2012), la incompresibilidad del tejido debido al alto contenido de agua (Alastrué et al., 2008; Peña et al., 2010), la anisotropía provocada por la orientación preferencial de las fibras de colágeno y musculares (Linden, 1998; Arruda et al., 2006) y la presencia de tensiones residuales (Peña et al., 2006, 2007).

Actualmente está aceptado que una formulación lagrangiana hiperelástica anisótropa es capaz de reproducir el comportamiento elástico de este tipo de tejidos, que corresponde al comportamiento habitual ante cargas fisiológicas (Holzapfel et al., 2000). El

comportamiento mecánico de los tejidos blandos se modela por medio de la definición de una función densidad energía de deformación expresada en función de invariantes cinemáticos (Spencer, 1971). Dado que el músculo está solicitado a tensiones, cuyo origen puede ser debido al comportamiento activo o pasivo, el comportamiento de los tejidos musculares se modela numéricamente como la adición de ambas contribuciones (Martins et al., 1998; Fernandez and Pandy, 2006; Bol and Reese, 2008; Stålhand et al., 2008; Ito et al., 2010; Stålhand et al., 2010).

La respuesta pasiva de los tejidos blandos viene dada por la suma de las contribuciones de la respuesta isótropa y anisótropa. Concretamente, los modelos pueden clasificarse en modelos *"fenomenológicos"* (Fung et al., 1979; Humphrey and Na, 2002), definidos como aquellos que únicamente reproducen la respuesta mecánica sin considerar los fenómenos físicos asociados en el tejido, y modelos *"estructurales"*, planteados de acuerdo a la composición física del tejido. Los modelos estructurales pueden a su vez clasificarse dos tipos de modelos: *"microestructurales"*, donde la anisotropía se considera a partir de la microestructura y, generalmente, a través de una función densidad de orientación que homogeiniza el comportamiento a nivel macroscópico (Lanir, 1979; Arruda and Boyce, 1993; Caner and Carol, 2006), y *"macroestructurales"*, donde la dirección de anisotropía se introduce explícitamente (Mooney, 1940; Demiray, 1972; Demiray et al., 1988; Arruda and Boyce, 1993; Yeoh, 1993; Holzapfel, 2000; Holzapfel et al., 2005; Calvo et al., 2009).

A continuación, las Secciones II.4.2.1 y II.4.2.2 incluyen un resumen de algunos de los trabajos existentes en la literatura relativos a la caracterización numérica de la respuesta pasiva y activa del tejido muscular, respectivamente.

II.4.2.1 Comportamiento pasivo. Estado del arte

La literatura relativa al modelado numérico de la repuesta pasiva de los tejidos blandos es muy amplia (Demiray et al., 1988; Weiss et al., 1996; Holzapfel et al., 2000; Lemos, 2001; Holzapfel, 2006; Holzapfel and Ogden, 2009; Calvo et al., 2010; Martins et al., 2010; Peña et al., 2010; Grasa et al., 2011). Sin embargo, los estudios focalizados en el músculo abdominal son escasos.

El modelado del comportamiento pasivo del tejido muscular se ha abordado tanto a nivel microscópico (Sharafi and Blemker, 2010) como nivel macroscópico (Hodgson et al., 2012; Martins et al., 2012). Existen formulaciones que modelan el comportamiento con modelos lineales (Boriek et al., 2000) y no lineales (Van Loocke et al., 2006) y, a su vez, el comportamiento en grandes deformaciones evidenciado en los tejidos musculares queda recogido en algunos modelos numéricos (Hodgson et al., 2012; Martins et al., 2012). Concretamente, Hodgson et al. (2012) analizó la calidad del ajuste numérico

utilizando cuatro funciones densidad energía de deformación y validó su estudio con ensayos experimentales en el músculo tibial anterior de rata. El mismo modelo de experimentación animal lo utilizó Ito et al. (2010) para validar su modelo constitutivo para músculo esquelético que describe la anisotropía, viscoelasticidad y el daño del tejido muscular. Odegard et al. (2008) propuso un modelo numérico para predecir la respuesta mecánica del tejido músculo esquelético pero no lo validó experimentalmente.

En lo que concierne al músculo abdominal, el modelado computacional se ha abordado desde un punto de vista macroscópico (Song et al., 2006a; Szymczak et al., 2009; Smietanski et al., 2012; Szymczak et al., 2012; Martins et al., 2012; Förstemann et al., 2011). Martins et al. (2012) modeló el comportamiento pasivo de la fascia del recto abdominal dentro de la teoría de la hiperelasticidad no lineal en grandes deformaciones. Por otra parte, Song et al. (2006a) estudió la respuesta del abdomen del humano en ensayos de inflado y modeló numéricamente el comportamiento utilizando la ecuación de Laplace para obtener la relación entre la presión de inflado y el radio de curvatura de la superficie abdominal. En estudios posteriores, López-Cano et al. (2007) propuso un modelo dinámico en 3D con el cual llevó a cabo la simulación del comportamiento dinámico de la región inguinal ante cargas fisiológicas.

Referente al abdomen humano, Song et al. (2006a) desarrolló un modelo tridimensional de la pared abdominal del humano basado en un modelo de experimentación en humano *"in vivo"*. Concretamente, su modelo permitió simular y analizar el patrón de movimiento que se produce en la cirugía laparoscópica donde la cavidad abdominal está solicitada a una presión intraabdominal y se produce un inflado de dicha cavidad. Posteriormente, Förstemann et al. (2011) definió la geometría de la parte frontal del abdomen a partir de imágenes de resonancia magnética (MRI), realizó ensayos uniaxiales sobre la zona de la línea alba y correlacionó los resultados obtenidos con el modelo computacional considerando una aproximación en pequeñas deformaciones y utilizando la ecuación de Laplace. A su vez, estos autores plantearon una relación entre las tensiones uniaxiales y biaxiales. En un estudio reciente, Szymczak et al. (2012) obtuvo las propiedades mecánicas del adomen humano mediante el método de análisis inverso y analizó las zonas del abdomen donde se producen mayores deformaciones.

Esta tesis abordará el modelado numérico de la respuesta pasiva de la pared abdominal ya que no se han encontrado trabajos que describan numéricamente dicha respuesta en el marco de la hiperelasticidad no lineal anisótropa, que es la necesaria para reproducir todos los patrones de comportamiento de la pared abdominal. Además, puesto que ningún modelo de la literatura propone un modelo de elementos finitos de abdomen completo, esta tesis describirá un modelo de abdomen que diferenciará las estructuras anatómicas principales de la anatomía del mismo.

II.4.2.2 Comportamiento activo. Estado del arte

Como se ha introducido con anterioridad, no existen trabajos previos focalizados en la simulación numérica de la respuesta activa del tejido abdominal. Por ello, esta tesis planteará un modelo numérico que reproducirá la respuesta activa del abdomen. Sin embargo, desde que surgieron los primeros modelos que caracterizan la respuesta activa de otros músculos se han desarrollado numerosos estudios que incorporan mejoras o que abordan el modelado desde otros enfoques. En general, los modelos se agrupan dentro de cuatro grupos: el modelo de Hill (1938), el modelo de Huxley o de los puentes cruzados Huxley (1957), modelos morfológicos (Huijing and Woittiez, 1984; Woittiez et al., 1984) y modelos morfo-mecánicos (Hunter and McCulloch, 1988; Martins et al., 1998).

El modelo desarrollado por Hill (1938), que ha sido utilizado ampliamente y que se basa en observaciones experimentales, consiste en un elemento contractil dispuesto en serie con un muelle. El elemento contractil representa el mecanismo de contracción mientras que el muelle representa la contribución pasiva del tendón y las aponeurosis. Finalmente, se añade un tercer elemento en paralelo que tiene en cuenta la propiedades pasivas del músculo (Hatze, 1981).

La dinámica de los puentes cruzados se tiene en cuenta en el modelo propuesto por Huxley (1957). Este modelo se desarrolló en base a ensayos experimentales para determinar la relación entre la fuerza y la velocidad. Otros modelos que parten del modelo de Huxley y que analizan la respuesta activa con más detalle son los publicados por Hill et al. (1975), Eisenberg et al. (1980), Ma and Zahalak (1987) y Zahalak (1981).

Los modelos morfologicos tienen en cuenta las características morfológicas de los músculos tales como la longitud de la fibras y el ángulo de las aponeurosis (Huijing and Woittiez, 1984; Woittiez et al., 1984; Otten, 1988; Leeuwen and Spoor, 1992, 1996). En lo que respecta a los músculos penados, estos modelos tienen en cuenta el ángulo de las fibras con respecto a la línea de acción de fuerza. La incompresibilidad se tiene en cuenta en el modelo planimétrico (Huijing and Woittiez, 1984) y en el correspondiente modelo tridimensional (Woittiez et al., 1984). Algunos modelos aseguran que la consideración de la geometría es fundamental para entender realmente la cantidad de fuerza que ejerce el músculo (Otten, 1988; Leeuwen and Spoor, 1992, 1996).

En la literatura existen estudios que proponen modelos morfo-mecánicos que se basan en la mecánica del músculo y que desarrollan modelos de elementos finitos aplicados a diferentes tejidos musculares (Hunter and McCulloch, 1988; McCullock et al., 1992; Martins et al., 1998). La potencialidad de estos modelos permite tener en cuenta no sólo las propiedades geométricas del músculo, sino que tienen en cuenta las propiedades

del material. Estos modelos consideran el músculo como un continuo y la capacidad de análisis de la respuesta es mayor.

Estudios recientes incorporan el modelado de las respuestas activa y pasiva, simultáneamente (Stålhand et al., 2008; Ito et al., 2010; Stålhand et al., 2010; Bol et al., 2011) y, generalmente, los modelos numéricos que se plantean en la literatura están validados con ensayos experimentales en músculos esqueléticos (Jenkyn et al., 2002; Fortuny et al., 2009a; Chi et al., 2010; Ito et al., 2010; Ramírez et al., 2010; Bol et al., 2011; Grasa et al., 2011; Hodgson et al., 2012) y músculos lisos (Stålhand et al., 2008, 2010). Sin embargo, hay estudios que proponen modelos numéricos para el comportamiento activo que no están validados experimentalmente, limitándose así su aplicabilidad (Bol and Reese, 2008; Odegard et al., 2008; Fortuny et al., 2009b).

II.5 Prótesis para reconstrucción herniaria

En la actualidad existen diferentes tipos de prótesis o mallas sintéticas. Esta sección describe los conceptos fundamentales relativos al estudio de dichas prótesis, que permiten clasificarlas atendiendo a diferentes criterios. Además, se realiza una revisión bibliográfica acerca de algunos de los trabajos existentes en la literatura relativos a la caracterización experimental y simulación numérica de dichas prótesis.

Se pueden establecer diferentes clasificaciones de las prótesis atendiendo a su estructura geométrica, al material del que están fabricadas y a su porosidad, ya que son los factores más determinantes en el comportamiento final de las mismas (Rosch et al., 2004; Bellón et al., 2009). Estas características determinan la flexibilidad y el tipo de respuesta, isótropa o anisótropa, de la prótesis, de modo que la orientación de la malla sobre el tejido abdominal receptor, que a su vez tiene un comportamiento anisótropo (Hwang et al., 2005), puede ser influyente en el resultado final de la cirugía. Por otra parte, tanto el material como el tamaño del poro determinan la forma en que se produce la integración tisular generando una mayor o menor fibrosis.

Atendiendo a la geometría o tejido de los hilos de la malla, las prótesis se pueden clasificar en reticulares, laminares y prótesis compuestas (ver Figuras II.17, II.18 y II.19) y dentro de dichos diseños se utilizan diferentes materiales. Las mallas reticulares pueden dividirse a su vez en no absorbibles, parcialmente absorbibles y totalmente absorbibles. En estas mallas, los filamentos se clasifican a su vez en monofilamentos o multifilamentos. Por otra parte, las mallas laminares pueden ser no absorbibles o absorbibles. En último lugar, las prótesis compuestas pueden ser de dos tipos: las que están formadas por componentes no absorbibles y una barrera física (diferente componente no absorbible), y las que lo están por componentes no absorbibles y una

barrera química (componente absorbible) (ver Figuras II.19 y II.20). Además, estos subgrupos se diferencian a su vez por el tipo de material del que están fabricadas.

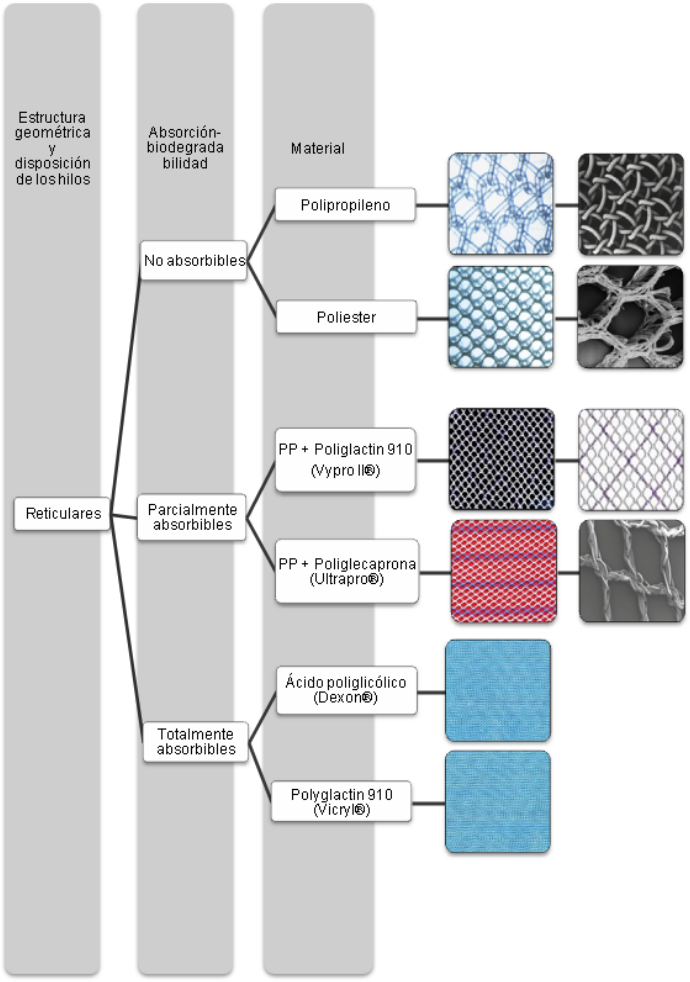

Figura II.17: Clasificación de las mallas sintéticas reticulares.

Desde el punto de vista de la porosidad, las prótesis se han clasificado en mallas de alto o bajo peso, dependiendo del parámetro de densidad g/m^2 que caracteriza las mismas (Klinge, 2007). Se consideran prótesis de alto peso o *"heavyweight"* (HW) aquellas que se sitúan por encima de 80 g/m^2, mediano peso o *"mediumweight"* (MW) entre $50 - 80$ g/m^2 (Cobb et al., 2006), y de bajo peso o *"lightweight"* (LW) las que se encuentran por debajo de 50 g/m^2. Incluso algunas clasificaciones introducen otra categoría de mallas sintéticas, consideradas como utraligeras o *"ultralightweight"* (ULW) que tienen un peso por unidad de superfice no superior a los 35 g/m^2 (Earle and Mark, 2008).

Hay que tener en cuenta que, a veces, el peso protésico es independiente del tamaño del poro. Ello es debido a que hay prótesis con un diseño de poro pequeño, con una

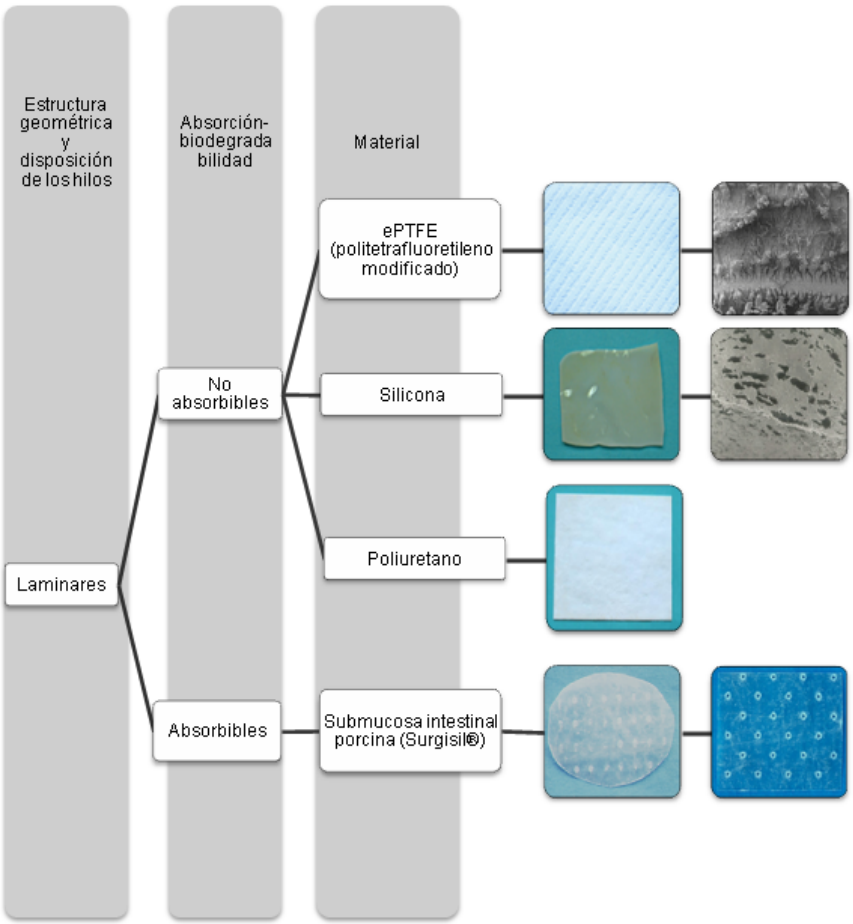

Figura II.18: Clasificación de las mallas sintéticas laminares.

estructura espacial y un anudado o entrecruzamiento simple y, a su vez, un filamento fino, que son LW por tener en su conjunto un peso en g/m^2 bajo. Este último aspecto es importante ya que, de acuerdo con la escuela alemana (Schumepelick and Klinge, 2003), se suele considerar que el tamaño de poro protésico es el principal parámetro para considerar a una prótesis como HW o LW. De esta manera, las prótesis HW tendrían un diseño con poro pequeño y las LW con poro grande.

A continuación se incluye una revisión bibliográfica de los trabajos disponibles en la literatura relativos a la caracterización experimental (Subsección II.5.1) y computacional (Subsección II.5.2) de prótesis. A pesar de que hay diversidad de estudios en la literatura, no se encuentran trabajos que consideren aspectos experimentales y computacionales simultáneamente. Por tanto, no hay un estudio completo que evalue la respuesta mecánica experimental de una malla quirúrgica y modele numéricamente su comportamiento. Esta tesis abordará estos dos aspectos, la caracterización mecánica experimental y computacional de tres mallas sintéticas representativas; concretamente

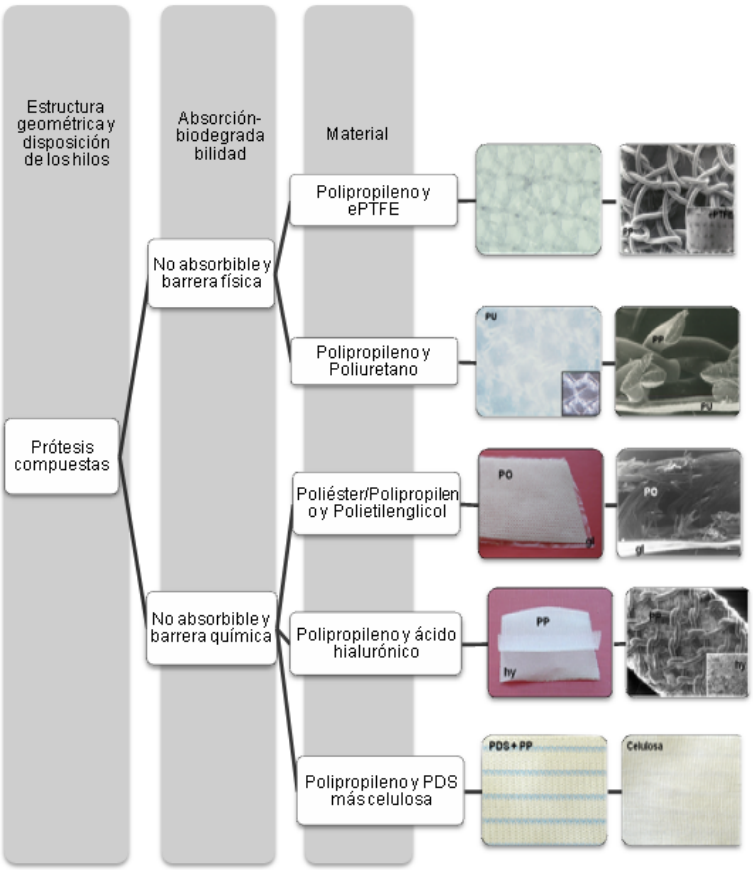

Figura II.19: Clasificación de las mallas sintéticas compuestas.

la malla Surgipro®, que está fabricada de polipropileno y es una malla de alto peso, la malla Optilene®, que es una malla de polipropileno y bajo peso y la malla Infinit®, fabricada de politetrafluoroetileno y de peso medio.

II.5.1 Caracterización mecánica experimental. Estado del arte

La caracterización experimental de prótesis utilizadas en la cirugía herniaria tiene como objetivo la determinación de las propiedades mecánicas de las mallas sintéticas (Afonso et al., 2008; Bellón, 2009; Saberski et al., 2010; Deeken et al., 2011). En la literatura se pueden encontrar numerosos estudios cuyo objetivo es la determinación del comportamiento mecánico de las prótesis. Saberski et al. (2010) llevó a cabo un estudio para comparar las propiedades anisótropas de diversas mallas comerciales utilizadas en la cirugía herniaria. Concretamente, utilizó las mallas Trelex®, ProLite^{TM}®, Ultrapro^{TM}®, Parietex^{TM}®, Dualmesh® e Infinit® y concluyó que todas ellas muestran un fuerte caracter anisótropo. Afonso et al. (2008) llevó a cabo ensayos uniaxiales

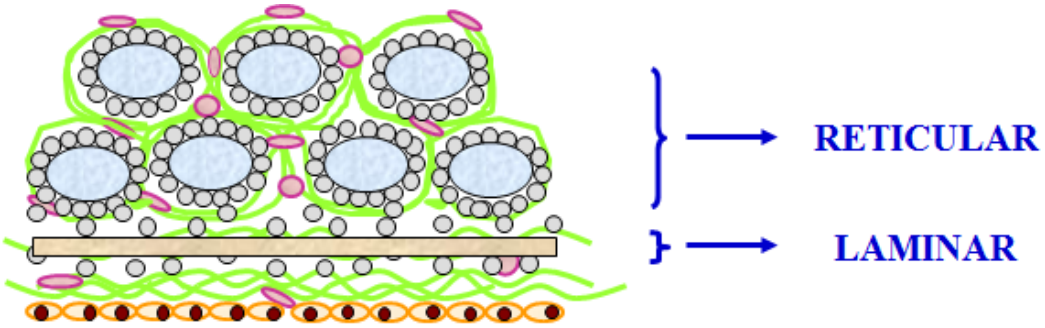

Figura II.20: Esquema transversal de una malla compuesta (Bellón, 2012).

y de compresión (utilizando una probeta en forma de anillo) y observó diferencias significativas en la respuesta mecánica de las prótesis Aris^{TM}®, TVTO^{TM}®, Auto Suture^{TM}®, Uretex^{TM}® y Avaulta^{TM}®. Por otra parte, Yoder and Elliott (2010) desarrollaron un estudio para medir las propiedades mecánicas de cuatro mallas diferentes: Alloderm®, Restore®, CuffPatch® y OrthADAPT®. En dicho trabajo, se evaluaron la anisotropía y la no linealidad de los materiales con el fin de entender las propiedades mecánicas en ensayos uniaxiales. Sus conclusiones indican que el tipo de prótesis que ha de elegirse depende del tipo de reparación para la que vaya a usarse.

Hollinsky et al. (2008) llevó a cabo una comparativa de las propiedades biomecánicas entre mallas ligeras y pesadas. La motivación del estudio fue que, además del tamaño de la malla, el coeficiente de fricción y la rigidez a flexión de la malla son aspectos cruciales para evitar la recurrencia de la hernia. El estudio experimental incluyó la realización de ensayos para determinar la tensión de rotura y el módulo de elasticidad de seis mallas ligeras y seis mallas pesadas utilizadas en la reparación de hernias inguinales por laparoscopia. Sus conclusiones fueron que las mallas con mayor rigidez a flexión o mallas ligeras bien fijadas con un solapamiento suficiente pueden ser utilizadas para el tratamiento de hernias de gran tamaño.

Otros estudios se centran en el estudio y análisis del comportamiento de las suturas que permiten la unión de la prótesis al tejido y que han de ser compatibles con las propiedades mecánicas de la malla. Concretamente, una fuerza de rotura de $16 - 32$ N se considera adecuada (Schwab et al., 2008). A pesar de que la fijación por laparoscopia tiene como objetivo minimizar el número de recurrencias tras la reparación, los sistemas de fijación tales como la sutura o grapado se asocian al dolor crónico (Schwab et al., 2008). Kes et al. (2004) evaluó el ratio de protusiones generadas a partir del uso de diferentes mallas comerciales: Marlex®, Parietene®, Prolene®, Mersilene®, Parietex®, Fluoromesh® y Vypro composite®. Como conclusión, se estableció un ranking basado en el mejor comportamiento de las mallas en función del tamaño del defecto reparado. Además, una de sus conclusiones fue que cuando se usa una malla

grande, la fijación no aporta necesariamente unión adicional porque la propia malla inmobiliza bastante por ella misma.

Binnebösel et al. (2007) evaluó la dependencia de la dislocación de la malla con respecto al tamaño del defecto, el solapamiento, la posición de la malla y la orientación de la malla en el caso de mallas anisótropas. Su estudio llevó a la conclusión de que un solapamiento de 3 cm es suficiente para prevenir la dislocación temprana de la prótesis.

II.5.2 Modelado numérico. Estado del arte

La información recabada en la caracterización experimental de mallas sintéticas se puede utilizar para el desarrollo de modelos constitutivos que sean capaces de reproducir la respuesta mecánica del material. Los modelos numéricos basados en formulaciones continuas no lineales permiten la simulación computacional del implante ante cargas fisiológicas, multidireccionales y cargas inhomogéneas y, a su vez, permiten la comparación del comportamiento mecánico de la malla quirúrgica con respecto al comportamiento del tejido que se quiere reemplazar.

Aparentemente, el comportamiento mecánico de las mallas sintéticas se atribuye a fenómenos que tienen lugar a diferentes escalas. Las evidencias experimentales indican una respuesta no lineal, cambios drásticos en la malla debido al colapso de los poros de la malla bajo condiciones de carga uniaxial y una fuerte componente anisótropa en algunas de las mallas comerciales existentes. Estos fenómenos se pueden estudiar a partir del análisis de la celda unidad o patrón que define, por repetición en el espacio, el tejido de la malla. Además, la fricción entre los hilos de la malla provoca fenómenos como histéresis, dependencia con la velocidad de deformación y procesos de deformación irreversibles que provocan cambios significantes en la geometría de la celda unidad durante ciclos de carga.

Algunos de los estudios que se encuentran en la literatura modelan numéricamente el comportamiento de las mallas sintéticas considerando el tejido de las mismas. Uno de dichos trabajos es el publicado por Kuwazuru and Yoshikawa (2004). Estos autores desarrollaron un modelo pseudo-continuo para analizar el comportamiento de mallas sintéticas desde el punto de vista de las propiedades micromecánicas no lineales. La validación del modelo la realizaron con un análisis biaxial.

Los modelos continuos son más eficientes y sencillos computacionalmente que los modelos discretos, puesto que se pueden incluir dentro de otros modelos mas complejos. A pesar de que los modelos continuos no reproducen el comportamiento individual de cada hilo, contienen información del comportamiento general de la malla. King et al. (2005) propuso un enfoque para desarrollar modelos continuos que reprodujesen

el comportamiento mecánico de mallas en deformación plana. La potencialidad de su estudio permite simular el comportamiento mecánico de prótesis existentes, así como predecir el comportamiento de nuevos diseños una vez conocido el patrón de tejido de la malla. La deformación macroscópica de la malla se relaciona con la configuración estructural del tejido a través de un método de minimización de la energía. Con dicho método, King et al. (2005) calculó las fuerzas internas que aparecen en los hilos de la prótesis y modeló por elementos finitos el comportamiento de mallas sintéticas bajo diferentes cargas.

Röhrnbauer et al. (2011) publicó una metodología para desarrollar un modelo constitutivo bidimensional que caracteriza numéricamente el comportamiento mecánico del tejido microestructural de mallas sintéticas. Su investigación dió como fruto dos modelos planteados en diferentes escalas: uno de ellos desarrolla el modelado del patrón de la prótesis, puesto que es una unidad repetitiva, y, a nivel macroscópico, otro modelo numérico que atiende a la respuesta continua de la malla sintética.

II.6 Proceso de integración tisular

Una vez que se ha realizado la cirugía abdominal y se ha colocado la prótesis, se inicia el proceso de integración tisular que provoca la formación de tejido nuevo sobre el área del defecto herniario, provocándo un cambio en las propiedades del conjunto tejido-malla. A continuación se describen los términos más importantes relativos al proceso de integración tisular y que son necesarios para el entendimiento de la tesis.

Tras la implantación de un biomaterial, el tejido receptor responde produciendo una reacción inflamatoria con una respuesta bioquímica y celular cuyo último objetivo es la cicatrización. Se originan, además, una serie de procesos que van encaminados a aislar el material implantado mediante la encapsulación. El grado de la respuesta tisular dependerá de la naturaleza y las características del material implantado, pero para que la cicatrización se complete es necesaria una correcta respuesta celular por parte del huésped. Además, la calidad del tejido neoformado viene dada por la estructura de la prótesis implantada (Pascual et al., 2008). Bellón et al. (1996) concluyó que es la estructura de la prótesis implantada la que condiciona el desarrollo del proceso reparativo, siendo la porosidad la característica más determinante para el desarrollo de la cicatrización.

Una vez realizada la implantación se suceden las distintas fases del proceso inflamatorio alrededor del biomaterial (García-Pumarino, 2010). Inicialmente, son los leucocitos polimorfonucleares las primeras células en llegar al lugar del implante. Tras una transitoria vasoconstricción (estrechamiento de los vasos sanguíneos), se produce

una hiperemia reactiva (aumento del flujo sanguíneo) en los pequeños vasos locales. El endotelio de dichos vasos se vuelve más permeable para el paso de proteínas y plasma. Coincidiendo con estos cambios, los leucocitos se adhieren a la superficie de las células endoteliales y, mediante diapedesis, salen de los vasos sanguíneos para concentrarse en el lugar de la lesión. En las primeras 24 a 48 horas la principal función de los leucocitos (sobre todo, los polimorfonucleares) es la fagocitosis de restos celulares y detritus del tejido lesionado.

Tras esta primera fase de emigración leucocitaria (diapedesis) y la lisis de los granulocitos, que liberan hidrolasas ácidas en el medio local, aumenta la proporción de monocitos-macrófagos (células del sistema inmunitario). Comienza entonces una importante actividad macrofágica tras la activación de los macrófagos en el medio extracelular. Los macrófagos cumplen un importante cometido en el proceso de cicatrización, posterior a la implantación de un biomaterial, y en la integración de éste en el tejido donde ha sido implantado. De este modo, una alteración en la reacción macrofágica podría conducir a procesos de cicatrización anómalos (Leibovich and Ross, 2007). Además, la liberación de diversos factores de crecimiento, que estimulan la migración de fibroblastos, células epiteliales y endoteliales, modulan los procesos de reparación tisular (Whal et al., 1989) (ver Figura II.21).

La valoración de la respuesta macrofágica en los implantes a lo largo del tiempo permite conocer el comportamiento del biomaterial y la tolerancia por parte del receptor. Según el estudio de Bellón et al. (1995), en la pared abdominal, el patrón de comportamiento macrofágico parece mantenerse a lo largo del tiempo, y este no depende de las características físicas de la prótesis, sino de la composición química del material (Pascual et al., 2012c).

Durante ciertos tipos de inflamación crónica, y siempre vinculadas a la presencia de un material extraño, los macrófagos forman células gigantes y multinucleadas mediante fusión celular que se denominan células gigantes a cuerpo extraño. Esta reacción inflamatoria crónica puede llegar a dañar las propiedades del biomaterial.

A medida que el proceso cicatricial evoluciona, comienzan a aumentar los fibroblastos en la herida (será la población celular predominante a partir del décimo día). Aumenta la síntesis de colágeno y de matriz extracelular, fundamental para formar el tejido conectivo cicatricial. Otros tipos celulares (plaquetas, linfocitos y macrófagos) sintetizan factores de crecimiento que modulan la respuesta mitótica, el desplazamiento y la síntesis de colágeno por parte de los fibroblastos. En esta fase, la angiogénesis, que es un proceso fisiológico que consiste en la formación de vasos sanguíneos nuevos a partir de los preexistentes, adquiere una vital importancia. Así, se originan nuevos capilares que aportan el oxígeno y nutrientes necesarios para la actividad de síntesis tisular (Border and Noble, 1994). Por tanto, se produce la formación de tejido conectivo que se ordena

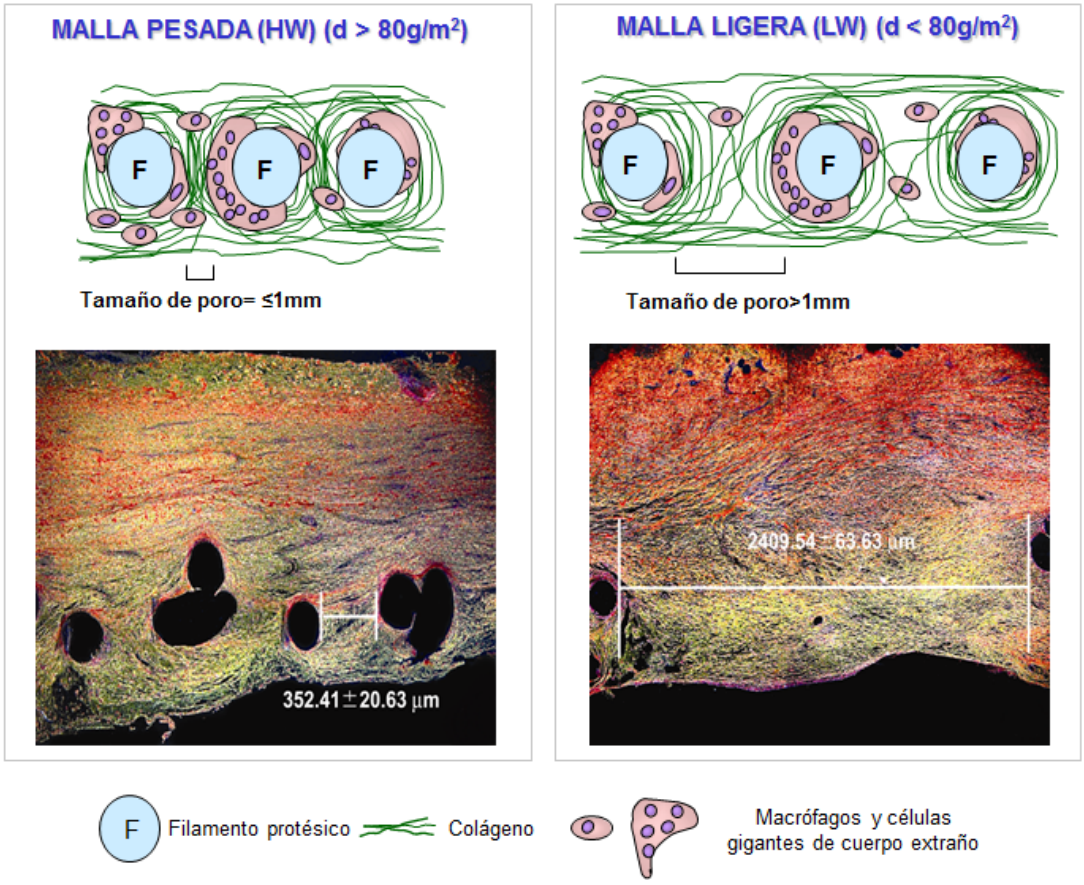

Figura II.21: Esquema de la integración tisular en mallas reticulares pesadas y ligeras (o de alto peso y bajo peso). Se diferencian los filamentos sintéticos de la prótesis (F), los macrófagos y las fibras de colágeno generadas en el proceso de regeneración tisular. En las imágenes inferiores, secciones tisulares de ambas mallas implantadas. Tinción Rojo Sirio donde se puede observar, en la matriz extracelular del tejido neoformado, el colágeno de tipo III en color amarillo y el de tipo I en rojo (Bellón, 2012).

alrededor del biomaterial, dando lugar a su encapsulación (ver Figura II.22).

Los fibroblastos desempeñan un papel importante en los procesos de remodelación tisular y en la posterior adaptación del implante. Hacia la cuarta o quinta semana el número de fibroblastos disminuye y el principal rasgo ultraestructural pasa a ser las fibras de colágeno de tipo III (colágeno inmaduro). Al principio la disposición de estos haces es al azar. Con el paso del tiempo, y por la interacción de las fuerzas de tensión mecánica de los tejidos, los haces de colágeno se reorganizan para resistir mejor la tracción y se convierten en colágeno tipo I (colágeno maduro). Los haces de colágeno cuya disposición no resulta útil, sufren procesos de degradación por la acción local de colagenasas, estableciéndose un equilibrio dinámico entre la síntesis y la destrucción de

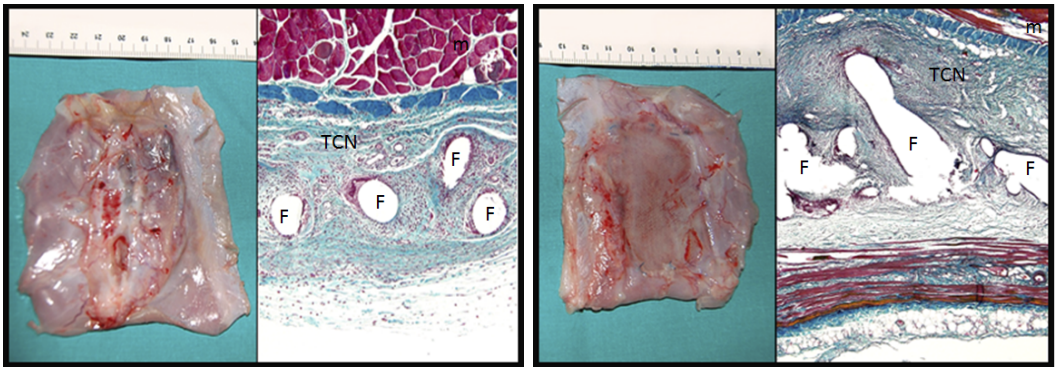

(a) (b)

Figura II.22: Integración tisular de dos prótesis en un tamaño de defecto de 6x4 cm a los 14 días tras el implante en un modelo experimental en conejo. Imágenes macroscópicas a la izquierda y de microscopía óptica, con Tinción Tricrómico de Masson, a la derecha (50x). (a) Malla Surgipro®. (b) Malla Progrip® (F: Filamento, m: tejido muscular, TCN: tejido conectivo neoformado) (Bellón, 2012).

haces de colágeno.

En lo que respecta a la prótesis implantada, el proceso de reparación provoca una retracción o acortamiento de la malla que queda plasmado en la reducción del tamaño de la misma (Konerding et al., 2011a).

II.7 Mecánica del tejido reparado tras la integración tisular. Nuevos diseños de prótesis

La gran diversidad de mallas disponibles en el mercado y la ausencia de criterios establecidos y científicamente reconocidos que indiquen qué malla es la más adecuada en cada situación particular, hacen que la elección de la malla sea una tarea difícil para el cirujano (Rosch et al., 2004). Además, si bien existen muchas prótesis comerciales, cada una de ellas puede provocar una serie de problemas sobre la zona del defecto que afectan al paciente tras la implantación de la misma. Por tanto, uno de los desafíos actuales en esta rama de la biomedicina es el diseño de nuevas prótesis y nuevos biomateriales que mejoren los resultados tras la cirugía herniaria (Bellón, 2009). En esta sección se describe la evolución en los diseños de prótesis en los últimos años, valorados en función de estudios experimentales del tejido reparado, cuyo objetivo es la evaluación de la respuesta final del conjunto tejido-malla tras la integración tisular.

Tras la cirugía, la formación de tejido en la zona del defecto, que provoca un in-

cremento en la rigidez del tejido reparado, es modulado en función de la prótesis implantada, siendo la respuesta del tejido abdominal diferente en función de la prótesis utilizada (Anurov et al., 2010). Por esta razón, se hace necesaria la caracterización experimental del conjunto tejido-malla para determinar las propiedades mecánicas del lugar del implante tras diferentes tiempos después de la operación, mediante ensayos uniaxiales (Hilger et al., 2006; Sergent et al., 2010) o de punzonamiento (Konerding et al., 2011b; Podwojewski et al., 2012), entre otros. Además, la obtención de imágenes a nivel microscópico aporta información sobre la formación de colágeno tipo III y sobre su posterior reconversión en colágeno tipo I conforme la prótesis se va integrando en el tejido (Pascual et al., 2008). De esta forma, es posible analizar en qué medida las propiedades del conjunto tejido-malla a lo largo del tiempo se modifican para mimetizar el comportamiento original del tejido abdominal sano (Cobb et al., 2006; Pascual et al., 2008; Bellón et al., 2009).

Uno de los materiales que más se ha utilizado para la reparación de defectos herniarios abdominales es el polipropileno en forma de prótesis reticular macroporosa. Su uso se remonta históricamente al siglo pasado, cuando Usher lo utilizó en las primeras reparaciones herniarias (Usher, 1959; Usher et al., 1960). A lo largo del tiempo se ha generalizado el uso de este biomaterial en las reparaciones de tipo tejido/tejido, incluyendo casos en los que existe infección (Antonopoulos et al., 2006; Alaedeen et al., 2007). En estos casos con infección, el polipropileno es de los pocos materiales con los que es posible el rescate parcial de la prótesis (Bellón-Caneiro et al., 2004; Jezupors and Mihelsons, 2006). Sin embargo, el polipropileno presenta el único inconveniente de que tiene mal comportamiento en la interfaz peritoneal, produciéndose complicaciones como fistulizaciones al intestino (Chew et al., 2000) y migraciones a órganos cavitarios (Chuback et al., 2000). Por tanto, cuando se trata de reparación de efectos en la interfaz, debe evitarse su uso. Experimentalmente *"in vitro"*, algunos estudios han demostrado la bioestabilidad del polipropileno (Kapischke et al., 2005). En lo que se refiere a ensayos *"in vivo"*, se han observado procesos de oxidación en la zona del implante, lo cual puede afectar al comportamiento del biomaterial mediante la biodegradación del mismo. Estos efectos se detectaron mediante la técnica de microscopía electrónica de barrido (Costello et al., 2007). A pesar de estas evidencias encontradas, la rigidez del polipropileno no se altera con el paso del tiempo.

Las prótesis han ido evolucionando para incorporar nuevos diseños que faciliten la integración tisular (ver Figura II.23). Uno de los requisitos imprescindibles que debe cumplir todo biomaterial es que su implantación no provoque reacciones deletéreas ni a nivel local ni sistémico. Ya que el medio que lo rodea no es estático, el biomaterial debe ser capaz de afrontar los cambios que experimenta el tejido huésped a largo plazo (Anderson, 1988). La biocompatibilidad de la prótesis se define como la respuesta del tejido ante la implantación de un cuerpo extraño. Esta reacción depende de la cantidad de material implantado, del tipo de material, de la estructura y del tipo de filamento

(monofilamento o multifilamento). Por otra parte, el diseño de una malla sintética debe considerar las propiedades mecánicas de la prótesis, incluyendo la rigidez y la tensión de rotura (Klinge et al., 1998). Las modificaciones que han sufrido las prótesis se han enfocado a la utilización de otros biomateriales y al diseño de mallas con poros de mayor tamaño.

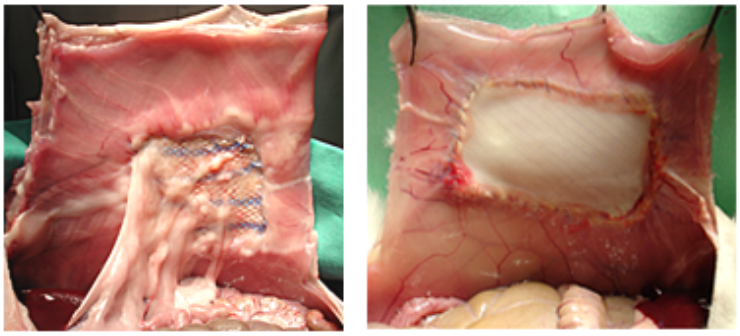

Figura II.23: Comparación de la fibrosis generada entre una prótesis reticular y una prótesis laminar (Bellón, 2012).

En lo que se refiere a la incorporación de nuevos biomateriales, una de las modificaciones que han sufrido las mallas reticulares de polipropileno es la incorporación parcial de materiales autodegradables. Estas prótesis se conocen como prótesis híbridas parcialmente degradables (Rosch et al., 2003; Junge et al., 2005). Es decir, la malla clásica de polipropileno incorpora materiales biodegradables que se degradan a medio o largo plazo. La ventaja que ofrecen estos diseños es que a medio o largo plazo, cuando la prótesis está prácticamente integrada, la cantidad de material que permanece en el lugar del implante, es menor. Además, una cantidad menor de material permanente en el tejido receptor hace que la reacción ante cuerpo extraño que se produce tras el implante sea menor y, por tanto, la fibrosis que se genera también lo sea (Klinge et al., 2002a; Cobb et al., 2006). Varios autores corroboran la importancia de este aspecto, puesto que numerosos pacientes sufren molestias (Welty et al., 2001; Holste, 2005) ya que la excesiva rigidez de la pared abdominal reduce la movilidad de la misma (Schimidbauer et al., 2005). El trabajo desarrollado por Langenbach et al. (2008) analizó la respuesta a largo tiempo de tres mallas sintéticas diferentes e indicó que la malla composite no ofrece ventajas con respecto a la función física ni con respecto al dolor provocado en el paciente. Sin embargo, Hilger et al. (2006) describió las propiedades histológicas y biomecánicas que aparecen con el uso de prótesis fabricadas con tejido colagenoso tras 6 y 12 semanas del implante. Sus conclusiones aseguran que, a pesar de que hay una disminución de la rigidez tras la implantación de las prótesis, la reacción inflamatoria es menor.

Otra de las modificaciones que se están considerando en las prótesis convencionales es la reducción de material implantado en la zona del defecto, por medio del diseño de

mallas con poros más amplios (Junge et al., 2002). Varios artículos recientes se han centrado en la evaluación del comportamiento de las prótesis LW y sus ventajas a corto plazo han sido mostradas en trabajos de la literatura (Conze et al., 2005; O'Dwyer et al., 2005). Especialmente, se centran en la evaluación del proceso de integración de las mallas en el tejido receptor y en la respuesta biomecánica del conjunto tejido-malla (Weyhe et al., 2006). Cobb et al. (2006) llevó a cabo un estudio experimental en cerdos tras 5 meses del implante y observaron que la respuesta mecánica era similar entre las mallas ligeras y pesadas. Otro estudio que corrobora esta evidencia a los 90 días del implante es el publicado por Bellón et al. (2007). Por otra parte, el uso de mallas LW provoca menor dolor crónico en los pacientes que las mallas HW (O'Dwyer et al., 2005), aunque se ha observado un mayor índice de recurrencia de la hernia. Algunos autores atribuyen el fenómeno de la recurrencia a factores asociados con el método de fijación de las mallas (O'Dwyer et al., 2005) mientras que otros indican casos de fallo de la malla por su parte central (Lintin and Kingsnorth, 2012). Otro estudio que compara la respuesta entre mallas LW y HW es el publicado por Klinge et al. (2002b). Las conclusiones de su estudio indican que con ambos tipos de mallas se produce una reacción inflamatoria en la zona del defecto. Sin embargo, se remarca que las mallas LW muestran una mejor integración del tejido y que el tamaño del poro es un factor muy importante de cara al proceso de incorporación de la prótesis (Bellón et al., 1996).

Entre las diferentes mallas comerciales que existen, algunas de ellas presentan un comportamiento mecánico anisótropo (Yoder and Elliott, 2010). En estos casos, una vez que la malla se integra en el tejido receptor, el conjunto resultante de tejido-malla sigue mostrando anisotropía en la respuesta mecánica (Ozog et al., 2011). Por tanto, si bien la adaptación final de la malla sintética ha de ser tal que mimetice la respuesta original del tejido sano, su disposición es fundamental (Anurov et al., 2010; Ozog et al., 2011). Anurov et al. (2010, 2012) estudió la influencia de la colocación de las prótesis en el abdomen de ratas. Concretamente, estudió los resultados obtenidos con las mallas Ultrapro® y DynaMesh®, concluyendo que las direcciones de anisotropía han de considerarse en la implantación. Concretamente, estos autores concluyen que la dirección más rígida de la malla ha de colocarse paralela a la dirección donde el esfuerzo muscular es mayor (Anurov et al., 2010) y a lo largo de la dirección donde estan dispuestas las fibras de las aponeurosis (Anurov et al., 2012).

A pesar de que hay infinidad de estudios experimentales sobre diferentes prótesis, los trabajos disponibles en la literatura evalúan principalmente la respuesta mecánica del conjunto tejido-malla tras cortos tiempos de estudio, siendo la literatura referente al estudio de la respuesta mecánica del conjunto tejido-malla a largo plazo mucho menor. Considerando las limitaciones de los estudios disponibles en la literatura, esta tesis estudiará el proceso de integración tisular desde el punto de vista mecánico e histológico a corto y largo plazo, en un defecto parcial con ausencia del músculo oblicuo externo, utilizando las tres mallas seleccionadas para el desarrollo de esta tesis.

Capítulo III

Resultados, publicaciones y conclusiones de la tesis

La motivación principal que ha llevado al desarrollo de esta tesis es el estudio del comportamiento mecánico de la pared abdominal y los problemas asociados a la cirugía abdominal de reparación de hernias. Comprender la respuesta mecánica de la pared podría ayudar a mejorar las técnicas quirúrgicas de colocación de mallas, por ejemplo, definiendo pautas para la elección de la malla más adecuada para cada paciente y tipo de defecto.

En esta tesis se ha estudiado la cirugía de reparación de hernias mediante la colocación de prótesis a través de un estudio experimental en un modelo animal, concretamente con conejos blancos de Nueva Zelanda, debido a la facilidad para posteriormente ensayar el tejido para diferentes tiempos de implantación. Los resultados obtenidos se han extrapolado a un modelo *"in silico"* de la cavidad abdominal humana.

El estudio ha sido abordado no sólo desde el punto de vista de la mecánica de medios continuos y modelado de tejidos en ingeniería, sino que además ha sido necesaria la contribución de biólogos y especialistas clínicos ya que son quienes definen la patología clínica, aportan experiencia en el tratamiento de la misma en pacientes y colaboran en la caracterización experimental e histológica. Por tanto, la formación de un grupo multidisciplinar de trabajo ha permitido obtener resultados desde el punto de vista ingenieril, clínico y biológico que han permitido aportar avances en el estudio de la patología herniaria en el estado del arte.

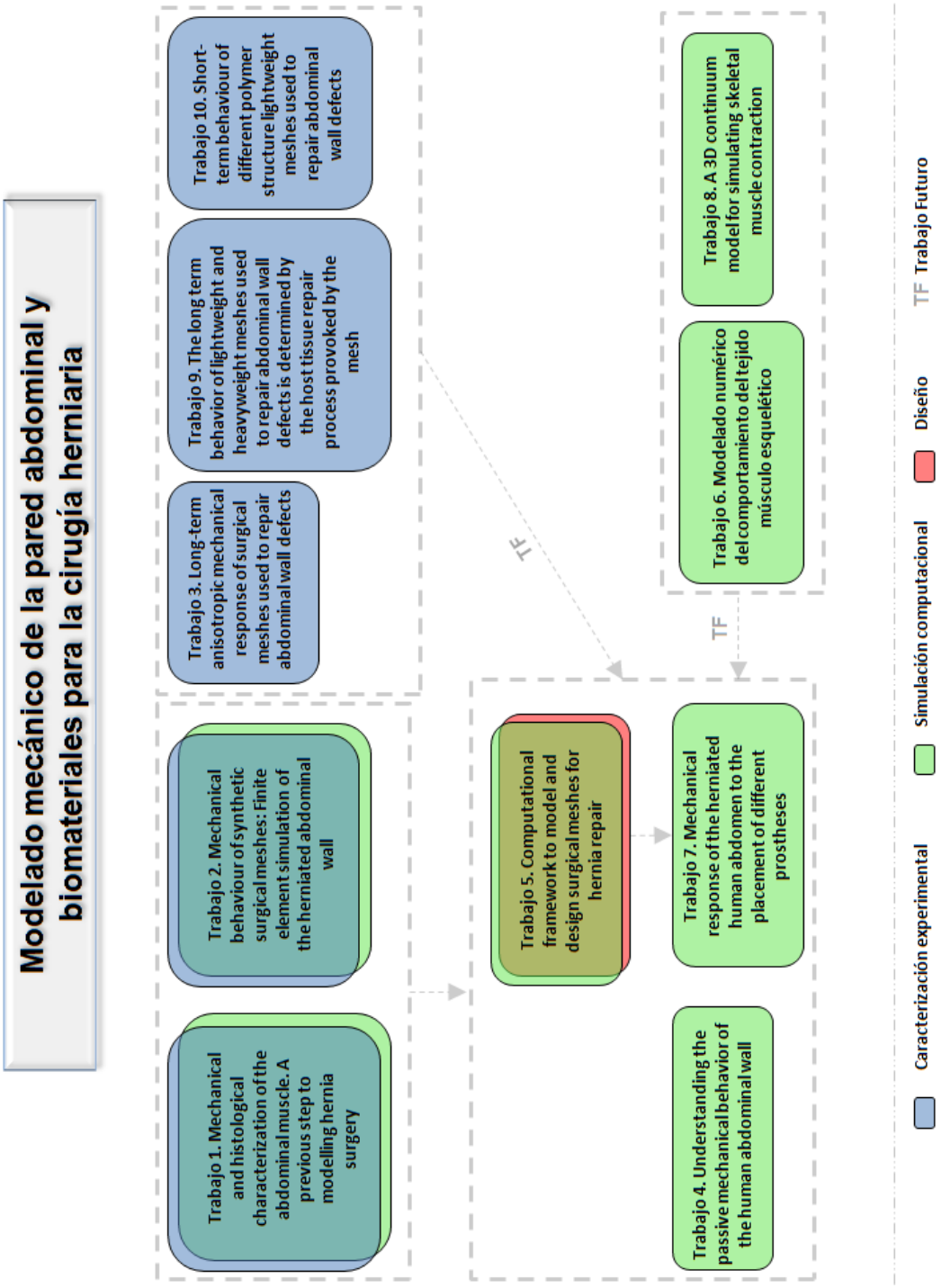

Figura III.1: Compendio de artículos que recogen el trabajo abordado en la realización de la tesis.

Los resultados alcanzados en el marco de la tesis doctoral se han recogido en 10 artículos con unidad temática que abarcan los objetivos planteados inicialmente en la

misma y que, a modo de resumen, se recogen en la Figura III.1 y en las Tablas III.1 y III.2. Todos los trabajos han sido publicados o aceptados para publicación en revistas del *Journal Citation Reports* a excepción de los trabajos 7 y 8 que se encuentran en proceso de revisión. En todos los trabajos incluidos, y en el desarrollo de todas las partes del mismo, la contribución máxima ha sido de la autora de la tesis, a excepción de los estudios histológicos incluidos en los trabajos 1 y 3 y los trabajos 9 y 10 donde únicamente el estudio mecánico ha sido realizado por la autora. Por tanto, se cumplen los requisitos establecidos por la Universidad de Zaragoza, siguiendo el acuerdo de 17 de diciembre de 2008 del Consejo de Gobierno de la Universidad por el que se aprueba el Reglamento sobre Tesis Doctorales y donde se contemplan las tesis elaboradas como compendio de publicaciones.

Table III.1: Artículos que conforman esta tesis. Parte I. (FI: Factor de impacto, EXP: Experimental, COM: Computacional, DIS: Diseño)

Trabajo	**Artículo**	**Autores**	**Revista**	**FI**	**Áreas**
1.	Mechanical and histological characterization of the abdominal muscle. A previous step to modelling hernia surgery	**B. Hernández**, E. Peña, G. Pascual, M. Rodríguez, B. Calvo, M. Doblaré, J. M. Bellón	Journal of the Mechanical Behavior of Biomedical Materials, 4 (3) (2011), pp: 392-404	2.814	EXP, COMP
2.	Mechanical behaviour of synthetic surgical meshes: Finite element simulation of the herniated abdominal wall	**B. Hernández-Gascón**, E. Peña, H. Melero, G. Pascual, M. Doblaré, M. P. Ginebra, J. M. Bellón, B. Calvo	Acta Biomaterialia, 7 (11) (2011), pp: 3905-3913	4.865	EXP, COMP
3.	Long-term anisotropic mechanical response of surgical meshes used to repair abdominal wall defects	**B. Hernández-Gascón**, E. Peña, G. Pascual, M. Rodríguez, J. M. Bellón, B. Calvo	Journal of the Mechanical Behavior of Biomedical Materials, 5 (1) (2012), pp: 257-271	2.814	EXP
4.	Understanding the passive mechanical behavior of the human abdominal wall	**B. Hernández-Gascón**, A. Mena, E. Peña, G. Pascual, J. M. Bellón, B. Calvo	Annals of Biomedical Engineering, In press (2012), DOI: 10.1007/s10439-012-0672-7	2.368	COM
5.	Computational framework to model and design surgical meshes for hernia repair	**B. Hernández-Gascón**, N. Espés, E. Peña, G. Pascual, J. M. Bellón, B. Calvo	Computer Methods in Biomechanics and Biomedical Engineering, In Press (2012), DOI:10.1080/10255842.2012.736967	1.169	DIS, COM
6.	Modelado numérico del comportamiento del tejido músculo esquelético	J. Grasa, **B. Hernández-Gascón**, A. Ramírez, J. F. Rodríguez, B. Calvo	Revista Internacional de Métodos Numéricos para Cálculo y Diseño en Ingeniería, 28 (3) (2012), pp: 177-186	0.167	COM

Table III.2: Artículos que conforman esta tesis. Parte II. (FI: Factor de impacto, EXP: Experimental, COM: Computacional, DIS: Diseño)

Trabajo	Artículo	Autores	Revista	FI	Áreas
7.	Mechanical response of the herniated human abdomen to the placement of different prostheses	**B. Hernández-Gascón**, E. Peña, J. Grasa, G. Pascual, J. M. Bellón, B. Calvo	Submitted	-	COM
8.	A 3D continuum model for simulating skeletal muscle contraction	**B. Hernández-Gascón**, J. Grasa, B. Calvo, J. F. Rodríguez	Submitted	-	COM
9.	The long term behavior of lightweight and heavyweight meshes used to repair abdominal wall defects is determined by the host tissue repair process provoked by the mesh	G. Pascual, **B. Hernández-Gascón**, M. Rodríguez, S. Sotomayor, E. Peña, B. Calvo, J. M. Bellón	Surgery, 152 (5) (2012), pp: 886-895	3.103	EXP
10.	Short-term behaviour of different polymer structure lightweight meshes used to repair abdominal wall defects	G. Pascual, **B. Hernández-Gascón**, S. Sotomayor, E. Peña, B. Calvo, J. Buján, J. M. Bellón	Histology and Histopathology, Accepted (2012)	2.480	EXP

A continuación se detallan los resultados principales obtenidos en la tesis, los cuales se agrupan según la metodología seguida para el desarrollo de la misma. Es decir, desde el punto de vista experimental (del tejido abdominal, de prótesis y del conjunto tejido-prótesis), numérico y de diseño (ver Figura III.1), justificándose así la unidad temática de los diferentes trabajos incluidos en el compendio de publicaciones de esta tesis, tal como se establece en los requisitos establecidos por la Universidad de Zaragoza:

(a) Caracterización mecánica experimental del comportamiento pasivo del músculo abdominal del modelo animal.

Se ha caracterizado experimentalmente, mediante ensayos uniaxiales, el comportamiento mecánico elástico pasivo de la pared abdominal, incluyendo las deformaciones iniciales, en un modelo de experimentación animal, el conejo blanco de Nueva Zelanda (Hernández et al., 2011) (*Artículo 1*). Concretamente, se ha estudiado la respuesta pasiva de los músculos abdominales de forma individual y conjuntamente. Además, se ha realizado un estudio histológico para analizar la disposición de las fibras de colágeno y musculares en el tejido abdominal. Los resultados del estudio han revelado que la retracción máxima que se produce al cortar el tejido abdominal alcanza un $26.4 \pm 6.76\%$ en la dirección craneo-caudal del animal y no se encuentran diferencias significativas entre la retracción en dicha dirección y la transversal. El estudio ha evidenciado una mayor rigidez de los tejidos en la dirección perpendicular a las fibras musculares que en la dirección de las mismas. Además, se ha observado que la anisotropía de cada uno de los músculos abdominales, estudiados de forma separada, es mayor que la que presenta la caracterización conjunta de todas capas musculares. En concreto, la dirección transversal del abdomen, a la altura de los músculos abdominales, presenta una rigidez mayor que en la dirección craneo-caudal (ver Figura III.2).

(b) Caracterización mecánica experimental del comportamiento de prótesis reticulares.

Se ha caracterizado la respuesta mecánica de tres mallas sintéticas reticulares frecuentemente utilizadas en la cirugía herniaria (*Surgipro*®, *Infinit*® y *Optilene*®, clasificadas como mallas de alto, medio y bajo peso, respectivamente), a través de ensayos uniaxiales de tracción, obteniéndose la curva tensión-alargamiento en dos direcciones ortogonales (Hernández-Gascón et al., 2011) (*Artículo 2*). Los resultados han sido comparados con la respuesta del tejido abdominal para identificar la prótesis que mejor reproduce el comportamiento del tejido abdominal sano. La caracterización mecánica de dichas prótesis revela una respuesta isótropa en la malla *Surgipro*®, mientras que la respuesta es anisótropa en las mallas *Optilene*® e *Infinit*® (ver Figura III.3).

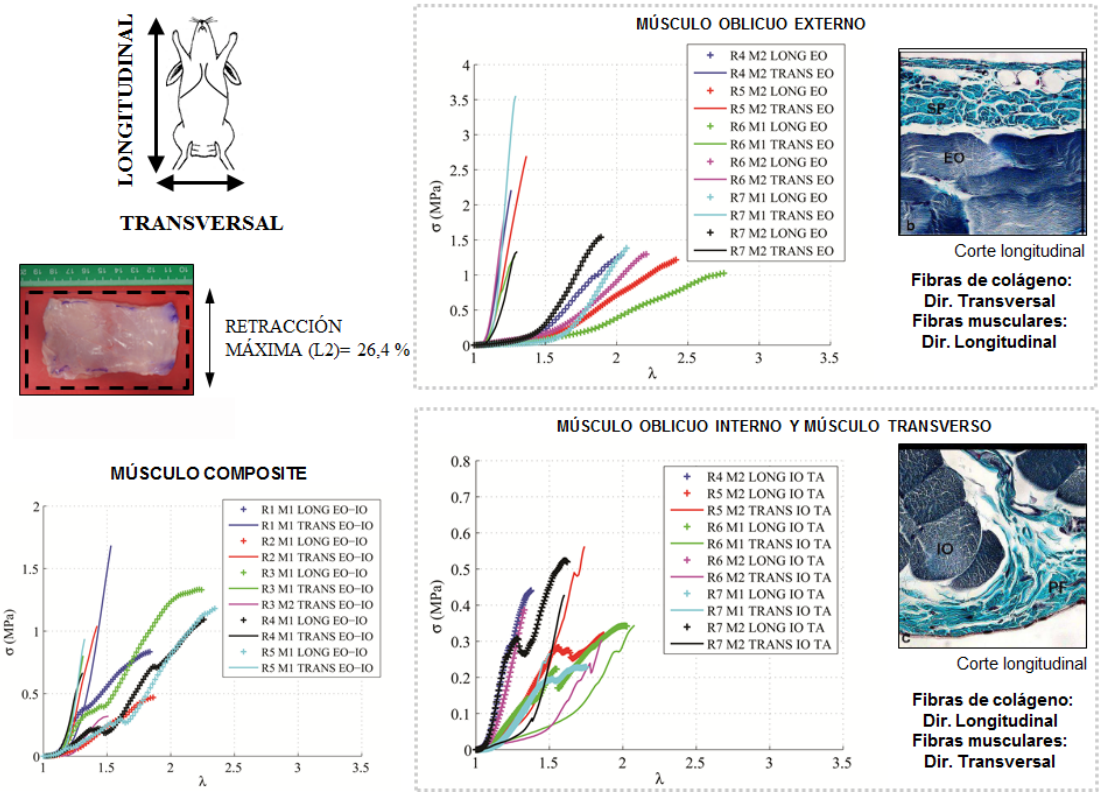

Figura III.2: Definición de las dos direcciones de ensayo uniaxial en el conejo, longitudinal y transversal. Imágen de la retracción de la muestra de tejido tras extraerla. Datos experimentales obtenidos en los ensayos uniaxiales para las muestras de composite EO-IO (Oblicuo externo e interno) y las capas de músculo individuales EO (oblicuo externo) e IO-TA (oblicuo interno y transverso) y correlación con los resultados del estudio histológico con microscopía óptica.

(c) Caracterización mecánica experimental del comportamiento pasivo del conjunto tejido-prótesis.

Se ha estudiado experimentalmente, mediante ensayos uniaxiales, el comportamiento mecánico elástico pasivo de la pared abdominal reparada con las tres prótesis seleccionadas para el estudio, tras diferentes tiempos post-implante (a 14, 90 y 180 días) (Hernández-Gascón et al., 2012e) (*Artículo 3*). Se ha observado que conforme el tiempo tras el implante aumenta, la integración tisular es mayor y, por tanto, la rigidez del conjunto tejido-malla se incrementa (ver Figura III.4). El comportamiento mecánico elástico pasivo de la pared abdominal se vuelve más rígido con la edad y sigue siendo anisótropo (ver Figura III.5.a). Además, se ha comparado el comportamiento del conjunto tejido-prótesis con el del tejido sano y el resultado indica que ninguna de las

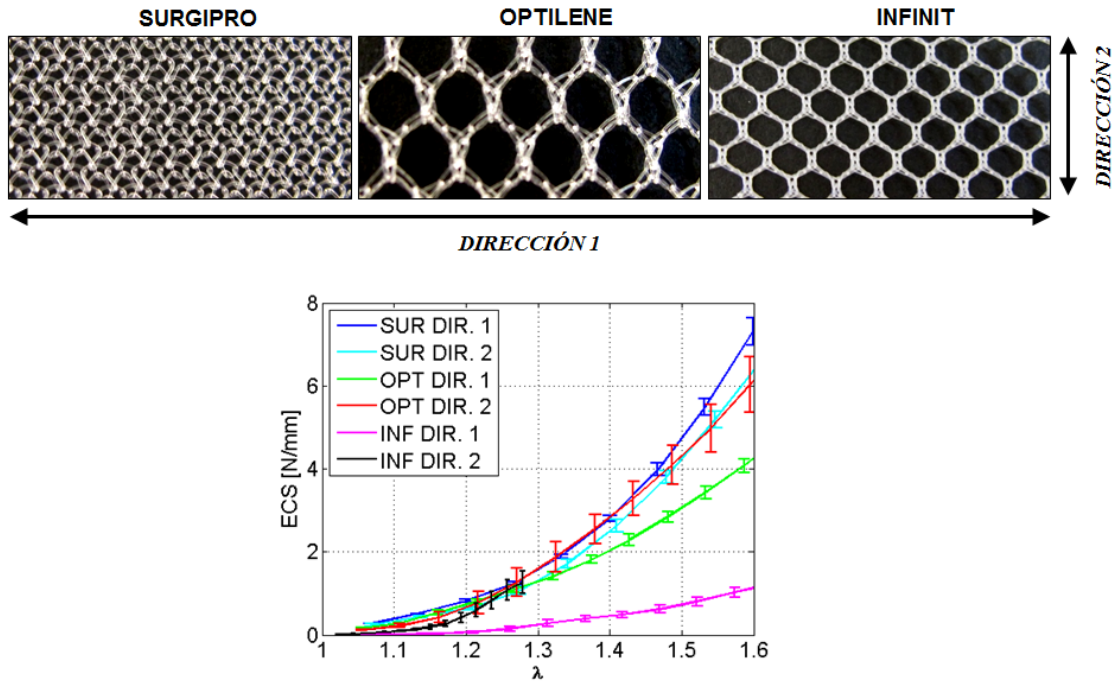

Figura III.3: Imágen de las tres mallas seleccionadas para el estudio con indicación de las dos direcciones de estudio. Datos experimentales (ECS=Tension/longitud vs. alargamiento) obtenidos en las dos direcciones de ensayo uniaxial.

mallas estudiadas es capaz de reproducir exactamente el comportamiento mecánico elástico del tejido abdominal en la dirección craneo-caudal del abdomen ni a 14 ni a 90 días tras el implante. Sin embargo, a largo plazo, la mejor adaptabilidad de la malla al tejido viene dada por las mallas de bajo peso ya que mantienen la anisotropía inicial (ver Figura III.5.a). Asimismo, se ha medido la retracción que sufre cada malla debido al proceso de integración tisular en función de las propiedades de la prótesis. Se ha apreciado que la retracción es significativamente diferente entre las dos direcciones perpendiculares estudiadas para la malla $Infinit^{®}$ mientras que no lo es en la malla $Surgipro^{®}$ para ningún tiempo de estudio. La retracción de la malla $Optilene^{®}$ es significativamente diferente entre las dos direcciones perpendiculares estudiadas solamente a 14 días. Por otra parte, se ha cuantificado histológicamente la cantidad de colágeno y macrófagos que se generan a consecuencia del proceso de integración tisular, dependiendo del tipo de prótesis implantada y del tiempo tras la implantación de la malla (Hernández-Gascón et al., 2012e; Pascual et al., 2012a,b) (*Artículos 3, 9 y 10*). El énfasis del estudio se ha enfocado en la comparación de una malla pesada ($Surgipro^{®}$) con una malla de medio peso ($Infinit^{®}$) y con otra de bajo peso ($Optilene^{®}$). Se ha observado que el crecimiento más notable de colágeno se produce a corto plazo y que a largo plazo el crecimiento de colágeno tiende a unificar la respuesta mecánica de las

tres mallas (ver Figura III.5.b). También se analiza el crecimiento de colágeno en función del tamaño de poro de la malla. Concretamente, a mayor tamaño de poro, mayor deposición de colágeno (ver Figura III.5.b). Finalmente, se observa que la respuesta macrofágica depende del material del que se ha fabricado la prótesis. Concretamente, la respuesta macrofágica es mayor en el caso de la malla fabricada de politetrafluoroetileno (*Infinit*®) que para las mallas de polipropileno (*Surgipro*® y *Optilene*®) (ver Figura III.6).

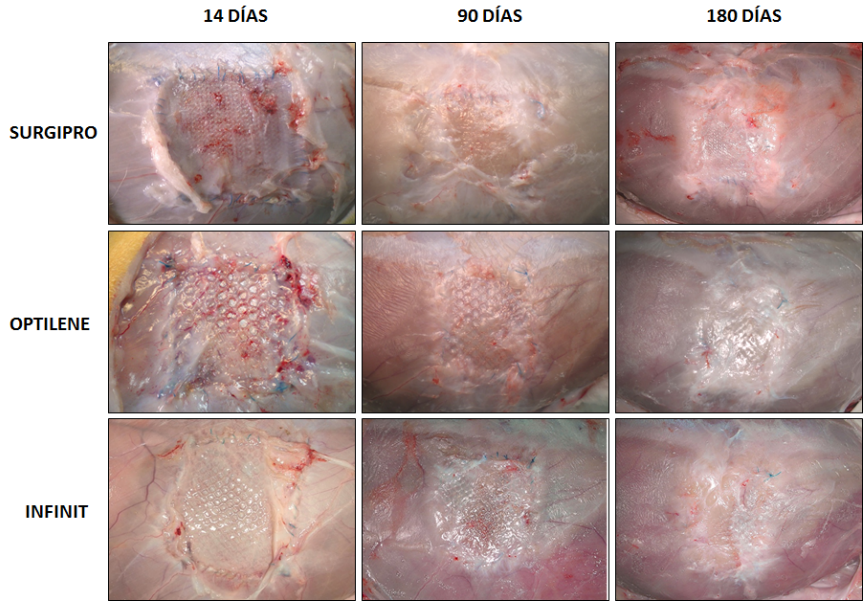

(a)

	SURGIPRO		OPTILENE		INFINIT	
	LONG	TRANS	LONG	TRANS	LONG	TRANS
14 días	7,5 ± 4,203	10,5 ± 7,549	16 ± 6	2,5 ± 2,887*	12,75 ± 3,775	0 ± 0*
90 días	5,5 ± 4,796	12,25 ± 1,5	5,25 ± 6,397	5,25 ± 6,397	12,25 ± 1,5	0 ± 0*
180 días	7 ± 4,761	6,5 ± 5,447	3,25 ± 6,5	0 ± 0	19,5 ± 6,403	0 ± 0*

(b)

Figura III.4: (a) Imágen macroscópica de las muestras obtenidas de la zona del defecto del conejo a diferentes tiempos post-implante (14, 90 y 180 días) y para las tres mallas estudiadas donde se aprecia la integración tisular. (b) Retracción (%) de las muestras de tejido extraídas del animal, en las direcciones longitudinal y transversal, para los diferentes tiempos de estudio (*$p<0.05$).

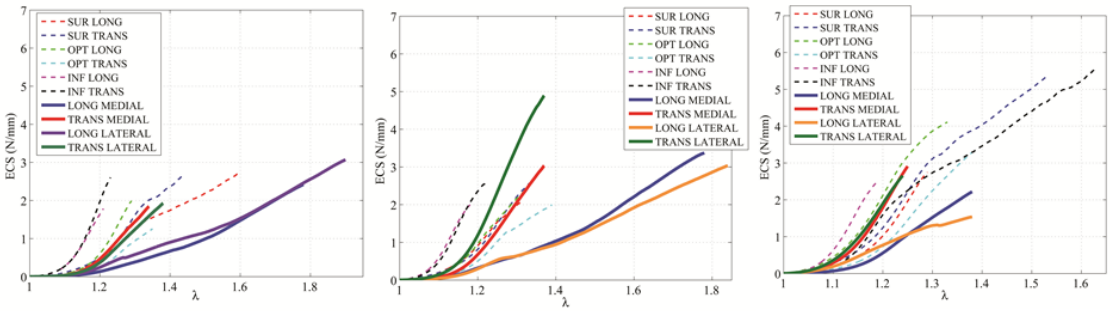

(a)

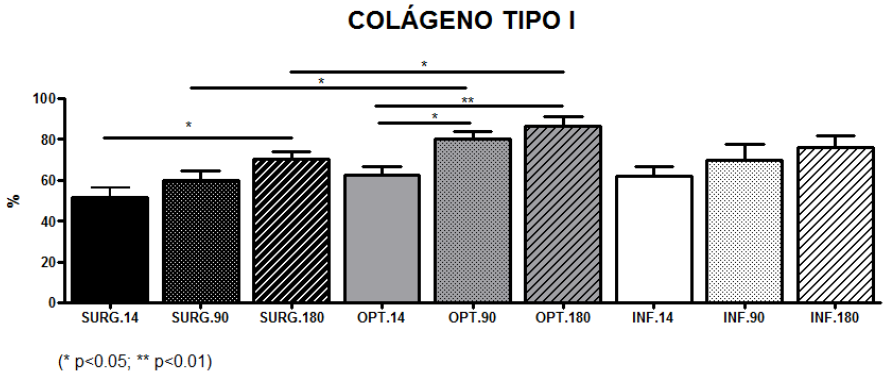

(b)

Figura III.5: (a) Comparación de los resultados experimentales de los ensayos uniaxiales entre el tejido abdominal del conejo control y el tejido abdominal reparado con las tres mallas de estudio a 14, 90 y 180 días. (b) Cuantificación de colágeno I (maduro) a 14, 90 y 180 días mediante tinción con Rojo Sirio para las tres mallas de estudio. Valores indicados con la media ± desviación típica.

(d) Modelado numérico de la respuesta mecánica del músculo abdominal y de prótesis.

Se ha planteado un modelo computacional tridimensional termodinámicamente consistente para la simulación del tejido muscular, reproduciendo tanto la respuesta mecánica activa como pasiva dentro del marco de la hiperelasticidad no lineal en grandes deformaciones (Hernández et al., 2011; Grasa et al., 2013; Hernández-Gascón et al., 2012b) (*Artículos 1, 6 y 8*). El modelo formulado permite incorporar las tensiones iniciales presentes en la cavidad abdominal. La respuesta mecánica activa del modelo se ha validado mediante resultados experimentales en el músculo tibial anterior de rata (Ramírez et al., 2010). Las funciones densidad energía de deformación correspondientes a la parte pasiva se han ajustado con los resultados experimentales obtenidos con el modelo de experimentación animal (Hernández et al., 2011) (*Artículo 1*) y también se

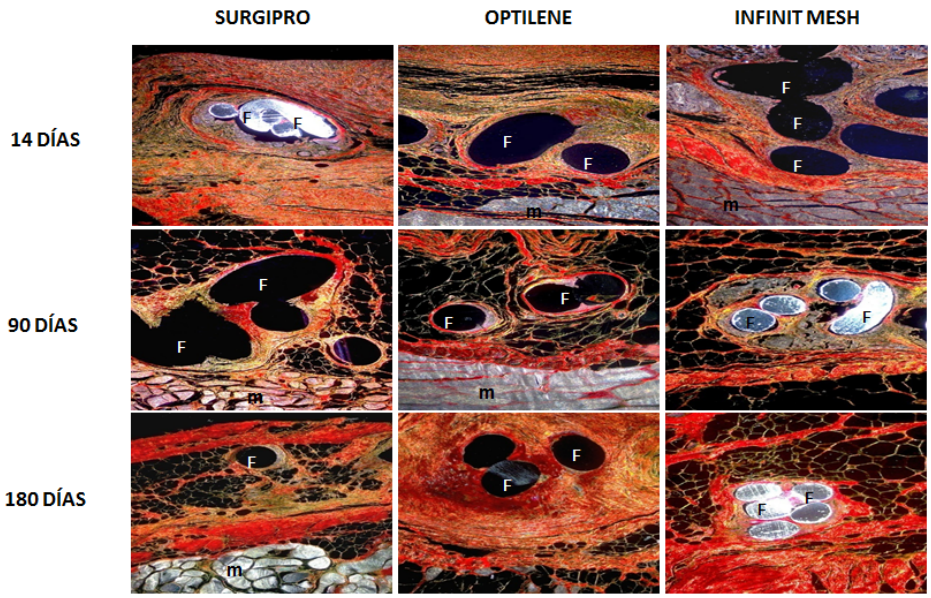

Figura III.6: Tinción con Rojo Sirio de muestras extraídas del conejo a diferentes tiempos post-implante y para las tres mallas estudiadas. El colágeno III (inmaduro) y I (maduro) se visualizan en color amarillo y rojo, respectivamente.

han tomado datos de la literatura (Calvo et al., 2010; Martins et al., 2012). Si bien desde el punto de vista anatómico la pared abdominal está formada por diferentes capas musculares (músculo oblicuo externo, músculo oblicuo interno y músculo transverso), se ha comprobado que la simulación de la respuesta conjunta de los músculos oblicuos considerados como un composite iguala a la respuesta mecánica de la pared abdominal definida como la unión de diferentes capas musculares (Hernández et al., 2011) (*Artículo 1*). Por tanto, la consideración de que los músculos oblicuos se comportan como un composite ha sido considerada a la hora de abordar el estudio de la respuesta del abdomen.

En lo que concierne al modelado del comportamiento mecánico de las prótesis, se han definido las funciones densidad energía de deformación que reproducen la respuesta mecánica de las mismas, a partir de los resultados experimentales obtenidos, y dentro de la teoría de la hiperelasticidad no lineal en grandes deformaciones (Hernández-Gascón et al., 2011) (*Artículo 2*).

Para extrapolar el estudio al cuerpo humano, se ha construido un modelo *"in silico"* del abdomen humano a partir de imágenes de resonancia magnética nuclear para estudiar la respuesta mecánica del abdomen ante cargas fisiológicas pasivas (Hernández-Gascón et al., 2012c) y activas (Hernández-Gascón et al., 2012b) (*Artículo 8*). En el modelo se han diferenciado las estructuras anatómicas principales del abdomen y se

han asignado las propiedades mecánicas anisótropas correspondientes a cada uno de los tejidos mediante la definición de las direcciones preferenciales de anisotropía (ver Figura III.7). Se ha obtenido que los desplazamientos máximos del abdomen se producen en la parte frontal (ver Figura III.8). En cuanto a las tensiones, los valores máximos se producen en las estructuras aponeuróticas. Concretamente, la línea alba es la estructura que más tensiones absorbe y, por tanto, la más solicitada en el abdomen.

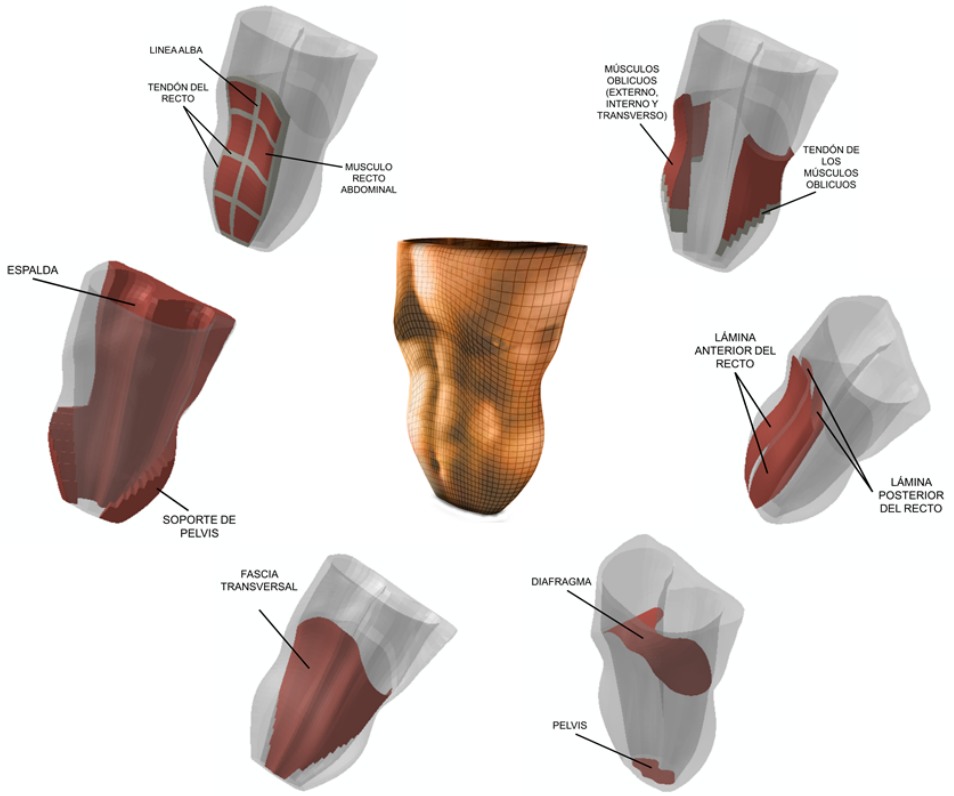

Figura III.7: Modelo de elementos finitos del abdomen humano completo e identificación de las estructuras anatómicas principales del abdomen.

Para simular el proceso quirúrgico de la reparación de hernias se ha construido un modelo de elementos finitos de un abdomen humano con una hernia total a lo largo de la línea alba a partir del modelo previo. Para ello, se ha simulado la colocación de la prótesis sobre la zona del defecto y se ha analizado la respuesta mecánica del abdomen herniado y reparado ante cargas fisiológicas dependiendo de la prótesis implantada y de la orientación de la misma en el abdomen (Hernández-Gascón et al., 2012d) (*Artículo 7*) (ver Figuras III.9 y III.10). Este estudio ha evidenciado que la malla *Surgipro*® es la que tiene peor adaptabilidad mientras que la malla *Infinit*® es la prótesis más flexible. Se ha detectado que la orientación de la prótesis influye en la respuesta mecánica y que los resultados están más cerca de mimetizar la respuesta original del abdomen sano cuando cuando la prótesis se orienta de tal forma que la dirección más rígida coincide

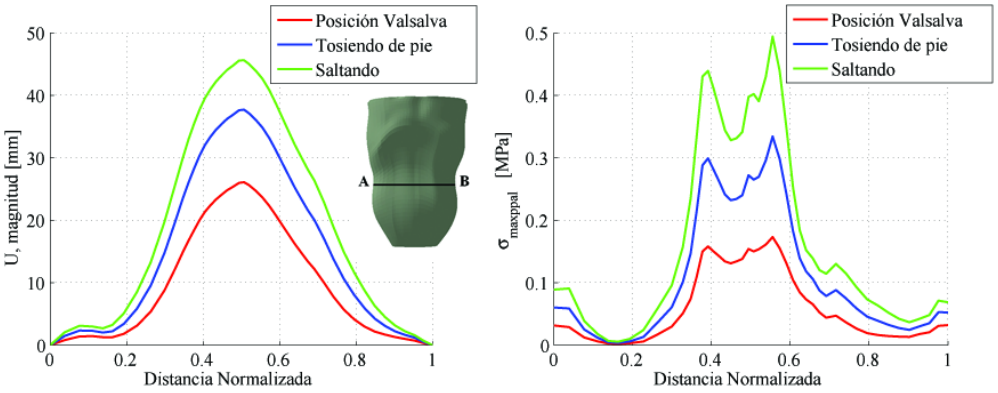

(a) (b)

Figura III.8: Desplazamientos máximos (mm) (a) y tensiones principales máximas (MPa) (b) a lo largo de la línea AB definida en (a). La distancia normalizada indica que $x = 0$ y $x = 1$ corresponden a los puntos A y B, respectivamente.

con la dirección transversal al abdomen (ver Figura III.10).

Figura III.9: Modelo de elementos finitos del abdomen humano herniado y reparado.

(e) Establecimiento de una metodología para el diseño de prótesis.

Se ha establecido un marco computacional que incluye dos modelos computacionales para el diseño y validación del comportamiento mecánico elástico de mallas quirúrgicas (Hernández-Gascón et al., 2012a) (*Artículo 5*) (ver Figura III.11). Primero se aborda el modelado considerando el tejido y disposición de los hilos de la malla utilizando elementos barra, mientras que el segundo modelo considera las mallas como un continuo dentro de la teoría de la hiperelasticidad no lineal en grandes deformaciones utilizando elementos membrana. Esta metodología se ha validado con la simulación de las tres mallas comerciales estudiadas previamente y su potencialidad viene dada por la reducción de costes de experimentación.

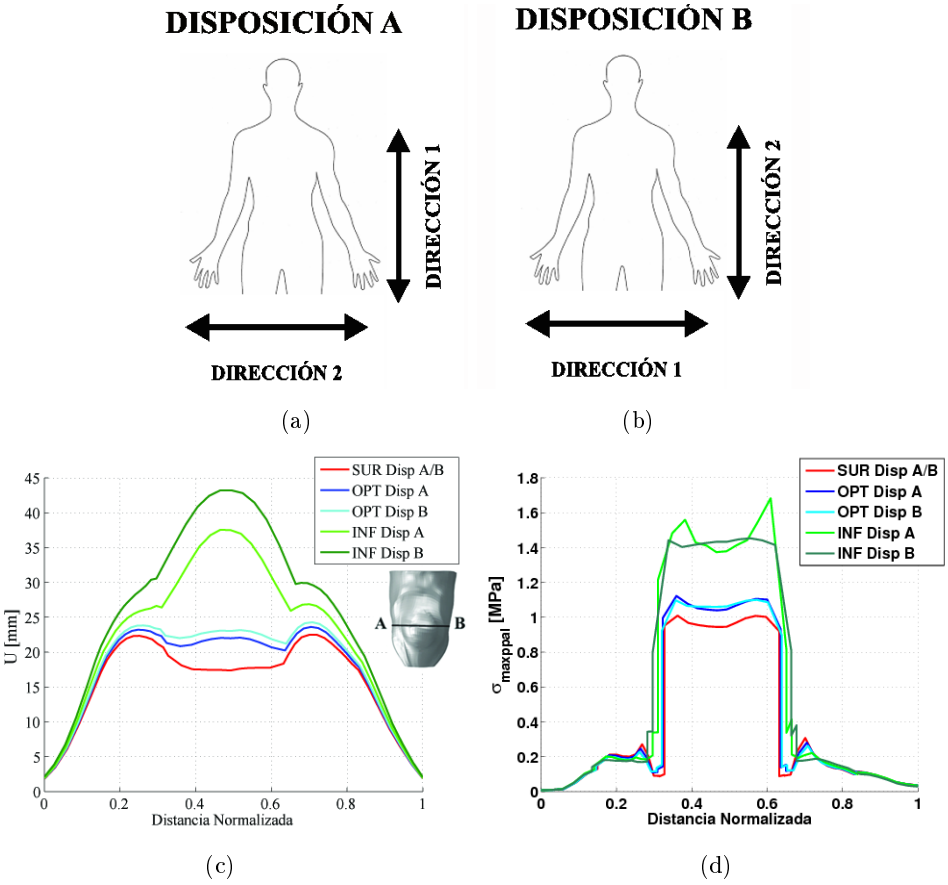

Figura III.10: Definición de las disposiciones A (a) y B (b) de la prótesis en el abdomen. Desplazamientos máximos (mm) (c) y tensiones principales máximas (MPa) (d) a lo largo de la línea AB definida en (c). La distancia normalizada indica que $x = 0$ y $x = 1$ corresponden a los puntos A y B, respectivamente.

III.1 Contribuciones originales

El desarrollo de esta tesis ha establecido una metodología de trabajo que abre las puertas a la automatización de la simulación de intervenciones quirúrgicas personalizadas, con el fin de seleccionar el tipo de malla más adecuada para cada paciente así como la orientación idónea en el defecto. Para ello, ha sido necesario trabajar dentro de un equipo multidisciplinar de trabajo, formado por especialistas en el campo de la mecánica de medios continuos dentro de la ingeniería, de la biología y de la medicina. El trabajo desarrollado de forma conjunta por un grupo amplio de investigadores de diferentes disciplinas, ha permitido abordar la patología de aparición de hernias de forma completa ya que se ha estudiado a varios niveles: a nivel experimental, incluyendo la caracterización mecánica e histológica de los tejidos abdominales en un modelo de experimentación animal, la caracterización mecánica de tres prótesis comerciales y la caracterización

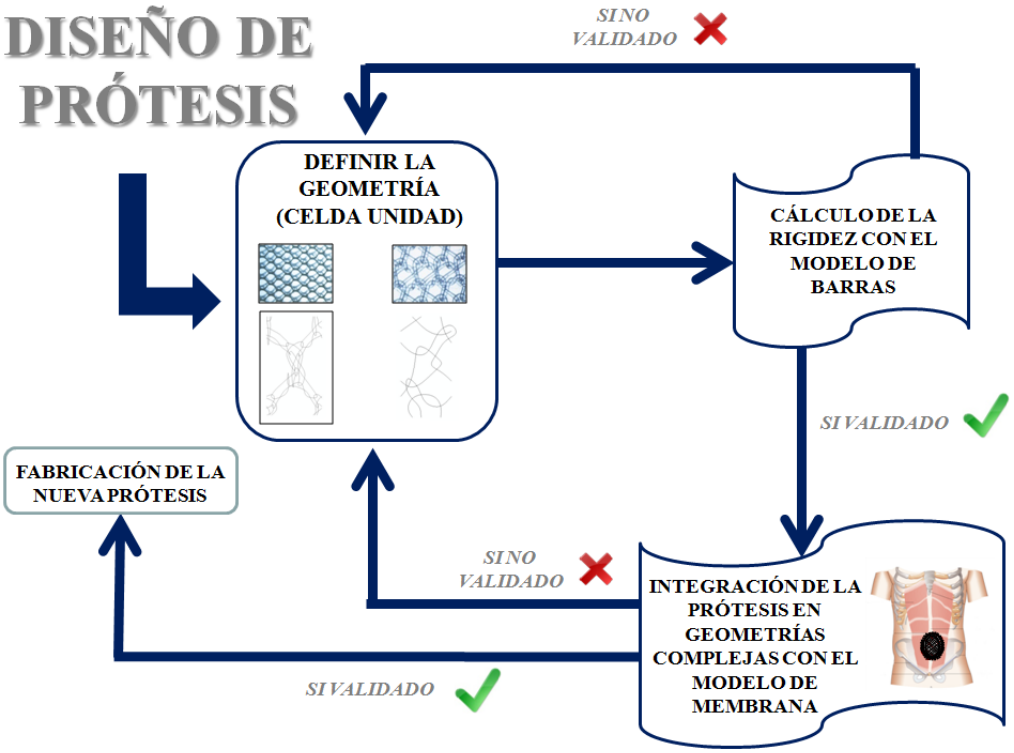

Figura III.11: Metodología del proceso definido para el diseño de prótesis. El marco computacional define dos modelos que utilizan elementos barra y membrana, respectivamente.

mecánica del conjunto tejido-prótesis a diferentes tiempos post-implante; y a nivel computacional, definiendo un modelo *"in silico"* del abdomen humano que ha permitido el análisis de la respuesta mecánica ante cargas fisiológicas, incluso después de la cirugía, y planteando una metodología de diseño y validación de prótesis. Particularmente, las principales contribuciones originales de esta tesis se enumeran a continuación:

- Se ha modelado la respuesta mecánica pasiva el tejido abdominal dentro del marco de la hiperelasticidad no lineal en grandes deformaciones a partir de los resultados experimentales obtenidos en ensayos uniaxiales en un modelo de experimentación animal, como es el conejo blanco de Nueva Zelanda.

- Se ha propuesto un modelo constitutivo para reproducir la respuesta mecánica de las prótesis $Surgipro^{®}$, $Optilene^{®}$ e $Infinit^{®}$ dentro del marco de la hiperelasticidad no lineal en grandes deformaciones y ha sido validado con la caracterización experimental de la respuesta mecánica a través de ensayos uniaxiales.

- Se ha cuantificado histológicamente la cantidad de colágeno y macrófagos que se generan tras el proceso de integración tisular con las mallas $Surgipro^{®}$, $Optilene^{®}$

e $Infinit^{®}$ a 14, 90 y 180 días después del implante. El énfasis del estudio se ha enfocado en la comparación de una malla pesada ($Surgipro^{®}$) con una malla de medio peso ($Infinit^{®}$) y otra de bajo peso ($Optilene^{®}$). Además, se ha caracterizado la respuesta mecánica del tejido reparado a los diferentes tiempos de estudio y se ha comparado dicha respuesta con el comportamiento del tejido abdominal sano, caracterizado a su vez a los diferentes tiempos de estudio.

- Se ha planteado y validado un modelo computacional tridimensional termodinámicamente consistente para la simulación de la respuesta mecánica activa y pasiva que ofrece el músculo esquelético. Dicho modelo se enmarca dentro de la teoría de la hiperelasticidad no lineal en grandes deformaciones.

- Se ha planteado una metodología para simular mediante elementos finitos el comportamiento mecánico (pasivo y activo) del abdomen humano durante movimientos fisiológicos. El modelo computacional utilizado se ha desarrollado a partir de imágenes de resonancia magnética nuclear e incorpora la distribución de tensiones iniciales propia del cuerpo humano. Asimismo, se diferencian las estructuras anatómicas principales del abdomen tanto geométricamente como respecto a las propiedades mecánicas de los tejidos y se consideran las tensiones iniciales presentes en los tejidos blandos.

- Se ha establecido una metodología para la simulación de la respuesta mecánica pasiva de un abdomen humano herniado y reparado mediante cirugía herniaria. Dicho modelo incluye el modelado de la prótesis y se analiza el comportamiento de la prótesis considerada y la influencia de su orientación en la respuesta mecánica del conjunto ante cargas fisiológicas comunes en el post-operatorio.

- Se ha establecido una metodología para el diseño y validación del comportamiento mecánico elástico de mallas quirúrgicas con la ventaja de reducir los costes de experimentación generados con los métodos tradicionales experimentales.

III.2 Conclusiones generales

A continuación se presentan las principales conclusiones que se extraen de esta tesis en función de los estudios experimentales y numéricos abordados:

- El comportamiento anisótropo de los músculos laterales abdominales considerados como un composite es menos pronunciado que la anisotropía de los músculos individuales. Concretamente, la dirección perpendicular a la dirección craneo-caudal (dirección transversal) del abdomen es más rígida que la dirección craneo-

caudal. El comportamiento mecánico elástico pasivo de la pared abdominal se vuelve más rígido con la edad y presenta el mismo patrón de anisotropía.

- Al extraer el tejido abdominal del animal, la retracción máxima que se produce alcanza un $26.4 \pm 6.76\%$ en la dirección longitudinal y no se detectan diferencias significativas entre la retracción en la dirección longitudinal y la transversal.

- El modelo constitutivo planteado para reproducir la respuesta mecánica elástica del músculo abdominal es termodinámicamente consistente y capaz de predecir la distribución de tensiones utilizando métodos computacionales.

- La respuesta mecánica, caracterizada mediante ensayos uniaxiales, de la malla *Surgipro*® es isótropa, la de la malla *Optilene*® es ligeramente anisótropa y la malla *Infinit*® presenta una respuesta altamente anisótropa.

- El proceso de integración tisular de las prótesis en el abdomen parcialmente herniado evidencia una retracción de las prótesis que difiere en función del tipo y orientación de la prótesis. Concretamente, la retracción es significativamente diferente entre las dos direcciones perpendiculares estudiadas para la malla *Infinit*® para todos los tiempos de estudio, mientras que no lo es en la malla *Surgipro*® para ningún tiempo de estudio. La malla *Optilene*® solamente presenta diferencias significativas en la retracción en las dos direcciones estudiadas a 14 días. Los tres implantes utilizados muestran una buena integración tisular debido a la formación de tejido conectivo alrededor de los poros.

- La formación de colágeno sobre la zona del defecto reparado provoca un incremento de rigidez notable que modifica las propiedades de la malla. Por tanto, la caracterización experimental mediante ensayos uniaxiales de una prótesis, previa al implante, proporciona información solamente orientativa. La formación de colágeno más notable se produce a corto plazo. Además, se observa relación entre la formación de colágeno y el tamaño de poro de la malla. Concretamente, a mayor tamaño de poro, mayor deposición de colágeno. A corto plazo, el material del que están fabricados los hilos (PP vs. PTFE) no influye en el crecimiento de colágeno. A largo tiempo, la formación de colágeno tiende a unificar la respuesta mecánica de las tres mallas.

- La respuesta macrofágica depende del material del que se ha fabricado la prótesis. Concretamente, la respuesta macrofágica es mayor en el caso de la malla fabricada de politetrafluoroetileno (*Infinit*®) que para las mallas de polipropileno (*Surgipro*® y *Optilene*®).

- Los ensayos uniaxiales evidencian que ninguna de las mallas estudiadas es capaz de reproducir exactamente el comportamiento mecánico elástico pasivo del tejido abdominal en la dirección craneo-caudal del abdomen ni a 14 ni a 90 días tras el

implante. A largo tiempo, la mejor adaptabilidad de la malla al tejido viene dada por las mallas de bajo peso ya que mantienen la anisotropía inicial.

- Los dos modelos computacionales planteados para el diseño y validación del comportamiento mecánico elástico de prótesis son capaces de reproducir el patrón de comportamiento experimental minimizando los largos tiempos y costes económicos requeridos en los métodos experimentales. El modelo continuo presenta la ventaja de que es más eficiente computacionalmente y permite incluir los modelos en otros modelos numéricos más complejos.

- Se ha definido una metodología para modelar el abdomen humano y para estudiar su respuesta mecánica ante cargas fisiológicas. Desde el punto de vista mecánico, este modelo permite predecir qué zonas son las más tensionadas y relacionarlo con el posible riesgo de formación de hernias en la pared abdominal. Las estructuras que más trabajan en el abdomen son las estructuras aponeuróticas, específicamente la línea alba. Por tanto, la línea alba es una de las unidades anatómicas más importantes desde el punto de vista de la estabilidad mecánica.

- La metodología presentada para el modelado computacional del abdomen humano es el punto de partida para futuros estudios en los que se simule automáticamente el comportamiento del abdomen humano. De esta forma, se podrán realizar estudios y procedimientos quirúrgicos personalizados.

- A partir del modelo computacional del abdomen herniado y reparado se concluye que las mallas *Surgipro*® y *Optilene*® podrían limitar la distensibilidad natural del abdomen mientras que no se recomienda utilizar la malla *Infinit*® en pacientes obesos o en pacientes con grandes defectos. La repuesta mecánica de las prótesis anisótropas en la zona del defecto influye notablemente en la adecuación tejido-malla. Se concluye que la dirección más rígida de las prótesis ha de estar alíneada con la dirección transversal del abdomen. Además, tanto la dirección más rígida como la más flexible deberían estar indicadas en la propia malla para que el cirujano no tenga dificultades a la hora de colocar la prótesis.

- Nuevos diseños de prótesis pueden ser validados con la metodología definida para la simulación computacional del abdomen humano herniado.

III.3 Líneas futuras

Considerando los estudios que se han llevado a cabo en la presente tesis, sus conclusiones y sus limitaciones, se proponen diferentes líneas de actuación para trabajos futuros:

- Se propone una línea de trabajo experimental para caracterizar la respuesta mecánica de los tejidos abdominales con ensayos biaxiales o de inflado. Estos nuevos protocolos, más similares al estado de carga real, aportarán información adicional sobre la caracterización de los tejidos. Asimismo, se propone determinar las propiedades plásticas y viscoelásticas del músculo y la pérdida de rigidez debido al daño como un proceso mecánico y previo a la aparición de la hernia.

- Dado que el comportamiento activo se ha caracterizado, en trabajos previos a esta tesis, con ensayos experimentales del músculo tibial anterior de rata (Ramírez et al., 2010), se propone realizar ensayos para caracterizar la respuesta activa de los diferentes músculos abdominales.

- También se propone la caracterización del comportamiento mecánico de mallas quirúrgicas mediante la realización de ensayos biaxiales. Esta caracterización permite reproducir estados de carga más similares al estado de carga real bajo el que trabajan las prótesis. Por otra parte, se propone llevar a cabo la determinación de las propiedades mecánicas de otras mallas comerciales diferentes, con el objetivo ampliar el campo de conocimiento sobre mallas sintéticas.

- La regeneración tisular ha sido abordada experimentalmente. Estos resultados nos permitirán una nueva línea de trabajo para plantear un modelo matemático de crecimiento tisular que, posteriormente, permita la simulación numérica del proceso de integración tisular, analizando la respuesta en función de las características de la malla.

- Se propone una línea experimental para la caracterización de la respuesta de la pared abdominal animal y humana, sana y herniada tras la cirugía, en ensayos *"in vivo"* mediante ensayos de inflado. Estos ensayos son equiparables a la acción fisiológica que impone la presión intraabdominal. La caracterización experimental del comportamiento mecánico, junto con la obtención de imágenes de resonancia magnética de dichos pacientes, permitirá la validación de la metodología propuesta en la presente tesis en los trabajos 2, 4, 5 y 7. El objetivo final es la automatización del proceso de simulación para cada paciente específico.

- Se propone la simulación numérica del abdomen humano combinando las respuestas activa y pasiva para entender cómo la malla puede dificultar la realización de movimientos (respiración, flexión, etc.), así como incorporar un comportamiento viscoelástico para analizar la respuesta en función de la velocidad de la carga y validarlo posteriormente con imágenes.

- Una problemática clínica que se produce en ciertos casos a consecuencia de la reparación herniaria es el síndrome compartimental (Sabbagh et al., 2011). El síndrome compartimental es una afección seria que implica aumento de la presión en un compartimento muscular. Puede provocar daño en nervios y músculos,

al igual que problemas con el flujo sanguíneo. Esta problemática surge a consecuencia de la reparación de hernias incisionales de gran tamaño, debido a que los órganos internos empujan a la cavidad torácica a través del diafragma. Una línea de aplicabilidad futura es la simulación de este proceso clínico para identificar las causas que lo generan y poder establecer métodos alternativos del cierre de la hernia que eviten la aparición del síndrome compartimental.

- Uno de los problemas más frecuentes de la reparación herniaria es la recidiva de la hernia. Generalmente, la recurrencia tiene lugar por la zona de la sutura. Considerando que la sutura es otro elemento que participa en el proceso quirúrgico, una nueva línea de trabajo que se propone es la caracterización experimental y numérica de la respuesta mecánica de diferentes tipos de hilos, así como de diferentes tipos de cierre. El objetivo es establecer qué hilos son más adecuados para cada tipo de cierre y de paciente, así como pautas de sutura de la prótesis al tejido receptor para disminuir el número de recidivas.

III.4 Conferencias

El estudio desarrollado en la presente tesis se ha presentado también en diferentes conferencias nacionales e internacionales enumeradas en las Tablas III.3 y III.4. Con el trabajo *"Caracterización del comportamiento pasivo del músculo abdominal del conejo. Aplicación al diseño de prótesis"*, presentado en el XXVII Congreso Anual de la Sociedad Española de Ingeniería Biomédia (CASEIB) en 2009, en Cádiz (España), la autora de la tesis obtuvo el segundo premio del concurso de estudiantes.

Table III.3: Trabajos en conferencias nacionales e internacionales. Parte I

	Título	Autores	Conferencia	Ciudad	Participación
1.	Mechanical modelling of the human abdomen applied to hernia surgery	**B. Hernández-Gascón**, E. Peña, G. Pascual, J.M. Bellón, B. Calvo	6th Annual Conference CIBER-BBN, 2012	Madrid (España)	Póster
2.	Respuesta mecánica del abdomen humano herniado y reparado	**B. Hernández-Gascón**, E. Peña, G. Pascual, J.M. Bellón, B. Calvo	Capítulo Nacional Español de la Sociedad Europea de Biomecánica, 2012	Sevilla (España)	Ponente
3.	Numerical modelling of skeletal muscle tissue. Application to human abdominal cavity	**B. Hernández-Gascón**, J. Grasa, J. F. Rodriguez, B. Calvo	European Congress on Computational Methods in Applied Sciences and Engineering (ECCOMAS), 2012	Viena (Austria)	Coautora
4.	Numerical modelling of the abdominal wall using MRI. Application to hernia surgery	**B. Hernández-Gascón**, A. Mena, J. Grasa, M. Malve, E. Peña, G. Pascual, J. M. Bellón, B. Calvo	3rd Edition Computational Modeling of Objects Presented in Images: Fundamentals, Methods and Applications (COMPIMAGE), 2012	Roma (Italia)	Ponente
5.	Numerical modelling of the abdominal wall applied to hernia surgery	**B. Hernández-Gascón**, J. Grasa, E. Peña, G. Pascual, J. M. Bellón, B. Calvo	18th Congress of the European Society of Biomechanics (ESB), 2012	Lisboa (Portugal)	Ponente
6.	Reconstruction and numerical modelling of the abdominal wall. Application to hernia surgery	**B. Hernández-Gascón**, J. Grasa, E. Peña, B. Calvo	I Jornada de Jóvenes Investigadores del I3A, 2012	Zaragoza (España)	Ponente
7.	Lightweight meshes, used to repair abdominal wall defects shows an anisotropic mechanical response at long term	G. Pascual, B. Hernández-Irizarri, **B. Hernández-Gascón**, M. Rodríguez, S. Sotomayor, E. Peña, B. Calvo, J. M. Bellón	5th International Hernia Congress the World Hernia Celebration, 2012	Nueva York (EEUU)	Coautora

Table III.4: Trabajos en conferencias nacionales e internacionales. Parte II

	Título	Autores	Conferencia	Ciudad	Participación
8.	Experimental and computational characterization of the abdominal muscle and surgical meshes. Modelling hernia surgery	**B. Hernández-Gascón**, G. Pascual, M. Rodríguez, S. Sotomayor, E. Peña, B. Calvo, M. Doblaré, J. M. Bellón	5th Annual Conference CIBER-BBN, 2011	Zaragoza (España)	Póster
9.	Modelling of the abdominal wall: Comparison of hexahedral and tetrahedral elements	**B. Hernández-Gascón**, P. Young, G. Pascual, E. Peña, J. M. Bellón, B. Calvo	Simpleware Users Meeting, 2011	Bristol (Reino Unido)	Póster
10.	Receptor tissue modulates long term behaviour of heavy and light weight prostheses in repair of abdominal wall defects	G. Pascual, **B. Hernández-Gascón**, E. Peña, M. Rodríguez, B. Calvo, M. Doblaré, J. M. Bellón	The 46th Congress of the European Society for Surgical Research, 2011	Aachen (Alemania)	Coautora
11.	Numerical modelling of abdominal wall. Application o hernia surgery	**B. Hernández-Gascón**, E. Peña, G. Pascual, M. Rodríguez, B. Calvo, M. Doblaré, J. M. Bellón	Congress on Numerical Methods in Engineering (CMNE), 2011	Coimbra (Portugal)	Ponente
12.	Computational model of the muscle of the rabbit and implanted meshes	**B. Hernández-Gascón**, E. Peña, B. Calvo, M. Doblaré	IV European Conference on Computational Mechanics (ECCM), 2010	París (Francia)	Coautora
13.	Caracterización del comportamiento pasivo del músculo abdominal del conejo. Aplicación al diseño de prótesis	**B. Hernández-Gascón**, E. Peña, B. Calvo, M. Doblaré, G. Pascual, J. M. Bellón	XXVII Congreso Anual de la Sociedad Española de Ingeniería Biomédica (CASEIB), 2009	Cádiz (España)	Ponente

GENERAL INTRODUCTION AND SUMMARY

Mechanical modelling of the abdominal wall and biomaterials for hernia surgery

Chapter 1

Motivation and objectives

Hernia appearance is one of the most common diseases in the medical field. A hernia is defined as the protrusion of one or several internal organs through an opening in the wall that contains them due to a weakening of the wall. According to statistics, more than 20 millions hernias are estimated to be repaired worldwide (Kingsnorth and LeBlanc, 2003). From another perspective, 3% of the population suffers throughout life some kind of hernia, being five times more common this disease in men than in women (Park et al., 2006). Although it is difficult to estimate the total cost that this disease poses to society, it is estimated to ascend to 2.5 billion euros per year in the United States.

Hernias can appear anywhere in the body, but they are most common in the abdominal or groin area. The abdominal cavity is not protected by any osseus cartilaginous structure, so the protection of this anatomical region is entirely in charge of the abdominal wall. Therefore, the integrity of the abdominal wall enables the proper functioning of the abdominal cavity, because functions as a dynamic system and is subjected to acute (cough, vomiting, etc.) or maintained pressure changes (obesity, pregnancy, etc.) (Cobb et al., 2005; Song et al., 2006b). The most common factors that cause hernia appearance include increased abdominal pressure due to chronic cough, constipation, urinary obstruction, heavy lifting, obesity and family history. Another cause of herniation is the weakening of the tissues and, consequently, the loss of their stiffness. Moreover, the weakening of the front abdominal region after a laparotomy incision through the linea alba to access the abdominal cavity or in other surgeries is very often.

Abdominal surgery using synthetic mesh implantation technique is the most frequently used to repair hernias nowadays. Over time, surgical techniques for hernia repair have evolved from autoplasty, using the individual's own tissues, to the use of

prosthetic materials (Deysine, 1998). Specifically, the therapeutic view of hernia defects located in the abdominal wall has changed with the results provided by the Lichtenstein group related to prostheses (Lichtenstein and Shulman, 1986; Lichtenstein et al., 1989). The use of biomaterials for hernia repair has gradually shown its effectiveness, although the repair of large incisional hernias is more complicated and is associated with high risk of complications in the postoperative period (Sabbagh et al., 2011). The polypropylene (PP) used in reticular prosthesis is one of the most used biomaterials to repair hernia defects. Over time, its use has become more widespread and is one of the best biomaterials for treating defects, even when there is infection (Alaedeen et al., 2007).

Although there are many commercial meshes used for hernia repair, each of them may cause, to a greater or lesser extent, a variety of problems which reduce the quality of life of the patient. One of the most frequent occurrences is the appearance of fibrosis, defined as the abnormal growth of tissue in the defect area due to the presence of a foreign body, and which can lead to incarceration or strangulation of the viscera. Hernia recurrence is considered one of the most important problems in hernia surgery and generally takes place in the suture between the prosthesis and tissue. In addition, a bad compliance between the host tissue and the prosthesis, due to a significant difference of their stiffness (Schimidbauer et al., 2005), can cause discomfort and even pain in patients (Welty et al., 2001; Holste, 2005). Moreover, surgeons do not have definitive and universally accepted guidelines for choosing the appropriate prosthesis for each patient and type of defect. Therefore, the choice of one or another mesh and its placement, is a decision to be made by the surgeon based on their experience.

Due to the fact that this medical pathology is very common, many scientists are focussed on its study from a clinical and biomechanical point of view. Particularly, biomechanics is a scientific discipline whose goal is the study of biological structures that exist in living organisms from the mechanical standpoint. This area of knowledge brings together different biomedical sciences, using knowledge of mechanics, engineering, anatomy, physiology and other disciplines aimed at studying the behaviour of the human body and addressing derived problems.

For a correct modelling and analysis of the problem, different considerations described below have to be taken into account. First, the mechanical properties of muscle tissues are given by their microstructural composition. Specifically, muscular tissues are formed by a network of muscular, collagen and elastin fibres embedded in a more or less isotropic matrix (Loocke et al., 2008; Ito et al., 2010) and are classified as soft tissues. The mechanical response of these soft tissues shows a nonlinear response in large deformations since large displacements are obtained at low load levels and tissues stiffen at high load levels (Calvo et al., 2010; Martins et al., 2012). Besides, the high water content in these tissues, around 70%, gives them an incompressible character.

The preferential orientation of muscular and collagen fibres leads to an anisotropic mechanical response. Collagen fibres are responsible for the passive response (Calvo et al., 2009; Martins et al., 2012), while muscular fibres are responsible for the active response of muscle (Linden, 1998; Arruda et al., 2006). The abdominal wall is subjected to a distribution of initial or residual stresses as a result of the growth process from the embryonic stage to adulthood. These residual stresses are revealed after an extraction of the tissue since it suffers shrinkage and the modification of the equilibrium configuration, due to the release of residual stresses, occurs (Fung, 1993; Gardiner et al., 2001; Peña et al., 2006).

The passive mechanical characterization of the abdominal tissue has been mainly addressed using experimental animal models (Nilsson, 1982a,b; Hwang et al., 2005). There are also studies that use experimental human models (Arampatzis et al., 2005; Song et al., 2006a,b), despite the obtention of human samples is complicated. The majority of the studies characterize the mechanical behaviour using uniaxial traction (Nilsson, 1982a,b; Gajdosik, 2001) and compression (Loocke et al., 2004) tests although biaxial (Hwang et al., 2005) or inflation (Song et al., 2006b) tests are also used, which are closer to the physiological situation. The mechanical response of the abdomen differs depending on the analyzed area of the abdomen (Nilsson, 1982a,b) and the test direction, so the response is anisotropic (Hwang et al., 2005; Song et al., 2006a,b; Martins et al., 2012). Specifically, the mechanical response is stiffer along the transversal direction than in the craneo-caudal direction (Song et al., 2006a,b). There are also studies indicating that the mechanical response depends on the age and sex of the subject (Junge et al., 2001) although other studies reject such evidence (Rath et al., 1996).

To the author's knowledge, there are no experimental studies that characterize the active response of the abdominal muscle, although there are studies in the literature of other muscles from both, animals (Hill, 1938; Ramsey and Street, 1940; Abbot and Wilkle, 1953; Huxley and Hanson, 1954; Huxley and Niedergerke, 1954; Huijing, 1998) and humans (Maganaris and Paul, 1999; Arampatzis et al., 2005).

The information obtained from the experimental characterization has been used for the definition of constitutive models that reproduce the mechanical response of the soft tissues (Bol and Reese, 2008; Odegard et al., 2008; Stålhand et al., 2008; Calvo et al., 2010; Morrow et al., 2010; Ramírez et al., 2010; Stålhand et al., 2010; Bol et al., 2011; Ehret et al., 2011; Grasa et al., 2011; Hodgson et al., 2012; Martins et al., 2012). The numerical modelling of the muscle tissue has been proposed at both microscopic (Sharafi and Blemker, 2010) and macroscopic (Martins et al., 2012) levels, through linear (Boriek et al., 2000) and nonlinear (Martins et al., 2012) models and even some models define their response within the large deformation hyperelasticity (Calvo et al., 2009; Chi et al., 2010; Ito et al., 2010; Hodgson et al., 2012). Numerical models proposed within the hyperelasticity theory require the definition of a strain energy function

(SEF) which is usually expressed in terms of kinematic invariants (Spencer, 1971) and consider additively the active (capable of generating force) and passive (resistance to deformation) responses. Furthermore, the passive component of these functions usually considers, in a decoupled way, the contributions of the isotropic (Yeoh, 1993; Ogden, 2001) and anisotropic (Demiray et al., 1988; Holzapfel et al., 2000; Calvo et al., 2009) responses.

Once the behaviour of the tissues has been characterized and the model that reproduces their behaviour has been selected, it is possible to address the numerical simulation using the finite element method and reproduce physiological and non-physiological loading conditions in a particular geometry whose analytical solution is not possible. The passive response of abdominal and inguinal regions has been simulated numerically in some studies with simple geometries or models (Song et al., 2006a,b; Szymczak et al., 2010; Förstemann et al., 2011; Smietanski et al., 2012; Szymczak et al., 2012). Fortuny et al. (2009a) and Fortuny et al. (2009b) simulated the dynamic response of the groin area but, to the author's knowledge, there are no studies that model the active response of the abdominal muscles. On the contrary, other studies in the literature report the computational simulation of the active mechanical behaviour of other smooth (Stålhand et al., 2008, 2010) or muscle skeletal (Blemker et al., 2005; Bol and Reese, 2008; Grasa et al., 2011) tissues.

Research and development in biomaterials intended for repairing abdominal wall defects have evolved and progressed in recent years, in order to find the "ideal prosthesis". With respect to the reticular prostheses, one objective of research was to assess the amount of implanted material. In addition, hybrid reticular prosthesis have been designed (Klosterhalfen et al., 2005), in which there are absorbable and nonabsorbable components. New designs also consider the pore size as an essential parameter, and other aspects such as the diameter of the filaments, the spatial distribution and the polymer used in the filament manufacture (Pandit and Henry, 2004; Rosch et al., 2004). Nowadays, in addition to polypropylene, other polymers such as expanded polytetrafluoroethylene (PTFE) are used for manufacturing these prostheses. Besides, the spatial distribution of the filaments generates an isotropic or an anisotropic mechanical response of the implant, so the placement of the mesh in the abdominal tissue, which also has an anisotropic behaviour (Hwang et al., 2005), is essential.

In general, reticular prostheses have been classified in biomaterials of low or high weight, depending on their density parameter g/m^2 (Klinge, 2007). Specifically, *"heavyweight"* (HW) prosthesis are those whose density parameter is above 80 g/m^2, in *"mediumweight"* (MW) prosthesis is between $50 - 80$ g/m^2 (Cobb et al., 2006) and in *"lightweight"* (LW) prosthesis is under 50 g/m^2. Tissular integration process after implantation depends on the prosthesis implanted (Schachtrupp et al., 2003). Specifically, the fibrosis caused by HW conventional prostheses could be diminished with the

implant of LW prostheses (Conze et al., 2005; O'Dwyer et al., 2005). Therefore, one of the purposes of the LW prostheses is to decrease the amount of residual foreign bodies that remain at the level of the recipient tissues. Thus, a lower foreign body reaction and a repair process generating less fibrosis can be obtained in the recipient tissues (Klinge et al., 2002b).

As previously mentioned, the abdominal wall works as a dynamic system and is under acute or maintained pressure changes over time (Cobb et al., 2005; Song et al., 2006b). Therefore, after the placement of a prosthetic material, some compliance that allows an unrestricted mobility of the wall (Junge et al., 2001; Klinge et al., 2002a) must exist without diminishing its final resistance.

The characterization of the behaviour of different prostheses has been addressed in numerous experimental studies found in the literature (Afonso et al., 2008; Hollinsky et al., 2008; Bellón, 2009; Saberski et al., 2010; Yoder and Elliott, 2010; Deeken et al., 2011). Other studies are focussed on the study and analysis of the behaviour of the sutures, that allow the union of the prosthesis to the tissue (Kes et al., 2004; Schwab et al., 2008), and in the size of the minimum overlap required to prevent early prosthesis dislocation (Binnebösel et al., 2007).

Regarding the modelling of the behaviour, constitutive models have to reproduce the observed behaviour patterns in prostheses at different loads. In general, the mechanical response of the prostheses is associated with phenomena occurring at different scales. Experimental evidences show a nonlinear response, drastic changes in the mesh due to the collapse of the pores of the mesh under uniaxial load conditions and a strong anisotropic component in some commercial meshes. Such phenomena may be studied by analyzing the cell or unit pattern that define, by repetition in space, the mesh fabric (Röhrnbauer et al., 2011). Moreover, the friction between the filaments of the mesh cause phenomena such as hysteresis, depending on the strain rate, and irreversible deformation processes that cause significant changes in the geometry of the cell during loading cycles. Some computational models reproduce the geometry of the filaments (Kuwazuru and Yoshikawa, 2004) while other authors propose continuous models (King et al., 2005; Röhrnbauer et al., 2011).

After surgery, the mechanical properties of the whole tissue-mesh change due to tissular integration process. For this reason, the main goal of the mechanical (Cobb et al., 2006; Bellón et al., 2007; Ozog et al., 2011) and histological (Hilger et al., 2006; Pascual et al., 2008) experimental characterization of the whole tissue-mesh is the determination of the mechanical properties of the implant site after different times after surgery. The stiffness of the whole tissue-prosthesis increases and has to reproduce the original behaviour of healthy abdominal tissue over time (Cobb et al., 2006; Pascual et al., 2008; Bellón et al., 2009). In cases with infection, only few materials such as the

PP allow the partial rescue of the prosthesis and its properties do not change over time. However, the PP has the drawback of having poor behaviour in the peritoneal interface and some complications such as intestinal fistulas (Chew et al., 2000) and migrations to cavitary organs appear (Chuback et al., 2000). As previously introduced, the abdominal tissue is anisotropic and some commercial prostheses also exhibit anisotropy (Yoder and Elliott, 2010). In these cases, once the mesh is integrated into the host tissue, the whole tissue-mesh remains anisotropic (Ozog et al., 2011). Therefore, since the final adaptation of synthetic mesh has to be such that it mimics the original response from healthy tissue, its placement in the abdomen is essential (Anurov et al., 2010; Ozog et al., 2011). Specifically, the stiffer direction of the mesh has to be placed parallel to the direction where muscular effort is higher and along the direction where fibres are arranged in the aponeurosis (Anurov et al., 2012).

Although there are existing works in the literature about the experimental characterization of the abdominal muscle, no data exist about the initial deformations in the abdomen and there is no complete study that determines the mechanical properties of all muscles in the same specimen. Besides, no work that describes numerically the passive response of abdominal tissue within the framework of the nonlinear anisotropic hyperelasticity, or work that models the active response of the abdomen was found. Moreover, to the author's knowledge, there are no work that models experimentally and numerically the behaviour of prostheses and, although the tissue integration process has been extensively studied in the literature, the analysis of the mechanical response of the whole tissue-mesh was mainly addressed in the short term. Thus, although there are existing works in the literature on experimental and computational characterization of the abdomen and prostheses, they are not enough to address our study completely. Because of the importance of the problem of abdominal surgery in today's society and the deficiencies of the available studies in the literature, this thesis focusses on the modelling of the mechanical behaviour of the abdominal wall and different synthetic meshes used in hernia repair.

Given the extent and complexity of the problem, the formation of a working multidisciplinary team is required. In this particular case, the team consists of specialists in continuum mechanics and modelling of tissues within the engineering field (Group of Applied Mechanics and Bioengineering, University of Zaragoza), biologists and clinical specialists with experience in the experimentation with animal models and with the innovative concern of giving solutions for hernia pathologies (Translational Research Group in Biomaterials and Tissue Engineering at the University of Alcalá de Henares). The formation of this team allowed us to approach the study of this disease under two different scenarios: first, a study in an animal model, the New Zealand white rabbit, was conducted and it enabled us to perform experimental tests to characterize the tissues, as well as evaluate the tissular integration using three common prosthesis. Furthermore, based on the experimental results obtained, numerical models of the mechanical be-

haviour have been proposed, defined and validated. Subsequently, the results obtained with the animal model have been spread to humans by defining an *"in silico"* model of the abdominal wall based on magnetic resonance imaging. This model allowed to study the response of the healthy wall and after the placement of the three types of selected meshes. The advantage of the proposed methodology is to reduce the cost of experimentation and clinical trials, which in the case of humans are difficult to perform.

The development of this thesis forms part of two research projects funded primarily by CIBBER-BBN and, subsequently, by the Ministry of Economy and Competitiveness: "Development and validation of a new concept of prosthetic implant for repairing abdominal wall defects" (ABDOMESH) and "Biomechanical modelling of the muscleskeletal abdominal tissue" (DPI2011-27939-C02-01), respectively. Furthermore, this thesis has been possible thanks to the grant FPI BES-2009-021515, awarded by the Ministry of Science and Innovation.

1.1 Objectives

The main objective of the thesis is to establish a working methodology that allows to analyze the response of prostheses in hernia surgery using experimental and computational techniques. To achieve this objective, the following partial objectives have to be achieved (see Figure 1.1):

- Experimental characterization and numerical modelling of the passive mechanical behaviour of the abdominal muscle using an experimental animal model.
- Experimental characterization and numerical modelling of the mechanical behaviour of different commercial synthetic meshes.
- Histological and experimental characterization in short and long term of the passive mechanical behaviour of the whole tissue-synthetic mesh after different times after the implant (14, 90 and 180 days) and types of implant.
- Definition of a methodology to design and validate the behaviour of prostheses.
- Definition of a simplified finite element computational model of the experimental animal to reproduce the abdominal behaviour without hernia and after surgery.
- Definition of a complete finite element computational model based on the human body geometry, obtained from nuclear magnetic resonance imaging to reproduce the mechanics of the healthy abdominal wall.

- Definition of a complete finite element computational model of the herniated and repaired human abdomen, using different prostheses, and analyses of the response of the whole depending on the commercial mesh and its placement in the abdomen.
- Numerical modelling of the active behaviour of the skeletal muscle tissue.

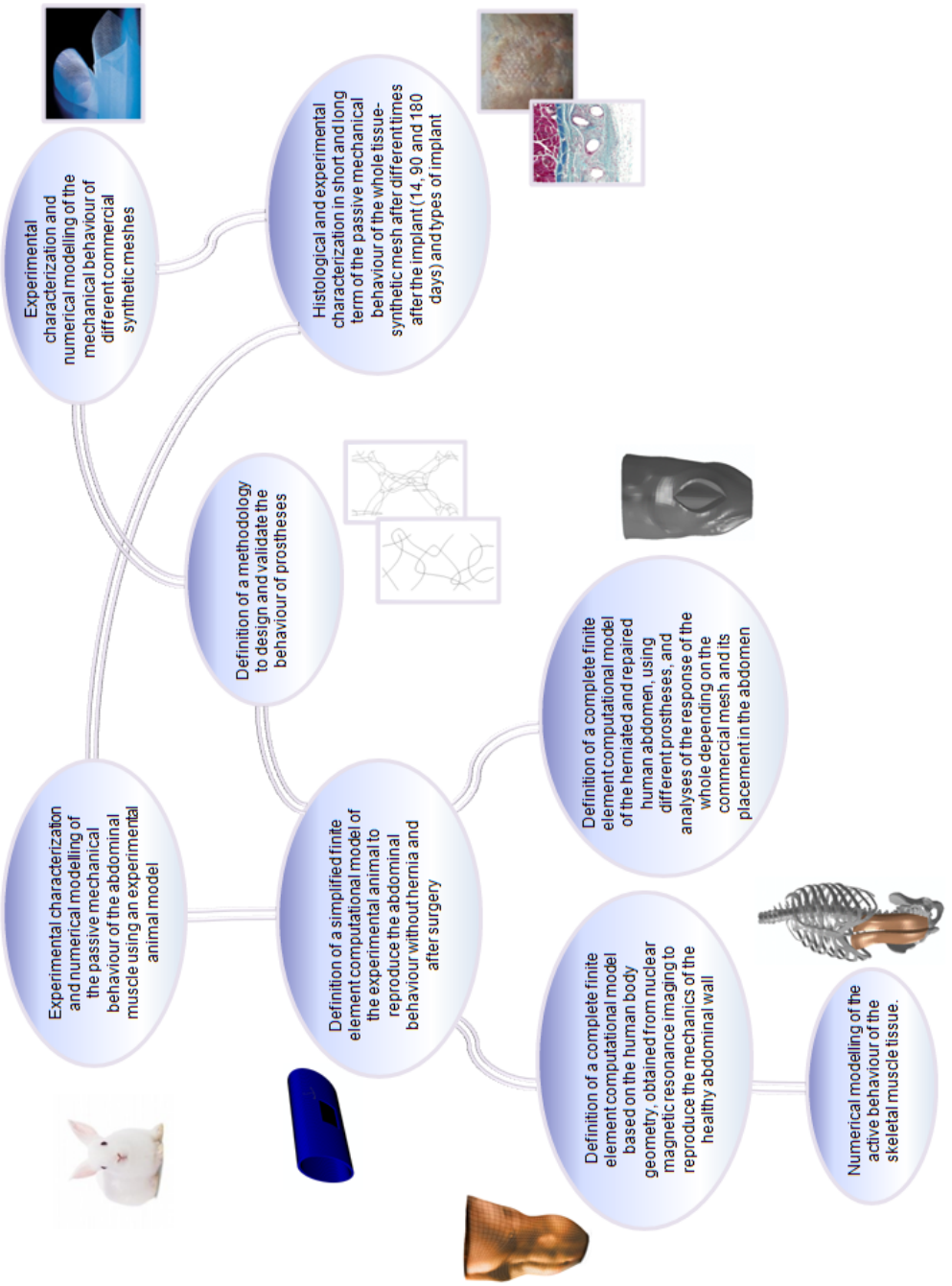

Figure 1.1: Partial objectives of the thesis.

1.2 Structure of the thesis

The thesis is presented as a compendium of publications and this document complies with the requirements established by the University of Zaragoza, following the agreement of the 17th of December 2008 of the Governing Council of the University that approves the Regulations on Doctoral Thesis and where thesis developed as a compendium of publications are contemplated.

On the home page it has been specified that the thesis is a compendium of publications and the complete references of each work that constitute the body of the thesis have been listed.

This thesis consists of five parts which are described below. First, Chapter 1, entitled ***Motivation and objectives***, presents the motivation of the study developed in the thesis and the research objectives.

Second, Chapter 2, entitled ***Abdominal wall and biomaterials for hernia surgery***, presents an overview and state of the art of the main topics related to mechanics, anatomy and physiology of the abdominal wall and the prostheses used in the implant, as well as to the tissue integration process. These concepts are important for understanding the results and scope of this thesis. Besides, detailed descriptions of the problem generated as a result of abdominal surgery are included from the mechanical standpoint, as well as considering clinical aspects relating to the treatment of hernias.

Third, Chapter 3, entitled ***Results, works and conclusions of the thesis***, presents the main results obtained in the thesis, which are grouped according to the methodology followed for its development, justifying the thematic unit of the works included in the compendium of publications. The original contributions of the thesis and the final conclusions, as well as the future lines of work are described.

Next, the works that comprise the compendium of publications are included and, finally, three appendixes are included. These appendixes include the characteristics of journals where articles were published in, the acceptance letter of the work 10 and the resignation of the non Doctors coauthors to present the works of which they are coauthors, as part of another doctoral thesis.

Chapter 2

Abdominal wall and biomaterials for hernia surgery

2.1 Introduction

Although hernias are usually small and relatively asymptomatic, they can cause pain and discomfort in patients affecting their quality of life. In addition, some hernias occasionally lead to incarceration and strangulation of the intestines and other organs, becoming a serious disease. Considering that one out of five patients that suffers intervention by laparotomy develop an incisional hernia, abdominal hernias have become a common pathology in the health system. Although it is difficult to estimate the total cost that this disease means for society, it is estimated to amount to 2.5 billion euros per year in the United States. The great medical relevance is this pathology has led many research groups to study this disease, among other fields, in the field of biomechanics.

Different sections describing the fundamental concepts needed to understand the contents of the thesis have been included in this chapter. The most important terms related to hernia surgery as well as anatomy and physiology of the abdominal wall have been described in Sections 2.2 and 2.3. After that, Sections 2.4, 2.5, 2.6 and 2.7 refer to the study of the abdominal wall and the prostheses used in hernia repair, the tissular integration process after surgery and the design of synthetic meshes, respectively. These sections describe the basic concepts and include a state of the art of the existing works in the literature for each topic.

2.2 Hernia surgery

A hernia occurs when a defect in the tissue appears, causing the protrusion of the internal organs outside the cavity that contains them (see Figure 2.1). Hernia appearance is due to diverse causes. A common factor is the increase in the abdominal pressure due to chronic cough, constipation, urinary obstruction, heavy lifting, belly hydropsy (fluid in the abdomen), previous abdominal surgery and obesity, among others. Moreover, the loss of stiffness in the tissue, nerve damage due to the weakening of the muscles, the presence of embryological channels in the case of congenital hernias (birth defects) and family history are other causes that can cause the appearance of hernias. Moreover, laparotomy incisions through the linea alba to access the peritoneal cavity is one of the most common approaches in abdominal surgery. This technique causes the weakening of the region where fibres from abdominal muscles intersect and this area becomes susceptible to suffer incisional hernia (see Figure 2.2).

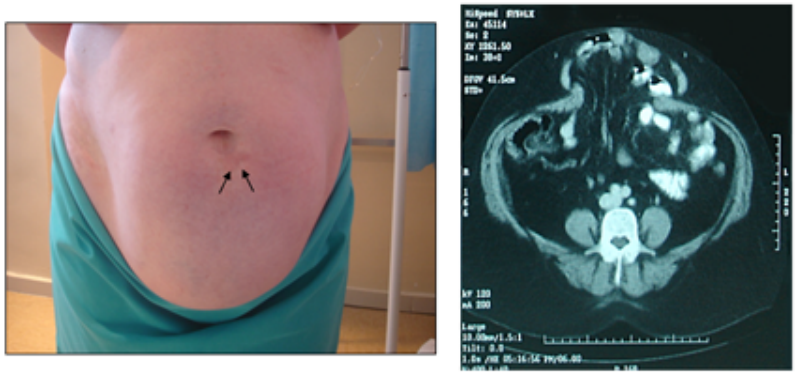

(a) (b)

Figure 2.1: (a) Macroscopic image of an abdominal hernia. (b) Hernia detection in (a) using magnetic resonance imaging (Bellón, 2012).

There are several types of hernias, depending on the area of the abdominal cavity where they appear (see Figure 2.3). The most common types of hernias are listed below:

- Inguinal hernia: it occurs when a defect in the muscle wall of the inguinal region allows the abdominal contents (usually intestine or bladder) to protrude under the skin covered by a peritoneal sac. There are two types of inguinal hernias: direct and indirect. In direct inguinal hernias, usually present in middle and old age, the abdominal contents, particularly the small intestine, pass through a muscle weakness and bulge in the area of the triangle of Hasselbach. Indirect inguinal hernias occur when abdominal contents protrude through the internal or deep inguinal ring, descend along the spermatic cord and, over time, often finish in the scrotum. The latter is usually present in young men and boys.

(a)

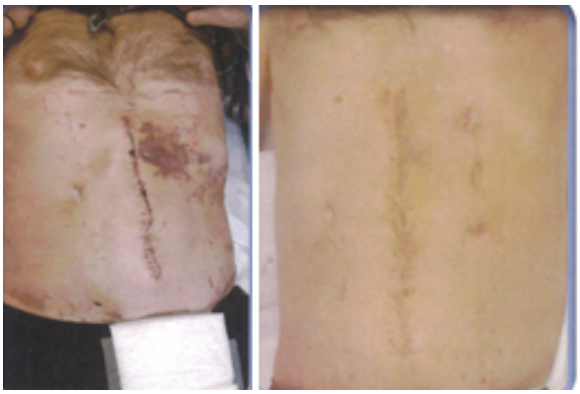

(b)

Figure 2.2: (a) Abdominal hernia along the linea alba. (b) Appearance of the abdomen after hernia surgery (Ramshaw, 2009).

- Femoral or crural hernia: it mainly affects older women, but can also occur in young women after pregnancy and childbirth. Appears in the groin, or just below. A portion of the intestine passes through the tube where femoral artery and vein normally run, under the inguinal ligament. They are easily strangulated, usually small and not very painful.

- Incisional hernia or eventration: it appears in places where surgery has been previously practiced (mainly after a longitudinal opening of the midline of the belly) since these regions of the abdominal wall are weakened: the young scar offers less resistance, and the intestine can create an opening and infiltrate.

- Umbilical hernia: they are developed when the umbilical ring weakens and the abdominal contents protrude. This part is frequently weakened by nature since it has blood vessels of the umbilical cord. Therefore, it is usually present from the birth due to a congenital weakness of the umbilical ring. They usually close spontaneously in the first years of a child's life, although it can occur at any age.

- Epigastric or ventral hernia: it is more usual in men aged between twenty and fifty years, and appears in the midline of the abdomen, between the sternum and the umbilicus (although it may occur below the umbilicus, slightly to the left or right). The relative weakness of the abdominal wall along the linea alba is the main cause of its appearance.

- Spiegel hernia: Spiegel line corresponds to the outer side edge of the rectus abdominis muscles, where the two sheaths of the rectus abdominis are formed from the aponeuroses of the oblique muscles. It appears in the so-called arc of Douglas, in the area between the anterior iliac spine and the umbilicus, at the level of the external rectus muscle, where the posterior rectus sheath finishes and the zone becomes less consistent. In this area, lateral ventral hernias may appear.

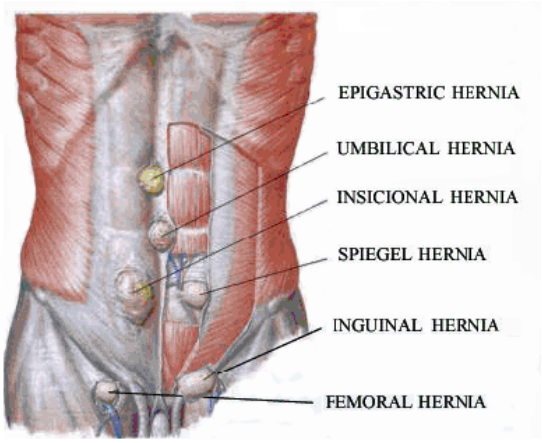

Figure 2.3: Types of hernias (Pqax, 2011).

Hernia repair is known as herniorrhaphy. This surgical procedure can be performed using two methods:

- Conventional method: an incision, or cut, on the area of the hernia is made, the protruding portion is placed back into the abdominal cavity and the hole or weakness in the abdominal wall defect is repaired stitching the surrounding muscles.

- Free tension technique: an incision on the area of the hernia is made, the protruding portion is repositioned in the abdominal cavity and a portion of synthetic mesh is used to cover the weakening in the abdominal wall without stitching the surrounding muscles. This technique can be performed using the laparoscopic method. With this method, three or four small incisions are performed in the abdomen near the area of the hernia. In one of them, a metal probe (called

laparoscope) is inserted with a light and a viewer. On the other incisions instruments are inserted to repair the hernia. The laparoscope viewer is connected to a screen that allows the surgeon to view the hernia. The protruding portion of tissue is placed back into the abdominal cavity and the hole or weakness in the abdominal wall is repaired by placing a mesh over the defect. Due to the fact that the conventional method causes problems such as the recurrence of hernias, the principle of anatomical reconstruction tended to be replaced by prosthetic replacement prosthesis where the resistant prosthesis covers the discontinuity and becomes a new wall. Four different positions can be considered when implanting the prosthesis, classified from the deeper to the superficial placements: intraperitoneal, preperitoneal, retromuscular prefascial and premusculoaponeurotic (see Figure 2.4):

- Intraperitoneal implantation: the prosthesis is implanted into the deeper side of the wall after the release of the viscera. This location has the advantage of not involving parietal dissection and being always usable wherever the hernia is placed since the abdominal pressure benefits the closure. To avoid intestinal adhesions, *"composite"* biomaterials with microporous visceral surface should be used since they cause less adhesions.

- Preperitoneal implantation: involves the placement (by simple apposition, or with the help of a stitch) of a prosthesis in the deeper side of the wall directly opposite the peritoneum, so that the edges of the mesh protrude significantly from the opening limits. Thus, the peritoneum is reinforced and a prosthetic-parietal adhesion is created such that the whole is equal to a new wall.

- Retromuscular prefascial implantation: the prosthesis is implanted between the muscular body and its posterior fascia and it is sutured externally. Hernia repair is effective, but requires parietal dissection and residual pain can appear due to accidental interposition of nerve fibres in the fixing points.

- Premusculoaponeurotic implantation: the principle is to reinforce, with a prosthetic, a parietal repair using suture and autoplasty. The drawback of this location is its superficial character, since there is no counterpressure but the skin. Thus, this is a cause of fragility when pressure increases. Any superficial infection or skin necrosis exposes the prosthesis. However, it is the site that makes easier tissular integration and generates greater vascularization (see Figure 2.5).

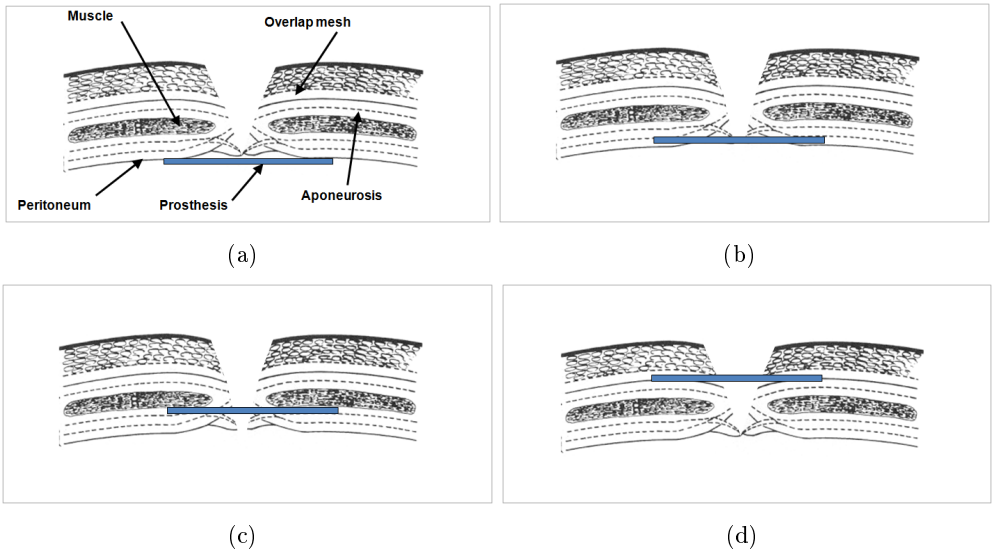

Figure 2.4: Different possible positions of the prosthesis from the deeper to the superficial placements: (a) intraperitoneal, (b) preperitoneal, (c) retromuscular prefascial, (d) premusculoaponeurotic (Bellón, 2012).

2.3 Anatomy and physiology of the anterior abdominal wall

The trunk is, in case of mammals, a vital anatomical area because it contains most of the vital organs belonging to the respiratory, digestive, urinary, cardiovascular and reproductive systems. It consists of the thoracic and abdominopelvic cavities, the latter being the subject of this study.

Contrary to the thoracic cavity, the abdominal cavity is not protected by any osseus cartilaginous structure, so the protection of this anatomical region is entirely given by the abdominal wall. Abdominal wall integrity involves performing normal activities automatically. Any injury at this level interferes with the functions of the abdominal wall, such as mobility (ventral flexion, rotation and lateral movements, standing, walking, bending, lifting efforts, etc.), protection and contention of the abdominal contents, breathing (together with the thoracic cavity) and pressure support (urination, defecation, childbirth, cough, vomiting, etc.).

Abdominal muscles have their fixation in the osseus cartilaginous structures that comprise the ribcage, including the spinal column and the pelvis. These structures provide the conditions for fixing and anchoring the abdominal wall muscles. The skin of the abdomen is loose and not attached unless at the level of the linea alba and the umbilicus. The development of this tissue in each individual relates to eating habits and surgical antecedents.

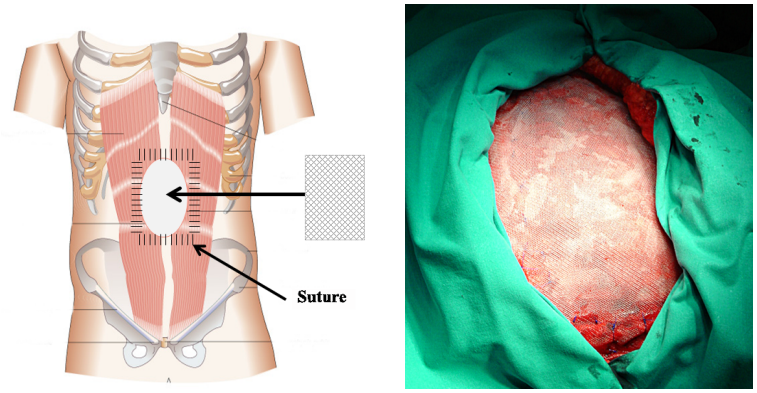

(a) (b)

Figure 2.5: (a) Scheme of a premusculoaponeurotic implantation of a prosthesis in hernia surgery. (b) Surgipro mesh® placed in a human abdominal hernia (Bellón, 2012).

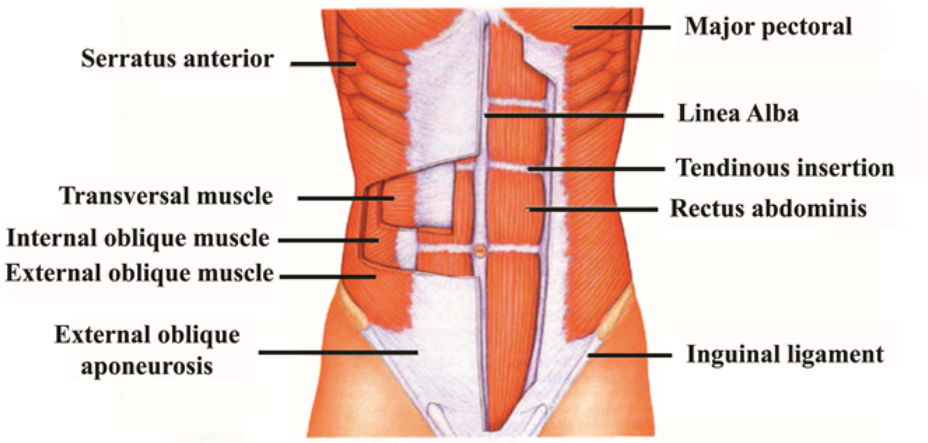

Figure 2.6: Main abdominal muscles (Murphy, 2010).

The anterolateral abdominal wall is composed of four pairs of major muscles and their fascial projections (Moore W., 2008) (see Figure 2.6). The four major muscles are the rectus abdominis, external oblique muscle, the internal oblique muscle and the transversus abdominis. Other muscle in the abdominal wall is the pyramidalis muscle of the abdomen, whose size is variable, it is usually small and may be absent (15-20% of the population does not have it) (see Figure 2.7). It originates from the crest of the pubis (pubic symphysis), being located immediately below the rectus and its frontal part, and is placed inside the rectus sheath inserting into the linea alba. Its function is the tensor of the linea alba.

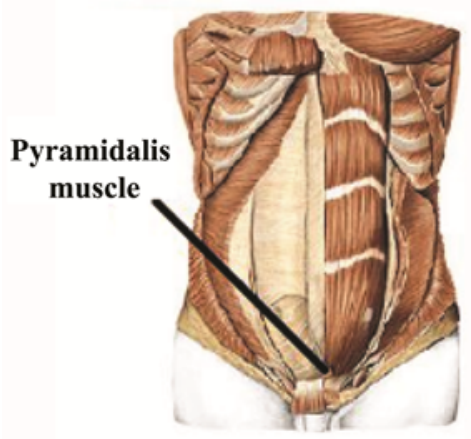

Figure 2.7: Pyramidalis muscle of the abdomen (Sistema-Muscular, 2012).

2.3.1 Rectus abdominis muscle

The rectus abdominis muscle is a double muscle (the muscle is divided into two symmetrical parts with each other) (see Figures 2.6 and 2.8) (Moore W., 2008). Their muscle fibres are arranged along the craneo-caudal direction of the body. Its origin appears in the symphysis and pubic crest and inserts into the costal cartilages V-VII and the xiphoid.

Each member of the rectus is separated by the so-called linea alba. Besides, each muscle is divided by three or four or aponeurotic intersections or tendons, called metameres. The rectus muscle is placed within a tendinous sheath (fascia or aponeurosis) which is formed by the aponeurosis of the oblique muscles (external oblique, internal oblique and trasversus abdominis). Specifically, the anterior rectus sheath extends over the entire surface of muscle and is attached to the periosteum of the bone insertions. The anterior rectus sheath comes from the external oblique aponeurosis and the anterior sheath of the aponeurosis of the internal oblique muscle (see Figure 2.8). Furthermore, the posterior sheath extends over the upper two thirds of the muscle and is formed by the posterior sheath of the internal oblique and the aponeurosis of the transversus abdominis. In the lower third, the posterior rectus sheath passes to the front of the rectus. In this area, the muscle contacts with the transversalis fascia and the extraperitoneal connective tissue (see Figure 2.8). The arcuate line is defined as the line where this change occurs and is located at the boundary between the upper two thirds and lower third of the rectus muscles.

The functions of this muscle are abdominal trunk flexion or elevation of the pelvis, thorax approach to the pelvis, collaboration in expiration and keep the tone of the abdominal wall (see Figure 2.9.a). It also helps in the abdominal press, which is the

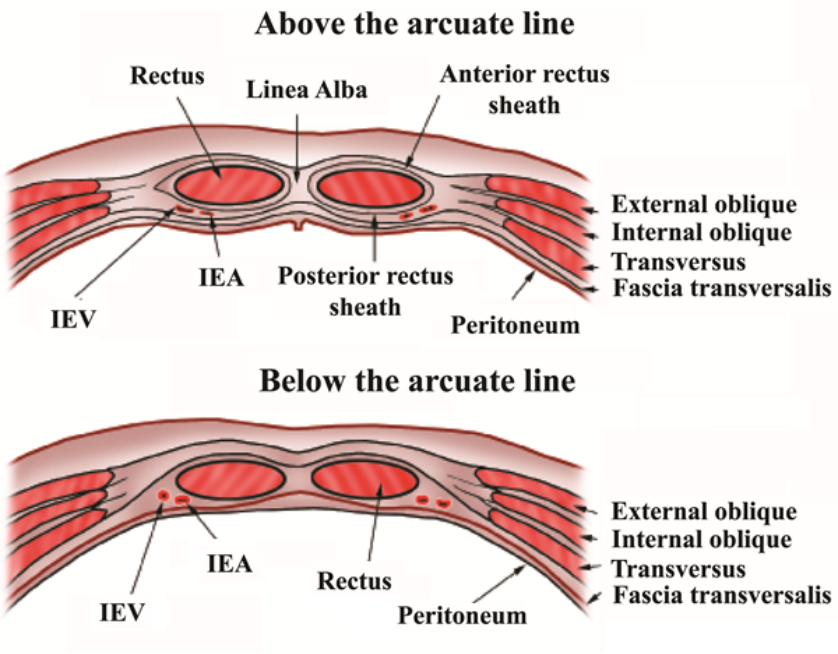

Figure 2.8: Transversal section of the rectus abdominis muscle. Arrangement of the anterior and posterior rectus sheaths of the muscle above (a) and below (b) the arcuate line, in the boundary located between the upper two thirds and one third lower rectus muscles (IEA: Inferior epigastric artery. IEV: Inferior epigastric vein) (WebMD-LLC, 1994).

process that provokes an increase in the abdominal pressure to perform a certain effort (cough, urination, defecation, etc.).

2.3.2 External oblique muscle

The external oblique muscle constitutes the most external of the lateral muscles of the abdomen (Moore W., 2008). Their muscular fibres are arraged from V-XII rib pairs to the iliac crest and the pubic area, i.e the direction of the muscular fibres is oblique to the lower and medial areas (see Figures 2.6, 2.10 and 2.11).

The origin of this anatomical structure is found in the outer face of the rib pairs V-XII, where interdigitates with thoracic wall muscles, serratus anterior and wide dorsal (see Figure 2.11). This muscle insertion occurs at the inner edge of the iliac crest, in the inguinal ligament through tendon insertions and in the pubic tubercle. In addition, this muscle is inserted within the external oblique aponeurosis (fascia or aponeurotic projection), which helps to form the anterior rectus sheath and the linea alba.

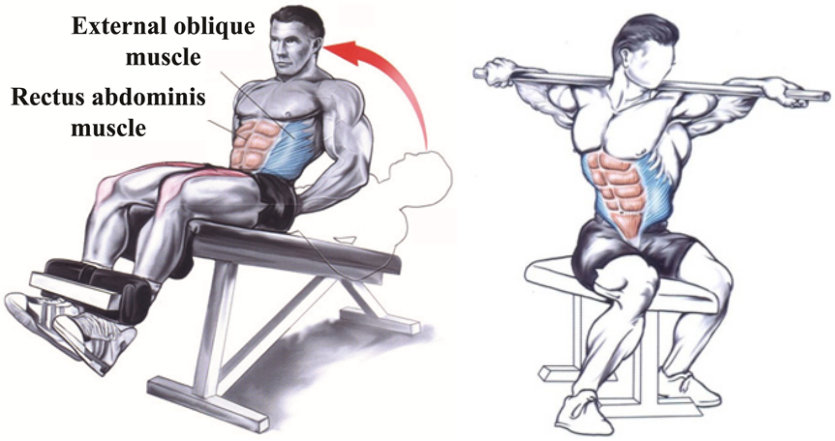

(a) (b)

Figure 2.9: Abdominal muscles activated in flexion (a) and rotation (b) movements of the abdominal trunk (WordPress, 2012).

The unilateral function of the external oblique muscle is the rotation of the trunk to the opposite side, trunk lateral bow and elevation of lateral pelvic edge (see Figure 2.9.b). Their bilateral actions are the trunk bow forward, lifting the pelvis and, also contributes to abdominal press during expiration.

2.3.3 Internal oblique muscle

The internal oblique muscle is located at an intermediate position of the lateral muscles of the abdomen (Moore W., 2008). The direction of their muscle fibres is approximately perpendicular to the external oblique fibres (Figures 2.6, 2.10 and 2.12), so fibres go from the costal margin to the spinous processes of the fifth lumbar vertebra, the inguinal ligament, the iliac crest and bone pubis.

Its origin is located in the inguinal ligament, iliac spine and thoracolumbar fascia, which in turn is anchored to the spinous apophysis of the last lumbar vertebra and the first sacrum. Its insertion occurs in the linea alba, the costal margin of the pairs X-XII by aponeurotic insertions and pectineal line. Above the arcuate line, the aponeurotic projection of the internal oblique muscle is divided in two, forming part of both, the posterior and the anterior rectus sheaths. Below the arcuate line, the aponeurotic projection of the internal oblique muscle becomes part of the anterior rectus sheath.

The function of the internal oblique muscle is the unilateral contraction by rotating the trunk on the same side and forward. Besides, the bilateral contraction occurs by bowing the trunk forwards and raising the anterior edge of the pelvis. It also works in

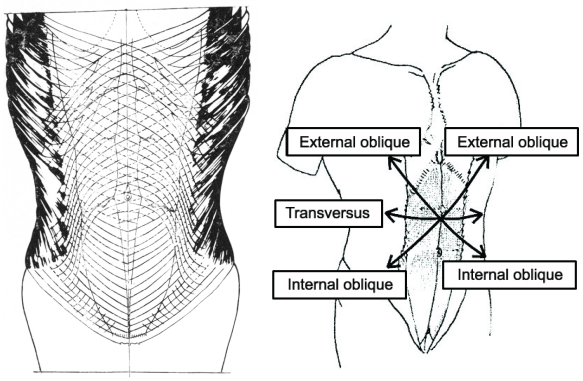

(a) (b)

Figure 2.10: (a) Arrangement of collagen fibres in the aponeurosis of the external and internal oblique that cover the anterior rectus sheath up to the linea alba (Askar, 1977). (b) Direction of muscular fibres in the external and internal oblique (symmetry with respect to the linea alba) and trasversus muscle (Axer et al., 2001a).

the press and abdominal expiration.

2.3.4 Transversus abdominis muscle

The transversus abdominis muscle is the deepest abdominal muscle (Moore W., 2008). Their muscle fibres are arranged from the linea alba to the lumbar spines apophysis, i.e their direction is approximately perpendicular to the craneo-caudal direction of the human body (see Figures 2.6, 2.10 and 2.13).

Its origin is found on the inside face of the ribs of the XI and XII pairs and on the costal cartilages of the VII to X pairs, where through digitations is intertwined with the diaphragm, in the thoracolumbar fascia, in the anterior two thirds of the inner part of the iliac crest and in the third lateral inguinal ligament through aponeurotic attachments. With respect to its insertion, this takes place in the linea alba, in the pectineal line and the pubic crest. Above the arcuate line, the aponeurotic projection of the transversus muscle muscle belongs to posterior rectus sheath. Below the arcuate line, this projection passes to the front of the abdominal muscles covering them. The posterior face of the transversus abdominis muscle is attached to the fibrous tissue called transversalis fascia.

Its functions are, in addition to maintaining the pressure and the tone of the abdominal cavity, the rotation of the trunk to the same side, the contraction and relaxation of the abdominal wall, mainly in bilateral contraction, and collaboration in the press and

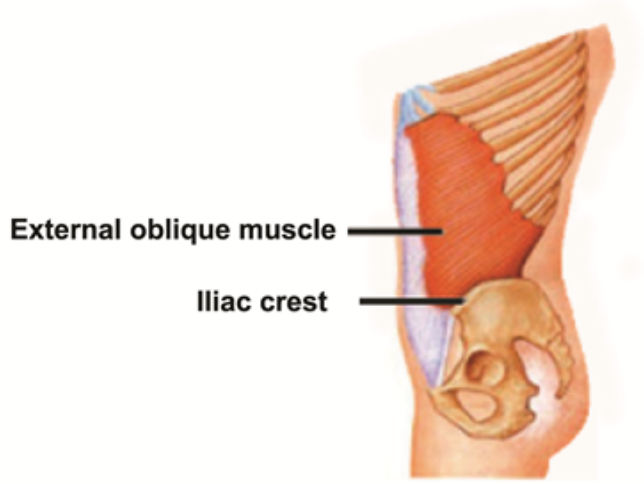

Figure 2.11: External oblique muscle of the abdomen (Automattic-Inc, 2005).

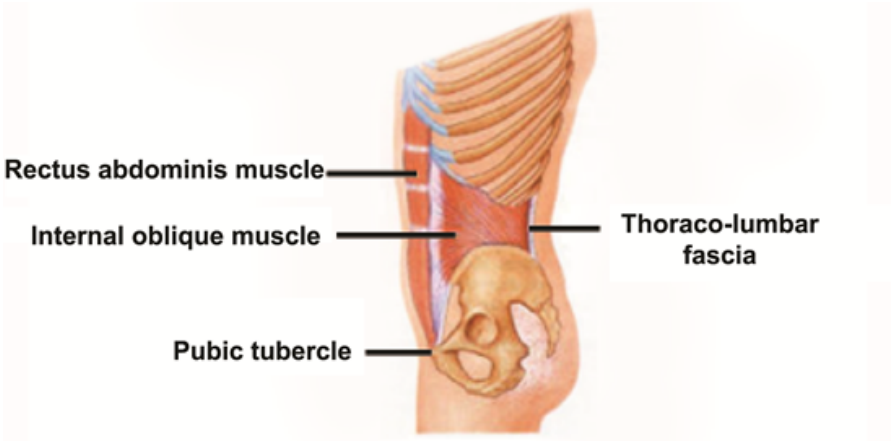

Figure 2.12: Internal oblique muscle of the abdomen (Automattic-Inc, 2005).

abdominal expiration.

2.3.5 Linea alba

The line alba is located between the medial borders of the rectus abdominis and extends from the xiphoid to the symphysis pubis (see Figures 2.6 and 2.8) (Moore W., 2008). It consists of a band of dense fibrous tissue formed by the fusion of the aponeurosis of the external and internal oblique and transversus muscles. The line alba expands as it reaches the xiphoid, going sometimes up to 1.25 - 2.5 cm width. In the supraumbilical portion of the linea alba the intertwined fibres of the aponeurosis leave small elliptical holes where the vessels and nerves pass through.

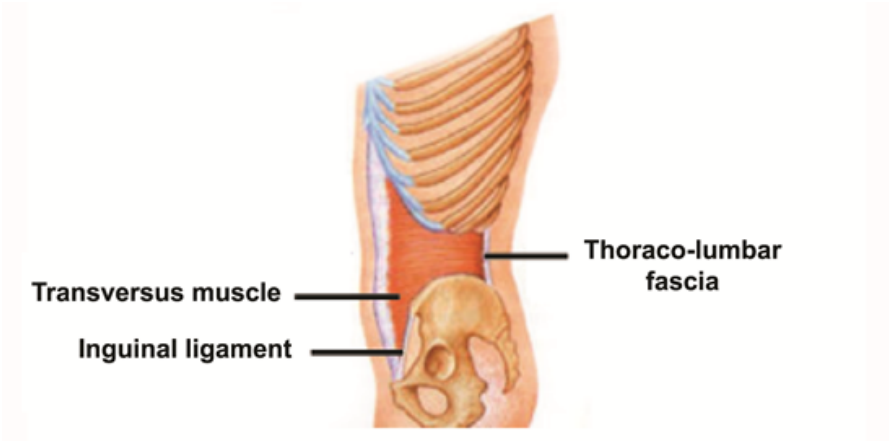

Figure 2.13: Transversus abdominis muscle of the abdomen (Automattic-Inc, 2005).

2.3.6 Transversalis fascia

The transversalis fascia is a sheath that covers the inside of the full abdominal muscle wall, and the deep surface of the transverse muscle (see Figure 2.8) (Moore W., 2008). Their collagen fibres are arranged perpendicularly to the craneo-caudal direction of the human body. This anatomical structure, in the upper half of the abdominal wall, is a very thin sheet attached to the subperitoneal fascia. Its structure becomes be stronger, and thus more consistent in its lower half.

Transversalis fascia covers therefore, the whole extension of the deep transversus muscle face, except for the part of the aponeurosis of this muscle which passes in front of the rectus abdominis, under the arch of Douglas. At this level, the transversalis fascia leaves the aponeurosis of the transversus abdominis and starts covering the back of the rectus muscle. Therefore, in this area, only the transversalis fascia and the peritoneum form the posterior rectus sheath. In the upper area of the abdomen this fascia is intimately fused with the diaphragm.

2.3.7 Other anatomical structures

In addition to the abdominal muscles and fascias described, there are other anatomical structures in the abdominal wall that are needed to be defined adequately to describe the abdominal cavity (Moore W., 2008):

- Diaphragm: this anatomical structure is the separation between the thoracic and abdominal-pelvic cavities, and its principal function is the respiratory movement.

In its normal position, relaxed, the diaphragm is convex, allowing the expulsion of air from the lungs and the expansion of distant organs in the abdominal cavity, whereas during inspiration, flattens, allowing the passage of air into the lungs and helping the intestinal transit. It consists of tendinous fibres, all converging in the center and higher area, denoted by phrenic center. Its insertion occurs at the edges of the rib cage, ends of the XI and XII ribs, xiphoid process of the sternum, lumbar vertebrae and some ligaments of the posterior abdominal wall.

- Arcuate line or line of Douglas: it defines the boundary between the upper two thirds and lower third of the rectus muscles. It is up to this line where the aponeurosis of the internal oblique belonging to the posterior rectus sheath and the aponeurosis of the transversus abdominis pass to cover the anterior rectus sheath.
- Semilunar line or line Spiegel: it is the one that marks the transition between the rectus and lateral muscles. It is located on both sides of the human anatomy and runs from the arch of the ribs to pubic bone.
- Inguinal ligament: it is considered as the edge of the external oblique aponeurosis running from the anterosuperior iliac spine to the pubic spine (see Figure 2.6).
- Pelvic floor: it is a system of muscles and ligaments of the abdomen that close the abdomen floor maintaining the correct position of the the bladder, vagina, uterus, etc.

2.4 Mechanics of the abdominal wall tissues

The abdominal tissue is a skeletal muscle that is cataloged as a soft tissue, from a mechanical point of view. Histologically, the abdominal muscles are composed of muscular, collagen and elastin fibres. This intertwined network of fibres is surrounded by the "ground substance" of polysaccharide type (proteoglycans), which acts as adhesive, lubricant and shock absorber (Kjaer, 2004; Loocke et al., 2008; Ito et al., 2010). Furthermore, the fascias or aponeurotic structures, that cover muscles, are essentially collagenous units in absence of muscle fibres.

Collagen fibres are responsible for the passive response of the muscle (Calvo et al., 2009; Martins et al., 2012), while muscle fibres are responsible for the active response of the muscle (Linden, 1998; Arruda et al., 2006). Specifically, the passive contribution appears in response to loads under which the muscle only provides resistance and does not contracts. However, when the muscle is stimulated by an electrical stimulus (either external or internal), muscle generates a contraction that produces an additional force. Active tension, provoked by muscle contraction, is the difference between total and

the passive stresses. Since, in general, there are two different mechanical responses in muscle, both have been addressed separately in this thesis.

Since the final goal in abdominal surgery is that the implanted prosthesis integrates into the abdominal tissue mimicking the original tissue behaviour, the study of its mechanical behaviour is essential. Its mechanical response depends on the nature and proportion of their components. Therefore, in this work we have experimentally addressed the study of the abdominal wall mechanics such that these results allow to select or define the required constitutive models for the numerical simulation.

This section is divided into two parts that describe the main concepts related to the experimental mechanical response pattern and the numerical modelling of the abdominal tissues, respectively. A state of the art of the studies described in the literature is also included.

2.4.1 Experimental mechanical characterization

Experimental tests provide information about muscle tissue behaviour (Nilsson, 1982a,b; Hwang et al., 2005; Calvo et al., 2010; Martins et al., 2010; Grasa et al., 2011; Martins et al., 2012). Specifically, experimental mechanical tests allow to establish the relation between the applied load and the tissue response. In addition, as more sophisticated computational models are developed, new experimental tests are required to validate these models.

To mechanically characterize the passive response of skeletal muscles in the short term, the most common experimental tests are uniaxial (Nilsson, 1982a), biaxial (Hwang et al., 2005) and inflation tests (Song et al., 2006b), while cyclic tests are used to determine the response in the long term.

Since the clinical application that this thesis aims to study is hernia surgery in humans, the human tissue should be characterized to reproduce the real behaviour of abdominal tissues. However, the obtention of human samples, which assure the desirable repeatability, is not always possible since the control of factors such as the type of feed, the movement restriction, the type and level of physical training, etc. is not possible. To solve this problems, animal models are used. Thus, there are some studies in the literature that use experimental animal studies such as dogs (Hwang et al., 2005), cats (Sandercock, 2003), pigs (Loocke et al., 2008), rabbits (Davis et al., 2003), rats (Grover et al., 2007), etc.

The passive mechanical behaviour pattern is given by a nonlinear response in large deformations to physiological loads (Calvo et al., 2010; Hodgson et al., 2012; Martins

et al., 2012). This nonlinear behaviour has been attributed to the wavy pattern of the collagen and elastin fibrils; at low load levels large displacements are obtained, since the fibre winding is easy to undo, and at high load levels tissues stiffen notably, since straightened fibres stretch elastically until failure. The preferential direction of muscular and collagen fibres addresses an anisotropic mechanical response (Hwang et al., 2005). Furthermore, the high water content in these tissues, next to 70%, provide a practically incompressible behaviour. Other feature of muscular tissues, similar to the rest of soft tissues, is that they are subjected to residual stresses due to the growth process from the embryonic stage to adulthood (Fung, 1993; Peña et al., 2006; Lanchares et al., 2008). These residual stresses are revealed when making a cut on a tissue free of external load. After this cut, there is a change in the equilibrium configuration due to the release of such residual stresses. This distribution is three-dimensional and its direct measurement is complex and impossible to perform *"in vivo"*. The determination of these initial deformations is very important due to the nonlinear behaviour of soft biological tissues (Fung, 1993; Gardiner et al., 2001; Peña et al., 2006). Furthermore, the muscle tissue shows a viscoelastic behaviour (relaxation and/or creep) which is attributed to the tangential interaction of collagen and muscle fibres with the matrix of proteoglycan (viscous lubricant between collagen fibres) (Loocke et al., 2008, 2009). This effect is observed when the tissue is stressed to a certain level and then is unloaded, causing a hysteresis. Also, if the tissue is deformed to a certain value and, next, this deformation remains constant, it is observed that, over time, the tension relaxes from the equilibrium initial stress. The reason of preconditioning in experimental tests resides in the viscoelastic nature of these tissues and the changes that take place in the structure during the first cycles. After a certain number of cycles, equilibrium is reached. Lastly, muscle tissue has the ability to change its structure depending on the environment and mechanical, biological or chemical stimuli that surround it (Taber, 1995). Growth occurs when there are changes in the mass and/or volume of muscle cells and the extracellular matrix and remodelling occurs when a modification of the microstructure, without changing its size and shape, is produced.

Regarding the active mechanical response of muscular tissues, active force is produced during activation or muscle contraction (Bol and Reese, 2008; Stålhand et al., 2010; Ramírez-Martínez, 2011). The mechanism of muscular contraction begins when a nerve impulse from the motor nerve reaches the neuromuscular junction. Then, the potential action depolarizes the muscle fibre membrane and T-tubules. T-tubules or transverse structures are structures that exist in skeletal or cardiac muscle cells. Specifically, they are membrane invaginations that connect the sarcolemma of the muscle fibres, forming the external fibre tube. Depolarization results in increased permeability and provokes the massive exit of ions $Ca2+$ from the endoplasmic reticulum to the inside of the cell, joining to troponin C. This union causes a change in the other components of the troponin complex, i.e, troponin I and troponin T. The change in troponin T causes a displacement of the tropomyosin and union sites between actin and myosin re-

main free. The liberalized energy produces the overlap between actin, or thin filaments, and myosin, or thick filaments, so sarcomere shortening and contraction occur. Experimentally in the laboratory, muscle activation is usually given by an external direct electric activation on the nerve or through the immersion of the tissue in calcium baths at different concentrations (see Figure 2.14). Activation tends to shorten the muscle. However, depending on the subject will or the relation between external resistances, three types or action exist (see Figure 2.15): shortening or concentric contraction when the developed force is able to move the external load, stretching or dynamic eccentric action when the external load is higher than the developed force and isometric action when muscular force is equivalent to the external load.

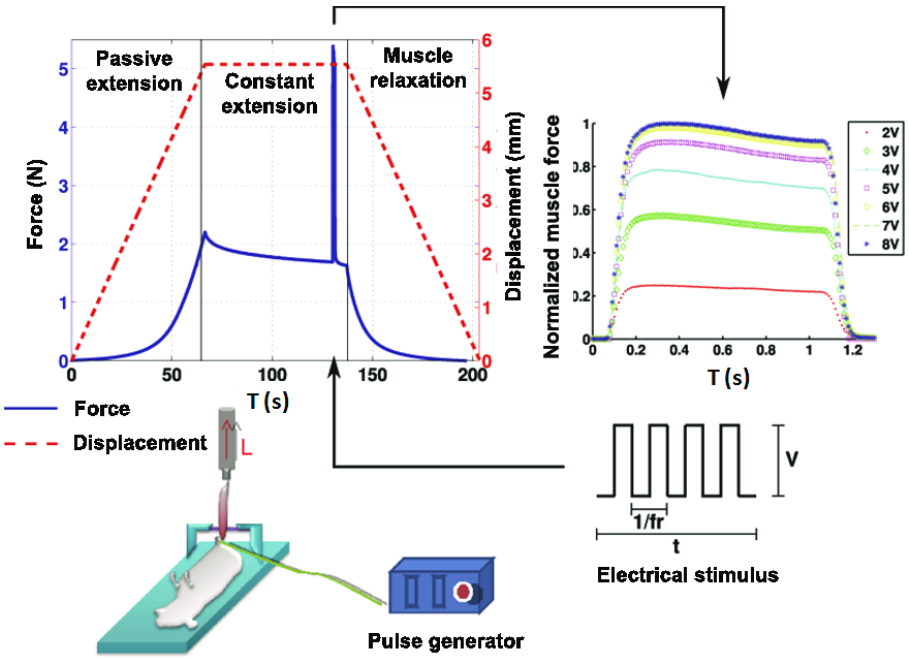

Figure 2.14: Active and passive force (N) of the muscle and displacement (mm) that appears depending on the electrical stimulus.

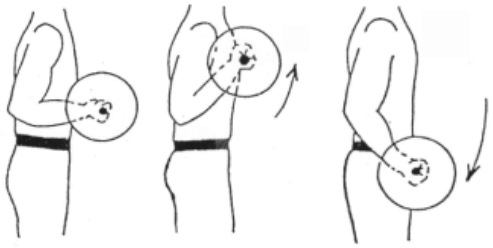

(a) (b) (c)

Figure 2.15: Types of muscular action: isometric (a), concentric (b) and eccentric (c).

Active force that a muscle can develop depends on different factors. The most

important ones are the length, the velocity and the excitation signal (Ramírez et al., 2010). Next, these factors are briefly described:

(a) Force-length relation.

Active force is developed due to the sliding of the actin filaments over myosin filaments, allowing Z-lines to get closer. Z-lines are the lines delimiting the functional unit of the muscle cell, the sarcomere. The energy needed in this process is obtained from the cross-bridges cycle, defined as the number of active points that are interacting between actin and myosin. Therefore, the level of muscle force depends on the number of free active cross-bridges. Specifically, the more number of cross-bridges, the more force developed. If sarcomere length varies, the overlap between actin and myosin changes, provoking changes in the number of actives places where actin filaments may contact with myosin ones. Thus, muscle force depends on the sarcomere length and on the number of cross-bridges (Huxley, 1966; Enoka, 2002; González-Badillo and Ribas, 2002) (see Figure 2.16.a). Indeed, there is an optimum length in at which muscle exerts the maximum force.

(b) Force-velocity relation.

Active force exerted by the muscle also depends on the contraction velocity of the muscle (see Figure 2.16.b). Velocity at which muscle shortens depends on the external load. The higher the load, the higher the force the muscle has to develop. Consequently, the velocity at which muscle shortens is lower. During concentric movements, the development of maximal force decreases progressively at higher velocities (when a heavy object is lifted, the movement is driven slowly, maximizing the exerted force).

(c) Force-excitation signal relation.

Muscle activation may be developed voluntary by means of a neuronal signal, or artificially, for example, using an electrode in contact with the nerve. With the artificial stimulation, the features of the input signal to the system are known. Therefore, intensity, voltage, frequency and time of stimuli can be controlled. During the stimulus, motoneurons are activated depending on whether the signal exceeds the threshold of

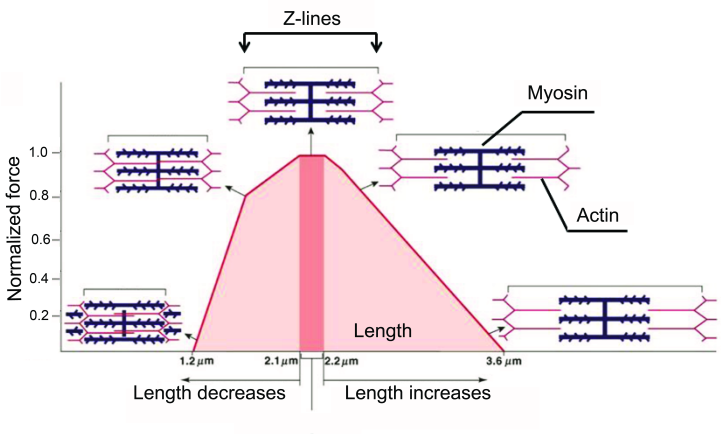

(a)

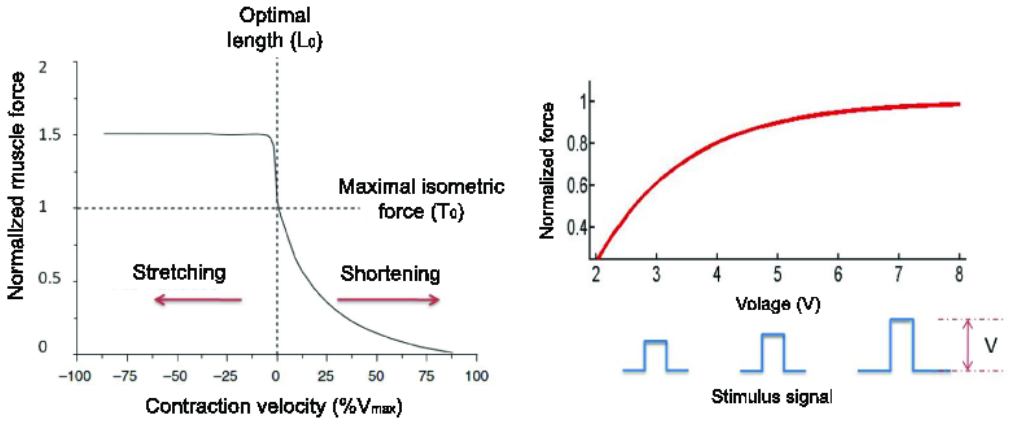

(b) (c)

Figure 2.16: Relation between active force and length (a), velocity (b) and excitation signal (c).

recruitment. Active force increases as the voltage increases (see Figure 2.16.c)

Having the main concepts of the experimental mechanical response pattern of muscle skeletal tissues described, a state of the art of the existing work in the literature regarding the experimental passive (Section 2.4.1.1) and active (Section 2.4.1.2) characterization of abdominal muscular tissue is introduced.

2.4.1.1 Passive behaviour. State of the art

In the literature there are several works that study the passive mechanical response of the abdominal muscles using animal or human experimentation and are focussed on the study of different muscles and fascias.

The majority of the studies in the literature about animal experimentation use uniaxial (Nilsson, 1982a,b; Gajdosik, 2001; Hwang et al., 2005) and compression (Loocke et al., 2004) tensile tests. There are also studies showing biaxial test protocols (Hwang et al., 2005), which agree more with the real behaviour of abdominal structures, and punching tests (Junge et al., 2001; Podwojewski et al., 2012). Nilsson (1982a,b) proved, performing tests on rabbits, that the passive mechanical behaviour of abdominal tissue is different in each zone of the abdomen. This evidence happens due to the fact that different muscles are located in each zone of the abdomen, and each of these muscles have its own fibre arrangement. Nilsson (1982b) found that the size of muscle samples influences the response and this fact was justified since the number of fibres in small samples that are clamped are higher than in longer samples. Results are presented in forces and displacements so, due to the lack of geometrical data of samples, these results can not be extrapolated to stresses, which are needed in our problem. Hwang et al. (2005) developed a comparative study between the internal oblique and transversus muscle through uniaxial and biaxial tests using abdominal tissue taken from dogs. These authors were focussed on analyzing differences on the passive behaviour of muscles studied all together and separately. Furthermore, the differences on the passive mechanical response along muscular direction, and perpendicularly, were studied. The main conclusions of this study indicated that the mechanical response is anisotropic and stiffer along the perpendicular direction of the muscular fibres than along them. Finally, Hwang et al. (2005) showed a less pronounced anisotropy in the muscles studied as a composite due to the presence of the extracellular connective tissue (Huijing, 1997) that allows to transmit forces through muscular layers.

Although the obtention of human tissue samples is difficult, there are some experimental studies that characterize the human abdominal wall response by means of *"in vivo"* and *"in vitro"* tests. Song et al. (2006a,b) studied the mechanical response of the abdominal wall through inflation tests in *"in vivo"* laparoscopic surgery. This surgical procedure is based on the inflation of the abdominal cavity and offers the possibility of measuring mechanical properties of the abdominal wall. These authors concluded that the abdomen is stiffer in the transversal plane than in the craneo-caudal one. Furthermore, Song et al. (2006b) justified this finding due to the different arrangement of muscular fibres in the abdomen.

Recently, inverse analysis methods have been applied to obtain the displacements of each point of interest by means of image processing. Szymczak et al. (2012) determined strains in the human abdomen using images. Smietanski et al. (2012) examined the behaviour of the abdomen front and their study aimed at describing the *"in vivo"* elasticity. The deformation of the abdomen was determined and these values were correlated with the stretch that the prosthesis can suffer and the stretch that can cause the failure of the tissue-mesh union.

Recent studies focussed on the study of the elasticity of the abdominal wall detect differences in tissue mechanical response between men and women (Junge et al., 2001). Junge et al. (2001) performed experimental punching tests indicating that the abdominal wall behaviour in one direction can not be extrapolated to the global response of the abdominal wall.

The architecture of the linea alba has been proposed by several authors (Rizk, 1980; Askar, 1977; Axer et al., 2001a,b). Specifically, models proposed by Rizk (1980) and Askar (1977) define six aponeurotic layers arranged obliquely in the linea alba, and they define this anatomical structure as a line where fibres end. Axer et al. (2001a,b) developed a detailed study about the fibre distribution on the linea alba and rectus sheaths. A new model of fibre architecture on the linea alba was proposed in that study (Axer et al., 2001a). Fibres were defined as a continuity through the linea alba and gender was considered as a factor that can cause differences on the fibre arrangement (Axer et al., 2001b). Considering these studies, Grassel et al. (2005) conducted a study to analyze the different proposals of fibre arrangement in the linea alba. Their results can not be directly extrapolated to the young people, but agree with the model proposed previously by Axer et al. (2001a).

The literature on experimental characterization of abdominal tissue includes other studies focussed on the mechanical response of the linea alba. The linea alba, like most soft tissues, shows a nonlinear elastic response. Rath et al. (1996) performed a biomechanical study of the linea alba to study its morphology and mechanical parameters such as resistance, strain and elasticity and observed that subumbilical region is more flexible that supraumbilical one. Konerding et al. (2011a) computed stresses generated on the supraumbilicar area of human cadavers after different intraabdominal pressures. For that purpose, Konerding et al. (2011a) performed tests where a balloon was inserted inside the abdominal cavity and, posteriorly, changed the intraabdominal pressure. Longitudinal stresses were not addressed since biomechanical studies on the linea alba point to the predominant role of transversally acting stress in incisional hernia formation (Klinge et al., 1998; Junge et al., 2001; Grassel et al., 2005; Song et al., 2006a).

The works published by Kirilova et al. (2009) and (Kirilova et al., 2010) were focussed on the study of the viscoelastic properties of *"in vitro"* human abdominal fascia through uniaxial tests. These authors studied the influence of direction and placement of the samples. Their conclusions showed that placement influences the viscoelastic response of the tissue. Kureshi et al. (2008) correlated the properties of non herniated and herniated transversalis fascia in experimental tests on *"in vitro"* human samples. Their protocol was based on the analysis of the mechanical response and collagen images from both tissues. Their findings proved that hernia damage and posterior tissue remodelling do not alter significantly transversalis fascia properties. Finally, a recent

study characterized the mechanical behaviour, by means of uniaxial tests, and modelled the damage process that occurs in the anterior rectus sheath along two directions (Martins et al., 2012). That study developed uniaxial tests along and perpendicularly to collagen fibres.

Considering the existing works about abdominal tissue, none of them provide information about initial strains that appear after obtaining samples from the experimental model. Furthermore, there is no complete characterization of all muscles in the same specimen. In addition, some data do not consider the thickness of the samples despite its importance in the stress obtention. Since existing works in the literature do not provide enough data, this thesis addresses the experimental characterization of the passive response of the abdominal wall in an animal model widely used in the literature, such as the New Zealand white rabbit (Nilsson, 1982a,b; García-Moreno, 2001; LeBlanc et al., 2002; Johnson et al., 2004; Judge et al., 2007; Pascual et al., 2008).

2.4.1.2 Active behaviour. State of the art

To the author's knowledge, there is no experimental studies that characterize the active response of the abdominal muscle tissue. However, the active mechanical response of other muscular tissues has been addressed in numerous studies in the literature, in other skeletal muscles from animals such as frogs (Hill, 1938; Ramsey and Street, 1940; Abbot and Wilkle, 1953; Huxley and Niedergerke, 1954) or rats (Ramírez et al., 2010) and also in humans (Maganaris and Paul, 1999; Arampatzis et al., 2005).

Hill (1938) was the first to experimentally determine the relationship between force and velocity of frog muscle shortening. His studies found that the velocity at which the muscle is shortened depends on the load that is applied. Thus, Hill (1938) obtained the force-velocity curve by applying different loads. When the load is maintained constant, contractions are denoted as isotonic. When the velocity of contraction is maintained constant, contractions are denoted as isokinetic. The force-velocity relationship was also described when muscle lengthens (Katz, 1939).

Regarding the dependency between the force exerted by the muscle and its length, several studies have obtained the force-length curve from data obtained in experimental contraction tests, developed for different muscle lengths and under isometric conditions (Ramsey and Street, 1940; Abbot and Wilkle, 1953). These studies demonstrate that the isometric force of frog muscle reaches a maximum value at a certain length, called optimal length. However, it must be considered that the characteristics of the force-length relationship are not constant for all test conditions (Huijing, 1998).

A few years later, in 1954, two published studies suggested that muscle contraction

is due to the interaction of actin and myosin filaments when one slides over the other (Huxley and Hanson, 1954; Huxley and Niedergerke, 1954). The force generated by the cross bridges generates the sliding filament (Huxley, 1957). This theory is considered as the most important with regard to the muscular active response and justifies the relationships between force, length and velocity. Specifically, Gordon et al. (1966) showed experimentally that the force-length relationship under isometric conditions of a fully activated sarcomere is related to the overlap of the actin and myosin filaments. The number of available cross bridges which can generate force depends on the overlap. Moreover, the contraction velocity depends on the formation ratio and disappearance of cross bridges (Huxley, 1957).

In general, to quantify the behaviour of muscle tendon unit, experiments were developed on the *"in vitro"* tendon (Colomo et al., 1997; Ciarletta et al., 2006), on the entire muscle (Davis et al., 2003; Grover et al., 2007; Ramírez et al., 2010; Grasa et al., 2011) and on muscle fibres (Konishi and Watanabe, 1998). Moreover, other studies on the literature provide the characterization of the active response in *"in vivo"* muscle models (Grover et al., 2007; Ramírez et al., 2010).

The development of observation techniques allows to quantify mechanical properties on human muscular contraction. For example, ultrasound is a technique that is used to visualize tissue located superficially under the body, rich of collagen, such as muscles, tendons or ligaments (Maganaris and Paul, 1999). It is used within a noninvasive medical protocol which measures the deformation and the cross section of the tissue in different positions of flexion and extension, while the articular moment is measured by an isokinetic dynamometer (Maganaris and Paul, 1999; Arampatzis et al., 2005).

A frequently used technique in the laboratory is the nerve stimulation by an electrical impulse that generates muscle contraction (Ramírez et al., 2010). This methodology is possible when there is a nerve that can be isolated from the rest of the muscle to perform the experiments, such as in fusiform muscles. However, in other muscles, such as the abdominal tissue, muscle activation has to be enforced through the immersion of the tissue in an ionic bath. With respect to the development of this thesis, the experimental characterization of the active response of the abdominal wall has not been performed since it is not within the scope of this thesis. However, nowadays, the experimental protocol is being established as part of another doctoral thesis. Therefore, data from the literature that address the active mechanical response of the tibialis anterior rat muscle have been considered (Ramírez et al., 2010). These data were obtained depending on muscle length, voltage and excitation signal.

2.4.2 Numerical modelling

Finite element simulation, within the biomechanic field, aims to evaluate approximately stresses and deformations to physiological or non-physiological load conditions using any geometry whose analytical solution is not possible to obtain. This methodology has been widely used in the literature to simulate different organs and structures: muscle skeletal tissue (Lemos, 2001), abdominal muscles (Smietanski et al., 2012), cartilage (Palomar and Doblaré, 2006), vena cava tissue (Alastrué et al., 2008), etc. For that purpose, the geometry of the study, the constitutive model, the material properties, the boundary conditions and loads have be defined.

The experimental characterization of tissues provides information which is used in the development and fitting of constitutive models that reproduce the mechanical response of the tissues (Fung, 1993; Weiss, 1994; Holzapfel, 2006; Calvo et al., 2010; Peña et al., 2010; Grasa et al., 2011). Constitutive models have to reproduce the behaviour patterns observed in soft tissues, such as the non linear response in large deformations (Lemos, 2001; Holzapfel and Ogden, 2009; Calvo et al., 2010; Martins et al., 2010; Grasa et al., 2011; Martins et al., 2012), the incompressibility of the material due to the high water content (Alastrué et al., 2008; Peña et al., 2010), the anisotropy given by the preferential arrangement of collagen and muscular fibres (Linden, 1998; Arruda et al., 2006) and the presence of residual stresses (Peña et al., 2006, 2007).

Nowadays, it is accepted that an anisotropic hyperelastic lagrangian formulation is capable of reproducing the elastic behaviour of this kind of tissues, which is the usual behaviour under physiological loads (Holzapfel et al., 2000). The mechanical behaviour of soft tissues is modelled by means of the definition of a strain energy function expressed as a function of cinematic invariants (Spencer, 1971). Since the muscle supports stresses, whose origin may be due to active or passive responses, muscular tissue behaviour is modelled numerically as the addition of both contributions (Martins et al., 1998; Fernandez and Pandy, 2006; Bol and Reese, 2008; Stålhand et al., 2008; Ito et al., 2010; Stålhand et al., 2010).

The passive response of soft tissues is given by the contribution of the isotropic and anisotropic responses. Specifically, models can be classified in *"phenomenological"* models (Fung et al., 1979; Humphrey and Na, 2002), defined as those which only reproduce the mechanical response without considering physical phenomena associated to the tissue, and *"structural"* models, expressed according to the physical composition of the tissue. Structural models can be also classified in two types of models: *"microstructural"*, where anisotropy is considered from the microstructure, and, generally, through an orientation density function that homogenize the behaviour at the macroscopic level (Lanir, 1979; Arruda and Boyce, 1993; Caner and Carol, 2006), and *"macrostructural"*,

where the direction of anisotropy is introduced explicitly (Mooney, 1940; Demiray, 1972; Demiray et al., 1988; Arruda and Boyce, 1993; Yeoh, 1993; Holzapfel, 2000; Holzapfel et al., 2005; Calvo et al., 2009).

Next, Sections 2.4.2.1 and 2.4.2.2 include a summary of some of the existing works in the literature related to the numerical characterization of the passive and active responses of the muscular tissue, respectively.

2.4.2.1 Passive behaviour. State of the art

Literature related to the numerical modelling of the passive response of soft tissues is very broad (Demiray et al., 1988; Weiss et al., 1996; Holzapfel et al., 2000; Lemos, 2001; Holzapfel, 2006; Holzapfel and Ogden, 2009; Calvo et al., 2010; Martins et al., 2010; Peña et al., 2010; Grasa et al., 2011). However, studies focussed on the abdominal muscles are limited.

The modelling of the passive behaviour of muscular tissue has been addressed at both, microscopic (Sharafi and Blemker, 2010) and macroscopic (Hodgson et al., 2012; Martins et al., 2012) levels. There are formulations that model the behaviour through linear (Boriek et al., 2000) and nonlinear (Van Loocke et al., 2006) models. Furthermore, the behaviour in large deformations shown by muscular tissues is reported in some numerical studies (Hodgson et al., 2012; Martins et al., 2012). Specifically, Hodgson et al. (2012) analyzed the quality of the numerical fitting using four strain energy functions and validated the study with experimental studies performed on the tibialis anterior rat muscle. The same experimental animal model was used by Ito et al. (2010) to validate its constitutive model that describe the anisotropy, viscoelasticity and muscle tissue damage in the skeletal muscle. Odegard et al. (2008) proposed a numerical model to predict the mechanical response of the skeletal muscle tissue but it was not experimentally validated.

Regarding the abdominal muscle, the computational modelling has been performed from a macroscopic standpoint (Song et al., 2006a; Szymczak et al., 2009; Smietanski et al., 2012; Szymczak et al., 2012; Martins et al., 2012; Förstemann et al., 2011). Martins et al. (2012) modelled the passive behaviour of the aponeurotic projection of the rectus abdominis within the nonlinear hyperelasticity in large deformations. Furthermore, Song et al. (2006a) studied the response of the human abdomen through inflation tests and modelled numerically its behaviour using Laplace's equation to obtain the relation between inflation pressure and radius of curvature of the abdominal surface. In posterior studies, López-Cano et al. (2007) proposed a three dimensional dynamic model to simulate the behaviour of the inguinal region to physiological loads.

Regarding the human abdomen, Song et al. (2006a) defined a three dimensional model of the human abdominal wall based on a *"in vivo"* human experimental model. Specifically, tgus model allowed to simulate and analyze the pattern of movement in laparoscopic surgery where an intraabdominal pressure is applied into the abdominal cavity and then the cavity inflates. Posteriorly, Förstemann et al. (2011) defined the geometry of the abdomen front from magnetic resonance imaging, performed uniaxial tests on samples from the linea alba and correlated the results obtained with the computational model, that considered an small deformation approach and used Laplace's equation. Furthermore, these authors established a relationship between uniaxial and biaxial stresses. In a recent study, Szymczak et al. (2012) obtained the mechanical properties of the human abdomen by means of the inverse analysis method and analyzed where maximal deformations in the abdomen appear.

This thesis addresses the numerical modelling of the passive response of the abdominal wall, since no numerical works describing its response within the framework of the nonlinear anisotropic hyperelasticity were found. In addition, no model in the literature defines a complete model of the abdomen, so this thesis describe a model of the abdomen that differentiates the main anatomical structures.

2.4.2.2 Active behaviour. State of the art

As previously introduced, there are no previous works focussed on the numerical simulation of the active response of abdominal tissues. Therefore, this thesis proposes a numerical model to reproduce the active response of the abdomen. However, since the appearance of the first studies addressing the active response of the other muscles, numerous studies have been developed to include improvements. In general, models are grouped into four groups: the Hill model (Hill, 1938), the Huxley or cross bridges model (Huxley, 1957), morphological models (Huijing and Woittiez, 1984; Woittiez et al., 1984) and morpho-mechanical models (Hunter and McCulloch, 1988; Martins et al., 1998).

The model developed by Hill (1938), which has been widely used and is based on experimental observations, consists of a contractile element arranged in series with a spring. The contractile element represents the contraction mechanism while the spring represents the passive contribution of the tendon and fascia. Finally, a third element is added in parallel and takes account the passive muscle properties (Hatze, 1981).

The dynamics of the cross bridges is taken into account in the model proposed by Huxley (1957). This model was developed based on experimental tests that determine the force-velocity relationship. Other models which are based on the Huxley model and analyze the active response in more detail are those published by Hill et al. (1975), Eisenberg et al. (1980), Ma and Zahalak (1987) and Zahalak (1981).

Morphological models take into account the morphologic characteristics of muscles such as the fibre length and the angle of the aponeurosis (Huijing and Woittiez, 1984; Woittiez et al., 1984; Otten, 1988; Leeuwen and Spoor, 1992, 1996). Regarding pennated muscles, these models take into account the angle of the fibres with respect to the of action line of force. The incompressibility is taken into account in the planimetric model (Huijing and Woittiez, 1984) and in the corresponding three dimensional model (Woittiez et al., 1984). Other models assure that the consideration of the geometry to really understand the amount of force exerted by the muscle is essential (Otten, 1988; Leeuwen and Spoor, 1992, 1996).

In the literature, there are studies that propose morpho-mechanical models based on the muscle mechanics and that develop finite element models applied to different muscular tissues (Hunter and McCulloch, 1988; McCullock et al., 1992; Martins et al., 1998). The potentiality of these models allows to take into account not only the geometrical properties of the muscle, but also the material properties.

Recent studies incorporate the modelling of the active and passive response simultaneously (Stålhand et al., 2008; Ito et al., 2010; Stålhand et al., 2010; Bol et al., 2011). Generally, numerical models proposed in the literature are validated with experimental tests in skeletal muscles (Jenkyn et al., 2002; Fortuny et al., 2009a; Chi et al., 2010; Ito et al., 2010; Ramírez et al., 2010; Bol et al., 2011; Grasa et al., 2011; Hodgson et al., 2012) and smooth muscles (Stålhand et al., 2008, 2010). However, some studies that propose numerical models to characterize the active response are not validated, thus limiting their applicability (Bol and Reese, 2008; Odegard et al., 2008; Fortuny et al., 2009b).

2.5 Prostheses in hernia reconstruction

Nowadays, different types of prostheses or synthetic meshes exist. This section describes the fundamental concepts related to the study of these prostheses, which allow to establish classifications depending on different criteria. In addition, a bibliographic review about some of the existing works in the literature related to the experimental characterization and numerical simulation of these prostheses is presented.

Different classifications can be established according to the geometric structure, the material composition of the prostheses and porosity, since they are the determinant factors in their final behaviour (Rosch et al., 2004; Bellón et al., 2009). Theses features determine the flexibility and type of response, isotropic or anisotropic. Since the abdomen is anisotropic (Hwang et al., 2005), the placement of the mesh on the abdomen is an influent factor in the final result of hernia surgery.

According to the geometry or the weaving of threads of the mesh, prostheses can be classified into reticular, laminar and composite prostheses (see Figures 2.17, 2.18 and 2.19), and different materials are used in these designs. Reticular meshes can be divided into non absorbable, partially absorbable and totally absorbable. In these meshes, filaments are also classified into monofilament and multifilaments. Furthermore, laminar meshes can be non absorbable or absorbable. Lastly, composite prostheses can be designed in two ways: they are formed by a non absorbable component and a physical barrier (different non absorbable component) or they are formed by a non absorbable component and a chemical barrier (absorbable component) (see Figures 2.19 and 2.20). In addition, these subgroups are differentiated according to the material composition.

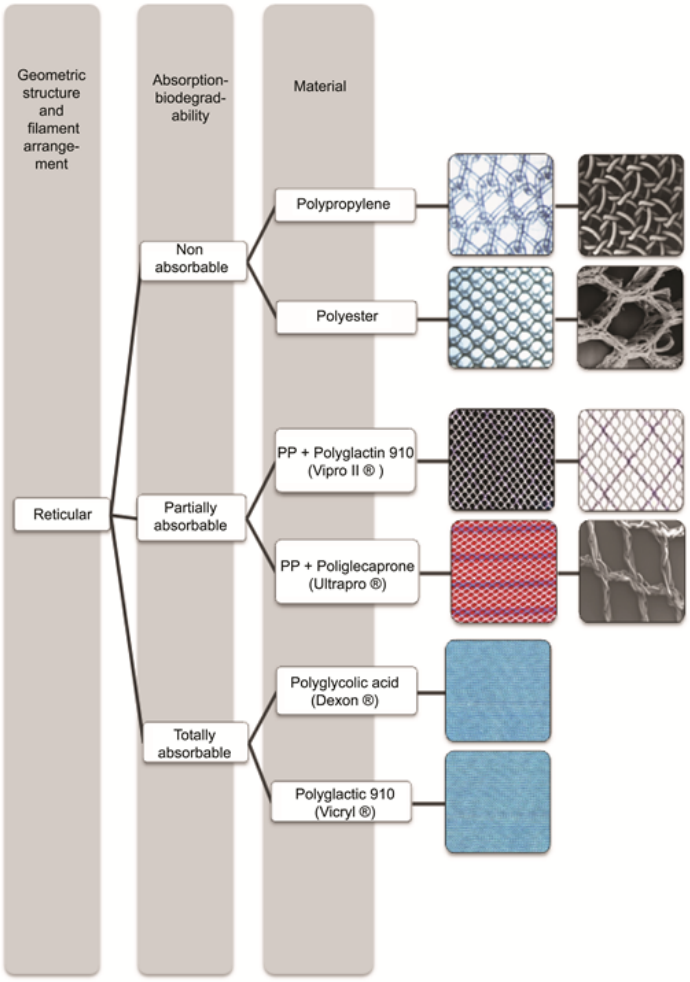

Figure 2.17: Classification of reticular synthetic meshes.

According to porosity, prostheses are classified into high or low weight, depending on the density parameter g/m^2 that characterizes them (Klinge, 2007). Specifically, *"heavyweight"* (HW) and *"lightweight* (LW) meshes have a density above 80 g/m^2 and below 50 g/m^2, respectively. A third type or *"mediumweight"* (MW) mesh has a density

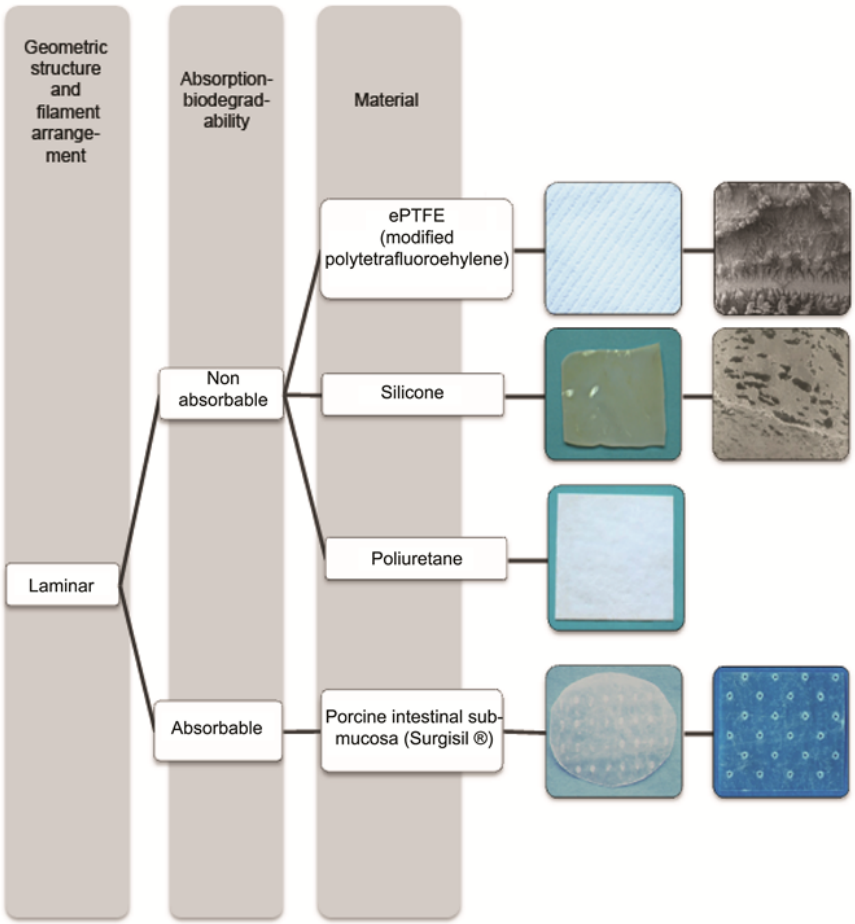

Figure 2.18: Classification of laminar synthetic meshes.

between 50 and 80 g/m^2 (Cobb et al., 2006). Some classifications even consider another type of meshes, denoted by *"ultralightweight"* (ULW), whose density is below 35 g/m^2 (Earle and Mark, 2008).

It is important to note that, prosthetic mesh density is, sometimes, independent on the pore size. Some designs, despite their small pore size are classified as LW since they are composed of a loosely woven monofilament that confers them a low density. This aspect is important since, according to the german school (Schumepelick and Klinge, 2003), pore size is considered the main parameter to consider a mesh as HW or LW. In that sense, HW and LW prosthesis would have a small and large pore size design, respectively.

Next, a bibliographic review of the existing works in the literature related to the experimental characterization (Subsection 2.5.1) and computational modelling (Subsection 2.5.2) of prostheses is included. Although the diversity of studies in the litera-

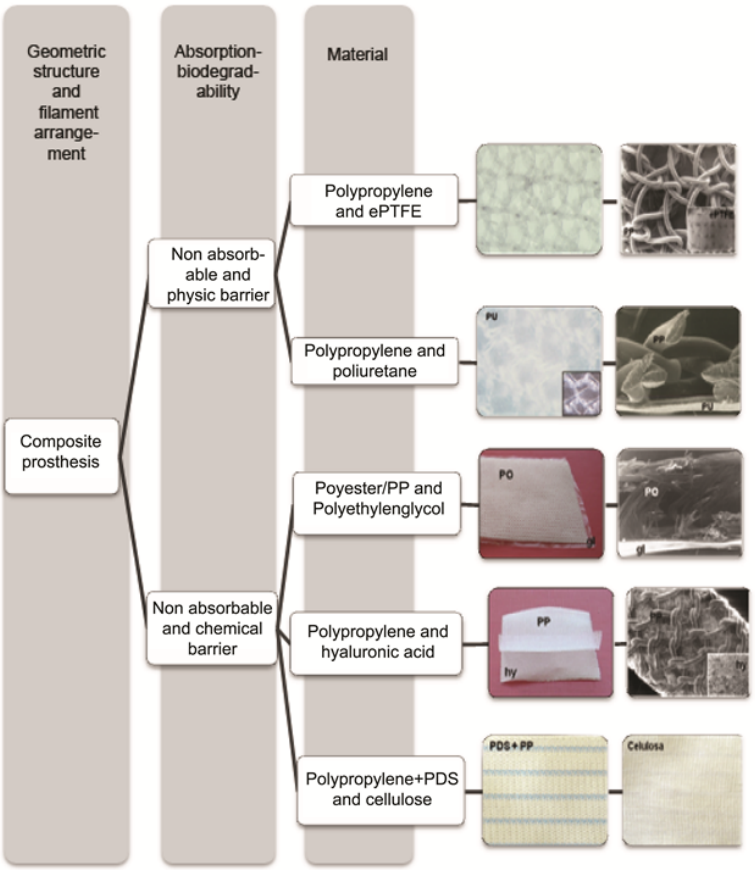

Figure 2.19: Classification of composite synthetic meshes.

ture, no jobs that consider simultaneously experimental and computational aspects are found. Therefore, there is no complete study that evaluates the experimental mechanical response of a surgical mesh and models numerically its behaviour. This thesis addresses both aspects, the experimental mechanical characterization and computational modelling of three representative synthetic meshes; specifically, Surgipro®, which is a polypropylene heavyweight mesh, Optilene®, which is a polypropylene lightweight mesh and Infinit®, which is a polytetrafluorethylene mediumweight mesh.

2.5.1 Experimental mechanical characterization. State of the art

The main goal of the experimental characterization of prostheses used in hernia surgery is the determination of their mechanical properties (Afonso et al., 2008; Bellón, 2009; Saberski et al., 2010; Deeken et al., 2011). Numerous studies whose objective is the determination of the mechanical properties of prostheses can be found in the literature. Saberski et al. (2010) compared the anisotropic properties of different commercial

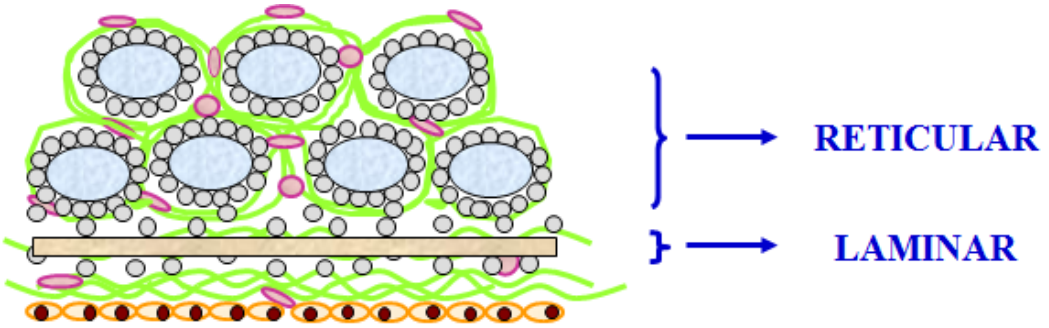

Figure 2.20: Transversal scheme of a composite mesh (Bellón, 2012).

meshes used in hernia surgery. Specifically, Trelex®, ProLite^{TM}®, Ultrapro^{TM}®, Parietex^{TM}®, Dualmesh® and Infinit® were studied and a high anisotropic response was found in all of them. Afonso et al. (2008) performed uniaxial and tape ring tests and observed significant differences in the mechanical response of the prostheses Aris^{TM}®, TVTO^{TM}®, Auto Suture^{TM}®, Uretex^{TM}® and Avaulta^{TM}®. Furthermore, Yoder and Elliott (2010) developed an study to measure mechanical properties of four different prostheses: Alloderm®, Restore®, CuffPatch® and OrthADAPT®. In this work, anisotropy and non linearity of the materials were evaluated with the aim of understanding the mechanical properties through uniaxial tests. Their conclusions indicated that the type of mesh has to be chosen depending on the type of hernia repair.

Hollinsky et al. (2008) developed a comparative study between the biomechanical properties of lightweight and heavyweight prostheses. The main concern of this study was found in the fact that mesh size, friction coefficient and flexion stiffness are crucial aspects to avoid hernia recurrence. The experimental study included tests to determine the breaking strength and the elastic modulus of six lightweight meshes and six heavyweight meshes used in laparoscopic inguinal hernia repair. These authors concluded that stiff prostheses or well-fixed lightweight meshes, with an enough overlap, can be used in the repair of large hernias.

Other studies are focussed on the study and analysis of the behaviour of sutures, that allow the union between tissue and prosthesis, and have to be compatible with the mechanical properties of the mesh. Specifically, a breaking force of $16 - 32\ N$ is considered appropriate (Schwab et al., 2008). Although laparoscopic fixation aims at minimizing the number or recurrences after surgery, fixation systems such as suture or stapling are associated to chronic pain (Schwab et al., 2008). Kes et al. (2004) evaluated the ratio of protrusions generated after using different commercial meshes: Marlex®, Parietene®, Prolene®, Mersilene®, Parietex®, Fluoromesh® and Vypro composite®. As a conclusion, a ranking based on the best behaviour offered by the meshes, depending on the repaired defect size, was established. In addition, Kes et al.

(2004) concluded that when a large mesh is used, fixation does not add necessarily additional union since the own mesh immobilizes in its own.

Binnebösel et al. (2007) evaluated the dependence of the dislocation of the mesh with respect to the defect size, the overlap, the position of the mesh and the mesh placement in the case of anisotropic meshes. Their study led to the conclusion that an overlap of 3 cm is enough to prevent early dislocation of the prosthesis.

2.5.2 Numerical modelling. State of the art

Information obtained in the experimental characterization of synthetic meshes can be used for the development of constitutive models that are capable of reproducing the mechanical response of the prostheses. Numerical models based on nonlinear continuous formulations allows the computational simulation of the implant to physiological, multidirectional and inhomogeneous loads and, besides, allow the comparison of the mechanical behaviour of the prostheses with respect to the healthy tissue.

Apparently, the mechanical behaviour of synthetic meshes is attributed to phenomena occurring at different scales. Experimental evidences show a nonlinear response, drastic changes in the mesh due to the collapse of the pores of the mesh under uniaxial load conditions and a strong anisotropic component in some existing commercial meshes. These phenomena may be studied by analyzing the unit cell or pattern that defines, by repetition in space, the mesh weave. Also, friction between filaments of the mesh causes phenomena such as hysteresis, depending on the strain rate and irreversible deformation processes that cause significant changes in the geometry of the unit cell during load cycles.

Some studies in the literature model numerically the behaviour of prostheses considering the mesh weave. One these works was published by Kuwazuru and Yoshikawa (2004) who developed a pseudo-continuous model to analyze the behaviour of synthetic meshes from the nonlinear micromechanical properties standpoint. The constitutive law proposed by these authors for the meshes is that of a nonlinear orthotropic elastic material. Model validation was performed using a biaxial analysis.

Continuous models are more efficient and computationally easier than discrete models, because they allow its inclusion in more complex models. Although continuous models do not reproduce the individual behaviour of each filament, they contain information of the general behaviour of the mesh. King et al. (2005) proposed an approach to develop continuous models that reproduce the mechanical behaviour of the mesh with plane strain. The potentiality of this study allows to simulate the mechanical behaviour of existing prostheses and predict the behaviour of new designs once the pattern of the

mesh fabric is known. The macroscopic deformation of the mesh is associated to the structural configuration of the weave through an energy minimization method. With this method, King et al. (2005) calculated internal forces that appear in filaments of the prostheses and modelled, using the finite element method, the synthetic mesh behaviour under different loads.

Röhrnbauer et al. (2011) published a methodology to develop a two-dimensional constitutive model that characterizes numerically the mechanical behaviour of the microstructural tissue of synthetic meshes. These authors proposed two models at different scales: one develops the modelling of the prosthesis weave pattern, since it is a repeating unit, and other model, in the macroscopic level, that addresses the continuum response of the synthetic mesh.

2.6 Tissular integration process

Once abdominal surgery has been performed and the prosthesis has been implanted, the tissular integration process starts provoking the formation of new tissue on the defect area, causing a change in the properties of the whole tissue-mesh. Next, the most important terms related to the tissue integration process, that are necessary for the understanding of the thesis, are described.

After the implantation of a biomaterial, the host tissue responds producing an inflammatory reaction with cellular and biochemical response whose ultimate goal is wound healing. In addition, a series of processes begin, which are intended to isolate the implanted material by encapsulation. The tissue response depend on the nature and characteristics of the implanted material, but for a complete wound healing a correct cellular response is needed by the host tissue. Furthermore, the quality of the new tissue is given by the structure of the implanted prosthesis (Pascual et al., 2008). Bellón et al. (1996) concluded that the structure of the implanted prosthesis influences the development of the reparative process and that the porosity is the most determinant feature in wound healing.

Once implantation is performed, different inflammation phases around the biomaterial occur (García-Pumarino, 2010). Initially, polymorphonuclear leukocytes are the first cells to arrive at the site of implantation. After a transient vasoconstriction (narrowing of blood vessels), a reactive hyperemia happens (increasing of the blood flow) in small local vessels. The endothelium of these vessels becomes more permeable to the passage of proteins and plasma. At the same time, the leukocytes adhere to the surface of endothelial cells, and by diapedesis, leukocytes leave blood vessels to concentrate at the site of injury. At the first 24 to 48 hours the main function of leukocytes (especially

polymorphonuclear) is the phagocytosis of cell debris and detritus of the injured tissue.

After this first phase of leukocyte emigration (diapedesis) and lysis of granulocytes, which release acid hydrolases in the local environment, the proportion of monocyte-macrophages (immune system cells) increases. Then, an important macrophage activity begins following activation of macrophages in the extracellular medium. Macrophages play an important role in the healing process, after implantation of a biomaterial, and in its integration into the tissue where it is implanted. Thus, a change in the macrophage response might lead to abnormal wound healing processes (Leibovich and Ross, 2007). Furthermore, the release of various growth factors, which stimulate the migration of fibroblasts, endothelial and epithelial cells modulate the tissue repair processes (Whal et al., 1989) (see Figure 2.21).

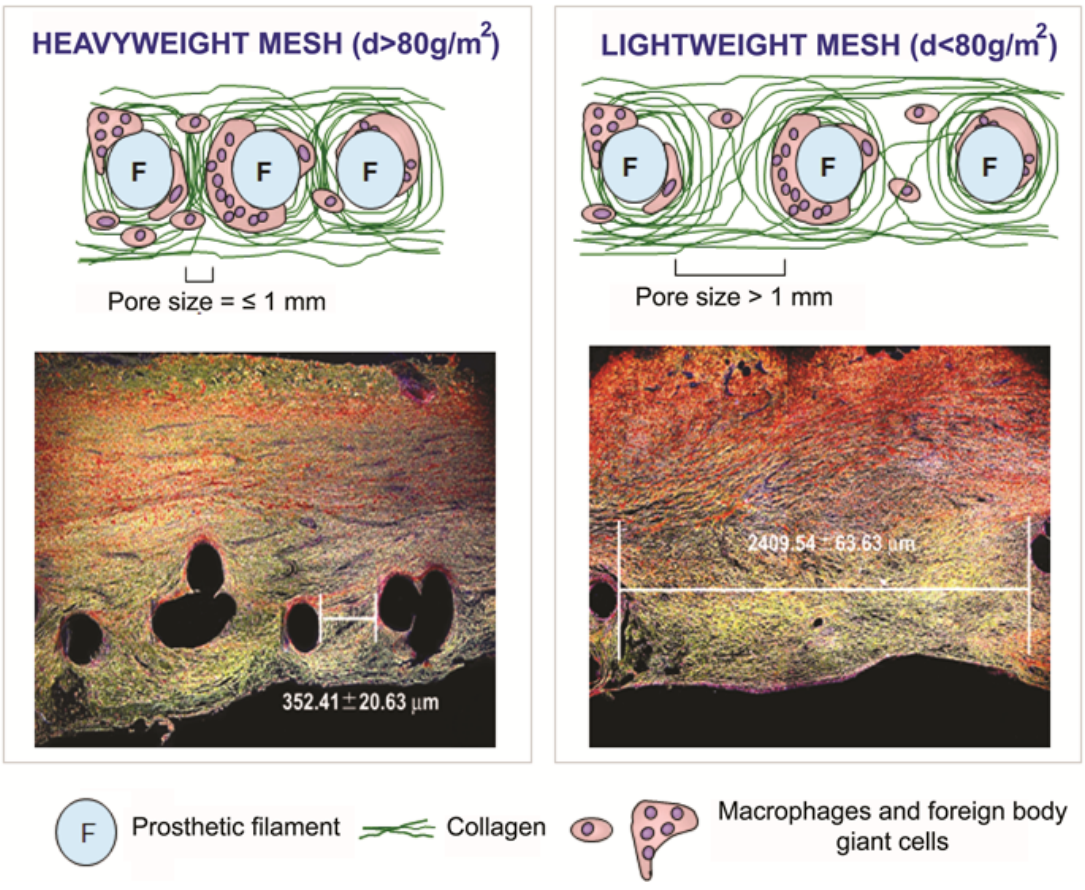

Figure 2.21: Scheme of tissular integration in reticular heavyweight and lightweight meshes. Synthetic filaments of the prosthesis (F), macrophages and collagen fibers generated in the tissue regeneration process are observed. In the images below, tissular sections from both implanted meshes. Sirius red staining where the extracellular matrix of neoformed tissue, collagen type III in yellow and red type I can be observed (Bellón, 2012).

The macrophage response assessment in implants over time allows us to know the biomaterial behaviour and tolerance by the recipient. According to the study of Bellón et al. (1995), in the abdominal wall, macrophage behaviour pattern seems to be maintained over time, and this does not depend on the physical characteristics of the prosthesis but on the chemical composition (Pascual et al., 2012c).

During certain types of chronic inflammation, and always linked to the presence of foreign material, macrophages form multinucleated giant cells by cell fusion which are called foreign body giant cells. This chronic inflammatory reaction may damage the properties of the the biomaterial.

As the cicatricial process progresses, fibroblasts begin to increase in the wound (fibroblast are the predominant cell population from the tenth day). The synthesis of collagen and extracellular matrix increases, which is essential for forming the connective tissue scar. Other cell types (platelets, lymphocytes and macrophages) synthesize growth factors that modulate the mitotic response, the displacement and the collagen synthesis by fibroblasts. In this phase, angiogenesis, which is a physiological process consisting of the formation of new blood vessels from the preexisting, acquired vital importance. Thus, new capillaries, that bring oxygen and nutrients needed for tissue synthesis activity, are originated (Border and Noble, 1994). Therefore, the formation of connective tissue around the biomaterial occurs, resulting in their encapsulation (see Figure 2.22).

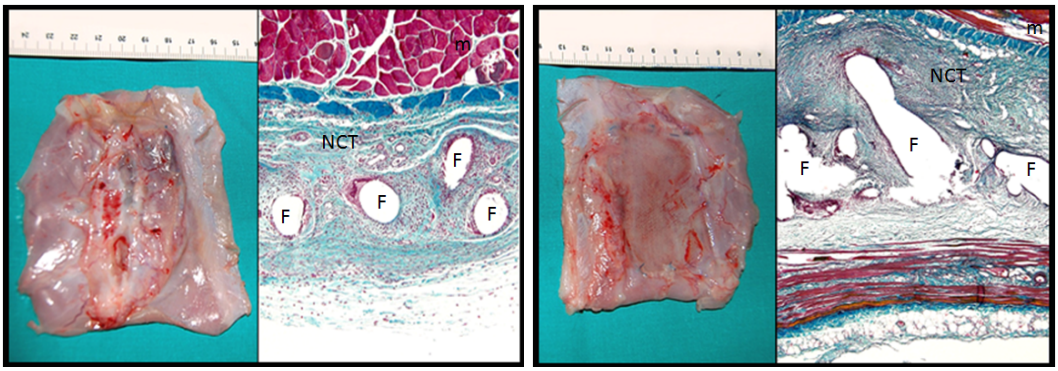

(a) (b)

Figure 2.22: Tissular integration with two prosthesis in a defect measuring 6x4 cm after 14 days after the implantation in an experimental model in rabbits. Macroscopic images on the left and light microscopy, Masson's trichrome staining, on the right (50x). (a) Surgipro® mesh. (b) Progrip® mesh (F: Filament, m: muscular tissue, NCT: neoformed connective tissue) (Bellón, 2012).

Fibroblasts play a major role in tissue remodelling processes and in the subsequent adaptation of the implant. By the fourth or fifth week the number of fibroblasts de-

creases and the main ultrastructural feature becomes collagen fibres of type III (immature collagen). At first, the arrangement of these bundles is random. In the course of time, and due to the interaction of mechanical tension forces of the tissues, collagen bundles are rearranged to better withstand the traction and become collagen type I (mature collagen). Collagen bundles, whose arrangement is not useful, suffer degradation processes due to the local action of collagenase, establishing a dynamic equilibrium between synthesis and destruction of collagen bundles.

With respect to the implanted prosthesis, the repair process provokes a shrinkage or shortening of the mesh that is reflected its size reduction (Konerding et al., 2011a).

2.7 Mechanics of the repaired tissue after tissular integration. New designs of prosthesis

The great variety of available meshes on the market and the absence of scientifically recognized established criteria that indicate which mesh is the most appropriate in each situation, make the choice of the mesh a difficult task for the surgeon (Rosch et al., 2004). Furthermore, although there are many commercial prostheses, each of them may cause a number of problems on the defect area that affect the patient after implantation. Therefore, one of the current challenges in the biomedicine field is the design of new prostheses and new biomaterials that improve the outcomes after hernia surgery (Bellón, 2009). This section describes the evolution of designs of prostheses in recent years, valued depending on repaired tissue experimental studies, whose objective is the evaluation of the final mechanical response of the whole tissue-mesh after tissue integration.

After surgery, tissue formation in the area of the defect, which causes an increase in the stiffness of the repaired tissue, is modulated depending on the implanted prosthesis, so the abdominal tissue response is different depending on the prosthesis used (Anurov et al., 2010). For this reason, the experimental characterization of the whole tissue-mesh is necessary to determine the mechanical properties of the implant site at different times after the surgery, using uniaxial tests (Hilger et al., 2006; Sergent et al., 2010) or punching tests (Konerding et al., 2011b; Podwojewski et al., 2012), between others. In addition, microscopic images provide information on the formation of collagen type III, and its subsequent conversion in collagen type I as the prosthesis is integrated in the tissue (Pascual et al., 2008). Thus, it is possible to analyze how the properties of the whole tissue-mesh over time are modified to mimic the original behaviour of healthy abdominal (Cobb et al., 2006; Pascual et al., 2008; Bellón et al., 2009).

Polypropylene, used as macroporous reticular meshes, is a very common material

used to repair abdominal hernia defects. Its use dates back historically to the last century, when Usher used it in the first hernia repairs (Usher, 1959; Usher et al., 1960). Over time, its use has been widespread in tissue/tissue repairs, including cases with infection (Antonopoulos et al., 2006; Alaedeen et al., 2007). In these cases with infection, the partial recovery of the prosthesis is possible with few materials, such as polypropylene (Bellón-Caneiro et al., 2004; Jezupors and Mihelsons, 2006). However, polypropylene has bad behaviour at the peritoneal interface, leading to complications such as bowel fistulas (Chew et al., 2000) and cavitary organ migrations (Chuback et al., 2000). Therefore, when hernia repair has to be performed on the interface, its use should be avoided. Some studies have demonstrated the biostability of polypropylene in *"in vitro"* experiments (Kapischke et al., 2005). Regarding *"in vivo"* experiments, oxidation processes have been observed in the implant area, and this process may affect the behaviour of the biomaterial due to its biodegradation. These effects were detected using scanning electron microscopy (Costello et al., 2007). Despite these evidences, the stiffness of polypropylene is not altered over time.

Prostheses have evolved to incorporate new designs that facilitate tissue integration (see Figure 2.23). One of the essential requirements any biomaterial has to satisfy is that its implantation does not cause deleterious reactions at local or systemic level. Since the surrounding environment is not static, the biomaterial should be able to cope with the changes in the host tissue in long-term (Anderson, 1988). The biocompatibility of the prosthesis is defined as the tissue response to the implantation of a foreign body. This reaction depends on the amount of implanted material, type of material, structure of the filament (monofilament or multifilament). Moreover, mesh design must consider the mechanical properties, including stiffness and breaking stress (Klinge et al., 1998). The modifications applied to the design of prostheses have been focussed on the use of other biomaterials with larger pore size.

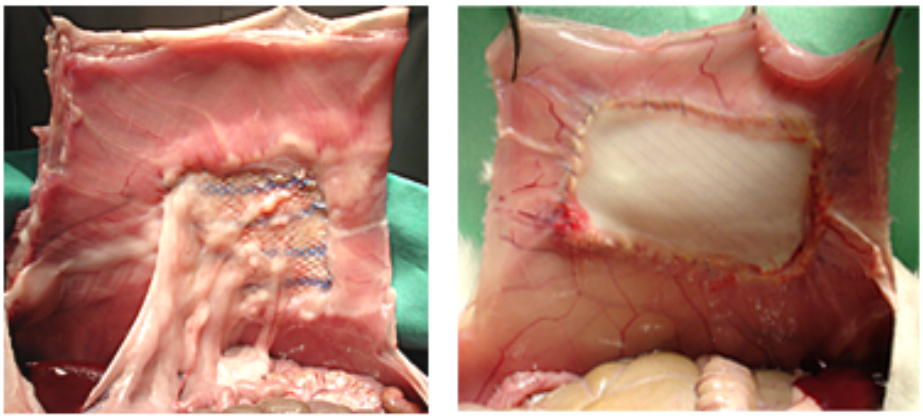

Figure 2.23: Comparison of the fibrosis generated with a reticular mesh and a laminar mesh (Bellón, 2012).

Regarding the incorporation of new biomaterials, one of the modifications undergone by reticular polypropylene meshes is the partial incorporation of auto degradable materials. These prostheses are known as partially degradable hybrid prostheses (Rosch et al., 2003; Junge et al., 2005). In other words, the classical polypropylene mesh incorporates biodegradable materials that are degraded in the medium to the long term. The advantage of these new designs is that in the medium to the long term, when the prosthesis is nearly integrated, the amount of material remaining at the implant site is less. In addition, the lesser amount of permanent material in the host tissue generates a lesser foreign body reaction after implantation and, therefore, the generated fibrosis is lower (Klinge et al., 2002a; Cobb et al., 2006). Several authors corroborate the importance of this aspect, since many patients suffer discomfort (Welty et al., 2001; Holste, 2005) due to the fact that excessive rigidity of the abdominal wall reduces its mobility (Schimidbauer et al., 2005). The work developed by Langenbach et al. (2008) analyzed the long term response of three different synthetic meshes and indicated that the composite mesh offers no advantages with respect to the physical function either regarding the pain caused to the patient. However, Hilger et al. (2006) described the histological and biomechanical properties of an implant repaired using a collagenous prosthesis after 6 and 12 weeks after implantation. They concluded that, although there is a decrease in stiffness after implantation of the prosthesis, the inflammatory reaction is lesser.

Prostheses have been also modified by designing meshes with larger pore size (Junge et al., 2002). Several recent articles have been focussed on the evaluation of the behaviour of lightweight prostheses and their advantages in the short term have been shown in some works in the literature (Conze et al., 2005; O'Dwyer et al., 2005). Specially, they are focussed on the evaluation of the integration process of the mesh into the host tissue and the biomechanical response of the whole tissue-mesh (Weyhe et al., 2006). Cobb et al. (2006) performed an experimental study on pigs after 5 months after the implant and they observed that the mechanical response was similar between lightweight and heavyweight meshes. Other study published by Bellón et al. (2007) corroborates this finding at 90 days after implantation. Furthermore, the use of lightweight prostheses provokes a lower chronic pain in patient than heavyweight meshes (O'Dwyer et al., 2005), although a higher hernia recurrence rate was observed. Some authors attribute the hernia recurrence to aspects related to the mesh fixation method (O'Dwyer et al., 2005) whereas others report mesh failure in its central part (Lintin and Kingsnorth, 2012). Lightweight and heavyweight meshes have been compared in the work published by Klinge et al. (2002b). Their findings assure that both types of meshes generate inflammatory reaction in the defect area. However, it is remarked that lightweight meshes exhibit better tissue integration and that the pore size is a very important factor regarding the incorporation process of the prosthesis (Bellón et al., 1996).

Among the different commercial meshes, some of them exhibit an anisotropic mechanical behaviour (Yoder and Elliott, 2010). In these cases, once the mesh is inte-

grated into the host tissue, the resulting mechanical response of the whole tissue-mesh is anisotropic (Ozog et al., 2011). Therefore, considering that the final adaptation of the synthetic mesh has to mimic the original response from healthy tissue, its placement is essential (Anurov et al., 2010; Ozog et al., 2011). Anurov et al. (2010, 2012) studied the influence of the placement of the prosthesis in the abdomen of rats. Specifically, they studied the results obtained with the meshes Ultrapro® and DynaMesh® and concluded that the directions of anisotropy have to be considered in the placement of the prosthesis. Specifically, these authors conclude that the stiffer direction of the mesh must be placed parallel to the direction where the muscular effort is greater (Anurov et al., 2010) and along the direction where the fibres are arranged in the aponeurosis (Anurov et al., 2012).

Although there are numerous experimental studies on different prostheses, the jobs available in the literature evaluate primarily the mechanical response of the whole tissue-mesh in the short term, while the literature on the study of the mechanical response of the whole tissue-mesh is limited in the long term. Considering the limitations of the available studies in the literature, this thesis examines the tissue integration process from the mechanical and histological standpoint in the short and long term, in a partial defect by removing the external oblique muscle, using the three meshes selected for the development of this thesis.

Chapter 3

Results, works and conclusions of the thesis

The main motivation that led to the development of this thesis is the study of the mechanical behaviour of the abdominal wall and the problems associated with abdominal surgery for hernia repair. Understanding the mechanical response of the abdominal wall may help to improve surgical techniques of mesh placement, for example, by defining guidelines for choosing the most appropriate mesh for each patient and type of defect.

In this thesis, hernia repair surgery was studied by placing prostheses through an experimental study in an animal model, specifically with New Zealand white rabbits, since the posterior experimentation with the tissues after different post-implant times can be easily performed. The results obtained were extrapolated to an *"in silico"* model of the human abdominal cavity.

The study was performed not only from the point of view of the continuum mechanics and tissue modelling in engineering, but also the contribution from biologists and clinicians specialists was necessary, since they are those who define the clinical pathology, provide expertise in the treatment of hernias in patients and collaborate in the experimental and histologic characterization. Therefore, the formation of a multidisciplinary working group allowed to obtain results from the engineering, clinical and biological points of view. These results provide advances in the state of the art of the study of hernia pathology.

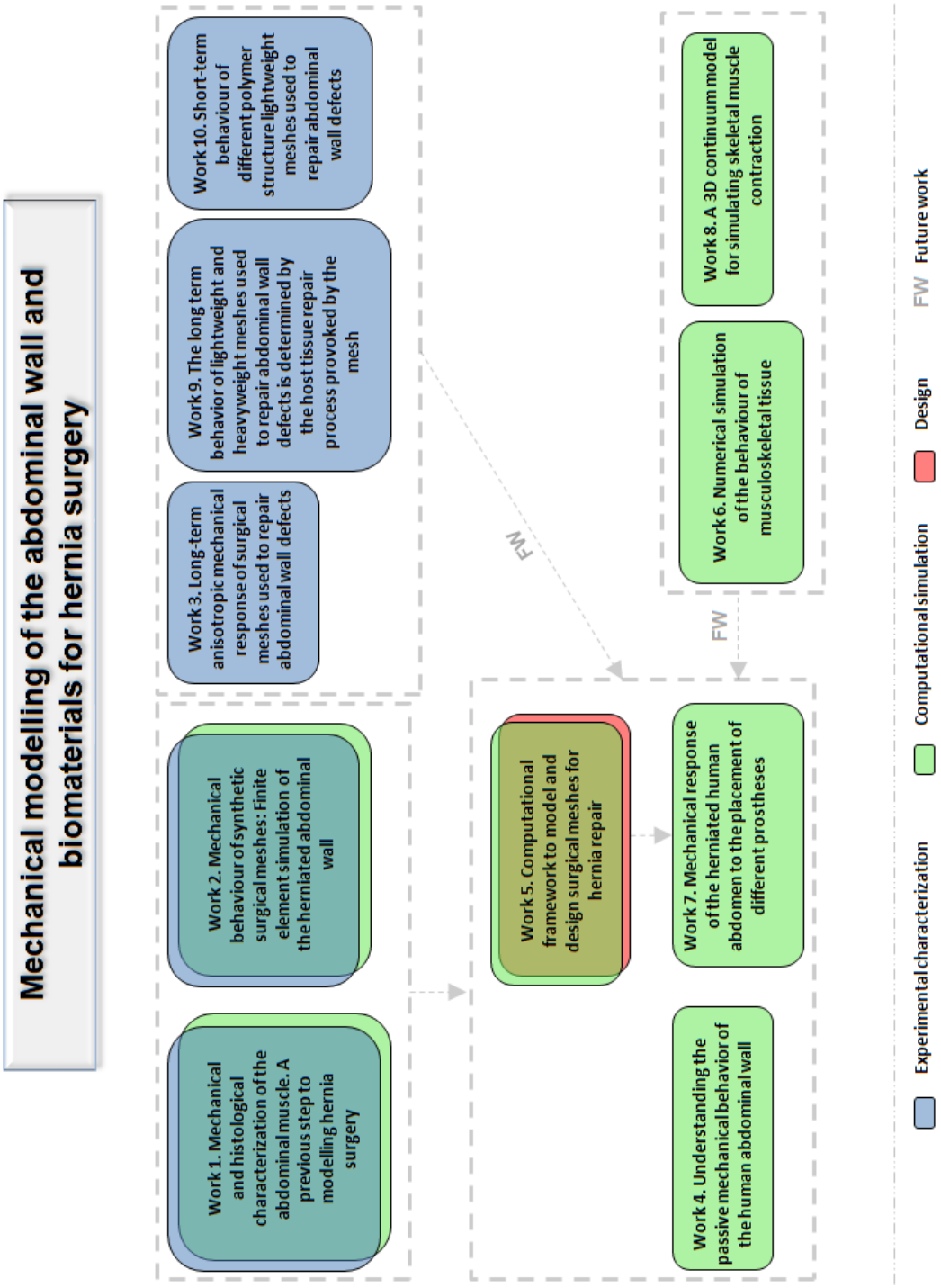

Figure 3.1: Compendium of publications that form the work performed in the development of the thesis.

The results achieved in the context of the doctoral thesis were collected on 10 articles with thematic unit, justifying the initial proposed objectives. These articles are shown

in Figure 3.1 and in Tables 3.1 and 3.2. All papers have been published or are accepted for publication in journals of the *Journal Citation Reports* with the exception of articles 7 and 8 which are under review. In all works included, and in the development of their parts, the maximum contribution is from the author of this thesis, except for the histological studies included in works 1 and 3 and articles 9 and 10 where only the mechanical study was conducted by the author. Therefore, the requirements established by the University of Zaragoza, following the agreement of the 17th of December 2008 of the Governing Council of the University that approves the Regulations on Doctoral Thesis and where thesis developed as a compendium of publications are contemplated.

Table 3.1: Articles that comprise this thesis. Part I. (IF: Impact factor, EXP: Experimental, COM: Computational, DES: Design)

Work	Article	Authors	Journal	IF	Areas
1.	Mechanical and histological characterization of the abdominal muscle. A previous step to modelling hernia surgery	**B. Hernández**, E. Peña, G. Pascual, M. Rodríguez, B. Calvo, M. Doblaré, J. M. Bellón	Journal of the Mechanical Behaviour of Biomedical Materials, 4 (3) (2011), pp: 392-404	2.814	EXP, COMP
2.	Mechanical behaviour of synthetic surgical meshes: Finite element simulation of the herniated abdominal wall	**B. Hernández-Gascón**, E. Peña, H. Melero, G. Pascual, M. Doblaré, M. P. Ginebra, J. M. Bellón, B. Calvo	Acta Biomaterialia, 7 (11) (2011), pp: 3905-3913	4.865	EXP, COMP
3.	Long-term anisotropic mechanical response of surgical meshes used to repair abdominal wall defects	**B. Hernández-Gascón**, E. Peña, G. Pascual, M. Rodríguez, J. M. Bellón, B. Calvo	Journal of the Mechanical Behaviour of Biomedical Materials, 5 (1) (2012), pp: 257-271	2.814	EXP
4.	Understanding the passive mechanical behaviour of the human abdominal wall	**B. Hernández-Gascón**, A. Mena, E. Peña, G. Pascual, J. M. Bellón, B. Calvo	Annals of Biomedical Engineering, In press (2012), DOI: 10.1007/s10439-012-0672-7	2.368	COM
5.	Computational framework to model and design surgical meshes for hernia repair	**B. Hernández-Gascón**, N. Espés, E. Peña, G. Pascual, J. M. Bellón, B. Calvo	Computer Methods in Biomechanics and Biomedical Engineering, In Press (2012), DOI:10.1080/10255842.2012.736967	1.169	DES, COM
6.	Numerical simulation of the behaviour of musculoskeletal tissue	J. Grasa, **B. Hernández-Gascón**, A. Ramírez, J. F. Rodríguez, B. Calvo	Revista Internacional de Métodos Numéricos para Cálculo y Diseño en Ingeniería, 28 (3) (2012), pp: 177-186	0.167	COM

Table 3.2: Articles that comprise this thesis. Part II. (IF: Impact factor, EXP: Experimental, COM: Computational, DES: Design)

Work	Article	Authors	Journal	IF	Areas
7.	Mechanical response of the herniated human abdomen to the placement of different prostheses	**B. Hernández-Gascón**, E. Peña, J. Grasa, G. Pascual, J. M. Bellón, B. Calvo	Submitted	-	COM
8.	A 3D continuum model for simulating skeletal muscle contraction	**B. Hernández-Gascón**, J. Grasa, B. Calvo, J. F. Rodríguez	Submitted	-	COM
9.	The long term behaviour of lightweight and heavyweight meshes used to repair abdominal wall defects is determined by the host tissue repair process provoked by the mesh	G. Pascual, **B. Hernández-Gascón**, M. Rodríguez, S. Sotomayor, E. Peña, B. Calvo, J. M. Bellón	Surgery, 152 (5) (2012), pp: 886-895	3.103	EXP
10.	Short-term behaviour of different polymer structure lightweight meshes used to repair abdominal wall defects	G. Pascual, **B. Hernández-Gascón**, S. Sotomayor, E. Peña, B. Calvo, J. Buján, J. M. Bellón	Histology and Histopathology, Accepted (2012)	2.480	EXP

Next, the main results obtained in the thesis are detailed, and they are grouped according to the methodology followed for its development. They are grouped from different standpoints: experimental (of the abdominal tissue, prostheses and the whole tissue-prosthesis), numerical and design (see Figure 3.1), thus justifying the thematic unit of the different papers included in the compendium of publications of this thesis, according to the requirements established by the University of Zaragoza:

(a) Experimental mechanical characterization of the passive behaviour of the abdominal muscle using an animal model.

The passive elastic mechanical behaviour of the abdominal wall, including initial strains, was characterized experimentally by means of uniaxial tests in an experimental animal model, the New Zealand white rabbit (Hernández et al., 2011) (*Article 1*). Specifically, the passive response of the abdominal muscles was studied considering separate muscle layers and all muscle layers together (composite). Furthermore, an histological study was performed to analyze the arrangement of collagen and muscular fibres in the abdominal tissue. Results from the study reveal that the maximum shrinkage that occurs when cutting the abdominal tissue reaches $26.4 \pm 6.76\%$ in the craneo-caudal direction of the animal and there are no significant differences between the shrinkage in this direction and the transversal one. The study showed a greater stiffness of the tissues in the perpendicular direction to the muscular fibres than along them. Furthermore, it was observed that the anisotropy of each of the abdominal muscles, studied separately, is greater than that exhibited by the characterization all muscle layers together. Specifically, the transverse direction of the abdomen, at the level of the abdominal muscles, presents higher stiffness than in the craneo-caudal direction (see Figure 3.2).

(b) Experimental mechanical characterization of the behaviour of reticular prostheses.

The mechanical response of three reticular synthetic prostheses frequently used in hernia surgery (*Surgipro*®, *Infinit*® and *Optilene*® classified as heavyweight, mediumweight and lightweight prostheses, respectively), was characterized using uniaxial traction tests and the stress-stretch curves along two perpendicular directions were obtained (Hernández-Gascón et al., 2011) (*Article 2*). Results were compared with the response of the abdominal tissue to identify the prosthesis that best reproduces the behaviour of the healthy abdominal tissue. The mechanical characterization of these prostheses reveals an isotropic response of *Surgipro*® mesh, while *Optilene*® and *Infinit*® meshes offer an anisotropic response (see Figure 3.3).

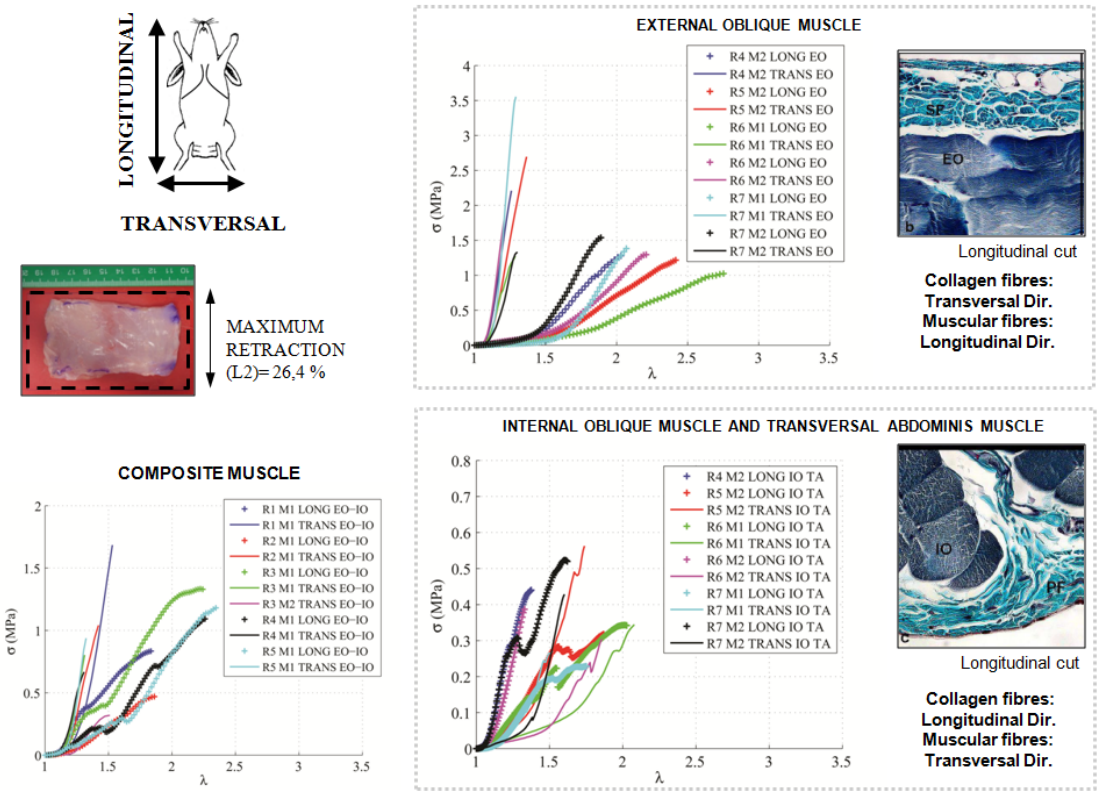

Figure 3.2: Definitions of longitudinal and transversal directions in the rabbit. Image of the shrinkage in the tissue patch after its extraction. Experimental data obtained in uniaxial tests in the composite EO-IO (External and internal oblique) and in the individual muscle layers EO (external oblique) and IO-TA (internal oblique) and correlation with the results from the histological study with light microscopy.

(c) Experimental mechanical characerization of the passive behaviour of the whole tissue-prosthesis.

The passive elastic mechanical behaviour of the repaired abdominal wall, using the three selected prostheses for the study, was studied experimentally by means of uniaxial tests, after different post-implant times (at 14, 90 and 180 days) (Hernández-Gascón et al., 2012e) (*Article 3*). It was observed that as the time increases, tissular integration is greater and, consequently, the stiffness of the whole tissue-mesh increases (see Figure 3.4). The passive elastic mechanical behaviour of the abdominal wall becomes stiffer with age and continues to be anisotropic (see Figure 3.5.a). In addition, the behaviour of the whole tissue-prosthesis was compared with the healthy tissue and the result indicates that none of the studied meshes is capable of exactly reproducing the elastic mechanical behaviour of the abdominal tissue in the craneo-caudal direction at 14 or

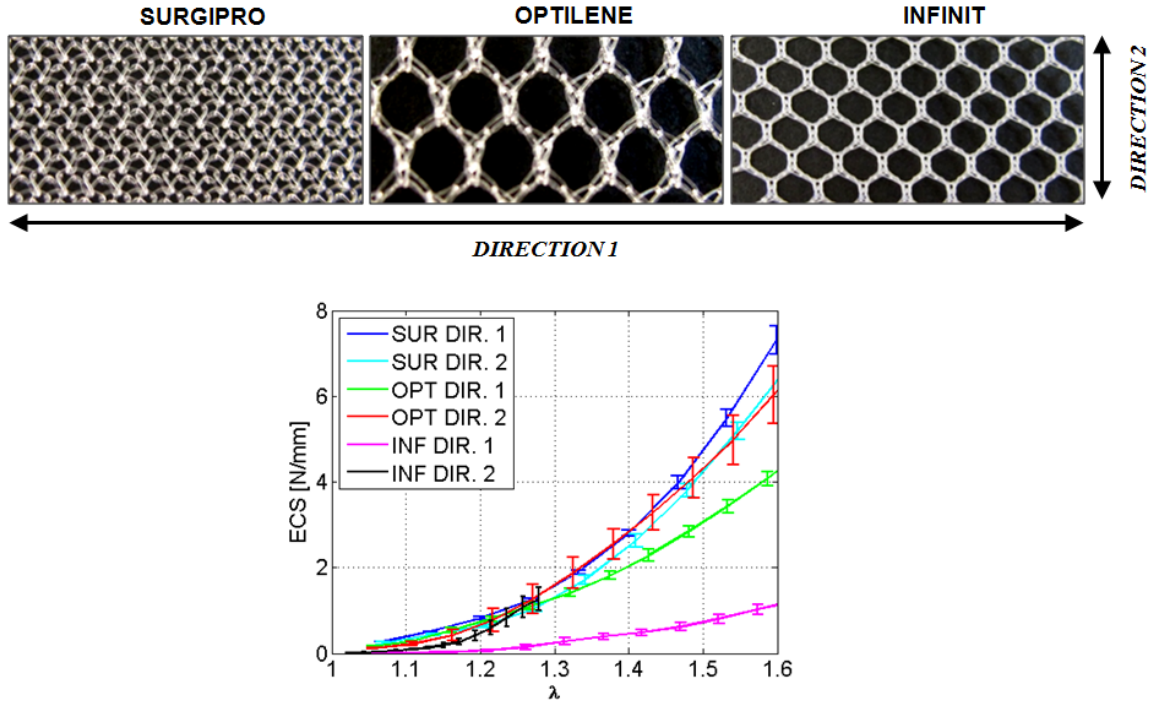

Figure 3.3: Image of the three meshes selected for the study where the two studied directions are indicated. Experimental data (ECS=Stress/length vs. stretch) obtained along the two directions of the uniaxial tests.

90 days after implantation. However, in the long term, the best compliance between mesh and tissue is given by the low weight prostheses since they maintain the initial anisotropy (see Figure 3.5.a). Furthermore, the shrinkage that suffers each mesh, due to the tissular integration process which depends on the properties of the prosthesis, was measured. The results reveal that the shrinkage is significantly different between the two orthogonal directions studied with $Infinit^{®}$ mesh, whereas is not with $Surgipro^{®}$ at any time of study. Shrinkage with $Optilene^{®}$ mesh is significantly different between the two perpendicular directions studied only at 14 days. Furthermore, the quantity of collagen and macrophages generated due to the tissular integration process, which depend on the type of prosthesis implanted and the time after implantation, were quantified (Hernández-Gascón et al., 2012e; Pascual et al., 2012a,b) (*Articles 3, 9 and 10*). The emphasis of the study was focussed on comparing a heavyweight mesh ($Surgipro^{®}$), a mediumweight mesh ($Infinit^{®}$) and a lightweight mesh ($Optilene^{®}$). It was observed that the most notable formation of collagen occurs in the short term and that the formation of collagen tends to unify the mechanical response of the three meshes in the long term (see Figure 3.5.b). Besides, the formation of collagen depending on the pore size of the mesh was analyzed. Specifically, the greater the pore size, the higher collagen deposition (see Figure 3.5.b). Finally, it was observed that the macrophagic

response depends on the material of the prosthesis. Specifically, the macrophagic response is greater when the mesh is made of polytetrafluoroethylene (*Infinit*®) than in polypropylene meshes (*Surgipro*® and *Optilene*®) (see Figure 3.6).

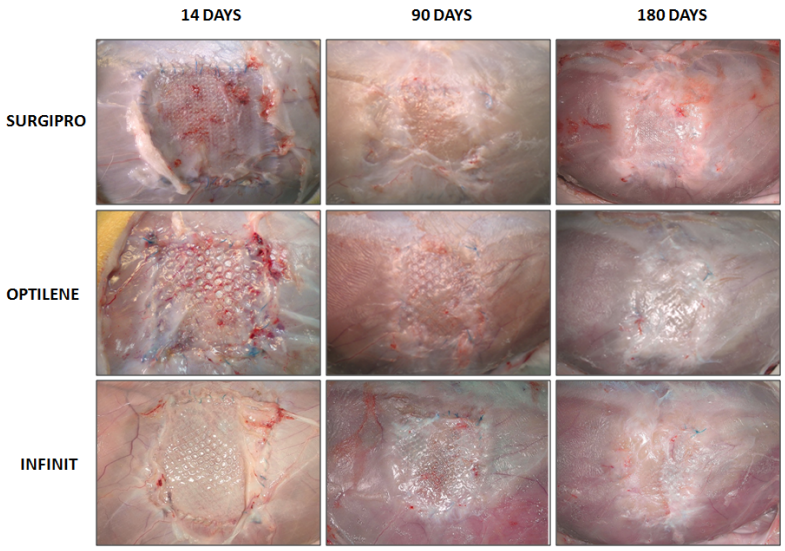

(a)

	SURGIPRO		OPTILENE		INFINIT	
	LONG	TRANS	LONG	TRANS	LONG	TRANS
14 days	7,5 ± 4,203	10,5 ± 7,549	16 ± 6	2,5 ± 2,887*	12,75 ± 3,775	0 ± 0*
90 days	5,5 ± 4,796	12,25 ± 1,5	5,25 ± 6,397	5,25 ± 6,397	12,25 ± 1,5	0 ± 0*
180 days	7 ± 4,761	6,5 ± 5,447	3,25 ± 6,5	0 ± 0	19,5 ± 6,403	0 ± 0*

(b)

Figure 3.4: (a) Macroscopic image of the tissue patches obtained from the defect area of the rabbit at different post-implat times (14, 90 and 180 days) and for the three different studied meshes, where tissular integration is appreciated. (b) Shrinkage (%) of the tissue patches obtained from the animal, in the longitudinal and transversal directions, at different times of study (*p<0.05).

(d) Numerical modelling of the mechanical response of the abdominal muscle and prostheses.

A thermodynamically consistent three-dimensional computational model for simulating muscle skeletal tissue was proposed to reproduce both, the active and passive mechanical responses within the framework of the nonlinear hyperelasticity in large de-

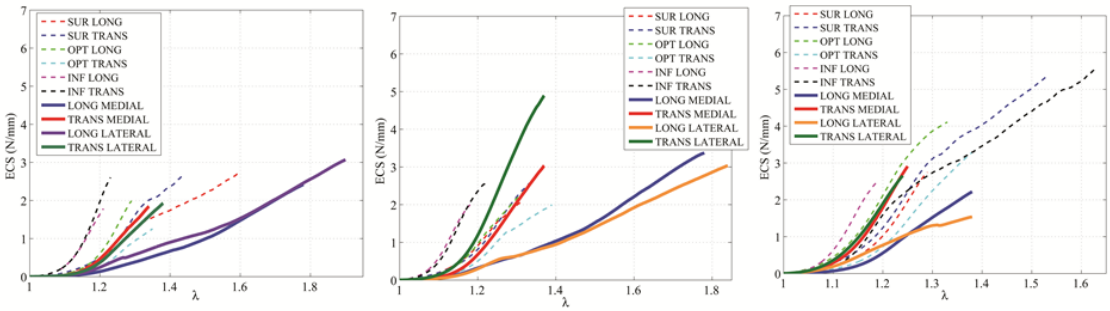

(a)

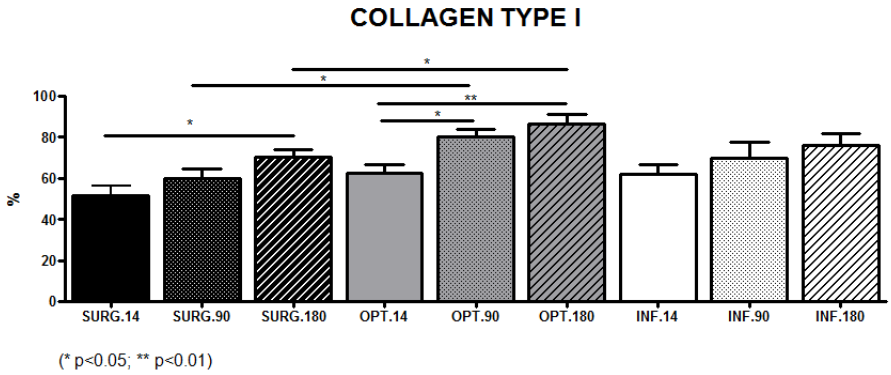

(b)

Figure 3.5: (a) Comparison of the experimental results from uniaxial tests between the abdominal tissue from control rabbits and the repaired abdominal tissue with the three studied meshes at 14, 90 and 180 days. (b) Quantification of collagen I (mature collagen) at 14, 90 and 180 days with the three studied prostheses using Sirius red staining. Values obtained as mean ± standard deviation.

formations (Hernández et al., 2011; Grasa et al., 2013; Hernández-Gascón et al., 2012b) (*Articles 1, 6 and 8*). The formulated model allows to incorporate initial stresses that are present in the abdominal cavity. The active mechanical response of the model was validated using experimental results from the tibialis anterior rat muscle (Ramírez et al., 2010). The strain energy functions corresponding to the passive contributions were fitted using the experimental results obtained with the experimental animal model (Hernández et al., 2011) (*Article 1*) and data from the literature were also taken (Calvo et al., 2010; Martins et al., 2012). Although from the anatomical point of view the abdominal wall is formed by muscle layers (external oblique muscle, internal oblique muscle and transversus abdominis muscle), it was found that the simulation of the behaviour of the composite, considering all muscle layers together, equals the mechanical response of the abdominal wall defined as the union of different muscle layers (Hernández et al., 2011) (*Article 1*). Therefore, the consideration that the oblique muscles behave as a composite was considered throughout the development of this thesis to study the response of

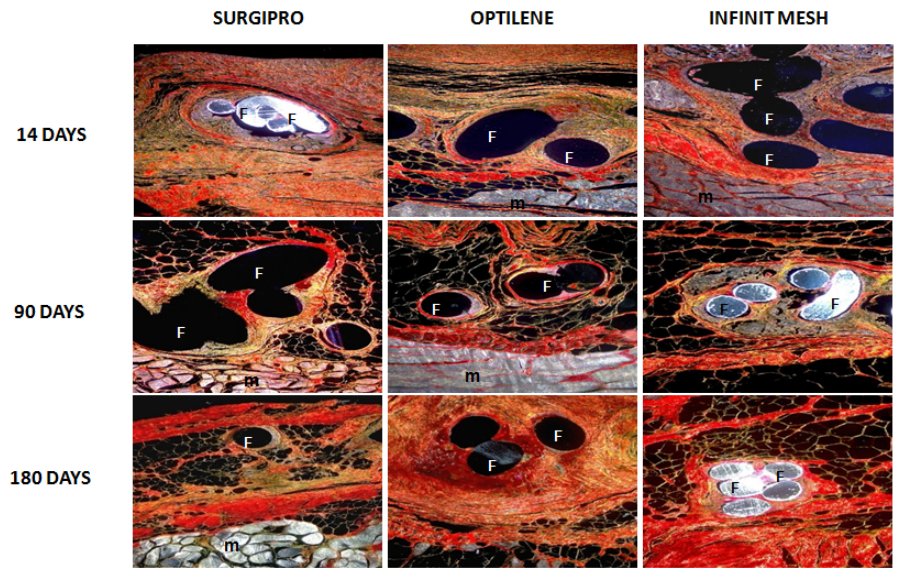

Figure 3.6: Sirius red staining of tissue patches taken from the rabbit at different post-implant times and for the three studied meshes. Collagen III (immature) and I (mature) are visualized in yellow and red, respectively.

the abdomen.

Regarding the modelling of the mechanical behaviour of the prostheses, strain energy functions that reproduce their mechanical response from the experimental results were defined within the nonlinear hyperelasticity theory in large deformations (Hernández-Gascón et al., 2011) (*Article 2*).

To extrapolate the study to the human body, an *"in silico"* model of the human abdomen, constructed from nuclear magnetic resonance imaging, was defined to study the mechanical response of the abdomen to passive (Hernández-Gascón et al., 2012c) and active (Hernández-Gascón et al., 2012b) physiological loads (*Article 8*). In the model, main anatomical structures of the abdomen were differentiated and the corresponding anisotropic mechanical properties were assigned to each tissue by means of the definition of preferential directions of anisotropy (see Figure 3.7). Maximal displacements addressed in the abdomen appear in the frontal part (see Figure 3.8). Regarding stresses, maximal values appear in the aponeurotic structures. Specifically, the linea alba is the structure that absorbs higher stresses meaning that this is the most requested structure in the abdomen.

To simulate the surgical procedure in hernia repair, a finite element model of the human abdomen bearing a total hernia along the linea alba was defined from the pre-

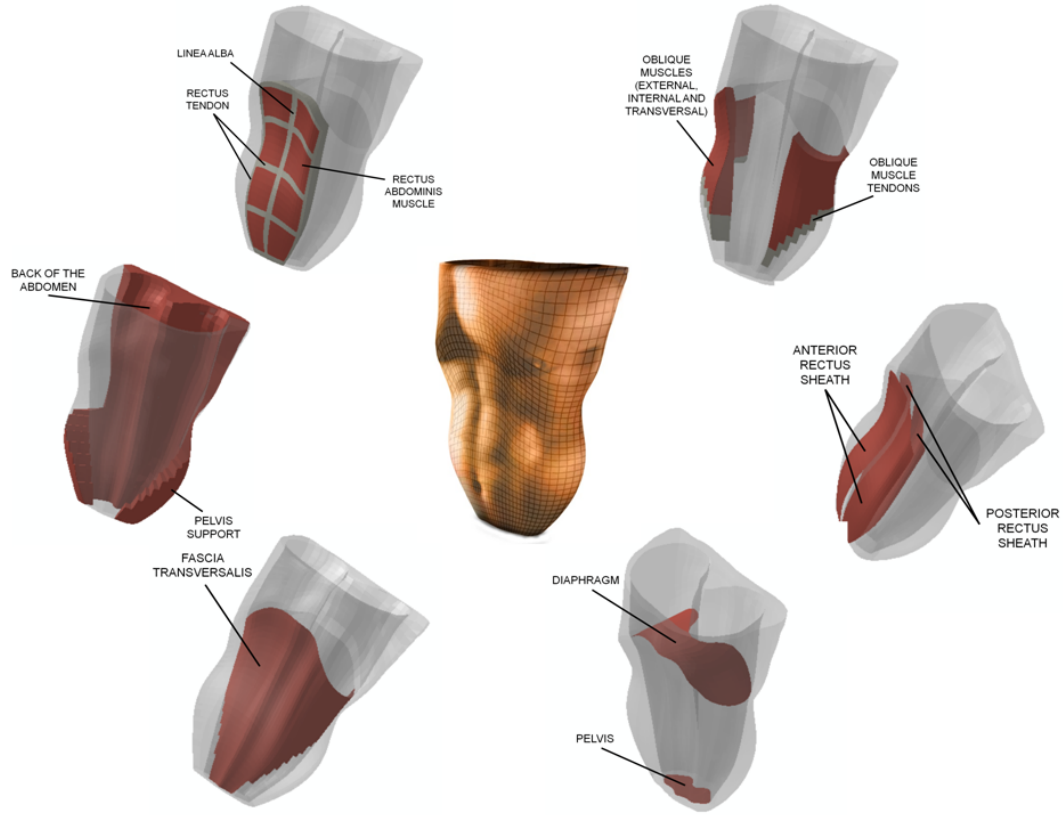

Figure 3.7: Finite element model of the complete human abdomen and identification of the main anatomical structures of the abdomen.

vious model. For that purpose, the implantation of the prosthesis in the defect area was simulated and the mechanical response of the herniated and repaired abdomen was analyzed to physiological loads depending on the implanted mesh and its placement in the abdomen (Hernández-Gascón et al., 2012d) (*Article 7*) (see Figures 3.9 and 3.10). This study showed that the worst compliance is given by *Surgipro*® mesh whereas *Infinit*® mesh is the most flexible. It was detected that the placement of the prosthesis influences the mechanical response and results are closer to mimic the original response of the healthy abdomen when the prosthesis is positioned such that the most compliant axis of the mesh coincides with the craneo-caudal direction of the body (see Figure 3.10).

(e) Establishment of a methodology for the design of prostheses.

A computational framework that includes two computational models was established to design and validate the elastic mechanical behaviour of surgical meshes (Hernández-Gascón et al., 2012a) (*Article 5*) (see Figure 3.11). First, the modelling is approached

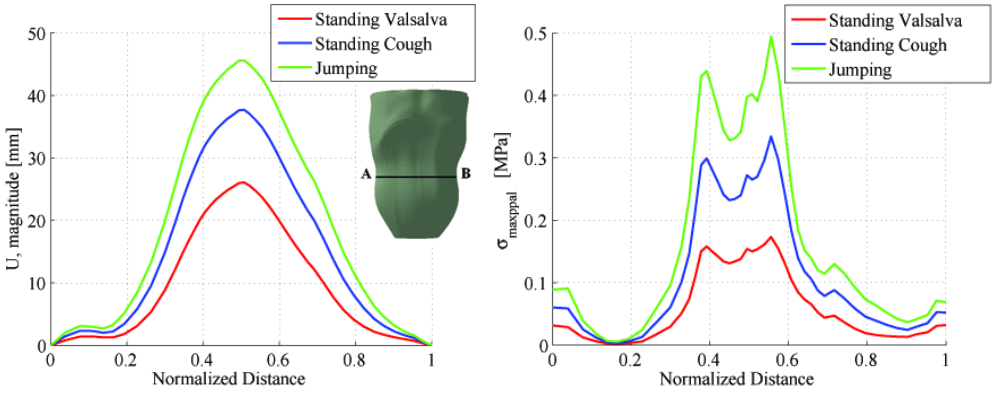

Figure 3.8: Maximal displacements (mm) (a) and maximal principal stresses (MPa) (b) along line AB defined in (a). The normalized distance indicates that $x = 0$ and $x = 1$ correspond to points A and B, respectively.

Figure 3.9: Finite element model of the herniated and repaired human abdomen.

considering the weave of the mesh using beam elements, while the second model considers the prosthesis as a continuum within the framework of the nonlinear hyperelasticity in large deformations using membrane elements. This methodology was validated with the simulation of the three commercial meshes studied previously and its potentiality is given by the experimental costs reduction.

3.1 Original contributions

The development of this thesis has established a methodology that opens the door to the automation of the simulation of personalized surgical interventions, in order to select the most appropriate mesh for each patient and the appropriate placement on the

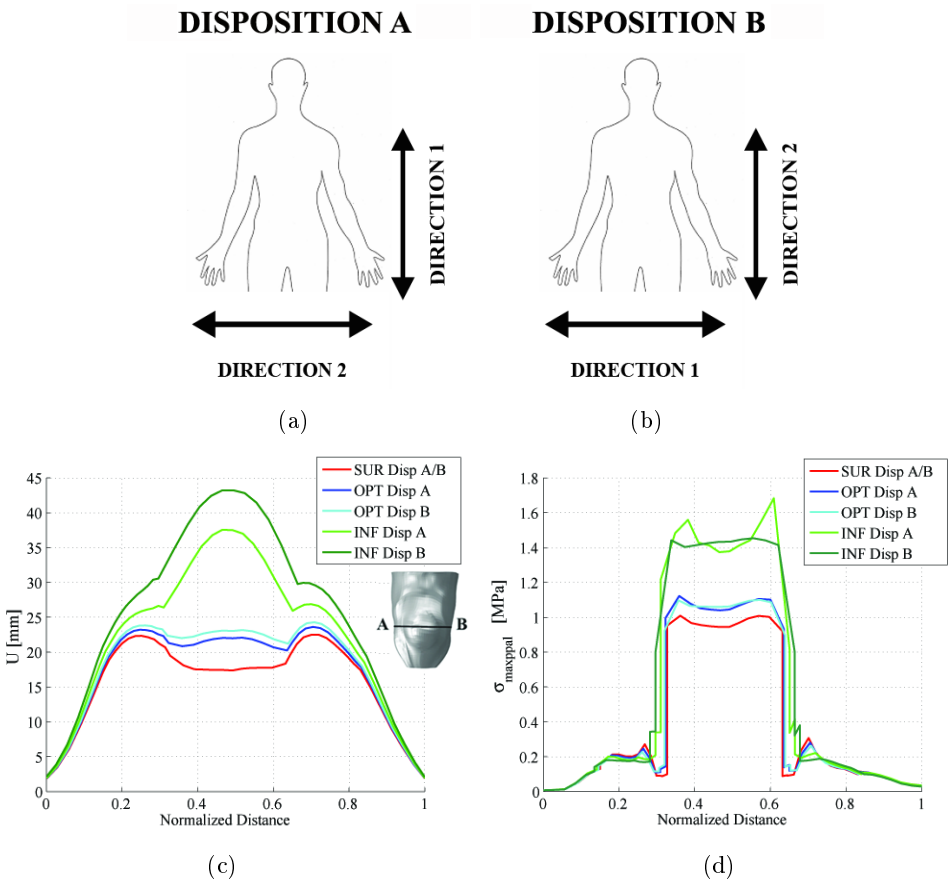

Figure 3.10: Definition of dispositions A (a) and B (b) of the prosthesis in the abdomen. Maximal displacements (mm) (c) and maximal principal stresses (MPa) (d) along the line AB defined in (c). The normalized distance shows that $x = 0$ and $x = 1$ corresponds to points A and B, respectively.

defect. For that purpose, it was necessary to work within a multidisciplinary working team, composed of specialists in the field of continuum mechanics in engineering, biology and medicine. The work developed by a large group of researchers from different disciplines helped to completely approach the pathology of hernia appearance since it was studied at various levels: experimental level, including mechanical and histological characterization of abdominal tissues in an experimental animal model, the mechanical characterization of three commercial prostheses and the experimental characterization of the whole tissue-mesh at different post-implant times; and at the computational level, by defining an *"in silico"* model of the human abdomen that allowed the analysis of the mechanical response to physiological loads, even after surgery, and by proposing a methodology to design and validate the behaviour of prostheses. Particularly, the main original contributions of this thesis are listed below:

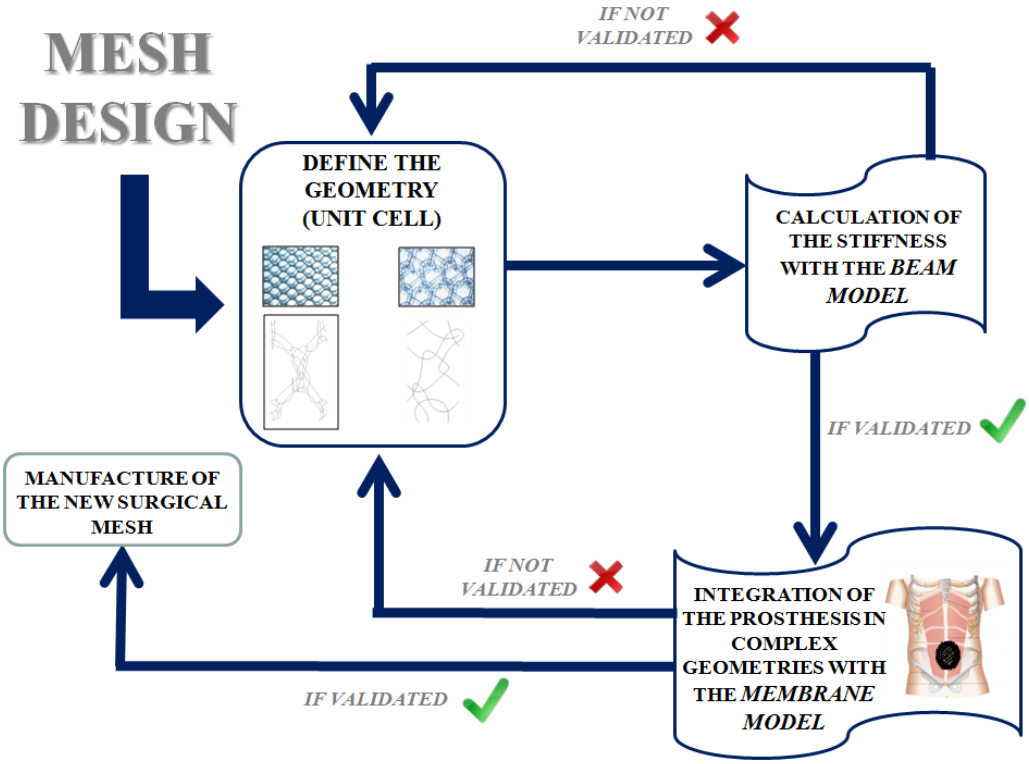

Figure 3.11: Methodology of the process defined to design prostheses. The computational framework define two models that use beam and membrane elements, respectively.

- The passive mechanical response of the abdominal tissue was modelled within the framework of the nonlinear hyperelasticity in large deformations, based on the experimental results obtained through uniaxial tests using an experimental animal model, such as the New Zealand white rabbit.

- A constitutive model was proposed to reproduce the mechanical response of the prostheses $Surgipro^{®}$, $Optilene^{®}$ and $Infinit^{®}$ within the framework of the nonlinear hyperelasticity in large deformations and the validation was addressed using the experimental characterization of their mechanical response through uniaxial tests.

- The quantity of collagen and macrophages generated with $Surgipro^{®}$, $Optilene^{®}$ and $Infinit^{®}$ prostheses due to the tissular integration process with was quantified histologically at 14, 90 and 180 days after the implantation. The emphasis of the study was focussed on the comparison of a heavyweight mesh ($Surgipro^{®}$), a mediumweight mesh ($Infinit^{®}$) and a lightweight mesh ($Optilene^{®}$). Furthermore, the mechanical response of the repaired tissue was characterized at different post-implant times and it was compared to the behaviour of the healthy abdominal tissue, which was characterized as well at the same times of study.

- A thermodynamically consistent three-dimensional computational model for simulating the active and passive responses of the skeletal muscle was proposed and validated. This model is defined within the nonlinear hyperelasticity theory in large deformations.
- A methodology to simulate the passive and active mechanical behaviour of the human abdomen to physiological movements, using the finite element method, is proposed. The computational model was developed from nuclear magnetic resonance imaging and incorporates the distribution of initial stresses of the human body. Furthermore, the main anatomical structures of the abdomen are differentiated in the geometry and the mechanical properties of the tissues were assigned correspondingly. Initial stresses in abdominal tissues are considered.
- A methodology to simulate the passive mechanical response of the herniated and repaired human abdomen after hernia surgery was established. This model includes the modelling of the prosthesis and analyzes the behaviour of the considered mesh and the influence of its placement in the mechanical response of the whole repaired abdomen to common physiological loads in the postoperative period.
- A methodology to design and validate the elastic mechanical behaviour of surgical meshes, whose major advantage is the reduction of the experimental costs that traditional experimental methods generate, was established.

3.2 General conclusions

The main conclusions drawn from this thesis, based on the experimental and numerical studies performed, are the following:

- The anisotropic behaviour of lateral abdominal muscles considered as a composite is less pronounce than the anisotropy of the individual muscle layers. Specifically, the perpendicular direction to the craneo-caudal one (transversal direction) in the abdomen is stiffer than the craneo-caudal direction. The passive elastic mechanical behaviour of the abdominal wall becomes stiffer with age and continues to be anisotropic.
- When removing the abdominal tissue of the animal, the maximum shrinkage goes up to $26.4 \pm 6.76\%$ in the longitudinal direction and no significative differences between the longitudinal and the transversal retraction are found.
- The constitutive model proposed to reproduce the elastic mechanical response of the abdominal muscles is thermodynamically consistent and is able to predict the stress distribution using computational methods.

- The mechanical response obtained in uniaxial tests is isotropic for *Surgipro*® mesh, lightly anisotropic in *Optilene*® mesh and *Infinit*® mesh exhibits a highly anisotropic response.

- Tissular integration process in the partially herniated abdomen shows a shrinkage of the prostheses that differs depending on the type and placement of the mesh. Specifically, the retraction is significantly different between the two perpendicular directions studied with the *Infinit*® mesh at all studied times, while is not with *Surgipro*® mesh at any time of study. The shrinkage between both directions in *Optilene*® mesh only exhibit significative differences at 14 days. The three implants used showed good tissular integration due to the formation of connective tissue around the pores.

- The formation of collagen in the repaired defect area provokes a notable increment on the stiffness which modifies the initial properties of the mesh. Therefore, the experimental characterization of prostheses using uniaxial tests before the implant, only addresses indicative information. The most notable formation of collagen occurs in the short term. Furthermore, a relationship between the formation of collagen and the pore size is observed. Specifically, the greater the pore size, the greater the collagen deposition. In the short term, the material composition of the filaments (PP vs. PTFE) does not influence the formation of collagen. In the long term, the formation of collagen tends to unify the mechanical response of the three meshes.

- The macrophagic response depends on the material composition of the prostheses. Specifically, the macrophagic response is higher when the mesh is made of polytetrafluoroethylene (*Infinit*®) than in cases where the prosthesis is made of polypropylene (*Surgipro*® and *Optilene*®).

- Uniaxial tests show that none of the studied prostheses is capable of exactly reproducing the passive elastic mechanical behaviour of the abdominal tissue along the craneo-caudal direction of the abdomen at 14 or 90 days after implantation. In the long term, the best compliance of the mesh is given by the low weight prostheses since they maintain the initial anisotropy.

- Both computational models proposed to design and validate the elastic mechanical behaviour of prostheses are capable of reproducing the patterns observed in the experiments. Furthermore, this methodology minimizes economic costs and long times required with experimental methods. The continuum model has the advantage of being more efficient computationally and allows the inclusion of the models in other models more complex.

- A methodology to model the human abdomen and to study its mechanical response to physiological loads was defined. From the mechanical standpoint, this

model allows to predict which areas are more stressed. These results can be related to the possible risk of hernia formation in the abdominal wall. The aponeurotic structures, specially the linea alba, are the structures that most work in the abdomen. Therefore, the linea alba is one of the most important units from the mechanical stability standpoint.

- The presented methodology in the computational modelling of the human abdomen is a starting point for future studies which automatically simulate the behaviour of the human abdomen. Thus, personalized surgical procedures and studies could be performed.

- Considering the computational model of the herniated and repaired human abdomen, it is concluded that *Surgipro*® and *Optilene*® prostheses could limit the natural distensibility of the abdomen whereas the use of *Infinit*® mesh is not recommended in obese patients or in patients with large defects. The mechanical response of the anisotropic meshes in the defect area influences notably the compliance between tissue and mesh. The study concludes that the stiffer direction of the prosthesis should be aligned with the transversal direction of the abdomen. Furthermore, both the stiffer and the most flexible directions should be indicated in the own mesh so that the surgeon will have no difficulties when placing the prosthesis.

- New designs of prosthesis could be validated with the methodology defined to simulate computationally the herniated human abdomen.

3.3 Future lines

Considering the studies developed in this thesis, its conclusions and limitations, different lines of action for future works are proposed:

- An experimental line of work to characterize the mechanical response of abdominal tissues using biaxial or inflation tests is proposed. These new protocols, which are more similar to the real load state, will provide additional information about tissue characterization. Furthermore, it is proposed to determine the plastic and viscoelastic properties of the muscle and the loss of stiffness due to damage as a mechanical process previous to hernia appearance.

- Since the active behaviour was characterized, in previous works to this thesis, with experimental test using the tibialis anterior rat muscle (Ramírez et al., 2010), new tests are proposed to characterize the active response of the different abdominal muscles.

- It is also proposed the mechanical characterization of surgical meshes through biaxial tests. This characterization allows to reproduce load states more similar to the real load state the prostheses work in. Furthermore, it is proposed to determine of the mechanical properties of other different commercial prostheses in order to broaden the scope of knowledge of synthetic meshes.

- Tissular regeneration process was addressed experimentally. These results will allow to define a new line of work to propose a mathematical model of tissular growth. Posteriorly, the numerical simulation of the tissular integration process could be performed to analyze the response according to the properties of the meshes.

- An experimental line is proposed to characterize the response of the animal and human, healthy and herniated abdominal wall after surgery, through *"in vivo"* inflation tests. These tests are comparable to the physiological action that the intraabdominal pressure imposes. The experimental characterization of the mechanical behaviour and the obtention of magnetic resonance imaging from the same animals or humans, will allow to validate the methodology proposed in works 2, 4, 5 and 7 of this thesis. The final objective is to automate the simulation process for each specific patient.

- The numerical simulation of the behaviour of the human abdomen by means of combining the active and passive responses is proposed to understand how the mesh can make difficult to carry out movements (breathing, flexion, etc.). Besides, the consideration of the viscoelastic properties, in order to analyze the response depending on the strain rate of the load, and the posterior validation of the model with images is proposed.

- A clinical problem that appears in some cases after hernia repair is the abdominal compartment syndrome (Sabbagh et al., 2011). The abdominal compartment syndrome is a serious condition which involves an increase of the pressure on muscle compartment. It may cause damage to nerves and muscles, as well as problems with blood flow. This problem arises as a result of repairing large incisional hernias, due to the fact that internal organs of the thoracic cavity pushes through the diaphragm. A line of future work consists of simulating this clinical process to identify the causes that generate the problem and establishing alternative methods of closure of the hernia to avoid the appearance of compartment syndrome.

- One of the most common problems after hernia repair is hernia recurrence. Generally, hernia recurrence takes place in the area of the sutures. Taking into account that the suture is another element that takes place in the surgical procedure, a new line of work proposes the experimental and numerical characterization of the mechanical response of different types of threads and suture techniques. The objective is to establish which threads are more appropriate for each type of closure

and patient and some guidelines to suture the prosthesis to the recipient tissue in order to diminish the number of hernia recurrences.

3.4 Conferences

The study developed in this thesis has been also presented in different national and international conferences listed in Tables 3.3 and 3.4. The author of this thesis obtained the second award on the student competition, with the work *"Caracterización del comportamiento pasivo del músculo abdominal del conejo. Aplicación al diseño de prótesis" (In Spanish)* in the XXVII Congreso Anual de la Sociedad Española de Ingeniería Biomédica (CASEIB) in 2009, in Cádiz (Spain).

Table 3.3: Works in national and international conferences. Part I

	Title	Authors	Conference	City	Participation
1.	Mechanical modelling of the human abdomen applied to hernia surgery	**B. Hernández-Gascón**, E. Peña, G. Pascual, J.M. Bellón, B. Calvo	6th Annual Conference CIBER-BBN, 2012	Madrid (Spain)	Poster
2.	Respuesta mecánica del abdomen humano herniado y reparado (In Spanish)	**B. Hernández-Gascón**, E. Peña, G. Pascual, J.M. Bellón, B. Calvo	Capítulo Nacional Español de la Sociedad Europea de Biomecánica, 2012	Seville (Spain)	Speaker
3.	Numerical modelling of skeletal muscle tissue. Application to human abdominal cavity	**B. Hernández-Gascón**, J. Grasa, J. F. Rodriguez, B. Calvo	European Congress on Computational Methods in Applied Sciences and Engineering (ECCOMAS), 2012	Vienna (Austria)	Coauthor
4.	Numerical modelling of the abdominal wall using MRI. Application to hernia surgery	**B. Hernández-Gascón**, A. Mena, J. Grasa, M. Malve, E. Peña, G. Pascual, J. M. Bellón, B. Calvo	3rd Edition Computational Modelling of Objects Presented in Images: Fundamentals, Methods and Applications (COMPIMAGE), 2012	Rome (Italy)	Speaker
5.	Numerical modelling of the abdominal wall applied to hernia surgery	**B. Hernández-Gascón**, J. Grasa, E. Peña, G. Pascual, J. M. Bellón, B. Calvo	18th Congress of the European Society of Biomechanics (ESB), 2012	Lisbon (Portugal)	Speaker
6.	Reconstruction and numerical modelling of the abdominal wall. Application to hernia surgery	**B. Hernández-Gascón**, J. Grasa, E. Peña, B. Calvo	I Jornada de Jóvenes Investigadores del I3A, 2012	Saragossa (Spain)	Speaker
7.	Lightweight meshes, used to repair abdominal wall defects shows an anisotropic mechanical response at long term	G. Pascual, B. Hernández-Irizarri, **B. Hernández-Gascón**, M. Rodríguez, S. Sotomayor, E. Peña, B. Calvo, J. M. Bellón	5th International Hernia Congress the World Hernia Celebration, 2012	New York (US)	Coauthor

Table 3.4: Works in national and international conferences. Part II

	Title	Authors	Conference	City	Participation
8.	Experimental and computational characterization of the abdominal muscle and surgical meshes. Modelling hernia surgery	**B. Hernández-Gascón**, G. Pascual, M. Rodríguez, S. Sotomayor, E. Peña, B. Calvo, M. Doblaré, J. M. Bellón	5th Annual Conference CIBER-BBN, 2011	Saragossa (Spain)	Poster
9.	Modelling of the abdominal wall: Comparison of hexahedral and tetrahedral elements	**B. Hernández-Gascón**, P. Young, G. Pascual, E. Peña, J. M. Bellón, B. Calvo	Simpleware Users Meeting, 2011	Bristol (United Kingdom)	Poster
10.	Receptor tissue modulates long term behaviour of heavy and light weight prostheses in repair of abdominal wall defects	G. Pascual, **B. Hernández-Gascón**, E. Peña, M. Rodríguez, B. Calvo, M. Doblaré, J. M. Bellón	The 46th Congress of the European Society for Surgical Research, 2011	Aachen (Germany)	Coauthor
11.	Numerical modelling of abdominal wall. Application o hernia surgery	**B. Hernández-Gascón**, E. Peña, G. Pascual, M. Rodríguez, B. Calvo, M. Doblaré, J. M. Bellón	Congress on Numerical Methods in Engineering (CMNE), 2011	Coimbra (Portugal)	Speaker
12.	Computational model of the muscle of the rabbit and implanted meshes	**B. Hernández-Gascón**, E. Peña, B. Calvo, M. Doblaré	IV European Conference on Computational Mechanics (ECCM), 2010	Paris (France)	Coauthor
13.	Caracterización del comportamiento pasivo del músculo abdominal del conejo. Aplicación al diseño de prótesis (In Spanish)	**B. Hernández-Gascón**, E. Peña, B. Calvo, M. Doblaré, G. Pascual, J. M. Bellón	XXVII Congreso Anual de la Sociedad Española de Ingeniería Biomédica (CASEIB), 2009	Cádiz (Spain)	Speaker

Bibliography

Abbot, B. C., Wilkle, D. R., 1953. The relation between velocity of shortening and the tension-length curve of skeletal muscle. The Journal of Physiology 120, 214–223.

Afonso, J., Martins, P., Girao, M., Natal Jorge, R., Ferreira, A., Mascarenhas, T., Fernandes, A., Bernardes, J., Baracat, E., Rodrigues de Lima, G., Patricio, B., 2008. Mechanical properties of polypropylene mesh used in pelvic floor repair. International Urogynecology Journal 19, 375–380.

Alaedeen, D. I., Lipman, J., Medalie, D., Rosen, M. J., 2007. The single-staged approach to the surgical management of abdominal wall hernias in contaminated fields. Hernia 11, 41–45.

Alastrué, V., Peña, E., Martínez, M. A., Doblaré, M., 2008. Experimental study and constitutive modelling of the passive mechanical properties of the ovine infrarenal vena cava tissue. Journal of Biomechanics 41, 3038–3045.

Anderson, J. M., 1988. Inflamatory response to implants. ASAIO Transactions 34, 101–107.

Antonopoulos, I. M., Nhas, W. C., Mazzuchi, E., Piovesan, A. C., Birolini, C., Lucon, A. M., 2006. Is polypropylene mesh safe and effective for repairing infected incisional hernia in renal transplant recipients? Urology 66, 874–877.

Anurov, M. V., Titkova, S. M., Oettinger, A. P., 2010. Impact of position of light mesh endoprosthesis with anisotropic structure for the efficiency of anterior abdominal wall reconstruction. Bulletin of Experimental Biology and Medicine 149(6), 779–783.

Anurov, M. V., Titkova, S. M., Oettinger, A. P., 2012. Biomechanical compatibility of surgical mesh and fascia being reinforced: dependence of experimental hernia defect repair results on anisotropic surgical mesh positioning. Hernia 16, 199–210.

Arampatzis, A., Stafilidis, S., DeMonte, G., Karamanidis, K., Morey-Klapsing, G., Brüggemann, G. P., 2005. Strain and elongation of the human gastrocnemius tendon

and aponeurosis during maximal plantarflexion effort. Journal of Biomechanics 38(4), 833–841.

Arruda, E. M., Boyce, M. C., 1993. A three-dimensional constitutive model for the large stretch behavior of rubber elastic materials. Journal of the Mechanics and Physics of Solids 41(2), 389–412.

Arruda, E. M., Mundy, K., Calve, S., Baar, K., 2006. Denervation does not change the ratio of collagen I and collagen II mRNA in extracellular matrix of muscle. American Journal of Physiology - Regulatory, Integrative and Comparative Physiology 292, 983–987.

Askar, O. M., 1977. Surgical anatomy of the aponeurotic expansions of the anterior abdominal wall. Annals of The Royal College of Surgeons of England 59, 313–321.

Automattic-Inc, 2005. WordPress. `http://wordpress.com/`, accessed September 25, 2012.

Axer, H., Keyserlingk, D. G., Graft, D., Prescher, A., 2001b. Collagen fibers in linea alba and rectus sheaths: II. Variability and biomechanical aspects. Journal of Surgical Research 96, 239–245.

Axer, H., Keyserlingk, D. G., Prescher, A., 2001a. Collagen fibers in linea alba and rectus sheaths: I. General scheme and morphological aspects. Journal of Surgical Research 96, 127–134.

Bellón, J. M., 2009. Role of the new lightweight prostheses in improving hernia repair. Cirugía Española 85(5), 268–273.

Bellón, J. M., 2012. Courtesy of Dr. Bellón, University of Alcalá (Spain).

Bellón, J. M., Buján, J., Contreras, L., Hernando, A., 1995. Integration of biomaterials implanted into abdominal wall: process of scar formation and macrophages response. Biomaterials 16, 381–387.

Bellón, J. M., Contreras, L., Buján, J., Carrera-San-Martín, A., Longas, G., Moreno, J., 1996. Influencia sobre el proceso cicatricial de la porosidad de biomateriales protésicos implantados en la pared abdominal. Cirugía Española 59, 296–302.

Bellón, J. M., Rodríguez, M., García-Honduvilla, N., Gómez-Gil, V., Pascual, G., Buján, J., 2009. Comparing the behavior of different polypropylene meshes (heavy and lightweight) in an experimental model of ventral hernia repair. Journal of Biomedical Materials Research. Part B, Applied Biomaterials 89B(2), 448–455.

Bellón, J. M., Rodríguez, M., García-Honduvilla, N., Pascual, G., Buján, J., 2007. Partially absorbable meshes for hernia repair offer advantages over nonabsorbable meshes. The American Journal of Surgery 194, 68–74.

Bellón-Caneiro, J. M., García-Carranza, A., García-Honduvilla, N., Carrera-San-Martín, A., Buján, J., 2004. Tissue integration and biomechanical behaviour of contaminated experimental polypropylene and expanded polytetrafluoroethylene implants. British Journal of Surgery 91, 489–494.

Binnebösel, M., Rosch, R., Junge, K., Flanagran, T., Schwab, R., Schumpelick, V., Klinge, U., 2007. Biomechanical analyses of overlap and mesh dislocation in an incisional hernia model in vivo. Surgery 142(3), 365–371.

Blemker, B. B., Pinsky, P. M., Delp, S. L., 2005. A 3D model of muscle reveals the causes of nonuniform strains in the biceps brachii. Annals of Biomedical Engineering 38, 657–665.

Bol, M., Reese, S., 2008. Micromechanical modelling of skeletal muscles based on the finite element method. Computer Methods in Biomechanics and Biomedical Engineering 11, 489–504.

Bol, M., Stark, H., Schilline, N., 2011. On a phenomenological model for fatigue effects in skeletal muscles. Jounal of Theoretical Biology 281, 122–132.

Border, W. A., Noble, N. A., 1994. Transforming growth factor beta in tissue fibrosis. New England Journal of Medicine 331, 1286–1292.

Boriek, A. M., Kelly, M. G., Rodarte, J. R., Wilson, T. A., 2000. Biaxial constitutive relations for the passive canine diaphragm. Journal of Applied Physiology 89, 2187–2190.

Calvo, B., Peña, E., Martins, P., Mascarenhas, T., Doblare, M., Natal, R., Ferreira, A., 2009. On modelling damage process in vaginal tissue. Journal of Biomechanics 42, 642–651.

Calvo, B., Ramírez, A., Alonso, A., Grasa, J., Soteras, F., Osta, R., Muñoz, M. J., 2010. Passive non linear elastic behaviour of skeletal muscle: Experimental results and model formulation. Journal of Biomechanics 43, 318–325.

Caner, F. C., Carol, I., 2006. Microplane constitutive model and computational framework for blood vessel tissue. Journal of Biomechanical Engineering 128(3), 419–427.

Chew, D. K., Choi, L. H., Rogers, A. M., 2000. Entero cutaneous fistula 14 years after prosthetic mesh repair of a ventral incisional hernia. Alife-long risk? Surgery 125, 101–111.

Chi, S., Hodgson, J., Chen, J. S., Edgerton, V. R., Shin, D. D., Roiz, R. A., Sinha, S., 2010. Finite element modeling reveals complex strain mechanics in the aponeuroses of contracting skeletal muscle. Journal of Biomechanics 43, 1243–1250.

Chuback, J. A., Sigh, R. S., Sill, C., Dick, L. S., 2000. Small bowel obstruction resulting from mesh plug migration after open inguinal hernia repair. Surgery 127, 475–466.

Ciarletta, P., Micera, S., Accoto, D., Dario, P., 2006. A novel microstructural approach in tendon viscoelastic modelling at the fibrillar level. Journal of Biomechanics 39 (11), 2034–2042.

Cobb, W. S., Burns, J. M., Kercher, K. W., Matthews, B. D., Norton, H. J., Heniford, B. T., 2005. Normal intraabdominal pressure in healthy adults. Journal of Surgical Research 129, 231–235.

Cobb, W. S., Burns, J. M., Peindl, R. D., Carbonell, A. M., Matthews, B. D., Kercher, K. W., Heniford, B. T., 2006. Textile analysis of heavy-weight, mid-weight and light-weight polypropylene mesh in a porcine ventral hernia model. Journal of Surgical Research 136, 1–7.

Colomo, F., Piroddi, N., Poggesi, C., te Kronnie, G., Tesi, C., 1997. Active and passive forces of isolated myofibrils from cardiac and fast skeletal muscle of the frog. Journal of Physiology 500(Pt 2), 535–548.

Conze, J., Kingsnorth, A. N., b. Flament, J., Simmermacher, R., Artl, G., Langer, C., 2005. Randomized clinical trial comparing lightweight composite mesh with polyester or polypropylene mesh for incisional hernia repair. British Journal of Surgery 92, 1488–1493.

Costello, C. R., Bachman, S. L., Grant, S. A., Cleveland, D. S., Loy, T. S., Ramshaw, B. J., 2007. Characterization of heavyweight and lightweight polypropylene prosthetic mesh explants from a single patient. Surgical Innovation 14, 168–176.

Davis, J., Kaufman, K. R., Lieber, R. L., 2003. Correlation between active and passive isometric force and intramuscular pressure in the isolated rabbit tibialis anterior muscle. Journal of Biomechanics 36(4), 505–512.

Deeken, C. R., Abdo, M. S., Frisella, M. M., Matthews, B., 2011. Physicomechanical evaluation of polypropylene, polyester, and polytetrafluoroethylene meshes for inguinal hernia repair. Journal of the American College of Surgeons 212(1), 68–79.

Demiray, H., 1972. A note on the elasticity of soft biological tissues. Journal of Biomechanics 5, 309–311.

Demiray, H., Weizsacker, H. W., Pascale, K., Erbay, H., 1988. A stress-strain relation for a rat abdominal aorta. Journal of Biomechanics 21, 369–374.

Deysine, M., 1998. Ventral herniorraphy: treatment evolution in a hernia service. Hernia 2, 15–18.

Earle, D. B., Mark, L. A., 2008. Prosthetic material in inguinal hernia repair: How do I choose? Surgical Clinics of North America 88, 179–201.

Ehret, A. E., Böl, M., Itskov, M., 2011. A continium constitutive model for the active behaviour of skeletal muscle. Journal of the Mechanics and Physics of Solids 59, 625–636.

Eisenberg, E., Hill, T. L., Chen, Y., 1980. Cross-bridge model of contraction, quantitative analysis. Biophysical Journal 29, 195–227.

Enoka, R. M., 2002. Activation order of motor axons in electrically evoked contractions. Muscle Nerve 25(6), 763–764.

Fernandez, J. W., Pandy, M. G., 2006. Integrating modelling and experiments to assess dynamic musculoskeletal function in humans. Experimental Physiology 91(2), 371–382.

Fortuny, G., Rodríguez-Navarro, J., Susín, A., Armengol-Carrasco, M., López-Cano, M., 2009a. A simulation finite element model for the mechanics of the internal oblique muscle: A defense mechanism against inguinal hernia formation? Computers in Biology and Medicine 39, 794–799.

Fortuny, G., Rodríguez-Navarro, J., Susín, A., López-Cano, M., 2009b. Simulation and study of the behaviour of the transversalis fascia in protecting against the genesis of inguinal hernias. Journal of Biomechanics 42, 2263–2267.

Förstemann, T., Trzewik, J., Holste, J., BAtke, B., Konerding, M. A., Wolloscheck, T., Hartung, C., 2011. Forces and deformations of the abdominal wall - A mechanical and geometrical approach to the linea alba. Journal of Biomechanics 44, 600–606.

Fung, Y. C., 1993. Biomechanics. Mechanical properties of living tissues. Springer-Verlag.

Fung, Y. C., Fronek, K., Patitucci, P., 1979. Pseudoelasticity of arteries and the choice of its mathematical expression. American Journal of Physiology 237, H620–H631.

Gajdosik, R. L., 2001. Passive extensibility of skeletal muscle: review of the literature with clinical implications. Clinical Biomechanics 16(2), 87–101.

García-Moreno, F., 2001. Reparación de defectos de la pared abdominal con biomateriales tipo composite. Evaluación y estudio del comportamiento a nivel peritoneal. Ph.D. thesis, University of Alcalá, Alcalá de Henares, Spain.

García-Pumarino, R., 2010. Comportamiento de diferentes bioprótesis de colágeno en presencia de contaminación bacteriana. estudio experimental “in vitro” e “in vivo”. Ph.D. thesis, University of Alcalá, Spain.

Gardiner, J. C., Weiss, J. A., Rosenberg, T. D., 2001. Strain in the human medial collateral ligament during valgus loading of the knee. Clinical Orthopaedics and Related Research 391, 266–274.

González-Badillo, J. J., Ribas, J., 2002. Programación del entrenamiento de fuerza. Inde Publicaciones.

Gordon, A., Huxley, A. F., Julian, F., 1966. The variations in isometric tension with sarcomere length in vertebrate muscle fibres. Journal of Physiology 84, 170–192.

Grasa, J., Hernández-Gascón, B., Ramírez, A., Rodríguez, J. F., Calvo, B., 2013. Numerical simulation of the behaviour of musculoskeletal tissue. Revista Internacional de Métodos Numéricos para Cálculo y Diseño en Ingeniería 28(3), 177–186.

Grasa, J., Ramírez, A., Osta, R., Muñoz, M. J., Soteras, F., Calvo, B., 2011. A 3D active-passive numerical skeletal muscle model incorporating initial tissue strains. Validation with experimental results on rat tibialis anterior muscle. Biomechanics and Modeling in Mechanobiology 10, 779–787.

Grassel, D., Prescher, A., Fitzed, S., Keyserlingk, D. G., Axer, H., 2005. Anisotropy of human linea alba: a biomechanical study. Journal of Surgical Research 124, 118–125.

Grover, J. P., Corr, D. T., Toumi, H., Manthei, D. M., Oza, A. L., Vanderby, R., Best, T. M., 2007. The effect of stretch rate and activation state on skeletal muscle force in the anatomical range. Clinical Biomechanics 22(3), 360–368.

Hatze, H., 1981. Myocybernetic control models of skeletal muscle. Biological Cybernetics 25(2), 103–119.

Hernández, B., Peña, E., Pascual, G., Rodríguez, M., Calvo, B., Doblaré, M., Bellón, J. M., 2011. Mechanical and histological characterization of the abdominal muscle. A previous step to model hernia surgery. Journal of the Mechanical Behavior of Biomedical Materials 4(3), 392–404.

Hernández-Gascón, B., Espés, N., Peña, E., Pascual, G., Bellón, J. M., Calvo, B., 2012a. Computational framework to model and design surgical meshes for hernia repair. Computer Methods in Biomechanics and Biomedical Engineering In Press, DOI:10.1080/10255842.2012.736967.

Hernández-Gascón, B., Grasa, J., Calvo, B., Rodríguez, J. F., 2012b. A 3D continuum model for simulating skeletal muscle contraction , Submitted.

Hernández-Gascón, B., Mena, A., Peña, E., Pascual, G., Bellón, J. M., Calvo, B., 2012c. Understanding the passive mechanical behavior of the human abdominal wall. Annals of Biomedical Engineering In Press, DOI: 10.1007/s10439–012–0672–7.

Hernández-Gascón, B., Peña, E., Grasa, J., Pascual, G., Bellón, J. M., Calvo, B., 2012d. Mechanical response of the herniated human abdomen to the placement of different prostheses , Submitted.

Hernández-Gascón, B., Peña, E., Melero, H., Pascual, G., Doblaré, M., Ginebra, M. P., Bellón, J. M., Calvo, B., 2011. Mechanical behaviour of synthetic surgical meshes. Finite element simulation of the herniated abdominal wall. Acta Biomaterialia 7(11), 3905–3913.

Hernández-Gascón, B., Peña, E., Pascual, G., Rodríguez, M., Bellón, J. M., Calvo, B., 2012e. Long-term anisotropic mechanical response of surgical meshes used to repair abdominal wall defects. Journal of the Mechanical Behavior of Biomedical Materials 5(1), 257–271.

Hilger, W. S., Walker, A., Zobitz, M. E., Leslie, K. O., Magtibay, P., Cornella, J., 2006. Histological and biomechanical evaluation of implanted graft materials in a rabbit vaginal and abdominal model. American Journal of Obstetrics and Gynecology 195, 1826–1831.

Hill, A. V., 1938. The heat of shortening and the dynamic constants of muscle. Proceedings of the Royal Society of London B 126, 136–195.

Hill, T. L., Eisenberg, E., Chen, Y., 1975. Some self-consistent two-state sliding filament models of muscle contractions. Biophysical Journal 15, 335–372.

Hodgson, J. A., Chi, S. W., Yang, J. P., Chen, J. S., Edgerton, V. R., Sinha, S., 2012. Finite element modeling of passive material influence on the deformation and force output of skeletal muscle. Journal of the Mechanical Behaviour of Biomedical Materials 9, 163–183.

Hollinsky, C., Sandberg, S., Koch, T., Seidler, S., 2008. Biomechanical properties of lightweight versus heavyweight meshes for laparoscopic inguinal hernia repair and their impact on recurrence rates. Surgical Endoscopy 22, 2679–2685.

Holste, J. L., 2005. Are meshes with lightweight construction strong enough? International Surgery 90(3 Suppl), S10–12.

Holzapfel, G. A., 2000. Nonlinear Solid Mechanics. Wiley, New York.

Holzapfel, G. A., 2006. Determination of material models for arterial walls from uniaxial extension tests and histological structure. Journal of Theoretical Biology 238, 290–302.

Holzapfel, G. A., Gasser, C. T., Sommer, G., Regitnig, P., 2005. Determination of the layer-specific mechanical properties of human coronary arteries with nonatherosclerotic intimal thickening, and related constitutive modelling. American Journal of Physiology - Heart and Circulatory Physiology 289, H2048–H2058.

Holzapfel, G. A., Gasser, T. C., Ogden, R. W., 2000. A new constitutive framework for arterial wall mechanics and a comparative study of material models. Journal of Elasticity 61, 1–48.

Holzapfel, G. A., Ogden, R. W., 2009. On planar biaxial tests for anisotropic nonlinearly elastic solids. A continuum mechanical framework. Mathematics and Mechanics of Solids 14(5), 474–489.

Huijing, P. A., 1997. Muscle as a collagen fiber reinforced composite: a review of force transmission in muscle and whole limb. Journal of Biomechanics 32, 329–345.

Huijing, P. A., 1998. Muscle the motor of movement: properties in function, experiment and modeling. Journal of Electromyography and Kinesiology 8, 61–77.

Huijing, P. A., Woittiez, R. D., 1984. The effect of architecture on skeletal muscle performance. Netherlands Journal of Zoology 34, 21–32.

Humphrey, J. D., Na, S., 2002. Elastodynamics and arterial wall stress. Annals of Biomedical Engineering 30(4), 509–523.

Hunter, P. J., McCulloch, A. D., 1988. Computational Methods in Bioengineering. The American Society of Mechanical Engineers, Ch. A finite element model of passive ventricular mechanics, pp. 387–397.

Huxley, A. F., 1957. Muscle structure and theories of contraction. Progress in Biophysics and Biophysical Chemistry 173, 257–318.

Huxley, A. F., Hanson, J., 1954. Changes in cross-striations of muscle during contraction and stretch and their structural interpretation. Nature 173, 973–976.

Huxley, A. F., Niedergerke, R., 1954. Interference microscopy of living muscle fibers. Nature 173, 971–973.

Huxley, H. E., 1966. The fine structure of striated muscle and its functional significance. Harvey Lectures 60, 85–118.

Hwang, W., Carvalho, J. C., Tarlovsky, I., Boriek, A. M., 2005. Passive mechanics of canine internal abdominal muscles. Journal of Applied Physiology 98(5), 1829–1835.

Ito, D., Tanaka, E., Yamamoto, S., 2010. A novel constitutive model of skeletal muscle taking into account anisotropic damage. Journal of Mechanical Behaviour of Biomedical Materials 3, 85–93.

Jenkyn, T. R., Koopman, B., Huijing, P., Lieber, R., Kaufman, K. R., 2002. Finite element model of intramuscular pressure during isometric contraction of skeletal muscle. Physics in Medicine and Biology 47(22), 4043–4061.

Jezupors, A., Mihelsons, M., 2006. The analysis of infection after polypropylene mesh repair of abdominal wall hernia. World Journal of Surgery 30(12), 2270–2278.

Johnson, E. K., Hoyt, C. H., Dinsmore, R. C., 2004. Abdominal wall hernia repair: a long-term comparison of Sepramesh and Dualmesh in a rabbit hernia model. American Journal of Surgery 70(8), 657–661.

Judge, T. W., Parker, D. M., Dinsmore, R. C., 2007. Abdominal wall hernia repair: a comparison of Sepramesh and Parietex composite mesh in a rabbit hernia model. Journal of the American College of Surgeons 204(2), 276–281.

Junge, K., Klinge, U., Prescher, A., Giboni, P., Niewiera, M., Shumpelick, V., 2001. Elasticity of the anterior abdominal wall and impact for reparation of incisional hernia using mesh implants. Hernia 5, 112–118.

Junge, K., Klinge, U., Rosch, R., Klosterhalfen, B., Shumpelick, V., 2002. Functional and morphologic properties of a modified mesh for inguinal hernia repair. World Journal of Surgery 26, 1472–1480.

Junge, K., r. Rosch, Krones, J., Klinge, U., Martens, P. R., Lynen, P., 2005. Influence of polyglecaprone 25 (monocryl) supplementation on the biocompatibility of a polypropylene mesh for hernia repair. Hernia 9, 212–217.

Kapischke, M., Prinz, K., Tepel, J., Tensfeldt, J., Schulz, T., 2005. Comparative investigation of alloplastic materials for hernia repair with improved methodology. Surgical Endoscopy 19, 1260–1265.

Katz, B., 1939. The relation between force and speed in muscular contraction. Journal of Physiology 96, 45–64.

Kes, E., Lange, J., Bonjer, J., Stoeckart, R., Mulder, P., Snijders, C., Kleinrensink, G., 2004. Protrusion of prosthetic meshes in repair of inguinal hernias. Surgery 135(2), 163–170.

King, M. J., Jearanaisilawong, P., Socrate, S., 2005. A continuum constitutive model for the mechanical behavior of woven fabrics. International Journal of Solids and Structures 42, 3867–3896.

Kingsnorth, A., LeBlanc, K., 2003. Hernias: inguinal and incisional. Lancet 362, 1561–1574.

Kirilova, M., Stoytchev, S., Pashkouleva, D., Kavardzhikov, V., 2010. Experimental study of the mechanical properties of human abdominal fascia. Medical Engineering & Physics 33(1), 1–6.

Kirilova, M., Stoytchev, S., Pashkouleva, D., Tsenova, V., Hristoskova, R., 2009. Viscoelastic mechanical properties of human abdominal fascia. Journal of Bodywork and Movement Therapies 13, 336–337.

Kjaer, M., 2004. Role of extracellular matrix in adaptation of tendon and skeletal muscle to mechanical loading. Physiological Reviews 84, 649–698.

Klinge, U., 2007. Experimental comparison of monofile light and heavy polypropylene meshes: less weight does not mean less biological response. World Journal of Surgery 31, 867–868.

Klinge, U., Junge, K., Stumpf, M., Klosterhalfen, B., 2002a. Functional and morphological evaluation of a low-weight monofilament polypropylene mesh for hernia repair. Journal of Biomedical Materials Research. Part B, Applied Biomaterials 63, 129–136.

Klinge, U., Klosterhalfen, B., Birkenhauer, V., Junge, K., Conze, J., Schumpelick, V., 2002b. Impact of polymer pore size on the interface scar formation in a rat model. Journal of Surgical Research 103, 208–214.

Klinge, U., Klosterhalfen, B., Conze, J., Limberg, W., Obolenski, B., Öttinger, A. P., Schumpelick, V., 1998. Modified mesh for hernia repair that is adapted to the physiology of the abdominal wall. European Journal of Surgery 164, 951–960.

Klosterhalfen, B., Junge, K., Klinge, U., 2005. The lightweight and large porous mesh concept for hernia repair. Expert Review of Medical Devices 2, 103–117.

Konerding, M. A., Bohn, M., Wolloscheck, T., Batke, B., Holste, J. L., Wohlert, S., Trzewik, J., Förstemann, T., Hartung, C., 2011a. Maximum forces acting on the abdominal wall: Experimental validation of a theoretical modeling in a human cadaver study. Medical Engineering & Physics 33(6), 789–792.

Konerding, M. A., Chantereau, P., v. Delventhal, Holste, J. L., Ackermann, M., 2011b. Biomechanical and histological evaluation of abdominal wall compliance with intraperitoneal onlay mesh implants in rabbits: A comparison of six different state-of-the-art meshes. Medical Engineering & Physics 34, 806–816.

Konishi, M., Watanabe, M., 1998. Steady state relation between cytoplasmic free Ca2+ concentration and force in intact frog skeletal muscle fibers. Journal of General Physiology 111(4), 505–519.

Kureshi, A., Vaiude, P., an A. Petrie, S. N. N., Brown, R. A., 2008. Matrix mechanical properties of transversalis fascia in inguinal herniation as a model for tissue expansion. Journal of Biomechanics 41, 3462–3468.

Kuwazuru, O., Yoshikawa, N., 2004. Theory of Elasticity for Plain-Weave Fabrics. Japan Society Mechanical Engineering International Journal 47(1), 17–25.

Lanchares, E., Calvo, B., Cristóbal, J. A., Doblaré, M., 2008. Finite element simulation of arcuates for astigmatism correction. Journal of Biomechanics 41, 797–805.

Langenbach, M. R., Schmidt, J., Ubrig, B., Zirngibl, H., 2008. Sixty-month follow-up after endoscopic inguinal hernia repair with three types of mesh: a prospective randomized trial. Surgical Endoscopy 22, 1790–1797.

Lanir, Y., 1979. A structural theory for the homogeneous biaxial stress-strain relationship in flat collageneous tissues. Journal of Biomechanics 12, 423–436.

LeBlanc, K. A., Bellanger, D., 5th, K. V. R., Baker, D. G., Stout, R. W., 2002. Tissue attachment strength of prosthetic meshes used in ventral and incisional hernia repair. A study in the New Zealand White rabbit adhesion model. Surgical Endoscopy 16(11), 1542–1546.

Leeuwen, J. L. V., Spoor, C. W., 1992. Modelling mechanically stable muscle architecture. Philosophical Transactions of the Royal Society B: Biological Sciences 336(1277), 275–292.

Leeuwen, J. L. V., Spoor, C. W., 1996. Modelling the pressure and force equilibrium in unipennate muscle with in-line tendons. Philosophical Transactions of the Royal Society B 342, 321–333.

Leibovich, S. J., Ross, R., 2007. The role of the macrophage in wound repair. American Journal of Pathology 78, 71–91.

Lemos, R., 2001. Realistic skeletal muscle deformation using finite element analysis. In: Proceedings of XIV Brazilian Symposium on Computer Graphics and Image Processing. Institute of Electrical and Electronics Engineers (IEEE) , pp. 192–199.

Lichtenstein, I. L., Shulman, A. G., 1986. Ambulatory outpatient hernia surgery including a new concept, introducing tension-free repair. International Surgery 71, 1–4.

Lichtenstein, I. L., Shulman, A. G., Amid, P. K., Montlor, M. M., 1989. The tension-free hernioplasty. American Journal of Surgery 157, 188–193.

Linden, V. D., 1998. Mechanical modeling of skeletal muscle functioning. Ph.D. thesis, University of Twente, The Netherlands.

Lintin, L. A. D., Kingsnorth, A. N., 2012. Mechanical failure of a lightweight polypropylene mesh. Hernia In Press, DOI: 10.1007/s10029–012–0959–5.

Loocke, M. V., Lyons, C., Simms, C., 2004. Stress-strain-time relations for soft connective tissues. In: Prendergast, P., McHugh, P. (Eds.), Topics in Bio-Mechanical Engineering. Trinity Centre for Bioengineering & National Centre for Biomedical Engineering Science, pp. 216–234.

Loocke, M. V., Lyons, C. G., Simms, C. K., 2008. Viscoelastic properties of passive skeletal muscle in compression: Stress-relaxation behaviour and constitutive modelling. Journal of Biomechanics 41(7), 1555–1566.

Loocke, M. V., Simms, C. K., Lyons, C. G., 2009. Viscoelastic properties of passive skeletal muscle in compression - cyclic behaviour. Journal of Biomechanics 42, 1038–1048.

López-Cano, M., Rodríguez-Navarro, J., Rodríguez-Baeza, A., Armengol-Carrasco, M., Susín, A., 2007. A real-time dynamic 3D model of the human inguinal region for surgical education. Computers in Biology and Medicine 37, 1321–1326.

Ma, S. P., Zahalak, G. I., 1987. A simple self-consistent distribution-moment model for muscle: Chemical energy and heat rates. Mathematical Biosciences 84, 211–230.

Maganaris, C. N., Paul, J. P., 1999. In vivo human tendon mechanical properties. Journal of Physiology 521, 307–313.

Martins, J. A. C., Pires, E. B., Salvado, R., Dinis, P. B., 1998. A numerical model of passive and active behavior of skeletal muscles. Computer Methods in Applied Mechanics and Engineering 151, 419–433.

Martins, P., Peña, E., Calvo, B., Doblaré, M., Mascarenhas, T., Jorge, R. N., Ferreira, A., 2010. Prediction of nonlinear elastic behavior of vaginal tissue: Experimental results and model formulation. Computer Methods in Biomechanics and Biomedical Engineering 13(3), 327–337.

Martins, P., Peña, E., Jorge, R. M. N., Santos, A., Santos, L., Mascarenhas, T., Calvo, B., 2012. Mechanical characterization and constitutive modelling of the damage process in rectus sheath. Journal of the Mechanical Behavior of Biomedical Materials 8, 111–122.

McCullock, A. D., Waldman, L., Rogers, J., Guccione, J., 1992. Large-scale finite element analysis of the beating heart. Critical Reviews in Biomedical Engineering 20(5-6), 427–449.

Mooney, M., 1940. A theory of large elastic deformation. Journal of Applied Physics 11, 582–592.

Moore W., 2008. Gray's Anatomy celebrates 150th anniversary. The Telegraph (Telegraph Media Group).

Morrow, D. A., Donahue, T. H., Odegard, G. M., Haufman, K. R., 2010. A method for assesing the fit of a constitutive material model to experimental stress-strain data. Computer Methods in Biomechanics and Biomedical Engineering 12, 247–256.

Murphy, T., 2010. MotionWorks. `/http://www.motionworkspt.com/`, accessed September 25, 2012.

Nilsson, T., 1982a. Biomechanical studies of rabbit abdominal wall. Part I.- The mechanical properties of specimens from different anatomical positions. Journal of Biomechanics 15(2), 123–129.

Nilsson, T., 1982b. Biomechanical studies of rabbit abdominal wall. Part II.- The mechanical properties of specimens in relation to length, width, and fibre orientation. Journal of Biomechanics 15(2), 131–135.

Odegard, G. M., Donahue, T. L. H., Morrow, D. A., Kaufman, K. R., 2008. Constitutive modeling of skeletal muscle tissue with an explicit strain-energy function. Journal of Biomechanical Engineering 130(6), 061017.

O'Dwyer, P. J., Kingsnorth, A. N., Mohillo, R. G., Small, P. K., Lammers, B., Horeysee, G., 2005. Randomized clinical trial assessing impact of a lightweight or heavyweight on chronic pain after inguinal hernia repair. British Journal of Surgery 92, 166–170.

Ogden, R. W., 2001. Nonlinear Elasticity, Anisotropy, Material Stability and Residual Stresses in Soft Tissue. Lecture Notes, CISM. Course on Biomechanics of Soft Tissue, Udine.

Otten, E., 1988. Concepts and models of functional arquitecture in skeletal muscle. Exercise and Sport Sciences Reviews 16, 89–137.

Ozog, Y., Konstantinovic, M. L., Werbrouck, E., Ridder, D. D., Mazza, E., Deprest, J., 2011. Persistence of polypropylene mesh anisotropy after implantation: an experimental study. Urogynaecology 118(10), 1180–1185.

Palomar, A. P. D., Doblaré, M., 2006. On the numerical simulation of the mechanical behaviour of articular cartilage. International Journal for Numerical Methods in Engineering 67, 244–1271.

Pandit, A. S., Henry, J. A., 2004. Design of surgical meshes - an engineering perspective. Technology and Health Care 12, 51–65.

Park, A. E., Roth, J. S., Kavic, S. M., 2006. Abdominal wall hernia. Current Problems in Surgery 43, 326–375.

Pascual, G., Hernández-Gascón, B., Rodríguez, M., Sotomayor, S., Peña, E., Calvo, B., Bellón, J. M., 2012a. The long term behavior of lightweight and heavyweight meshes used to repair abdominal wall defects is determined by the host tissue repair process provoked by the mesh. Surgery 152(5), 886–895.

Pascual, G., Hernández-Gascón, B., Sotomayor, S., Peña, E., Calvo, B., Buján, J., Bellón, J. M., 2012b. Short-term behaviour of different polymer structure lightweight meshes used to repair abdominal wall defects. Histology and Histopathology , Accepted.

Pascual, G., Rodríguez, M., Gómez-Gil, V., García-Honduvilla, N., Buján, J., Bellón, J. M., 2008. Early tissue incorporation and collagen deposition in lightweight polypropylene meshes: bioassay in an experimental model of ventral hernia. Surgery 144, 427–435.

Pascual, G., Rodríguez, M., Sotomayor, S., Perez-Köhler, B., Bellón, J. M., 2012c. Inflammatory reaction and neotissue maturation in the early host tissue incorporation of polypropylene prostheses. Hernia In Press, DOI 10.1007/s10029–012–0945–y.

Peña, E., Calvo, B., Martínez, M. A., Martins, P., Mascarenhas, T., Jorge, R. M. N., Ferreira, A., Doblare, M., 2010. Experimental study and constitutive modeling of the viscoelastic mechanical properties of the human prolapsed vaginal tissue. Biomechanics and Modeling in Mechanobiology 9, 35–44.

Peña, E., del Palomar, A. P., Calvo, B., Martínez, M. A., Doblaré, M., 2007. Computational modelling of diarthrodial joints. Physiological, pathological and pos-surgery simulations. Archives of Computational Methods in Engineering 14(1), 47–91.

Peña, E., Martinez, M. A., Calvo, B., Doblaré, M., 2006. On the numerical treatment of initial strains in soft biological tissues. International Journal for Numerical Methods in Engineering 68, 836–860.

Podwojewski, F., Otténio, M., Beillas, P., Guérin, G., Turquier, F., Mitton, D., 2012. Mechanical response of animal abdominal walls in vitro: Evaluation of the influence of a hernia defect and a repair with a mesh implanted intraperitoneally. Journal of Biomechanics DOI: 10.1016/j.jbiomech.2012.09.014.

Pqax, 2011. Pqax Wikispaces. `http://pqax.wikispaces.com/`, accessed September 25, 2012.

Ramírez, A., Grasa, J., Alonso, A., Soteras, F., Osta, R., Muñoz, M. J., Calvo, B., 2010. Active response of skeletal muscle: *in vivo* experimental results and model formulation. Journal of Theoretical Biology 267, 546–553.

Ramírez-Martínez, A. M., 2011. Modelado y simulación del tejido músculo-esquelético. Ph.D. thesis, University of Zaragoza, Spain.

Ramsey, R. W., Street, S. F., 1940. The isometric length-tension diagram of isolated skeletal muscle fibers of the frog. Journal of Cellular and Comparative Physiology 15, 11–34.

Ramshaw, B., 2009. Novus Scientific. `www.novusscientific.com`, accessed September 25, 2012.

Rath, A. M., Attali, P., Dumas, J. L., Goldlust, D., Zhang, J., 1996. The abdominal linea alba: an anatomoradiologic and biomechanical study. Surgical and Radiologic Anatomy 18, 281–288.

Röhrnbauer, B., Kress, G., Mazza, E., 2011. Procs. International Conference on Computational Plasticity - Fundamentals and Applications (COMPLAS XI), Barcelona, Spain. Multi-Scale Characterization and Modeling of Medical Mesh Implants .

Rizk, N., 1980. A new description of the anterior abdominal wall in man and mammals. Journal of Anatomy 131, 373–385.

Rosch, R., Junge, K., Hölzl, F., Schachtrupp, A., Stumpf, M., Klinge, U., 2004. Meshes: Benefits and risks. Springer-Verlag, Berlin,Heidelberg,New York, Ch. How to construct a mesh? Impact of structure, filament and pore size for tissue ingrowth, pp. 179–188.

Rosch, R., Junge, K., Quester, R., Klinge, U., Klosterhalfen, B., Schumpelick, V., 2003. Vypro II mesh in hernia repair: impact of polyglactin on long-term incorporation in rats. European Surgical Research 35, 445–450.

Sabbagh, C., Dumont, F., Robert, B., Badaoui, R., Verhaeghe, P., Regimbeau, J. M., 2011. Peritoneal volume is predictive of tension-free fascia closure of large incisional hernias with loss of domain: a prospective study. Hernia 15(5), 559–565.

Saberski, E. R., Orenstein, S. B., Novitsky, Y. W., 2010. Anisotropic evaluation of synthetic surgical meshes. Hernia 15(1), 47–52.

Sandercock, T. G., 2003. Nonlinear summation of force in cat tibialis anterior: a muscle with intrafascicularly terminating fibers. Journal of Applied Physiology 94(5), 1955–1963.

Schachtrupp, A., Klinge, U., Junge, K., Rosch, R., Bhardwaj, R. S., Schumpelick, V., 2003. Individual inflammatory response of human blood monocyte to mesh biomaterials. British Journal of Surgery 90, 114–120.

Schimidbauer, S., Ladurner, R., hallfeldt, K. K., Mussack, T., 2005. Heavy-weight versus low-weight polypropylene meshes for open sublay mesh repair of incisional hernia. European Journal of Medical Research 10, 247–253.

Schumepelick, V., Klinge, U., 2003. Prosthetic implants for hernia repair. British Journal of Surgery 90, 1457–1458.

Schwab, R., Schumacher, O., Junge, K., Binnebösel, M., Klinge, U., Becker, H. P., Schumpelick, V., 2008. Biomechanical analyses of mesh fixation in TAPP and TEP hernia repair. Surgical Endoscopy 22(3), 731–738.

Sergent, F., Desilles, N., Lacoume, Y., Tuech, J. J., Marie, J. P., Bunel, C., 2010. Biomechanical analysis of polypropylene prosthetic implants for hernia repair: an experimental study. The American Journal of Surgery 200, 406–412.

Sharafi, B., Blemker, S. S., 2010. A micromechanical model of skeletal muscle to explore the effects of fiber and fascicle geometry. Journal of Biomechanics 43, 3207–3213.

Sistema-Muscular, 2012. Sistema Muscular. `http://elsistemamuscular.blogspot.com.es/`, accessed October 15, 2012.

Smietanski, M., Bury, K., Tomaszewska, A., Lubowiecka, I., Szymczak, C., 2012. Biomechanics of the front abdominal wall as a potential factor leading to recurrence with laparoscopic ventral hernia repair. Surgical Endoscopy 26(5), 1461–7.

Song, C., Alijani, A., Frank, T., Hanna, G., Cuschieri, A., 2006a. Elasticity of the living abdominal wall in laparoscopic surgery. Journal of Biomechanics 39, 587–591.

Song, C., Alijani, A., Frank, T., Hanna, G., Cuschieri, A., 2006b. Mechanical properties of the human abdominal wall measured in vivo during insufflation for laparoscopic surgery. Surgical Endoscopy 20, 987–990.

Spencer, A. J. M., 1971. Theory of invariants. In: Continuum Physics. Academic Press, New York, pp. 239–253.

Stålhand, J., Klarbring, A., Holzapfel, G. A., 2008. Smooth muscle contraction: mechanochemical formulation for homogeneous finite strains. Progress in Biophysics & Molecular Biology 96, 465–481.

Stålhand, J., Klarbring, A., Holzapfel, G. A., 2010. A micromechanical 3D continuum model for smooth muscle contraction under finite strains. Journal of Theoretical Biology 268(1), 120–130.

Szymczak, C., Lubowiecka, I., Tomaszewska, A., Smietanski, M., 2010. Modeling of the fascia-mesh system and sensitivity analysis of a junction force after a laparoscopic ventral hernia repair. Journal of Theoretical and Applied Mechanics 48(4), 933–950.

Szymczak, C., Lubowiecka, I., Tomaszewska, A., Smietanski, M., 2012. Investigation of abdomen surface deformation due to life excitation: Implications for implant selection and orientation in laparoscopic ventral hernia repair. Clinical Biomechanics 27, 105–110.

Szymczak, C., Tomaszewska, A., Lubowiecka, I., Smietanski, M., 2009. Mathematical study of a tissue-implant connection in a ventral hernia repair in a context of the system's parameters. Proceedings in Applied Mathematics and Mechanics 9, 167–168.

Taber, L. A., 1995. Biomechanics of growth, remodeling, and morphogenesis. Applied Mechanics Reviews 48, 487–545.

Usher, F. C., 1959. A new plastic prosthesis for repairing tissue defects of the chest and abdominal wall. Americal Journal of Surgery 97, 629–633.

Usher, F. C., Cogan, J. E., Lowry, T., 1960. A new technique for the repair of inguinal and incisional hernias. Archives of Surgery 84, 847–850.

Van Loocke, M., Lyons, C. G., Simms, C. K., 2006. A validated model of passive muscle in compression. Journal of Biomechanics 39(16), 2999–3009.

WebMD-LLC, 1994. MedScape. `http://emedicine.medscape.com/`, accessed September 25, 2012.

Weiss, J. A., 1994. A constitutive model and finite element representation for transversely isotropic soft tissues. Ph.D. thesis, University of Utah, United States.

Weiss, J. A., Maker, B. N., Govindjee, S., 1996. Finite element implementation of incompressible, transversely isotropic hyperelasticity. Computer Methods in Applied Mechanics of Engineering 135, 107–128.

Welty, G., Klinge, U., Klosterhalfen, B., Kaspeck, R., Schumpelick, V., 2001. Functional impairment and complaints following incisional hernia repair with different polypropylene meshes. Hernia 5, 142–147.

Weyhe, D., Schmitz, I., Belyaev, O., Grabs, R., Muller, K. M., Uhl, W., 2006. Experimental comparison of monofile light and heavy polypropylene meshes: less weight does not mean less biological response. World Journal of Surgery 30, 1586–1591.

Whal, S. M., h. Wong, McCartney-Francis, N., 1989. Role of growth factors in inflammation and repair. Journal of Cellular Biochemistry 40, 193–199.

Woittiez, R. D., Huijing, P. A., Boom, H. B. K., Rozendal, R. H., 1984. A three-dimensional muscle model: A quantified relation between form and function of skeletal muscles. Journal of Morphology 182, 95–113.

WordPress, 2012. Elite Culturismo. `http://www.eliteculturismo.com/`, accessed September 25, 2012.

Yeoh, O. H., 1993. Some forms of the strain energy function for rubber. Rubber Chemistry and Technology 66, 754–771.

Yoder, J. H., Elliott, D. M., 2010. Nonlinear and anisotropic tensile properties of graft materials. Clinical Biomechanics 25, 378–382.

Zahalak, G., 1981. A distributed moment approximation for kinetic theories of muscular contraction. Mathematical Biosciences 55, 89–114.

COMPENDIUM OF PUBLICATIONS

Work 1: Mechanical and histological characterization of the abdominal muscle. A previous step to modelling hernia surgery

Journal: *Journal of the mechanical behavior of biomedical materials*, **4**(3) (2011): 392-404.
Journal impact factor: 2.814

JOURNAL OF THE MECHANICAL BEHAVIOR OF BIOMEDICAL MATERIALS 4 (2011) 392–404

available at www.sciencedirect.com

ScienceDirect

journal homepage: www.elsevier.com/locate/jmbbm

Research paper

Mechanical and histological characterization of the abdominal muscle. A previous step to modelling hernia surgery

B. Hernández[a,d], E. Peña[a,d], G. Pascual[b,d], M. Rodríguez[c,d], B. Calvo[a,d,*], M. Doblaré[a,d], J.M. Bellón[c,d]

[a] Group of Structural Mechanics and Materials Modelling (GEMM), Aragón Institute of Engineering Research (I3A), University of Zaragoza, Spain
[b] Departament of Medical Specialities, Faculty of Medicine, University of Alcalá, Spain
[c] Departament of Surgery, Faculty of Medicine, University of Alcalá, Spain
[d] Centro de Investigación Biomédica en Red en Bioingeniería, Biomateriales y Nanomedicina (CIBER-BBN), Spain

ARTICLE INFO

Article history:
Received 9 July 2010
Received in revised form
11 November 2010
Accepted 25 November 2010
Published online 3 December 2010

Keywords:
Abdominal muscle
Initial strain
Passive behaviour
Collagen fibres
Muscle fibres
Anisotropy
Hyperelasticity

ABSTRACT

The aims of this study are to experimentally characterize the passive elastic behaviour of the rabbit abdominal wall and to develop a mechanical constitutive law which accurately reproduces the obtained experimental results. For this purpose, tissue samples from New Zealand White rabbits 2150 ± 50 (g) were mechanically tested *in vitro*.

Mechanical tests, consisting of uniaxial loading on tissue samples oriented along the craneo–caudal and the perpendicular directions, respectively, revealed the anisotropic non-linear mechanical behaviour of the abdominal tissues. Experiments were performed considering the composite muscle (including external oblique-EO, internal oblique-IO and transverse abdominis-TA muscle layers), as well as separated muscle layers (i.e., external oblique, and the bilayer formed by internal oblique and transverse abdominis). Both the EO muscle layer and the IO–TA bilayer demonstrated a stiffer behaviour along the transversal direction to muscle fibres than along the longitudinal one. The fibre arrangement was measured by means of a histological study which confirmed that collagen fibres are mainly responsible for the passive mechanical strength and stiffness. Furthermore, the degree of anisotropy of the abdominal composite muscle turned out to be less pronounced than those obtained while studying the EO and IO–TA separately.

Moreover, a phenomenological constitutive law was used to capture the measured experimental curves. A Levenberg–Marquardt optimization algorithm was used to fit the model constants to reproduce the experimental curves.

* *Corresponding author at:* Group of Structural Mechanics and Materials Modelling (GEMM), Aragón Institute of Engineering Research (I3A), University of Zaragoza, Spain.
E-mail address: bcalvo@unizar.es (B. Calvo).

1751-6161/$ - see front matter © 2010 Elsevier Ltd. All rights reserved.
doi:10.1016/j.jmbbm.2010.11.012

1. Introduction

Hernia repair by implantation of synthetic meshes is the most widely used surgery for the treatment of this type of abdominal pathology. In technical terms, the repair of a hernial defect in the abdominal wall using a biomaterial has become routine clinical practice. However, hernia recurrences as well as other problems such as inflammatory reactions or adhesions between the implanted material and organs are still frequent (Rosch et al., 2004; Schippers, 2007).

Nowadays, there is a great variety of meshes available in the market which makes the choice of the optimal mesh a hard task for surgeons. For tissue repair, polypropylene is still the preferred material (Afonso et al., 2008; Pascual et al., 2008; Bellón, 2009), however, a wide variety of modifications regarding the structure and the porosity of the material can be applied to this material, aiming to improve the adaptation to the host tissue as well as to reduce the foreign body reaction and fibrosis provoked at the implant site. Despite these improvements, the "ideal prosthesis", in terms of pore size and spatial structure, which best adapts to the mechanical conditions of the host tissue has not been achieved yet.

The abdominal wall contains four expiratory muscles: the rectus abdominis, the external oblique (EO), the internal oblique (IO), and the transverse abdominis (TA). Anatomically, the IO lies internal to the EO muscle in the lateral abdominal wall, whereas the TA, the innermost abdominal muscle, lies in the lateral and ventral abdominal wall between the internal surface of the IO and the costal cartilage. The passive mechanical properties of these muscles from different animals have been studied by several authors. Hwang et al. (2005) studied the IO and TA separately, whereas Nilsson (1982a,b) focused on analysing different anatomical positions, geometric variables and fibre orientation, although no results regarding cross section areas were provided.

Regarding the constitutive behaviour of the muscular tissue, it has been usually considered as a network of muscle fibres, collagen and elastin embedded in a more or less isotropic matrix (Loocke et al., 2008; Ito et al., 2010). In the case of the abdominal muscle it is necessary to distinguish between collagen fibres, which are mainly responsible for the passive passive mechanical response, and muscular fibres, which are associated to the contractile muscle behaviour. Furthermore, muscular and collagen fibres are frequently not aligned in the same direction (Linden, 1998). The direction of collagen fibres is assumed to determine the direction of material anisotropy in order to study the passive behaviour of the tissue (Arruda et al., 2006), whereas muscle fibres have to be considered in the modelling of the active behaviour. The purely passive response of these soft tissues is often modelled within the framework of hyperelasticity by means of a strain energy function (SEF) expressed in terms of kinematic invariants (Spencer, 1954). Muscle tissue, in addition, has the unique characteristic of generating forces through fibre contraction. In order to incorporate this feature to models, it is common to describe the material behaviour as the addition of both passive and active contributions in the SEF (Martins et al., 1998; Fernandez and Pandy, 2006; Bol and Reese, 2008; Stalhand et al., 2008; Ito et al., 2010).

In the context of mathematical modelling and finite element (FE) simulation, appropriate experimental data are needed to estimate the model parameters (Palevski et al., 2006; Loocke et al., 2009; Morrow et al., 2010b). Furthermore, initial strains are needed to take into account the actual initial configuration and associated strain and stress distributions. To the authors' knowledge, there is no study including all the steps described above and carried out upon the same samples in abdominal tissue.

In this work, we present a systematic study of the *in vitro* passive mechanical characterization of muscle tissue within the framework of the continuum theory of large deformation hyperelasticity. An in-depth analysis of the mechanical properties of the implant site, namely, the abdominal wall, is essential. Thus, using the New Zealand White rabbit as a well known and extensively used animal model (Nilsson, 1982a,b; LeBlanc et al., 2002; Johnson et al., 2004; Judge et al., 2007; Pascual et al., 2008), the lateral wall of the abdomen was mechanically characterized. In addition, a histological study is included in order to provide a complete characterization of the abdominal wall. Because of the different fibre orientation in each layer of the abdominal wall (collagen and muscular fibres), we analysed separated layers in comparison to the muscle as a whole considered as a composite material. Furthermore, it was also necessary to investigate the behaviour of the external oblique muscle layer since partial hernia repair is more frequent in abdominal surgery when only the EO muscle layer is replaced.

2. Materials and methods

2.1. *Experimental data*

Experimental tests were developed on New Zealand White rabbits, a frequently used animal model in the study of muscle behaviour (Nilsson, 1982a,b; Pascual et al., 2008; Bellón et al., 2009). The experiments developed in the study were governed according to the provisions of the European Council (ETS 123) and the European Union (Council Directive 86/609/EEC) regarding the protection of animals used for experimental and other scientific purposes. Seven male rabbits were acclimatized to the experimental laboratories. The animals were maintained in a controlled temperature room (22 ± 1 (°C)) with 12 h light–dark cycles and free access to water and food according to European Union guidelines for animal care (EEC 28871-22A9). The body weight of the rabbits was 2150 ± 50 (g). The animals were sacrificed by an intravenous injection of sodium pentobarbital (300 (mg/kg)). Immediately afterwards, each animal was placed on its back and the abdominal wall and the skin were dissected (see Figs. 1 and 2(a), respectively).

2.2. *Muscle patch preparation*

Abdominal wall tissue patches were harvested from all the animals, Fig. 2(a). The procedure was carried out by making marks in the abdominal wall of the rabbit by using a 60×100 (mm) rectangular template in order to minimize patch size variability (Fig. 1). The long side of the template was

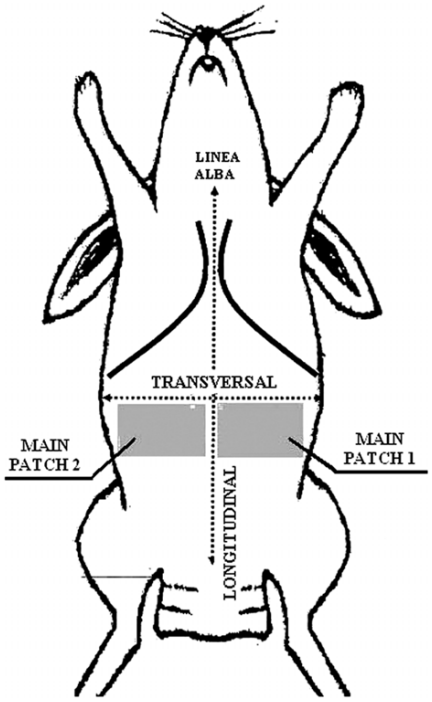

Fig. 1 – Definitions of longitudinal and transversal directions in the rabbit.

perpendicularly oriented to the craneo–caudal direction (note that, for the sake of simplicity, the craneo–caudal direction will be referred to as the longitudinal direction, whereas the perpendicular to the craneo–caudal direction will be referred as the transversal direction in the following, see Fig. 1).

Two tissue patches, one from the left side and another from the right side of the linea alba, immediately next to the rectus, were cut from each animal, see Fig. 1. Two zones were differentiated for the study in each patch. The first one, located close to the rectus abdominis and the linea alba, was composed of two muscles: the EO and the IO, whereas the second one, located close to the para-spinous muscle, comprised three muscles, namely, the EO, the IO and the TA, see Fig. 2(c). Some of the patches were used to analyse the whole tissue as a composite material, whereas the behaviour of the separated layers was studied in others by dissecting the EO layer and the IO–TA bilayer. Also two rectus abdominis samples were harvested, see Fig. 2(c). In all cases, the tissue patches were carefully examined and those patches with holes, cuts or apparent damage were rejected for the experiments.

2.3. *Initial strains*

Initial or residual strains, which are found in many soft biological tissues (Fung, 1993), usually have a strong influence on the mechanical response of the biological tissue. A widely used methodology to assess the amount of residual stresses is based on the measurement of the displacement field appearing in the unloaded tissue when subjected to a cut. In order to evaluate the initial strain distribution in the abdominal wall, the first step of this study was to evaluate the muscle retraction happening on tissue patches after harvesting.

Prior to cutting each patch into smaller samples for mechanical and histological testing, the shortening of the tissue in the longitudinal and transversal directions was measured. In order to evaluate the muscle retraction avoiding undesired viscoelastic effects, a photograph of the patch was

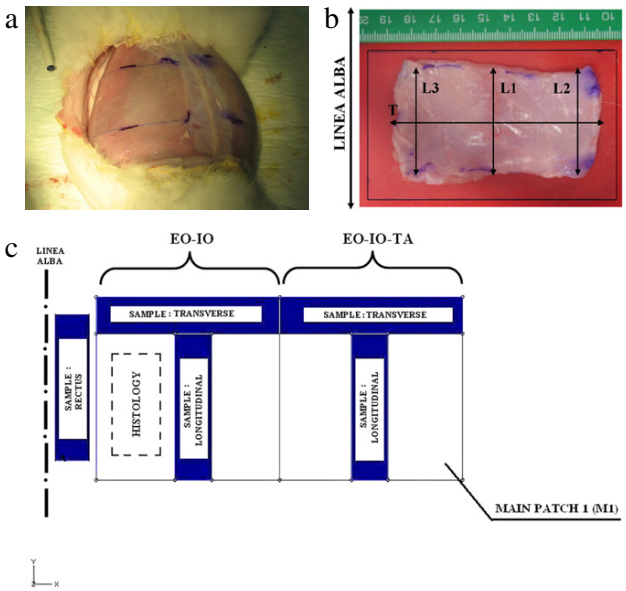

Fig. 2 – (a) Marks in the abdominal wall of the animals using a 60 × 100 mm template. (b) Tissue patch after retraction. (c) The patch was sectioned into four samples for tensile testing. The main patch 2 (M2) is placed in the same area but at the left side of the linea alba. Samples for the histologies were obtained from the area included within the dotted line.

Table 1 – Average dimensions of studied samples (mean ± standard deviation).

Tissue	Sample	Length (mm)	Width (mm)	CSA (mm^2)	Thickness (mm)	Density (mg/mm^3)
EO–IO composite	LONG	44.535 ± 10.557	7.925 ± 0.219	24.633 ± 5.425	3.100 ± 0.599	1.08 ± 0.115
	TRANS	40.195 ± 3.670	9.470 ± 0.325	28.513 ± 6.983	3.025 ± 0.841	
EO–IO–TA composite	LONG	33.565 ± 1.534	8.855 ± 0.007	36.761 ± 8.595	4.151 ± 0.967	1.296 ± 0.419
	TRANS	35.890 ± 4.525	8.205 ± 0.318	33.281 ± 3.968	4.069 ± 0.641	
EO muscle layer	LONG	36.435 ± 3.756	6.755 ± 0.851	10.930 ± 1.382	1.635 ± 0.280	0.998 ± 0.153
	TRANS	42.935 ± 0.599	7.198 ± 1.526	12.487 ± 1.046	1.770 ± 0.234	
IO–TA muscle bilayer	LONG	39.31 ± 4.645	7.090 ± 1.133	15.41303 ± 2.676	2.175 ± 0.123	1.007 ± 0.133
	TRANS	32.092 ± 4.974	7.485 ± 0.518	17.8265 ± 1.139	2.383 ± 0.082	
RECTUS muscle layer	LONG	44.312 ± 3.652	7.680 ± 1.304	18.9235 ± 3.139	2.495 ± 0.472	0.992 ± 0.147

taken 15 min after being cut. Then, variations in size and shape were determined by comparing the patch dimensions with the template used to perform the cuts. Since patch length was considerable (100 (mm)), distance variations at three locations (L1, L2 and L3) were measured in order to evaluate the retraction variability as a function of the position, whereas a single measurement was taken in the transversal direction (T), see Fig. 2(b).

2.4. *Histology*

The tissue remaining in the patch after harvesting the samples for the mechanical tests (white areas in Fig. 2(c)) was used for the histological studies. A total of seven animals were used in this study. This tissue remaining was fragmented into small pieces and oriented longitudinally to the anatomical plane of the animal for the different analyses.

2.4.1. *Light microscopy*

The samples were fixed in Bouin's solution, embedded in paraffin and cut into 5 (μm) sections. Once cut, the sections were stained with Masson's trichrome (Goldner–Gabe) and examined under the light microscope (Zeiss Axiophot, Carl Zeiss, Oberkochen, Germany). The orientation of the muscle fibres of the abdominal wall and the localization of the collagen fascias between them were observed using these stainings.

2.4.2. *Collagen content*

In the same sections, Sirius red staining was used to localize and assess collagen types I and III in the abdominal wall. This technique is based on the orientation and interaction between the sulphone groups of the dye, the amine groups of lysin and hydrolysin and the guanidine groups of arginine in the collagen fibres, giving rise to different colours depending on the type of collagen. Collagen type I appears as a reddish–orangey stain while type III collagen takes on a yellow–greenish shade when observed under polarized light microscopy. Finally, 10 digitalized histological images per animal were obtained using a digital camera fitted to the microscope (Axiocam HR, Zeiss) and analyzed using image analysis software Axiovision AC 4.1. The percentages of collagens I and III were measured in 5 (μm) thick cross sections.

2.4.3. *Transmission electron microscopy*

For ultrastructural analysis, small tissue fragments were fixed for 1 h in 3% glutaraldehyde, stored in Millonig buffer (pH 7.3) and postfixed in 2% osmium tetroxide. Once dehydrated in a graded series of acetone, the tissue fragments were embedded in Araldite to obtain thin cuts. These sections were counterstained with lead citrate and examined using a Zeiss 109 transmission electron microscope. The ultrastructural study was used to observe the orientation of the collagen fibres in the different collagen fascias.

2.5. *Experimental characterization of the muscle samples*

After retraction, the tissue patches were immersed in a saline solution at 4 (°C) in order to prevent them from drying. In total, 6 patches of composite muscle, 6 patches in which the EO muscle layer and IO–TA muscle bilayer had been dissected and 10 samples of the rectus were obtained.

For the mechanical testing, several samples with a width/length ratio around 1/7 were cut from each tissue patch in order to preserve the uniaxial tension hypothesis. Specifically, one sample in both the longitudinal and transversal directions were harvested from each of the zones of the tissue patch, Fig. 2(c). A total of 11 of EO–IO composite, 9 of EO–IO–TA composite, 12 of EO muscle layer, 11 of IO–TA muscle bilayer and 10 of rectus abdominis feasible samples were obtained after rejecting those damaged or holed ones.

Samples length, width and thickness, were measured using a digital calibre. Volume was obtained by measuring the water level variation occurring when the sample was introduced in a tube-test filled with water, whereas weight was measured with a precision weighting balance. The cross-section area was straightforwardly determined by dividing the muscle mass m by the product of the length L and the density $\rho\left(\text{CSA}\ (mm^2) = \frac{m\ (mg)}{L\ (mm)\cdot\rho\ (mg/mm^3)}\right)$. The measured magnitudes for each type of sample are shown in Table 1.

Uniaxial tensile tests were performed under displacement control on an INSTRON 3340 microtester with a 1 (kN) full scale load cell. Each abdominal muscle sample was preconditioned with three cycles at a nominal strain of 40% or 20% for the composite muscle or the separated layers, respectively. These deformation levels were chosen aiming to compensate for the measured initial strains, so that the tissue

was subjected to physiological loading states. The applied displacement rate was 5 (mm/min) in order to preserve quasi-static testing conditions. Load and displacement were recorded till complete sample rupture.

Load and displacements were recorded from the tests in order to calculate the stretch of the sample as $\lambda = \frac{L_0+\Delta L}{L_0}$, where L_0 is the initial length between the clamps, ΔL is the clamp displacement and the Cauchy stress in the direction of the stretch was computed as $\sigma = \frac{N}{CSA}\lambda$, where N is the applied load.

2.6. Statistical analysis

A statistical analysis was performed in order to study the possible significant variations in the retraction between longitudinal and transversal directions as well as to study possible significant variations in the mechanical behaviour between longitudinal and transversal directions in the different tested groups: for the composite, the compared groups were EO–IO layer and EO–IO–TA one, whereas the EO single layer and IO–TA one were compared for the separate muscle layers. Besides, a statistical analysis was performed in order to study the possible significant variations in the mechanical behaviour in the longitudinal direction for composite and separated muscle layers between the different described zones, Fig. 2(c). The same procedure was applied in the transversal direction for the two compared groups. All comparisons were made by means of an independent t-test. A $p < 0.05$ was established to indicate statistical significance.

2.7. Constitutive modelling

A frequently used methodology to formulate an elastic constitutive law for fibred soft tissues is to postulate the existence of a strain energy function that depends on the orientation of the family of fibres represented by a material vector $\mathbf{m}_0$ at point $\mathbf{X}$ of the reference configuration (Weiss et al., 1996; Holzapfel et al., 2000; Peña et al., 2007). Then, the stretch of the fibres is defined as:

$$\lambda_m^2 = \mathbf{m}_0 \cdot \mathbf{C}\mathbf{m}_0, \tag{1}$$

where $\mathbf{F} = \frac{\partial \mathbf{x}}{\partial \mathbf{X}}$ and $\mathbf{C} = \mathbf{F}^T\mathbf{F}$ are the standard deformation gradient and the corresponding right Cauchy–Green strain measure, respectively. In order to handle the quasi-incompressibility constraint more easily, a multiplicative decomposition of $\mathbf{F} = J^{\frac{1}{3}}\bar{\mathbf{F}}$ and $\mathbf{C} = J^{\frac{2}{3}}\bar{\mathbf{C}}$ into volume-changing and volume-preserving parts is usually established (Flory, 1961).

Then, we postulate the existence of a unique decoupled representation of the strain–energy density function (SEF):

$$\Psi(\mathbf{C}, \mathbf{M}) = \Psi_{vol}(J) + \bar{\Psi}(\bar{\mathbf{C}}, \mathbf{M}) = \Psi_{vol}(J) + \bar{\Psi}(\bar{I}_1, \bar{I}_2, \bar{I}_4), \tag{2}$$

where $\Psi_{vol}(J)$ and $\bar{\Psi}$ are given scalar-valued functions of J, $\bar{\mathbf{C}}$, $\mathbf{M} = \mathbf{m}_0 \otimes \mathbf{m}_0$, respectively, that describe the volumetric and isochoric responses of the material (Weiss et al., 1996; Holzapfel, 2000); $\bar{I}_1$ and $\bar{I}_2$ are the first and second modified strain invariants of the symmetric modified Cauchy–Green tensor $\bar{\mathbf{C}}$. Finally, the invariant $\bar{I}_4 \geq 1$ characterizes the constitutive response of the fibres:

$$\bar{I}_4 = \bar{\mathbf{C}} : \mathbf{M} = \bar{\lambda}_m^2. \tag{3}$$

The constitutive equation for quasi-compressible hyperelastic materials can be defined from the Clausius–Planck inequality as

$$\mathbf{S} = 2\frac{\partial \Psi(\mathbf{C}, \mathbf{M})}{\partial \mathbf{C}} = \mathbf{S}_{vol} + \bar{\mathbf{S}} = Jp\mathbf{C}^{-1} + 2\frac{\partial \bar{\Psi}(\bar{\mathbf{C}}, \mathbf{M})}{\partial \mathbf{C}}, \tag{4}$$

where the second Piola–Kirchhoff stress $\mathbf{S}$ consists of a purely volumetric contribution $\mathbf{S}_{vol}$ and a purely isochoric one $\bar{\mathbf{S}}$, being $p = \frac{d\Psi_{vol}(J)}{dJ}$ the hydrostatic pressure. The Cauchy stress tensor $\boldsymbol{\sigma}$ is $1/J$ times the push-forward of $\mathbf{S}$ ($\boldsymbol{\sigma} = J^{-1}\boldsymbol{\chi}_*(\mathbf{S})$) (Holzapfel, 2000).

The experimental data showed several relevant features of the muscle tissue that should be considered in order to mathematically model the tissue behaviour, Fig. 7. First, the samples experienced finite strains for small loads. Second, a strongly marked non-linear response was found. Third, there was a remarkable anisotropic behaviour in a single muscle layer, being less pronounced in the whole composite muscle. Therefore, a suitable mechanical framework had to be adopted in order to properly model its mechanical behaviour. The isotropic response was modelled by means of the SEF proposed by Demiray et al. (1988) whereas the anisotropic response was represented by the phenomenological exponential SEF by Holzapfel et al. (2000), i.e.,

$$\begin{aligned}\bar{\Psi} &= \bar{\Psi}_{iso} + \bar{\Psi}_{ani} \\ &= \frac{c_1}{c_2}\left[\exp\left(\frac{c_2}{2}[\bar{I}_1 - 3]\right) - 1\right] + \frac{c_3}{2c_4}\left[\exp\left(c_4[\bar{I}_4 - 1]^2\right) - 1\right],\end{aligned} \tag{5}$$

where $c_1 > 0$ and $c_3 > 0$ are stress-like parameters and $c_2 > 0$ and $c_4 > 0$ are dimensionless (note that $\bar{\Psi}_{ani} = 0$ if $\bar{I}_4 \leq 1$).

2.7.1. Estimation of the model parameters

Following the approach generally adopted in soft tissue mechanics, the tissue was assumed as incompressible in order to estimate the material parameters, that is, $I_3 = J^2 = 1$ (Ogden, 2001). Since the collagen fibre orientation is different from the test direction, the deformation gradient resulting from the application of stretch to the samples was assumed as

$$\mathbf{F} = \begin{bmatrix} \lambda_x & 0 & \kappa \\ 0 & [\lambda_x\lambda_z]^{-1} & 0 \\ 0 & 0 & \lambda_z \end{bmatrix}, \tag{6}$$

where λ_x is the stretch along the x direction, $[\lambda_x\lambda_z]^{-1}$ is the stretch in the y direction, κ is the amount of shear stretch in the xz transversal direction and λ_z is the stretch in the z direction (Ogden, 2001). Note that the z direction was assumed to correspond to the stretching direction in the mechanical tests, so λ_z was straightforwardly calculated from the experimental data, Fig. 3.

Fitting of the mean curves of experimental data was performed using a Levenberg–Marquardt minimization algorithm (Marquardt, 1963). This algorithm, widely used for experimental data fitting of soft biological tissues (Holzapfel et al., 2005), is based upon the minimization of an objective function (Morrow et al., 2010a), which takes the form represented in (7) for the uniaxial tension test:

$$\chi^2 = \sum_{i=1}^{n}\left[\left[\sigma^{exp} - \sigma^{\Psi}\right]_{iL}^2 + \left[\sigma^{exp} - \sigma^{\Psi}\right]_{iT}^2\right], \tag{7}$$

Table 2 – Retraction obtained for the abdominal muscle tissue. Mean and SD (standard deviation).

	Retraction—L1 (%)	Retraction—L2 (%)	Retraction—L3 (%)	Retraction—T (%)
Patch 1	12.9	28.2	14.5	22.7
Patch 2	21.5	27.9	12.9	23.4
Patch 3	18.6	18.7	21.6	28.7
Patch 4	23.5	22.6	17.9	28.8
Patch 5	20.5	21.2	11.1	24.0
Patch 6	24.1	25.9	12.7	16.8
Patch 7	23.3	25.3	24.6	29.8
Patch 8	36.3	41.0	34.7	28.1
Mean	22.6	26.4	18.8	25.3
SD	6.63	6.76	7.97	4.40

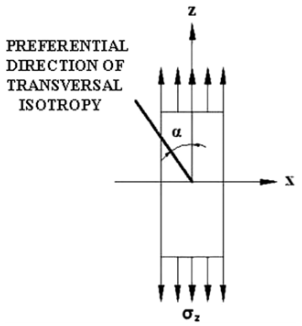

Fig. 3 – Different orientations between the uniaxial test and the preferential direction of transversal isotropy.

where σ_i^{exp} and σ_i^{Ψ} represent the measured and the fitted stress values for the ith point data, respectively. The L and T subscripts indicate the direction of the test, longitudinal and transversal respectively, Fig. 2(c). The quality of the fittings was evaluated by computing the coefficient of determination R^2 and the normalized mean square root error ε, i.e.,

$$\varepsilon = \frac{\sqrt{\frac{\chi^2}{n-q}}}{\mu}, \tag{8}$$

where q is the number of parameters of the SEF, n is the number of data points, $n - q$ is the number of degrees of freedom, and μ is the mean stress defined as $\mu = \frac{1}{n}\sum_{i=1}^{n}[\sigma]_i$ (Holzapfel et al., 2005).

In order to prove that the mathematical model can reproduce the behaviour of the tissue, a FEM simulation of the experimental uniaxial test in the ABAQUS commercial code was done using a UMAT subroutine. This simulation was carried out considering both the sample as a composite in a unique layer and as the junction of two muscle layers Fig. 10(a) and (b). The material parameters used were the constants obtained in the fitting procedure.

The FE model was constructed with 2745 nodes and 1920 C3D8H elements. Boundary conditions reproducing the uniaxial test conditions were applied by clamping one of the ends of the model and applying a displacement corresponding to a nominal strain value of 50% to the other end. Higher deformation ranges were not considered since experimental observations showed that muscle delamination occurs for stretch levels higher than 1.5.

3. Results

3.1. *Initial strains*

The measurements of the muscle retraction in the composite in the longitudinal and transversal directions at locations in L1, L2 and L3, and T, respectively (see Fig. 2(b)) are presented in Table 2.

Considering the average, the maximum value of the retraction was 26.4% in the longitudinal direction (L2), where the muscle is comprised of three layers. On the other hand, the minimum value was 18.8%, also in the longitudinal direction (L3) but close to the rectus, where only two muscles form the tissue (see Fig. 2(b)). No significant variations were found in the retraction between longitudinal and transversal directions ($p > 0.0675$).

3.2. *Histology*

3.2.1. *Light microscopy*

In the section stained with Masson's trichrome localization of the different collagen fascias was observed in green in the subcutaneous and peritoneal sides, and also between the two muscular layers of the abdominal wall (Fig. 4(a)). Light microscopy allowed observing the orientation of the muscle fibres. In sections made in the longitudinal anatomical plane in the abdominal wall, the external oblique muscle layer showed the muscle fibres in an oblique orientation, and the internal oblique muscle layer in a transversal orientation with respect to the longitudinal axis of the animal (Fig. 4(b) and (c)). These observations allowed us to establish a pattern of arrangement of the muscle fibres in the outer and inner layers of the abdominal wall of rabbits, as shown in Fig. 5.

3.2.2. *Collagen content*

The Sirius red staining showed that the different fascias were formed by the mature type of collagen, type I (Fig. 6). Quantification of the percentage of collagen in the different fascia with respect to the total components of the abdominal wall was analysed. The subcutaneous fascia represented 11.2% ± 3.9% of the total components of the abdominal wall, while only 2.5%±1.1% was immature collagen. This fascia was mostly loose, with collagen fibres packed less densely than in the other fascias and sometimes with the presence of adipose tissue in the highest area. The fascia between the external

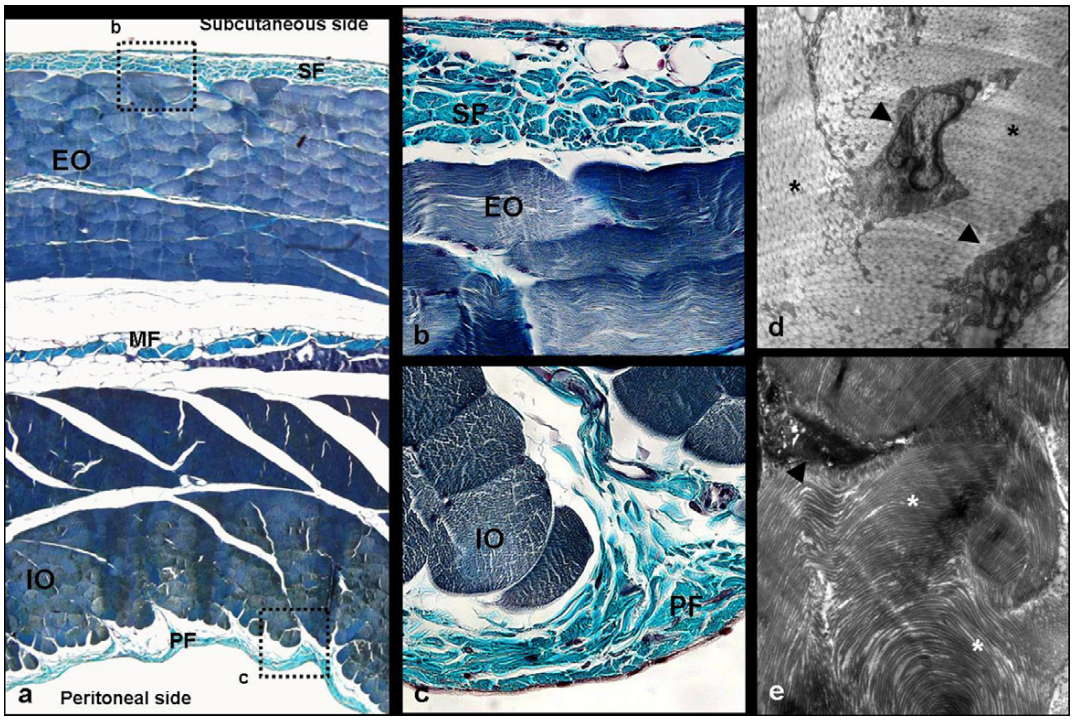

Fig. 4 – (a) Panoramic view of a longitudinal section of the abdominal wall of the New Zealand white rabbit. Light microscopy, Masson's trichrome staining, 100×. (b) Magnification of the limited area in the dotted square from image (a), in the subcutaneous side, showing muscle fibres in oblique disposition in EO muscle layer. Light microscopy Masson's trichrome staining, 400×. (c) Magnification of the limited area in the dotted square from image (a), in the peritoneal side, showing muscle fibres in transversal disposition in IO muscle layer. Light microscopy Masson's trichrome staining, 400×. (d) TEM image of an area from the SF showing collagen fibres in transversal disposition 8000×. (e) High magnification of TEM image of an area from the PF showing collagen fibres preferentially arranged in longitudinal disposition. 2500×. (EO: external oblique; IO: internal oblique muscular layers; SF: subcutaneous fascia; PF: peritoneal fascia; MF: medial fascia; Black arrows: fibroblasts; * in black: collagen fibres in the transversal section and * in white: in the longitudinal section).

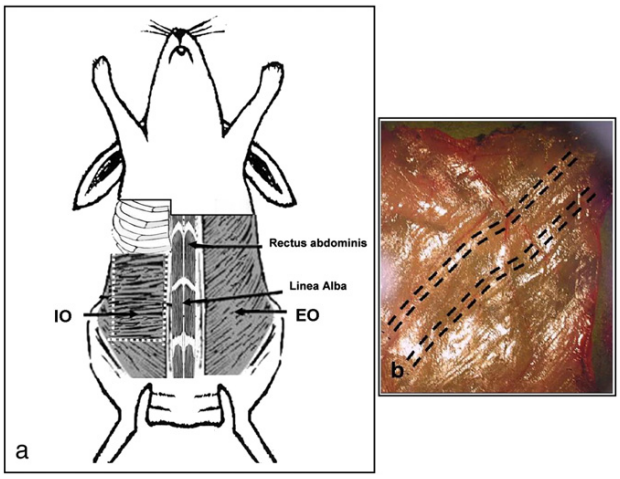

Fig. 5 – (a) Model of the arrangement of the muscle fibres in the abdominal wall of the New Zealand white rabbit (EO: external oblique; IO: internal oblique muscular layers). (b) Macroscopic image of the superficial skeletal muscle layer in the left side of the abdominal wall of the experimental animal. The dotted lines represent the direction of the muscle fibres in this area.

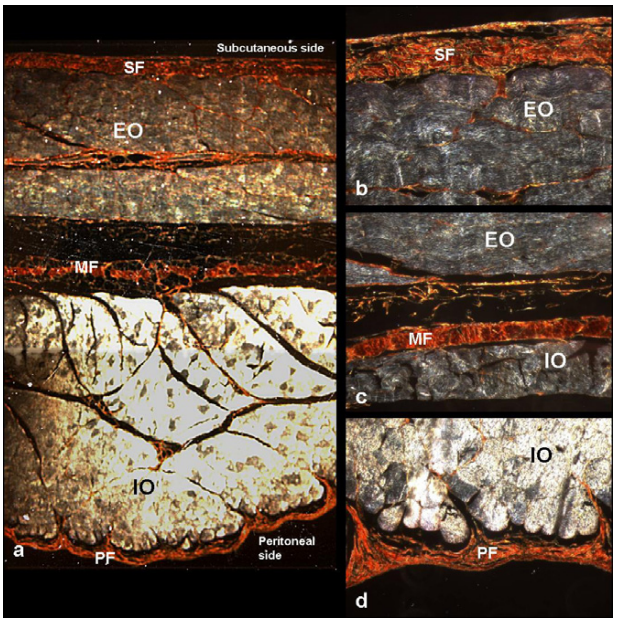

Fig. 6 – (a) Image of Sirius red staining showing a panoramic view of a longitudinal section of the abdominal wall of the experimental animals showing that the different fascias are formed by the mature type of collagen (type I). A small amount of collagen type III (in yellow) was observed in the samples. Polarized light microscopy, 100×. (b) Magnification of an area in the subcutaneous side, showing the subcutaneous fascia (SF). Polarized light microscopy, 200×. (c) Magnification of an area between the outer and inner muscle layers, showing the medial fascia composition (MF). Polarized light microscopy, 200×. (d) Magnification of the peritoneal fascia (PF). Polarized light microscopy, 200×. (EO: external oblique; IO: internal oblique muscular layers). (For interpretation of the references to colour in this figure legend, the reader is referred to the web version of this article.)

and the internal muscle layer represented approximately 8.6% ± 4.1% of collagen I and 0.6% ± 0.3% of collagen III. The innermost fascia, in the peritoneal side, represented the 7.2% ± 3.3% collagen I and 0.9% ± 0.4% collagen type III of the total components of the abdominal wall.

3.2.3. *Transmission electron microscopy*

The ultrastructural analysis was used to observe the orientation of the collagen fibres in the fascial areas. In a longitudinal section, the TEM images showed in the fascial tissue a collagen layer composed of interwoven strands of collagen in different directions, but most of the collagen fibres in the subcutaneous fascia were cross-sectional indicating that they preferentially arranged parallel to the transverse anatomical plane of the animal (Fig. 4(d)). However, the collagen fibres were preferentially arranged parallel to the longitudinal axis of the animal in the fascia on the peritoneal side (Fig. 4(e)).

3.3. *Mechanical tests*

The Cauchy stress–stretch curve is represented in Fig. 7 for the different groups of studied samples. In which the EO muscle layer is concerned, Fig. 7(a), the longitudinal direction was less stiff than the transversal one, and the rupture stress was also lower in the longitudinal than in the transversal direction. Note that a remarkable anisotropy is found in the separated muscle layers ($p < 0.043$). The IO–TA muscle bilayer had lower failure stress than the EO tissue, Fig. 7(b). In this case, the longitudinal direction was stiffer, whereas similar rupture stress values were measured in both directions, Fig. 7(b). In this case, significant variations in stiffness for $\lambda > 1.25$ ($p < 0.05$) were found. Fig. 7(c) and (d) show the muscle composite behaviour. For the EO–IO composite, close to the rectus abdominis tissue, the rupture stress value was higher than for the EO–IO–TA. No remarkable anisotropy was detected and similar results were measured in the longitudinal and transversal directions. Significant variations in stiffness for $\lambda > 1.21$ and $\lambda > 1.31$ in the EO–IO composite ($p < 0.025$) and the EO–IO–TA ($p < 0.05$), respectively, were observed. Fig. 7(e) shows that the rectus muscle has a high rupture stress compared with the other studied areas.

No significant variations in the mechanical properties of the composite were found neither in the longitudinal ($p > 0.2360$) nor in the transversal direction ($p > 0.1316$) between the two muscle (EO–IO) and the three muscle areas (EO–IO–TA). However, significant mechanical property variations were found between the EO and IO–TA separated muscle layers ($p < 0.043$) for $\lambda > 1.21$ in the longitudinal direction, whereas significant variations ($p < 0.0184$) in all the stretch ranges in the transversal direction.

In order to analyse the behaviour of the tissue *in-situ*, the effect of passive physiological loading was incorporated by representing the Cauchy stress versus the measured stretch divided by the initial stretch, Fig. 8. This plot shows a more pronounced anisotropic response.

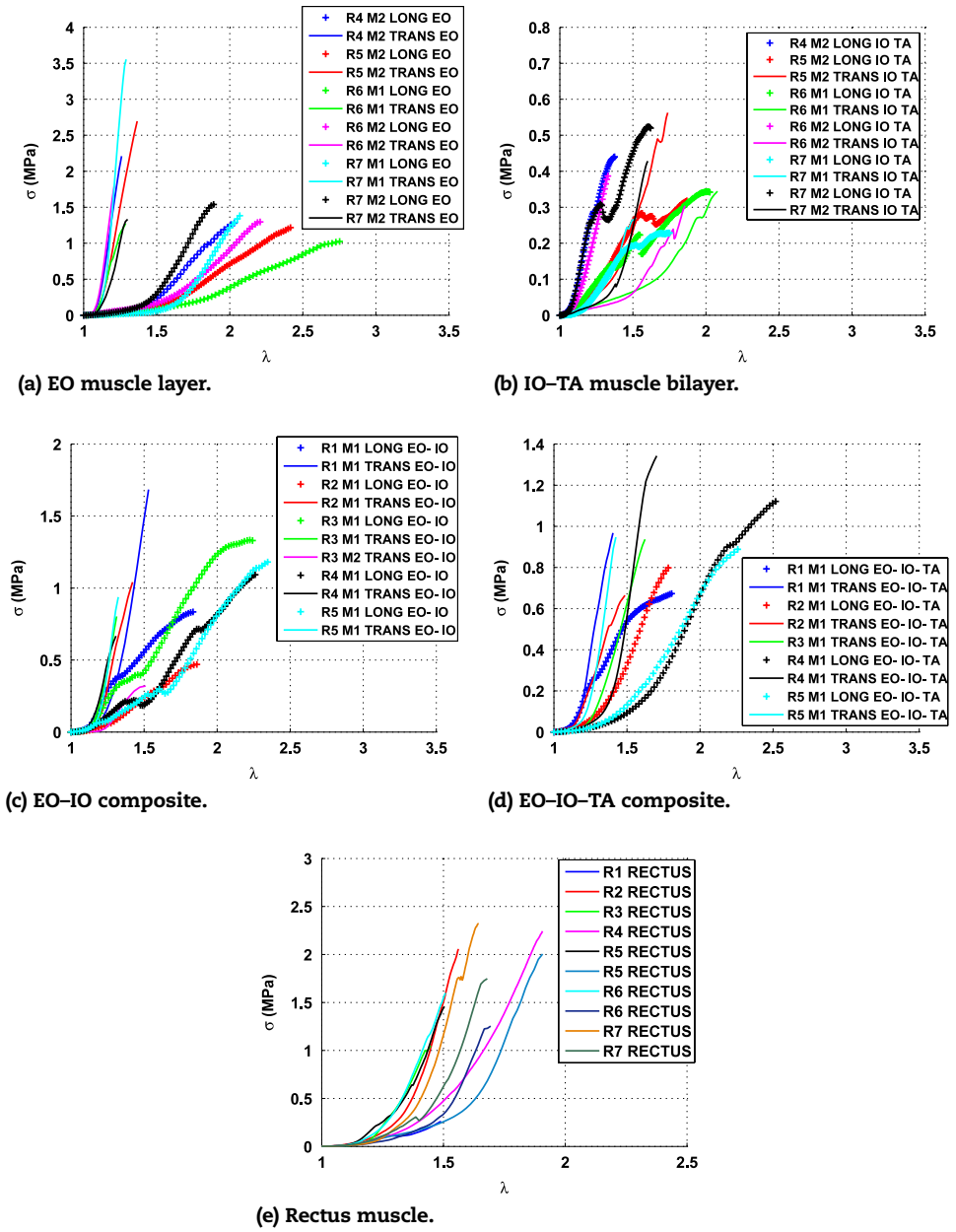

(a) EO muscle layer. **(b) IO–TA muscle bilayer.**

(c) EO–IO composite. **(d) EO–IO–TA composite.**

(e) Rectus muscle.

Fig. 7 – Experimental data. All experimental curves were truncated before the maximum stress point.

3.4. *Data fitting*

Table 3 shows the results of the parameter estimation for the muscle tissue including the values obtained for the mean curves in longitudinal and transversal directions. In all cases, R^2 values were close to 1 and very low ε values were obtained, which confirmed the goodness of the fitting. In Fig. 9, the fitted mean curves are shown, where it is observed that the fitted curves do not show an agreement with the experimental data in low stretch ranges, which is due to the exponential character of the curves.

The results obtained from the uniaxial test FEM simulation corresponding to the composite and separated muscle layer models together with the experimental curves in longitudinal direction are depicted in Fig. 10(b). The three shown curves are quite similar, which points out that assuming the tissue as a composite or as two separate muscle layers is a feasible hypothesis in the studied stretch range.

4. Discussion and conclusions

The passive elastic behaviour of the abdominal wall including initial strains has been studied in the present work. Several samples extracted from experimental animals were tested

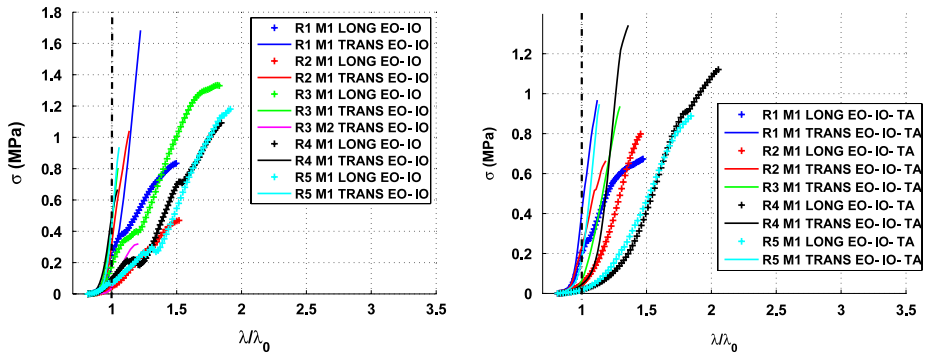

(a) EO–IO composite. (b) EO–IO–TA composite.

Fig. 8 – Experimental data considering retraction for composite muscle layers. All experimental curves were truncated before the maximum stress point.

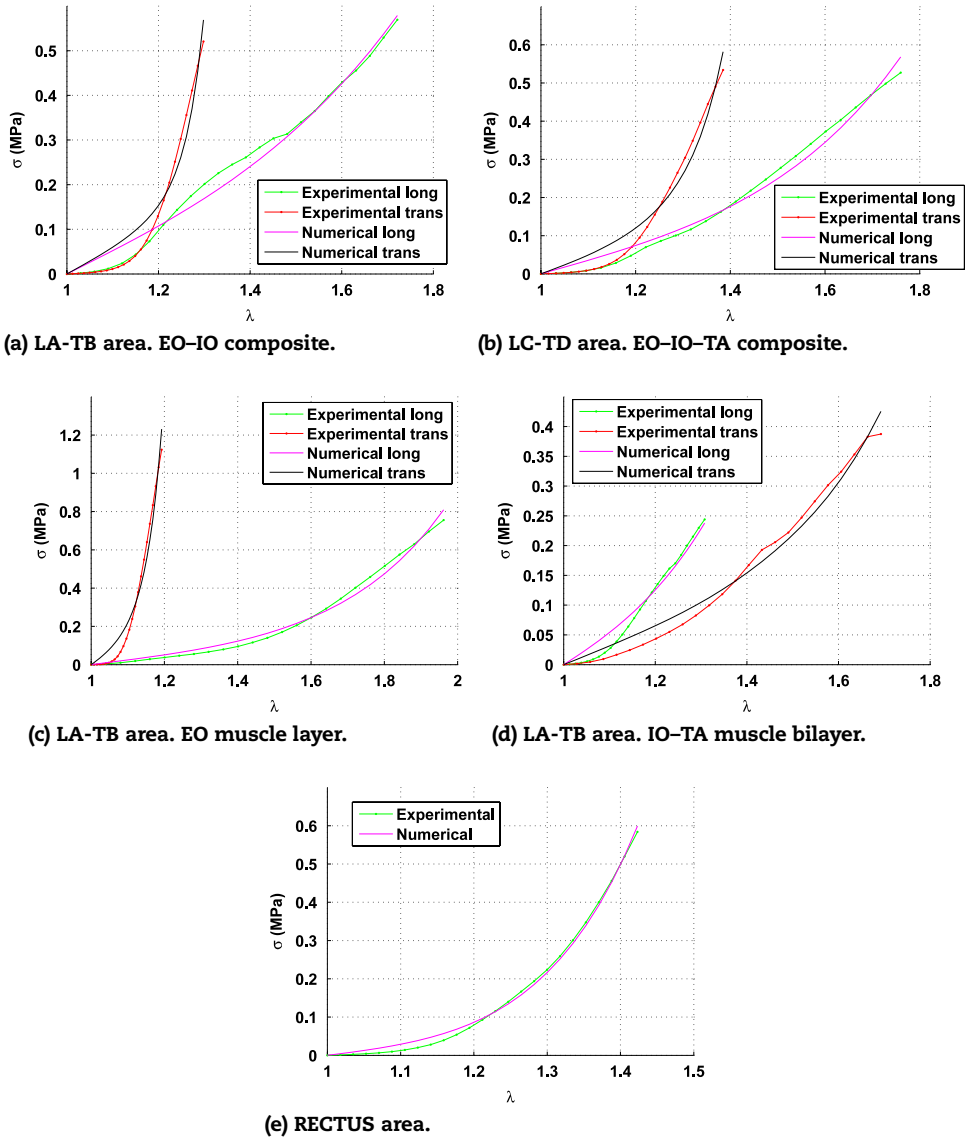

(a) LA-TB area. EO–IO composite. (b) LC-TD area. EO–IO–TA composite.

(c) LA-TB area. EO muscle layer. (d) LA-TB area. IO–TA muscle bilayer.

(e) RECTUS area.

Fig. 9 – Experimental *versus* numerical stress–stretch relationships for each muscle sample.

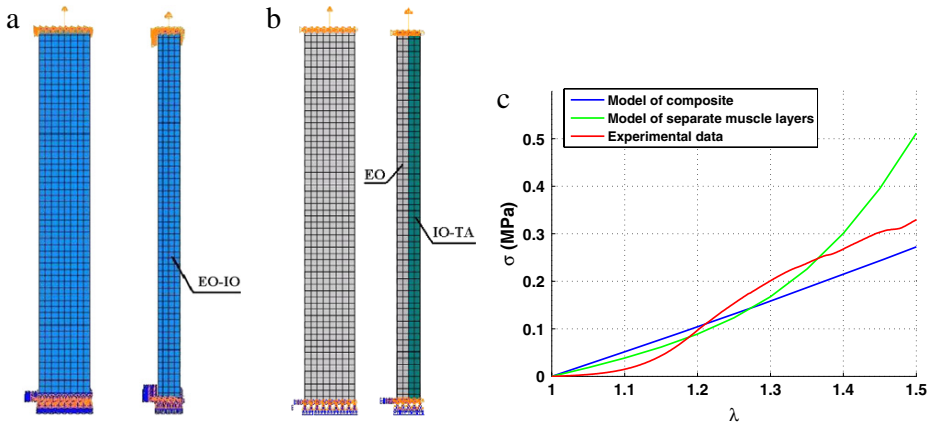

Fig. 10 – (a) Front and lateral view of the FE simulation of the model of the tissue as a composite. (b) Front and lateral view of the FE simulation of the model of the tissue using separate muscle layers. (c) Obtained curves considering two models, separate muscle layers and composite, and curve of experimental longitudinal EO–IO sample.

Table 3 – Material model parameters obtained from the fitting procedure. The angle α is considered between the longitudinal direction and the preferential direction of transversal isotropy.

	c_1 (MPa)	c_2 (–)	c_3 (MPa)	c_4 (–)	α (°)	ε (–)
EO–IO	0.16832	0.6319	0.01219	5.68158	87.8	0.17873
EO–IO–TA	0.11092	1.12568	0.02568	1.87174	83.6	0.16118
EO	0.06577	1.26785	0.28146	7.02349	88.2	0.17782
IO–TA	0.10768	0.11071	0.05814	2.03275	15	0.13871
RECTUS	0.03092	3.68821	0.52764	2.07285	21.64	0.07379

in order to characterize the mechanical properties of the abdominal wall. The mechanical properties and initial strains were then evaluated using the classical rabbit model for these kinds of pathologies.

Biological soft tissues are usually subjected to a complex distribution of *in vivo* initial strains. This is a consequence of the continuous growth and remodelling that these living materials suffer throughout their whole lives. The real strain distribution of the tissue is three-dimensional and heterogeneous and direct measurement poses significant problems. Due to the non-linear behaviour of this tissue, an erroneous inclusion of the initial strain state in computational models can lead to large errors (Peña et al., 2006). In this work, shortening of the tissue along different directions was measured in order to estimate the initial strain field. After contraction the shape of the patch remained approximately rectangular which indicated that the patch has been taken more or less along its preferential directions of anisotropy.

It has been proved that the achievement of good clinical results in abdominal hernia surgery strongly depends on obtaining a perfect correspondence between the mechanical properties of the abdominal wall and the mechanical properties of the biomaterial used for repair (Conze and Klinge, 1999). Other studies can be found in the literature related to abdominal wall behaviour, each of them focusing on similar aspects but not directly comparable with the present results. On the one hand, a comparative study has been carried out between IO and TA canine muscles (Hwang et al., 2005), while here both are studied as a composite. In the cited paper, similar conclusions are obtained in terms of anisotropy and muscle compliance comparing a single muscle layer and a composite. On the other hand, mechanical properties of samples from different anatomical positions as well as in relation to geometric variables and fibre orientation have also studied. For example, Nilsson (1982a,b) obtained results relating force and stretch but no data referring to cross sectional area were given, so stress data could not be obtained and therefore the results cannot be compared with ours. Nevertheless, the stress–stretch relationships obtained in the present study showed similar non-linear patterns to those previously published for soft tissues in general, also undergoing large deformations (Quapp and Weiss, 1998; Davis et al., 2003; Hwang et al., 2005; Lopez et al., 2008; Calvo et al., 2009; Martins et al., 2010).

Regarding the passive behaviour, we have found in this study that the anisotropic behaviour of the internal abdominal muscles considered as a composite muscle is less pronounced than the individual muscles, Fig. 7. The transversal direction in the composite is stiffer than the longitudinal direction, Fig. 7(c) and (d). Similar results were found by Morrow et al. (2010b). Focusing on the external oblique muscle layer, the transversal direction is stiffer than the longitudinal, Fig. 7(a), and this result is related to histological results based on collagen fibre orientation, Fig. 4(b). Fascial tissue in the subcutaneous side is formed preferentially by collagen fibres arranged in the transversal direction, making this direction stiffer than the perpendicular, Fig. 7(a). On the other hand, the internal oblique muscle layer is stiffer in the longitudinal direction, Fig. 7(b), and the results from the histology showed that the inner fascia next to the peritoneal side is formed

preferentially by collagen fibres in an oblique arrangement, Fig. 4(c). The correlation between this fibre arrangement and passive behaviour supports the hypothesis that collagen fibres are responsible for passive mechanical strength and stiffness while muscle fibres take care of the contraction (Linden, 1998; Arruda et al., 2006). Focusing on the collagen content, Fig. 6, the subcutaneous fascia has the greater quantity of collagen and this can explain why the EO muscle layer has a higher rupture stress than the IO–TA muscle layer. Besides, when dissecting the external oblique free from the internal abdominal wall the fascia between the muscle layers may remain with the EO muscle layer.

As discussed previously, the abdominal muscles are arranged in multiple layers, each with collagen and muscle fibres oriented along a different axis from that of the adjacent layer. In the presence of extracellular connective tissue matrix, this arrangement of muscle layers allows for the transmission of muscle forces between adjacent muscle layers called myofascial force transmission (Hwang et al., 2005). Therefore, rather than bearing a transverse stress with increased abdominal pressure during inspiratory activity, muscle layers can transmit this transverse stress to the adjacent abdominal muscle layer. Due to this fact, composites behave in an intermediate way between separated muscle layers.

Concerning the model formulation, a constitutive model has been proposed that can be used to study muscle tissue mechanics. Fig. 9 indicates that this constitutive model is sufficiently accurate to guarantee the prediction of reliable stress distributions using finite element computations. The good fit in the range of the physiological work guarantee the correct response of the tissue in further FE simulations. To demonstrate this, a FE simulation with ABAQUS has been developed, Fig. 10(a). The correspondence between the two FE models and experimental results validates our assumption, so it is possible to simulate the tissue as a composite or as two separate muscle layers using the material parameters previously fitted, Table 3.

Some limitations of this study should be mentioned. Only the elastic properties of the tissues have been determined here. Damage and viscoelastic properties were not included and remain issues for subsequent work (Calvo et al., 2009; Ito et al., 2010; Peña et al., 2010). Further tests are needed to determine the plastic and viscoelastic properties of muscle (Loocke et al., 2008, 2009), as well as the stiffness loss due to damage. Additional information from other kinds of tests (e.g., biaxial tests) would provide useful additional information for muscle tissue characterization. Moreover, biaxial tests reproduce the physiological deformation and loading conditions of muscle tissue. Besides, subsequent work will include the characterization of active behaviour which may provide additional information for muscle tissue.

Despite these limitations, the proposed constitutive model can be used to study muscle tissue mechanics as it seems to be sufficiently accurate to guarantee the prediction of reliable stress distributions using finite element computations. Within the broader aim of developing a validated 3D computational model of the muscle of the rabbit capable of simulating abdominal wall movement in healthy conditions and with different kinds of implanted meshes, this paper provides a material model for the passive elastic behaviour of abdominal muscle tissues.

Acknowledgements

The authors gratefully acknowledge research support from the Spanish Ministry of Science and Technology through research projects DPI2008-02335/DPI2010-20746-C03-01 and the Instituto de Salud Carlos III (ISCIII) through the CIBER initiative project SOFT-TISSUES-BIOSCAFF. CIBER-BBN is an initiative funded by the VI National R&D&i Plan 2008-2011, Iniciativa Ingenio 2010, Consolider Program, CIBER Actions and financed by the Instituto de Salud Carlos III with assistance from the European Regional Development Fund. Finally, we also thank the Spanish Ministry of Science and Technology for the financial support to B. Hernández through grant BES-2009-021515.

REFERENCES

Afonso, J., Martins, P., Girao, M, Natal Jorge, R., Ferreira, A., Mascarenhas, T., Fernandes, A., Bernardes, J., Baracat, E., Rodrigues de Lima, G., Patricio, B., 2008. Mechanical properties of polypropylene mesh used in pelvic floor repair. International Urogynecology Journal 19, 375–380.

Arruda, E.M., Mundy, K., Calve, S., Baar, K., 2006. Denervation does not change the ratio of collagen I and collagen II mRNA in extracellular matrix of muscle. American Journal of Physiology — Regulatory, Integrative and Comparative Physiology 292, 983–987.

Bellón, J.M., 2009. Role of the new lightweight prostheses in improving hernia repair. Cirugía española 85 (5), 268–273.

Bellón, J.M., Rodríguez, M., García-Honduvilla, N., Gómez-Gil, V., Pascual, G., Buján, J., 2009. Comparing the behavior of different polypropylene meshes (heavy and lightweight) in an experimental model of ventral hernia repair. Journal of Biomedical Materials Research. Part B, Applied Biomaterials 89B (2), 448–455.

Bol, M., Reese, S., 2008. Micromechanical modelling of skeletal muscles based on the finite element method. Computer Methods in Biomechanics and Biomedical Engineering 11, 489–504.

Calvo, B., Peña, E., Martins, P., Mascarenhas, T., Doblare, M., Natal, R., Ferreira, A., 2009. On modelling damage process in vaginal tissue. Journal of Biomechanics 42, 642–651.

Conze, J., Klinge, U., 1999. Biocompatibility of Biomaterials-Clinical and Mechanical Aspects. Springer, Berlin, Heidelberg, New York, pp. 169–177 (Chapter 14).

Davis, J., Kaufman, K.R., Lieber, R.L., 2003. Correlation between active and passive isometric force and intramuscular pressure in the isolated rabbit tibialis anterior muscle. Journal of Biomechanics 36 (4), 505–512.

Demiray, H., Weizsacker, H.W., Pascale, K., Erbay, H., 1988. A stress–strain relation for a rat abdominal aorta. Journal of Biomechanics 21, 369–374.

Fernandez, J.W., Pandy, M.G., 2006. Integrating modelling and experiments to assess dynamic musculoskeletal function in humans. Experimental Physiology 91 (2), 371–382.

Flory, P.J., 1961. Thermodynamic relations for high elastic materials. Transaction of the Faraday Society 57, 829–838.

Fung, Y.C., 1993. Biomechanics. Mechanical Properties of Living Tissues. Springer-Verlag.

Holzapfel, G.A., 2000. Nonlinear Solid Mechanics. Wiley, New York.

Holzapfel, G.A., Gasser, C.T., Sommer, G., Regitnig, P., 2005. Determination of the layer-specific mechanical properties of human coronary arteries with non-atherosclerotic intimal thickening, and related constitutive modelling. American Journal of Physiology-Heart and Circulatory Physiology 289, H2048–H2058.

Holzapfel, G.A., Gasser, T.C., Ogden, R.W., 2000. A new constitutive framework for arterial wall mechanics and a comparative study of material models. Journal of Elasticity 61, 1–48.

Hwang, W., Carvalho, J.C., Tarlovsky, I., Boriek, A.M., 2005. Passive mechanics of canine internal abdominal muscles. Journal of Applied Physiology 98 (5), 1829–1835.

Ito, D., Tanaka, E., Yamamoto, S., 2010. A novel constitutive model of skeletal muscle taking into account anisotropic damage. Journal of Mechanical Behaviour of Biomedical Materials 3, 85–93.

Johnson, E.K., Hoyt, C.H., Dinsmore, R.C., 2004. Abdominal wall hernia repair: a long-term comparison of sepramesh and dualmesh in a rabbit hernia model. American Journal of Surgery 70 (8), 657–661.

Judge, T.W., Parker, D.M., Dinsmore, R.C., 2007. Abdominal wall hernia repair: a comparison of sepramesh and parietex composite mesh in a rabbit hernia model. Journal of the American College of Surgeons 204 (2), 276–281.

LeBlanc, K.A., Bellanger, D., 5th, K.V.R., Baker, D.G., Stout, R.W., 2002. Tissue attachment strength of prosthetic meshes used in ventral and incisional hernia repair. A study in the New Zealand White rabbit adhesion model. Surgical Endoscopy 16 (11), 1542–1546.

Linden, V.D., 1998. Mechanical modeling of skeletal muscle functioning. Ph.D. Thesis, University of Twente, The Netherlands.

Loocke, M.V., Lyons, C.G., Simms, C.K., 2008. Viscoelastic properties of passive skeletal muscle in compression: stress-relaxation behaviour and constitutive modelling. Journal of Biomechanics 41 (7), 1555–1566.

Loocke, M.V., Simms, C.K., Lyons, C.G., 2009. Viscoelastic properties of passive skeletal muscle in compression-cyclic behaviour. Journal of Biomechanics 42, 1038–1048.

Lopez, M., Pardo, P., Cox, G., Boriek, A., 2008. Early mechanical dysfunction of the respiratory pump in the muscular dystrophy with myositis (ttn^{mdm}) model. American Journal of Physiology-Cell Physiology 295, C1092–C1102.

Marquardt, D.W., 1963. An algorithm for least-squares estimation of nonlinear parameters. SIAM Journal on Applied Mathematics 11, 431–441.

Martins, J., Pires, E., Salvado, R., Dinis, P., 1998. A numerical model of passive and active behavior of skeletal muscles. Computer Methods in Applied Mechanics and Engineering 151, 419–433.

Martins, P., Peña, E., Calvo, B., Doblaré, M., Mascarenhas, T., Jorge, R.N., Ferreira, A., 2010. Prediction of nonlinear elastic behavior of vaginal tissue: experimental results and model formulation. Computer Methods in Biomechanics and Biomedical Engineering 327–337.

Morrow, D.A., Donahue, T.H., Odegard, G.M., Haufman, K.R., 2010a. A method for assessing the fit of a constitutive material model to experimental stress–strain data. Computer Methods in Biomechanics and Biomedical Engineering 12, 247–256.

Morrow, D.A., Donahue, T.L.H., Odegard, G.M., Haufman, K.R., 2010b. Transversely isotropic tensile material properties of skeletal muscle tissue. Journal of the Mechanical Behaviour of Biomedical Materials 3, 124–129.

Nilsson, T., 1982a. Biomechanical studies of rabbit abdominal wall. Part I. — The mechanical properties of specimens from different anatomical positions. Journal of Biomechanics 15 (2), 123–129.

Nilsson, T., 1982b. Biomechanical studies of rabbit abdominal wall. Part II. — The mechanical properties of specimens in relation to length, width, and fibre orientation. Journal of Biomechanics 15 (2), 131–135.

Ogden, R.W., 2001. Nonlinear Elasticity, Anisotropy, Material Stability and Residual Stresses in Soft Tissue. Lecture Notes, CISM. Course on Biomechanics of Soft Tissue, Udine.

Palevski, A., Glaich, I., Portnoy, S., Linder-Ganz, E., Gefen, A., 2006. Stress relaxation of porcine gluteus muscle subjected to sudden transverse deformation as related to pressure sore modeling. Journal of Biomechanical Engineering Transactions of the ASME 128, 782–787.

Pascual, G., Rodríguez, M., Gómez-Gil, V., García-Honduvilla, N., Buján, J., Bellón, J.M., 2008. Early tissue incorporation and collagen deposition in lightweight polypropylene meshes: bioassay in an experimental model of ventral hernia. Surgery 144 (3), 427–435.

Peña, E., Calvo, B., Martínez, M.A., Martins, P., Mascarenhas, T., Jorge, R.M.N., Ferreira, A., Doblare, M., 2010. Experimental study and constitutive modeling of the viscoelastic mechanical properties of the human prolapsed vaginal tissue. Biomechanics and Modeling in Mechanobiology 9, 35–44.

Peña, E., Calvo, M.A.M.B., Doblaré, M., 2006. On the numerical treatment of initial strains in soft biological tissues. Int. J. Numer. Meth. Engrg. 68, 836–860.

Peña, E., del Palomar, A.P., Calvo, B., Martínez, M.A., Doblaré, M., 2007. Computational modelling of diarthrodial joints. Physiological, pathological and pos-surgery simulations. Archives of Computational Methods in Engineering 14 (1), 47–91.

Quapp, K.M., Weiss, J.A., 1998. Material characterization of human medial collateral ligament. ASME Journal of Biomechanical Engineering 120, 757–763.

Rosch, R., Junge, K., Hölzl, F., Schachtrupp, A., Stumpf, M., Klinge, U., 2004. How to construct a mesh? Impact of structure, filament and pore size for tissue ingrowth. In: Meshes: Benefits and Risks. Springer-Verlag, pp. 179–188.

Schippers, E., 2007. Central mesh rupture—Myth or real concern? In: Recurrent Hernia. Springer, Berlin Heidelberg, pp. 371–376.

Spencer, A.J.M., 1954. Theory of invariants. In: Continuum Physics. Academic Press, New York, pp. 239–253.

Stalhand, J., Klarbring, A., Holzapfel, G.A., 2008. Smooth muscle contraction: mechanochemical formulation for homogeneous finite strains. Progress in Biophysics & Molecular Biology 96, 465–481.

Weiss, J.A., Maker, B.N., Govindjee, S., 1996. Finite element implementation of incompressible, transversely isotropic hyperelasticity. Computer Methods in Applied Mechanics of Engineering 135, 107–128.

Work 2: Mechanical behaviour of synthetic surgical meshes: Finite element simulation of the herniated abdominal wall

Journal: *Acta Biomaterialia*, **7**(11) (2011): 3905-3913.
Journal impact factor: 4.865

Acta Biomaterialia 7 (2011) 3905–3913

Contents lists available at ScienceDirect

Acta Biomaterialia

journal homepage: www.elsevier.com/locate/actabiomat

Mechanical behaviour of synthetic surgical meshes: Finite element simulation of the herniated abdominal wall

B. Hernández-Gascón [a,d], E. Peña [a,d], H. Melero [d,e], G. Pascual [b,d], M. Doblaré [a,d], M.P. Ginebra [d,e], J.M. Bellón [c,d], B. Calvo [a,d,*]

[a] Group of Structural Mechanics and Materials Modelling (GEMM), Aragón Institute of Engineering Research (I3A), University of Zaragoza, Spain
[b] Department of Medical Specialities, Faculty of Medicine, University of Alcalá, Spain
[c] Department of Surgery, Faculty of Medicine, University of Alcalá, Spain
[d] Centro de Investigación Biomédica en Red en Bioingeniería, Biomateriales y Nanomedicina (CIBER-BBN), Spain
[e] Biomaterials, Biomechanics and Tissue Engineering Group, Department of Materials Science and Metallurgy, Technical University of Catalonia (UPC), Spain

ARTICLE INFO

Article history:
Received 9 February 2011
Received in revised form 20 June 2011
Accepted 21 June 2011
Available online 26 June 2011

Keywords:
Polypropylene
PTFE
Anisotropy
FE simulation
Partial hernia defect

ABSTRACT

The material properties of meshes used in hernia surgery contribute to the overall mechanical behaviour of the repaired abdominal wall. The mechanical response of a surgical mesh has to be defined since the haphazard orientation of an anisotropic mesh can lead to inconsistent surgical outcomes. This study was designed to characterize the mechanical behaviour of three surgical meshes (Surgipro®, Optilene® and Infinit®) and to describe a mechanical constitutive law that accurately reproduces the experimental results. Finally, through finite element simulation, the behaviour of the abdominal wall was modelled before and after surgical mesh implant.

Uniaxial loading of mesh samples in two perpendicular directions revealed the isotropic response of Surgipro® and the anisotropic behaviour of Optilene® and Infinit®. A phenomenological constitutive law was used to reproduce the measured experimental curves.

To analyze the mechanical effect of the meshes once implanted in the abdomen, finite element simulation of the healthy and partially herniated repaired rabbit abdominal wall served to reproduce wall behaviour before and after mesh implant. In all cases, maximal displacements were lower and maximal principal stresses higher in the implanted abdomen than the intact wall model. Despite the fact that no mesh showed a behaviour that perfectly matched that of abdominal muscle, the Infinit® mesh was able to best comply with the biomechanics of the abdominal wall.

1. Introduction

Since the introduction of Lichtenstein's tension-free mesh procedure [1,2], the classic suture techniques have gradually given way to the use of a biomaterial for the surgical repair of an abdominal wall hernia, which is today practically standard practice. A great variety of meshes are available showing different mechanical properties. However, since these properties have not yet been clearly established, it is difficult to select the best prosthesis for each type of hernial defect and for each type of patient. In addition, several studies have shown that the behaviour of the abdominal wall is not isotropic [3–5]. There is therefore a need to define the best mesh material and mesh orientation for each clinical situation such that the behaviour of the mesh matches that of the abdominal wall as closely as possible.

Research into prosthetic materials for hernia repair has sought to find the "ideal prothesis". Studies examining the behaviour of macroporous prosthetic materials, mainly polypropylene (PP), have focussed on assessing the geometry and quantity of implanted material. Attempts to reduce the amount of foreign material persisting in the host have led to the design of macroporous composite meshes with both absorbable and non-absorbable components [6]. Pore size has also been considered a key factor for new designs, as well as the diameter of the prosthetic filaments and their spatial distribution. According to pore size, or density, the German authors classify prosthetic meshes into heavyweight (HW) or lightweight (LW) for densities above 80 or below 50 g/m^2, respectively [7]. In addition, materials with a density between 50 and 80 g/m^2 are designated mediumweight (MW) [8]. Prosthetic mesh density is, however, sometimes independent of pore size and some designs, despite their small pore size are classified as LW since they are composed of a loosely woven monofilament that

* Corresponding author at: Group of Structural Mechanics and Materials Modelling (GEMM), Aragón Institute of Engineering Research (I3A), University of Zaragoza, Spain. Tel.: +34 976761912; fax: +34 976762578.
E-mail address: bcalvo@unizar.es (B. Calvo).

1742-7061/$ - see front matter © 2011 Acta Materialia Inc. Published by Elsevier Ltd. All rights reserved.
doi:10.1016/j.actbio.2011.06.033

confers them a low density. All these features: filament composition, mesh weave and the spatial arrangement of the filaments, along with pore size will determine the mechanical anisotropic behaviour of a surgical mesh.

For tissue repair, the macroporous PP mesh continues to be the material of choice [9–11] after its generalized use since the middle of last century [12], including its use for hernia repair even in the presence of infection [13]. One of the principal objectives of a PP–LW mesh is to reduce the amount of foreign material implanted in the host [14]; the main idea being that a LW mesh will consequently provoke less fibrosis than a HW implant [15].

The mechanical properties of the different meshes have been previously studied. Saberski et al. [16] compared the anisotropic properties of several synthetic meshes used in hernia repair (Trelex®, ProLite™, Ultrapro™, Parietex™, Dualmesh® and Infinit®). With the exception of Dualmesh®, all the mehes showed significant anisotropic behaviour. In another study, Afonso et al. [9] subjected five different meshes (Aris™, TVTO™, Auto Suture™, Uretex™ and Avaulta™) to uniaxial and compression tests and noted significant differences in the mechanical properties of these uro-gynaecological meshes. Other authors have focussed on analysing the postimplant behaviour of different surgical meshes [8,10,17]. Bellón et al. [17] compared the functional and morphologic properties of several meshes (Surgipro®, Parietene® and Optilene®) and recorded similar tensile strengths 14–90 days after their implant in the abdominal wall. These authors concluded that LW prostheses have the benefit of minimizing the amount of implanted foreign material while preserving the flexibility of host tissue. In an assessment of the burst strength and stiffness of three meshes ((Marlex®, Prolene Soft® and Ultrapro®), Cobb et al. [8] concluded that long-term implantation led to improved physiological abdominal wall compliance after LW–PP mesh implant. Finally, Pascual et al. [10] examined the early host tissue incorporation of several meshes (Surgipro®, Parietene®, Ultrapro® and Optilene®) and observed that LW meshes with a large pore size induced the genetic overexpression of collagen types I and III.

To analyze the mechanical behaviour of a mesh implanted in the abdominal wall, tests need to be conducted in two perpendicular directions since the size and spatial arrangement of its pores and filaments can provoke an anisotropic response of the mesh. The importance of considering this anisotropy is directly related to the *in vivo* behaviour of abdominal muscle tissue [5]. Once the mesh is implanted, overall behaviour (tissue plus mesh) should resemble that of the intact healthy tissue. The abdominal wall works as a dynamic system that is able to withstand intense pressure changes (coughing, vomiting, etc.) or sustained pressure increases (obesity, pregnancy, etc.) [18,19]. This means that after the implant of a surgical mesh, some of the flexibility of the abdominal wall needs to be preserved [20,3] and this is achieved by carefully matching the anisotropy of the abdominal muscle with that of the implanted mesh.

An abdominal hernia can affect all the muscle layers of the wall or only a single layer. Partial hernias are today the most frequent and it is usually the external oblique (EO) muscle that fails in this type of hernia. Here we propose a finite element (FE) simulation of the rabbit abdomen, in which a partial hernial defect is simulated to address the mechanical behaviour of the abdomen after mesh implantation.

The present study was designed to examine the anisotropic mechanical properties of three commercially available surgical meshes (Surgipro®, Optilene® and Infinit®) and thus identify the prosthesis closest to showing an ideal behaviour in mechanical terms. After mechanically characterizing the materials, their postimplant behaviour was reproduced by FE simulation. This model is based on the results of a previous study in which we characterized the passive mechanical behaviour of the abdominal wall of New Zealand White rabbits [5]. Here each mesh as well as abdominal muscle tissue is modelled through a strain energy function under the continuum theory of large deformation hyperelasticity, and the anisotropic response is described by defining a preferred direction of anisotropy [21].

2. Materials and methods

2.1. Specimen preparation

The three non-absorbable, biocompatible surgical meshes tested were: Surgipro® (SUR), a HW (84 g/m^2) polypropylene monofile mesh with a small pore size; Optilene® (OPT) a LW (48 g/m^2) polypropylene monofile mesh but with a large pore size. Both are indicated for abdominal and inguinal hernia repair as well as tissue reinforcement; and Infinit® (INF), a MW mesh (70 g/m^2) with a large pore size composed of a PTFE monofilament. This mesh is indicated for the repair of a hernia or other soft tissue defects. The geometry and pore size characteristics of the three meshes are provided in Fig. 1. This figure also indicates the two perpendicular directions (designated 1 and 2) selected to determine the anisotropy of the materials. The mesh samples tested in both directions were 20 mm wide by 190 mm long. Five samples of each mesh were tested in each direction.

2.2. Experimental test

The mesh samples were immersed in Hanks solution for 24 h. Uniaxial tensile tests were performed in an INSTRON 5548 microtester with a 50 N load cell. Contact between the sample and the clamps was improved by attaching sandpaper using double-sided duct tape to the sample. Before the test, a preload of 2 N was applied to each sample and then a displacement rate of 10 mm min^{-1} was maintained until the rupture of the sample. Stretch data were computed as $\lambda = \frac{L_0+\triangle L}{L_0}$, where L_0 is the initial distance between the clamps and $\triangle L$ is the displacement. The value of the thickness of the meshes can not be measured due to its discontinuous cross sectional area, where filaments and empty areas exist and are interspersed so Cauchy stress $\left(\sigma_{\text{Cauchy}} = \frac{\text{Force(N)}}{\text{Width(mm)Thickness(mm)}}\lambda\right)$ can not be computed. Thus, to compare the three meshes, force per unit width multiplied by stretch (Equivalent Cauchy Stress, ECS) was obtained using the expression $\frac{\text{Force(N)}}{\text{Width(mm)}}\lambda$, where Force (N) is the load applied during the test. Due to the nonlinear character of the curves, the stiffness of the curves was computed as the rate between the ECS variation and the stretch variation in the lineal range of the curve.

2.3. Statistical analysis

Possible significant variations in mechanical behaviour between directions 1 and 2 in the different meshes were analysed to establish the anisotropy of each mesh. We also compared the mechanical behaviour in each direction of the abdominal muscle tissue and each direction of the meshes. The Mann–Whitney *U*-test was used for all comparisons since the normal distribution of data could not be asserted. The level of significance was set at $p < 0.05$.

3. Calculation

3.1. Constitutive modelling

A frequently used methodology to formulate an elastic constitutive law for anisotropic materials is to postulate the existence of a strain energy function (SEF), Ψ, that depends on the preferential

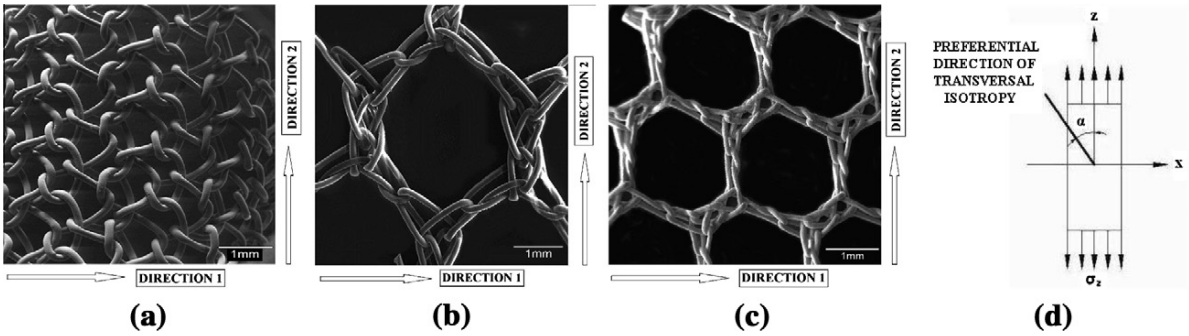

Fig. 1. Details of the three meshes tested indicating the directions 1 and 2 of the tests. (a) Surgipro® mesh. (b) Optilene® mesh. (c) Infinit® mesh. (d) Uniaxial tests were conducted in direction *z*, which differs from the preferential direction of transverse isotropy. Direction *z* is equivalent to direction 2 of the meshes and to the longitudinal direction of abdominal muscle tissue.

direction of anisotropy represented by a unit vector $\mathbf{m}_0$ and the Cauchy Green tensor, $\mathbf{C}$, [5,22–24] defined as:

$$\Psi(\mathbf{C},\mathbf{M}) = \Psi_{\text{vol}}(J) + \bar{\Psi}(\bar{\mathbf{C}},\mathbf{M}) = \frac{1}{D}(J-1) + \bar{\Psi}(\bar{I}_1,\bar{I}_2,\bar{I}_4), \tag{1}$$

where $\Psi_{\text{vol}}(J = \frac{1}{D}(J-1)^2)$ and $\bar{\Psi}$ are given scalar-valued functions of J, $\bar{\mathbf{C}} = \bar{\mathbf{F}}^T\bar{\mathbf{F}}$, $\mathbf{M} = \mathbf{m}_0 \otimes \mathbf{m}_0$, respectively, that describe the volumetric and isochoric responses of the material [22,25]; $\mathbf{F} = \frac{\partial \mathbf{x}}{\partial \mathbf{X}}$ is the standard deformation gradient, J = det ($\mathbf{F}$), $\bar{\mathbf{F}} = J^{-\frac{1}{3}}\mathbf{F}$, $\bar{I}_1$ and $\bar{I}_2$ are the first and second modified strain invariants of the symmetric modified Cauchy-Green tensor $\bar{\mathbf{C}} = J^{-\frac{2}{3}}\mathbf{C}$. Finally, the invariant $\bar{I}_4 = \bar{\mathbf{C}} : \mathbf{M} = \bar{\lambda}_m^2 \geqslant 1$ characterizes the anisotropic behaviour of the material. Furthermore, the Cauchy stress tensor $\boldsymbol{\sigma}$ can then be obtained from the second Piola–Kirchhoff $\mathbf{S}$ [25] which is defined as:

$$\mathbf{S} = 2\frac{\partial \Psi(\mathbf{C},\mathbf{M})}{\partial \mathbf{C}} = 2\frac{\partial \Psi_{\text{vol}}(J)}{\partial \mathbf{C}} + 2\frac{\partial \bar{\Psi}(\bar{\mathbf{C}},\mathbf{M})}{\partial \mathbf{C}}. \tag{2}$$

To fit the experimental results obtained, a strain energy function (SEF) which reproduces anisotropic responses was considered:

$$\bar{\Psi} = \bar{\Psi}_{\text{iso}} + \bar{\Psi}_{\text{ani}} = \frac{c_1}{c_2}\left(\exp^{\frac{c_2}{2}(\bar{I}_1-3)} - 1\right) + \frac{c_3}{2c_4}\left(\exp^{c_4(\bar{I}_4-1)^2} - 1\right), \tag{3}$$

where $c_1 > 0$ and $c_3 > 0$ are stress-like parameters and $c_2 > 0$ and $c_4 > 0$ are dimensionless parameters (*Note:* $\bar{\Psi}_{\text{ani}} = 0$ if $\bar{I}_4 \leqslant 1$). In this SEF, the isotropic part was modelled using Demiray's SEF [26] while the anisotropic response was represented by Holzapfel's SEF [23]. In the uniaxial test, a preferential direction of anisotropy is considered through the angle α referred to direction *z*, Fig. 1d.

Since mesh thickness is small, in the constitutive 3D model for materials, normal stresses were assumed to be zero such that we considered a membrane model according to the algorithm proposed by Klinkel et al. [27]. We computed ECS by Cauchy Stress using a thickness of 1 mm.

Material parameters and the preferential direction of anisotropy, angle α, were fitted by an iterative process minimizing the error between experimental and analytical curves. There are two approaches to obtain the material parameters: in the first the curved are averaged and then fit once, or in the second each experiment curve was fit and then constants averaged. In this work we used the first approach, so experimental mean data were fitted only once using the Levenberg–Marquardt minimization algorithm [28]. This algorithm is based upon minimization of an objective function, which takes the form represented in (4) for the uniaxial tension test:

$$\chi^2 = \sum_{i=1}^{n}\left[\left(ECS^{\text{exp}} - ECS^{\Psi}\right)_{i2}^2 + \left(ECS^{\text{exp}} - ECS^{\Psi}\right)_{i1}^2\right], \tag{4}$$

where ECS_i^{exp} and ECS_i^{Ψ} represent the measured and analytical ECS values for the *i*th data point, respectively. Subscripts 1 and 2 indicate the directions 1 and 2 of the test. The quality of data fitting was assessed by calculating the normalized mean square root error $\varepsilon = \frac{\sqrt{\frac{\chi^2}{n-q}}}{\mu}$, were q is the number of parameters of the SEF, n is the number of data points, $n-q$ is the number of degrees of freedom, and μ is the mean stress defined as $\mu = \frac{1}{n}\sum_{i=1}^{n}[ECS]_i$.

3.2. FE Simulation of meshes

A FE membrane model of each sample (20 mm × 160 mm) was used to reproduce the uniaxial tests on the meshes in directions 1 and 2. The FE model consisted of 165 nodes and 128 membrane elements; the thickness was established at 1 mm. The material model of each mesh was implemented using the previously proposed SEF, Eq. (3).

Boundary conditions mimic the uniaxial test. Displacements are fixed in all directions at the lower clamp. On the upper side, a preload of 2 N is applied and, next, a displacement corresponding to 100% strain is applied in the axial direction. Computations were conducted for directions 1 and 2. The results obtained were compared with the experimental data.

3.3. FE simulation of the hernia repair

To analyse the effects of the meshes in the abdominal wall just after mesh implantation – at time-zero without tissue in-growth – a FE simulation was conducted for the rabbit abdomen, whose geometry was approximated by an extruded ellipse. The dimensions of the ellipse were based on measurements of the abdomen of rabbits weighing 2150 ± 50 g. The long axis of the ellipse was 140 mm and the short axis was 60 mm. The thickness of the complete abdomen was taken as 3.5 mm and the length was fixed at 160 mm (length of the rabbit abdomen), Fig. 2a. Two lids were included at the top and bottom the abdomen to reproduce the abdominal cavity. For the boundary conditions, displacements of the nodes at the back of the abdomen were fixed to simulate the constraints imposed by the shoulders. Finally, an internal pressure of 60 mm Hg (8 kPa) was applied to the interior abdominal wall to reproduce the abdominal load during the standing Valsalva manoeuvre [18]. The craneo-caudal direction of the rabbit was considered the longitudinal direction and the direction perpendicular to this was considered the transversal direction, Fig. 2a.

According to the procedure of Hernández et al. [5], we reproduced the response of the abdominal muscle tissue using the proposed SEF in Eq. (3) and the material parameters fitted in [5] for EO (external oblique layer)–IO (internal oblique layer) composite muscle layer (c_1 = 0.16832 MPa, c_2 = 0.6319, c_3 = 0.01219 MPa, c_4 = 5.68158, α = 87.8°). The angle α represents the preferential

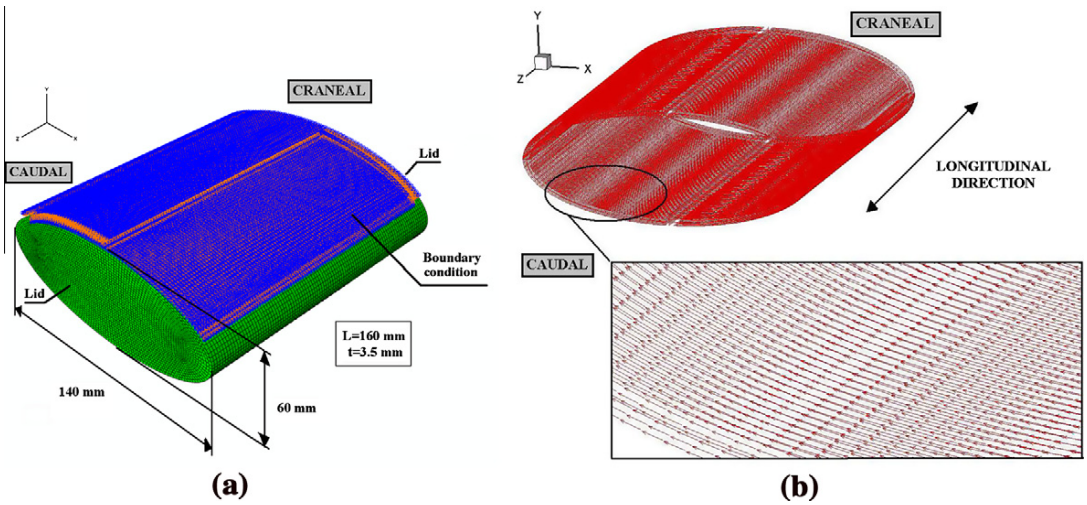

Fig. 2. (a) Complete model of the rabbit abdomen. (b) Preferential direction of anisotropy for healthy muscle tissue ($\alpha = 87.8°$ referred to the craneo-caudal direction).

direction of anisotropy of the muscle tissue and is referred to the longitudinal direction of the abdomen of the rabbit (equivalent to direction *z*, Fig. 1d). In the FE simulation, the preferential direction of anisotropy for healthy muscle tissue is included at each integration point through a unit vector, Fig. 2b. The numbers of linear hexahedral elements and nodes were 41856 and 62790, respectively.

The partial hernia was modelled at the front of the abdomen, at midlength along the abdomen and adjacent to the linea alba by removing the elements corresponding to the EO layer, Fig. 3a. The dimensions of the defect were 40 × 40 mm. A total of 62376 nodes, 41400 linear hexahedral elements for the abdominal wall and 456 linear quadrilateral membrane elements for the mesh were included. The thickness of the membrane elements was 1 mm. The surgery process was modelled by simulating the SUR, OPT and INF meshes. In all cases, the direction 2 of the meshes was coincident with the transversal direction of the abdomen corresponding to the perpendicular one to the craneo-caudal direction. To model the running sutures used to fix the meshes, the nodes of the boundaries of the meshes were matched with the abdominal nodes.

4. Results

4.1. Mechanical test of meshes

Fig. 4a–c provides the mean ECS vs. stretch curves obtained in the mechanical tests for SUR, OPT and INF, respectively. The stretch values recorded were 1.949 ± 0.024 and 2.009 ± 0.0814 in directions 1 and 2, respectively, for SUR and 1.822 ± 0.049 and 1.811 ± 0.051, respectively for OPT (see Table 1). The stretch values obtained for INF were 1.762 ± 0.067 in direction 1, but only 1.321 ± 0.038 in direction 2.

Our ECS data also revealed differences among the meshes (see Table 1). SUR emerged as the stiffest mesh showing similar behaviour in each direction such that it can be considered isotropic ($p > 0.1$) and the maximum ECS were 20.629 ± 0.282 N/mm and 18.363 ± 2.413 N/mm in directions 1 and 2, respectively. For the OPT mesh, the maximum ECS recorded in direction 2 was lower (10.785 ± 1.047 N/mm) than that shown by SUR and indicated greater stiffness in this direction than in direction 1 (7.573 ± 0.735 N/mm) and the anisotropy of the material for $\lambda > 1.33$ ($p < 0.0158$). Finally, for INF, maximum ECS were 2.075 ± 0.548

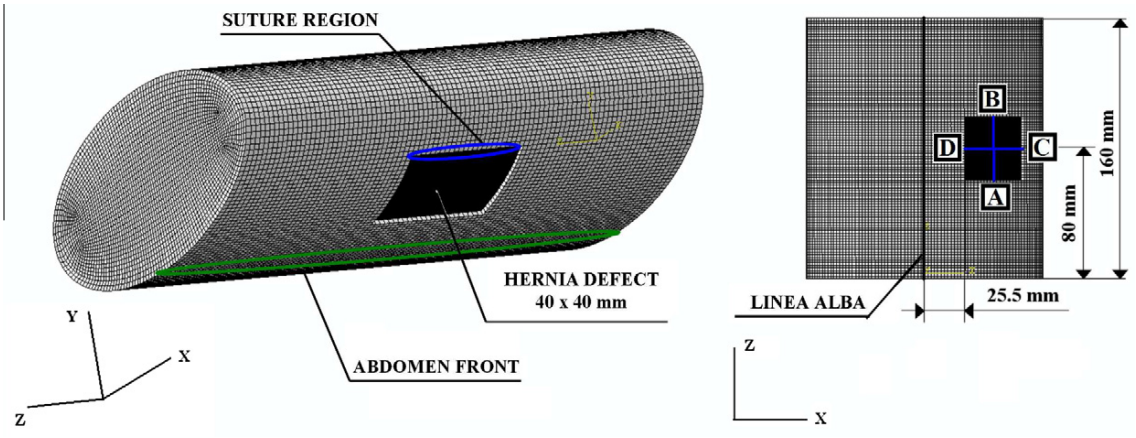

Fig. 3. Simplified model of the rabbit abdomen with a partial hernial defect. The figure shows the areas of the model to which the results refer to. The lines AB and CD, defined for post-processing purpose, are indicated.

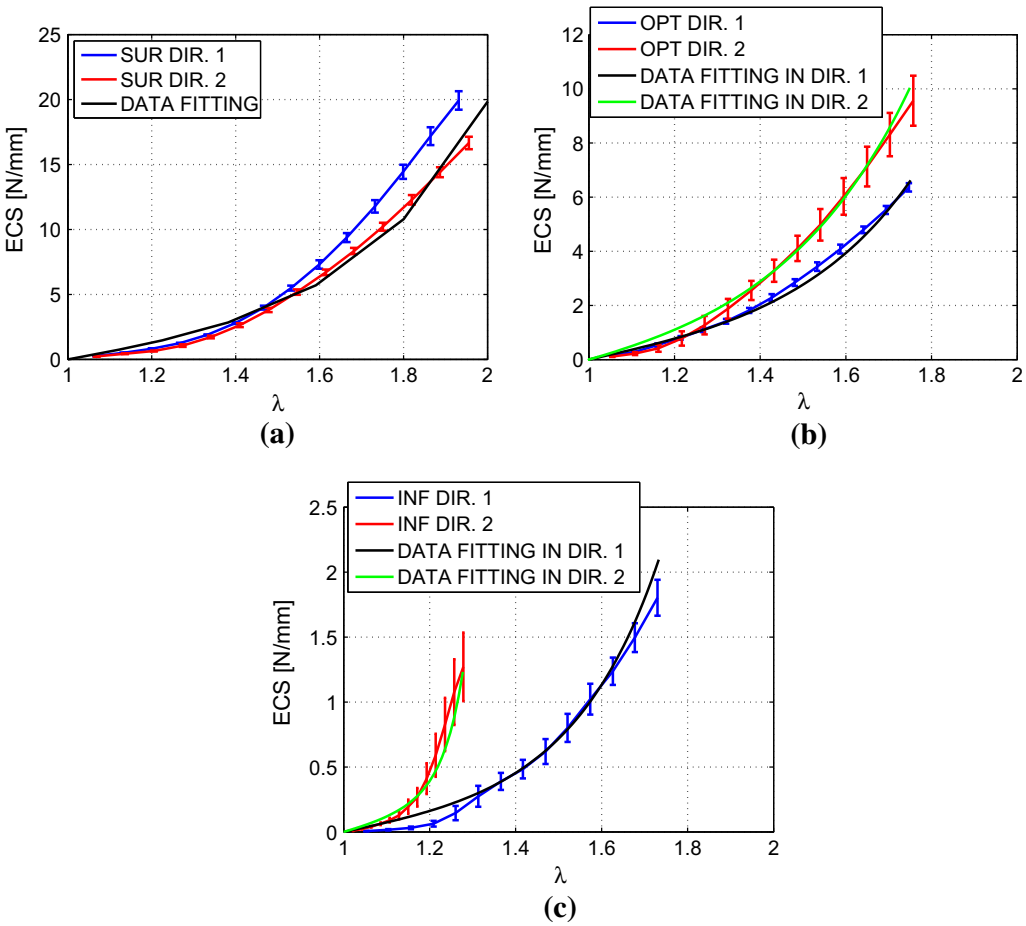

Fig. 4. Experimental and fitting results. (a) SUR mesh. The data fitting was obtained using the isotropic part of the SEF. (b) OPT mesh. The data fitting was obtained using the Demiray-Holzapfel SEF. (c) INF mesh. The data fitting was obtained using the Demiray-Holzapfel SEF.

Table 1
Average properties for the different meshes in directions 1 and 2 (mean ± standard deviation); Maximum ECS (N/mm), maximum stretch and stiffness (N/mm). The stiffness was computed in the linear region of the curves.

	ECS_{max} (N/mm)		λ_{max}		Stiffness (N/mm)	
	Dir. 1	Dir. 2	Dir. 1	Dir. 2	Dir. 1	Dir. 2
Surgipro®	20.629 ± 0.282	18.363 ± 2.413	1.949 ± 0.024	2.009 ± 0.081	32.456 ± 1.343	24.819 ± 0.727
Optilene®	7.573 ± 0.735	10.785 ± 1.047	1.822 ± 0.049	1.811 ± 0.051	12.838 ± 0.161	19.785 ± 2.205
Infinit®	2.075 ± 0.548	1.637 ± 0.204	1.762 ± 0.067	1.321 ± 0.038	4.045 ± 0.436	10.244 ± 2.456

N/mm and 1.637 ± 0.204 N/mm in directions 1 and 2, respectively, indicating its remarkable anisotropy ($p < 0.0001$).

To identify the "ideal prothesis" that was best able to mimic the mechanical behaviour of the healthy abdominal wall, we compared our results to those reported by Hernández et al. [5], Fig. 5. This comparison revealed that only the INF mesh displayed the intense anisotropy of the abdominal muscle tissue showing, in direction 2, a response that was close to the tissue response in a transverse direction ($p > 0.181$). In contrast, the response of INF in direction 1 most resembled that produced in the longitudinal direction of the tissue but only for $\lambda > 1.48$ ($p > 0.1811$). The mechanical behaviour of OPT in both directions was similar to the crossways behaviour of the tissue ($p > 0.1601$ and $p > 0.0735$, respectively). However, although anisotropic, its mechanical behaviour was far from that observed in the longitudinal direction of the tissue. The isotropic behaviour of the SUR mesh was only comparable to the mechanical response shown in the transverse direction by the muscle tissue ($p > 0.1428$).

4.2. Model parameters

The Demiray SEF, the isotropic part in Eq. (3), was used to model the isotropic behaviour of the SUR mesh. Only one mean plot for one direction (longitudinal) was needed to fit the isotropic response. In contrast, the anisotropic responses shown by OPT and INF were reproduced using the Demiray-Holzapfel SEF, Eq. (3).

The results of parameter estimation for all meshes obtained by fitting the experimental curves are shown in Table 2. In all cases, ε values were close to 0 confirming the goodness of fit. However, agreement was poor when fitting the INF data across the low stretch range, and the ε value for the INF mesh was accordingly higher. This is due to the highly exponential nature of the curves.

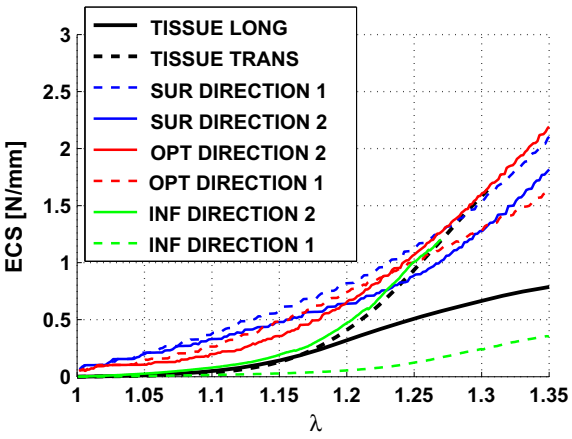

Fig. 5. ECS vs. stretch for healthy tissue, SUR, OPT and INF. Plot shows the experimental means up to $\lambda = 1.35$.

Table 2
Material parameters for the SUR, OPT and INF meshes generated by the fitting procedure. Angle α is referred to direction 2 (equivalent to direction z), Fig. 1d.

	c_1 (MPa)	c_2 (−)	c_3 (MPa)	c_4 (−)	α (°)	ε
Surgipro®	2.10163	1.17805	–	–	–	0.1467
Optilene®	1.25112	1.5	0.28	0.03062	0.0	0.0807
Infinit®	0.25	2.5	0.07804	5.49131	0.0	0.3714

Fig. 4a–c provide the results of the fitting process. Curves constructed using the experimental uniaxial test data and the results of the simulation are compared. The plots of ECS vs. stretch indicate the good fit of the parameters.

4.3. FE simulation of the hernia repair

These results are provided for the three different areas of the model indicated in Fig. 3: the abdomen front (where there is no surgical mesh), the area of the repaired hernial defect and the suture zone.

The maximal principal stress (MPS) of the healthy abdominal wall at the front of the abdomen was about 0.195 MPa, Fig. 6. When the hernial defect was computed, MPS were also modified at the abdomen front and the three surgical meshes returned relatively higher values of MPS than the healthy wall: 0.205, 0.2048 and 0.2029 MPa for SUR, OPT and INF respectively, Fig. 6.

MPS in the area of the hernial defect were not evenly distributed, Fig. 6. For all three implanted meshes, stresses were higher close to the suture zone. When an element in the centre of the hernial defect was examined in the implant simulations, MPS were 0.1678 MPa (for the underlying tissue) and 0.3883 MPa (for the surgical mesh) for INF, 0.0412 MPa (underlying tissue) and 0.5694 MPa (surgical mesh) for SUR and 0.0574 MPa (underlying tissue) and 0.5494 MPa (surgical mesh) for OPT. In the healthy muscle tissue, in the same reference element, MPS was 0.1881 MPa. Fig. 8a and b shows the MPS in the tissue along the lines AB and CD (See Fig. 3). MPS for INF are very similar to those obtained in the healthy muscle tissue whereas MPS for SUR and

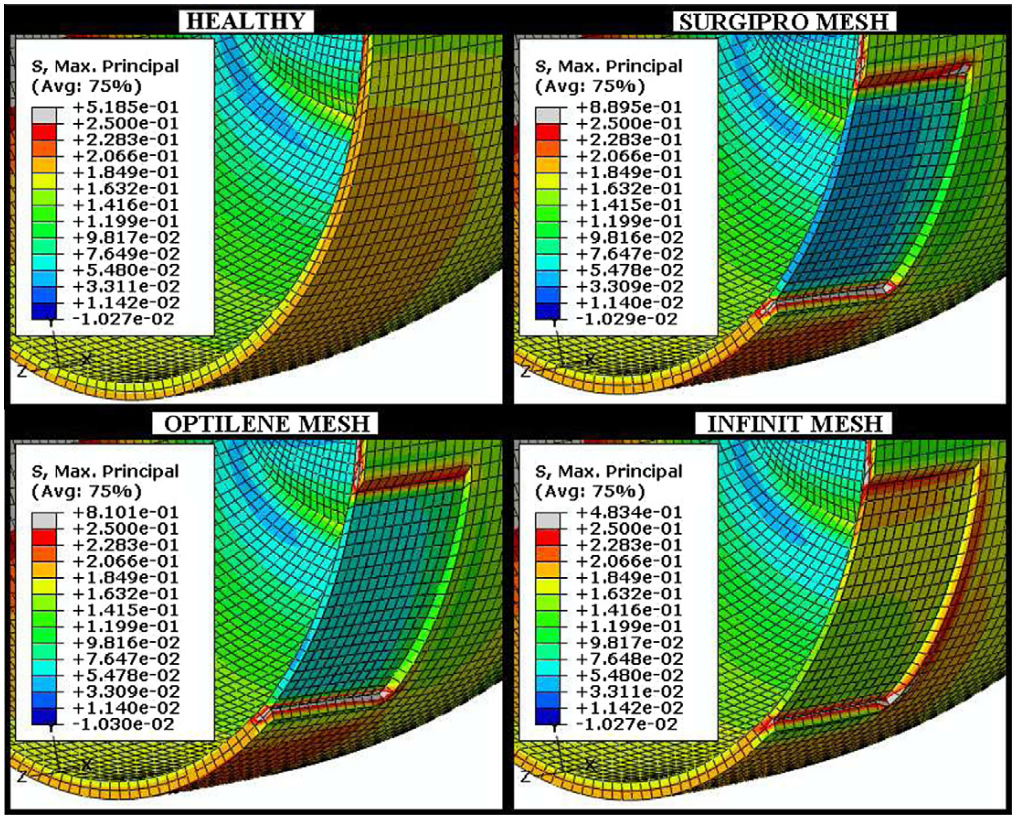

Fig. 6. Maximal principal stress (MPS) computed for the hernial defect area. The zones compared are the healthy abdominal wall with no defect and the three implanted meshes. Note that only half the model is represented.

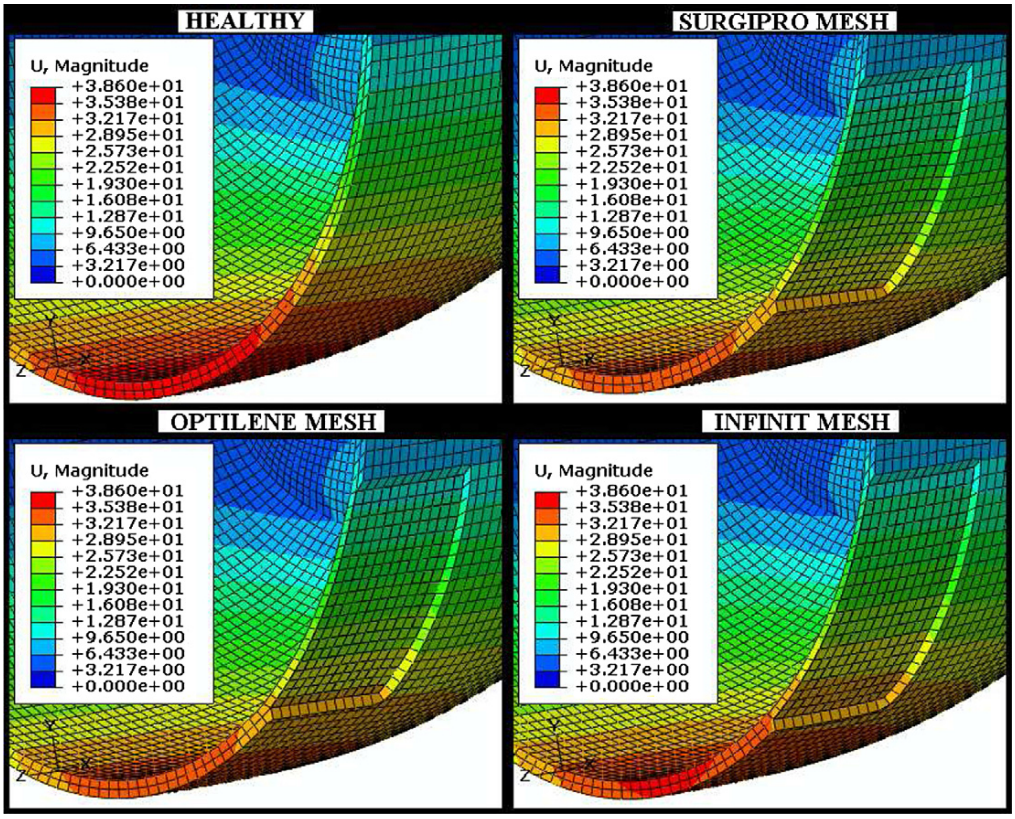

Fig. 7. Displacements computed for the hernial defect area. The zones compared are the healthy abdominal wall with no defect and the three implanted meshes. Note that only half the model is represented.

OPT meshes are very low. Close to the suture zones, where there is a stress concentration due to the discontinuity provoked by the surgical mesh, stresses provoked by the biomaterial in the tissue were 0.1238, 0.138 and 0.2424 MPa for SUR, OPT and INF, respectively. For the surgical meshes themselves in the suture zone, SUR, OPT and INF attained MPS values of 0.4501, 0.4364 and 0.3001 MPa, respectively. At both the elements in the mesh centre and the suture zone, MPS for SUR and OPT were higher than for INF; in this last mesh, MPS were well balanced between the underlying muscle tissue and surgical mesh whereas MPS in the underlying tissue for SUR and OPT are very low so they could cause further atrophy of the defect muscle (see Fig. 8a and b). For the healthy abdominal wall, maximum stress in the area corresponding to the equivalent suture zone was 0.2132 MPa, which is higher compared to SUR and OPT and lower compared to INF.

It may be seen in Fig. 7 that maximum displacements (MD) are produced at the abdomen front and that these diminish after mesh implantation. MD values for the healthy abdominal muscle were 36.8207 and 33.3926, 33.5978 and 34.5293 mm, respectively, for SUR, OPT and INF. When the central hernial defect area was analysed, results revealed that the healthy abdominal wall induces displacements of 24.7077 mm whereas this value was reduced for the SUR, OPT and INF meshes (20.1438, 20.5787 and 22.6789 mm, respectively). Considering an element in the suture zone, displacements were 16.0061 mm for the intact wall compared to displacements of 13.3397, 13.4775 and 14.2138 mm induced by SUR, OPT and INF in the tissue, respectively. Fig. 8c and d shows the MD along the lines AB and CD (see Fig. 3). The closer MD to the healthy muscle tissue are those obtained for the INF mesh whereas MD for SUR and OPT are lower. Thus, SUR and OPT provoke a more restrictive mobility of the abdominal wall. The FE simulation of the INF mesh indicated least variation in displacements compared to healthy abdominal wall.

5. Discussion

For good clinical results in abdominal hernia surgery, the mechanical properties of the abdominal wall need to perfectly match the mechanical properties of the biomaterial used for its repair [29].

In this study, we addressed the mechanical response of three surgical meshes (SUR, OPT and INF). Uniaxial test curves for the meshes were compared to the response of the abdominal tissue to identify the "ideal prothesis" from a purely mechanical point of view. To model the mechanical response of the meshes, a homogenization methodology was used. For each mesh, a SEF was proposed and the parameters of the materials were accordingly adjusted. Finally, these properties were included in a model of the rabbit abdomen.

The experimental data reported here indicate that the SUR mesh shows an isotropic mechanical response while OPT and INF display an anisotropic response. Thus, the SUR mesh yielded similar experimental data when tested in two different directions, Fig. 4a. This is because the spatial arrangement of its filaments is very similar between both directions, Fig. 1a. On the contrary, the OPT and INF meshes are LW biomaterials and the anisotropic behaviour of OPT was less pronounced than that of INF, Fig. 4b and c, respectively. The anisotropic response shown by both these meshes can also be attributed to the spatial arrangement of their filaments since in both cases, there were more filaments running in direction 2 than in direction 1, Fig. 1b and c. Thus, both the

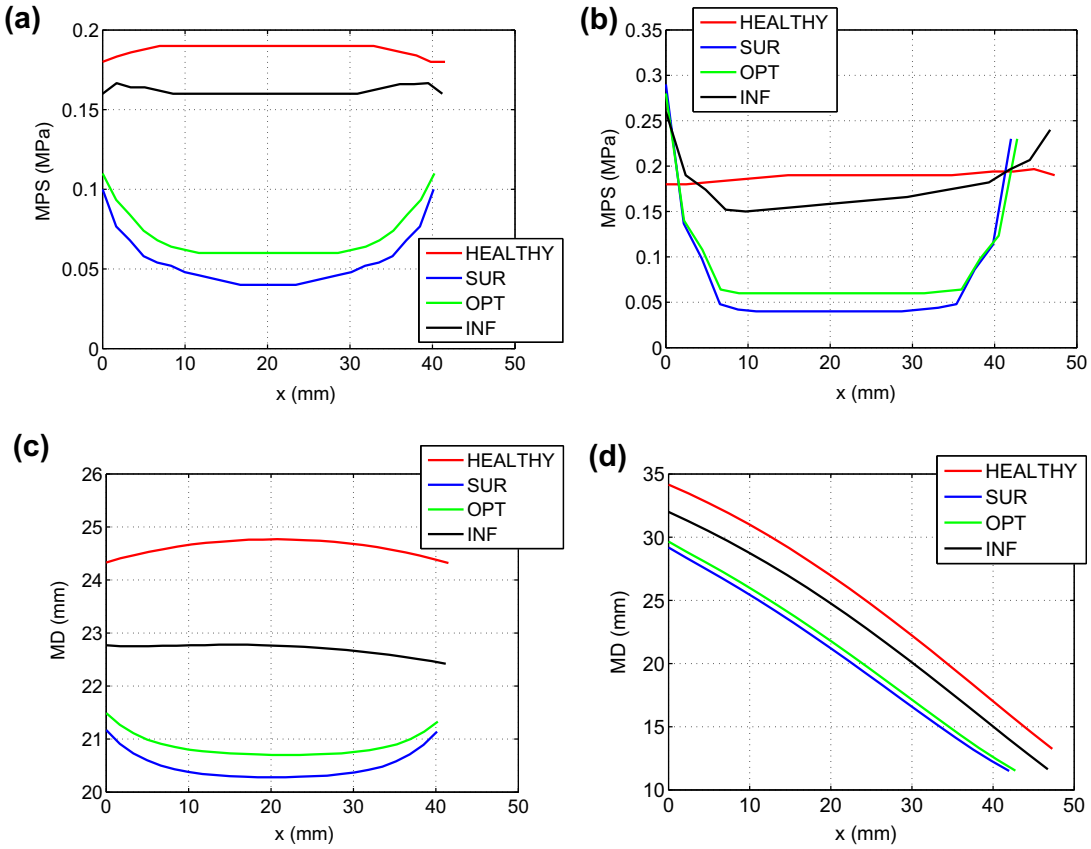

Fig. 8. (MPS along the lines AB (a) and CD (b) (see Fig. 3). MD along the lines AB (c) and CD (d). The abscissa shows the deformed coordinates of the defect. $x = 0$ and 40 mm correspond to points A,C and B,D in the undeformed configuration of the abdomen.

OPT and INF meshes are stiffer in direction 2. The direction of anisotropy (α) obtained for the OPT and INF meshes was equal to 0°, Table 2, and this once again indicates that direction 2 is much stiffer than direction 1. If we consider the breakage points of the samples, SUR mesh showed the greatest rupture stress, approximately doubling that of OPT, and the INF mesh showed the lowest rupture stress point. Furthermore, due to the discontinuous cross sectional area of the meshes ECS was defined and used instead of Cauchy Stress. Fig. 4 shows the good fit of the parameters so the assumption of membrane model instead of the porous mesh is validated.

If at this point we consider the abdominal muscle tissue, the transverse direction (perpendicular to the craneo-caudal) is the stiffer direction [3–5]. In our comparison of the mechanical responses of abdominal muscle tissue [5] and the different meshes we were able to conclude that the INF mesh is the one that best complies with the anisotropic mechanical behaviour of the abdominal wall. The isotropic SUR mesh and direction 2 of the OPT mesh showed a similar response to the transverse mechanical behaviour of the abdominal wall. Neither SUR nor OPT complied with the longitudinal response of the wall such that if these meshes are implanted, poor compliance between muscle tissue and mesh will cause pain and discomfort. Thus, to ensure good mechanical matching between the abdominal muscle and these surgical meshes, the stiffer direction of the mesh should be aligned with the transverse direction of the abdomen, Fig. 1. Given that direction 2 of OPT and INF proved here to be the stiffest, the surgeon should align this axis with the transverse direction of the abdomen, whereas SUR can be aligned either way because of its isotropic behaviour.

We here propose a constitutive model to reproduce the mechanical behaviour of the surgical meshes. Fig. 4d–f shows that the membrane model used is sufficiently accurate to predict this behaviour. Our models not only reproduce the nonlinear behaviour of the material but also describe the anisotropy of the materials.

Including a surgical mesh in the healthy abdominal wall clearly modifies the distribution of stresses. This means that the surgical repair procedure does not fully restore normal physiological conditions. Besides the inhomogeneous distribution of MPS, stresses seem to concentrate in the hernial defect area, and are greatest close to the suture zone, Fig. 6. This build-up of stress could lead to hernia recurrence in the suture zone. When simulation was conducted for the implanted meshes, MPS values were always higher than for the healthy abdominal wall front. The highest values were induced by the SUR and OPT meshes, while INF provoked slightly lower stress values in all the zones assessed. Maximum displacements were also affected by mesh implant and no mesh was able to match the displacements of the abdominal wall. The higher MD computed for the healthy abdominal wall indicates that the meshes compromise abdominal compliance. SUR and OPT behaved similarly allowing comparable displacements in all zones, while greater MD were observed for INF. This indicates the better compliance of the abdominal wall after the implant of the INF mesh.

Our study is not devoid of certain simplifications and limitations. Thus, the ECS vs. stretch plots were based on the assumption of a homogeneous thickness of the meshes so that we could directly compare the abdominal tissue and meshes. Further information from other mechanical tests (e.g. biaxial) would be useful to

complete our characterization of these materials. In addition, the host tissue remodelling process produced in response to the different implants including collagen synthesis would need to be addressed in future works since these biological processes will affect the mechanical response. Finally, our simulations were based on a simplified geometry of the mesh sample through a continuum membrane sheet, which does not take into account the deformation of the pores, and the rabbit abdomen. These geometries, nevertheless, are considered useful for analyzing both, the response of the meshes from uniaxial tests and the response of the tissue after surgery. In spite of these limitations, given the potentiality of the presented work, minor modifications would be enough to apply it to the modelling of human abdomen.

Our findings provide direction for future studies designed to examine the long term behaviour of the abdominal wall after mesh implantation. Mechanical properties as well as histological factors should provide further insight into the host tissue incorporation process determined by the pore size and filament spatial distribution of the surgical meshes.

6. Conclusions

In this study, we characterize the mechanical behaviour of three surgical meshes, SUR, OPT and INF, and observe an isotropic mechanical response in SUR and an anisotropic one in OPT and INF.

We conclude that the stiffer direction of a surgical mesh should be aligned with the transverse direction of the abdominal muscle tissue [3–5]. Our findings indicate that the anisotropic behaviour of OPT and INF needs to be considered by surgeons during mesh placement in the abdomen.

Finally, our FE simulations of the different meshes reveal that no mesh is able to reproduce the displacements of the abdominal wall. Despite the fact that no ideal mesh seems to exist, best abdominal wall compliance was observed for INF. Thus, the INF mesh was best able to reproduce abdominal wall displacements compared to SUR and OPT and the stresses provoked by INF were lower than those observed for SUR and OPT when occupying an anterior abdominal position. Finally, the FE simulation of this PTFE mesh indicated equalized MPS between the muscle tissue and mesh both in the central mesh zone and suture zone determining less stiffness in this region compared to SUR and OPT.

Disclosures

The authors declare no commercial or personal interests in any of the materials or procedures mentioned in this study.

Acknowledgments

This research was supported by the Spanish Ministry of Science and Technology through projects DPI2008-02335/DPI2010-20746-C03-01/DPI2011-27939 and the Instituto de Salud Carlos III (ISCIII) through the CIBER Initiative Project ABDOMESH. CIBER-BBN is an initiative funded by the VI National R& D& i Plan 2008–2011, Iniciativa Ingenio 2010, Consolider Program, CIBER Actions and financed by the Instituto de Salud Carlos III with assistance from the European Regional Development Fund. The authors also acknowledge the Spanish Ministry of Science and Technology for a Grant (BES-2009-021515) awarded to B. Hernández-Gascón. The authors are indebted to Gore and Associates, Flagstaff, Arizona, USA for providing the meshes used in this study.

Appendix A. Figures with essential colour discrimination

Certain figures in this article, particularly Figures 2–8, are difficult to interpret in black and white. The full colour images can be found in the on-line version, at doi:10.1016/j.actbio.2011.06.033.

References

[1] Lichtenstein IL, Shulman AG. Ambulatory outpatient hernia surgery including a new concept introducing tension-free repair. Int Surg 1986;71:1–4.
[2] Lichtenstein IL, Shulman AG, Amid PK, Montlor MM. The tension-free hernioplasty. Am J Surg 1989;157:188–93.
[3] Junge K, Klinge U, Prescher A, Giboni P, Niewiera M, Shumpelick V. Elasticity of the anterior abdominal wall and impact for reparation of incisional hernia using mesh implants. Hernia 2001;5:112–8.
[4] Grassel D, A P, Fitzed S, Keyserlingk DG, Axer H. Anisotropy of human linea alba: a biomechanical study. J Surg Res 2005;124:118–25.
[5] Hernández B, Peña E, Pascual G, Rodriguez M, Calvo B, Doblaré M, et al. Mechanical and histological characterization of the abdominal muscle: a previous step to model hernia surgery. J Mech Behav Biomed Mater 2011;4:392–404.
[6] Klosterhalfen B, Junge K, Klinge U. The lightweight and large porous mesh concept for hernia repair. Expert Rev Med Devices 2005;2:103–17.
[7] Klinge U. Experimental comparison of monofile light and heavy polypropylene meshes: less weight does not mean less biological response. World J Surg 2007;31:867–8.
[8] Cobb WS, Burns JM, Peindl RD, Carbonell AM, Matthews BD, Kercher KW, et al. Textile analysis of heavy-weight, mid-weight and light-weight polypropylene mesh in a porcine ventral hernia model. J Surg Res 2006;136:1–7.
[9] Afonso J, Martins P, Girao M, Natal Jorge R, Ferreira A, Mascarenhas T, et al. Mechanical properties of polypropylene mesh used in pelvic floor repair. Int Urogynecol J 2008;19:375–80.
[10] Pascual G, Rodríguez M, Gómez-Gil V, García-Honduvilla N, Buján J, Bellón JM. Early tissue incorporation and collagen deposition in lightweight polypropylene meshes: bioassay in an experimental model of ventral hernia. Surgery 2008;144(3):427–35.
[11] Bellón JM. Role of the new lightweight prostheses in improving hernia repair. Cir Esp 2009;85(5):268–73.
[12] Usher FC, Cogan JE, Lowry T. A new technique for the repair of inguinal and incisional hernias. Arch Surg 1960;84:847–50.
[13] Alaedeen DI, Lipman J, Medalie D, Rosen MJ. The single-staged approach to the surgical management of abdominal wall hernias in contaminated fields. Hernia 2007;11:41–5.
[14] Klinge U, Klosterhalfen B, Birkenhauer V, Junge K, Conze J, Schumpelick V. Impact of polymer pore size on the interface scar formation in a rat model. J Surg Res 2002;103:208–14.
[15] Schachtrupp A, Klinge U, Junge K, Rosch R, Bhardwaj RS, Schumpelick V. Individual inflammatory response of human blood monocyte to mesh biomaterials. British J Surg 2003;90:114–20.
[16] Saberski ER, Orenstein SB, Novitsky YW. Anisotropic evaluation of synthetic surgical meshes. Hernia 2010:1–6.
[17] Bellón JM, Rodríguez M, García-Honduvilla N, Gómez-Gil V, Pascual G, Buján J. Comparing the behavior of different polypropylene meshes (heavy and lightweight) in an experimental model of ventral hernia repair. J Biomed Mater Res B Appl Biomater 2009;89B(2):448–55.
[18] Cobb WS, Burns JM, Kercher KW, Matthews BD, Norton HJ, Heniford BT. Normal intraabdominal pressure in healthy adults. J Surg Res 2005;129:231–5.
[19] Song C, Alijani A, Frank T, Hanna G, Cuschieri A. Mechanical properties of the human abdominal wall measured in vivo during insufflation for laparoscopic surgery. Surg Endoscopy 2006;20:987–90.
[20] Klinge U, Junge K, Stumpf M, Klosterhalfen B. Functional and morphological evaluation of a low-weight monofilament polypropylene mesh for hernia repair. J Biomed Mater Res B Appl Biomater 2002;63:129–36.
[21] Spencer AJM. Theory of invariants. In: Continuum Phys. New York: Academic Press; 1954. p. 239–53.
[22] Weiss JA, Maker BN, Govindjee S. Finite element implementation of incompressible transversely isotropic hyperelasticity. Comp Methods Appl Mech Eng 1996;135:107–28.
[23] Holzapfel GA, Gasser TC, Ogden RW. A new constitutive framework for arterial wall mechanics and a comparative study of material models. J Elasticity 2000;61:1–48.
[24] Peña E, del Palomar AP, Calvo B, Martínez MA, Doblaré M. Computational modelling of diarthrodial joints. Physiological, pathological and pos-surgery simulations,. Arch Comput Methods Eng 2007;14(1):47–91.
[25] Holzapfel GA. Nonlinear Solid Mechanics. New York: Wiley; 2000.
[26] Demiray H, Weizsacker HW, Pascale K, Erbay H. A stress–strain relation for a rat abdominal aorta. J Biomech 1988;21:369–74.
[27] Klinkel S, Govindjee S. Using finite strain 3D-material models in beam and shell elements. Eng Comput 2002;19(8):902–21.
[28] Marquardt DW. An algorithm for least-squares estimation of nonlinear parameters. SIAM J Appl Math 1963;11:431–41.
[29] Conze J, Klinge U. Biocompatibility of biomaterials-clinical and mechanical aspects. Berlin, Heidelberg, New York: Springer; 1999. Chapter 14, pp. 169–177.

Work 3: Long-term anisotropic mechanical response of surgical meshes used to repair abdominal wall defects

Journal: *Journal of the mechanical behavior of biomedical materials*, **5**(1) (2012): 257-271.
Journal impact factor: 2.814

Available online at www.sciencedirect.com

SciVerse ScienceDirect

journal homepage: www.elsevier.com/locate/jmbbm

Research paper

Long-term anisotropic mechanical response of surgical meshes used to repair abdominal wall defects

B. Hernández-Gascón[a,d], E. Peña[a,d], G. Pascual[b,d], M. Rodríguez[c,d], J.M. Bellón[c,d], B. Calvo[a,d,*]

[a] Aragón Institute of Engineering Research (I3A), University of Zaragoza, Spain
[b] Department of Medical Specialities, Faculty of Medicine, University of Alcalá, Spain
[c] Department of Surgery, Faculty of Medicine, University of Alcalá, Spain
[d] Centro de Investigación Biomédica en Red en Bioingeniería, Biomateriales y Nanomedicina (CIBER-BBN), Spain

ARTICLE INFO

Article history:
Received 11 May 2011
Received in revised form
6 September 2011
Accepted 9 September 2011
Published online 17 September 2011

Keywords:
Hernia repair
Polypropylene prostheses
Biomechanical response
Mesh repair
Partial hernia

ABSTRACT

Routine hernia repair surgery involves the implant of synthetic mesh. However, this type of procedure may give rise to pain and bowel incarceration and strangulation, causing considerable patient disability. The purpose of this study was to compare the long-term behaviour of three commercial meshes used to repair the partially herniated abdomen in New Zealand White rabbits: the heavyweight (HW) mesh, *Surgipro*® and lightweight (LW) mesh, *Optilene*®, both made of polypropylene (PP), and a mediumweight (MW) mesh, *Infinit*®, made of polytetrafluoroethylene (PTFE). The implanted meshes were mechanical and histological assessed at 14, 90 and 180 days post-implant. This behaviour was compared to the anisotropic mechanical behaviour of the unrepaired abdominal wall in control non-operated rabbits.

Both uniaxial mechanical tests conducted in craneo-caudal and perpendicular directions and histological findings revealed substantial collagen growth over the repaired hernial defects causing stiffness in the repair zone, and thus a change in the original properties of the meshes. The mechanical behaviour of the healthy tissue in the craneo-caudal direction was not reproduced by any of the implanted meshes after 14 days or 90 days of implant, whereas in the perpendicular direction, SUR and OPT achieved similar behaviour. From a mechanical standpoint, the anisotropic PP-lightweight meshes may be considered a good choice in the long run, which correlates with the structure of the regenerated tissue.

1. Introduction

Hernia repair is a common surgical procedure when an abdominal wall defect exists. Mechanically speaking, the abdominal hernia is an opening in the abdominal wall layer that makes it impossible for the wall to maintain intra-abdominal pressure. Since the introduction of Lichtenstein's tension-free mesh procedure (Lichtenstein and Shulman, 1986; Lichtenstein et al., 1989), the classic suture techniques have gradually given way to the use of a biomaterial for

* *Corresponding author at:* Aragón Institute of Engineering Research (I3A), University of Zaragoza, Spain.
E-mail address: bcalvo@unizar.es (B. Calvo).

1751-6161/$ - see front matter © 2011 Elsevier Ltd. All rights reserved.
doi:10.1016/j.jmbbm.2011.09.005

the surgical repair of an abdominal wall hernia, which is a practically standard practice today. Prosthetic mesh was first used for ventral hernia repair in the 1960s, when Usher (Usher, 1959; Usher et al., 1960; Usher, 1970) described the advantages of knitted polypropylene (PP) mesh for the repair of anterior abdominal wall hernias. Since then several studies have shown that closing hernial defects with mesh leads to a lower recurrence rate (Morris-Stiff and Hughes, 1998; Luijenkijk et al., 2000).

There are a variety of meshes made of different materials available to the surgeon when contemplating hernia repair. Currently, PP and expanded polytetrafluoroethylene (ePTFE) meshes are the most commonly employed, although their physical characteristics differ considerably (Bellón et al., 1996). These traditional biomaterials have been gradually modified over the years including modifications to pore size and the spatial arrangement or diameter of their filaments. According to the German school, density is the main feature that serves to classify a mesh into heavyweight (HW) or lightweight (LW) (Klinge, 2007) such that the classic HW meshes have a density above 80 g/m^2 and the LW meshes below 50 g/m^2. A third type or mediumweight (MW) mesh has a density between 50 and 80 g/m^2 (Cobb et al., 2006). When used to repair a tissue defect, PP and ePTFE confer clinical strength to the repair site (Simmermacher et al., 1994; Holzman et al., 1997) but they also elicit an intense inflammatory tissue response (Brown et al., 1985; Law and Ellis, 1988; Saiz et al., 1996; Morris-Stiff and Hughes, 1998). PP shows excellent host tissue incorporation and is relatively inexpensive (Bellón et al., 1998) but unfortunately induces adhesion formation to underlying viscera (Law and Ellis, 1988; Bleichrodt et al., 1993; Saiz et al., 1996; Bellón et al., 1999; LeBlanc et al., 2000; Dinsmore et al., 2000; LeBlanc et al., 2002; Van't et al., 2003). These adhesions may eventually result in bowel erosion, fistulization or obstruction (Simmermacher et al., 1994; Szymanski et al., 2000). In contrast, ePTFE meshes provoke minimal inflammation and adhesion formation (Law and Ellis, 1988; Buján et al., 1997; Bellón et al., 1999; Johnson et al., 2004) and also seem to show some resistance to infection (Brown et al., 1985).

Good clinical results in abdominal hernia surgery are known to strongly depend on a perfect match between the mechanical properties of the abdominal wall and those of the biomaterial used for repair in the long term (Conze and Klinge, 1999). Thus, once the mesh has adapted to the host tissue, the behaviour of the implant site (tissue and mesh) should reproduce the behaviour of healthy tissue. The abdominal wall works as a dynamic system that can withstand sudden pressure changes (coughing, vomiting, etc.) or sustained pressures (obesity, pregnancy, etc.) (Cobb et al., 2005; Song et al., 2006). After the surgical mesh is implanted, the wound repair process causes the mesh to shrink and this is reflected by a reduction in mesh size. However, following mesh shrinkage the implanted material should still show some distensibility to allow movement of the abdominal wall (Klinge et al., 2002; Junge et al., 2001). This determines a need for knowledge of the long term mechanical behaviour of the different biomaterials.

To address the concerns of Bleichrodt et al. (1993) regarding poor host tissue ingrowth into ePTFE implants compromising the strength of clinical repair, LeBlanc et al. (2002) compared the strength achieved by three different implanted meshes; a PP mesh and two ePTFE meshes (a dual-surface mesh DLM and a modified surface mesh DLMC). Having already established that considerable tissue ingrowth occurs within 7–14 days of implant (LeBlanc et al., 1998), LeBlanc et al. (2002) examined the early stage of host tissue ingrowth (3 days). These authors observed that modified forms of ePTFE mesh could achieve abdominal wall repairs that were as strong or stronger than with the use of PP through early host tissue incorporation, while still avoiding adhesions (LeBlanc et al., 1998, 2002). Johnson et al. (2004) compared Sepramesh (SM) and Dualmesh (DM) in terms of strength of tissue incorporation (SOI), mesh shrinkage and adhesiogenesis at 30 days and 5 months post implant. These authors concluded that the SOI achieved by DM increases over time such that at 5 months it becomes comparable to that achieved by SM. Though DM undergoes more mesh shrinkage, similar adhesions are induced by the two materials. In a similar comparison of SM and Parietex composite mesh (PCM) in terms of SOI, adhesion formation and mesh shrinkage at 1 and 5 months, Judge et al. (2007) reported a substantially better SOI for PCM that improved over time, compared to a decline in SOI observed for SM. PCM was also better at avoiding adhesions but underwent considerably more shrinkage.

The functional, morphological and histological properties of HW versus LW PP meshes have also been addressed by several authors. Thus, Bellón et al. (2009) concluded that the lower amount of foreign material implanted when a LW rather than a HW was used resulted in better abdominal wall compliance. Cobb et al. (2006) also reported that physiological abdominal wall compliance could be achieved in the long term after LW mesh implantation used for hernia repair. In a histological study, Pascual et al. (2008) examined the early host tissue incorporation of several LW and HW meshes and observed that the larger pore LW meshes induced the genetic overexpression of collagen types I and III, more collagen type III deposition, its faster conversion to collagen I and that these features conferred these LW meshes greater tensile strengths 14 days after implant.

In the present study, we examine the *in vitro* passive mechanical behaviour of healthy and partially herniated repaired muscle tissue from the short to the long term in the New Zealand White rabbit. As far we are aware, this is the first investigation of this type to include a 6-month time point. First, we characterized the healthy abdominal muscle tissue in terms of its anisotropy and stiffness at 14, 90 and 180 days. Next, we mechanically characterized the partially herniated repaired muscle tissue, and also determined mesh shrinkage at the different post-implant times and the effects of mesh material, pore size, the spatial arrangement of filaments, etc. This was followed by a histological study in which the tissue incorporation process was monitored over time. Finally, in an effort to explain current clinical results, we also determined mechanical correspondence between the intact abdominal muscle and muscle repaired using the three different meshes.

2. Materials and methods

2.1. *Experimental data*

Experimental tests were conducted on New Zealand White rabbits, an animal model frequently used for the study of

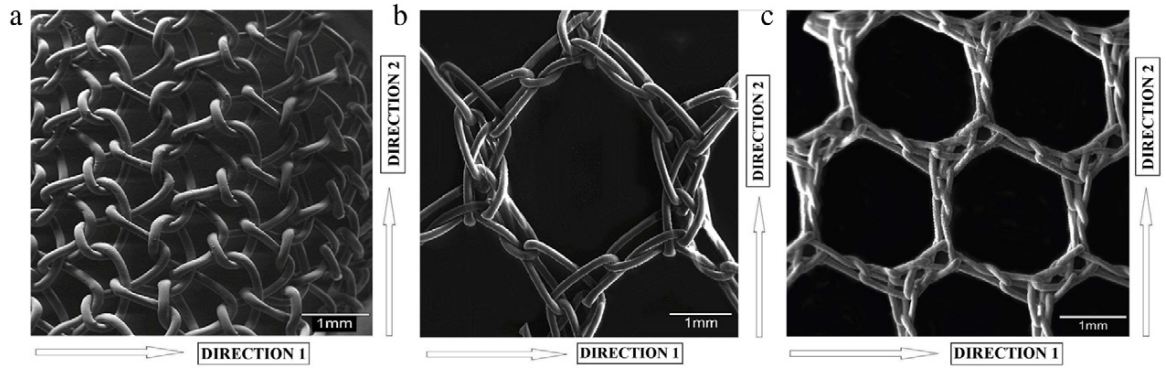

Fig. 1 – Details of the three implanted meshes showing the defined directions 1 and 2. (a) *Surgipro* ®. (b) *Optilene* ®. (c) *Infinit* ®.

muscle behaviour (Nilsson, 1982a,b; LeBlanc et al., 2002; Johnson et al., 2004; Hilger et al., 2006; García-Urena et al., 2007; Judge et al., 2007; Pascual et al., 2008; Bellón et al., 2009; Pierce et al., 2009). All experiments were performed in line with the directives of the European Council (ETS 123) and European Union (Council Directive 86/609/EEC) regarding the protection of animals used for experimental or other scientific purposes. 61 male rabbits were acclimatized to the experimental laboratory. During the entire study period, the animals were maintained in a controlled temperature room (22 ± 1 (°C)) with a 12 h light-dark cycle and free access to water and food according to European Union guidelines for animal care (EEC 28871-22A9). The body weight of the rabbits was 2150 ± 50 (g) at the beginning of the experiment (baseline, 3 months). All established time points (14, 90 and 180 days) are hereafter referred to this baseline.

The three non-absorbable, biocompatible surgical meshes tested were (see Fig. 1): *Surgipro* ® (SUR), a HW (84 g/m^2) PP monofile mesh with a small pore size (pore surface area = 0.26 ± 0.03 mm^2); *Optilene* ® (OPT), a LW (48 g/m^2) PP monofile mesh but with a large pore size (pore surface area = 7.64 ± 0.32 mm^2); and *Infinit* ® (INF), a MW mesh (70 g/m^2) with a large pore size composed of a PTFE monofilament (pore surface area = 4.05 ± 0.22 mm^2). So between the 3 meshes described above, both the pore size and density were different. Four study groups were established as follows: a control group (n = 7) of rabbits not subjected to surgery and Groups 1 (n = 18), 2 (n = 18) and 3 (n = 18) comprised of animals implanted with SUR, OPT and INF meshes, respectively. At each of the established time points (14, 90 and 180 days post implant) six animals were sacrificed in each group with the exception of the control group in which 2, 2 and 3 animals were sacrificed respectively.

So between the 3 meshes described above, both the pore size and density were different.

2.2. *Surgical procedure*

To minimize pain, all animals were given 0.05 (mg/kg) buprenorphine 1 h before and three days after the surgical procedure. Anaesthesia was induced with a mixture of ketamine hydrochloride (70 (mg/kg)), diazepam (1.5 (mg/kg)) and chlorpromazine (1.5 (mg/kg)) administered intramuscularly.

Using a sterile surgical technique, 40 × 40 (mm) defects were created in the lateral wall of the abdomen comprising the plane of the external oblique (EO) and sparing the internal oblique (IO) and transversal abdominis (TA) muscle, parietal peritoneum and skin (see Figs. 2 and 3). The defects were then repaired by fixing a mesh of the same size to the edges of the defect using a running 4/0 polypropylene suture interrupted at the four corners. In all cases, direction 2 of the mesh (see Fig. 1) was longitudinally aligned in the rabbit (see Figs. 2(a) and 3(a)) whereas mesh direction 1 (see Fig. 1) was transversally aligned (see Figs. 2(a) and 3(a)). The skin was closed over the mesh patches by 3/0 polypropylene running suture. After surgery, the animals were returned to their cages and subjected to regular examinations to check their surgical wounds.

At the established time points, animals in each group including the control non-operated animals were sacrificed in a CO_2 chamber. Immediately afterwards, each animal was placed on its back and the abdominal wall and the skin were dissected to obtain a patch consisting, in the operated animals, of the repaired defect including the sutures (see Fig. 2(a) for groups 1, 2 and 3).

2.2.1. *Muscle patch preparation*

Two protocols were followed, one for the control group and the other for the remaining groups.

The protocol used for the control group specimens has been previously described by Hernández et al. (2011). Abdominal wall tissue patches were harvested using a template from each animal. Patch size was 60 × 100 (mm) with the long side perpendicular to the craneo-caudal direction. Two tissue patches were cut from each animal: one from the left side and another from the right side of the linea alba immediately adjacent to the rectus muscle. In each patch, we defined two zones. The first zone close to the rectus abdominis and linea alba (medial area) was composed of two muscles: the EO and IO, and the second zone, close to the para-spinous muscle (lateral area), was comprised of the muscles EO, IO and TA.

In groups 1, 2 and 3, prior to harvesting each patch from the animals, mesh shrinkage was determined in the longitudinal and transverse directions. For this purpose, before their removal, we traced the outlines of the meshes on

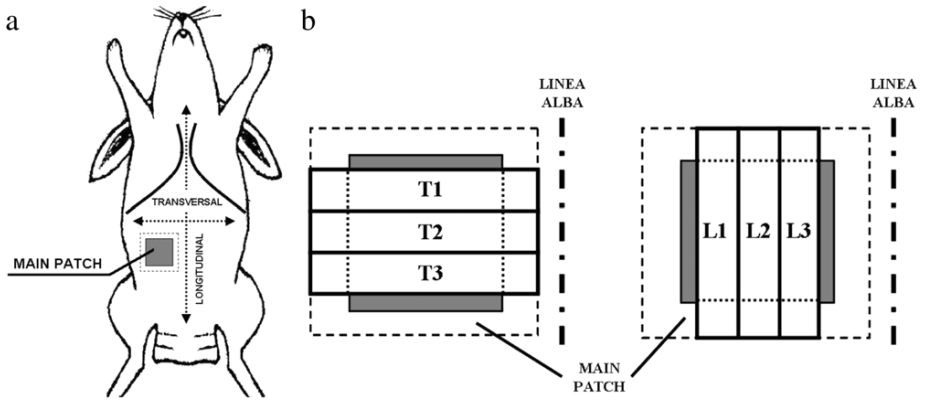

Fig. 2 – (a) Longitudinal (craneo-caudal) and transverse (perpendicular) directions defined in the rabbit. The grey area is the implant site and the outer dotted line is the cutting line used to harvest the main patch. (b) The main patch was cut into three strips in the transverse (left) or longitudinal (right) directions. The fine dotted lines on the strips are the sutures. Specimens for histology were obtained from the grey areas.

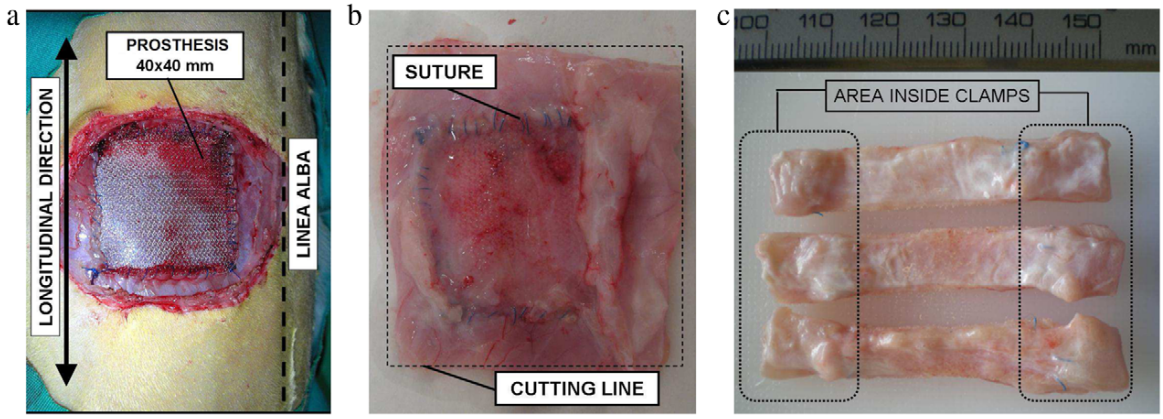

Fig. 3 – (a) Placement of the prosthesis (SUR) indicating the longitudinal direction of the rabbit and the linea alba. (b) Harvested muscle patch (SUR at 14 days). (c) Three strips of muscle/mesh patch ready to start the test (SUR).

40 × 40 (mm) square transparent templates (same dimensions as the original mesh). Using a calibrated system, a single measurement was then made in both directions on 4 patches at each time point for each group (1, 2 and 3). After measuring mesh shrinkage, abdominal wall tissue patches were harvested from all the animals, Figs. 2 and 3(b). This was done by marking a 50 × 50 (mm) square on the abdominal wall of the rabbit using a transparent template (dashed line in Figs. 2(b) and 3(b), lightly larger than the dimensions of the original prostheses). One tissue patch was cut from each animal (see Fig. 2(a)).

2.3. *Histology*

2.3.1. *Light microscopy*

After harvesting the strips for the mechanical tests, the tissue remaining in the patch was used for the histological study (see Fig. 2(b)). For light microscopy, tissue specimens obtained in the craneo-caudal direction of the animal were fixed in F13 solution, embedded in paraffin and cut into 5 (μm) sections. Once cut, the sections were stained with Masson's trichrome (Goldner-Gabe) and examined under a light microscope (Zeiss Axiophot, Carl Zeiss, Oberkochen, Germany).

2.3.2. *Collagen quantification*

Collagen contents were determined in the same sections by Sirius red staining of collagen types I and III. This technique (Junqueira et al., 1978) is based on the orientation and interaction between the sulphone groups of the dye, the amine groups of lysin and hydrolysin and the guanidine groups of arginine in the collagen fibres, giving rise to different colours depending on the type of collagen. Collagen type I, or mature collagen, appears as a reddish-orangey stain while type III collagen (immature) takes on a yellow-greenish shade when observed under the polarized light microscope (Zeiss Axiophot, Carl Zeiss, Oberkochen, Germany).

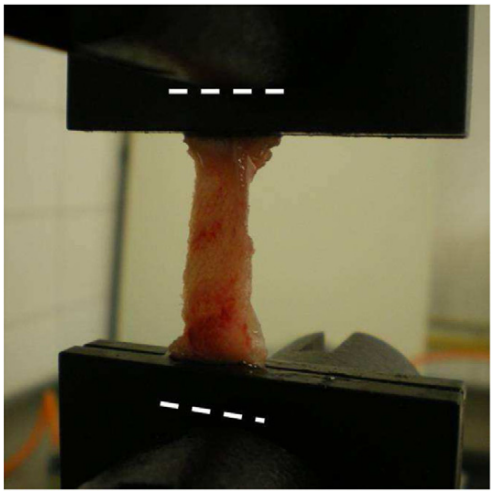

Fig. 4 – Uniaxial test under displacement control on an INSTRON 3340. The sutures fall within the clamp (indicated by the dotted lines) to avoid their effect during the tests.

Table 1 – Number of strips taken in both directions at the three post-implant times in the control rabbits.

	14 days	90 days	180 days
Medial area (EO-IO muscle)	6	6	11
Lateral area (EO-IO-TA muscle)	5	5	8

For each type of collagen, percentage staining was assessed in 10 digitalized histological images per animal that were captured using a digital camera fitted to the microscope (Axiocam HR, Zeiss) and analysed using image analysis software Axiovision AC 4.1. Each section was divided into 4 zones and one microscope field (×100) was randomly selected from each zone to estimate the extent of staining. Percentages of collagen I and III were assessed on (5 μm) cross sections by two independent observers in a blinded fashion. The Student's *t*-test was used to compare percentages of collagen I and III among the different study groups. The level of significance was set at $p < 0.05$.

2.4. *Experimental characterization of the muscle samples*

After harvesting the patches, they were immersed in a saline solution at 4 (°C) until sample preparation to prevent them from drying out.

From the control rabbits, 4, 4 and 6 patches of intact abdominal muscle were obtained at 14, 90 and 180 days, respectively. For the mechanical tests, several strips were cut from each tissue patch. Specifically, one strip in each direction, longitudinal and transverse, was harvested from each zone (medial and lateral) of the tissue patch giving rise to the total number of feasible samples shown in Table 1.

In the remaining groups (1, 2 and 3), 6 patches of each implanted mesh (SUR, OPT or INF) were obtained at each time point. For the mechanical tests, three strips were obtained from each tissue patch (see Figs. 2 and 3). Longitudinal strips were obtained from 3 patches and transverse strips from the remaining 3 patches. The total number of feasible strips is shown in Table 2.

Table 2 – Number of feasible strips obtained in both directions at the different post-implant times.

Mesh		14 days	90 days	180 days
SURGIPRO	LONG	6	9	5
	TRANS	5	8	6
OPTILENE	LONG	6	8	5
	TRANS	5	7	6
INFINIT	LONG	9	8	8
	TRANS	7	6	5

All tissue patches and strips were carefully examined and any with holes, cuts or apparent damage were rejected.

Sample lengths and widths were measured using a digital calliper. These measurements for each type of sample are shown in Tables 3 and 4. Uniaxial tensile tests were performed under displacement control on an INSTRON 3340 microtester with a 1 (kN) full scale load cell (Fig. 4). Each abdominal muscle sample was preconditioned with three cycles at a nominal strain of 40% (Hernández et al., 2011). The applied displacement rate was 5 (mm/min) to preserve quasi-static testing conditions. Stretch data were computed as $\lambda = \frac{L_0+\Delta L}{L_0}$, where L_0 is the initial distance between the clamps and ΔL is the displacement. The value of the thickness of the meshes cannot be defined due to its discontinuous cross sectional area including filaments and interspersed empty areas. Thus, Cauchy stress could not be defined when testing the whole tissue-mesh. In its place, force per unit width multiplied by stretch (Equivalent Cauchy Stress, ECS, defined in large deformations) was obtained using the expression $\frac{\text{Force (N)}}{\text{Width (mm)}}\lambda$, where Force (N) is the load applied during the test.

Data were statistically compared among the groups to detect significant variations in the mechanical behaviour of the meshes and healthy muscle tissue at all post-implant times in both directions. Mesh shrinkage in both directions was also compared. An independent *t*-test was used for all comparisons. The level of significance was set at $p < 0.05$.

3. Results

None of the operated animals died and there were no signs of infection and/or rejection at the level of the different implants. Seroma was detected in two animals implanted with an INF mesh.

3.1. *Initial measurements*

After surgical mesh implantation, wound repair process causes the shrinkage of the mesh. Consequently, mesh size is reduced. Thus, the shrinkage, which is different depending on the implanted surgical mesh, may limit the distensibility of the abdominal wall, being a contributing factor for recurrences and patient discomfort.

Table 3 – Average dimensions of the tissue strips obtained from control rabbits (mean ± standard deviation).

	Tissue	Sample	Length (mm)	Width (mm)
14 days	Medial area	LONG	34.533 ± 3.186	11.186 ± 1.295
		TRANS	30.256 ± 2.276	9.813 ± 0.278
	Lateral area	LONG	34.04 ± 7.385	10.77 ± 2.867
		TRANS	24.625 ± 0.361	7.785 ± 2.1
90 days	Medial area	LONG	44.05 ± 5.387	13.463 ± 1.352
		TRANS	37.31 ± 1.14	11.673 ± 1.268
	Lateral area	LONG	41.837 ± 5.413	14.43 ± 1.247
		TRANS	44.385 ± 3.938	12.535 ± 0.686
180 days	Medial area	LONG	37.238 ± 3.879	11.616 ± 0.964
		TRANS	38.44 ± 4.159	10.648 ± 1.829
	Lateral area	LONG	40.735 ± 5.237	12.747 ± 0.706
		TRANS	40.382 ± 2.899	9.422 ± 1.26

Table 4 – Average dimensions of implanted tissue/mesh strips (mean ± standard deviation).

	Tissue	Sample	Length (mm)	Width (mm)
14 days	SURGIPRO	LONG	62.75167 ± 6.15894	9.10 ± 1.00737
		TRANS	64.718 ± 3.32569	8.524 ± 0.66127
	OPTILENE	LONG	71.065 ± 10.25784	7.96 ± 1.08395
		TRANS	67.23 ± 9.5322	8.154 ± 0.48896
	INFINIT	LONG	61.77444 ± 3.68581	10.47222 ± 0.86371
		TRANS	67.93286 ± 2.89323	8.36571 ± 0.88921
90 days	SURGIPRO	LONG	69.47333 ± 5.49226	9.89111 ± 0.86642
		TRANS	69.56625 ± 4.27752	9.28875 ± 0.75005
	OPTILENE	LONG	67.21125 ± 3.49823	9.40375 ± 0.91046
		TRANS	73.99142 ± 6.25912	9.19 ± 0.73487
	INFINIT	LONG	62.10375 ± 3.12556	10.4775 ± 0.57271
		TRANS	68.58666 ± 1.43158	8.82166 ± 1.02626
180 days	SURGIPRO	LONG	69.04 ± 5.54487	10.278 ± 1.87085
		TRANS	72.46166 ± 3.30391	9.93333 ± 1.53947
	OPTILENE	LONG	63.52 ± 5.74161	10.116 ± 0.80289
		TRANS	75.63166 ± 2.06553	9.05166 ± 0.53251
	INFINIT	LONG	66.86625 ± 5.32182	11.915 ± 1.31802
		TRANS	71.866 ± 9.5569	9.43 ± 1.35965

Table 5 – Mesh shrinkage observed at 14 days post-implant.

	Surgipro®		*Optilene®*		*Infinit®*	
	LONG (%)	TRANS (%)	LONG (%)	TRANS (%)	LONG (%)	TRANS (%)
Patch 1	10	17	13	5	10	0
Patch 2	12	17	13	5	10	0
Patch 3	5	5	13	0	18	0
Patch 4	3	3	25	0	13	0
Mean	7.5	10.5	16	2.5*	12.75	0*
SD	4.203	7.549	6	2.887	3.775	0

*$p < 0.05$.

Table 6 – Mesh shrinkage observed at 90 days post-implant.

	Surgipro®		*Optilene®*		*Infinit®*	
	LONG (%)	TRANS (%)	LONG (%)	TRANS (%)	LONG (%)	TRANS (%)
Patch 1	3	13	0	0	13	0
Patch 2	0	13	0	13	13	0
Patch 3	10	10	8	8	10	0
Patch 4	9	13	13	0	13	0
Mean	5.5	12.25	5.25	5.25	12.25	0*
SD	4.796	1.5	6.397	6.397	1.5	0

*$p < 0.05$.

Tables 5–7 provide the percentage mesh shrinkage values recorded in the longitudinal and transverse directions of the animals at the different time points post-implant. No significant variations were produced in mesh shrinkage at any time point between the longitudinal and transverse directions for the SUR mesh ($p > 0.0617$). In contrast, the shrinkage suffered by the INF mesh was significantly greater in the longitudinal direction at each time point ($p < 0.0089$), and the same occurred for the OPT mesh at 14 days ($p < 0.0132$) but not at the remaining time points ($p > 0.391$).

3.2. *Morphological analysis*

3.2.1. *Light microscopy*

At 14 days post-implant, the three biomaterials had become infiltrated with a disorganized, well-vascularized, loose,

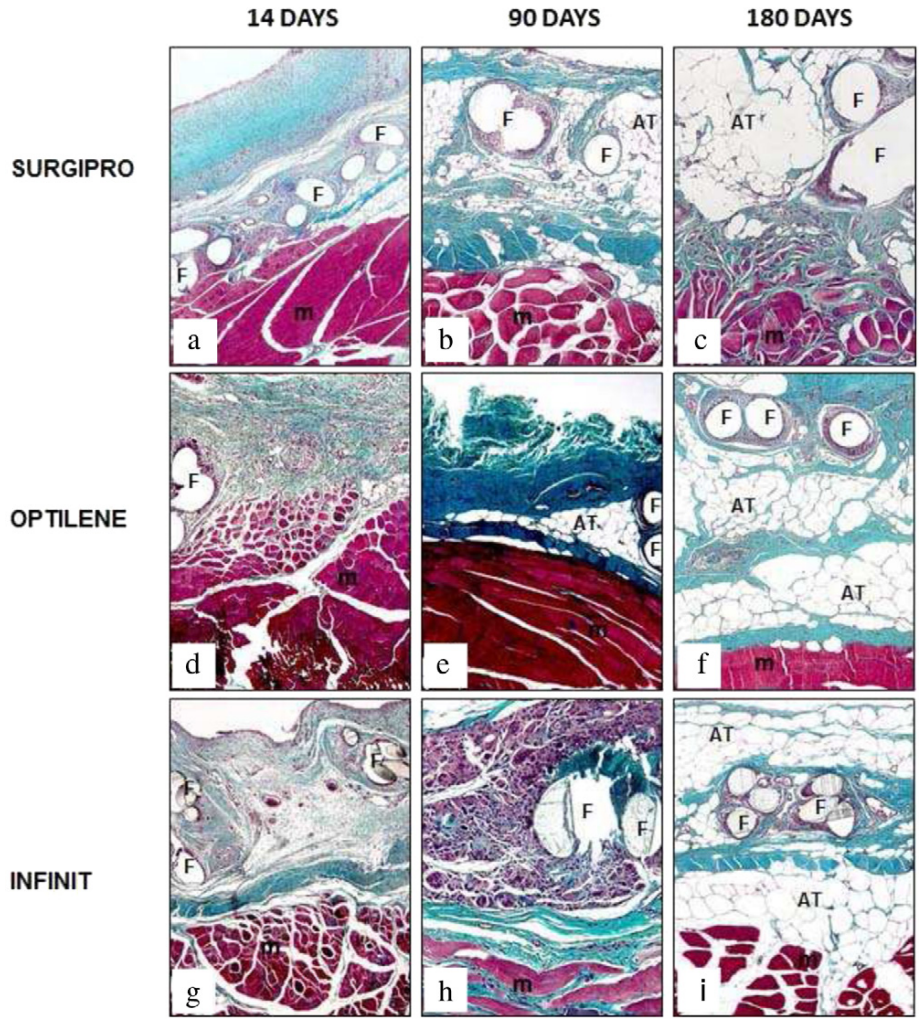

Fig. 5 – Histological findings on Masson's trichrome staining of the implanted meshes. Surgipro (a–c), Optilene (d–f) and Infinit (g–i) after 14 (a, d, g), 90 (b, e, h) or 180 (c, f, i) days of implant in the experimental animals. (F: prosthetic filaments, AT: adipose tissue. m: muscle tissue).

Table 7 – Mesh shrinkage observed at 180 days post-implant.

	Surgipro®		*Optilene®*		*Infinit®*	
	LONG (%)	TRANS (%)	LONG (%)	TRANS (%)	LONG (%)	TRANS (%)
Patch 1	10	13	0	0	15	0
Patch 2	0	5	0	0	13	0
Patch 3	8	0	13	0	25	0
Patch 4	10	8	0	0	25	0
Mean	7	6.5	3.25	0	19.5	0*
SD	4.761	5.447	6.5	0	6.403	0

*$p < 0.05$.

connective scar tissue (see Fig. 5). This neoformed tissue occupied all the spaces between the PP or PTFE filaments. By 90 days, this neoformed tissue had thickened considerably. In these specimens, the zones of loose neoformed connective tissue were interspersed with areas in which the ingrowth of adipose tissue could be observed in all the mesh types. After 180 days, there was a significant increase in adipose tissue ingrowth. Most neoformed connective tissue was observed around the prosthetic filaments. The spared IO and TA muscles in the lower zone of the partial defect showed no evident morphological alterations at any of the follow up times in any of the study groups.

3.2.2. *Collagen*

Following implantation of the different meshes, it is desirable that a well-structured regenerated tissue, where there is optimal synthesis and deposition of collagen (mainly type I that helps to modulate and give strength to the repair area), will be formed around the filaments of the prostheses.

Collagen fibres could be seen to run parallel to the mesh surface in zones far from the filaments or were arranged concentrically to these filaments in areas closer to the implant edges (see Figs. 6–8).

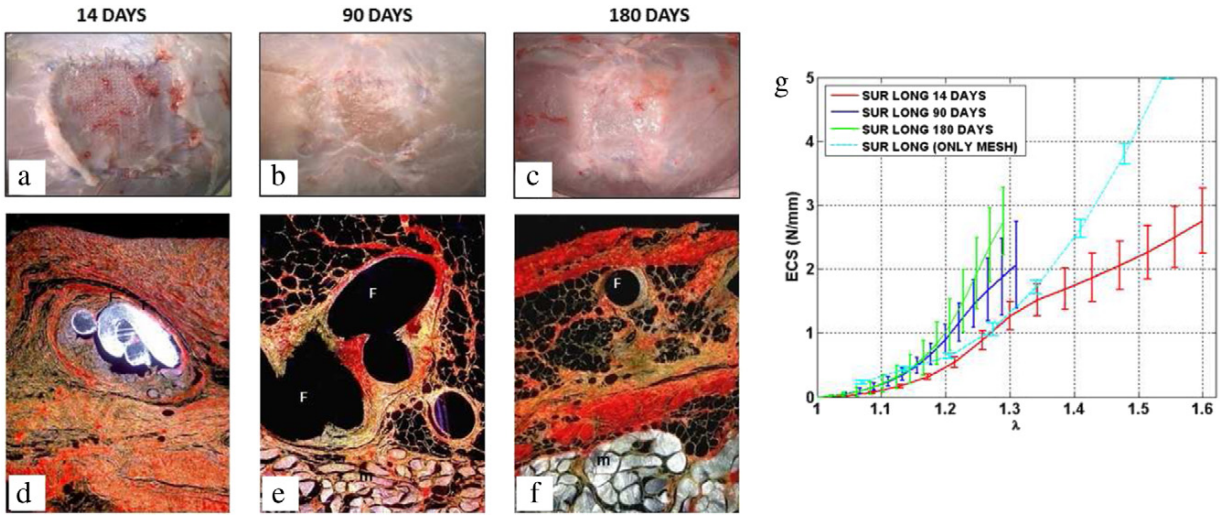

Fig. 6 – Macroscopic appearance of the implant site in the SUR group, 14 (a), 90 (b) and 180 (c) days after implant. Sirius red staining of these meshes at 14 (d), 90 (e) and 180 (f) days post-implant. Collagen III appears yellow while collagen I (mature collagen) stains red. (g) Mean ECS curves constructed using the data obtained in the mechanical tests at 14, 90 and 180 days for the tissue/SUR mesh patches and the SUR mesh alone (from Hernández-Gascón et al., in press). (For interpretation of the references to colour in this figure legend, the reader is referred to the web version of this article.)

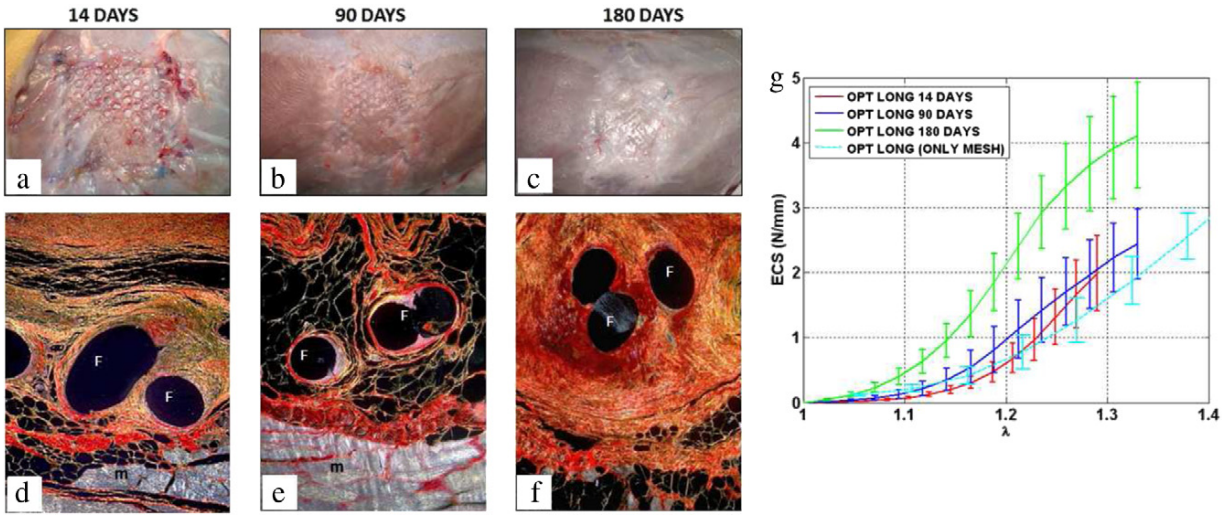

Fig. 7 – Macroscopic appearance of the implant site in the OPT group, 14 (a), 90 (b) and 180 (c) days after implant. Sirius red staining of these meshes at 14 (d), 90 (e) and 180 (f) days post-implant. Collagen III appears yellow while collagen I (mature collagen) stains red. (g) Mean ECS curves constructed using the data obtained in the mechanical tests at 14, 90 and 180 days for the tissue/OPT mesh patches and the OPT mesh alone (from Hernández-Gascón et al., in press). (For interpretation of the references to colour in this figure legend, the reader is referred to the web version of this article.)

Collagen contents, quantified by Sirius red staining after 14 days of implant, revealed higher collagen type I levels in the INF and OPT meshes relative to SUR. In the short term, immature or type III collagen was least expressed in the INF mesh, although no significant differences emerged for either collagen type at the first time point (14 days).

Generally in the three groups of prosthetic meshes, type I collagen increased gradually throughout the time of implant (see Fig. 9). This increase was statistically significant ($p < 0.016$) when amounts at 14 and 180 days were compared in the SUR group. OPT showed a significantly greater amount of this type of collagen at both 90 ($p < 0.0153$) and 180 ($p < 0.0058$) days, along with a considerable reduction in the percentage of collagen type III ($p < 0.0025$ and $p < 0.0018$), whose expression was practically null in the mid- and long term.

When the different prostheses were compared within the same study time, we observed that OPT showed significantly

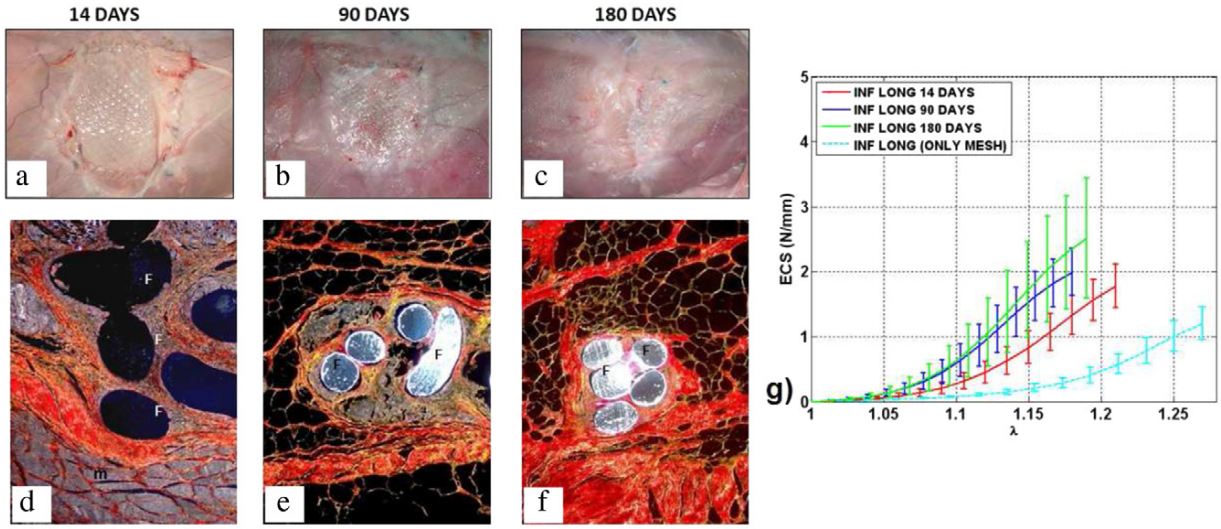

Fig. 8 – Macroscopic appearance of the implant site in the INF group, 14 (a), 90 (b) and 180 (c) days after implant. Sirius red staining of these meshes at 14 (d), 90 (e) and 180 (f) days post-implant. Collagen III appears yellow while collagen I (mature collagen) stains red. (g) Mean ECS curves constructed using the data obtained in the mechanical tests at 14, 90 and 180 days for the tissue/INF mesh patches and the INF mesh alone (from Hernández-Gascón et al., in press). (For interpretation of the references to colour in this figure legend, the reader is referred to the web version of this article.)

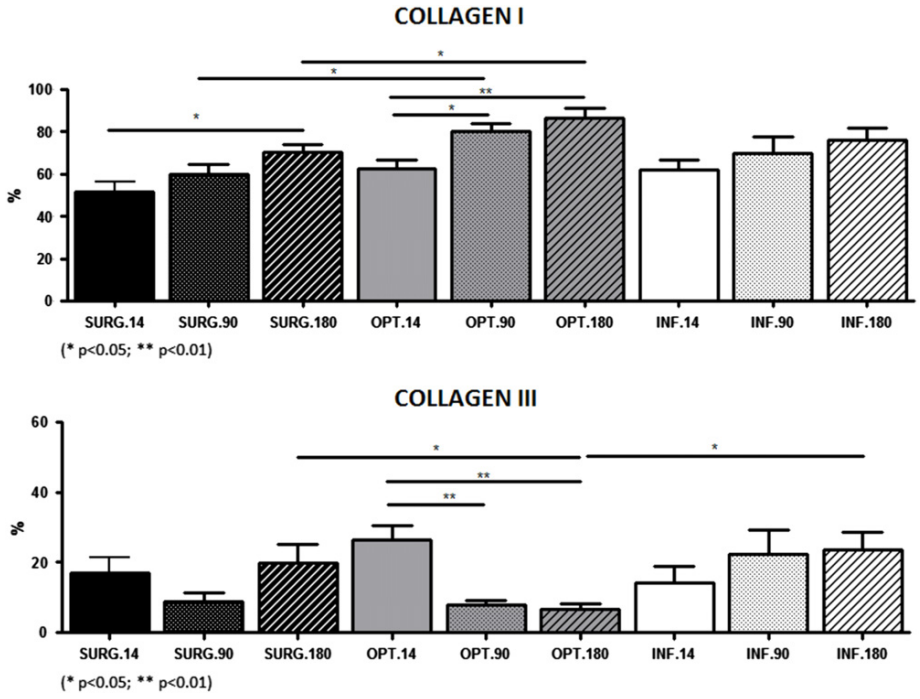

Fig. 9 – Experimental data (percentages) for collagen I and collagen III quantified by image analysis on Sirius red-stained samples recorded in the three groups at the different implant times. Values are given as the mean ± standard deviation. (For interpretation of the references to colour in this figure legend, the reader is referred to the web version of this article.)

greater collagen type I at 90 ($p < 0.0107$) and 180 ($p < 0.0308$) days than SUR. Collagen III expression at 180 days was significantly lower in the OPT group when compared with the other two prostheses, SUR ($p < 0.0414$) and INF ($p < 0.0126$).

3.3. *Mechanical tests*

Since the whole tissue/mesh should mimic the mechanical response of the healthy abdominal wall, both whole tissue/mesh and healthy tissue are characterized along time and compared.

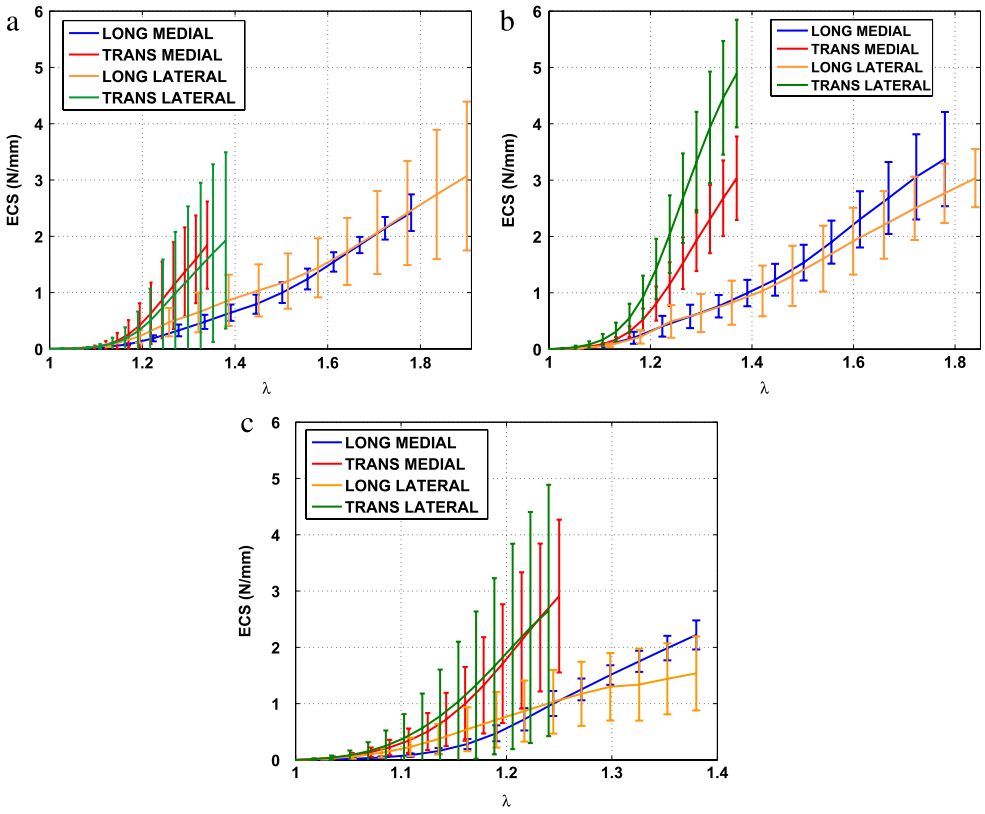

Fig. 10 – Experimental data obtained in the mechanical tests for the control muscle specimens. All experimental curves were truncated before the maximum stress point. Time points: (a) 14 days (b) 90 days (c) 180 days.

The experimental data recorded for the intact abdominal muscle in the mechanical tests at the time points 14, 90 and 180 days are provided in Fig. 10. When we compared mechanical behaviour between the medial and lateral zones in the control group at 14, 90 and 180 days similar behaviour was observed both in the transverse ($p > 0.1583$) and longitudinal ($p > 0.1259$) directions of the rabbits. According to these results, for the statistical analysis we assumed equal behaviour in the medial and lateral regions. When we compared the overall behaviour of longitudinal and transverse tissue specimens, both returned values indicating greater tissue stiffness at 180 days than after 14 days ($p < 0.013$ and $p < 0.0087$, respectively). On the other hand, after 14, 90 or 180 days, significant differences in mechanical behaviour were observed between the longitudinal and transverse directions ($p < 0.0487, p < 0.0335$ and $p < 0.0451$, respectively).

The course of stiffness values observed for the partially herniated repaired muscle tissue is shown in Figs. 6(g), 7(g) and 8(g). The curves showing the response of the meshes alone are from Hernández-Gascón et al. (in press). It may be observed that both the SUR and INF meshes were stiffer at 90 days than 14 days ($p < 0.0026$ and $p < 0.0039$, respectively) whereas values recorded at 180 days were similar to those observed at 90 days ($p > 0.05$ and $p > 0.3206$, respectively). In contrast, the stiffness of the OPT mesh was elevated at both 90 and 180 days ($p < 0.0428$ and $p < 0.0035$, respectively). The mechanical responses shown by the non-implanted meshes are far from the behaviour shown by the repaired muscle tissue such that the muscle became stiffer over time due to the growth of collagen over the hernial defect.

Fig. 11 provides the ECS curves obtained for groups 1, 2 and 3. At 14 days post-implant (see Fig. 11(a)), the SUR and INF meshes showed an isotropic response such that similar behaviour was observed in the longitudinal and transverse direction of the rabbit ($p > 0.0593$ and $p > 0.5031$, respectively) whereas the response of the OPT mesh was anisotropic and the longitudinal direction was stiffer than the transverse ($p < 0.0469$). At 90 days post-implant (see Fig. 11(b)), the response of the SUR and the INF meshes was again isotropic ($p > 0.4272$ y $p > 0.3952$) whereas the transverse direction of the tissue bearing the OPT mesh was less stiff than the longitudinal ($p < 0.0401$). In the long term (180 days), only the SUR mesh was isotropic ($p > 0.0562$) (see Fig. 11(c)). For both the OPT and INF meshes, the longitudinal direction was stiffer ($p < 0.006$ y $p < 0.009$).

When comparing the behaviour of the transverse and longitudinal strips of the implanted meshes, at 14 days post-implant, the OPT mesh showed a similar behaviour in the longitudinal direction than the SUR mesh in the transverse direction ($p > 0.05$) (see Fig. 11(a)). After 90 and 180 days, the behaviour of the OPT mesh in the longitudinal direction was the same as that shown by the SUR mesh in both the longitudinal and transverse directions ($p > 0.0983$) (see Fig. 11(b) and (c)). At 180 days, the implanted OPT and the INF meshes behaved similarly in both directions ($p > 0.05$).

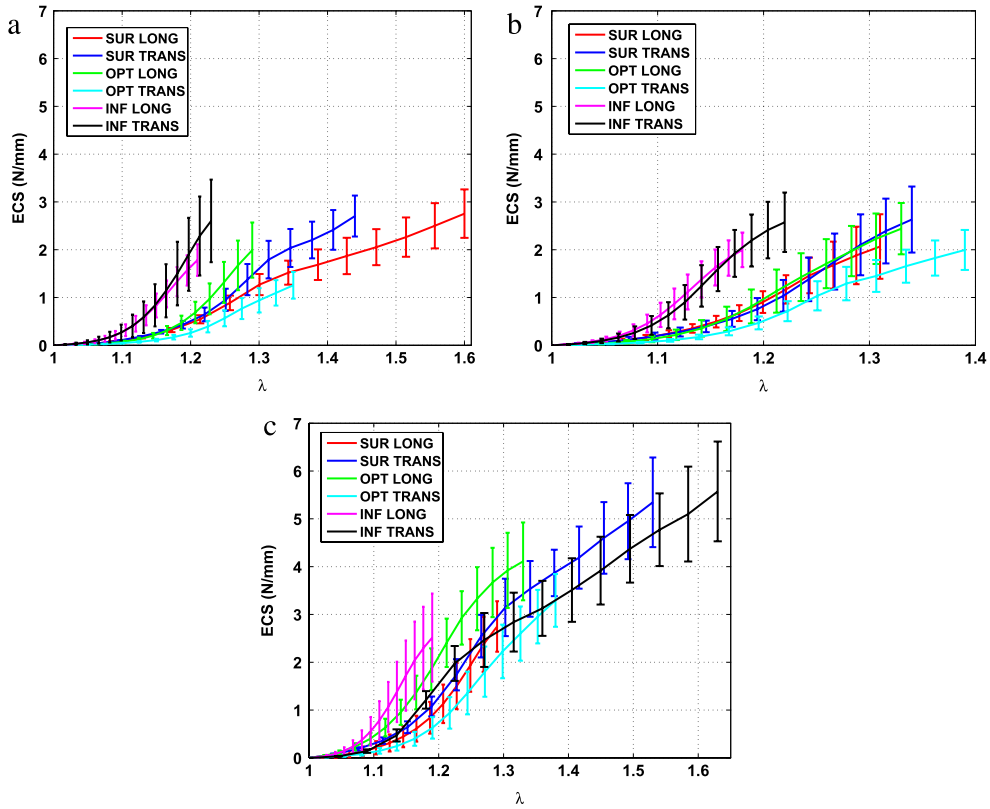

Fig. 11 – Mean ECS curves obtained in the mechanical tests for groups 1, 2 and 3. All curves were truncated before the maximum stress point. Time points: (a) 14 days, (b) 90 days and (c) 180 days post-implant.

Finally, uniaxial tests conducted in a longitudinal direction on the SUR meshes revealed the same response as that shown in the transverse direction by the OPT and INF meshes ($p > 0.05$ y $p > 0.05$, respectively).

In Fig. 12, we compare the mechanical behaviour of the healthy and herniated-repaired tissue. This figure shows that at 14 days post-implant, the INF mesh does not reproduce the mechanical behaviour of the abdominal muscle in any direction. The tests in the transverse direction of the healthy abdominal wall were mimicked by the tests conducted in the longitudinal and transverse direction on the OPT mesh ($p > 0.0918$) and SUR mesh ($p > 0.1848$). After 90 days, the SUR mesh mimicked the transverse behaviour of the healthy tissue ($p > 0.076$). Besides, the tests run in the longitudinal and transverse directions on the implanted OPT mesh also reproduced this behaviour in the transverse direction of the healthy tissue ($p > 0.1008$). However, the behaviour of the healthy tissue in the longitudinal direction was not reproduced by any implanted mesh after 14 days or 90 days, whereas at 180 days post-implant its response was mimicked by the tests conducted transversally on the OPT mesh ($p < 0.0622$). Also at 180 days post-implant, the mechanical behaviour of the healthy muscle in the transverse direction was similar to that shown in both the longitudinal and transverse directions by the SUR mesh ($p > 0.0942$) and the INF mesh ($p > 0.05$). Finally, the response of the tests in the longitudinal direction on the OPT mesh also mimicked that of the healthy abdominal tissue when tested in the transverse direction ($p > 0.0567$).

4. Discussion

In this study, we examined the passive elastic behaviour over time of the healthy abdominal wall and of the partially herniated muscle tissue repaired with one of the three meshes: SUR, OPT or INF. Mechanical properties were evaluated using the classic rabbit model used for hernia repair. Shrinkage of the meshes implanted in the animals was also determined.

The characteristics of an implanted mesh are such that it usually undergoes some shrinkage. This shrinkage may compromise the functionality of the abdomen since the mesh becomes integrated within abdominal tissue. Our findings indicate that the SUR mesh always suffered the same amount of shrinkage in both tissue directions whereas OPT and INF underwent more longitudinal than transverse shrinkage. This could be because SUR has a small pore size, Fig. 1(a), and the spatial arrangement of its filaments is that of a compact weave, i.e., it is a HW mesh, or because of its isotropic behaviour. Conversely, the shrinkage shown by the OPT and INF meshes could also be attributed to their anisotropic behaviour or to the spatial arrangement of their filaments since in both cases, there were more filaments running in direction 2, along which more shrinkage was produced, than in direction 1, Fig. 1(b) and (c).

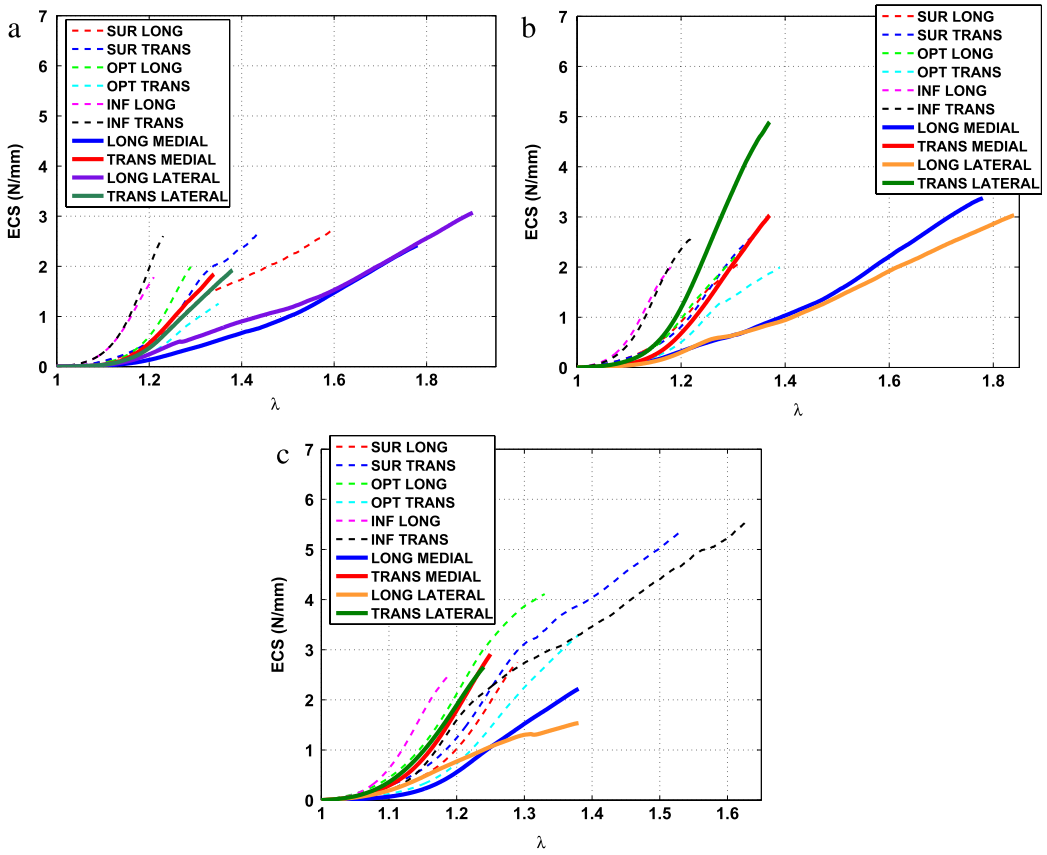

Fig. 12 – Comparing the mechanical test results in the control group and groups 1, 2 and 3 at (a) 14 days (b), 90 days and (c) 180 days post-implant.

It was confirmed here that the medial and lateral areas of the healthy abdominal wall behaved similarly in mechanical terms such that abdominal muscle tissue can be considered homogeneous. Moreover, our study of the mechanical behaviour of the healthy abdominal tissue indicated that this tissue became stiffer over time and that it is anisotropic, the transverse direction always being stiffer than the longitudinal one. Similar conclusions were drawn by Hernández et al. (2011) at the baseline.

In our study, partial defects were created in the lateral wall of the abdomen to avoid involving the peritoneum in the repair process. Although we included a short term time point (14 days), the main objective was to examine mesh behaviour in the long term (180 days). We compared post-implant behaviour in terms of tissue regeneration of a conventional PP-HW mesh to that of a LW mesh and MW mesh, one composed of PP and the other of non-expanded PTFE. In terms of tissue regeneration, the three implant types showed good behaviour showing a well vascularized neoformed connective tissue around all the spaces between the prosthetic filaments that became infiltrated with adipose tissue in the mid- and long term, Fig. 5.

Collagen I, or mature collagen, is the main fibrillar protein responsible for the mechanical properties of neoformed tissue, hence our interest in correlating the presence of this protein with the results of our mechanical studies. Type III collagen is also a fibrillar collagen and the second most abundant collagen in human tissues and occurs particularly in tissues exhibiting elastic properties. This type of collagen is found in extensible connective tissues and very common in fast growing tissue, particularly at the early stages of wound repair. Much of it is replaced later by the type stronger and tougher type I collagen, that is why it has given more importance to the levels of collagen I, that form the mesh largely responsible for the mechanical properties. At 14 days, more type I collagen was deposited in the INF and OPT meshes relative to SUR, although there were no significant differences. Generally speaking, levels of type I collagen increased gradually during the course of implant in all three meshes, provoking an increase in mechanical stiffness (see Figs. 6–8) although most significant host tissue incorporation had occurred within 14 days (see Fig. 9), in line with the findings of others (LeBlanc et al., 2002). In a prior study (Pascual et al., 2008), our group also observed in the short term (14 days) significantly greater gene expression levels for collagens I and III in the neoformed tissue that forms around the filaments comprising meshes with pores larger than 3 mm. This finding could be correlated with the greater amount of the protein observed here in the OPT group and also with the increased stiffness shown by these meshes in the mechanical tests. If we compare our results with those reported by Hernández-Gascón et al. (in press) (see Figs. 6(g),

7(g) and 8(g)), the increase in mechanical stiffness produced at 14 days is greater for the INF mesh than the SUR and OPT meshes. The contribution of collagen I to the stiffness of SUR and OPT is probably negligible compared to that of the mesh alone (Hernández-Gascón et al., in press) whereas this contribution is much more marked for the INF mesh due to its inherently low stiffness (see Fig. 8(g)). On the other hand, although collagen I contents peaked at 180 days in all three meshes, it was the greatest *pore size* mesh OPT that showed significantly greater amounts of this type of collagen at both 90 and 180 days when compared with SUR. Greca et al. (2001, 2008) also observed greater type I collagen deposition following the implant of large-pore prosthetic materials. Our observations suggest that the repair process induced by placement of a LW mesh, whether composed of PP or PTFE, is modulated by ingrowing host tissue, with correlation observed between collagen deposition and prosthetic pore size. However, the polymer forming the prosthesis (PP or PTFE), may be conditioning, in some way, the development and behaviour of newly formed tissue. As previous studies conducted by our group (data pending publication) shown, there is a significant increase in the inflammatory reaction after implantation of meshes consisting of PTFE (INF).

Once a mesh is implanted in the host, its behaviour as a whole (tissue and mesh) should reproduce that of the healthy tissue. Given the anisotropy of healthy abdominal muscle tissue, at the different post-implant times the tissue/mesh should similarly provoke an anisotropic mechanical response so that there is good compliance between mesh and tissue. Our results indicate that neither the SUR mesh nor INF mesh are able to mimic the response of the healthy abdominal wall at 14 and 90 days post implant because of their isotropy which cannot mimic the anisotropic response of healthy tissue. However, despite the anisotropic response of the OPT mesh at 14 and 90 days, in neither direction was the behaviour similar to that shown by the healthy tissue in the longitudinal direction due to the high stiffness of the mesh which is provoked by the growth of collagen in the area of the defect. In the long term, the synthesis, the deposit and the orientation of the collagen fibres tends to unify the mechanical response of the meshes. The OPT mesh displayed a similar response to the healthy muscle and, from a mechanical standpoint, may be considered a suitable prosthetic mesh because of its anisotropic mechanical response which is able to mimic the anisotropic response of healthy tissue. This mechanical behaviour of the LW mesh, correlates with the structure of a newly formed tissue more abundant in type I collagen in the repair zone, revealed in our morphological analysis. Therefore, these LW prostheses would be the best at reproducing the formation of a repair tissue of structural and mechanical characteristics similar to healthy tissue, compared with HW. If we consider the INF mesh, despite its anisotropic behaviour at 180 days, it was only able to mimic the mechanical behaviour of the healthy abdominal muscle in the transverse direction due to its high stiffness at this late stage of implant. The isotropic behaviour of SUR mesh dictates that only the mechanical response of one direction of the healthy tissue can be mimicked. These findings are similar to those obtained by Bellón et al. (2009) and Cobb et al. (2006) who described more physiological abdominal wall compliance after LW mesh implantation when less foreign material remains in the host tissue. We also found that our LW mesh OPT offered the best abdominal wall compliance.

In a previous study, Hernández-Gascón et al. (in press) addressed the mechanical response of three non-implanted surgical meshes (SUR, OPT and INF) and observed an isotropic mechanical response in SUR and an anisotropic one in OPT and INF. Besides, these authors noted that INF was best able to reproduce abdominal wall behaviour. Here we found that the growth of a connective tissue rich in collagen over the hernial defect, and the proper deposit of the collagen fibres in the regenerated tissue, substantially modifies the original properties of the mesh increasing their biomechanical strength making the whole tissue/mesh stiffer. Moreover, INF was anisotropic only at 180 days post-implant and did not comply with the mechanics of the healthy abdomen. This suggests that the mechanical characterization of a surgical mesh before implant can lead to erroneous interpretations and conclusions about the mechanics of hernia repair.

Our study is not devoid of certain simplifications and limitations. Information provided by other types of test (e.g., biaxial tests) would be useful to complement our tissue characterization. Biaxial tests reproduce the physiological deformation and loading conditions of muscle tissue. Besides, only three commercial surgical meshes are considered whereas the mechanical characterization of other commercially available surgical meshes would also provide further insight. Determining active mechanical behaviour in addition to the passive response would also help us model the post-implant behaviour of a mesh.

Despite these limitations, our paper describes a new systematic method to characterize the mechanical behaviour of the healthy abdominal wall or the herniated muscle tissue repaired by mesh implant. Mesh behaviour was also assessed by determining mesh shrinkage in both the longitudinal and transverse directions. In addition, we examined the mechanical properties of healthy abdominal muscle and of repaired abdominal muscle over time up until the long term. This mechanical behaviour of the abdominal wall repaired using three different meshes was characterized with tests conducted in two perpendicular directions. Finally, after statistical analysis, we were able to conclude which mesh was best able to mimic the behaviour of the intact healthy abdominal wall. Our characterization of the mechanical properties of the rabbit abdominal wall could be modified to model the behaviour of the human abdomen with minor modifications. This would provide suitable guidelines to help surgeons select the best prosthetic mesh in mechanical terms and its best orientation.

5. Conclusions

The growth of collagen over a mesh used to repair a hernial defect induces an increase in stiffness that substantially modifies the original properties of the mesh. This means that the mechanical characterization of a surgical mesh before implant provides no meaningful information. In the long term, this growth of collagen tends to unify the mechanical response of the different meshes.

The behaviour of healthy abdominal muscle tissue in the longitudinal direction of the experimental animal was not reproduced by any of the implanted meshes after 14 days or 90 days due to the high stiffness of the meshes. In the longer term, best correspondence between the anisotropic behaviour of healthy tissue and the mesh used for its repair was observed only for the PP-lightweight mesh included in our study. In this type of prosthesis the steady increase in synthesis and proper deposit of collagen type I in the newly formed tissue over time, would contribute to increased resistance in the area and in turn maintain the initial anisotropy of the mesh at long term, resembling healthy tissue.

Acknowledgements

This study was supported by the Spanish Ministry of Science and Technology through research projects DPI2008-02335/IPT-010000-2010-22/DPI2011-27939 and the Instituto de Salud Carlos III (ISCIII) through the CIBER initiative project ABDOMESH. CIBER-BBN is an initiative funded by the VI National R&D&i Plan 2008–2011, Iniciativa Ingenio 2010, Consolider Program, CIBER Actions and financed by the Instituto de Salud Carlos III with assistance from the European Regional Development Fund. B. Hernández-Gascón was funded by a grant (BES-2009-021515) from the Spanish Ministry of Science and Technology. Finally, the authors are indebted to Gore and Associates, Flagstaff, Arizona, USA for providing the meshes used in this study. No conflicts of interest declared.

REFERENCES

Bellón, J.M., Buján, J., Contreras, L.A., Martín, A.C.-S., Jurado, F., 1996. Comparison of a new type of polytetrafluoroethylene patch (Mycro Mesh) and polypropylene prosthesis (Marlex) for repair of abdominal wall defects. Journal of the American College of Surgeons 183, 11–18.

Bellón, J.M., Contreras, L.A., Buján, J., Palomares, D., Martín, A.C.-S., 1998. Tissue response to polypropylene meshes used in the repair of abdominal wall defects. Biomaterials 19, 669–675.

Bellón, J.M., Contreras, L.A., Pascual, G., Buján, J., 1999. Neoperitoneal formation after implantation of various biomaterials in the repair of abdominal wall defects in rabbits. European Journal of Surgery 165, 145–150.

Bellón, J.M., Rodríguez, M., García-Honduvilla, N., Gómez-Gil, V., Pascual, G., Buján, J., 2009. Comparing the behavior of different polypropylene meshes (heavy and lightweight) in an experimental model of ventral hernia repair. Journal of Biomedical Materials Research Part B: Applied Biomaterials 89B (2), 448–455.

Bleichrodt, R.P., Simmermacher, R.K.J., Lei, B.V.D., Schakenraad, J.M., 1993. Expanded polytetrafluoroethylene patch versus polypropylene mesh for the repair of contaminated defects of the abdominal wall. Surgery Gynecology & Obstetrics 176, 18–24.

Brown, G.L., Richardson, J.D., Malangoni, M.A., Tobin, G.R., Ackerman, D., Polk, H.C., 1985. Comparison of prosthetic materials for abdominal wall reconstruction in the presence of contamination and infection. Annals of Surgery 210, 705–711.

Buján, J., Contreras, L.A., Martin, A.C.-S., Bellón, J.M., 1997. The behaviour of different types of polytetrafluoroethylene (PTFE) prostheses in the reparative sparring process of abdominal wall defects. Histology and Histopathology 12, 683–690.

Cobb, W.S., Burns, J.M., Kercher, K.W., Matthews, B.D., Norton, H.J., Heniford, B.T., 2005. Normal intraabdominal pressure in healthy adults. Journal of Surgical Research 129, 231–235.

Cobb, W.S., Burns, J.M., Peindl, R.D., Carbonell, A.M., Matthews, B.D., Kercher, K.W., Heniford, B.T., 2006. Textile analysis of heavy-weight, mid-weight and light-weight polypropylene mesh in a porcine ventral hernia model. Journal of Surgical Research 136, 1–7.

Conze, J., Klinge, U., 1999. Biocompatibility of Biomaterials—Clinical and Mechanical Aspects. Springer, Berlin, Heidelberg, New York, (Chapter 14).

Dinsmore, R.C., Calton, W.C., Harvey, S.B., 2000. Prevention of adhesions to polypropylene mesh in a traumatized bowel model. Journal of the American College of Surgeons 191, 131–136.

García-Urena, M.A., Vega, V., Díaz, A., Báez, J.M., Marín, L.M., Carnero, F.J., Velasco, M.A., 2007. Differences in polypropylene shrinkage depending on mesh position inan experimental study. The American Journal of Surgery 193, 538–542.

Greca, F.H., Paula, J.B.D., Biondo-Simoes, M.P.L., Costa, F.D., Silva, A.P.G.D., Time, S., Mansur, A., 2001. The influence of differing pore sizes on the biocompatibility of two polypropylene meshes in the repair of abdominal defect: experimental study in dogs. Hernia 5, 59–64.

Greca, F.H., Souza-Filho, Z.A., Giovanini, A., Rubin, M.R., Kuenzer, R.F., Reese, F.B., Araujo, L.M., 2008. The influence of porosity on the integration histology of two polypropylene meshes for the treatment of abdominal wall defects in dogs. Hernia 12, 45–49.

Hernández, B., Peña, E., Pascual, G., Rodriguez, M., Calvo, B., Doblaré, M., Bellón, J.M., 2011. Mechanical and histological characterization of the abdominal muscle. A previous step to model hernia surgery. Journal of the Mechanical Behavior of Biomedical Materials 4, 392–404.

Hernández-Gascón, B., Peña, E., Melero, H., Pascual, G., Doblaré, M., Ginebra, M.P., Bellón, J.M., Calvo, B., 2011. Mechanical behaviour of synthetic surgical meshes. Finite element simulation of the herniated abdominal wall. Acta Biomaterialia (in press).

Hilger, W.S., Walker, A., Zobitz, M.E., Leslie, K.O., Magtibay, P., Cornella, J., 2006. Histological and biomechanical evaluation of implanted graft materials in a rabbit vaginal and abdominal model. American Journal of Obstetrics & Gynecology 195, 1826–1831.

Holzman, M.D., Purut, C.M., Reintgen, K., Eubanks, S., Pappas, T.N., 1997. Laparoscopic ventral and incisional hernioplasty. Surgical Endoscopy 11, 32–35.

Johnson, E.K., Hoyt, C.H., Dinsmore, R.C., 2004. Abdominal wall hernia repair: a long-term comparison of sepramesh and dualmesh in a rabbit hernia model. The American Journal of Surgery 70 (8), 657–661.

Judge, T.W., Parker, D.M., Dinsmore, R.C., 2007. Abdominal wall hernia repair: a comparison of sepramesh and parietex composite mesh in a rabbit hernia model. Journal of the American College of Surgeons 204 (2), 276–281.

Junge, K., Klinge, U., Prescher, A., Giboni, P., Niewiera, M., Shumpelick, V., 2001. Elasticity of the anterior abdominal wall and impact for reparation of incisional hernia using mesh implants. Hernia 5, 112–118.

Junqueira, L.C., Cossermelli, W., Brentani, R., 1978. Differential staining of collagen type I, II and III by Sirius Red and polarization microscopy. Archivum Histologicum Japonicum 41, 267–274.

Klinge, U., 2007. Experimental comparison of monofile light and heavy polypropylene meshes: less weight does not mean less biological response. World Journal of Surgery 31, 867–868.

Klinge, U., Junge, K., Stumpf, M., Klosterhalfen, B., 2002. Functional and morphological evaluation of a low-weight monofilament polypropylene mesh for hernia repair. Journal of Biomedical Materials Research Part B: Applied Biomaterials 63, 129–136.

Law, N.W., Ellis, H., 1988. Adhesion formation and peritoneal healing on prosthetic materials. Clinical Materials 3, 95–101.

LeBlanc, K.A., Bellanger, D., Rhynes, K.V., Baker, D.G., Stout, R.W., 2002. Tissue attachment strength of prosthetic meshes used in ventral and incisional hernia repair. A study in the New Zealand White rabbit adhesion model. Surgical Endoscopy 16 (11), 1542–1546.

LeBlanc, K.A., Booth, W.V., Whitaker, J.M., Baker, D., 1998. In vivo study of meshes implanted over the inguinal ring and external iliac vessels in uncastrated pigs. Surgical Endoscopy and Other Interventional Techniques 12, 247–251.

LeBlanc, K.A., Booth, W.V., Whitaker, J.M., Bellanger, D.E., 2000. Laparoscopic incisional and ventral herniorrhaphy in 100 patients. The American Journal of Surgery 180, 193–197.

Lichtenstein, I.L., Shulman, A.G., 1986. Ambulatory outpatient hernia surgery including a new concept, introducing tension-free repair. International Journal of Surgery 71, 1–4.

Lichtenstein, I.L., Shulman, A.G., Amid, P.K., Montlor, M.M., 1989. The tension-free hernioplasty. The American Journal of Surgery 157, 188–193.

Luijenkijk, R.W., Hop, W.C., den Tol, M.P.V., 2000. A comparison of suture repair with mesh repair for incisional hernia. The New England Journal of Medicine 343, 392–398.

Morris-Stiff, G.J., Hughes, L.E., 1998. The outcomes of nonabsorbible mesh paced within the abdominal cavity: literature review and clinical experience. Journal of the American College of Surgeons 186, 352–367.

Nilsson, T., 1982a. Biomechanical studies of rabbit abdominal wall. Part I—the mechanical properties of specimens from different anatomical positions. Journal of Biomechanics 15 (2), 123–129.

Nilsson, T., 1982b. Biomechanical studies of rabbit abdominal wall. Part II–the mechanical properties of specimens in relation to length, width, and fibre orientation. Journal of Biomechanics 15 (2), 131–135.

Pascual, G., Rodríguez, M., Gómez-Gil, V., García-Honduvilla, N., Buján, J., Bellón, J.M., 2008. Early tissue incorporation and collagen deposition in lightweight polypropylene meshes: bioassay in an experimental model of ventral hernia. Surgery 144, 427–435.

Pierce, L.M., Grunlan, M.A., Hou, Y., Baumann, S.S., Kuehl, T.J., Muir, T.W., 2009. Biomechanical properties of synthetic and biologic graft materials following long-term implantation in the rabbit abdomen and vagina. American Journal of Obstetrics & Gynecology 200, 549.e1–549.e8.

Saiz, A.A., Willis, I.H., Paul, D.K., Sivina, M., 1996. Laparoscopic hernia repair: a community hospital experience. The American Surgeon 62, 336–338.

Simmermacher, R.K.J., Schakenraad, J.M., Bleichrodt, R.P., 1994. Reherniation after repair of the abdominal wall with expanded polytetrafluoroethylene. Journal of the American College of Surgeons 178, 613–616.

Song, C., Alijani, A., Frank, T., Hanna, G., Cuschieri, A., 2006. Mechanical properties of the human abdominal wall measured in vivo during insufflation for laparoscopic surgery. Surgical Endoscopy 20, 987–990.

Szymanski, J., Votik, A., Joffe, J., Alvarez, C., Rosenthal, F., 2000. Technique and early results of outpatient laparoscopic mesh only repair of ventral hernias. Surgical Endoscopy and Other Interventional Techniques 14, 582–584.

Usher, F.C., 1959. A new plastic prosthesis for repairing tissue defects of the chest and abdominal wall. The American Journal of Surgery 97, 629–633.

Usher, F.C., 1970. The repair of incisional and inguinal hernias. Surgery Gynecology and Obstetrics with International Abstracts of Surgery 131, 525–530.

Usher, F.C., Cogan, J.E., Lowry, T., 1960. A new technique for the reparir of inguinal and incisional hernias. Archives of Surgery 84, 847–850.

Van't, R.M., van Steenwijk, P.J.V., Bonthuis, F., 2003. Prevention of adhesion to prosthetic mesh: comparison of different barriers using an incisional hernia model. Annals of Surgery 237, 123–128.

Work 4: Understanding the passive mechanical behavior of the human abdominal wall

Journal: *Annals of Biomedical Engineering*, **In press**, (2012): DOI: 10.1007/s10439-012-0672-7.
Journal impact factor: 2.368

Annals of Biomedical Engineering (© 2012)
DOI: 10.1007/s10439-012-0672-7

BMES BIOMEDICAL ENGINEERING SOCIETY™ www.bmes.org

Understanding the Passive Mechanical Behavior of the Human Abdominal Wall

B. HERNÁNDEZ-GASCÓN,[1,4] A. MENA,[4] E. PEÑA,[1,4] G. PASCUAL,[2,4] J. M. BELLÓN,[3,4] and B. CALVO[1,4]

[1]Mechanical Engineering Department, Aragón Institute of Engineering Research (I3A), University of Zaragoza, María de Luna, 3, 50018, Zaragoza, Spain; [2]Department of Medical Specialities, Faculty of Medicine, University of Alcalá, Alcalá de Henares, Madrid, Spain; [3]Department of Surgery, Faculty of Medicine, University of Alcalá, Alcalá de Henares, Madrid, Spain; and [4]CIBER-BBN, Centro de Investigación en Red en Bioingeniería, Biomateriales y Nanomedicina, Zaragoza, Spain

(Received 25 June 2012; accepted 29 September 2012)

Associate Editor Peter E. McHugh oversaw the review of this article.

Abstract—The aim of this work is to present a methodology to model the passive mechanical behavior of the human abdomen during physiological movements. From a mechanical point of view, it is possible to predict where hernia formation is likely to occur since the areas that support higher stresses can be identified as the most vulnerable ones. For this purpose, a realistic geometry of the human abdomen is obtained from magnetic resonance imaging. The model defines different anatomical structures of the abdomen, including muscles and aponeuroses, and anisotropic mechanical properties are assigned. The finite element model obtained from the geometric human model, which includes initial strains, is used to simulate the anisotropic passive behavior of the healthy human abdomen under intra-abdominal pressure. This study demonstrates that the stiffest structures, namely aponeuroses and particularly the linea alba, are the structures that perform the most work in the abdomen. Thus, the linea alba is the most important unit contributing to the mechanical stability of the abdominal wall.

Keywords—Hyperelasticity, Collagen fibers, Initial strains, Intra-abdominal pressure.

ABBREVIATIONS

RA	Rectus abdominis
ARS	Anterior lamina of the rectus sheath
PRS	Posterior lamina of the rectus sheath
LA	Linea alba
FT	Fascia transversalis
RT	Rectus tendon
RAM	Rectus abdominis muscle
OMT	Oblique muscle tendon
OM	Oblique muscles
EO	External oblique
IO	Internal oblique
TA	Transversus abdominis

Address correspondence to E. Peña, Mechanical Engineering Department, Aragón Institute of Engineering Research (I3A), University of Zaragoza, María de Luna, 3, 50018, Zaragoza, Spain. Electronic mail: fany@unizar.es

INTRODUCTION

The exact pathogenesis of the development of abdominal hernias is not well understood. There are a variety of factors that are known to contribute to hernia development, including physiological changes in fascial integrity, proteolysis associated with cigarette smoking,[39] physical overexertion, significant obesity, connective tissue disorders[6,17,36,37] and familial genetic tendency. However, the most common mechanism of hernia formation in the abdominal midline occurs in the postoperative setting. This mechanism represents the simplest conceptual scenario of hernia development, in which the traumatized tissue loses a portion of its structural integrity, allowing the protrusion of an organ or viscera.[5,35]

The field of medical imaging has significantly changed over the years. New imaging methods and minimally invasive instruments have revolutionized the routine practice in surgery.[28] Currently, computer modeling of human movements, such as FE simulations using anatomical models and even simulations of simple surgical procedures, are possible.[41]

There are limited experimental data regarding the material properties of the human abdominal wall in the literature. Using a motion analysis system with infrared cameras, Song *et al.*[40] performed a study of the

Published online: 13 October 2012

mechanical properties of abdominal tissue from measurements taken from patients during laparoscopic surgery. They observed that the abdominal wall changed from a cylindrical to a dome-like shape during the insufflation process. Additionally, some works have investigated the collagen and elastin fiber content of the abdominal wall layers that are rich in connective tissue, such as the skin, the rectus sheath, the transversalis fascia and the peritoneum.[34] A significant step towards a better understanding of the morphology and biomechanics of the rectus sheath was carried out by Axer *et al.*[3,4] and Martins *et al.*[27] These authors provided information on the collagen fiber orientations of the rectus sheath, fiber diameter and distribution,[4] material properties of the rectus sheath[27] and interpretations of the biomechanical roles of different fiber groups.[3]

In the field of hernia surgery, several authors have proposed FE models with idealized geometries that address the mechanical responses of various tissues. Fortuny *et al.*[13] modeled muscular contraction using the FE method to study the dynamics of the inguinal area. They also studied the effects of various biological parameters on the genesis of inguinal hernias. López-Cano *et al.*[25] described a dynamic 3D model for the human inguinal region that allows real-time simulation of its behavior. However, to the authors' knowledge, there has been no computational study defining a realistic geometry of the entire human abdomen, including the different anatomical structures, to be used to simulate the mechanical behavior under different physiological loads.

The primary goal of this study is to present a methodology to model the passive mechanical behavior of the human abdomen during physiological movements. With this methodology is possible to establish some guidelines to predict where hernia formation is likely to occur on the abdominal wall from a mechanical point of view. For that purpose, this work presents a systematic procedure to obtain a complete FE model of the human abdomen using magnetic resonance imaging (MRI). The model includes the different anatomical structures of the abdomen, and the mechanical properties and initial physiological state are assigned according to the human anatomy. The human model was used to simulate the passive mechanical behavior of the abdominal wall under several intra-abdominal pressures.

MODEL OF THE HUMAN ABDOMEN

Geometry and Mesh

To obtain the abdominal geometry, DICOM (Digital Imaging and Communication in Medicine) files from the MRI of a healthy 38-year-old man were used (see Fig. 1a). We obtained informed consent from the patient and this study was approved by Quirón Hospital Ethics Committee, in Zaragoza. The anatomic cross-sections of the abdomen used to build the 3D model of the upper trunk represent 48 slices, each separated by 7.9 mm. The image resolution corresponds to a discretization of $512 \times 512 \times 48$ cells whose size is $0.664 \times 0.664 \times 7.9$ mm ^{3}. Using the commercial software MIMICS®, a manual segmentation of the 3D DICOM images was made, and a geometrical model of the abdomen was obtained. Three masks were defined in the segmentation process: linea alba (LA), rectus abdominis (RA) and flat muscles, namely oblique muscles (OM), as shown in Figs. 2a and 2b. Flat muscles comprise the external oblique (EO), the internal oblique (IO) and the transversus abdominis (TA) (see Fig. 1c). However, the three flat muscles were not separated in different masks because they were not clearly differentiated in the slices. Therefore, we established that the entire front abdominal wall comprising the oblique muscles is a composite of the layers and aponeuroses.[18] Although the different muscle layers of the flat muscles are considered to be a monolayer and EO, IO and TA were not differentiated, 5 elements were defined in the thickness so that approximately 2 elements represent the EO, 2 elements represent the IO and the last element represents the TA (see Fig. 1c). These proportions were established using the measurements described by Norasteh *et al.*[32] Skin and fat were not included because their stiffness is negligible compared to that contributed by the muscle and aponeuroses.[15] Mesh features were analyzed by means of the comparison between tetrahedral and hexahedral elements[19] and mesh size was determined reaching a compromise between convergence and computation time. Finally, using the geometrical model previously obtained and the software ABAQUS®, a structured volumetric mesh employing 13200 hybrid linear hexahedral elements was used (see Fig. 1b).

Aponeuroses were not visible in the MRI data due to their small thickness.[27] However, according to the human anatomy,[29] the structures that form the aponeuroses around muscles were defined over the previously created mesh using the software ABAQUS®. The aponeuroses that wrap around the muscles were modeled using membrane elements of 1 mm [27] whose nodes were coincident with the underlying nodes to simulate contact between aponeuroses and muscles. These membrane elements were divided into fascia transversalis (FT), anterior rectus sheath (ARS) and posterior rectus sheath (PRS) (see Figs. 2d and 2e). Specifically, a total of 2092 membrane elements were defined. The tendinous structures (aponeuroses) inside the muscles, specifically the rectus abdominis tendon (RT) and oblique muscle tendons (OMT), were part of the structured volumetric mesh previously made

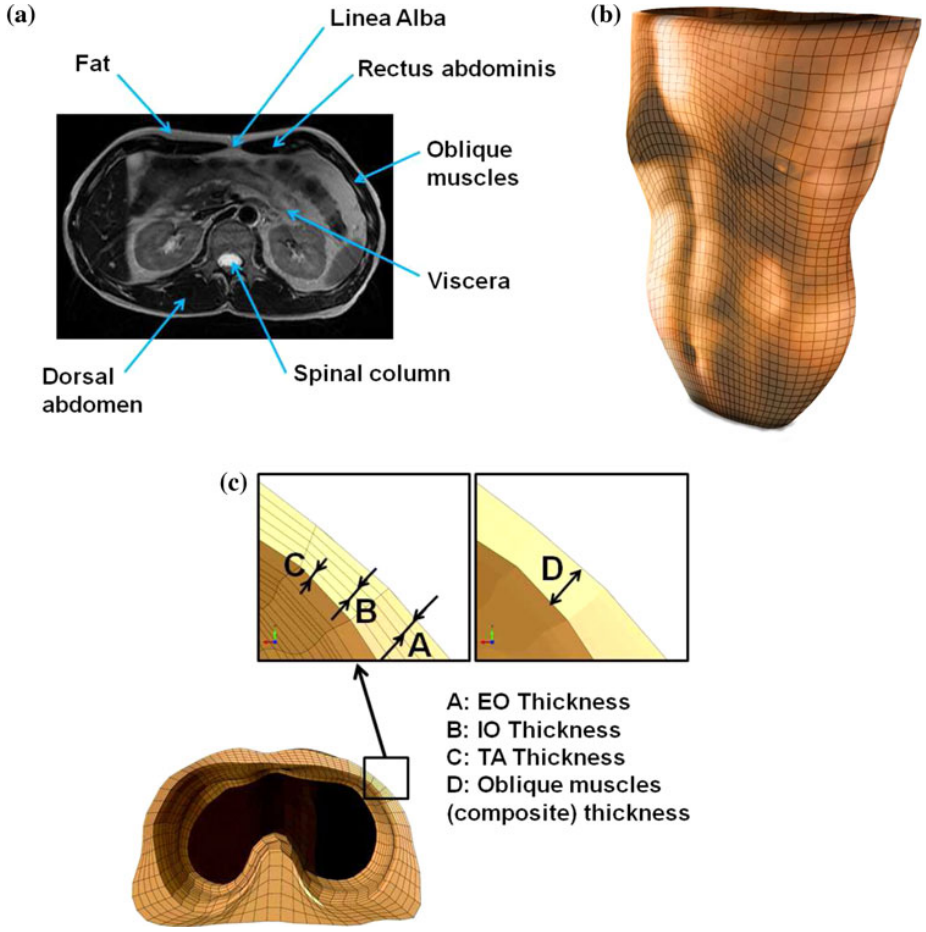

FIGURE 1. (a) MRI data. (b) 3D reconstructed model and meshing of the human abdomen. (c) Upper view of the reconstructed model and detail of the thickness for the different muscle layers (EO, IO and TA) and the oblique muscles as a composite (see Fig. 2b).

with hexahedral elements (represented by the greyish areas in Figs. 2a and 2b). Therefore, two groups were differentiated in the rectus abdominis, namely the rectus tendon and the rectus abdominis muscle (RAM), and two groups were differentiated in the flat muscles as well, namely the OMT and the oblique muscles.

Finally, the diaphragm and pelvis were modeled to close the abdominal cavity. For that purpose, 432 reduced shell elements of 3 mm were added to the model using the FEMAP® software (Siemens Software) (see Fig. 2c).

In summary, hexahedral elements were used for different groups: the linea alba, rectus abdominis muscle, rectus tendon, oblique muscles (comprising the EO, IO and TA), OMT, chest, dorsal part of the abdomen and pelvis support. The fascia transversalis and the anterior and PRSs were membrane elements. Finally, the shell elements were subdivided into the diaphragm and pelvis (see Fig. 2).

The FE analysis of the model was developed using the commercial software *ABAQUS STANDARD*® and using an implicit formulation.

Material Properties and Preferential Direction of Anisotropy

Regarding the constitutive modeling, the purely passive response of the abdominal muscle is modeled within the framework of large deformation anisotropic hyperelasticity using a strain energy function (SEF),[18] $\bar{\Psi}(\mathbf{C}, \mathbf{M})$. This function depends on the scalar-valued functions of $\bar{\mathbf{C}} = \bar{\mathbf{F}}^T\bar{\mathbf{F}}$ and $\mathbf{M} = \mathbf{m}_0 \otimes \mathbf{m}_0$, respectively. The preferential direction of anisotropy is represented by a unit vector $\mathbf{m}_0$.

The material properties were obtained from the literature for each anatomical structure.[18,27] Because the reported experimental data on the mechanical properties of the human abdominal wall are limited,

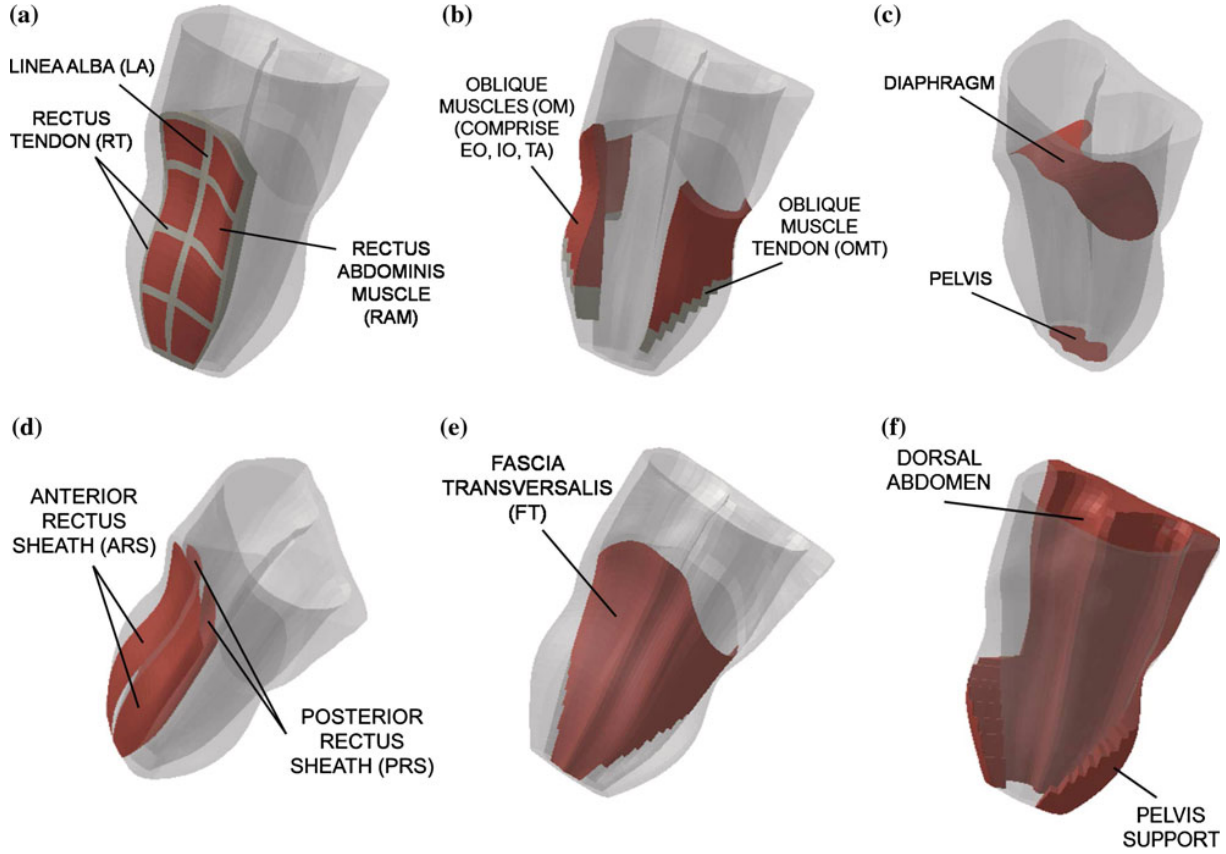

FIGURE 2. Different element sets defined in the model. (a) RAM (reddish area), LA (grayish area running longitudinally between the right and left RAM) and RT (remaining grayish areas). (b) OM (reddish area) and OMT (grayish area). (c) Diaphragm and pelvis. (d) ARS and PRS. (e) FT. (f) Area in which the boundary conditions are applied.

experimental animal data are used when there are no data from humans.

In the case of the abdominal muscles, it is necessary to distinguish between collagen fibers, which are mainly responsible for the passive mechanical response, and muscular fibers (MF), which are associated with contractile muscle behavior.[18] Because our model was only used to simulate the passive mechanical behavior of the abdominal wall, MF were not considered. The anisotropic behavior associated with the passive response is modeled by introducing a preferential direction of anisotropy (PDA)[1] (see Fig. 3).

Referencing experimental and numerical results from the literature,[18,27] two types of SEFs were used to model the mechanical behavior of the soft tissues. Specifically, an uncoupled SEF, divided into two terms (isotropic and anisotropic), was considered $\bar{\Psi} = \bar{\Psi}_{\text{iso}} + \bar{\Psi}_{\text{ani}}$. For both meshes, the isotropic response was modeled using Demiray's SEF[12]:

$$\bar{\Psi}_{\text{iso}} = \frac{c_1}{c_2}\left[\exp\left(\frac{c_2}{2}[\bar{I}_1 - 3]\right) - 1\right]. \tag{1}$$

To model the anisotropic response of human aponeuroses,[27] Calvo's SEF[9] was considered:

$$\begin{aligned} \bar{\Psi}_{\text{ani}} &= 0 \qquad\qquad \bar{I}_4 < \bar{I}_{4_0} \\ \bar{\Psi}_{\text{ani}} &= \frac{c_3}{c_4}\left(e^{c_4(\bar{I}_4 - \bar{I}_{4_0})} - c_4(\bar{I}_4 - \bar{I}_{4_0}) - 1\right), \\ &\qquad\qquad \bar{I}_4 > \bar{I}_{4_0} \text{ and } \bar{I}_4 < \bar{I}_{4_{\text{ref}}} \\ \bar{\Psi}_{\text{ani}} &= c_5\sqrt{\bar{I}_4} + \frac{1}{2}c_6 \ln(\bar{I}_4) + c_7 \bar{I}_4 > \bar{I}_{4_{\text{ref}}}, \end{aligned} \tag{2}$$

where $\bar{I}_1$ is the first modified strain invariant of the symmetric modified right Cauchy–Green tensor, $\mathbf{C}$, and the invariant $\bar{I}_4 \geq 1$ characterizes the anisotropic constitutive response.[18,27] $\bar{I}_{4_{\text{ref}}}$ characterizes the stretch at which collagen fibers begin to straighten. It was assumed that the strain energy corresponding to the anisotropic terms only contributes to the global mechanical response of the tissue when stretched, that is when $\bar{I}_4 > \bar{I}_{4_0}$. In Eqs. (1) and (2), $c1 > 0$, $c3 > 0$, $c5 > 0$ and $c6 > 0$ are stress-like parameters, $c2 > 0$ and $c4 > 0$ are dimensionless parameters and $c7 > 0$ is an energy-like parameter. Note that $c5$, $c6$ and $c7$ are

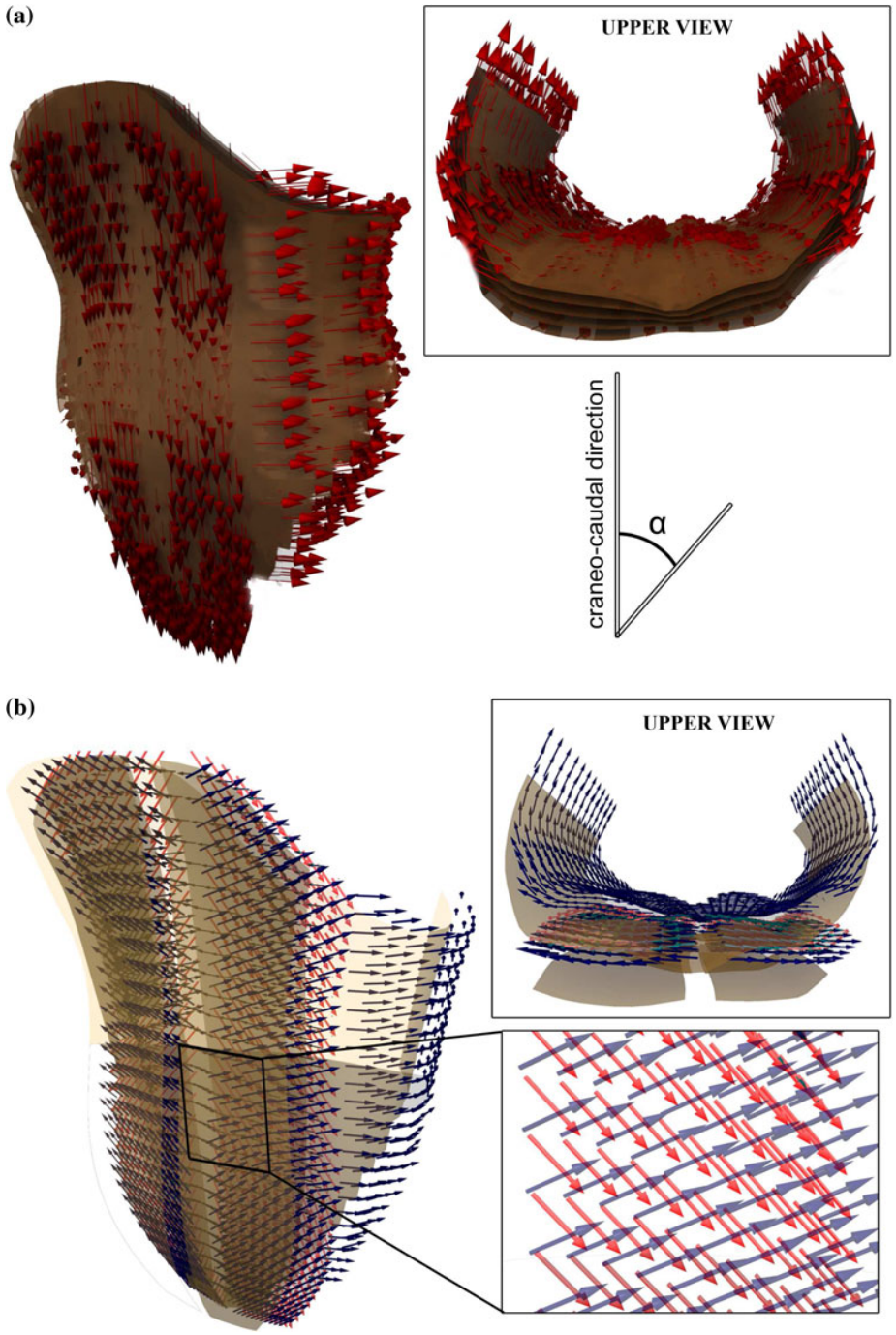

FIGURE 3. (a) Visualization of the PDA in the abdominal muscles according to the fitting procedure. The angle α that indicates the PDA is considered from the craneo-caudal direction. (b) Visualization of the collagen fiber directions in the anterior and PRSs (enlarged image) and the FT.

not independent parameters as they enforce strain, stress and stress derivative's continuity.

The anisotropic response of the abdominal muscles[18] was fitted using the SEF proposed by Holzapfel *et al.*[21]:

$$\bar{\Psi}_{\text{ani}} = \frac{c_3}{2c_4}\left[\exp\left(c_4[\bar{I}_4 - 1]^2\right) - 1\right]. \qquad (3)$$

In this equation, $c_1 > 0$ and $c_3 > 0$ are stress-like parameters, and $c_2 > 0$ and $c_4 > 0$ are dimensionless ($\Psi_{\text{ani}} = 0$ if $\bar{I}_4 \leq 1$).

Fitting of the mean curves of experimental data was performed using a Levenberg–Marquardt minimization algorithm.[26] This algorithm is based upon the minimization of an objective function,[30] which takes the form represented in (4) for the uniaxial tension test:

$$\chi^2 = \sum_{i=1}^{n} \left[\left[\sigma^{\exp} - \sigma^{\Psi} \right]_{i1}^2 + \left[\sigma^{\exp} - \sigma^{\Psi} \right]_{i2}^2 \right], \qquad (4)$$

where $\sigma_i^{\exp}$ and σ_i^{Ψ} represent the measured and the fitted stress values for the ith point data, respectively. The 1 and 2 subscript indicates the direction of the test, perpendicular one to each other.[18,27] The quality of the fittings was evaluated by computing the normalized mean square root error $\varepsilon = \frac{\sqrt{\frac{\chi^2}{n-q}}}{\mu}$. Convergence to the global minimum is difficult to achieve and the final results depend on the initial guess. For this reason, the fits were performed many times starting with randomized parameters until ε was sufficiently small.

The material parameters that fit the experimental behavior in each case are shown in Table 1. Because our primary goal was to analyze the results in the frontal part of the abdomen, the behavior of the diaphragm and pelvis was simply modeled using a Neo-Hookean model.[22,33]

There are two methods to include the direction of anisotropy. First, when the angle α is obtained by the fitting procedure, it represents a PDA but is not necessarily related to the direction of the collagen fibers. Second, with the aim of introducing the anisotropy direction in the aponeuroses or collagenous structures, guidelines published in other studies are followed by assuming that collagen fibers in the fascias have the same disposition as the muscle fibers in the muscles.[29]

Thus, the PDA in the rectus abdominis (including the RAM and RT) is disposed in the craneo-caudal direction, whereas the PDA for the oblique muscle unit runs transversally to the abdomen (see Fig. 3a). However, according to the literature,[29,35] the collagen fiber disposition in the FT is disposed transversally to the abdomen (see Fig. 3b). We assume in our work that all aponeurotic fibers from the EO and IO are included in the anterior lamina of the rectus sheath, and the aponeurotic fibers from the TA are included in the posterior lamina of the rectus sheath. Therefore, the collagen fiber patterning in the posterior rectus sheath runs transversally to the abdomen, whereas the fiber patterning in the anterior sheath, where two families of fibers exist (coming from the EO and IO), is as shown in Fig. 3b. The LA is formed by the junction of the aponeuroses coming from the anterior and posterior lamina of the rectus sheath[16,29]; therefore, collagen fiber disposition of the LA is that of the anterior and PRSs. In all cases, the constitutive equations and PDA were included in ABAQUS® by a user material (UMAT).

Displacement Boundary Conditions

In a physiological state, the ribs prevent movement of the dorsal part of the abdomen. Thus, boundary conditions were defined in the model as follows. The constraint imposed by the ribs in the dorsal part of the abdomen and lower part of the abdomen is included by fixing the nodes at the back of the abdomen and those corresponding to the pelvis support (see Fig. 2f).

Including the Initial Strains in the FE Model

The MRI data were obtained from a live subject in a supine position. Thus, the abdomen is not stress free due to the residual stresses of the living tissues and the intra-abdominal pressure (IAP) (3.6 mmHg).[10] However, the obtained geometrical model from the MRI does not provide this information so these initial stresses are unknown. The objective of the following iterative procedure is to establish the initial stresses that equilibrate the IAP in the supine position in the geometry of the MRI data.[24,11] The idea is to include

TABLE 1. Material model parameters obtained from the fitting procedure of the experimental *in vitro* results.[18,22,27]

	c_1 (MPa)	c_2 (–)	c_3 (MPa)	c_4 (–)	c_5 (MPa)	c_6 (MPa)	c_7 (MPa)	I_{40} (–)		ε (–)
*Sets**[27]	0.2434	0.8	0.0064	9.63	31.8214	−36.9188	−31.4118	1.0	–	0.1483
	c_1 (MPa)	c_2 (–)	c_3 (MPa)	c_4 (–)					α (°)	ε (–)
OM[18]	0.16832	0.6319	0.01219	5.68158	–	–	–	–	87.8	0.17873
RAM[18]	0.10445	6.86123	0.001	0.00491	–	–	–	–	0.0	0.10923
*Sets***[18]	0.16832	0.6319	0.01219	5.68158	–	–	–	–	–	0.17873
*Sets****[22]	0.18	–	–	–	–	–	–	–	–	–

The angle α is considered from the craneo-caudal direction (see Fig. 3a). These properties are assigned to the following sets of elements: (*) LA, RAT, OMT, FT, ARS and PRS, (**) chest and dorsal part of the abdomen and (***) diaphragm and pelvis.

initial strains ($\mathbf{F}_0$) that produces a stress distribution which equilibrate the IAP without displacements.

In the iterative numerical process, the supine position configuration (Ω_0) is initially stress-free, so the initial strain is $\mathbf{F}_0^0 = \mathbf{I}$. When an IAP of 0.48 kPa (3.6 mmHg), corresponding to the supine position,[10] was applied, a new deformed configuration Ω_1 is obtained with the corresponding deformation gradient ($\mathbf{F}_0^1$), and the resultant stress distribution balances the IAP applied. After that, the IAP and $\mathbf{F}_0^1$ are the inputs applied again to Ω_0, and a new configuration Ω_2, corresponding to $\mathbf{F}_0^2$ results. This iterative process is repeated until the deformed configuration is such that the displacements of the nodes in the front of the abdomen are lower than a given tolerance and can be considered to be null. At this point, the initial strains of our geometry correspond to the deformation gradient $\mathbf{F}_0^n = \mathbf{F}_{n-1}^n \mathbf{F}_0^{n-1}$ (see Fig. 4).[24,38]

Modeling Physiological Loads

Once the reference configuration is achieved by balancing the IAP and the initial strains, the next step is the simulation of physiological loads. To analyze the effects of the loads on the anterior abdominal wall, different increments of the IAP are applied perpendicularly in the inner surface of the abdominal cavity following the data presented by Cobb *et al.*[10]

The Motion of Standing

The change from a supine position to a standing position is modeled taking into account both the body mass (gravity), which includes the weight of the viscera and the muscles, and the IAP in this position. Thus, in a first load step, the IAP corresponding to the standing position (20 mmHg)[10] is applied to the reference configuration of the abdominal wall (see Fig. 4).

IAP in Other Physiological Maneuvers

After the motion of standing is simulated and during the second load step, the IAPs corresponding to the standing Valsalva maneuver (P1 = 56.25 mmHg), standing cough (P2 = 112.51 mmHg) and jumping motion (P3 = 168.76 mmHg) were applied.[10]

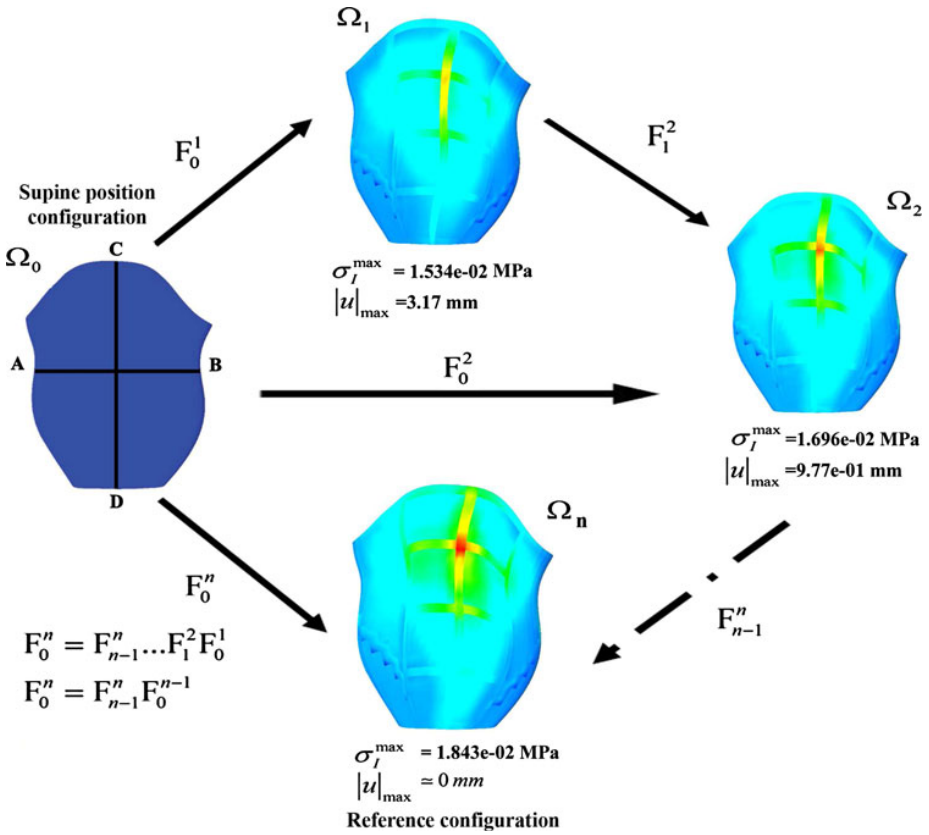

FIGURE 4. **Iterative process used to include the initial strains in the finite element model. MPS distribution, σ_I (MPa), is shown.**

RESULTS

Physiological Loads

The abdomen changes from a cylindrical to a dome-like shape during the insufflation process. The results show that after standing, the maximal displacements (MD) reach 12.35 mm in the front of the abdomen (see Fig. 5a), and the maximal principal stresses (MPS) addressed in the model are equal to 0.1003 MPa (see Figs. 5b, 5c, and 5d). As previously described, in the frontal part of the abdomen, there are different anatomical structures through the entire thickness of the model (RAM, RT, ARS, PRS and FT) (see Figs. 2a, 2d, and 2e). To clarify the representation of the results, Figs. 5b, 5c, and 5d represent the stresses experienced in the linea alba, rectus abdominis muscle and rectus tendon, linea alba, the anterior and posterior lamina of the rectus sheath and the FT, respectively. In this way, it is possible to analyze the stresses reported in each anatomical structure. The highest stresses are obtained in the linea alba (see Figs. 5b and 5c). This is likely because of the high collagen content in the LA, making it the stiffest structure. The rectus tendon and anterior and PRSs experience high stress values (approximately 0.055 and 0.065 MPa, respectively) as well. The values obtained in the RAM are lower because the stiffness of the muscle is not as high as in the aponeuroses.[18,27] Specifically, the stresses are lower than 0.04 MPa. This difference between the muscle and aponeuroses is clear in Fig. 5b, where a significant difference is displayed between the stresses identified in the rectus abdominis muscle and tendon. The stresses obtained in the

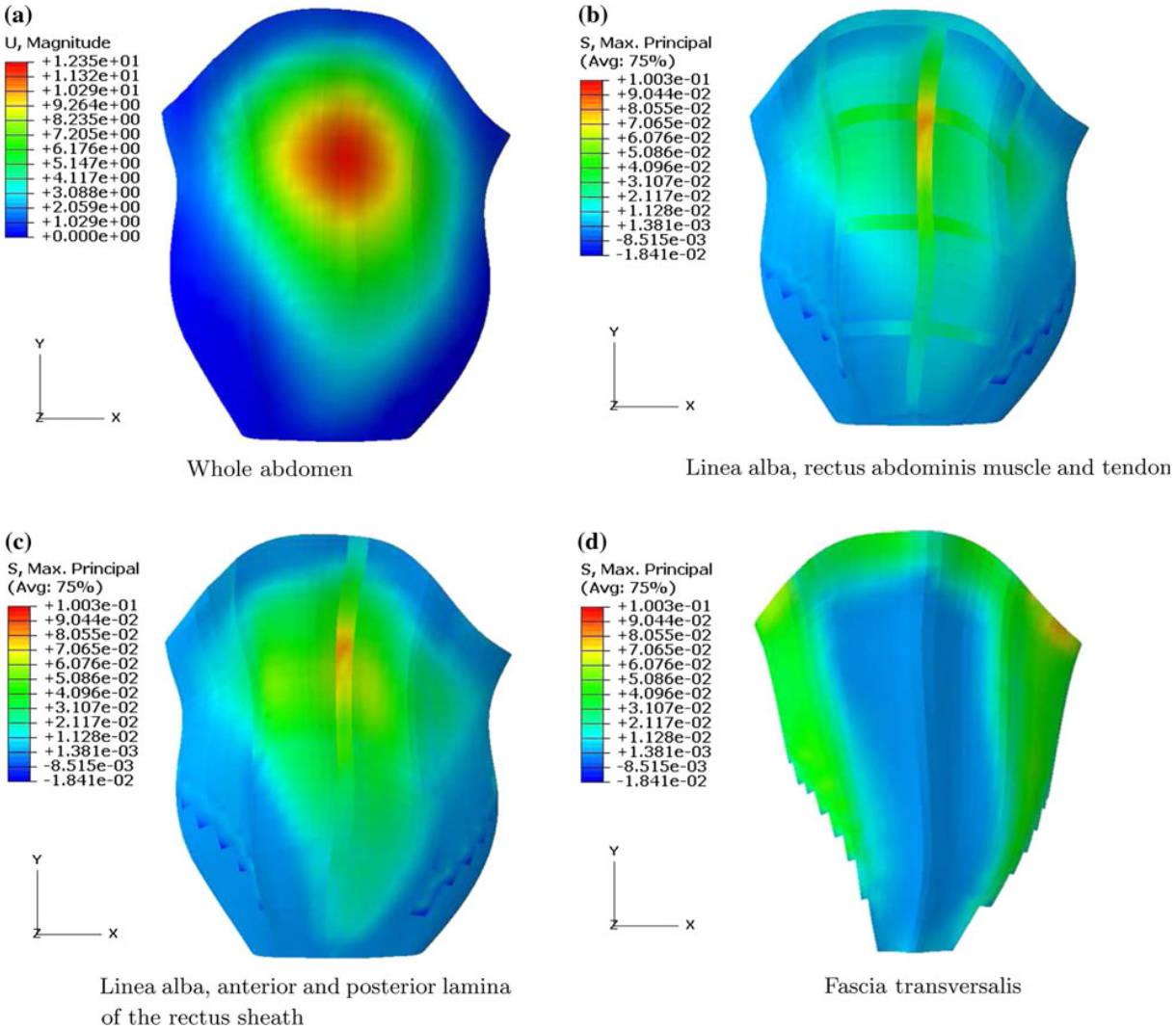

FIGURE 5. Displacement distribution (mm) (a) and stress distribution (MPa) (b–d) after the standing up motion. Stresses are shown for the different anatomical structures through the thickness of the model in the frontal part of the abdomen.

oblique muscles are even lower than those in the RAM because the highest displacements take place in the frontal part of the abdomen. Regarding the FT, the area corresponding to the frontal part of the abdomen experiences minimal stresses (lower than 0.015 MPa), whereas the areas under the oblique muscles reach higher values (>0.05 MPa). This stress distribution is justified considering the stiffness of the anatomical structures that are in contact with the FT. In the frontal part of the abdomen, the stiffest structures (LA) or structures with similar stiffness (ARS and PRS) exist over the FT. In contrast, when the oblique muscles and the FT appear together, the stiffest structure in that zone is the latter. As a consequence, in that area, the highest stresses are supported by the fascia transversalis.

To understand the effects of the applied load, Figs. 6a and 6b show the MD obtained with the three different applied IAPs, along the transversal (AB) and craneo-caudal (CD) lines, defined in Fig. 4. Regarding the stress distribution, MPS in the tissue along lines AB and CD are compared in Figs. 6c and 6d. In general, the distributions of the MD and MPS obtained with the different IAPs are similar to each other. Figure 6 shows that the MD and MPS occur in the central part of the abdomen. Along line CD, the MD and MPS occur at approximately 30% of the total distance of the line from the diaphragm (see Figs. 6b and 6d). Despite P2 ≃ 2P1 and P3 ≃ 3P1, neither the MD nor the MPS are proportional because of the nonlinear behavior of the tissues. Thus, the extensibility of the abdominal wall is higher at a lower IAP. The MD reach 45.6 mm while jumping, whereas this value is equal to 26.08 and 37.7 mm during the standing valsalva maneuver and standing cough, respectively (see Figs. 6a and 6b).

Similar to the MD, the MPS increase as the IAP increases. The MPS increase from the boundaries to the frontal part of the abdomen. Along line AB, there is a perturbation of the MPS because of the transition between the rectus abdominis and linea alba where material properties change (see Fig. 6c). Following line CD, which corresponds to the LA, the computed MPS are equal to 0.176, 0.295, and 0.427 MPa during the standing Valsalva maneuver, during the standing cough and while jumping, respectively.

DISCUSSION

The main objective of this work is to present a methodology to model the passive mechanical

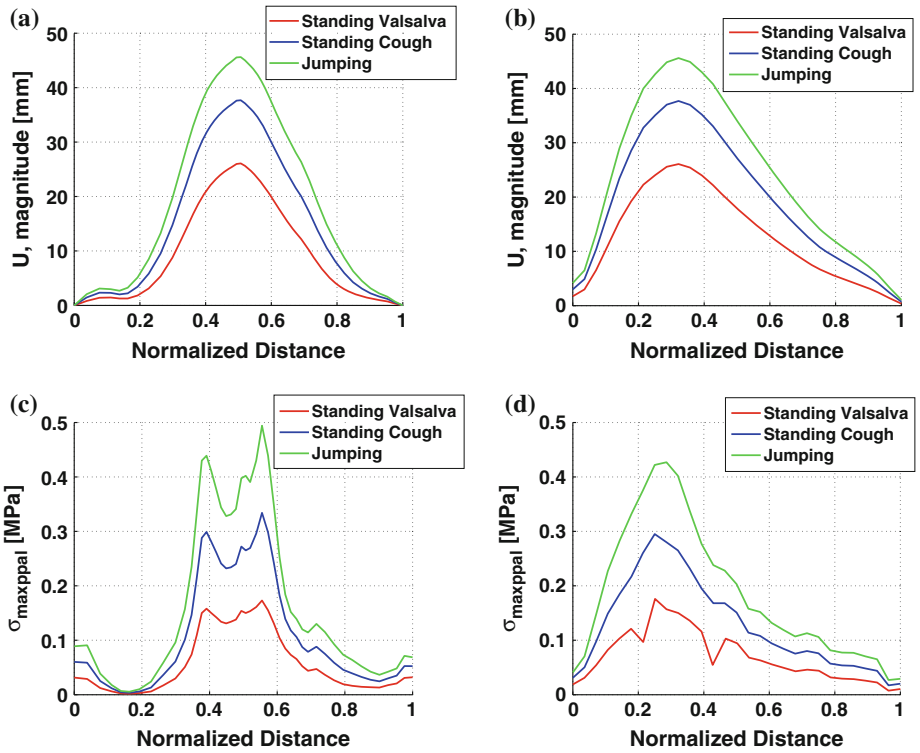

FIGURE 6. MD along lines AB (a) and CD (b) and MPS along lines AB (c) and CD (d) in a model of the healthy abdomen (See Fig. 4). The abscissa shows the normalized distance of lines AB and CD. $x = 0$ and $x = 1$ correspond to points A, B and C, D, respectively.

behavior of the human abdomen during physiological movements. With this methodology, it is possible to establish some guidelines to predict where hernia formation is likely to occur on the abdominal wall from a mechanical point of view.

Because of the high collagen content in the fascias and aponeuroses, they are stiffer than the muscles.[18,27] According to the material properties assigned to each tissue, the stresses obtained in the aponeuroses are higher than the values obtained in the muscles. In the healthy abdomen, the MD and MPS appear in the front of the abdomen (see Figs. 5 and 6). Specifically, the MPS appear in the linea alba. This area becomes stiffer because it is composed mostly of collagen connective tissue and is the zone where the MD occur. Traditionally, the linea alba and the rectus sheaths are regarded as the most important structures for the stability of the abdominal wall from a mechanical point of view.[4] However, in some cases, the LA may be weaker. Naraynsingh *et al.*[31] hypothesized that the LA is a weak layer and varies widely in individuals with respect to its anatomy. Thus, the highest probability of hernia appearance corresponds to elderly, obese and multiparous patients. In addition, Korenkov *et al.*[23] have asserted that a combination of low density and thin fibers in the LA could be a predisposing factor for the development of midline incisional hernias. Usually, a midline incision is preferred in clinical practice because it gives wide access to the abdomen during laparotomy.[7] However, it is known that the most common mechanism of hernia formation in the abdominal midline (LA) is in the postoperative setting after laparotomy.[7] Hernia recurrence in these cases is in agreement with our results because the MD and MPS appear in the LA. If the mechanical properties of the LA are altered, this anatomical structure could be incapable of maintaining high loads, and the integrity of the abdominal wall could deteriorate. Thus, our findings suggest that laparotomy through the upper area of the linea alba may not be the best choice.

Other authors have published studies regarding the behavior of the abdominal wall. For example, Song *et al.*[40] reported on the mechanical properties of abdominal tissue. However, instead of using large deformation hyperelasticity to mechanically characterize the abdominal wall, Laplace's equation was applied to obtain the relationship between the inflation pressure and the radii at the center of the abdominal surface. The typical Laplace's equation assumes that the stresses are directly proportional to the applied pressure,[40] and we demonstrated that the MD and MPS are not proportional as the pressure increases. Förstemann *et al.*[14] compared the results from an experimental study of the mechanical properties of the LA and the simulation of this anatomical unit using a reconstructed model obtained using MRI. The authors considered the anisotropy of the LA and the nonlinear response of the tissue. However, they also considered small deformations using the Laplace's equation. Since these authors do not apply the large deformation hyperelasticity, their hypotheses are not completely correct, and our results in stresses are not directly comparable with theirs. Because the material properties of the tissue are not considered using Laplace's equation, and this formulation is not valid in large deformations or with high thickness geometries, it would not be an adequate approach to evaluate the mechanical behavior of the abdominal wall.

Our study is not devoid of certain simplifications. Because of the great complexity of the abdominal anatomy, some anatomical structures are simplified. Regarding the modeling of the aponeuroses, we assume that all aponeurotic fibers from the external and internal obliques are included in the ARS, and those from the transversus abdominis are included in the PRS. However, the exact disposition is more complex.[29,35] Furthermore, because the reported experimental data on the mechanical behavior of human tissues are limited, experimental animal data are used when there are no data from human tissue. In both cases, uniaxial experimental data are taken but these tests are not sufficient for the mechanical characterization of multidimensional material models aimed at predicting the behaviour in physiological loading states.[20] Thus, further information from other mechanical multiaxial tests (e.g., biaxial, inflation) would be useful to complete our characterization of these materials. In addition, the different flat muscles are not differentiated, but a composite muscle is modeled.[8,18] This assumption was based on the work published by Brown *et al.*[8] These authors have shown that the layers of the abdomen do not express separate movements but only change their thickness. Thus, the flat muscles move as a monolayer component under IAP. Furthermore, Hernández *et al.*[18] demonstrated that it is possible to simulate the passive mechanics of the abdominal tissue as a composite or as separate muscle layers. Despite the study is only focused on the mechanical response, further considerations such as chemical and biological should be included in that methodology in future works to study other kinds of tissue abnormalities. Besides, since only elastic properties of the tissues have been considered, the methodology would be improved by means of considering the active response, the viscoelastic properties of muscle, as well as the stiffness loss due to damage. Finally, an important limitation of this study is that the applied IAP are non-patient-specific and the results can only be analyzed from a qualitative point of view. Thus, the results obtained have to be validated with

experimental *in vivo* studies. Those *in vivo* experiments have to measure the patient-specific IAP so that they reproduce physiological states. In addition, the geometry of the abdominal wall is different for each patient considered. Besides, features such as wall thickness or radii of curvature strongly influence on the mechanical behavior of the abdomen (Laplace Law). For those reasons, the experimental validation using experiments of the literature is difficult.

In spite of these limitations, this work is the first study that defines a realistic geometry of the entire real human abdomen, including the different anatomical structures. Furthermore, the model can be used to simulate the mechanical behavior under different physiological loads. The main advantage of this study is that our findings provide direction for future studies designed to automatically simulate the mechanical behavior of the abdominal wall in personalized studies. The anatomical structures that perform the most work in the healthy abdomen were identified. Thus, the analysis of the anatomy of a specific patient can provide some guidelines to predict where hernia formation is likely to occur on the abdominal wall. Specifically, weak abdominal tissues that support higher stresses than in the healthy abdomen would indicate they tend to mechanically fail. Furthermore, the ideal surgical procedure would be personalized. Before surgery, the geometry of interest of each particular patient could be processed using a three-dimensional computational tool. The reconstructed geometry would be simulated using finite element (FE) analysis incorporating the properties of human tissue. This methodology would allow surgical procedures to be planned to predict and improve the outcomes of a customized surgery.[2] Thus, simulating the surgical procedure before the actual surgery would predict the outcomes and the best results could be achieved.

CONCLUSIONS

A methodology to model the human abdomen and to study its mechanical response after physiological movements is defined. Furthermore, from a mechanical point of view it is possible to predict where hernia formation is likely to occur on the abdominal wall since the areas that support higher stresses can be identified as the most vulnerable ones. Specifically, the stiffest structures, namely aponeuroses, are the structures that most work in the abdomen, specially, the linea alba. Thus, the linea alba is the most important unit for the stability of the abdominal wall from a mechanical point of view. Finally, our findings provide direction for future studies designed to automatically simulate the mechanical behavior of the abdominal wall in personalized studies and surgical procedures.

ACKNOWLEDGMENTS

This study was supported by the Spanish Ministry of Economy and Competitiveness through research project DPI2011-27939-C02-01/C02-02 and the Instituto de Salud Carlos III (ISCIII) through the CIBER-BBN initiative project ABDOMESH. B. Hernández-Gascón was funded by a grant (BES-2009-021515) from the Spanish Ministry of Science and Technology.

REFERENCES

[1]Arruda, E. M., K. Mundy, S. Calve, and K. Baar. Denervation does not change the ratio of collagen I and collagen II mRNA in extracellular matrix of muscle. *Am. J. Physiol.* 292:983–987, 2006.

[2]Audettea, M. A., H. Delingetteb, A. Fuschsc, Y. Kosekia, and K. Chinzeia. A procedure for computing patient-specific anatomical models for finite element-based surgical simulation. *Int. Cong. Ser.* 1256:356–361, 2003.

[3]Axer, H., D. G. Keyserlingk, D. Graft, and A. Prescher. Collagen fibers in linea alba and rectus sheaths: II. Variability and biomechanical aspects. *J. Surg. Res.* 96:239–245, 2001.

[4]Axer, H., D. G. Keyserlingk, and A. Prescher. Collagen fibers in linea alba and rectus sheaths: I. General scheme and morphological aspects. *J. Surg. Res.* 96:127–134, 2001.

[5]Bartlett, D. C., and A. N. Kingsnorth. Abdominal wound dehiscence and incisional hernia. *Surgery* 24(7):234–238, 2006.

[6]Bellón, J. M., A. Bajo, N. Ga-Honduvilla, M. J. Gimeno, G. Pascual, A. Guerrero, and J. Buján. Fibroblasts from the transversalis fascia of young patients with direct inguinal hernias show constitutive MMP-2 overexpression. *Ann. Surg.* 233(2):287–291, 2001.

[7]Bellón-Caneiro, J. M. Abdominal wall closure in laparotomy. *Cir. Esp.* 77(3):114–123, 2004.

[8]Brown, S. H. M., and S. M. McGill. A comparison of ultrasound and electromyography measures of force and activation to examine the mechanics of abdominal wall contraction. *Clin. Biomech.* 25:115–123, 2010.

[9]Calvo, B., E. Peña, P. Martins, T. Mascarenhas, M. Doblare, R. Natal, and A. Ferreira. (2009) On modelling damage process in vaginal tissue. *J. Biomech.* 42:642–651, 2009.

[10]Cobb, W. S., J. M. Burns, K. W. Kercher, B. D. Matthews, H. J. Norton, and B. T. Heniford. Normal intraabdominal pressure in healthy adults. *J. Surg. Res.* 129:231–235, 2005.

[11]De Putter, S., B. J. B. M. Wolters, M. C. M. Rutten, M. Breeuwer, F. A. Gerritsen, and F. N. van de Vosse. Patient-specific initial wall stress in abdominal aortic aneurysms with a backward incremental method. *J. Biomech.* 40:1081–1090, 2007.

[12]Demiray, H., H. W. Weizsacker, K. Pascale, and H. Erbay. A stress-strain relation for a rat abdominal aorta. *J. Biomech.* 21:369–374, 1988.

[13]Fortuny, G., J. Rodríguez-Navarro, A. Susín, M. López-Cano. Simulation and study of the behaviour of the transversalis fascia in protecting against the genesis of inguinal hernias. *J. Biomech.* 42:2263–2267, 2009.

[14]Föstemann, T., J. Trzewik, J. Holste, B. Batke, M. A. Konerding, Wolloscheck T., Hartung C. (2011) Forces and deformations of the abdominal wall—a mechanical and geometrical approach to the linea alba. *J. Biomech.* 44:600–606, 2011.
[15]Gerovichev, O., P. Marayong, and A. M. Okamura. The effect of visual and haptic feedback on manual and teleoperated needle insertion. In: Medical Image Computing and Computer-Assisted Intervention—MICCAI 2002, vol. 2488. Springer, Berlin, pp. 147–154, 2002.
[16]Grassel, D., A. Prescher, S. Fitzed, D. G. Keyserlingk, and H. Axer. Anisotropy of human linea alba: a biomechanical study. *J. Surg. Res.* 124:118–125, 2005.
[17]Henriksen, N. A., D. H. Yadete, L. T. Sorensen, M. S. Agren, and L. N. Jorgensen. Connective tissue alteration in abdominal wall hernia. *Br. J. Surg.* 98(2):210–219, 2011.
[18]Hernández, B., E. Peña, G. Pascual, M. Rodriguez, B. Calvo, M. Doblaré, and J. M. Bellón. Mechanical and histological characterization of the abdominal muscle. A previous step to model hernia surgery. *J. Mech. Behav. Biomed.* 4:392–404, 2011.
[19]Hernández-Gascón, B., P. Young, G. Pascual, E. Peña, J. M. Bellon, and B. Calvo. Modelling of the abdominal wall: comparison of hexahedral and tetrahedral elements. In: 2011 Simpleware Users Meeting. Simpleware, November 2011.
[20]Holzapfel, G. A. (2006) Determination of material models for arterial walls from uniaxial extension tests and histological structure. *J. Theor. Biol.* 238:290–302, 2006.
[21]Holzapfel, G. A., T. C. Gasser, and R. W. Ogden. A new constitutive framework for arterial wall mechanics and a comparative study of material models. *J. Elasticity* 61:1–48, 2000.
[22]Kauer, M. Inverse Finite Element Characterization of Soft Tissues with Aspiration Experiments. Ph.D. thesis, Swiss Federal Institute of Technology, Zürich, 2001.
[23]Korenkov, M., A. Beckers, J. Koebke, R. Lefering, T. Tiling, and H. Troidl. Biomechanical and morphological types of the linea alba and its possible role in the pathogenesis of midline incisional hernia. *Eur. J. Surg.* 167:909–914, 2001.
[24]Lanchares, E., B. Calvo, J. A. Cristóbal, and M. Doblaré. Finite element simulation of arcuates for astigmatism correction. *J. Biomech.* 41:797–805, 2008.
[25]López-Cano, M., J. Rodríguez-Navarro, A. Rodríguez-Baeza, M. Armengol-Carrasco, and A. Susín. A real-time dynamic 3D model of the human inguinal region for surgical education. *Comput. Biol. Med.* 37:1321–1326, 2007.
[26]Marquardt, D. W. An algorithm for least-squares estimation of nonlinear parameters. *SIAM J. Appl. Math.* 11:431–441, 1963.
[27]Martins, P., E. Peña, R. M. Natal Jorge, A. Santos, L. Santos, T. Mascarenhas, and B. Calvo. Mechanical characterization and constitutive modelling of the damage process in rectus sheath. *J. Mech. Behav. Biomed.* 8:111–122, 2012.
[28]Meier, A. H., C. L. Rawn, and T. M. Krummel. Virtual reality: surgical application-challenge for the new millennium. *J. Am. Coll. Surgeons* 192:372–374, 2001.
[29]Moore, W. Gray's Anatomy celebrates 150th anniversary. The Telegraph (Telegraph Media Group), 2008.
[30]Morrow, D. A., T. H. Donahue, G. M. Odegard, and K. R. Haufman. A method for assesing the fit of a constitutive material model to experimental stress-strain data. *Comput. Methods Biomech. Biomed. Eng.* 12:247–256, 2010.
[31]Naraynsingh, V., R. Maharaj, D. Dan, and S. Hariharan. Strong linea alba: Myth or reality? *Med. Hypotheses* 78:291–292, 2012.
[32]Norasteh, A., E. Ebrahimi, M. Salavati, J. Rafiei, and E. Abbasnejad. Reliability of B-mode ultrasonography for abdominal muscles in asymptomatic and patients with acute low back pain. *J. Bodywork Mov. Ther.* 11:17–20, 2007.
[33]Ogden, R. W. Non-Linear Elastic Deformations. Dover, New York, 1996.
[34]Ozdogan, M., F. Yildiz, A. Gurer, S. Orhun, H. Kulacoglu, and R. Aydin. Changes in collagen and elastic fiber contents of the skin, rectus sheath, transversalis fascia and peritoneum in primary inguinal hernia patients. *Bratisl Med. J.* 107:235–238, 2006.
[35]Park, A. E., J. S. Roth, and S. M. Kavic. Abdominal wall hernia. *Curr. Prob. Surg.* 43:326–375, 2006.
[36]Pascual, G., C. Corrales, V. Gómez-Gil, J. Buján, and J. M. Bellón. TGF-Beta1 overexpression in the transversalis fascia of patients with direct inguinal hernia. *Eur. J. Clin. Invest.* 37(6):516–521, 2007.
[37]Pascual, G., M. Rodríguez, V. Gómez-Gil, C. Trejo, J. Buján, and J. M. Bellón. Active matrix metalloproteinase-2 upregulation in the abdominal skin of patients with direct inguinal hernia. *Eur. J. Clin. Invest.* 40(12):1113–1121, 2010.
[38]Peña, E., M. A. Martinez, B. Calvo, and M. Doblaré. On the numerical treatment of initial strains in soft biological tissues. *Int. J. Numer. Methods Eng.* 68:836–860, 2006.
[39]Read, R. C. A review: the role of protease-antiprotease imbalance in the pathogenesis of herniation and abdominal aortic aneurysm in certain smokers. *Postgrad. Gen. Surg.* 4:161– 165, 1992.
[40]Song, C., A. Alijani, T. Frank, G. Hanna, and A. Cuschieri. Elasticity of the living abdominal wall in laparoscopic surgery. *J. Biomech.* 39:587–591, 2006.
[41]Spitzer, V. M., and D. G. Whitlock. The visible human data set: the anatomical platform for human simulation. *Anat. Rec.* 253:49–57, 1998.

Work 5: Computational framework to model and design surgical meshes for hernia repair

Journal: *Computer Methods in Biomechanics and Biomedical Engineering*, **In Press**, (2012): DOI:10.1080/10255842.2012.736967.
Journal impact factor: 1.169

Computer Methods in Biomechanics and Biomedical Engineering
iFirst article, 2012, 1–15

Taylor & Francis
Taylor & Francis Group

Computational framework to model and design surgical meshes for hernia repair

B. Hernández-Gascón[a,b], N. Espés[a], E. Peña[a,b]*, G. Pascual[b,c], J.M. Bellón[b,d] and B. Calvo[a,b]

[a]*Aragón Institute of Engineering Research, University of Zaragoza, Agustin Betancourt Building, Maria de Luna s/n, 50018 Zaragoza, Spain;* [b]*Centro de Investigación Biomédica en Red en Bioingeniería, Biomateriales y Nanomedicina (CIBER-BBN), Spain;* [c]*Departament of Medical Specialities, Faculty of Medicine, University of Alcalá, Madrid, Spain;* [d]*Departament of Surgery, Faculty of Medicine, University of Alcalá, Madrid, Campus Universitario Crta. de Madrid-Barcelona, Km. 33.600, Alcalá de Henares, Spain*

(*Received 21 September 2011; final version received 2 October 2012*)

Surgical procedures for hernia surgery are usually performed using prosthetic meshes. In spite of all the improvements in these biomaterials, the perfect match between the prosthesis and the implant site has not been achieved. Thus, new designs of surgical meshes are still being developed. Previous to implantation in humans, the validity of the meshes has to be addressed, and to date experimental studies have been the gold standard in testing and validating new implants. Nevertheless, these procedures involve long periods of time and are expensive. Thus, a computational framework for the simulation of prosthesis and surgical procedures may overcome some disadvantages of the experimental methods. The computational framework includes two computational models for designing and validating the behaviour of new meshes, respectively. Firstly, the beam model, which reproduces the exact geometry of the mesh, is set to design the weave and determine the stiffness of the surgical prosthesis. However, this implies a high computational cost whereas the membrane model, defined within the framework of the large deformation hyperelasticity, is a relatively inexpensive computational tool, which also enables a prosthesis to be included in more complex geometries such as human or animal bodies.

Keywords: beam model; membrane model; hyperelasticity; finite element model

1. Introduction

Classic suture techniques have gradually given way to the use of biomaterials for the surgical repair of abdominal wall hernias since the introduction of Lichtenstein's tension-free mesh procedure which is today practically standard practice (Lichtenstein and Shulman 1986; Lichtenstein et al. 1989). For tissue repair, there are a great variety of meshes available showing different mechanical properties, but macroporous polypropylene (PP) meshes continue to be the gold-standard material (Afonso et al. 2008; Pascual et al. 2008; Bellón 2009). The 'ideal prothesis' characteristics are inertness, resistance to infection, early host tissue incorporation, a non-carcinogenic response, the ability not to produce recurrences and the ability to mimic physiological behaviour. However, current surgical meshes exhibit many but not all of these characteristics, and the perfect correspondence between the anisotropy of the abdominal muscle (Junge et al. 2001; Grassel et al. 2005; Hernández et al. 2011) and that of the implanted mesh has not yet been achieved (Hernández-Gascón et al. 2011). Thus, new designs of surgical implants are still being developed.

The available meshes on the market can be classified according to different criteria. Depending on their geometric structure, implants are classified as reticular, laminar and compound meshes. Reticular meshes can be subdivided into absorbable, partially absorbable and non-absorbable. Laminar meshes can be absorbable and non-absorbable while compound meshes are formed by a non-absorbable component and a physical or a chemical component.

According to density, German authors classify prosthetic meshes into heavyweight (HW) or lightweight (LW) for densities above 80 or below 50 g/m^2, respectively (Klinge 2007). In addition, materials with a density between 50 and 80 g/m^2 are designated as mediumweight (Cobb et al. 2006). Prosthetic mesh density is, however, sometimes independent of pore size and some designs, despite their small pore size, are classified as LW since they are composed of a loosely woven monofilament that confers on them a low density. Finally, as regards the material, meshes can be made of PP, expanded polytetrafluoroethylene, polyester, silicone, polyurethane, etc. All these features, the filament composition, mesh weave and the spatial arrangement of the filaments, along with pore size will determine the mechanical anisotropic behaviour of a surgical mesh.

Nowadays, the response of surgical meshes is usually analysed through experimental studies, which involve high costs and long periods of time. However, the computational simulation of multiple real situations from different fields is possible by using the finite element

*Corresponding author. Email: fany@unizar.es

ISSN 1025-5842 print/ISSN 1476-8259 online

http://dx.doi.org/10.1080/10255842.2012.736967
http://www.tandfonline.com

method (FEM). Specifically, biomechanical materials and surgical procedures can be simulated once the geometry, the load and the boundaries are completely defined. Therefore, the use of the FEM may have advantages in the biomechanical field for several reasons. A first approach to the real situation may predict the validity or invalidity of a new design without having to spend the long period of time required by experimental studies. Besides, the cost of the study will be reduced because most of the resources needed for experiments are not required.

The whole process of designing a new prosthesis for hernia repair may be made following the computational framework that is presented in this study which includes two computational models (see Figure 1). Complications associated with surgical mesh materials and geometry have been debated by other authors (Pandit and Henry 2004) regarding the amount of prosthetic material employed in the design of the prosthesis. The inflammatory response may be reduced by a reduction in the amount of material by reducing the mesh weight along with an increase in the mesh pore size. In this study, these concerns are addressed by a first computational model in which the geometry of the unit cell is defined. Then, the beam model validates the geometry and the stiffness comparing the computational and the experimental results (see Figure 1). The stiffness is achieved when the computational results mimic the real mechanical behaviour of the prostheses obtained experimentally. Once the stiffness is validated with the experimental results using the beam model, the second approach of the computational framework, which uses a membrane model, simplifies the geometry and its potentiality permits the reproduction of surgical procedures as well as the inclusion of the prosthesis in complex models of human or animal bodies (see Figure 1). The integration of the prosthesis in these complex models using the membrane model reproduces the whole behaviour which can consequently be addressed. Finally, once good compliance and patient comfort are achieved in the simulation with the membrane model, the manufacture of the surgical mesh may be developed.

The main objective of this study was to define an efficient computational framework in order to design and simulate the mechanical behaviour of surgical meshes. In addition to reducing the high cost of experimental studies, these computational tools may help to achieve better designs of implants for hernia surgery and the correspondence between the abdominal wall and the prosthesis can be analysed before the implant. On the other hand, complex models that simulate the geometries of human or animal bodies may reproduce surgical procedures where prostheses need to be included. We may include the prosthesis in a complex model of a body and simulate the whole behaviour prior to developing an experimental study of a surgical procedure. There are some papers that simulate plain weave fabrics (King et al. 2005); however, to the best of the authors' knowledge, there are no similar previous studies simulating the mechanical behaviour of meshes in surgical applications.

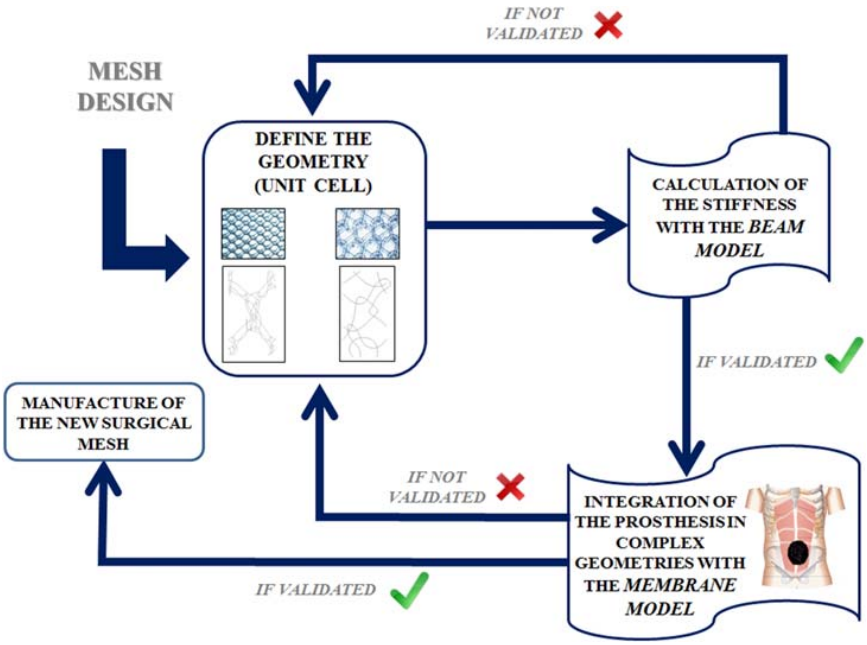

Figure 1. Sketch of the process to design a surgical mesh. The computational framework is applied by means of two computational models: the beam and the membrane models.

This paper is structured as follows. Following this introduction, Section 2 presents a computational approach to mesh design. In Section 2.1, the geometry is completely reproduced through beam elements in the finite element (FE) simulation to determine the stiffness of the mesh, whereas the second computational tool in Section 2.2 simplifies the geometry into a membrane model. In Section 3, two commercial surgical meshes are modelled using both strategies and compared with experimental results. An FE simulation of hernia surgery is presented in Section 4. Finally, Section 5 sets out the principal conclusions obtained in this study.

2. Computational approach to mesh design

The computational framework includes two computational models that are described in this section: the beam and the membrane approaches. The first approach has been considered to design the woven fabrics and determine the stiffness of the woven, whereas the membrane model has been used to simplify the geometry and reduce the computational time cost in order to include the mesh in complex clinical applications and to characterise the whole response of the abdominal wall.

2.1 Mesh modelling with beam model

To reproduce the behaviour of the filaments of the prosthesis, the exact model would have to be designed using truss elements. However, such elements have a high instability when the geometry of the model is complex and compression may appear. This fact entails numerical problems and a high computational cost (Hibbit, Karlsson and Sorensen, Inc. 2008). With the aim of modelling the global response of the surgical meshes, beam elements were used. However, these elements include bending stiffness so the computational response is stiffer than the real response. To avoid this, reduced material properties were considered, and this fact was taken into account when determining Young's modulus of the filaments which had to be lower than the theoretical one. Specifically, we adjusted Young's modulus until it fitted the experimental results. For this purpose, we applied an optimisation method [recursive quadratic programming (RQP)] in order to obtain Young's modulus capable of mimicking the experimental tests. Another approach that could be used is maintaining the axial stiffness and only reducing the bending stiffness. This methodology is less systematic than the proposed methodology in our study.

The beam model considers the exact geometry of the mesh in order to define the stiffness of the prosthesis. With this method, the interweave of the mesh is reproduced and the shape of the mesh allows the study of the behaviour in the two perpendicular directions. Besides, the nodes where the filaments interweave are distinguished. The real interweave in surgical meshes makes possible the gliding between wires. However, due to the high number of contact points that exist in the surgical mesh, the exact reproduction and the computational simulation of the sliding between wires are too complex. Therefore, the geometry is generated without considering contact between the filaments. Thus, the interweave is considered through rigid nodes.

Surgical meshes are designed and woven following a repeated pattern namely, for the sake of simplicity, unit cells. Thus, these cells are repeated in space and symmetric conditions can be assumed when simulating them. Therefore, as the size of the FE model is reduced by symmetry, the computational cost is reduced. The constitutive modelling is that of linear elastic material with large deformations (Timoshenko and Goodier 1972). The geometry and the linear elastic properties of the beams determine the response in stiffness and the deformed shape.

2.2 Mesh modelling with membrane model

With the aim of reducing the computational cost of the previous model, a membrane model is proposed, where the geometry and weave of the surgical mesh are homogenised, using a 3D anisotropic hyperelastic formulation. This way, the prosthesis may be simulated inside complex geometries, such as human or animal bodies.

The constitutive modelling for this method is that of the continuum theory of large deformation hyperelasticity. Membrane models in the commercial software used do not include anisotropic behaviours. Thus, the following formulation is needed and was programmed in a user subroutine.

Let $\mathcal{B}_0 \subset \mathbb{R}^3$ be a reference or rather material configuration of a body B of interest. The notation $\boldsymbol{\chi} : \mathcal{B}_0 \times \mathcal{T} \rightarrow \mathcal{B}_t$ represents the one-to-one mapping, continuously differentiable, transforming a material point $\mathbf{X} \in \mathcal{B}_0$ to a position $\mathbf{x} = \boldsymbol{\varphi}(\mathbf{X}, t) \in \mathcal{B}_t \subset \mathbb{R}^3$, where $\mathcal{B}_t$ represents the deformed configuration at time $t \in \mathcal{T} \subset \mathbb{R}$. The mapping $\boldsymbol{\chi}$ represents a motion of the body B that establishes the trajectory of a given point when moving from its reference position $\mathbf{X}$ to $\mathbf{x}$. The two-point deformation gradient tensor is defined as $\mathbf{F} = \nabla\chi(\mathbf{X}, \mathbf{t}) : \mathrm{T}\mathcal{B}_0 \rightarrow \mathrm{T}\mathcal{B}_t$ that defines the linear tangent map from the material tangent space $\mathrm{T}\mathcal{B}_0$ to the spatial tangent space $\mathrm{T}\mathcal{B}_t$, with $J(\mathbf{X}) = \det(\mathbf{F}) > 0$ the local volume variation and $\mathbf{C} = \mathbf{F}^{\mathrm{T}}\mathbf{F}$ the corresponding right Cauchy–Green tensor as a characteristic material deformation measure. It is sometimes useful to consider the multiplicative decomposition of $\mathbf{F} = J^{1/3}\mathbf{I} \cdot \bar{\mathbf{F}}$. Hence, deformation is split into a dilatational part, $J^{1/3}\mathbf{I}$, where $\mathbf{I}$ represents the second-order identity tensor, and an isochoric contribution, $\bar{\mathbf{F}}$, so that $\det(\bar{\mathbf{F}}) = 1$ (Flory 1961; Simo and Taylor 1991). With these quantities at hand, the isochoric counterparts of the right Cauchy–Green deformation tensor associated with $\bar{\mathbf{F}}$ are defined as $\bar{\mathbf{C}} := \bar{\mathbf{F}}^{\mathrm{T}} \cdot$

$\bar{\mathbf{F}} = J^{-2/3}\mathbf{C}$. In general, for materials with anisotropy it is necessary to introduce two unit vectors $\mathbf{m}_0$ and $\mathbf{n}_0$, describing the anisotropy direction, and the concept of the anisotropic invariants, describing the invariants associated with this vector and the deformation tensor. Therefore, the following isochoric invariants were used (Spencer 1971; Holzapfel 2000):

$$\begin{aligned} &\bar{I}_4 = \bar{\mathbf{C}} : \mathbf{M} = \bar{\lambda}_m^2, \;\; \bar{I}_5 = \bar{\mathbf{C}}^2 : \mathbf{M}, \;\; \bar{I}_6 = \bar{\mathbf{C}} : \mathbf{N} = \bar{\lambda}_n^2, \\ &\bar{I}_7 = \bar{\mathbf{C}}^2 : \mathbf{N}, \;\; \bar{I}_8 = [\mathbf{m}_0 \cdot \mathbf{n}_0]\mathbf{m}_0 \cdot \bar{\mathbf{C}}\mathbf{n}_0, \;\; \bar{I}_9 = [\mathbf{m}_0 \cdot \mathbf{n}_0]^2, \end{aligned} \tag{1}$$

where $\mathbf{M} = \mathbf{m}_0 \otimes \mathbf{m}_0$ and $\mathbf{N} = \mathbf{n}_0 \otimes \mathbf{n}_0$ are structural tensors.

To characterise isothermal processes, we postulate the existence of a unique decoupled representation of the strain-energy density function Ψ (Simo et al. 1985). Based on the kinematic description, the free energy can be rewritten in decoupled form as

$$\Psi(\mathbf{C}, \mathbf{M}, \mathbf{N}) = \Psi_{\text{vol}}(J) + \Psi_{\text{ich}}(\bar{\mathbf{C}}, \mathbf{M}, \mathbf{N}), \tag{2}$$

where $\Psi_{\text{vol}}(J)$ and $\Psi_{\text{ich}}(\bar{\mathbf{C}}, \mathbf{M}, \mathbf{N})$ are given scalar-valued functions of J, $\bar{\mathbf{C}}$, $\mathbf{m}_0$ and $\mathbf{n}_0$, respectively, that describe the volumetric and isochoric responses of the material (Holzapfel 2000). In terms of the strain invariants, Ψ can be written as

$$\Psi = \Psi_{\text{vol}}(J) + \Psi_{\text{ich}}(\bar{I}_1, \bar{I}_2, \bar{I}_4, \bar{I}_5, \bar{I}_6, \bar{I}_7, \bar{I}_8). \tag{3}$$

Usually, the formulation is only expressed with the invariants $\bar{I}_1, \bar{I}_2, \bar{I}_4$ and $\bar{I}_6$. The second Piola–Kirchhoff stress tensor is obtained by derivation of (2) and (3) with respect to the right Cauchy–Green tensor. Thus, the stress tensor consists of a purely volumetric and a purely isochoric contribution, i.e. $\mathbf{S}_{\text{vol}}$ and $\mathbf{S}_{\text{ich}}$, so the total stress is

$$\begin{aligned} \mathbf{S} &= \mathbf{S}_{\text{vol}} + \mathbf{S}_{\text{ich}} = 2\frac{\partial \Psi_{\text{vol}}(J)}{\partial \mathbf{C}} + 2\frac{\partial \Psi_{\text{ich}}(\bar{\mathbf{C}}, \mathbf{M}, \mathbf{N})}{\partial \mathbf{C}} \\ &= 2\left[\frac{\partial \Psi_{\text{vol}}(J)}{\partial J}\frac{\partial J}{\partial \mathbf{C}} + \frac{\partial \Psi_{\text{ich}}(\bar{\mathbf{C}}, \mathbf{M}, \mathbf{N})}{\partial \bar{\mathbf{C}}}\frac{\partial \bar{\mathbf{C}}}{\partial \mathbf{C}}\right] \\ &= Jp\mathbf{C}^{-1} + 2\sum_{j=1,2,4,6} \mathsf{P} : \frac{\partial \Psi_{\text{ich}}}{\partial \bar{I}_j}\frac{\partial \bar{I}_j}{\partial \bar{\mathbf{C}}}. \end{aligned} \tag{4}$$

Moreover, one obtains the following noticeable relations $\partial_{\mathbf{C}} J = (1/2)J\mathbf{C}^{-1}$ and $\mathsf{P} = \partial_{\mathbf{C}}\bar{\mathbf{C}} = J^{-2/3}[\mathsf{I} - (1/3)\mathbf{C}\otimes\mathbf{C}^{-1}]$. P is the fourth-order projection tensor and I denotes the fourth-order unit tensor, which, in index notation, has the form $\mathsf{I}_{IJKL} = (1/2)[\delta_{IK}\delta_{JL} + \delta_{IL}\delta_{JK}]$. Note that it is possible to obtain the Cauchy stress tensor by applying the push-forward operation to (4) $\sigma = J^{-1}\chi_*(\mathbf{S})$ (Marsden and Hughes 1994).

Based on the kinematic decomposition of the deformation gradient tensor, the tangent operator, also known as the elasticity tensor when dealing with elastic constitutive laws, is defined in the reference configuration as

$$\begin{aligned} \mathbf{C} &= 2\frac{\partial \mathbf{S}(\mathbf{C}, \mathbf{M}, \mathbf{N})}{\partial \mathbf{C}} = 4\left[\frac{\partial^2 \Psi_{\text{vol}}(J)}{\partial \mathbf{C} \otimes \partial \mathbf{C}} + \frac{\partial^2 \Psi_{\text{ich}}(\bar{\mathbf{C}}, \mathbf{M}, \mathbf{N})}{\partial \mathbf{C} \otimes \partial \mathbf{C}}\right] \\ &= \mathbf{C}_{\text{vol}} + \mathbf{C}_{\text{ich}}. \end{aligned} \tag{5}$$

Note that its spatial counterpart of (5) is obtained from the application of the push-forward operation to (5) $\mathsf{c} = J^{-1}\chi_*(\mathrm{C})$ (Holzapfel 2000).

Since the prosthesis thickness is small, surgical meshes are simplified into a membrane model. In this case, stresses in the direction of the thickness have to be zero. Thus, in order to use a membrane model, the constitutive modelling in 3D for anisotropic materials has to be modified. In this study, the method proposed by Klinkel and Govindjee (2002) is used. The hyperelastic formulation for membrane elements presented in this study was included in the commercial software Abaqus by a UMAT subroutine with the Klinkel and Govindjee algorithm.

To model the membrane behaviour, the code uses a local system of coordinates defined by three vectors. $\mathbf{e}_1$ and $\mathbf{e}_2$ are placed in the membrane plane and $\mathbf{e}_3$ is perpendicular to this plane. These vectors rotate along with the rigid solid and strains are expressed in the local system. The standard deformation gradient $\mathbf{F}$ is expressed as follows:

$$\mathbf{F} = \begin{pmatrix} F_{11} & F_{12} & 0 \\ F_{21} & F_{22} & 0 \\ 0 & 0 & F_{33} \end{pmatrix}. \tag{6}$$

However, in 3D formulation, the C_{33} component of the right Cauchy–Green strain tensor as well as the S_{33} component is not null. The final objective of the algorithm is to ensure $S_{33} = 0$.

In order to start the algorithm, the constitutive 3D law is expressed grouping the second Piola–Kirchhoff stress $\mathbf{S}$ and the elastic tensor $\mathbb{C}$ in null terms ($\mathbf{S}_z = (S_{33}) = 0$) and in non-null terms ($\mathbf{S}_m = (S_{11}, S_{22}, S_{12}, S_{13}, S_{23})^T$):

$$\begin{pmatrix} \mathrm{d}\mathbf{S}_m \\ \mathrm{d}\mathbf{S}_z \end{pmatrix} = \begin{pmatrix} \mathbb{C}_{mm} & \mathbb{C}_{mz} \\ \mathbb{C}_{zm} & \mathbb{C}_{zz} \end{pmatrix} \begin{pmatrix} \mathrm{d}\mathbf{C}_m \\ \mathrm{d}\mathbf{C}_z \end{pmatrix}. \tag{7}$$

Considering Equation (7), $\mathbf{S}_z = 0$ and $\mathbf{C}_z$ is the unknown component in the deformation gradient. The algorithm is developed by means of a Taylor series:

$$\mathbf{S}_z^{(i+1)} = \mathbf{S}_z^{(i)} + \frac{\partial \mathbf{S}_z^{(i)}}{\partial \mathbf{C}_z^{(i)}}\Delta\mathbf{C}_z + \cdots \doteq 0, \tag{8}$$

where the superscript i is the number of the local iteration. In the following iterations, $\mathbf{C}_z$ is modified until the

condition $\mathbf{S}_z = 0$ is reached. Depreciating the high order terms in the Taylor series $\mathbb{C}^i_{zz} = (\partial \mathbf{S}^{(i)}_z / \partial \mathbf{C}^{(i)}_z)$ is obtained. The incremental deformation is:

$$\Delta \mathbf{C}_z = -[\mathbb{C}^i_{zz}]^{-1} \mathbf{S}^{(i)}_z. \tag{9}$$

Thus, in the next iteration, the deformation is expressed as follows:

$$\mathbf{C}^{(i+1)}_z = \mathbb{C}^{(i)}_z + \Delta \mathbf{C}_z. \tag{10}$$

The stiffness tangent matrix $\mathbb{C}^i_{zz}$, used in each iteration in the Newton–Raphson algorithm, should be associated with the variation of $\mathbf{S}_m = 0$ with respect to $\mathbf{C}_m$, but it will depend on the complete deformation state $\mathbf{C}$. In order to obtain the stiffness tangent matrix, considering the imposed stress in the membrane element ($\mathbf{S}_z = (S_{33}) = 0$), it will have to be condensed. If $\mathrm{d}\mathbf{C} = 0$ in the second equation of (7):

$$\mathrm{d}\mathbf{C}_z = -\mathbb{C}^{-1}_{zz} \mathbb{C}_{zm}\, \mathrm{d}\mathbf{C}_m. \tag{11}$$

Inserting (11) in (7):

$$\begin{aligned} \mathrm{d}\mathbf{S}_m &= \mathbb{C}_{psc}\, \mathrm{d}\mathbf{C}_m \quad \text{con} \\ \mathbb{C}_{psc} &= [\mathbb{C}_{mm} - \mathbb{C}_{mz} \mathbb{C}^{-1}_{zz} \mathbb{C}_{zm}], \end{aligned} \tag{12}$$

where $\mathbb{C}_{psc}$ is the stiffness tangent matrix corresponding to the membrane element [for more details of the algorithm, see Klinkel and Govindjee (2002)].

3. Application of the methodologies to the mesh design

With the aim of verifying the defined methods, two surgical meshes were simulated in this study using both the beam and the membrane models. The numerical results were compared with experimental results previously published by Hernández-Gascón et al. (2011). The two non-absorbable, biocompatible surgical meshes simulated were *Surgipro*® (SUR), a HW (84 g/m^2) PP monofile mesh with a small pore size and *Optilene*® (OPT), a LW (48 g/m^2) PP monofile mesh but with a large pore size (see Figure 2). Both are used for abdominal and inguinal hernia repair as well as tissue reinforcement.

3.1 Beam model

For each mesh, the coordinates of multiple points are registered in a python code, and this is processed using the commercial software Abaqus, generating the geometry. As the number of registered points increases, the better geometry is achieved. Nevertheless, the greater the number of points considered, the heavier the FE model becomes.

In Figures 3(b) and 4(b), the unit cells are represented for both surgical meshes, SUR and OPT, and Figures 3(a) and 4(a) show the FE model for each mesh in which four unit cells are linked in order to have a representative area of the surgical mesh. These FE models consisted of 806 nodes and 858 beam elements and of 3148 nodes and 3420 beam elements when simulating SUR and OPT, respectively (see Table 2). The greater amount of nodes and elements for the OPT mesh is justified because the unit cell in OPT has more filaments and its interweave is more complicated (see Figures 3(b) and 4(b)).

Here, symmetry conditions are supposed. Boundary conditions of the FE model mimic the uniaxial test developed in the laboratory. Symmetrical conditions are imposed at two sides of the mesh. On the other edge, the corresponding load or displacement is imposed (see Figures 5–8).

Young's modulus proposed here is different from those values previously reported in the literature (Shackelford 2008). The material of the filaments of both prostheses is PP, and Young's modulus of $E = 300$ MPa was obtained after applying an optimisation method (RQP) and Poisson's coefficient $\nu = 0.36$ was taken from Shackelford (2008).

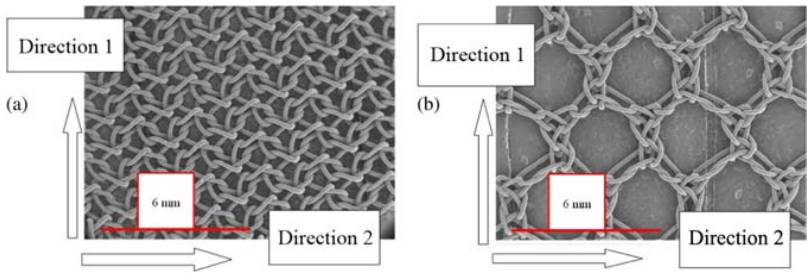

Figure 2. Macroscopic photographs of the two commercial meshes showing the considered Directions 1 and 2. (a) SUR mesh. (b) OPT mesh.

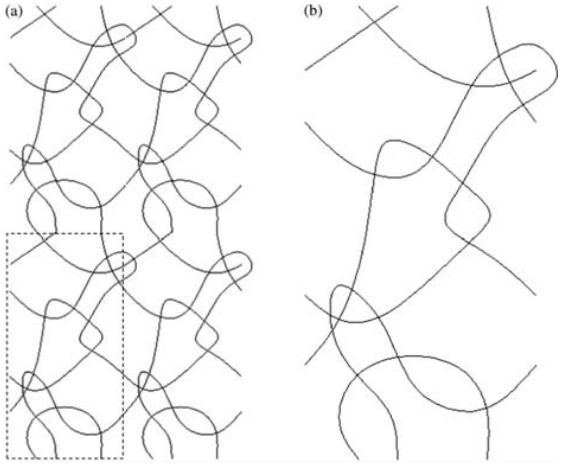

Figure 3. (a) The FE model is formed by four unit cells (2.2 mm × 4.31 mm) (unit cell inside the dotted line). (b) Unit cell from SUR mesh with beam elements (1.1 mm × 2.155 mm).

3.2 Membrane model

The geometry included in the FE model is shown in Figure 10(a) (20 mm × 160 mm). This FE membrane model consists of 165 nodes and 128 membrane elements for both meshes, SUR and OPT.

The material parameters for this method are obtained by defining one strain energy function (SEF) to fit the experimental results. The behaviour of the meshes was reproduced by the following SEF in which the isotropic part was modelled using Demiray's SEF (Demiray et al. 1988) while the anisotropic response was represented by Holzapfel's SEF (Holzapfel et al. 2000) which depends on a preferential direction of anisotropy:

$$\Psi_{\text{ich}} = \Psi_{\text{ich}}^{\text{iso}} + \Psi_{\text{ich}}^{\text{ani}} = \frac{c_1}{c_2}(\exp^{(c_2/2)(\bar{I}_1-3)} - 1) + \frac{c_3}{2c_4}(\exp^{c_4(\bar{I}_4-1)^2} - 1), \tag{13}$$

where $c_1 > 0$ and $c_3 > 0$ are stress-like parameters and $c_2 > 0$ and $c_4 > 0$ are dimensionless parameters (Note: $\Psi_{\text{ich}}^{\text{ani}} = 0$ if $\bar{I}_4 \leq 1$). In Equation (13), only the isochoric part is expressed.

Material parameters were fitted by an iterative process minimising the error between experimental and analytical curves. The value of the thickness of the meshes cannot be measured due to the discontinuous cross-sectional area, where filaments and empty areas exist and are interspersed so that the Cauchy stress ($\sigma_{\text{Cauchy}} = (\text{Force(N)}/\text{Width(mm)}\,\text{Thickness(mm)})\lambda$) cannot be computed. Thus, inside large deformations, force per unit width multiplied by stretch [equivalent Cauchy stress (ECS)] was obtained using the expression (Force(N)/Width(mm))λ, where Force(N) is the load applied during the test. A simple tension test is considered in the direction Y, so $\lambda_y = \lambda$; $\lambda_x = \lambda_z = \lambda^{-1/2}$. The Cauchy stress tensor σ_e becomes diagonal with $\sigma_{yy} = \sigma$; $\sigma_{xx} = \sigma_{zz} = 0$. Experimental data were fitted using the Levenberg–Marquardt minimisation algorithm (Marquardt 1963). This algorithm is based upon minimisation of an objective function, which takes the form represented in Equation (14) for the uniaxial tension test:

$$\chi^2 = \sum_{i=1}^{n} \left[(\text{ECS}^{\text{exp}} - \text{ECS}^{\Psi})_{i1}^2 + (\text{ECS}^{\text{exp}} - \text{ECS}^{\Psi})_{i2}^2\right], \tag{14}$$

where $\text{ECS}_i^{\text{exp}}$ and ECS_i^{Ψ} represent the measured and analytical ECS values for the ith data point, respectively. Subscripts 1 and 2 indicate the Directions 1 and 2 of the test. The quality of data fitting was assessed by calculating the normalised mean square root error $\varepsilon = (\sqrt{(\chi^2/(n-q))}/\mu)$, where q is the number of parameters of the SEF, n is the number of data points, $n - q$ is the number of degrees of freedom and μ is the mean stress defined as $\mu = 1/n\sum_{i=1}^{n}[\text{ECS}]_i$.

The boundary conditions mimic the uniaxial test developed in the laboratory. Displacements are fixed in all directions at the lower clamp and, on the upper side, the corresponding load and displacement are applied (see Section 3.3).

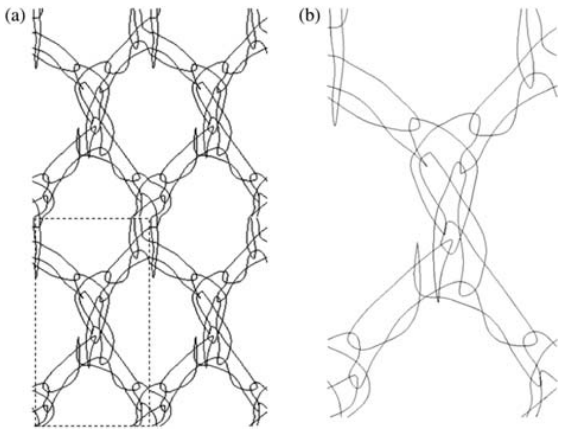

Figure 4. (a) The FE model is formed by four unit cells (5.72 mm × 10.22 mm) (unit cell inside the dotted line). (b) Unit cell from OPT mesh with beam elements (2.86 mm × 5.11 mm).

3.3 Validation of the methodologies by experimental data

Hernández-Gascón et al. (2011) performed uniaxial tests in an INSTRON 5548 microtester with a 50 N load cell

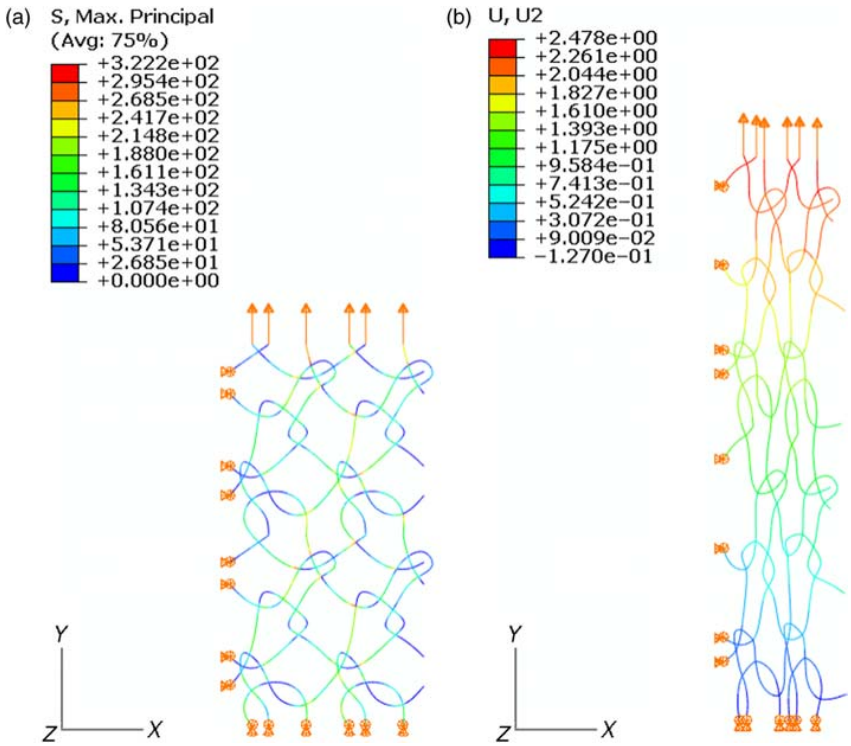

Figure 5. Beam model: FE model of SUR mesh computed in Direction 1 as the arrows indicate. The boundary conditions show the symmetry conditions. (a) MPS in the undeformed shape. (b) Displacements in the deformed shape at 55% of deformation ($\lambda = 1.55$).

using 20 mm × 160 mm samples. Before the test, a preload of 2 N was applied to each sample, and then a displacement rate of 10 mm min^{-1} was maintained until the rupture of the sample. Stretch data were computed as $\lambda = ((L_0 + \Delta L)/L_0)$, where L_0 is the initial distance between the clamps and ΔL is the displacement [see Hernández-Gascón et al. (2011) for further details]. An isotropic mechanical response was observed in SUR, and an anisotropic mechanical response was observed in OPT. Note that for a complete experimental characterisation the lateral contraction has to be measured.

Following the experimental protocol, the FE simulations compute both the preload and the displacement. Computations were conducted for Directions 1 and 2 of the mesh (see Figure 2).

Regarding the beam model, as the size of the FE model is different from the experimental protocol, the applied preload should be proportional to the experimental one depending on the width of the reduced geometry. Experimentally, a preload of 2 N was applied to each sample for which the width was 20 mm. Thus, in the FE simulation, in each node of the clamp where the preload is applied, the value is equal to 0.0366 and 0.0476 N for SUR and OPT, respectively, in Direction 1. In Direction 2, these values are equal to 0.0538 and 0.0638 N for SUR and OPT, respectively.

Figures 5–8 provide the undeformed geometry and the deformed geometry of SUR and OPT meshes computed in both Directions 1 and 2, respectively. The deformed shape shows how the mesh lengthens along the direction of the applied load whereas it becomes narrower in the perpendicular direction, causing the pores to become distorted. The maximal principal stress (MPS) appears in the rigid nodes where the filaments interweave. Since the interweave is considered to be rigid nodes, we conclude that the MPS is higher than in the real case.

The ECS versus stretch curves obtained from the FE simulation are presented in Figure 9 and compared with the experimental results previously reported by Hernández-Gascón et al. (2011). Specifically, the curves are only compared within the physiological range of stretch up to 1.6. The ECS values are computed as the sum of all the reaction forces (in the nodes where the load and displacements are applied) per unit width multiplied by stretch.

In the FE simulation of the OPT mesh, the results for Direction 2 are similar to the experimental results, but those for Direction 1 are slightly less stiff than those for the experimental tests. On the other hand, the curves of the FE simulation of the SUR mesh for Directions 1 and 2 are close to those reported in the experimental tests.

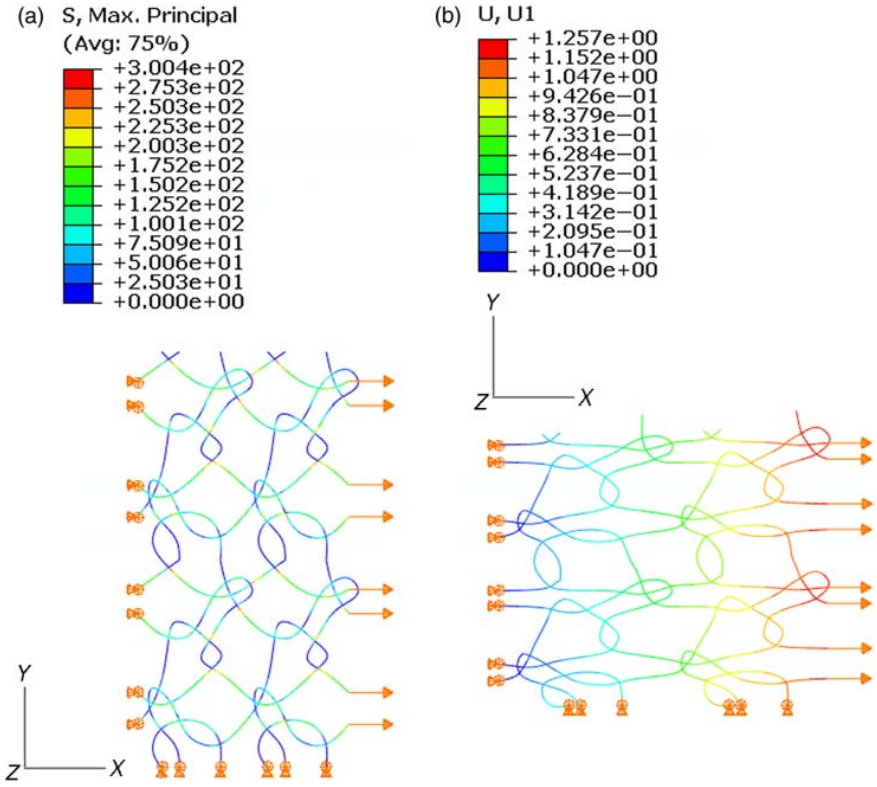

Figure 6. Beam model: FE model of SUR mesh computed in Direction 2 as the arrows indicate. The boundary conditions show the symmetry conditions. (a) MPS in the undeformed shape. (b) Displacements in the deformed shape at 55% of deformation ($\lambda = 1.55$).

Regarding the membrane model, the preload and displacements are applied in the upper clamp (see Figure 10(a)). The necessary load to compute the ECS is that reported in the central node of the upper clamp where the sum of all the reactions from all the upper nodes is included.

With the aim of characterising the material properties, the Demiray SEF, being the isotropic part in Equation (13), was used to model the isotropic behaviour of the SUR mesh. Only one mean plot for one direction (Direction 2) was needed to fit the isotropic response. In contrast, the anisotropic response shown by OPT was reproduced using the Demiray–Holzapfel SEF, Equation (13).

The results of parameter estimations used in the membrane model for all meshes obtained by fitting the experimental curves are shown in Table 1. In all cases, ε values were close to 0 confirming the goodness of fit.

After the FE simulation computed in both directions using the membrane model, in both cases a homogeneous distribution of MPS is appreciated except in the lower clamp where no results are considered. Despite the anisotropic behaviour of the OPT mesh, no tangential deformation appears in the simulations because the preferential direction of transversal isotropy (angle α) is aligned with the direction of the test when simulating Direction 2 and perpendicular to it when computing the response in Direction 1 (see Table 1).

The ECS versus stretch curves obtained from the FE simulation and the experimental curves reported by Hernández-Gascón et al. (2011) are presented in Figure 10. The behaviour of SUR and OPT surgical meshes is mimicked by the FEM because these curves are very close to the experimental curves showing the good agreement of the membrane method.

Focusing on the computational cost, the total CPU time (TCT) needed when simulating SUR mesh with the beam model is 0.8 and 0.7 s for Directions 1 and 2, respectively. However, the TCT is reduced to 0.31 s when applying the membrane model, Table 2. The TCT needed to simulate the OPT mesh with the beam model is equal to 1.5 and 1.6 s for Directions 1 and 2, respectively. These times are five times the TCT needed with the membrane model, for which the TCT is reduced to 0.3 and 0.31 for Directions 1 and 2, respectively, Table 2.

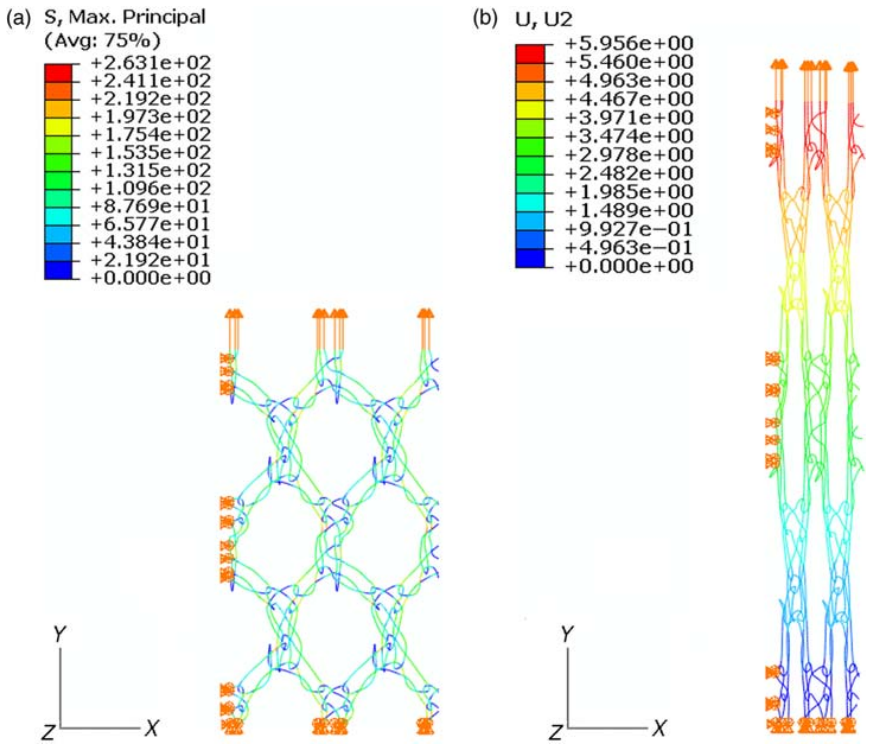

Figure 7. Beam model: FE model of OPT mesh computed in Direction 1 as the arrows indicate. The boundary conditions show the symmetry conditions. (a) MPS in the undeformed shape. (b) Displacements in the deformed shape at 55% of deformation ($\lambda = 1.55$).

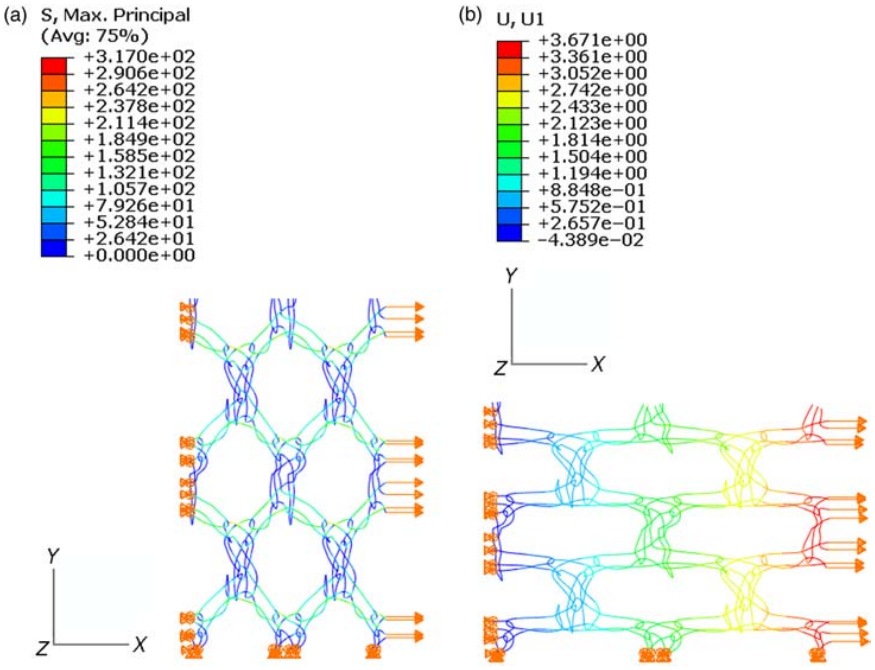

Figure 8. Beam model: FE model of OPT mesh computed in Direction 2 as the arrows indicate. The boundary conditions show the symmetry conditions. (a) MPS in the undeformed shape. (b) Displacements in the deformed shape at 55% of deformation ($\lambda = 1.55$).

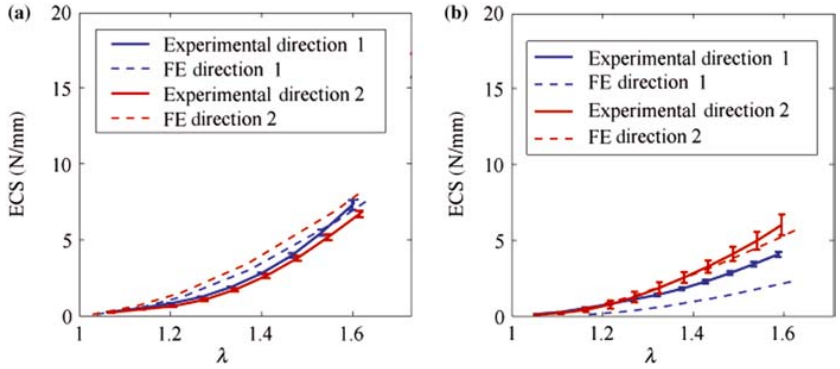

Figure 9. Experimental and FEM results with the beam model. (a) SUR mesh. (b) OPT mesh.

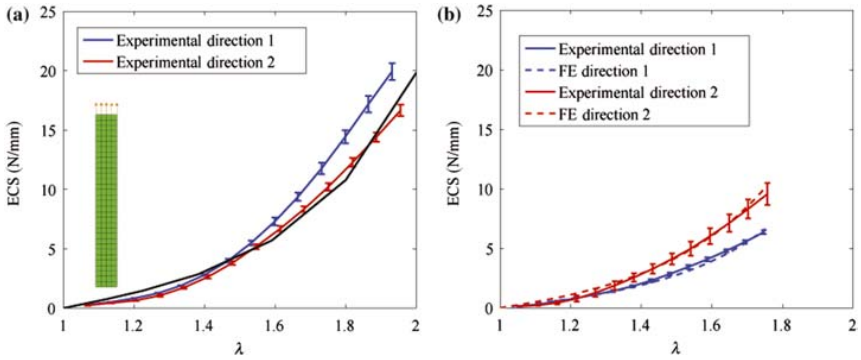

Figure 10. Experimental and FEM results with the membrane model. (a) SUR mesh. The FE model of surgical meshes with M3D4 elements (20 mm × 160 mm) is shown and the applied load in the upper clamp is shown. (b) OPT mesh.

4. Application to modelling hernia surgery

With the aim of simulating a complex model, an FE simulation of a surgical procedure is developed. Specifically, a simplified model that reproduces hernia surgery in a human abdomen is presented.

In order to compare the behaviour of the abdomen before and just after surgery (at time zero without tissue ingrowth), a simplified model of the human abdomen is proposed. The geometry of the model was approximated by an extruded ellipse. A magnetic resonance from a person aged 52 years was used to determine the dimensions of the ellipse. The anteroposterior axis and the lateromedial axis of the ellipse were 175 and 250 mm, respectively, and the length was fixed at 280 mm (length of the human abdomen; Figure 11). Although the abdomen is composed of different muscle layers depending on the area, the simplified model considers a single layer and the thickness of the complete abdomen was taken as 15 mm. Two lids were included at the top and bottom in order to model the abdominal cavity.

Due to the non-existence of experimental data characterising abdominal muscle tissue for humans, properties from an animal model were considered as a first approach. Specifically, properties from rabbits were used according to the procedure of Hernández et al. (2011). The material parameters for the complete thickness in the case of the human abdomen were those fitted in Hernández et al. (2011) for the external oblique layer–internal oblique layer composite muscle layer ($c_1 = 0.16832$ MPa, $c_2 = 0.6319$, $c_3 = 0.01219$ MPa, $c_4 = 5.68158$, $\alpha = 87.8°$). The angle α represents the

Table 1. Material parameters used in the membrane model for the SUR and OPT meshes generated by the fitting procedure (Hernández-Gascón et al. 2011).

	c_1 (MPa)	c_2	c_3 (MPa)	c_4	α (°)	ε
SUR	2.10163	1.17805	–	–	–	0.1467
OPT	1.25112	1.5	0.28	0.03062	0.0	0.0807

Note: The preferential direction of transversal isotropy is defined by the angle α which is referred to as Direction 2.

Table 2. Comparison of the computational cost between the beam and the membrane model.

	FE model	TCT (s)	Nodes	Elements
Beam model	SUR Dir. 1	0.8	806	858
	SUR Dir. 2	0.7		
	OPT Dir. 1	1.5	3148	3420
	OPT Dir. 2	1.6		
Membrane model	SUR Dir. 1	0.31	165	128
	OPT Dir. 1	0.3		
	OPT Dir. 2	0.31		

preferential direction of anisotropy of the muscle tissue, and is referred to as the craneo-caudal direction of the human abdomen. The high angle α means that the craneo-caudal direction of the human is less stiff than the transversal direction (Song et al. 2006). In the FE simulation, the preferential direction of anisotropy for healthy muscle tissue is included at each integration point through a unit vector. The numbers of linear hexahedral elements and nodes were 253,056 and 295,246, respectively.

Regarding the boundary conditions, displacements of the nodes at the back of the abdomen were fixed to simulate the constraints imposed by the shoulders. Besides, an internal pressure of 171 mmHg (23 kPa) was applied to the interior abdominal wall in order to reproduce the abdominal load when jumping (Cobb et al. 2005).

To simulate the surgery, a partial hernia was modelled at the front of the abdomen, at its midlength and adjacent to the linea alba by removing the elements corresponding to the external half of the total thickness (Figure 12(a)). The dimensions of the defect were fixed at 80 mm × 80 mm (Sabbagh et al. 2011). The surgery process was modelled by simulating the SUR and OPT meshes through membrane elements. The thickness of the membrane elements was 1 mm. A total of 292,549 nodes, 250,176 linear hexahedral elements for the abdominal wall and 960 linear quadrilateral membrane elements for the mesh were included. As in the healthy muscle tissue, the preferential direction of anisotropy for the OPT mesh was included at each integration point of the membrane elements through a unit vector. In all cases, Direction 2 of the meshes was coincident with the transversal direction of the abdomen, the perpendicular corresponding to the craneo-caudal direction. The nodes of the meshes were matched with the abdominal nodes in order to model the running sutures used to fix the meshes and the contact between both surfaces.

Regarding the maximum displacements (MDs) in the tissue, these are shown in Figure 13(a),(b) along the lines 1–2 and 3–4 (see Figure 12(b)) at the abdomen front (see Figure 14). After mesh implantation, the MDs are higher than those attained in the healthy abdomen (see Figure 13(a),(b)). This is due to the low stiffness of the abdominal wall in the area of the hernia defect because, in this case, just after mesh implantation, the regeneration process has not yet occurred. Therefore, MDs were affected by mesh implant and, just after mesh implantation, no mesh was able to match the displacements of the abdominal wall.

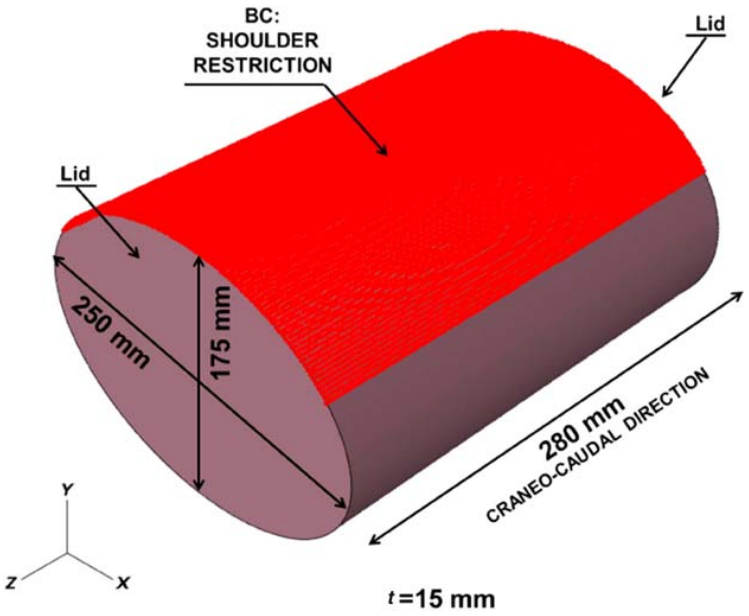

Figure 11. Simplified model of the human abdomen (lying face-down).

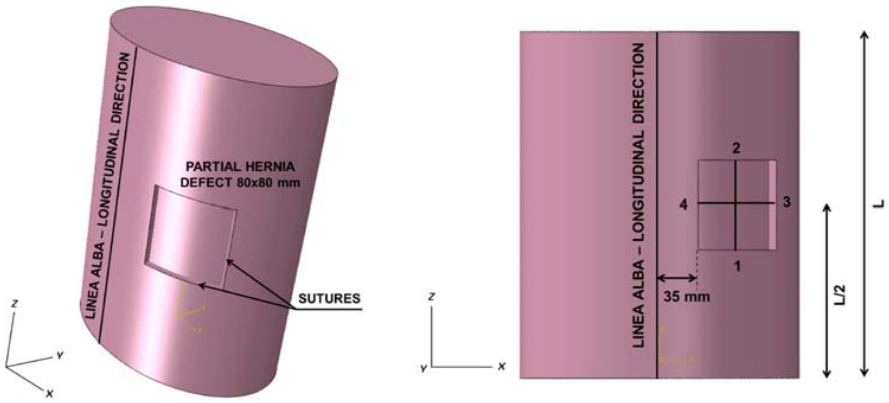

Figure 12. (a) Simplified model of the human abdomen with a partial hernial defect. The figure shows the areas of the model to which the results refer. (b) Lines 1–2 and 3–4, defined for post-processing purpose, are indicated.

Furthermore, the strains were analysed in order to obtain the range of stretching of the abdominal muscle. In the healthy abdomen, the maximal stretch reaches 1.291 whereas this value increases until 1.463 and 1.456 in the abdominal wall when SUR and OPT are placed, respectively. These high stretches take place in the suture zone where the stiffness is very low just after mesh implantation when the regeneration process has not yet occurred. On the other hand, the maximal stretches that appear in the surgical meshes are equal to 1.222 and 1.2335 for SUR and OPT, respectively.

Figure 13(c),(d) shows the MPS in the tissue along the lines 1–2 and 3–4 (see Figure 12(b)). When simulation was conducted for the implanted meshes, the MPS values were always higher than for the healthy abdominal wall. Besides, the SUR mesh provokes a slightly stiffer response on the tissue than the OPT mesh. The high MD previously referred justifies the existence of such high MPS in the

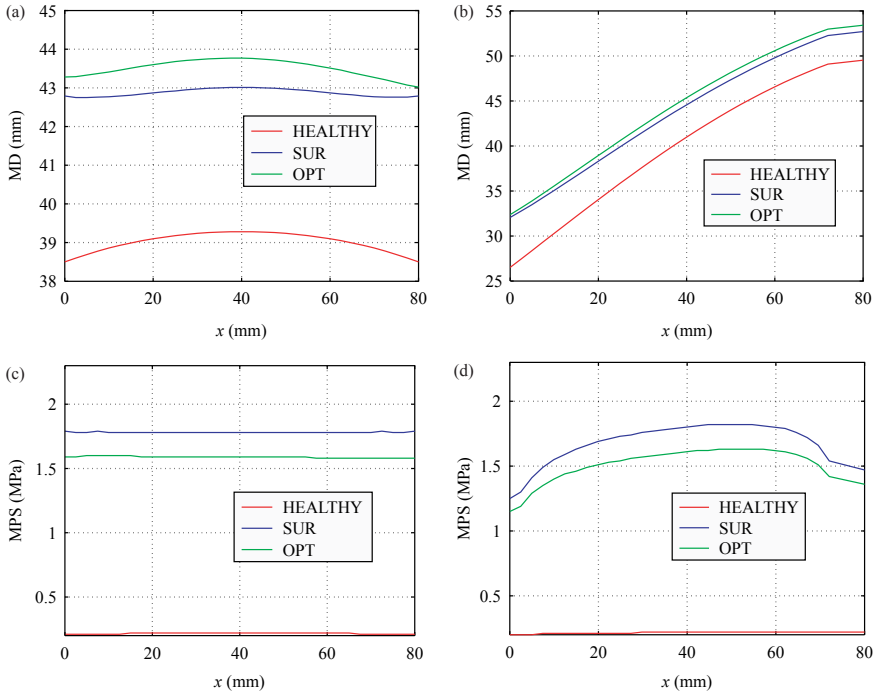

Figure 13. MD along the lines 1–2 (a) and 3–4 (b) (see Figure 12(b)). MPS along the lines 1–2 (c) and 3–4 (d). The abscissa shows the undeformed coordinates of the defect. $x = 0$ and $x = 80$ mm correspond to points 1, 3 and 2, 4 in the undeformed configuration of the abdomen, respectively.

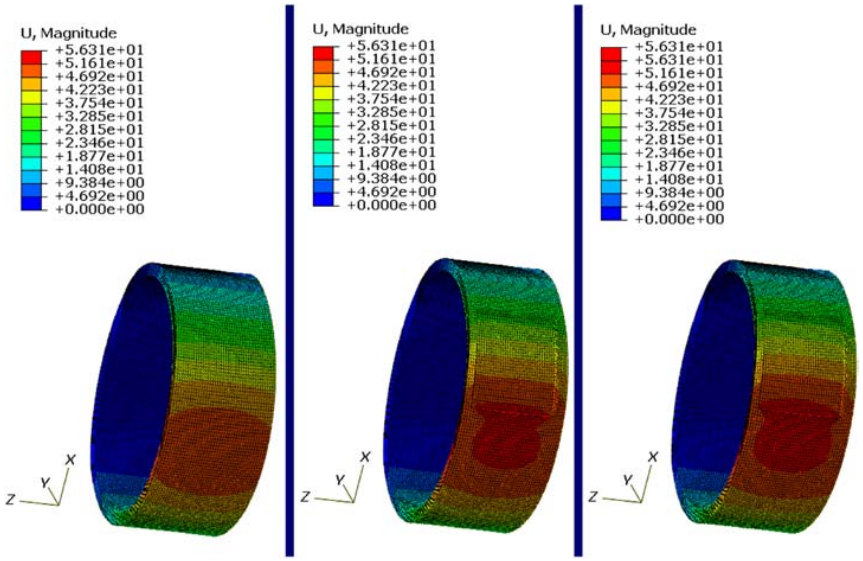

Figure 14. Displacements computed for the hernial defect area. The zones compared are the healthy abdominal wall with no defect (left) and the two implanted meshes, SUR (centre) and OPT (right). Note that only the central section of the model is represented.

area of the hernial defect which undergoes large deformations. Focusing on Figure 15, the MPS in the area of the hernial defect was not evenly distributed. Close to the suture zones, there is a stress concentration due to the discontinuity provoked by the surgical mesh and the large MD that takes place. Thus, stresses provoked by the biomaterial in the tissue were significantly higher (DuBay et al. 2006). This build-up of stress could lead to hernia recurrence in the suture zone.

Therefore, the distribution of stresses is modified when including a surgical mesh in the healthy abdominal wall. This means that the surgical repair procedure does not fully restore normal physiological conditions just after mesh implantation. The results obtained for the FE simulations are consistent with the real situation just after surgery when the area of the hernia defect is still weak and the risk of hernia recurrence is high due to the stress concentration in the sutures. At this point, a good

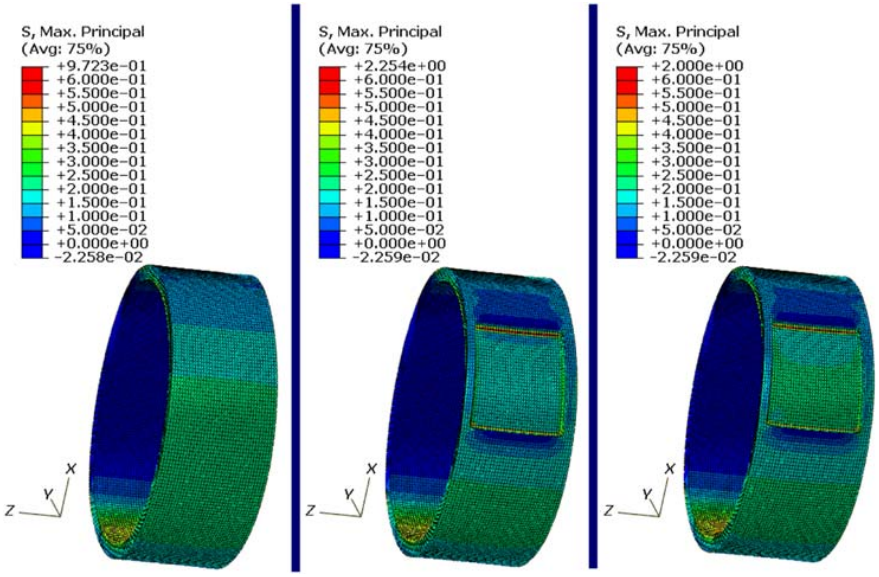

Figure 15. MPS computed for the hernial defect area. The zones compared are the healthy abdominal wall with no defect (left) and the two implanted meshes, SUR (centre) and OPT (right). Note that only the central section of the model is represented.

compliance between the prosthesis and the implant site has not yet been achieved so the patient may suffer discomfort.

5. Conclusions

With the aim of achieving better designs of prostheses for hernia repair, an efficient computational framework is proposed comprising two computational approaches to design surgical meshes. In the first, the beam model is proposed to define the geometry of the unit cell and establish the stiffness of the prosthesis and, in the second, the membrane model is aimed at reducing the geometry and the computational cost to reproduce complex surgical procedures that address patient comfort by means of compliance between the prosthesis and the implant site.

The beam model is based upon the formulation of large displacements for linear elastic materials, whereas the constitutive modelling for the membrane model is described in the context of large deformation hyperelasticity with anisotropy. The validation of both methodologies showed that the results from the FEM agree with the experimental results previously published by Hernández-Gascón et al. (2011).

Focusing on the computational cost, we observed a reduction in the TCT when applying the membrane model. Besides, it is important to remark that the geometries used with both methodologies are different because the beam model only considers four unit cells with symmetry conditions instead of reproducing the real size of the sample. Thus, the TCT is not directly comparable between both. However, these differences give us an idea of how much higher the computational cost would be with the beam model if the complexity of the mesh increases or if more realistic models, such as a human abdomen with a hernia defect, are simulated.

Comparing both approaches, both models are considered useful and complementary. The beam model is a computational tool which helps with the design of new prostheses. With this approach, the stiffness as well as the geometry of the surgical mesh is defined. The geometry of the mesh is fundamental because it determines the tissue ingrowth in the area of the hernia defect and influences the inflammatory response. The main disadvantage of this approach is that the beam model implies a high computational cost due to the high number of nodes and elements that are necessary (see Table 2), whereas the membrane model is more efficient. The latter also enables a prosthesis to be used in more complex geometries from real clinical applications. Regarding the fitting procedure, we can observe in Figure 10 that the strains in the abdomen were 1.291 whereas this value increases until 1.463 and 1.456 in the abdominal wall when SUR and OPT are placed, respectively. So, in the range of the interest the fitting procedure is acceptable for both, SUR and OPT, meshes.

In this study, a simplified model of the human abdomen is presented in order to reproduce the behaviour of a complex geometry. In the FE simulation, the response of the abdomen under internal pressure just after mesh implantation is simulated and the results obtained mimic reality in the sense that the attained tendency is the same as that obtained in real surgery. Thus, the membrane model was validated in order to reproduce surgical procedures within complex models.

Our study is not devoid of certain simplifications. In order to avoid numerical problems and to reduce the computational cost, the first approach has been developed using beam elements instead of truss elements which do not include bending stiffness. Since Young's modulus of the polypropylene is unknown, the first step consists of an optimisation methodology to determine it using the experimental tests for the SUR mesh. After that, this Young's modulus is used to reproduce the behaviour of the OPT mesh and to check whether the FE results mimic the experimental curves. Once these results are validated, this strategy would be used in following new designs in the future. Another approach in which bending stiffness could be progressively adjusted by repeated calculations until a desired value and, at the same time, controlling possible numerical problems, may be used. However, this methodology is less systematic than that proposed in our study. Besides, in the beam model, yarn slip at the crossover points is neglected, where stress concentrations occur. This assumption implies that the crossover points deform in an affine manner with the fabric continuum. Drawing the weave of the mesh is a long process and the greater the precision achieved in the geometry, the higher is the computational cost. Besides, further information from other mechanical tests (e.g. biaxial or shear tests) or other data from the uniaxial test (e.g. lateral contraction) would be useful to complete and validate the computational framework. To mimic the lateral contraction with the proposed methodology, the incompressibility condition would not be enforced and some modifications should be included in the model. Finally, in the last FE simulations, we only studied the surgery just after mesh implantation without taking into account the interaction between tissue and mesh, the tissue regeneration process (Hernández-Gascón et al. 2012).

The computational framework presented in this study starts by applying the beam model to define the geometry of the unit cell and to address the stiffness of the prosthesis comparing the computational results experimentally (see Figure 1). Then, the membrane model may be applied to reproduce complex surgical procedures. Not drawing the exact geometry gives this method a great advantage over the beam model because it is so much easier to generate the FE model. Besides, the number of nodes and elements that are involved as well as the computational cost is minor (see Table 2). At this point, once the compliance between prosthesis and implant site is achieved, the design of a prosthesis can be validated up to the manufacturing stage.

In spite of the limitations, the two proposed models within a computational framework can be used to design and validate the behaviour of new meshes. Both models are sufficiently accurate to guarantee the prediction of reliable displacements and stress distributions using FE computations. Continuum models allow greater computational efficiency and are easily integrated into more complex clinical problems. With the broader aim of developing a validated 3D computational framework to minimise traditional animal studies, which involve long periods of time and are expensive, this paper provides an efficient computational framework including two different models.

Acknowledgements

This study was supported by the Spanish Ministry of Science and Technology through research projects DPI2011-27939-C02-01/IPT-010000-2010-22 and the Instituto de Salud Carlos III (ISCIII) through the CIBER initiative project ABDOMESH. CIBER-BBN is an initiative funded by the VI National R&D&i Plan 2008–2011, Iniciativa Ingenio 2010, Consolider Program, CIBER Actions and financed by the Instituto de Salud Carlos III with assistance from the European Regional Development Fund. B. Hernández-Gascón was funded by a grant (BES-2009-021515) from the Spanish Ministry of Science and Technology.

References

Afonso J, Martins P, Girao M, Natal Jorge R, Ferreira A, Mascarenhas T, Fernandes A, Bernardes J, Baracat E, Rodrigues deLima G, et al. 2008. Mechanical properties of polypropylene mesh used in pelvic floor repair. Int Urogynecol J. 19:375–380.

Bellón JM. 2009. Role of the new lightweight prostheses in improving hernia repair. Cirugía Española. 85(5):268–273.

Cobb WS, Burns JM, Kercher KW, Matthews BD, Norton HJ, Heniford BT. 2005. Normal intraabdominal pressure in healthy adults. J Surg Res. 129:231–235.

Cobb WS, Burns JM, Peindl RD, Carbonell AM, Matthews BD, Kercher KW, Heniford BT. 2006. Textile analysis of heavy-weight, mid-weight and light-weight polypropylene mesh in a porcine ventral hernia model. J Surg Res. 136:1–7.

Demiray H, Weizsacker HW, Pascale K, Erbay H. 1988. A stress-strain relation for a rat abdominal aorta. J Biomech. 21:369–374.

DuBay DA, Wang X, Adamson B, Kuzon WM, Dennis RG, Franz MG. 2006. Mesh incisional herniorrhaphy increases abdominal wall elastic properties: a mechanism for decreased hernia recurrences in comparison with suture repair. Surgery. 140(1):14–24.

Flory PJ. 1961. Thermodynamic relations for high elastic materials. Trans Faraday Soc. 57:829–838.

Grassel D, Prescher A, Fitzed S, Keyserlingk DG, Axer H. 2005. Anisotropy of human linea alba: a biomechanical study. J Surg Res. 124:118–125.

Hernández-Gascón B, Peña E, Melero H, Pascual G, Doblaré M, Ginebra MP, Bellón JM, Calvo B. 2011. Mechanical behaviour of synthetic surgical meshes. Finite element simulation of the herniated abdominal wall. Acta Biomater. 7:3905–3913.

Hernández-Gascón B, Peña E, Pascual G, Rodríguez M, Bellón JM, Calvo B. 2012. Long-term anisotropic mechanical response of surgical meshes used to repair abdominal wall defects. J Mech Behav Biomed Mater. 5:257–271.

Hernández B, Peña E, Pascual G, Rodriguez M, Calvo B, Doblaré M, Bellón JM. 2011. Mechanical and histological characterization of the abdominal muscle. A previous step to model hernia surgery. J Mech Behav Biomed Mater. 4:392–404.

Hibbit, Karlsson and Sorensen, Inc. 2008. Abaqus user's guide, v. 6.9. Pawtucket, RI: HKS Inc.

Holzapfel GA. 2000. Nonlinear solid mechanics. New York: Wiley.

Holzapfel GA, Gasser TC, Ogden RW. 2000. A new constitutive framework for arterial wall mechanics and a comparative study of material models. J Elasticity. 61:1–48.

Junge K, Klinge U, Prescher A, Giboni P, Niewiera M, Shumpelick V. 2001. Elasticity of the anterior abdominal wall and impact for reparation of incisional hernia using mesh implants. Hernia. 5:112–118.

King MJ, Jearanaisilawong P, Socrate S. 2005. A continuum constitutive model for the mechanical behavior of woven fabrics. Int J Solids Struct. 42:3867–3896.

Klinge U. 2007. Experimental comparison of monofile light and heavy polypropylene meshes: less weight does not mean less biological response. World J Surg. 31:867–868.

Klinkel S, Govindjee S. 2002. Using finite strain 3D-material models in beam and shell elements. Eng Comput. 19(8):902–921.

Lichtenstein IL, Shulman AG. 1986. Ambulatory outpatient hernia surgery including a new concept, introducing tension-free repair. Int Surg. 71:1–4.

Lichtenstein IL, Shulman AG, Amid PK, Montlor MM. 1989. The tension-free hernioplasty. Am J Surg. 157:188–193.

Marquardt DW. 1963. An algorithm for least-squares estimation of nonlinear parameters. SIAM J Appl Math. 11:431–441.

Marsden JE, Hughes TJR. 1994. Mathematical foundations of elasticity. New York: Dover.

Pandit AS, Henry JA. 2004. Design of surgical meshes – an engineering perspective. Technol Health Care. 12:51–65.

Pascual G, Rodríguez M, Gómez-Gil V, García-Honduvilla N, Buján J, Bellón JM. 2008. Early tissue incorporation and collagen deposition in lightweight polypropylene meshes: bioassay in an experimental model of ventral hernia. Surgery. 144:427–435.

Sabbagh C, Dumont F, Robert B, Badaoui R, Verhaeghe P, Regimbeau JM. 2011. Peritoneal volume is predictive of tension-free fascia closure of large incisional hernias with loss of domain: a prospective study. Hernia. 15(5):559–565.

Shackelford JF. 2008. Introduction to materials science for engineers. University of California, Davis: Prentice Hall.

Simo JC, Taylor RL. 1991. Quasi-incompresible finite elasticity in principal stretches. Continuum basis and numerical algorithms. Comput Methods Appl Mech Eng. 85:273–310.

Simo JC, Taylor RL, Pister KS. 1985. Variational and projection methods for the volume constraint in finite deformation elasto-plasticity. Comput Methods Appl Mech Eng. 51:177–208.

Song C, Alijani A, Frank T, Hanna G, Cuschieri A. 2006. Mechanical properties of the human abdominal wall measured in vivo during insufflation for laparoscopic surgery. Surg Endos. 20:987–990.

Spencer AJM. 1971. Theory of invariants. In: Continuum physics. New York: Academic Press. p. 239–253.

Timoshenko S, Goodier JN. 1972. Teoría de la Elasticidad. Bilbao: Editorial Urmo.

Work 6: Modelado numérico del comportamiento del tejido músculo esquelético (*Numerical simulation of the behaviour of musculoskeletal tissue)*

Journal: *Revista Internacional de Métodos Numéricos para Cálculo y Diseño en Ingeniería*, **28**(3) (2012): 177-186.
Journal impact factor: 0.167

Rev. int. métodos numér. cálc. diseño ing. 2012;**28(3)**:177–186

Revista Internacional de Métodos Numéricos para Cálculo y Diseño en Ingeniería

www.elsevier.es/rimni

Modelado numérico del comportamiento del tejido músculo-esquelético

J. Grasa*, B. Hernández-Gascón, A. Ramírez, J.F. Rodríguez y B. Calvo

Instituto de Investigación en Ingeniería de Aragón (I3A), Universidad de Zaragoza, Ed. Betancourt, C/ María de Luna s/n, 50018, Zaragoza, Spain

INFORMACIÓN DEL ARTÍCULO

Historia del artículo:
Recibido el 8 de junio de 2011
Aceptado el 3 de febrero de 2012
On-line el 3 de julio de 2012

Palabras clave:
Elementos finitos
Tejido músculo-esquelético
Comportamiento activo y pasivo

R E S U M E N

En este trabajo se muestra un modelo computacional tridimensional para la simulación del comportamiento mecánico de la unidad músculo tendón (UMT). El modelo ha sido formulado a través de una función densidad energía de deformación para materiales hiperelásticos que incorpora tanto el comportamiento pasivo de los tejidos conectivos como el activo, considerando para ambos casos direcciones de comportamiento preferencial no necesariamente coincidentes en el espacio. Las tensiones iniciales, presentes habitualmente en tejidos blandos, han sido implementadas mediante la definición de un gradiente de deformación para llevar a cabo la simulación de la UMT. El modelo se ha particularizado para un modelo de experimentación animal. La geometría utilizada se corresponde con la del músculo tibial anterior de rata reconstruido a partir de imagen médica procedente de resonancia magnética obtenida «*in-vivo*». También se estudia el efecto que sobre el comportamiento pasivo ejerce la fascia ajustando un modelo de comportamiento hiperelástico para la misma a partir de ensayos experimentales.

Numerical simulation of the behaviour of musculoskeletal tissue

Keywords:
Finite elements
Musculoskeletal tissue
Active and passive behavior

A B S T R A C T

This paper presents a three dimensional computational model to simulate the mechanical behavior of the muscle-tendon unit (MTU). The model has been formulated through a strain energy density function for hyperelastic materials incorporating both the passive and active behavior of the connective tissues, and taking into account preferential directions for both behaviours, not necessarily coincident. The initial stresses, usually present in soft tissues, have been considered when performing the MTU simulation. The geometry used corresponds to the rat tibialis anterior muscle reconstructed from «*in-vivo*» magnetic resonance images. This paper also studies the effect of the fascia on the MTU passive behaviour and the setting of a hyperelastic model for this tissue by means of experimental tests.

1. Introducción

El tejido músculo-esquelético es un tejido biológico blando responsable, fundamentalmente, del movimiento del cuerpo y de mantener la postura corporal. El cuerpo humano contiene aproximadamente 650 músculos, con formas diferentes en función del tipo de movimiento, representando aproximadamente el 40% del peso corporal [1]. Cada uno de estos músculos puede ser considerado como un conjunto de fibras musculares (elemento contractil) rodeadas, en diferentes niveles, por tejido conectivo (elemento elástico) que, de forma pasiva, es el responsable de absorber los alargamientos del músculo. Es bien sabido además que, las fibras musculares también contribuyen al comportamiento pasivo (elemento elástico en serie) [2,3]. El tejido conectivo está constituido por fibras de colágeno y elastina embebidas en la sustancia fundamental y organizadas en tres niveles, el epimisio, perimisio y endomisio, que juegan un papel importante en la transmisión lateral de las fuerzas generadas por las fibras y, a través de los cuales, se distribuyen los vasos sanguíneos y ramificaciones nerviosas.

Los recientes avances en la adquisición de imágenes, en la caracterización experimental de los tejidos biológicos y en el desarrollo de nuevos algoritmos de comportamiento han permitido el desarrollo de modelos 3D que permiten obtener el campo de tensiones y deformaciones en el interior de los tejidos vivos. En la mayoría de las ocasiones, la construcción de dichos modelos lleva asociada la adopción de hipótesis simplificativas, por ejemplo, las

* Autor para correspondencia.
Correo electrónico: jgrasa@unizar.es (J. Grasa).

0213-1315/$ – see front matter © 2011 CIMNE (Universitat Politècnica de Catalunya). Publicado por Elsevier España, S.L. Todos los derechos reservados.
doi:10.1016/j.rimni.2012.03.005

propiedades mecánicas se determinan mediante ensayos «*in-vitro*» [4,5], o se combinan parámetros de diferentes tejidos [6], o bien se adoptan geometrías idealizadas [7–11], lo que hace difícil validar los resultados obtenidos y por lo tanto poder extrapolar los resultados numéricos a estudios clínicos.

Con el objetivo de minimizar las posibles causas de error atribuidas a las simplificaciones anteriores, en este trabajo se presenta el modelado del músculo tibial anterior (TA) de rata, partiendo de imagen procedente de resonancia magnética (RM). Se ha utilizado un modelo de comportamiento hiperelástico anisótropo capaz de reproducir la respuesta pasiva y activa del músculo partiendo de los resultados experimentales. También se han incorporado las deformaciones iniciales habituales en los tejidos blandos [12,13]. El modelo parte de la caracterización experimental, tanto activa como pasiva de la UMT llevada a cabo por los autores en trabajos previos [14–16].

Los resultados obtenidos en la simulación son validados con los resultados experimentales procedentes de ensayos uniaxiales a tracción «*in-vivo*» de la UTM, en el caso del comportamiento pasivo [14], y de la estimulación eléctrica en condiciones isométricas, en el caso activo [15].

2. Modelo matemático

En este apartado se resumen las ecuaciones que definen el modelo de comportamiento hiperelástico anisótropo habitualmente empleado en la simulación de tejidos biológicos blandos, dentro siempre del dominio elástico. Dicho modelo estructural se plantea en el marco de la mecánica del continuo no lineal y teniendo en cuenta la posibilidad de ser incorporado en un código de elementos finitos.

2.1. Definición de la deformación

Se entiende por sólido tridimensional, Ω_o, a un subconjunto de $\mathbb{R}^3$ cuyos puntos se identifican mediante sus coordenadas en un sistema de referencia. Matemáticamente, podemos interpretar lo anterior a través de una función biunívoca de tres componentes $\boldsymbol{\varphi_o}$ aplicada sobre el sólido Ω_o tal que, a cada punto $\boldsymbol{P} \in \Omega_o$, adscribe tres valores que corresponden a las coordenadas de dicho punto $\boldsymbol{P}$ en el sistema de referencia elegido, es decir:

$$\boldsymbol{\varphi}_o : \Omega_o \to \mathbb{R}^3 \quad \boldsymbol{\varphi}_o \equiv \mathbf{X}; \qquad \varphi_o^I = X^I \tag{1}$$

A $\boldsymbol{\varphi_o}$ la denominaremos *configuración inicial del sólido* Ω_0, *configuración de referencia* o *configuración indeformada*. A lo largo del movimiento del sólido, la posición de cada uno de los puntos del mismo va variando. La configuración correspondiente define las coordenadas de los puntos del sólido en ese instante Ω_t respecto a un sistema de referencia (que en general también puede variar con el tiempo) a través de una expresión similar a (1), es decir:

$$\begin{aligned} &\boldsymbol{\varphi}_t : \Omega_t \to \mathbb{R}^3 \quad \boldsymbol{\varphi}_t \equiv \mathbf{x}; \\ &\boldsymbol{\varphi}_t^I = x^i \quad \text{con} \quad t \in \mathbb{I} \in \mathbb{R} \end{aligned} \tag{2}$$

A $\boldsymbol{\varphi}_t$ la denominaremos *configuración actual del sólido* Ω_t o *configuración deformada*.

Dado un movimiento $\boldsymbol{\varphi_t} : \Omega_t \to \mathbb{R}^3 \quad C^1-regular$, se define el gradiente de deformación $\mathbf{F}$, como el campo tensorial sobre la configuración indeformada $\boldsymbol{\varphi}_o(\Omega)$, $\mathbf{F} = \frac{\partial \mathbf{x}}{\partial \mathbf{X}}$, siendo $J \equiv det\mathbf{F} > 0$ el jacobiano de la transformación.

Una de las características más relevantes de los tejidos biológicos blandos, en general, y del músculo en particular, es la *incompresibilidad*. Esta indica que el cuerpo al ser sometido a fuerzas o deformaciones no presenta un cambio de volumen, lo que se representa matemáticamente como que el jacobiano del gradiente de deformación es igual a la unidad, $J \cong 1$. Siguiendo a [17], definimos la siguiente descomposición multiplicativa del gradiente de deformación:

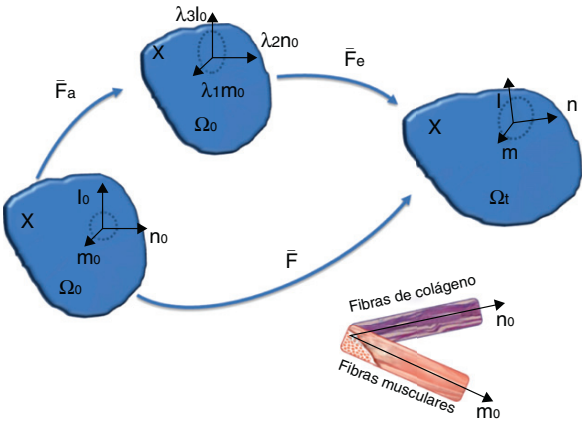

Figura 1. Esquema de la deformación pasiva y activa [18]. Sobre el punto $\mathbf{X}$ de la configuración indeformada Ω_0, consideramos dos direcciones preferenciales definidas por $\mathbf{m}_0$ y $\mathbf{n}_0$. Esta configuración se transforma en la misma dirección por la contracción activa $\bar{\mathbf{F}}_a$, donde los nuevos vectores serán $\lambda_1\mathbf{m}_0$, $\lambda_2\mathbf{n}_0$ y $\lambda_3\mathbf{l}_0$. La deformación elástica transforma esta configuración intermedia activa a la configuración deformada Ω_t por medio del gradiente de deformación $\bar{\mathbf{F}}_e$.

$$\mathbf{F} = J^{\frac{1}{3}}\bar{\mathbf{F}}, \qquad \bar{\mathbf{F}} = J^{-\frac{1}{3}}\mathbf{F} \tag{3}$$

$$\mathbf{C} = \mathbf{F}^T\mathbf{F}, \qquad \bar{\mathbf{C}} = J^{-\frac{2}{3}}\mathbf{C} = \bar{\mathbf{F}}^T\bar{\mathbf{F}} \tag{4}$$

$$\mathbf{b} = \mathbf{F}\mathbf{F}^T, \qquad \bar{\mathbf{b}} = J^{-\frac{2}{3}}\mathbf{b} = \bar{\mathbf{F}}\bar{\mathbf{F}}^T \tag{5}$$

el término $J^{\frac{1}{3}}\mathbf{I}$ representa la deformación volumétrica y $\bar{\mathbf{F}}$ la deformación desviadora. Denotamos por $\bar{\mathbf{F}}$, $\bar{\mathbf{C}}$ y $\bar{\mathbf{b}}$ al gradiente de deformación y los tensores de deformación de Cauchy-Green por la derecha e izquierda modificados, respectivamente.

La anisotropía del material en un punto $\mathbf{X} \in \Omega_0$, va asociada a la dirección de la fibras musculares, en el caso del comportamiento activo, y a la dirección de las fibras de colágeno en el caso del comportamiento pasivo. En los músculos fusiformes como es el caso del TA, la dirección de anisotropía coincide para ambos comportamientos, es decir, el comportamiento preferencial pasivo coincide con la dirección de las fibras musculares, pero no es así en músculos planos, como pueden ser los de la pared abdominal [5]. Por tanto, en una situación general, se puede partir de la hipótesis de que la dirección de anisotropía, asociada al comportamiento activo, se define por un vector unitario $\mathbf{m}_0(\mathbf{X})$, y la asociada al comportamiento pasivo mediante el vector $\mathbf{n}_0(\mathbf{X})$, con $|\mathbf{m}_0| = 1$, $|\mathbf{n}_0| = 1$. Definimos la base $\mathbf{E}_i = (\mathbf{m}_0, \mathbf{n}_0, \mathbf{l}_0)$, donde el vector $\mathbf{l}_0 = \mathbf{m}_0 \otimes \mathbf{n}_0$ está fuera del plano formado por los otros dos vectores.

La deformación asociada a la actividad muscular (ver figura 1) se puede modelar mediante un proceso ficticio de dos pasos [18]: el primero de ellos asociado al desplazamiento relativo de las proteínas actina y miosina y, el segundo, a una deformación elástica asociada a los puentes cruzados y a la titina. Esto puede ser expresado mediante una descomposición multiplicativa de $\bar{\mathbf{F}}$ [18]:

$$\bar{\mathbf{F}} = \bar{\mathbf{F}}_e\bar{\mathbf{F}}_a \tag{6}$$

donde $\bar{\mathbf{F}}_a$ representa la deformación asociada a la contracción muscular por el movimiento relativo de los filamentos de actina y miosina y $\bar{\mathbf{F}}_e$ representa la deformación elástica asociada a los puentes cruzados y a la titina. El tensor $\bar{\mathbf{F}}_a$ no corresponde a una transformación integrable, partes infinitesimales de Ω_0 se deforman de manera independiente y su unión puede dar lugar a configuraciones no compatibles. El tensor $\bar{\mathbf{F}}_e$ representa

la deformación elástica y garantiza la compatibilidad de la nueva configuración.

Si las fibras musculares se contraen en la dirección definida por el vector de comportamiento preferencial $\mathbf{m}_0$ y se supone que dicha dirección no cambia, el tensor de contracción activo vendrá dado por:

$$\bar{\mathbf{F}}_a = \bar{\lambda}_1 \mathbf{e}_1 \otimes \mathbf{E}_1 + \bar{\lambda}_2 \mathbf{e}_2 \otimes \mathbf{E}_2 + \bar{\lambda}_3 \mathbf{e}_3 \otimes \mathbf{E}_3 \tag{7}$$

donde los vectores $\mathbf{E}_i$ forman una base dual a $\mathbf{e}_i$ definida como $\mathbf{e}_i \cdot \mathbf{E}_j = \delta_{ij}$ con δ_{ij} la delta de Kronecker. $\bar{\lambda}_1 = \bar{\lambda}_a$ y el valor de $\bar{\lambda}_2 = \bar{\lambda}_3$ se determina al considerar el material incompresible.

$$det\bar{\mathbf{F}}_a = 1 = \bar{\lambda}_1 \bar{\lambda}_2 \bar{\lambda}_3 \tag{8}$$

Sustituyendo los valores de $\bar{\lambda}_2$ y $\bar{\lambda}_3$ obtenidos al aplicar (8), la ecuación (7) se reduce a:

$$\bar{\mathbf{F}}_a = \bar{\lambda}_a \mathbf{e}_1 \otimes \mathbf{E}_1 + \bar{\lambda}_a^{-1/2} \mathbf{e}_2 \otimes \mathbf{E}_2 + \bar{\lambda}_a^{-1/2} \mathbf{e}_3 \otimes \mathbf{E}_3 \tag{9}$$

el tensor de contracción sólo depende del alargamiento de contracción $\bar{\lambda}_a$. Aplicando la regla de la cadena, la variación de $\bar{\mathbf{F}}_a$ con respecto al tiempo (9) viene dada como:

$$\dot{\bar{\mathbf{F}}}_a = \frac{\partial \bar{\mathbf{F}}_a}{\partial \bar{\lambda}_a} \dot{\bar{\lambda}}_a \tag{10}$$

donde $\dot{\bar{\lambda}}_a$ es la velocidad de contracción en la dirección de comportamiento preferencial que debe ser conocida y $\frac{\partial \bar{\mathbf{F}}_a}{\partial \bar{\lambda}_a}$ puede obtenerse como:

$$\frac{\partial \bar{\mathbf{F}}_a}{\partial \bar{\lambda}_a} = \mathbf{e}_1 \otimes \mathbf{E}_1 - \frac{1}{2}\bar{\lambda}_a^{-3/2} \mathbf{e}_2 \otimes \mathbf{E}_2 - \frac{1}{2}\bar{\lambda}_a^{-3/2} \mathbf{e}_3 \otimes \mathbf{E}_3 \tag{11}$$

Se supone que las fibras de colágeno se mueven de forma conjunta con la matriz extracelular, por lo que, el alargamiento $\bar{\lambda}$ es definido como la relación entre las longitudes de las fibras en las configuraciones deformada y de referencia, es decir:

$$\begin{aligned} &\bar{\lambda}\mathbf{n}(\mathbf{x}, t) = \bar{\mathbf{F}}(X, t)\mathbf{n}_0(\mathbf{X}) \\ &\bar{\lambda}^2 = \mathbf{n}_0 . \bar{\mathbf{F}}^T \bar{\mathbf{F}} . \mathbf{n}_0 = \mathbf{n}_0 . \bar{\mathbf{C}} . \mathbf{n}_0 \end{aligned} \tag{12}$$

donde $\bar{\mathbf{C}} = \bar{\mathbf{F}}^T \bar{\mathbf{F}}$ es el tensor de deformación de Cauchy-Green por la derecha modificado. Podemos definir $\bar{\mathbf{C}}_e = \bar{\mathbf{F}}_e^T \bar{\mathbf{F}}_e = \bar{\mathbf{F}}_a^{-T} \bar{\mathbf{C}} \bar{\mathbf{F}}_a^{-1}$ como la medida de deformación de los puentes cruzados y la titina (no es una variable de estado ya que depende de $\bar{\mathbf{C}}$ y $\bar{\lambda}_a$), $\mathbf{m}$ y $\mathbf{n}$ son los vectores unitarios que definen la dirección de comportamiento preferencial (asociada a las fibras musculares y de colágeno, respectivamente) en la configuración deformada (fig. 1).

2.2. Respuesta tensional hiperelástica

Para caracterizar un proceso isotermo en materiales reversibles sin disipación de energía, se suele postular la existencia de una única representación de la función densidad energía de deformación Ψ [19], en este caso, expresada de forma desacoplada como suma de la energía volumétrica y desviadora, para evitar los problemas de incompresibilidad, empleando en la hipótesis cinemática (3) y siguiendo a [20]. A su vez, para el tejido muscular, la energía de deformación desviadora se puede expresar de forma aditiva como la energía pasiva almacenada en el tejido y asociada principalmente al colágeno y elástina, $\bar{\Psi}_p$, más la energía almacenada en la fibra muscular, que denominaremos energía activa, $\bar{\Psi}_a$. La energía almacenada dependerá de $\mathbf{F}$ y de las variables de estado $\bar{\lambda}_a$, β y de los tensores estructurales $\mathbf{M}$, $\mathbf{N}$ definidos como $\mathbf{M} = \mathbf{m}_0 \otimes \mathbf{m}_0$ y $\mathbf{N} = \mathbf{n}_0 \otimes \mathbf{n}_0$:

$$\Psi = \Psi_{vol}(J) + \bar{\Psi}_p(\bar{\mathbf{C}}, \mathbf{N}) + \bar{\Psi}_a(\bar{\mathbf{C}}_e, \bar{\lambda}_a, \mathbf{M}, \beta) \tag{13}$$

con Ψ_{vol}, $\bar{\Psi}_p$ y $\bar{\Psi}_a$ las partes volumétrica y desviadora asociadas a las componentes pasiva y activa, respectivamente, de la función densidad de energía de deformación. El tensor $\bar{\mathbf{C}}_e$ no es una variable de estado ya que depende de $\bar{\mathbf{C}}$ y $\bar{\lambda}_a$, pero es necesario para formular la energía libre. β representa el nivel de activación con el tiempo o, lo que es lo mismo, la variación de la fuerza activa generada con el tiempo.

La función densidad energía de deformación Ψ puede expresarse en función de los invariantes definidos por:

$$\begin{aligned} &\bar{I}_1 = tr\bar{\mathbf{C}}, \qquad \bar{I}_2 = \frac{1}{2}((tr\bar{\mathbf{C}})^2 - tr\bar{\mathbf{C}}^2) \\ &\bar{I}_4 = \mathbf{n}_0 . \bar{\mathbf{C}} \mathbf{n}_0, \qquad \bar{I}_5 = \mathbf{n}_0 . \bar{\mathbf{C}}^2 . \mathbf{n}_0 \end{aligned} \tag{14}$$

$\bar{I}_1$ y $\bar{I}_2$ son el primer y segundo invariante de $\bar{\mathbf{C}}$ y los pseudo-invariantes $\bar{I}_4, \bar{I}_5$ caracterizan la anisotropía asociada al comportamiento pasivo. $\bar{I}_4$ tiene un claro significado físico ya que se define como el alargamiento de la fibras de colágeno al cuadrado e $\bar{I}_5$ está asociado a la deformación transversal de las fibras de colágeno. De forma análoga se definirán los pseudo-invariantes asociados a las fibras musculares, donde el tensor de deformación $\bar{\mathbf{C}}$ se ha sustituido por $\bar{\mathbf{C}}_e$:

$$\bar{J}_4 = \mathbf{m}_0 . \bar{\mathbf{C}}_e \mathbf{m}_0, \qquad \bar{J}_5 = \mathbf{m}_0 . \bar{\mathbf{C}}_e^2 . \mathbf{m}_0 \tag{15}$$

Es norma habitual en biomecánica omitir la dependencia de la función Ψ de los invariantes $\bar{I}_5, \bar{J}_5$, como consecuencia de la fuerte correlación de $\bar{I}_5$ con $\bar{I}_4$ y de $\bar{J}_5$ con $\bar{J}_4$ [21]. Con lo cual se consigue disminuir el número de parámetros del material y, por lo tanto, facilitar el ajuste a los resultados experimentales. Adicionalmente, los invariantes $\bar{I}_4$ y $\bar{J}_4$ poseen una clara interpretación física. En lo que sigue, se planteará la formulación únicamente considerando los invariantes $\bar{I}_4$ y $\bar{J}_4$, con lo que la ecuación (13) vendrá dada como:

$$\Psi = \Psi_{vol}(J) + \bar{\Psi}_p(\bar{I}_1, \bar{I}_2, \bar{I}_4) + \bar{\Psi}_a(\bar{J}_4, \bar{\lambda}_a, \beta) \tag{16}$$

La respuesta en tensiones se puede obtener a partir de la Ψ teniendo en cuenta la desigualdad de Clausius-Planck:

$$\mathcal{D}_{int} = -\dot{\Psi} + \frac{1}{2}\mathbf{S} : \dot{\mathbf{C}} + S_a \dot{\bar{\lambda}}_a + S_c \dot{\beta} \geq 0 \tag{17}$$

siendo S_a la tensión generada por el golpe de fuerza en los puentes cruzados y S_c por la variación del impulso en el tiempo. Teniendo en cuenta las ecuaciones (16) y (17) se obtiene:

$$\begin{aligned} &\left(\frac{1}{2}\mathbf{S} - \frac{\partial \Psi}{\partial \bar{\mathbf{C}}}\right) : \dot{\mathbf{C}} - \frac{\partial \Psi}{\partial \bar{\mathbf{C}}_e} : \dot{\mathbf{C}}_e \\ &+ \left(S_a - \frac{\partial \Psi}{\partial \bar{\lambda}_a}\right) \dot{\bar{\lambda}}_a + \left(S_c - \frac{\partial \Psi}{\partial \beta}\right) \dot{\beta} \geq 0 \end{aligned} \tag{18}$$

Si suponemos que el primer término de la ecuación (18) no depende de $\dot{\bar{\lambda}}_a$ y $\dot{\beta}$, el segundo tensor de tensiones de Piola-Kirchhoff vendrá dado por:

$$\begin{aligned} \mathbf{S} &= 2\frac{\partial \Psi}{\partial \mathbf{C}} \\ &= \mathbf{S}_{vol} + \bar{\mathbf{S}}_p + \bar{\mathbf{S}}_a \\ &= Jp\mathbf{C}^{-1} + J^{-\frac{2}{3}}(\mathbb{I} - 1/3\mathbf{C}^{-1} \otimes \mathbf{C}) : (\tilde{\mathbf{S}}_p) \\ &+ \bar{\mathbf{F}}_a^{-1}(J^{-\frac{2}{3}}(\mathbb{I} - 1/3\mathbf{C}_e^{-1} \otimes \mathbf{C}_e) : (\tilde{\mathbf{S}}_a))\bar{\mathbf{F}}_a^{-T} \\ &= Jp\mathbf{C}^{-1} + J^{-\frac{2}{3}} DEV[\tilde{\mathbf{S}}_p] + \bar{\mathbf{F}}_a^{-1}(J^{-\frac{2}{3}} DEV_e[\tilde{\mathbf{S}}_a])\bar{\mathbf{F}}_a^{-T} \end{aligned} \tag{19}$$

con:

$$p = \frac{d\Psi_{vol}(J)}{dJ}$$
$$\tilde{\mathbf{S}}_p = 2\frac{\partial\overline{\Psi}(\bar{I}_1,\bar{I}_2,\bar{I}_4)}{\partial\overline{\mathbf{C}}} \quad \tilde{\mathbf{S}}_a = 2\frac{\partial\overline{\Psi}(\bar{J}_4,\bar{\lambda}_a,\beta)}{\partial\overline{\mathbf{C}}_e} \tag{20}$$

siendo p la presión hidrostática, $\tilde{\mathbf{S}}_p$ y $\tilde{\mathbf{S}}_a$ los tensores de tensiones de Piola-Kirchhoff modificados correspondientes a la parte pasiva y activa respectivamente y *DEV* el operador desviador en descripción material definido como:

$$DEV[\,\cdot\,] = (\,\cdot\,) - 1/3(\mathbf{C} : (\,\cdot\,))\mathbf{C}^{-1} \tag{21}$$

El valor del segundo tensor de Piola-Kirchhoff, **S**, en función de los invariantes $\bar{I}_1, \bar{I}_2, \bar{I}_4$ y $\bar{J}_4$ vendrá dado por:

$$\begin{aligned}\mathbf{S} &= Jp\mathbf{C}^{-1}\\ &+2\left[\left(\frac{\partial\overline{\Psi}_p}{\partial\bar{I}_1}+\bar{I}_1\frac{\partial\overline{\Psi}_p}{\partial\bar{I}_2}\right)\mathbf{I}-\frac{\partial\overline{\Psi}_p}{\partial\bar{I}_2}\mathbf{C}+\bar{I}_4\frac{\partial\overline{\Psi}_p}{\partial\bar{I}_4}\mathbf{n}_0\otimes\mathbf{n}_0\right.\\ &-\frac{1}{3}\left(\frac{\partial\overline{\Psi}_p}{\partial\bar{I}_1}\bar{I}_1+2\frac{\partial\overline{\Psi}_p}{\partial\bar{I}_2}\bar{I}_2+\frac{\partial\overline{\Psi}_p}{\partial\bar{I}_4}\bar{I}_4\right)\mathbf{C}^{-1}\Bigg]\\ &+2\overline{\mathbf{F}}_a^{-1}\left[\left(\bar{J}_4\frac{\partial\overline{\Psi}_a}{\partial\bar{J}_4}\right)\mathbf{m}_0\otimes\mathbf{m}_0-\frac{1}{3}\left(\frac{\partial\overline{\Psi}_a}{\partial\bar{J}_4}\bar{J}_4\right)\mathbf{C}_e^{-1}\right]\overline{\mathbf{F}}_a^{-T}\end{aligned} \tag{22}$$

El tensor de tensiones de Cauchy $\boldsymbol{\sigma}$ es $1/J$ veces el empuje (*push-forward*) de **S** ($\boldsymbol{\sigma} = J^{-1}\boldsymbol{\varphi}_*(\boldsymbol{S})$), o en notación indicial, $\sigma_{ij} = J^{-1}F_{iI}F_{jJ}S_{IJ}$. Utilizando la relación entre el operador $DEV[\bullet]$, definido en la descripción material, y el operador $dev[\bullet]$, definido en la espacial [22]:

$$J^{-2/3}\mathbf{F}(DEV[\bullet])\mathbf{F}^T = dev[\overline{\mathbf{F}}(\bullet)\overline{\mathbf{F}}^T] \tag{23}$$

se obtiene la descripción espacial de (22), es decir, el tensor de Cauchy. Para obtener la componente asociada al comportamiento activo, el empuje se ha de realizar con el tensor $\overline{\mathbf{F}}_e$ en lugar del tensor $\overline{\mathbf{F}}$ utilizado para la componente volumétrica y pasiva. Operando, se obtiene:

$$\begin{aligned}\boldsymbol{\sigma} &= p\mathbf{1}\\ &+\frac{2}{J}\left[\left(\frac{\partial\overline{\Psi}_p}{\partial\bar{I}_1}+\bar{I}_1\frac{\partial\overline{\Psi}_p}{\partial\bar{I}_2}\right)\overline{\mathbf{b}}-\frac{\partial\overline{\Psi}_p}{\partial\bar{I}_2}\overline{\mathbf{b}}^2+\bar{I}_4\frac{\partial\overline{\Psi}_p}{\partial\bar{I}_4}\mathbf{n}\otimes\mathbf{n}\right.\\ &-\frac{1}{3}\left(\frac{\partial\overline{\Psi}_p}{\partial\bar{I}_1}\bar{I}_1+2\frac{\partial\overline{\Psi}_p}{\partial\bar{I}_2}\bar{I}_2+\frac{\partial\overline{\Psi}_p}{\partial\bar{I}_4}\bar{I}_4\right)\mathbf{1}\\ &+\bar{J}_4\frac{\partial\overline{\Psi}_a}{\partial\bar{J}_4}\mathbf{m}\otimes\mathbf{m}-\frac{1}{3}\frac{\partial\overline{\Psi}_a}{\partial\bar{J}_4}\bar{J}_4\mathbf{1}\Bigg]\end{aligned} \tag{24}$$

con **1** el tensor identidad de segundo orden, $\mathbf{m}\otimes\mathbf{m}$ y $\mathbf{n}\otimes\mathbf{n}$ los tensores estructurales asociados a las fibras musculares y de colágeno, respectivamente, en la configuración espacial.

2.3. Tensor de comportamiento elástico

Para obtener la solución numérica del problema no lineal empleando una técnica iterativa tipo Newton, es necesario obtener la linealización de las ecuaciones constitutivas [23]. Conocido el segundo tensor de tensiones de Piola-Kirchhoff, **S**, en un punto, su variación con respecto al tensor de Cauchy-Green por la derecha **C** puede escribirse de la forma:

$$d\mathbf{S} = \mathbb{C} : \frac{1}{2}d\mathbf{C}, \qquad \mathbb{C} = 2\frac{\partial\mathbf{S}(\mathbf{C})}{\partial\mathbf{C}} \tag{25}$$

con $\mathbb{C}$ *el tensor elástico* en la configuración material [24]. Partiendo de la ecuación (19) se obtiene la contribución volumétrica y desviadora del tensor, esta última expresada como la suma de la componente pasiva y activa:

$$\mathbb{C} = \mathbb{C}_{vol} + \overline{\mathbb{C}}_p + \overline{\mathbb{C}}_a = 2\frac{\partial\mathbf{S}_{vol}}{\partial\mathbf{C}} + 2\frac{\partial\overline{\mathbf{S}}_p}{\partial\mathbf{C}} + 2\frac{\partial\overline{\mathbf{S}}_a}{\partial\mathbf{C}} \tag{26}$$

donde $\mathbb{C}_{vol}$, $\overline{\mathbb{C}}_p$ y $\overline{\mathbb{C}}_a$ pueden escribirse de la forma siguiente:

$$\begin{aligned}\mathbb{C}_{vol} &= 2\mathbf{C}^{-1}\otimes\left(p\frac{\partial J}{\partial\mathbf{C}}+J\frac{\partial p}{\partial\mathbf{C}}+2Jp\frac{\partial\mathbf{C}^{-1}}{\partial\mathbf{C}}\right)\\ &= J\tilde{p}\mathbf{C}^{-1}\otimes\mathbf{C}^{-1}-2Jp\mathbf{C}^{-1}\odot\mathbf{C}^{-1}\end{aligned} \tag{27}$$

Por conveniencia, se introduce la función escalar $\tilde{p}$, definida por:

$$\tilde{p} = p + J\frac{dp}{dJ} \tag{28}$$

con la ecuación constitutiva para p dada por (20).

$$\begin{aligned}\overline{\mathbb{C}}_p &= -\frac{4}{3}J^{-\frac{4}{3}}\left(\frac{\partial\overline{\Psi}_p}{\partial\overline{\mathbf{C}}}\otimes\overline{\mathbf{C}}^{-1}+\overline{\mathbf{C}}^{-1}\otimes\frac{\partial\overline{\Psi}_p}{\partial\overline{\mathbf{C}}}\right)\\ &+\frac{4}{3}J^{-\frac{4}{3}}\left(\frac{\partial\overline{\Psi}_p}{\partial\overline{\mathbf{C}}}:\overline{\mathbf{C}}\right)\left(\mathbb{I}_{\overline{C}}^{-1}-\frac{1}{3}\overline{\mathbf{C}}^{-1}\otimes\overline{\mathbf{C}}^{-1}\right)\\ &+J^{-\frac{4}{3}}\overline{\mathbb{C}}_{\overline{w}}^{p}\end{aligned} \tag{29}$$

con:

$$\begin{aligned}(\mathbb{I}_{C^{-1}})_{IJKL} &= \frac{\partial C_{IJ}^{-1}}{\partial C_{KL}} = -(\mathbf{C}^{-1}\odot\mathbf{C}^{-1})_{IJKL} =\\ &-\frac{1}{2}(C_{IK}^{-1}C_{JL}^{-1}+C_{IL}^{-1}C_{JK}^{-1})\end{aligned} \tag{30}$$

y

$$\begin{aligned}\overline{\mathbb{C}}_{\overline{w}}^{p} &= 4\frac{\partial^2\overline{\Psi}_p}{\partial\overline{\mathbf{C}}\partial\overline{\mathbf{C}}}-\frac{4}{3}\left[\left(\frac{\partial^2\overline{\Psi}_p}{\partial\overline{\mathbf{C}}\partial\overline{\mathbf{C}}}:\overline{\mathbf{C}}\right)\otimes\overline{\mathbf{C}}^{-1}\right.\\ &+\overline{\mathbf{C}}^{-1}\otimes\left(\frac{\partial^2\overline{\Psi}_p}{\partial\overline{\mathbf{C}}\partial\overline{\mathbf{C}}}:\overline{\mathbf{C}}\right)\Bigg]\\ &+\frac{4}{9}\left(\overline{\mathbf{C}}:\frac{\partial^2\overline{\Psi}_p}{\partial\overline{\mathbf{C}}\partial\overline{\mathbf{C}}}:\overline{\mathbf{C}}\right)\overline{\mathbf{C}}^{-1}\otimes\overline{\mathbf{C}}^{-1}\end{aligned}$$

Para calcular la componente desviadora del tensor elástico asociada al comportamiento activo, se parte de la hipótesis de que las actualizaciones de $\bar{\lambda}_a$ se calcularán de forma explícita en cada incremento, por lo tanto $\overline{\mathbf{S}}_a$ no dependerá de $\overline{\mathbf{F}}_a$. Operando se obtiene:

$$\begin{aligned}\overline{\mathbb{C}}_a &=\\ &\overline{\mathbf{F}}_a^{-1}\odot\overline{\mathbf{F}}_a^{-1}\left[-\frac{4}{3}J^{-\frac{4}{3}}\left(\frac{\partial\overline{\Psi}_a}{\partial\overline{\mathbf{C}}_e}\otimes\overline{\mathbf{C}}_e^{-1}+\overline{\mathbf{C}}_e^{-1}\otimes\frac{\partial\overline{\Psi}_a}{\partial\overline{\mathbf{C}}}_e\right)\right.\\ &+\frac{4}{3}J^{-\frac{4}{3}}\left(\frac{\partial\overline{\Psi}_a}{\partial\overline{\mathbf{C}}_e}:\overline{\mathbf{C}}_e\right)\left(\mathbb{I}_{\mathbf{C}_e^{-1}}-\frac{1}{3}\overline{\mathbf{C}}_e{}^{-1}\otimes\overline{\mathbf{C}}_e^{-1}\right)\\ &+J^{-\frac{4}{3}}\overline{\mathbf{C}}_{e\overline{w}}^{a}\Bigg]\overline{\mathbf{F}}_a^{-T}\odot\overline{\mathbf{F}}_a^{-T}\end{aligned} \tag{31}$$

con:

$$\overline{\mathbb{C}}^{a}_{e\overline{w}} = 4\frac{\partial^2\overline{\Psi}_a}{\partial\overline{\mathbf{C}}_e\partial\overline{\mathbf{C}}_e} - \frac{4}{3}\left[\left(\frac{\partial^2\overline{\Psi}_a}{\partial\overline{\mathbf{C}}_e\partial\overline{\mathbf{C}}_e} : \overline{\mathbf{C}}_e\right)\otimes\overline{\mathbf{C}}_e^{-1} + \overline{\mathbf{C}}_e^{-1}\otimes\left(\frac{\partial^2\overline{\Psi}_a}{\partial\overline{\mathbf{C}}_e\partial\overline{\mathbf{C}}_e} : \overline{\mathbf{C}}_e\right)\right] + \frac{4}{9}\left(\overline{\mathbf{C}}_e : \frac{\partial^2\overline{\Psi}_a}{\partial\overline{\mathbf{C}}_e\partial\overline{\mathbf{C}}_e} : \overline{\mathbf{C}}_e\right)\overline{\mathbf{C}}_e^{-1}\otimes\overline{\mathbf{C}}_e^{-1} \tag{32}$$

como puede observarse el valor de (31) es idéntico a (29) reemplazando $\overline{\mathbf{C}}$ por su componente elástica $\overline{\mathbf{C}}_e$ y posteriormente realizar la operación tirón (*pull-back*).

El tensor elástico en la configuración espacial, denotado por $\mathbb{C}$, se define como el empuje de $\mathbb{C}$ escalado por el factor J^{-1}, esto es:

$$\mathbb{C} = J^{-1}\boldsymbol{\varphi}_*(\mathbb{C}), \quad \mathbb{C}_{abcd} = J^{-1}F_{aA}F_{bB}F_{cC}F_{dD}\mathbb{C}_{ABCD} \tag{33}$$

Operando, se obtiene la expresión volumétrica y desviadora en la configuración deformada:

$$\mathbb{C} = \mathbb{C}_{vol} + \mathbb{C}_p + \mathbb{C}_a \tag{34}$$

siendo:

$$\mathbb{C}_{vol} = (\tilde{p}\mathbf{1}\otimes\mathbf{1} - 2p\mathbb{I}),$$
$$\overline{\mathbb{C}}_p = \frac{2}{3}tr(\tilde{\boldsymbol{\sigma}}_p)\mathbb{P} - \frac{2}{3}(\mathbf{1}\otimes\overline{\boldsymbol{\sigma}}_p + \overline{\boldsymbol{\sigma}}_p\otimes\mathbf{1}) + \mathbb{C}^{p}_{w} \tag{35}$$

con:

$$\tilde{\boldsymbol{\sigma}}_p = \frac{2}{J}\left[\left(\frac{\partial\overline{\Psi}_p}{\partial\bar{I}_1} + \bar{I}_1\frac{\partial\overline{\Psi}_p}{\partial\bar{I}_2}\right)\overline{\mathbf{b}} - \frac{\partial\overline{\Psi}_p}{\partial\bar{I}_2}\overline{\mathbf{b}}^2 + \bar{I}_4\frac{\partial\overline{\Psi}_p}{\partial\bar{I}_4}\mathbf{n}\otimes\mathbf{n}\right] \tag{36}$$

$$\overline{\boldsymbol{\sigma}}_p = \frac{2}{J}\left[\left(\frac{\partial\overline{\Psi}_p}{\partial\bar{I}_1} + \bar{I}_1\frac{\partial\overline{\Psi}_p}{\partial\bar{I}_2}\right)\overline{\mathbf{b}} - \frac{\partial\overline{\Psi}_p}{\partial\bar{I}_2}\overline{\mathbf{b}}^2 + \bar{I}_4\frac{\partial\overline{\Psi}_p}{\partial\bar{I}_4}\mathbf{n}\otimes\mathbf{n} - \frac{1}{3}\left(\frac{\partial\overline{\Psi}_p}{\partial\bar{I}_1}\bar{I}_1 + 2\frac{\partial\overline{\Psi}_p}{\partial\bar{I}_2}\bar{I}_2 + \frac{\partial\overline{\Psi}_p}{\partial\bar{I}_4}\bar{I}_4\right)\mathbf{1}\right] \tag{37}$$

y $\mathbb{P}$ el tensor proyección:

$$\mathbb{P} = \mathbb{I} - \frac{1}{3}\mathbf{1}\otimes\mathbf{1}. \tag{38}$$

Para calcular la parte desviadora de la componente activa en la configuración espacial es necesario realizar el empuje con el tensor $\overline{\mathbf{F}}_e$:

$$\overline{\mathbb{C}}_a = \frac{2}{3}tr(\tilde{\boldsymbol{\sigma}}_a)\mathbb{P} - \frac{2}{3}(\mathbf{1}\otimes\overline{\boldsymbol{\sigma}}_a + \overline{\boldsymbol{\sigma}}_a\otimes\mathbf{1}) + \mathbb{C}^{a}_{w} \tag{39}$$

con:

$$\tilde{\boldsymbol{\sigma}}_a = \frac{2}{J}\left[\bar{J}_4\frac{\partial\overline{\Psi}_a}{\partial\bar{J}_4}\mathbf{m}\otimes\mathbf{m}\right] \tag{40}$$

y

$$\overline{\boldsymbol{\sigma}}_a = \frac{2}{J}\left[\bar{J}_4\frac{\partial\overline{\Psi}_a}{\partial\bar{J}_4}\mathbf{m}\otimes\mathbf{m} - \frac{1}{3}\frac{\partial\overline{\Psi}_a}{\partial\bar{J}_4}\bar{J}_4\mathbf{1}\right] \tag{41}$$

$\overline{\mathbb{C}}^{i}_{\overline{w}}$, $i = p, a$, es el empuje de $\overline{\mathbb{C}}^{i}_{\overline{w}}$ y su valor también se puede expresar mediante:

$$\overline{\mathbb{C}}^{i}_{w} = \mathbb{P} : \overline{\mathbb{C}}^{i} : \mathbb{P} \tag{42}$$

Operando se puede llegar a la expresión del tensor constitutivo desviador $\overline{\mathbb{C}}$ expresado en función de los invariantes $\bar{I}_1, \bar{I}_2, \bar{I}_4$ y $\bar{J}_4$.

2.4. Imposición de deformaciones iniciales

El músculo, al igual que la mayoría de los tejidos blandos, se encuentra sometido a deformaciones iniciales en la configuración de referencia. Para su incorporación en la formulación hiperelástica se sigue la metodología propuesta por [25]. Se supone que el tensor gradiente de deformación correspondiente al estado deformado $\mathbf{F}_r$ se puede expresar mediante una descomposición multiplicativa $\mathbf{F}_r = \mathbf{F}\mathbf{F}_0$, donde, $\mathbf{F}_0$ representa el gradiente de deformación correspondiente a las deformaciones iniciales y $\mathbf{F}$ es el gradiente de deformación correspondiente a la aplicación de las cargas desde la configuración inicial Ω_0 (ver figura 2).

Como $\mathbf{F}_0$ no es fácil de evaluar, en este caso se supone que $\mathbf{F}_0$ corresponde al alargamiento longifudinal λ_0 en la dirección de las fibras musculares $\mathbf{m}_0$ en el estado de referencia Ω_0 [25]. En un sistema local de coordenadas (*) donde la dirección de las fibras musculares $\mathbf{m}_0$ está alineada con el eje X_1, $\mathbf{F}^*_0$ puede ser expresado por:

$$\left[\mathbf{F}^*_0\right] = \begin{bmatrix} \lambda_0 & 0 & 0 \\ 0 & \dfrac{1}{\sqrt{\lambda_0}} & 0 \\ 0 & 0 & \dfrac{1}{\sqrt{\lambda_0}} \end{bmatrix} \tag{43}$$

y trasformado al sistema global mediante el tensor de rotación $\mathbf{F}_0 = \mathbf{R}\mathbf{F}^*_0\mathbf{R}^T$ [13].

2.5. Extensión al elemento membrana

A la hora de abordar el modelado mediante elementos finitos de distintas unidades musculares, aparece la dificultad de que determinados tejidos presentan un espesor despreciable frente a los tejidos circundantes. Una posible alternativa sería despreciar su contribución mecánica, lo cual es factible siempre que su rigidez sea inferior a la de los otros tejidos. Sin embargo, no es posible despreciar la contribución de las estructuras que aportan rigidez, como es el caso de la fascia. En este caso se ha optado por modelar el tejido fascial mediante elementos membrana, por lo que las tensiones normales en la dirección del espesor se consideran despreciables. Por lo tanto, las seis componentes del tensor de tensiones considerado en la formulación 3D (ecuaciones (22) y (24)) se han de reducir en la formulación de membrana, por lo que la condición de tensiones nulas en el espesor del elemento ha de ser incorporada si se trabaja con la ley constitutiva planteada (ecuaciones (26) y (34)) para materiales hiperelásticos anisótropos. Este ha sido el esquema seguido en este trabajo, para el cual se ha empleado el algoritmo propuesto por [26], que ha sido implementado en el código Abaqus [27] mediante una subrutina UMAT.

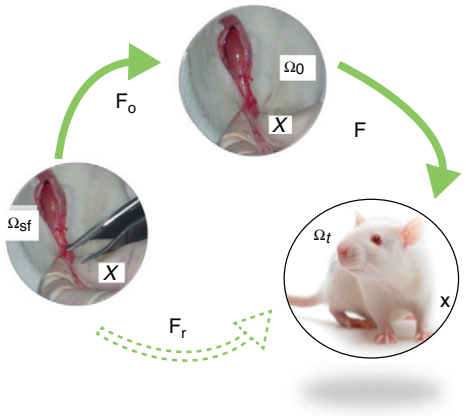

Figura 2. Descomposición multiplicativa del gradiente de deformación. Ω_{sf}, estado libre de tensiones (una vez diseccionado el tendón); Ω_0, estado de referencia o configuración libre de cargas (configuración fisiológica) y Ω_t, estado deformado actual.

Para el modelado del comportamiento de la membrana, se utiliza un sistema de coordenadas local definido por tres vectores. e_1 y e_2 están incluidos en el plano de la membrana y e_3 es perpendicular a dicho plano. Estos vectores giran como lo hace el sólido rígido y las deformaciones se expresan en el sistema local. El gradiente de deformación **F** en notación matricial, para el elemento membrana, viene dado por:

$$\mathbf{F} = \begin{pmatrix} F_{11} & F_{12} & 0 \\ F_{21} & F_{22} & 0 \\ 0 & 0 & F_{33} \end{pmatrix} \tag{44}$$

por lo que las componentes C_{33} y b_{33} del tensor de deformaciones de Cauchy Green por la derecha y la izquierda no son nulas, así como las componentes S_{33} y σ_{33}.

Para comenzar con el algoritmo, la ley constitutiva 3D se expresa agrupando los tensores de tensión y deformación en los términos no nulos $\mathbf{S}_m = (S_{11}, S_{22}, S_{12}, S_{13}, S_{23})^T$ y los que tendrían que ser nulos $\mathbf{S}_z = (S_{33}) = 0$.

$$\begin{pmatrix} d\mathbf{S}_m \\ d\mathbf{S}_z \end{pmatrix} = \begin{pmatrix} \mathbb{C}_{mm} & \mathbb{C}_{mz} \\ \mathbb{C}_{zm} & \mathbb{C}_{zz} \end{pmatrix} \begin{pmatrix} d\mathbf{C}_m \\ d\mathbf{C}_z \end{pmatrix} \tag{45}$$

Para desarrollar el algoritmo de imposición de tensión plana de forma local, se parte de la ecuación (45) y se considera que $\mathbf{S}_z = 0$ y $\mathbf{C}_z$ es la componente desconocida del tensor de deformación. Expresando la tensión en serie de Taylor:

$$\mathbf{S}_z^{(i+1)} = \mathbf{S}_z^{(i)} + \frac{\partial \mathbf{S}_z^{(i)}}{\partial \mathbf{C}_z^{(i)}} \Delta \mathbf{C}_z + \ldots \doteq 0 \tag{46}$$

donde el superíndice i indica el número de la iteración local. En las iteraciones sucesivas se modifica la componente en z del tensor de deformación de Cauchy Green por la derecha, $\mathbf{C}_z$ hasta alcanzar la condición de $\mathbf{S}_z = 0$. Despreciando los términos de alto orden en la ecuación (46) se obtiene $\mathbb{C}_{zz}^{(i)} = \frac{\partial \mathbf{S}_z^{(i)}}{\partial \mathbf{C}_z^{(i)}}$ y con ello la deformación incremental:

$$\Delta \mathbf{C}_z = -[\mathbb{C}_{zz}^{(i)}]^{-1} \mathbf{S}_z^{(i)} \tag{47}$$

con lo que la deformación en la siguiente iteración viene dada por:

$$\mathbf{C}_z^{(i+1)} = \mathbf{C}_z^{(i)} + \Delta \mathbf{C}_z \tag{48}$$

La matriz de rigidez tangente, utilizada en cada iteración en el algoritmo de Newton-Raphson, podría estar asociada con la variación de $\mathbf{S}_m$ con respecto a $\mathbf{C}_m$ pero dependerá del estado de deformación completo **C**. Para obtener la matriz de rigidez tangente consistente, con la condición de tensión impuesta por la formulación del elemento, la matriz de rigidez tangente se ha de condensar. En este caso concreto, la condición es que la tensión sea nula en el espesor de la membrana. Si $d\mathbf{C}_z = 0$, de la segunda ecuación de (45) se obtiene:

$$d\mathbf{C}_z = -\mathbb{C}_{zz}^{-1} \mathbb{C}_{zm} d\mathbf{C}_m \tag{49}$$

Insertando (49) en la primera ecuación de (45) se obtiene

$$d\mathbf{S}_m = \mathbb{C}_{psc} d\mathbf{C}_m \tag{50}$$

con:

$$\mathbb{C}_{psc} = [\mathbb{C}_{mm} - \mathbb{C}_{mz} \mathbb{C}_{zz}^{-1} \mathbb{C}_{zm}] \tag{51}$$

donde $\mathbb{C}_{psc}$ es la matriz de rigidez tangente correspondiente al elemento membrana.

3. Ejemplos

Es esta sección se presentan diferentes resultados obtenidos de la simulación del músculo TA de rata que muestran tanto su respuesta pasiva como activa. Con el objetivo de validar el modelo numérico propuesto en la sección anterior, estas simulaciones se comparan con ensayos experimentales llevados a cabo sobre el mismo músculo.

3.1. Modelo geométrico del músculo TA

La geometría del músculo TA se reconstruyó a partir de la imagen axial de resonancia magnética (RM) de una rata adulta Wistar de 215 ± 15 g de peso tal y como se describe en [16]. Dicha geometría se discretizó con elementos hexaédricos utilizando el software ABAQUS [27].

Es necesario tener en cuenta que la geometría del músculo se ha obtenido «*in-vivo*», es decir, en la configuración fisiológica, por lo que está sujeto a tensiones iniciales que es necesario introducir en el modelo numérico. En este caso se introduce un gradiente de deformación inicial, $\mathbf{F}_0$, definido por el acortamiento $\lambda_0 = 1.2035$ obtenido experimentalmente al diseccionar el tendón en la zona distal (4.54 ± 1.325 mm) [16].

3.2. Función densidad energía de deformación

Para caracterizar el comportamiento pasivo de la UMT, se utilizó la siguiente función densidad energía de deformación:

$$\begin{aligned} &\overline{\Psi}_p = c_1(\bar{I}_1 - 3) + \overline{\Psi}_{pf} \\ &\overline{\Psi}_{pf} = 0 \quad \bar{I}_4 < \bar{I}_{4_0} \\ &\overline{\Psi}_{pf} = \frac{c_3}{c_4}(e^{c_4(\bar{I}_4 - \bar{I}_{4_0})} - c_4(\bar{I}_4 - \bar{I}_{4_0}) - 1) \quad \bar{I}_4 > \bar{I}_{4_0} \text{ y } \bar{I}_4 < \bar{I}_{4_{ref}} \\ &\overline{\Psi}_{pf} = c_5\sqrt{\bar{I}_4} + \frac{1}{2}c_6 \ln(\bar{I}_4) + c_7 \qquad \bar{I}_4 > \bar{I}_{4_{ref}} \end{aligned} \tag{52}$$

donde $\bar{I}_1$ representa el primer invariante del tensor de deformación de Cauchy-Green modificado, $\bar{I}_4 > \bar{I}_{4_0}$ caracteriza la respuesta mecánica en la dirección de las fibras de colágeno, $\bar{I}_{4_{ref}}$ alargamiento de transición entre la zona lineal y exponencial. $c_1 > 0$, $c_3 > 0$, $c_5 > 0$ y $c_6 < 0$ son parámetros con unidades de tensión, siendo $c_3 > 0$ una escala de la parte exponencial, $c_4 > 0$ es un parámetro adimensional y c_7 es un parámetro con unidades de energía de deformación. Nótese que $c_5 > 0$, $c_6 > 0$ y $c_7 > 0$ no son parámetros independientes, sino que vienen determinados por las condiciones de continuidad de la energía, de la tensión y de la primera derivada de la tensión (en términos globales del tensor elástico tangente).

Para caracterizar el comportamiento pasivo de la fascia se utilizó la función isótropa de Yeoh:

$$\overline{\Psi}_p = c_{10}(\bar{I}_1 - 3) + c_{20}(\bar{I}_1 - 3)^2 + c_{30}(\bar{I}_1 - 3)^3 \tag{53}$$

donde $c_{10} > 0$, $c_{20} > 0$ y $c_{30} > 0$ son parámetros con unidades de tensión. En las ecuaciones (52) y (53) solo se expresa la parte isocórica.

Para caracterizar el comportamiento activo, proponemos la función $\overline{\Psi}_a$ expresada como una serie de funciones adimensionales que escalan la magnitud de la tensión isométrica máxima σ_0 [15]. Estas funciones se obtienen de la relación tensión-alargamiento $f_1(\bar{\lambda}_a)$ asociada al solapamiento efectivo entre los filamentos de miosina y actina en el elemento contráctil, de la relación tensión-velocidad $f_2(\dot{\bar{\lambda}}_a)$, de la deformación asociada a los puentes cruzados $f_3(\bar{J}_4)$ y del nivel de activación $f(f_r, t)$:

$$\overline{\Psi}_a = \sigma_0 f_1(\bar{\lambda}_a) f_2(\dot{\bar{\lambda}}_a) f_3(\bar{J}_4) \beta(f_r, t) \tag{54}$$

Tabla 1
Parámetros que caracterizan el comportamiento pasivo del músculo y tendón. Constantes en MPa [14].

	c_1	c_3	c_4	c_5	c_6	c_7	$\bar{I}_{4_0}$	$\bar{I}_{4_{ref}}$
Músculo	0,001	0,053915	0,782802	5,742780	−9,035709	−4,875961	1,254400	3,189796
Tendón	0,01	0,054292	6,860021	57,738461	−66,243575	−57,078409	1,0	1,44

La función $f_1(\bar{\lambda}_a)$ ha sido formulada por diferentes autores [28,10], en este trabajo utilizamos la función propuesta por [15]:

$$f(\bar{\lambda}_a) = \int_{0,5}^{1,5} e^{\frac{-(\bar{\lambda}_a - \lambda_{opt})^2}{2(1-\alpha)^2}} d\bar{\lambda}_a \tag{55}$$

siendo λ_{opt} el alargamiento óptimo del músculo y α corresponde a la curvatura de la función. La relación tensión-velocidad $f_2(\dot{\bar{\lambda}}_a)$ tomará el valor unidad en el caso de contracciones isométricas, para el caso en el que varíe la longitud del músculo durante la contracción, se adopta la propuesta por [10]. La deformación asociada a los puentes cruzados:

$$f_3(\bar{J}_4) = \frac{2}{3}\left(2\bar{J}_4^{3/2} - \frac{3}{2}\bar{J}_4 + 1\right) \tag{56}$$

Finalmente la función de activación $\beta(f_r, t)$ puede expresarse como [15]:

$$\beta(f_r, t) = \sum_{i=1}^{n}\left[\left(1 - re^{(f_r T')/c}\right)\left(P'\frac{t - t_i}{T'}e^{1-(\frac{t-t_i}{T'})}\right)\right] \tag{57}$$

siendo T' el tiempo de contracción aparente para todo el músculo generado en un pulso y P' es la amplitud aparente de la tensión generada en el mismo pulso, t_i es el intervalo de tiempo entre estímulos que corresponde a $1/f_r$, r determina la tasa entre la tensión en un pulso y un tétano, c es la tasa de incremento de fuerza conforme aumenta la frecuencia y n es el número de estímulos.

3.3. *Simulación ensayo uniaxial*

Para validar el modelo de comportamiento pasivo se ha reproducido numéricamente un ensayo de tracción uniaxial sobre la UMT de dos formas, considerando la inclusión de la fascia a través de elementos membrana y sin incluirla. Después, se comparan los resultados numéricos obtenidos con los experimentales [14]. En ambos casos, las fibras se consideran en la dirección fusiforme y el espesor de la fascia, medido previamente en ensayos experimentales [29], se toma igual a 0.3 mm. Las constantes de la función densidad energía de deformación para el músculo, tendón y fascia se recogen en las tablas 1 y 2, respectivamente. Es necesario destacar aquí que, si bien los parámetros que caracterizan el comportamiento pasivo de músculo y tendón son bien conocidos de un trabajo previo [14], aquellos que caracterizan la fascia han sido determinados ajustando la respuesta numérica a los ensayos experimentales. Para reproducir el ensayo se fijan los desplazamientos de la zona proximal del músculo TA y se aplica un desplazamiento impuesto de 10 mm en la zona distal (nodos correspondientes al tendón). Como el ensayo se realiza una vez que se ha producido la disección del tendón, se ha de partir en la simulación de la configuración libre de tensiones iniciales (Ω_{sf}), por lo que inicialmente se ha de obtener dicha configuración liberando las tensiones iniciales.

Tabla 2
Parámetros que caracterizan el comportamiento pasivo de la fascia. Constantes en MPa.

	D	C_{10}	C_{20}	C_{30}
Fascia	0,01	0,008	0,05	1,0

La figura 3a presenta el modelo de elemenos finitos para el músculo TA, donde se ha indicado una región central del vientre muscular sobre la que se visualizan los campos de tensiones máximas principales (TMP). Las TMP que se muestran en la figura 3b se corresponden con la simulación del modelo sin incluir la fascia mientras que la figura 3c incluye este tejido. Para establecer una comparación directa entre ambas imágenes, los elementos correspondientes a la fascia han sido suprimidos en la figura 3c. Se observa que la distribución de TMP evidencia valores mayores en la figura 3b, donde no está considerada la fascia.

Las relaciones fuerza-desplazamiento obtenidas en las simulaciones numéricas se muestran en la figura 3.d donde, a su vez, se comparan con las curvas experimentales. Aquí se aprecia la diferencia de rigidez entre ambas situaciones, evidenciando una rigidez notablemente mayor para el caso en el que se incluye la fascia.

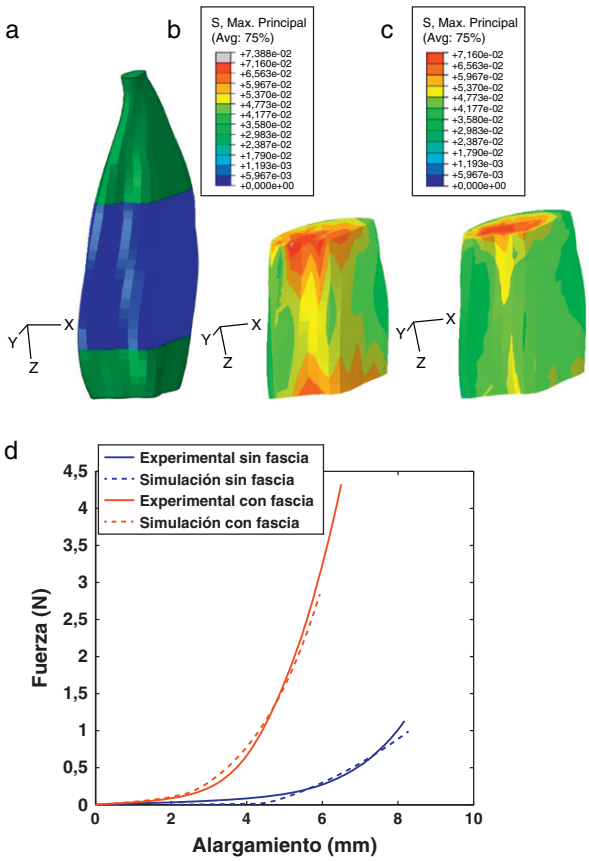

Figura 3. (a) Modelo de elementos finitos del TA. En azul se indica la parte central del músculo, donde se visualizan los campos de TMP. (b) Campo de TMP en el músculo cuando no se incluye la fascia. (c) Campo de TMP en el músculo cuando se considera la fascia. La fascia ha sido retirada para visualizar solamente el músculo y poder comparar con (b). (d) Fuerza vs. alargamiento obtenido de las simulaciones del ensayo uniaxial, con y sin fascia, comparadas con los resultados experimentales [14].

Tabla 3
Parámetros que caracterizan el comportamiento activo del músculo [15].

σ_0 (MPa)	λ_{opt}	α	T (s)	P (N)	t_i (s)	r	c
0,8	1	0,83616	0,04	0,11	0,01667	1,0535	1,1245

3.4. Simulación de la contracción

Se han llevado a cabo 2 grupos diferentes de simulaciones para estudiar la contracción isométrica (la longitud del músculo es constante) y la contracción concéntrica (la longitud del músculo disminuye) a velocidad constante (isotónica). La tabla 3 recoge los parámetros utilizados para las simulaciones.

En primer lugar, para estudiar la contracción isométrica, se fijan ambos extremos de la malla manteniendo fijos los grados de libertad de los nodos en dichas regiones. Puesto que en una contracción isométrica, la unidad mínima funcional del músculo (sarcómero) no altera su longitud inicial, no existe desplazamiento relativo entre los filamentos de actina y miosina. Es por ello que, en la descomposición multiplicativa del gradiente de deformación $\overline{\mathbf{F}}_a = \mathbf{1}$, por lo tanto $\overline{\mathbf{F}} = \overline{\mathbf{F}}_e$. El valor de la función $f(\dot{\overline{\lambda}}_a)$ en la ecuación (54) al no existir dependencia con la velocidad se toma como $f(\dot{\overline{\lambda}}_a) = 1$.

La figura 4 muestra la fuerza de reacción total registrada en los nodos de la malla del extremo superior para cuatro frecuencias del estímulo. El efecto que la frecuencia del estímulo ejerce sobre la deformación y la TMP del tejido se observa en la figura 5.

Por otro lado, para llevar a cabo la simulación de una contracción concéntrica, se liberan las condiciones de contorno establecidas en el caso anterior para los nodos del extremo superior de la malla. De esta manera, el músculo acortará su longitud inicial libremente.

Bajo estas condiciones, y realizando sucesivos incrementos de tiempo en un análisis estático, es necesario definir la velocidad de la contracción. En las simulaciones llevadas a cabo en este trabajo se ha considerado que la contracción se realiza a velocidad constante (contracción isotónica) tomando un valor $\dot{\overline{\lambda}}_a = -5$ [1/s] [34] por ello, $\overline{\mathbf{F}}_a$ se supone conocida y, en la dirección de la fibra muscular tendrá la siguiente forma, con $\overline{\lambda}_a^{n+1} = \overline{\lambda}_a^n + \dot{\overline{\lambda}}_a \triangle t$:

$$[\mathbf{F}_a] = \begin{bmatrix} \overline{\lambda}_a & 0 & 0 \\ 0 & \dfrac{1}{\sqrt{\overline{\lambda}_a}} & 0 \\ 0 & 0 & \dfrac{1}{\sqrt{\overline{\lambda}_a}} \end{bmatrix} \tag{58}$$

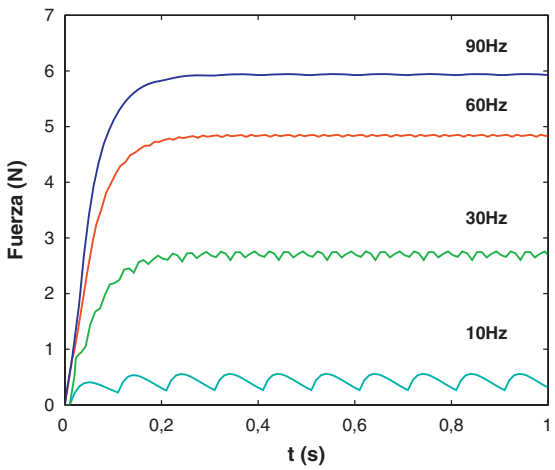

Figura 4. Fuerza de reacción isométrica para cuatro frecuencias de estímulo.

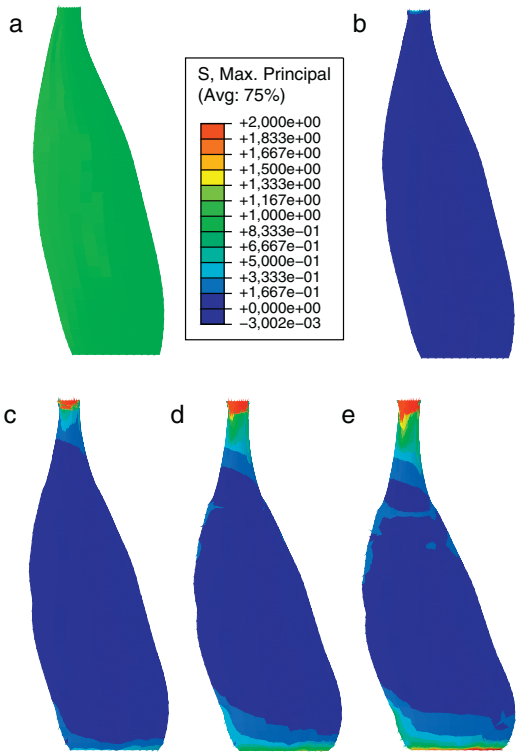

Figura 5. (a) Configuración inicial de la UMT. TMP alcanzada para el estímulo a (b) 10Hz. (c) 30Hz. (d) 60Hz. (e) 90Hz. Nota: tensiones por encima de 2, 0 MPa se alcanzan en la región del tendón.

En esta situación, el valor de $f(\dot{\overline{\lambda}}_a)$ se ha tomado como $f(\dot{\overline{\lambda}}_a) = 0.5$ [10].

La figura 6 representa el desplazamiento del extremo superior de la UMT para las cuatro diferentes frecuencias consideradas. La figura 7 representa, junto con la configuración inicial del tejido, la deformada y el campo de desplazamientos en la dirección longitudinal para los 4 estímulos. Se observa cómo para la frecuencia mayor se obtiene el mayor acortamiento del músculo.

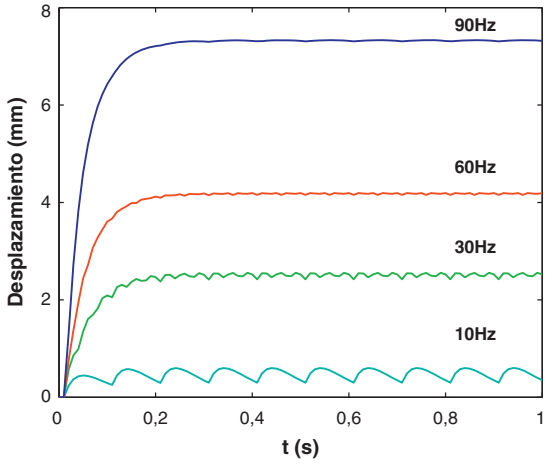

Figura 6. Desplazamiento del extremo superior de la UMT para 4 frecuencias de estímulo.

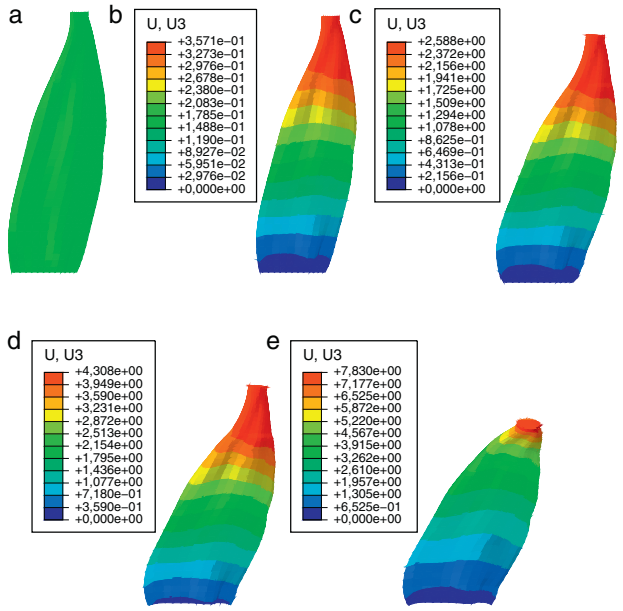

Figura 7. Campo de desplazamientos en la dirección longitudinal del músculo para una contracción concéntrica a 4 diferentes frecuencias del estímulo. (a) Configuración indeformada. (b) 10Hz. (c) 30Hz. (d) 60Hz. (e) 90Hz.

4. Conclusiones

En este trabajo se ha presentado y validado un modelo numérico de comportamiento 3D que permite simular la respuesta mecánica del tejido músculo-esquelético de mamíferos. Esta respuesta está fuertemente influenciada por la geometría y la arquitectura de las fibras musculares [30]. Por ello, en este trabajo se ha modelado el músculo TA partiendo de imagen de RM considerando una distribución de dichas fibras siguiendo la geometría fusiforme del tejido. En la mayoría de los trabajos de la literatura se parte de geometrías de músculos procedentes de cadáveres [31,10] o bien utilizan geometrías idealizadas [9,28,10,32].

El modelo numérico propuesto se ha particularizado para el músculo TA de rata. Para ello, las constantes que definen el comportamiento pasivo y activo se han tomado de trabajos experimentales previos desarrollados por los autores [14,15]. El comportamiento pasivo se ha validado comparando los resultados numéricos con los experimentales cuando a la UMT se le solicita a un estado uniaxial de tracción (fig. 3d). Este procedimiento ha permitido, a través de las curvas fuerza-desplazamiento obtenidas experimentalmente, ajustar un modelo de comportamiento isótropo para la fascia que envuelve el tejido muscular. De esta forma se ha conseguido estimar las constantes que definen su comportamiento indirectamente a través de la simulación computacional. Este hecho permite caracterizar de manera precisa el tejido evitando llevar a cabo ensayos experimentales de extrema dificultad técnica. La figura 3 muestra además el efecto que ejerce la fascia sobre la distribución de tensiones en el vientre muscular. Este tejido, debido a que presenta una rigidez mayor, disminuye la tensión que soporta el músculo para un mismo nivel de extensión pasiva [33].

En el caso de la simulación del comportamiento activo, la fuerza de reacción obtenida para la contracción isométrica (figura 4) coincide con la observada experimentalmente en [15] para las frecuencias de estímulo de 30, 60 y 90 Hz. Una limitación importante del modelo bajo contracción isométrica consiste en haber considerado $\bar{\mathbf{F}}_a = \mathbf{1}$. Si bien es cierto que para este tipo de contracción no hay desplazamiento de los extremos de la UMT, las fibras musculares se acortan hasta alcanzar una posición de equilibrio en la dirección formada por los dos extremos fijos. En el caso de contracciones concéntricas los resultados presentan la misma tendencia obtenida por otros autores para geometrías diferentes [9,10,34]. La simplificación llevada a cabo de no considerar la masa y efectos inerciales del tejido así como la ausencia de cargas exteriores condiciona que la simulación se acerque a la realidad del comportamiento de la UMT.

Agradecimientos

Esta investigación ha sido financiada por el Ministerio de Economía y Competitividad de España mediante el proyecto DPI2011-27939-C02-01 y el Instituto de Salud Carlos III (ISCIII) mediante la iniciativa CIBER. Los autores también agradecen al Ministerio de Ciencia e Innovación por la beca (BES-2009-021515) concedida a B. Hernández-Gascón.

Bibliografía

[1] B.R. MacIntosh, P.F. Gardiner, A.J. McComas, Skeletal Muscle Form and Function, 2nd edition, Human Kinetics, 2006.
[2] A.V. Hill, The heat of shortening and the dynamic constants of muscle, en: P. ROY. SOC. B-BIOL. SCI., Vol. 126, 1938, pp. 136–195.
[3] A. Magid, D.J. Law, Myofibrils bear most of the resting tension in frog skeletal muscle, Science 230 (4731) (1985) 1280–1282.
[4] J.A.C. Martins, E.B. Pires, R. Salvado, P.B. Dinis, Numerical model of passive and active behavior of skeletal muscles, Comput. Methods Appl. Mech. Eng. 151 (1998) 419–433.
[5] B. Hernández-Gascón, E. Peña, G. Pascual, M. Rodríguez, B. Calvo, M. Doblaré, J.M. Bellón, Mechanical and histological characterization of the abdominal muscle. a previous step to modelling hernia surgery, J. Mech. Behav. Biomed. Mater. 4 (3) (2011) 392–404.
[6] J.W. Fernandez, M.L. Buist, D.P. Nickerson, P.J. Hunter, Modelling the passive and nerve activated response of the rectus femoris muscle to a flexion loading: a finite element framework, Med. Eng. Phys. 27 (10) (2005) 862–870.
[7] T. Johansson, P. Meier, R. Blickhan, A finite-element model for the mechanical analysis of skeletal muscles, J. Theor. Biol. 206 (1) (2000) 131–149.
[8] C.A. Yucesoy, B.H.F.J.M. Koopman, P.A. Huijing, H.J. Grootenboer, Three-dimensional finite element modeling of skeletal muscle using a two-domain approach: linked fiber-matrix mesh model, J. Biomech. 35 (9) (2002) 1253–1262.
[9] C.P. Tsui, C.Y. Tang, C.P. Leung, K.W. Cheng, Y.F. Ng, D.H. Chow, C.K. Li, Active finite element analysis of skeletal muscle-tendon complex during isometric, shortening and lengthening contraction, Bio-Med. Mater. Eng. 14 (2004) 271–279.
[10] M. Böl, S. Reese, Micromechanical modelling of skeletal muscles based on the finite element method, Comput. Methods Biomech. Biomed. Eng. 11 (2008) 489–504.
[11] S.-W. Chi, J. Hodgson, J.-S. Chen, V. Reggie Edgerton, D.D. Shin, R.A. Roiz, S. Sinha, Finite element modeling reveals complex strain mechanics in the aponeuroses of contracting skeletal muscle, J. Biomech. 43 (7) (2010) 1243–1250.
[12] J.C. Gardiner, J.A. Weiss, T.D. Rosenberg, Strain in the human medial collateral ligament during valgus lading of the knee, Clin. Orthop. Relat. Res. 391 (2001) 266–274.
[13] E. Peña, M.A. Martinez, B. Calvo, M. Doblaré, On the numerical treatment of initial strains in biological soft tissues, Int. J. Numer. Methods Engin. 68 (8) (2006) 836–860.
[14] B. Calvo, A. Ramírez, A. Alonso, J. Grasa, F. Soteras, R. Osta, M.J. Muñoz, Passive nonlinear elastic behavior of skeletal muscle: Experimental results and model formulation, J. Biomech. 43 (2) (2010) 318–325.
[15] A. Ramírez, J. Grasa, A. Alonso, F. Soteras, R. Osta, M. Muñoz, B. Calvo, Active response of skeletal muscle: In vivo experimental results and model formulation, J. Theor. Biol. 267 (4) (2010) 546–553.
[16] J. Grasa, A. Ramírez, R. Osta, M.J. Muñoz, F. Soteras, B. Calvo, A 3D active-passive numerical skeletal muscle model incorporating initial tissue strains. validation with experimental results on rat tibialis anterior muscle, Biomech. Model. Mechanobio. 10 (2011) 779–787.
[17] P.J. Flory, Thermodynamic relations for high elastic materials, Trans. Faraday Soc. 57 (1961) 829–838.
[18] J. Staalhand, A. Klarbring, G.A. Holzapfel, A mechanochemical 3d continuum model for smooth muscle contraction under finite strains, J. Theor. Biol. 268 (1) (2011) 120–130.
[19] J.C. Simo, R.L. Taylor, Quasi-incompresible finite elasticity in principal stretches. continuum basis and numerical algorithms, Comput. Methods Appl. Mech. Eng. 85 (1991) 273–310.
[20] A. Spencer, Continuum Physics. Theory of Invariants, Academic Press, New York, 1954.
[21] G.A. Holzapfel, Nonlinear Solid Mechanics, A continuum approach for engineering, Wiley, 2000.

[22] J.C. Simo, T.J.R. Hughes, Computational Inelasticity, Springer-Verlag, New York, 1998.
[23] T.J.R. Hughes, K.S. Pister, Consistent linearization in mechanics of solids and structures, Comput. Struct. 8 (1978) 391–397.
[24] R.W. Ogden, Non-linear Elastic Deformations, Dover, New York, 1996.
[25] J.C. Gardiner, J.A. Weiss, Subject-specific finite element analysis of the human medial collateral ligament during valgus knee loading., J. Orthop. Res. 21 (6) (2003) 1098–1106.
[26] S. Klinkel, S. Govindjee, Using finite strain 3d-material models in beam and shell elements, Eng. Comput. 19 (8) (2002) 902–921.
[27] Hibbit, Karlsson, Sorensen, Abaqus user's guide, v. 6.5, HKS inc. Pawtucket, RI, USA., 2005.
[28] B.B. Blemker, P.M. Pinsky, S.L. Delp, A 3d model of muscle reveals the causes of nonuniform strains in the biceps brachii, Ann. Biomed. Eng. 38 (2005) 657–665.
[29] A. Ramírez, Modelado y simulación del tejido músculo-esquelético. validación experimental con el músculo tibial anterior de rata, Ph.D. thesis (2011).
[30] B.B. Blemker, S.L. Delp, Three-dimensional representation of complex muscle architectures and geometries, Ann. Biomed. Eng. 33 (2005) 661–673.
[31] D. d'Aulignac, J.A. Martins, E.B. Pires, T. Mascarenhas, R.M. Jorge, A shell finite element model of the pelvic floor muscles, Comput. Methods Biomech. Biomed. Eng. 8 (5) (2005) 339–347.
[32] C.Y. Tang, G. Zhang, C.P. Tsui, A 3d skeletal muscle model coupled with active contraction of muscle fibres and hyperelastic behaviour., J. Biomech. 42 (7) (2009) 865–872.
[33] J.M. Rijkelijkhuizen, H.J.M. Meijer, G.C. Baan, P.A. Huijing, Myofascial force transmission also occurs between antagonistic muscles located within opposite compartments of the rat lower hind limb, J. Electromyogr. Kinesiol. 17 (6) (2007) 690–697.
[34] P. Meier, R. Blickhan, Skeletal muscle mechanics: from mechanisms to function, Ch. FEM-Simulation of Skeletal Muscle: The Influence of Inertia During Activation and Deactivation, 1st ed. New York, 2000, pp. 207-223.

Work 7: Mechanical response of the herniated human abdomen to the placement of different prostheses

Journal: *Submitted* (2012)

Mechanical response of the herniated human abdomen to the placement of different prostheses

B. Hernández-Gascón[a,d], E. Peña[a,d], J. Grasa[a,d], G. Pascual[b,d], J. M. Bellón[c,d] and B. Calvo[a,d]

[a] *Aragón Institute of Engineering Research (I3A) University of Zaragoza. Spain*
[b] *Department of Medical Specialities. Faculty of Medicine. University of Alcalá. Spain*
[c] *Department of Surgery. Faculty of Medicine. University of Alcalá. Spain*
[b] *CIBER-BBN. Centro de Investigación en Red en Bioingeniería, Biomateriales y Nanomedicina. Spain*

Abstract

This paper describes a method designed to model the repaired herniated human abdomen just after surgery and examine its mechanical response to a physiological movement (standing cough). The model is based on the real geometry of the human abdomen bearing a large incisional hernia with several anatomical structures differentiated by MRI. To analyze the outcome of hernia repair, the surgical procedure was simulated by modeling a prothesis placed over the hernia. Three surgical meshes with different mechanical properties were considered: an isotropic heavy-weight mesh ($Surgipro^{®}$), a slightly anisotropic light-weight mesh ($Optilene^{®}$) and a highly anisotropic medium-weight mesh ($Infinit^{®}$). Our findings suggest that anisotropic implants need to be positioned such that the most compliant axis of the mesh coincides with the craneo-caudal direction of the body.

Keywords: hernia surgery, anisotropy, intra-abdominal pressure, hyperelasticity, finite element model.

1 Introduction

Over the course of time, surgical techniques in hernia surgery have evolved from autoplasty, using the patient's own tissue, to the use of prosthetic materials. These materials have changed the therapeutic view of abdominal hernia repair since the publication of Lichtenstein's tension-free repair procedure[23,24]. The recent use of biomaterials to repair a primary incisional hernia has gradually demonstrated their efficacy for this purpose, though the repair of large incisional hernias is more difficult and has been linked to a high risk of postoperative complications[31].
Despite the appearance of many new prosthetic materials designed to repair abdominal wall defects, polypropylene (PP) continues to be the most widely employed. This is because of the good cost/benefits and excellent biocompatibility of PP, along with an improved tolerance to infection over that of other materials. Research and development in prosthetic materials has aimed to improve the wound repair process elicited by prosthetic mesh implants. Thus, macroporous meshes have been subjected to modifications to their structure, porosity and composition. This has led to the construction of new large-pore meshes composed of other polymers such as polytetrafluoroethylene (PTFE) and polyvinylidene fluoride (PVDF).
Pore size has also been considered an important factor in new mesh designs along with other characteristics such as the diameter and spatial distribution of fibers. These new designs have led to the classification of macroporous meshes as heavy-weight (HW), medium-weight (MW) or low-weight (LW), respectively, according to whether their density values are above 80 g/m^2, between 50 and 80 g/m^2 or below 50 g/m^2. Some authors even define an ultra-lightweight material whose density is under 35 g/m^2.
In general, PP-LW protheses attempt to reduce the amount of foreign material that remains in the host tissue after implant. The features pursued are a less intense immune response and a tissue regeneration process that induces less fibrosis in the recipient tissue[20]. It should be noted that the abdominal wall works as a dynamic system under intense pressure changes (coughing, vomiting, etc.) or sustained pressures (obesity, pregnancy, etc.)[6]. Thus, after mesh implantation, the distensibility of the abdomen has to permit non-restrictive movements without compromising the final mechanical resistance of the abdominal wall[22]. Besides, the prosthesis has to be capable of absorbing stresses provoked by intraabdominal pressures (IAP). Such stresses have been described as responsible for the adverse effects of trauma and other abdominal diseases such as the formation or recurrence of hernias.
Numerous experimental animal studies have examined the outcome of the use of different prothetic materials[1,2,13,14]. Other studies have focussed on analyzing the effects of the anisotropy of a surgical mesh once implanted[1,2,30]. However, the distensibility and stress produced to the tissues and implant cannot be experimentally addressed. We propose a computational approach to the topic with the advantage that traditional animal studies, which involve long periods of time and are expensive, are minimized. Several authors have proposed FE models with idealized geometries to evaluate the mechanical responses of inguinal human tissues[9,25]. However, to the authors' knowledge, no computational study has defined the real geometry of the entire herniated human abdominal wall including the different anatomical structures of the abdomen to simulate the mechanical response to the implant of a surgical mesh.
This study was designed to compare the mechanical response of different meshes shortly after

their implant over a large incisional hernia and of the repaired abdominal wall. Here we present an FE model of an abdominal wall fully herniated along the linea alba. The surgical procedure of hernia repair is simulated for the different prostheses to analyze immediate outcomes under the load of standing cough. This physiological load is common in patients during post-operative recovery. The three surgical meshes considered were: an isotropic heavy-weight mesh, a slightly anisotropic light-weight mesh and a highly anisotropic medium-weight mesh.

2 Methods

2.1 Model of the herniated human abdomen

An FE model of a completely herniated abdomen was constructed to simulate its condition just after hernia surgery (at time-zero without tissue in-growth, see Figures 1 and 2) by creating a large 120 x 200 mm incisional hernia[31]. This FE model was based on a model of the human abdomen obtained using DICOM files generated by magnetic resonance imaging (MRI) of a healthy 38-year-old man[12]. Different anatomical structures including muscles and aponeuroses were considered whereas skin and fat were not included since their stiffness is negligible compared to that of the former structures (see Figure 1)[10]. Specifically, the structures distinguished by the FE model were: linea alba (LA), rectus abdominis muscle (RAM), rectus tendon (RT), oblique muscles (comprising the external and internal obliques and the transversus abdominis), oblique muscle tendon (OMT), fascia transversalis (FT), anterior and posterior rectus sheath (ARS and PRS, respectively), diaphragm, chest, back and pelvis.

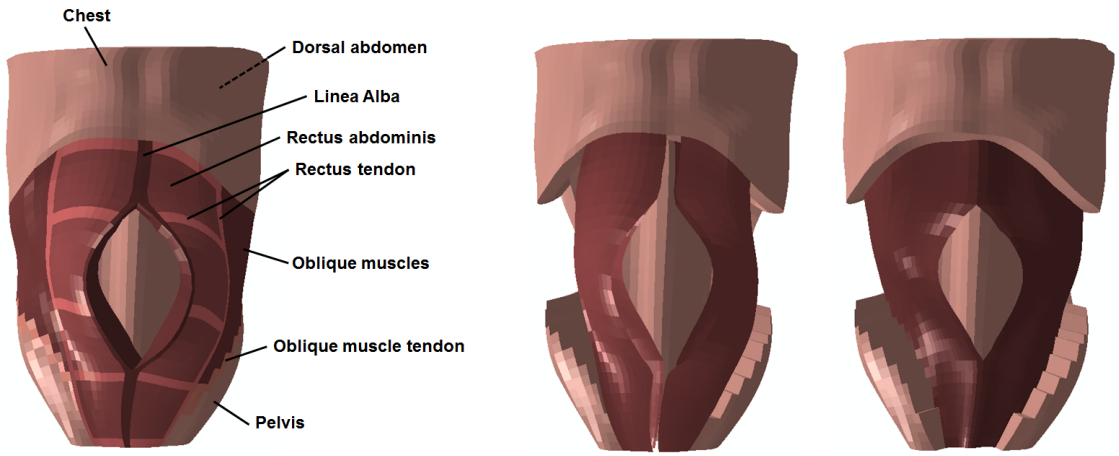

(a) (b) (c)

Figure 1: Anatomical structures defined in the model of the herniated human abdomen. (a) Linea alba, rectus abdominis muscle, rectus tendon, oblique muscles, oblique muscle tendon, chest, dorsal abdomen and pelvis. (b) Anterior and posterior rectus sheaths in dark color. (c) Fascia transversalis in dark color.

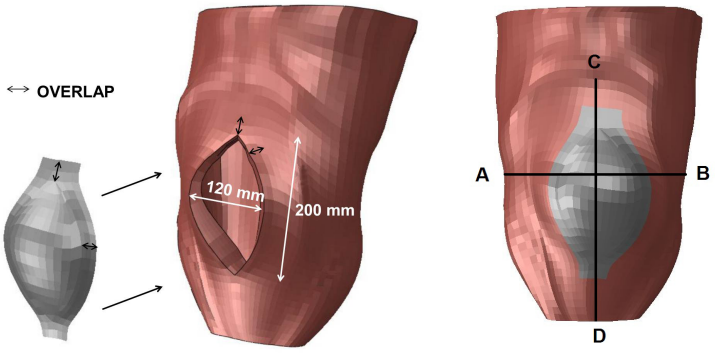

(a) (b)

Figure 2: FE model of the herniated human abdomen including a large incisional hernia along the LA and FE model of the surgical mesh. The placement direction and the overlap between prosthesis and tissue is shown. (b) Whole FE model with the prosthesis in place.

In the model, a surgical mesh was placed over the hernia defect simulating the onlay mesh technique. The prosthesis was thus modeled using membrane elements with the software *ANSYS ICEM CFD*®. The thickness considered for membrane elements was 1 mm[13]. As in real surgery, overlap exists between the prosthesis and abdominal wall (see Figure 2.a). Overlap was created by placing 3 elements on the lateral edges and 2 elements on the upper and lower sides of the overlap (see Figure 2). Despite several techniques are used to suture the surgical mesh, in this study two running sutures were modeled[17]. Nodes corresponding to the overlap between tissue and prosthesis were matched to model these running sutures. Specifically, the FE model includes a total of 13200 hexahedral elements, 2257 membrane elements and 432 shell elements.

2.2 Material properties and preferential direction of anisotropy

To define the material properties through constitutive modeling, the purely passive response of the abdominal muscle was modeled within the framework of large deformation anisotropic hyperelasticity by means of a strain energy function (SEF)[11], $\Psi(\mathbf{C}, \mathbf{M})$. The SEF depends on the scalar-valued functions of $\bar{\mathbf{C}} = \bar{\mathbf{F}}^T\bar{\mathbf{F}}$ and $\mathbf{M} = \mathbf{m}_0 \otimes \mathbf{m}_0$, respectively. The preferential direction of anisotropy (PDA) is represented by a unit vector $\mathbf{m}_0$[3]. Specifically, an uncoupled SEF, divided into two terms (isotropic and anisotropic), was considered ($\bar{\Psi} = \bar{\Psi}_{\text{iso}} + \bar{\Psi}_{\text{ani}}$). Material properties were obtained from the literature for each anatomical structure[11,27]. The isotropic behavior of the abdominal tissues was modeled using Demiray's SEF[8]:

$$\bar{\Psi}_{\text{iso}} = \frac{c_1}{c_2}\left[\exp\left(\frac{c_2}{2}[\bar{I}_1 - 3]\right) - 1\right], \tag{1}$$

whereas the anisotropic response was modeled using two different SEF depending on the tissues. For the anisotropic response of human aponeuroses[27], the Calvo's SEF[5] was considered:

$$
\begin{aligned}
\bar{\Psi}_{\text{ani}} &= 0 \qquad\qquad \bar{I}_4 < \bar{I}_{4_0} \\
\bar{\Psi}_{\text{ani}} &= \frac{c_3}{c_4}(e^{c_4(\bar{I}_4-\bar{I}_{4_0})} - c_4(\bar{I}_4 - \bar{I}_{4_0}) - 1), \qquad \bar{I}_4 > \bar{I}_{4_0} \text{ and } \bar{I}_4 < \bar{I}_{4_{ref}} \\
\bar{\Psi}_{\text{ani}} &= c_5\sqrt{\bar{I}_4} + \frac{1}{2}c_6\ln(\bar{I}_4) + c_7 \qquad \bar{I}_4 > \bar{I}_{4_{ref}},
\end{aligned}
\tag{2}
$$

where $\bar{I}_1$ is the first modified strain invariant of the symmetric modified right Cauchy-Green tensor, $\bar{\mathbf{C}}$, and the anisotropic constitutive response is characterized by the invariant $\bar{I}_4 \geq 1$. The stretch point at which collagen fibers begin to straighten is represented by $\bar{I}_{4_{ref}}$. It was assumed that the strain energy corresponding to the anisotropic terms only contributes to the global mechanical response of the tissue when stretched, that is, when $\bar{I}_4 > \bar{I}_{4_0}$. In Equations 1 and 2, $c1 > 0$, $c3 > 0$, $c5 > 0$ and $c6 > 0$ are stress-like parameters, $c2 > 0$ and $c4 > 0$ are dimensionless parameters and $c7 > 0$ is an energy-like parameter. Note that $c5$, $c6$ and $c7$ are not independent parameters as they enforce strain, stress and stress derivative's continuity.
For the anisotropic response of abdominal muscles[11], we considered Holzapfel's SEF[16]:

$$
\bar{\Psi}_{\text{ani}} = \frac{c_3}{2c_4}\left[\exp\left(c_4[\bar{I}_4 - 1]^2\right) - 1\right], \tag{3}
$$

where $c_1 > 0$ and $c_3 > 0$ are stress-like parameters, and $c_2 > 0$ and $c_4 > 0$ are dimensionless ($\bar{\Psi}_{\text{ani}} = 0$ if $\bar{I}_4 \leq 1$).
Mean experimental data curves were fitted using a Levenberg-Marquardt minimization algorithm[26]. Table 1 shows the material parameters obtained after fitting the experimental data[13,11,27]. Finally, a Neo-Hookean model was used to model the mechanical behavior of the diaphragm and pelvis[18].
Following a previous model of a healthy abdomen[12], two methods were used to include the direction of anisotropy. First, when the angle α is obtained by the fitting procedure, it is taken to represent a PDA. Second, collagen fibers in fascias were assumed to show a similar spatial arrangement to muscle fibers in muscles[28]. Accordingly, anisotropy in the fascia transversalis appears in the transverse direction of the abdomen. In addition, we considered that the aponeurotic fibers of the external and internal obliques occur along the anterior lamina of the rectus sheath. Here two families of obliquely running fibers exist (from the external oblique and internal oblique) whereas the fibers of the transversal abdominis run transversally along the posterior lamina[28]. Finally, the ends of both aponeuroses arising from the anterior and posterior lamina of the rectus sheath form the LA.
Three non-reabsorbable, biocompatible surgical meshes with different mechanical properties were analyzed: *Surgipro*® (SUR), a HW (84 g/m^2) polypropylene monofile isotropic mesh with a small pore size; *Optilene*® (OPT) a LW (48 g/m^2) polypropylene monofile, slightly anisotropic mesh but with a large pore size and *Infinit*® (INF), a MW highly anisotropic mesh (70 g/m^2) with a large pore size composed of a woven PTFE monofilament. Using a method described elsewhere[13], the protheses were modeled within the framework of large deformation anisotropic hyperelasticity. The material properties were taken from Hernández-Gascón et al. [13].
The isotropic response of all meshes was modeled using Demiray's SEF[8] (see Equation 1) while

Table 1: Material parameters obtained from prior works[13,11,27]. Angle α is considered from the craneo-caudal direction. * Set 1: LA, RAT, OMT, FT, ARS and PRS. Set 2: oblique muscles. Set 3: Rectus abdominis muscle. Set 4: chest, back and pelvis. Set 5: diaphragm and pelvis.

	c_1 [MPa]	c_2 [-]	c_3 [MPa]	c_4 [-]	c_5 [MPa]	c_6 [MPa]	c_7 [MPa]	I_{40} [-]		ε [-]
Set 1* [27]	0.2434	0.8	0.0064	9.63	31.8214	-36.9188	-31.4118	1.0	-	0.1483
	c_1 [MPa]	c_2 [-]	c_3 [MPa]	c_4 [-]					α[°]	ε [-]
Set 2* [11]	0.16832	0.6319	0.01219	5.68158	-	-	-	-	87.8	0.17873
Set 3* [11]	0.10445	6.86123	0.001	0.00491	-	-	-	-	0.0	0.10923
Set 4* [11]	0.16832	0.6319	0.01219	5.68158	-	-	-	-	-	0.17873
Set 5* [18]	0.18	-	-	-	-	-	-	-	-	-
SURⓇ [13]	2.10163	1.17805	-	-	-	-	-	-	-	0.1467
OPTⓇ [13]	1.25112	1.5	0.28	0.03062	-	-	-	-	0.0	0.0807
INFⓇ [13]	0.25	2.5	0.07804	5.49131	-	-	-	-	0.0	0.3714

the anisotropic responses of OPT and INF were represented by Holzapfel's SEF [16] (see Equation 3), Figure 3. In all cases, constitutive equations and PDA were included in *ABAQUSⓇ* by a user material subroutine (UMAT).

The meshes OPT and INF are anisotropic so their placement in the abdomen should lead to different outcomes depending on the orientation of the mesh. To examine the effects of anisotropy and placement of the protheses, two directions, 1 and 2 (see Figure 3), defined in prior experimental tests by Hernández-Gascón et al.[13], were considered. Direction 1 runs parallel to the main axis of the human body, craneo-caudal, and Direction 2 is perpendicular to this (denoted the transverse direction). Thus, we defined mesh alignments A and B in which directions 1 or 2 were aligned with the craneo-caudal direction, respectively (see Figure 4). According to experimental results, this means that the stiffest axis of the protheses was placed in the transverse direction or perpendicular to this as orientations A or B, respectively.

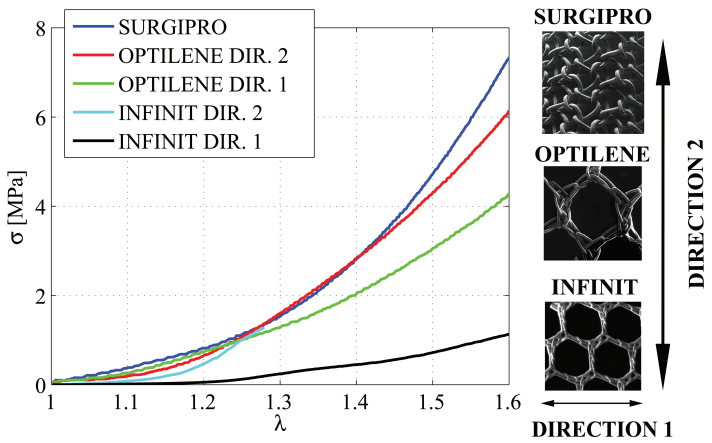

Figure 3: Experimental data from uniaxial mechanical tests conducted on the protheses examined obtained from the literature (figure inspired on the image in B. Hernández-Gascón et al.[13])

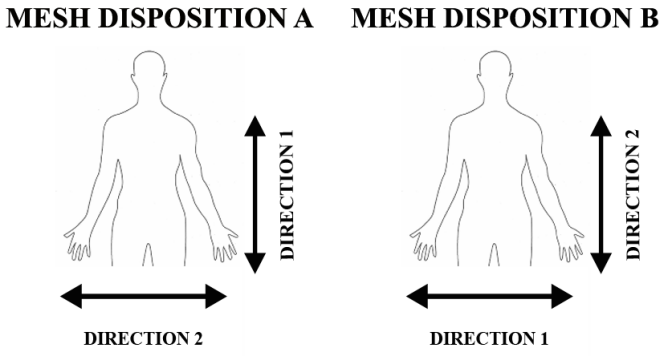

Figure 4: Two orientations are defined to place the mesh so that it covers the hernia. (a) Orientation A: the most compliant direction of the mesh, direction 1, is aligned with the craneo-caudal axis. (b) Orientation B: the stiffest direction of the mesh, direction 2, is aligned with the craneo-caudal axis.

2.3 Boundary conditions

DICOM images were taken with the subject lying down[12] and the defect created in that position. Thus, during a first load step, the change from the supine position to the standing position was modeled considering both body mass (gravity $= 4.64 \cdot 10^{-6}\ \frac{Kg}{mm^3}$), including the weight of the viscera and muscles, and IAP in the standing position (20 mmHg)[6]. Since IAP has been considered responsible for adverse effects in trauma and other abdominal diseases such as hernia formation or recurrence, we simulated its effect. Thus, during a second load step, a high physiological IAP commonly observed in the post-operative course was considered. Specifically, we used the IAP corresponding to a standing cough motion (P=107.6 mmHg).
In a physiological state under IAP the ribs prevent movement of the dorsal part of the abdomen so boundary conditions were defined in the model as follows. The constraint imposed by the ribs on the dorsal and lower part of the abdomen was entered by fixing the nodes in the dorsal abdomen and pelvis (see Figure 1.a).
FE analysis of the model was conducted using *ABAQUS v.11*® software and an implicit formulation.

3 Results

Figures 5.a and 5.c show the maximal displacements (MD) simulated for the three surgical meshes along the lines AB and CD defined in Figure 2.b, in the most external anatomical structures. Maximal principal stresses (MPS) along the lines AB and CD are presented in Figures 5.b and 5.d.
Along line AB, MD in the overlap zone was slightly lower because mesh stiffness is greater than that of the abdomen (see Figures 5.a and 5.c). Besides, MD decreased throughout the protheses when simulating SUR and OPT. In other words, SUR and OPT restrict movement in the

overlap zone and also restrict movement throughout of the repaired defect due to their stiffness. In contrast, the MD recorded throughout the INF mesh notably exceeded the displacement corresponding to the natural distensibility of the abdomen (see Figures 5.a and 5.c).
Among the three protheses, maximal restriction of the natural movement of the abdomen was provoked by SUR mesh. The low displacements obtained for this mesh in the area of the defect would clearly prevent the natural movement of the abdomen. Despite OPT also preventing the natural movement of the abdomen, its compliance was better than that observed for SUR. The maximum displacement obtained for INF was 95.8% and 149% higher than the MD recorded for OPT and SUR, respectively.
The distribution of MD and the maximum stretch values for each mesh are provided in Figure 6. The values obtained for INF mesh placed in orientation A differed significantly from those recorded in position B. Specifically, displacements were 18% higher for orientation B than position A. This means that, when a mesh is placed in orientation B, wall resistance may not be enough to maintain the pull-out forces of the viscera in large defects. Under IAP, the deformation of the abdomen is greater in the craneo-caudal direction than the transvere direction.
The greater stiffness of the prostheses compared to that of the tissue led to a marked increase in MPS in the area of the defect. These stresses concentrated in the overlap zone as depicted in Figures 5.b and 5.d.
The distribution of MPS for each mesh is shown in Figure 7. The central area of the defect supports different stresses depending on the prothesis implanted and on the placement direction. This can be clearly seen for the INF mesh. Thus, stresses in the lower area of the defect were higher than those obtained for SUR and OPT. Further, orientation A returned higher stress values. Stresses were also lower in the overlap zone than in the area of the defect.
To determine qualitatively which prothesis is the most vulnerable to relaxation under physiological loads, we examined MPS in the center of the protheses, Table 2. These values were compared with the experimental data[13].
Figure 8 shows that MPS for human tissues under the overlap are slightly higher than in the remaining areas. This stress concentration is due to the great stiffness of the protheses relative to that of the muscles and aponeuroses. In addition, stresses obtained for the aponeuroses were higher than those observed in muscles due to the greater stiffness of collagenous tissues.

4 Discussion

The mechanical properties of surgical meshes vary depending on the material used, spatial arrangement of the filaments, pore size and filament thickness. Such properties need to be adapted to the mechanical behavior of the abdominal tissues. Is most cases, surgeons are unaware of the mechanical properties of the implants they use. Furthermore, there are no guidelines indicating their correct orientation.
In this paper, we present a method to model the herniated human abdomen and study its mechanical response to physiological motion. Our main objective was to examine the response of the human abdominal wall to standing cough, as a common load, just after surgery using different prostheses. The model proposed is based on the simulated geometry of the repaired

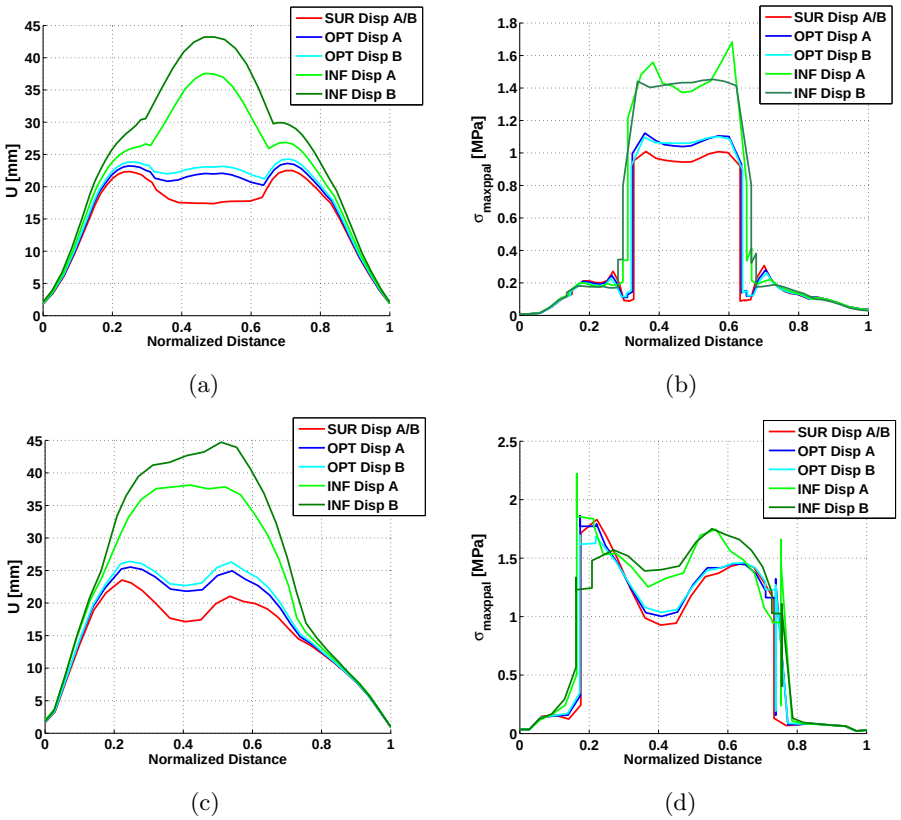

Figure 5: MD along the lines AB (a) and CD (c), and MPS along the lines AB (b) and CD (d) in the model of the herniated abdomen just after surgery (see Figure 2). The abscissa shows the normalized distance of the line AB. $x = 0$ and $x = 1$ correspond to points A and B, respectively.

herniated human abdomen differentiating several anatomical structures by MRI and includes the mechanical behavior of the different prostheses.

General findings. One of the main findings of this work was that the implant of a SUR mesh led to the worse compliance of the abdominal wall under physiological loads (see Figures 5.a and 5.c). This could translate to patient discomfort. The OPT mesh was found to restrict the natural movement of the abdomen to a lesser extent while the INF mesh emerged as very compliant. Moreover, INF mesh permited greater displacements to those needed to mimic the natural distensibility of the abdomen[12].

Maximal principal stresses for the healthy tissue areas (outside the defect) were slightly lower than values provided in the literature for the healthy abdomen[12]. Thus, MPS for simulation of the healthy abdomen undergoing a coughing motion are about 0.4 MPa[12]. However, in our model of the herniated human abdomen, MPS reached 0.25 MPa in the healthy tissue areas. The orientations of the muscles and aponeuroses justify this finding. In the human abdomen, the stiffer structures (linea alba, anterior and posterior rectus sheath and rectus tendons) occur in the front part of the abdomen so these support high stresses. However, in the herniated

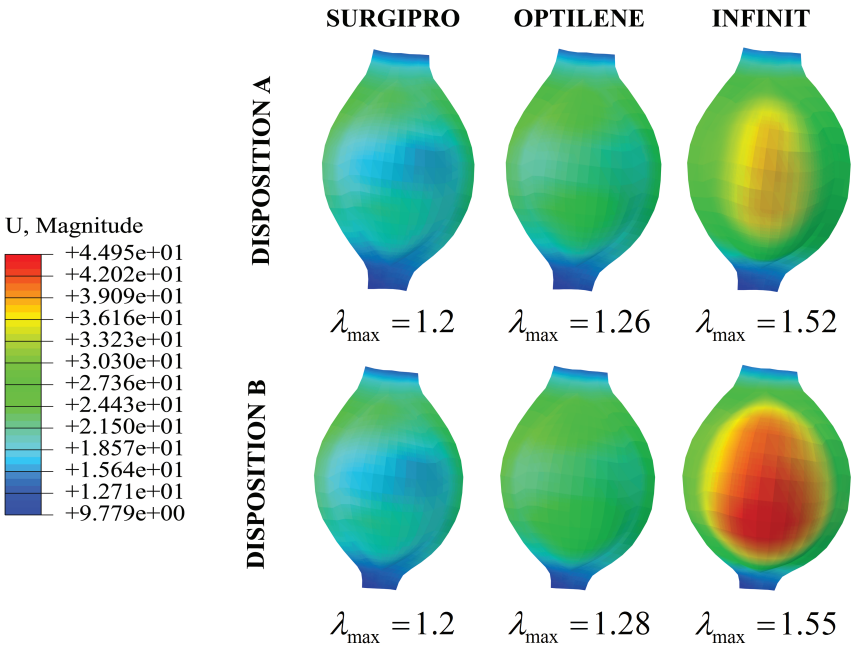

Figure 6: Displacements (mm) produced in the protheses after a coughing motion just after surgery. Note the similar distribution of displacements in SUR for both orientations due to its isotropic behavior.

abdomen, the stiffer structures rather than occupying a frontal position are laterally displaced by the defect. Thus, since IAP provokes higher displacements in the frontal abdomen, rather than being supported by the stiffer structures, stresses are supported by the prothesis.

Relation to previous studies. It has been widely established that the abdominal wall is anisotropic [11,33], the craneo-caudal direction being the most compliant and the transverse direction being stiffer. We observed that the response of the prothesis in the area of the defect is strongly determined by the alignment chosen (see Figures 6 and 7). In effect, an improved tissue regeneration process has been reported when a prosthetic implant is correctly aligned in relation to the direction of the host tissue [2]. Thus, due to anisotropy, the orientation of the mesh must be taken into account during surgery. Specifically, anisotropic protheses have to be placed so that the most compliant direction coincides with the craneo-caudal direction of the human body [1,13,7]. In addition, anisotropic directions in the mesh itself should be indicated as well as the stiffest and more compliant direction.

Clinical hernia recurrence occurs mainly at the implant margins. Several experimental studies have confirmed that some "overlap" is necessary [4,19]. Accordingly, for both conventional and laparoscopic surgery, besides the defect, the prothesis has to also cover approximately 3-5 cm of host tissue. Morris et al. [29] examined the outcomes of non-absorbable meshes placed within

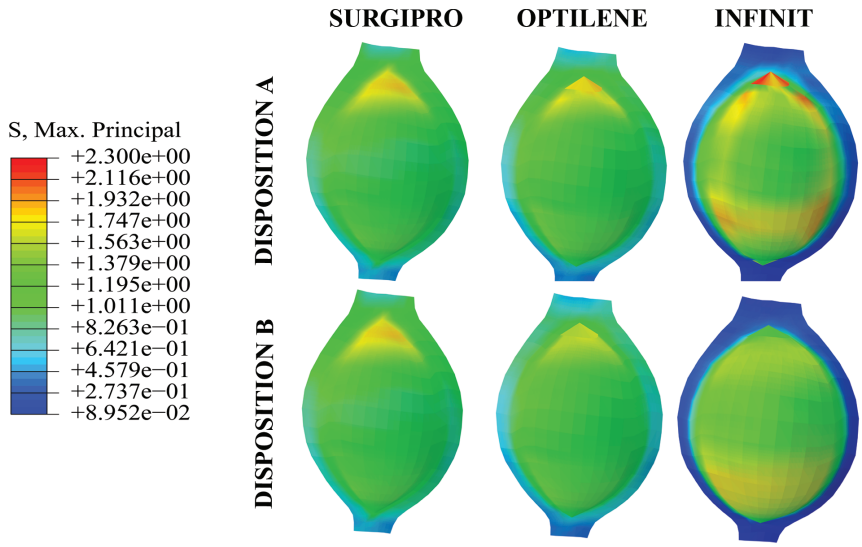

Figure 7: Distribution of maximal principal stresses (MPa) produced in the protheses after a coughing motion just after surgery.

Table 2: Experimental breaking stress (MPa) of the studied prothesis protheses examined [13], considering a thickness of 1 *mm*. These stresses are, compared to the simulated maximal principal stresses [MPa] obtained in the simulation in a representative model element located of the model in the center of the protheses.

		Experimental data	FEM Orientation A	FEM Orientation B
SURGIPRO	Dir. 1	19.926	0.93308	0.93308
	Dir. 2	16.655		
OPTILENE	Dir. 1	6.3598	1.02324	1.04889
	Dir. 2	9.5601		
INFINIT	Dir. 1	1.8028	1.3623	1.43092
	Dir. 2	1.2044		

the abdominal cavity. These authors concluded that all recurrences were reported as occurring laterally to the mesh and no cases of mesh weakness were identified in any of the studied materials. Langer et al. [21] provided the first description of central mesh rupture after incisional hernia repair using a mesh and Schippers et al. [32] observed broken filaments of meshes after histological examination. Deeken et al. [7] described the standard techniques used, underwent

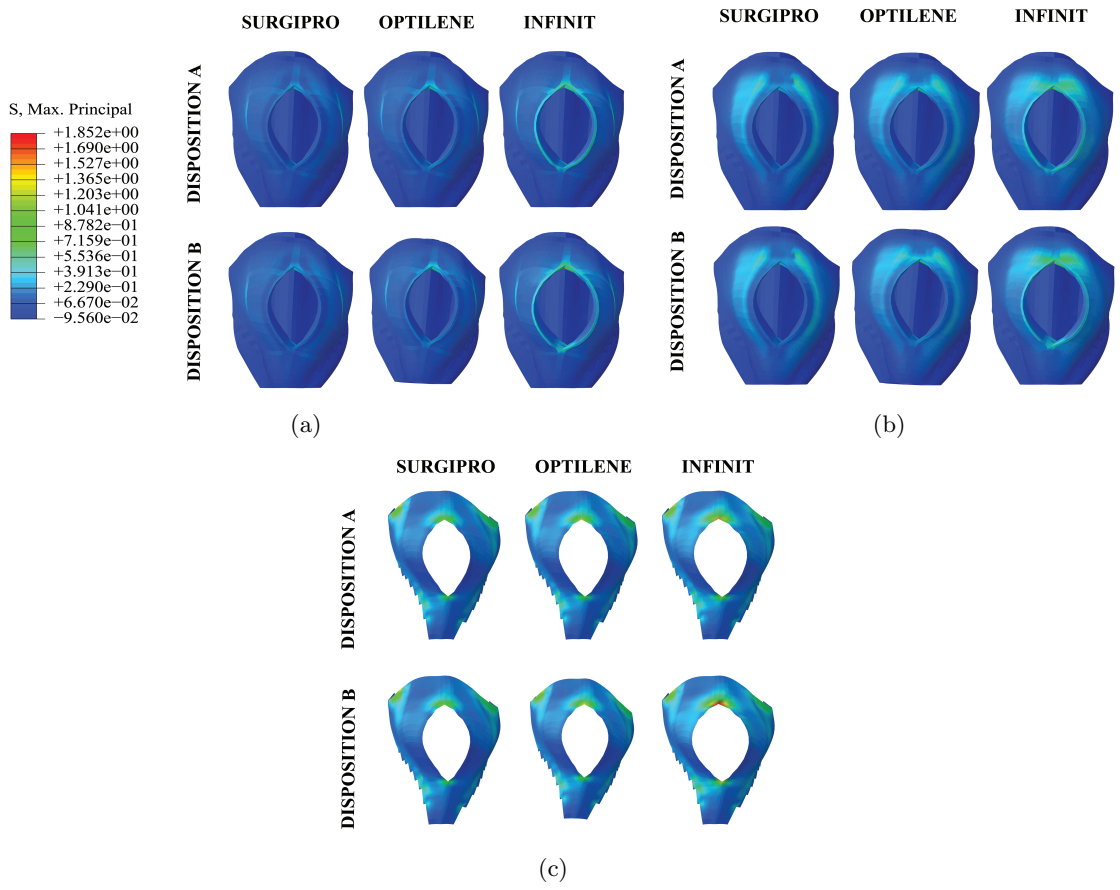

Figure 8: Maximal principal stress distributions (MPa) in the abdominal tissues: rectus abdominis and their tendons (a), anterior rectus sheath (b) and fascia transversalis (c). In all cases, results are shown for the linea alba and oblique muscles.

physicomechanical testing and classified materials commonly used for hernia repair. In line with our findings, these authors concluded that the orientation of anisotropic meshes is critical for implant success and that INF mesh should not be used when a high tensile strength is required. We observed that maximal experimental stresses related to the implant of SUR and OPT[13] were higher than the values provided by our simulation (see Table 2). However, our experimental data for INF along direction 2[13] indicate that, just after surgery and while standing to cough, the stresses generated in this prothesis exceed the maximal stress it may support (see Table 2). Qualitatively, this suggests that INF is the most vulnerable prothesis to relaxation under physiological loads from a mechanical point of view. Consequently, this surgical mesh should not be used, for instance, in extremely obese patients or for the repair of a very large defect without tissue reinforcement[7].

Limitations. Some limitations of this study should be mentioned. First, since experimental data for the mechanical characterization of human tissue are limited, animal data were sometimes

used. In all cases, the experimental data used were derived from uniaxial tests and these tests are not sufficient for the mechanical characterization of multidimensional material models aimed at predicting the behaviour in physiological loading states[15]. Thus, further information from other mechanical multiaxial tests (e.g. biaxial, inflation) would be useful to complete our characterization of these materials. Our simulations included a simplified geometry of the prothesis through a continuum membrane sheet and the behaviour of the meshes were characterized by uniaxial tests. In addition, our work did not consider host tissue in-growth in the prostheses. Thus, our findings only correspond to time zero after surgery. Modeling of tissue incorporation in the implant would provide useful information about the wound repair process, which differs according to factors such as the pore size or composition of the prosthetic material. Also, since we only considered the elastic mechanical response, future studies should examine the active response, the viscoelastic properties of muscle and stiffness loss due to damage. The results obtained in this study also need validation in an experimental *in vivo* study that reproduces the physiological state represented here, as they are only qualitative. In addition, since the geometry of the abdomen markedly affects the results, the same subject should be used to compare computational and experimental results when validating the model.

5 Conclusions

In this study, we have described a method designed to model the repaired herniated human abdomen just after surgery and examine its mechanical response to a physiological movement (standing cough). In particular, we sought to analyze the mechanical response of the herniated human abdomen to the placement of different prostheses. Our findings suggest that anisotropic implants need to be positioned such that the most compliant axis of the mesh coincides with the craneo-caudal direction of the body. The major drawback of this study is that it is not validated in an experimental *in vivo* study. Despite the limitations of this study, our model may have applications in the computational testing of new synthetic prosthetic designs before clinical trials.

6 Acknowledgments

This study was supported by the Spanish Ministry of Economy and Competitiveness through research project DPI2011-27939-C02-01/C02-02 and the Instituto de Salud Carlos III (ISCIII) through the CIBER initiative project ABDOMESH. B. Hernández-Gascón was also funded by a grant (BES-2009-021515) from the Spanish Ministry of Science and Technology.

References

[1] M. V. Anurov, S. M. Titkova, and A. P. Oettinger. Impact of position of light mesh endoprosthesis with anisotropic structure for the efficiency of anterior abdominal wall reconstruction. *Bulletin of Experimental Biology and Medicine*, 149(6):779–83, 2010.

[2] M. V. Anurov, S. M. Titkova, and A. P. Oettinger. Biomechanical compatibility of surgical mesh and fascia being reinforced: dependence of experimental hernia defect repair results on anisotropic surgical mesh positioning. *Hernia*, 16:199–210, 2012.

[3] E. M. Arruda, K. Mundy, S. Calve, and K. Baar. Denervation does not change the ratio of collagen I and collagen II mRNA in extracellular matrix of muscle. *American Journal of Physiology - Regulatory, Integrative and Comparative Physiology*, 292:983–987, 2006.

[4] M. Binnebösel, R. Rosch, K. Junge, T. Flanagran, R. Schwab, V. Schumpelick, and U. Klinge. Biomechanical analyses of overlap and mesh dislocation in an incisional hernia model in vivo. *Surgery*, 142(3):365–71, 2007.

[5] B. Calvo, E. Peña, P. Martins, T. Mascarenhas, M. Doblare, R. Natal, and A. Ferreira. On modelling damage process in vaginal tissue. *Journal of Biomechanics*, 42:642–651, 2009.

[6] W. S. Cobb, J. M. Burns, K. W. Kercher, B. D. Matthews, H. J. Norton, and B. T. Heniford. Normal intraabdominal pressure in healthy adults. *Journal of Surgical Research*, 129:231–235, 2005.

[7] C. R. Deeken, M. S. Abdo, M. M. Frisella, and B Matthews. Physicomechanical evaluation of polypropylene, polyester, and polytetrafluoroethylene meshes for inguinal hernia repair. *Journal of the American College of Surgeons*, 212(1):68–79, 2011.

[8] H. Demiray, H. W. Weizsacker, K. Pascale, and H. Erbay. A stress-strain relation for a rat abdominal aorta. *Journal of Biomechanics*, 21:369–374, 1988.

[9] G. Fortuny, J. Rodríguez-Navarro, A. Susín, and M. López-Cano. Simulation and study of the behaviour of the transversalis fascia in protecting against the genesis of inguinal hernias. *Journal of Biomechanics* , 42:2263–2267, 2009.

[10] O. Gerovichev, P. Marayong, and A. M. Okamura. The Effect of Visual and Haptic Feedback on Manual and Teleoperated Needle Insertion. In *Medical Image Computing and Computer-Assisted Intervention - MICCAI 2002*, volume 2488, pages 147–154. Springer Berlin / Heidelberg, 2002.

[11] B. Hernández, E. Peña, G. Pascual, M. Rodríguez, B. Calvo, M. Doblaré, and J. M. Bellón. Mechanical and histological characterization of the abdominal muscle. A previous step to model hernia surgery. *Journal of the Mechanical Behavior of Biomedical Materials*, 4 (3):392–404, 2011.

[12] B. Hernández-Gascón, A. Mena, E. Peña, G. Pascual, J. M. Bellón, and B. Calvo. Understanding the passive mechanical behavior of the human abdominal wall. *Annals of Biomedical Engineering*, In Press:DOI: 10.1007/s10439–012–0672–7, 2012.

[13] B. Hernández-Gascón, E. Peña, H. Melero, G. Pascual, M. Doblaré, M. P. Ginebra, J. M. Bellón, and B. Calvo. Mechanical behaviour of synthetic surgical meshes. Finite element simulation of the herniated abdominal wall. *Acta Biomaterialia*, 7 (11):3905–3913, 2011.

[14] B. Hernández-Gascón, E. Peña, G. Pascual, M. Rodríguez, J. M. Bellón, and B. Calvo. Long-term anisotropic mechanical response of surgical meshes used to repair abdominal wall defects. *Journal of the Mechanical Behavior of Biomedical Materials*, 5 (1):257–271, 2012.

[15] G. A. Holzapfel. Determination of material models for arterial walls from uniaxial extension tests and histological structure. *Journal of Theoretical Biology*, 238:290–302, 2006.

[16] G. A. Holzapfel, T. C. Gasser, and R. W. Ogden. A new constitutive framework for arterial wall mechanics and a comparative study of material models. *Journal of Elasticity*, 61:1–48, 2000.

[17] A. Kald, B. Anderberg, P. Carlsson, P. O. Park, and K. Smedh. Surgical outcome and cost-minimisation-analyses of laparoscopic and open hernia repair: a randomised prospective trial with one year follow up. *Eur J Surg*, 163(7):505–10, 1997.

[18] M. Kauer. *Inverse Finite Element Characterization of Soft Tissues with Aspiration Experiments*. PhD thesis, Swiss Federal Institute of Technology, Zürich, 2001.

[19] E. Kes, J. Lange, J. Bonjer, R. Stoeckart, P. Mulder, C. Snijders, and G. Kleinrensink. Protrusion of prosthetic meshes in repair of inguinal hernias. *Surgery*, 135(2):163–170, 2004.

[20] U. Klinge, B. Klosterhalfen, V. Birkenhauer, K. Junge, J. Conze, and V. Schumpelick. Impact of polymer pore size on the interface scar formation in a rat model. *Journal of Surgical Research*, 103:208–214, 2002.

[21] C. Langer, T. Neufang, C. Kley, T. Liersch, and H. Becker. Central mesh recurrence after incisional hernia repair with marlex- are the meshes strong enough? *Hernia*, 5:164–167, 2001.

[22] K. A. LeBlanc, D. Bellanger, K. V. Rhynes 5th, D. G. Baker, and R. W. Stout. Tissue attachment strength of prosthetic meshes used in ventral and incisional hernia repair. A study in the New Zealand White rabbit adhesion model. *Surgical Endoscopy*, 16(11):1542–6, 2002.

[23] I. L. Lichtenstein and A. G. Shulman. Ambulatory outpatient hernia surgery including a new concept, introducing tension-free repair. *International Surgery*, 71:1–4, 1986.

[24] I. L. Lichtenstein, A. G. Shulman, P. K. Amid, and M. M. Montlor. The tension-free hernioplasty. *American Journal of Surgery*, 157:188–193, 1989.

[25] M. López-Cano, J. Rodríguez-Navarro, A. Rodríguez-Baeza, M. Armengol-Carrasco, and A. Susín. A real-time dynamic 3D model of the human inguinal region for surgical education. *Computers in Biology and Medicine*, 37:1321–1326, 2007.

[26] D. W. Marquardt. An algorithm for least-squares estimation of nonlinear parameters. *SIAM Journal on Applied Mathematics*, 11:431–441, 1963.

[27] P. Martins, E. Peña, R. M. Natal Jorge, A. Santos, L. Santos, T. Mascarenhas, and B. Calvo. Mechanical characterization and constitutive modelling of the damage process in rectus sheath. *Journal of the Mechanical Behavior of Biomedical Materials*, 8:111–122, 2012.

[28] Moore W. *Gray's Anatomy celebrates 150th anniversary.* The Telegraph (Telegraph Media Group), 2008.

[29] G. J. Morris-Stiff and L. E. Hughes. The outcomes of nonabsorbible mesh paced within the abdominal cavity: literature review and clinical experience. *Journal of the American College of Surgeons*, 186:352–367, 1998.

[30] Y. Ozog, M. L. Konstantinovic, E. Werbrouck, D. De Ridder, E. Mazza, and J. Deprest. Persistence of polypropylene mesh anisotropy after implantation: an experimental study. *Urogynaecology*, 118(10):1180–5, 2011.

[31] C. Sabbagh, F. Dumont, B. Robert, R. Badaoui, P. Verhaeghe, and J. M. Regimbeau. Peritoneal volume is predictive of tension-free fascia closure of large incisional hernias with loss of domain: a prospective study. *Hernia*, 15 (5):559–65, 2011.

[32] E. Schippers. *Recurrent hernia*, chapter Central mesh rupture- Myth or real concern?, pages 371–376. Springer Berlin Heidelberg, 2007.

[33] C. Song, A. Alijani, T. Frank, G. Hanna, and A. Cuschieri. Mechanical properties of the human abdominal wall measured in vivo during insufflation for laparoscopic surgery. *Surgical Endoscopy*, 20:987–990, 2006.

Work 8: A 3D continuum model for simulating skeletal muscle contraction

Journal: *Submitted* (2012)

A 3D continuum model for simulating skeletal muscle contraction

B. Hernández-Gascón[a,b], J. Grasa[a,b], B. Calvo[a,b] and J. F. Rodríguez[a,b]

[a] *Aragón Institute of Engineering Research. University of Zaragoza (Spain)*
[b] *CIBER-BBN. Centro de Investigación en Red en Bioingeniería, Biomateriales y Nanomedicina (Spain)*

Abstract

A thermodynamically consistent three-dimensional electro-mechanical continuum model for simulating skeletal muscle contraction is presented. Active and passive response are accounted for by means of a decoupled strain energy function into passive and active contributions. The active force is obtained as the maximum tetanic force penalized by two functions that consider the external stimulus frequency and the overlap between actin and myosin filaments. Passive response is model by a transversely isotropic strain energy function. The response of the model is analyzed by means of finite element simulations that reproduce the one dimensional isometric, concentric and eccentric contractions in a simplified model of a muscle. The model has also been implemented to reproduce isometric and concentric contraction on three dimensional finite element models of the tibialis anterior rat muscle and the human rectus abdominis muscle. Both finite element models were obtained from magnetic resonance imaging and considered the preferential directions associated with the collagen and muscular fibres. The proposed model has been validated using experimental data of the active force generated by isolated tibialis anterior rat muscles during isometric contractions.

Keywords: muscular fibres, collagen fibres, contraction, hyperelasticity, finite element model.

1 Introduction

Skeletal muscles exist throughout the human body and are under control of the nervous system. The main functions of these muscles are the body motion and posture support and most of them are attached to bones by bundles of collagen fibres known as tendons. Skeletal muscles are made up of individual components known as muscle fibres that contribute not only to the active response but also the passive one. In addition, muscle fibres are surrounded by connective tissue capable of absorbing the muscle lengthening. Connective tissue has a major role in protection and covering of muscle fibres and is composed of a ground substance, collagen fibres and elastin fibres of varying proportions. In muscle, the connective tissue is largely responsible for transmitting forces, for example the transmission of forces from the muscle to the bone by the tendon. Muscle fibres generate force through the action of actin and myosin cross-bridge cycling and, consequently, muscle may lengthen in a eccentric contraction, shorten in a concentric contraction, or remain the same in an isometric contraction.

Computational models offer the possibility of simulating experimental observations and obtaining internal variables such as stresses and deformations. Thus, the mechanical effects of muscular, collagen, elastin fibres interaction can be implemented into numerical models to predict the outcome of skeletal muscle contraction. Specifically, contraction in skeletal muscles can be propagated due to an electrical, mechanical or chemical stimuli. Some researches have focussed their works on modelling skeletal muscle contraction within the continuum mechanics framework to model muscle contraction.

The Hill model[19] has been widely used in the literature. This model is based on experimental observations in frogs. The model explains the relationship between force and velocity on the whole muscle and consists of a contractile element, representing the contraction mechanism or active response, in series with an elastic one that symbolizes the passive contribution of muscle fibres. Besides, a parallel element considers passive properties of muscle associated to connective tissue and collagen and elastin fibres. In 1977, Hatze[16] suggested an improvement of the Hill model by means of including the influence of the fibre length on the activation process. Microstructural details were considered in the model proposed by Huxley[20] where the cross-bridges theory considers the interaction between actin and myosin filaments in two different states, i.e, coupled or uncoupled.

The contraction of a whole muscle has been studied in the literature in simulations where different muscles are included but these studies do not include information about the geometry[8,11,25]. Geometrical information has been considered in other studies that use macroscopic description of the tissue and include the active behaviour in one-dimensional models through micromechanical approaches[3,21,24,31]. The three-dimensional modelling of the active behaviour through micromechanical models has been reported in other studies focussed on skeletal[4] and smooth muscles[28,29].

To the authors's knowledge, the first study to incorporate the chemical kinetics of smooth muscle contraction and nonlinear kinematics was published by Stålhand et al.[28]. These authors used the chemical state law of Hai and Murphy[15] to connect the chemical influence to the active behaviour in a one-dimensional study. Several years later, the three-dimensional extension of this model was published by Stålhand et al.[29]. This work is based on the idea presented by

these authors, who consider that the deformation associated to the smooth muscle activity can be modelled as two fictitious processes and can be expressed as a multiplicative decomposition of the deformation gradient [29]. However, the model proposed in our work is translated to skeletal muscle.

The aim of this work is to present a thermodynamically consistent electro-mechanical continuum model, based on Stålhand et al. [29], to simulate the skeletal muscle contraction within the 3D continuum mechanics framework. The modelling reproduces both contributions of skeletal muscle, the passive and active responses, being the last one modelled through an electrical signal. One of the major challenges of this work is to propose a model which does not depend on a velocity function, as other works in the literature suggest [4,13], but the model is capable of reproducing such effect. The simulation of skeletal muscle contraction is developed using two finite element (FE) models that reproduces the geometry of the rat tibialis anterior muscle and the human rectus abdominis muscle.

2 Mathematical model

2.1 Kinematics

Let Ω_0 be a three-dimensional solid defined by a set of points which are identified by their coordinates in a reference configuration. The bijective time dependent function $\boldsymbol{\varphi_o}$, namely initial, material, reference or undeformed configuration, governs the motion of any point $\boldsymbol{P} \in \Omega_o$ according to:

$$\boldsymbol{\varphi}_o : \Omega_o \to \mathbb{R}^3 \quad \boldsymbol{\varphi}_o \equiv \mathbf{X}; \qquad \varphi_o^I = X^I. \tag{1}$$

The motion of the solid, after a time t, defines the current configuration, Ω_t, with regard to a reference system which can also vary with time, according to:

$$\begin{aligned} &\boldsymbol{\varphi}_t : \Omega_t \to \mathbb{R}^3 \quad \boldsymbol{\varphi}_t \equiv \mathbf{x}; \\ &\boldsymbol{\varphi}_t^i = x^i \quad \text{with} \quad t \in \mathbb{I} \in \mathbb{R}, \end{aligned} \tag{2}$$

where $\boldsymbol{\varphi}_t$ is denoted the current, spatial or deformed configuration.

Let $\mathbf{F}$ be the deformation gradient associated with the motion $\boldsymbol{\varphi}_t$. $\mathbf{F}$ is defined as the tensor field on the undeformed configuration $\boldsymbol{\varphi}_o(\Omega)$, $\mathbf{F} = \frac{\partial \mathbf{x}}{\partial \mathbf{X}}$, where $J \equiv det\mathbf{F} > 0$ is the Jacobian of the transformation.

In order to handle more easily the quasi-incompressibility constraint presented by soft tissues ($J \cong 1$), a multiplicative decomposition of the deformation gradient into volume-changing and volume-preserving parts is usually established [10] as follows:

$$\mathbf{F} = J^{\frac{1}{3}}\bar{\mathbf{F}}, \qquad \bar{\mathbf{F}} = J^{-\frac{1}{3}}\mathbf{F} \tag{3}$$

$$\mathbf{C} = \mathbf{F}^T\mathbf{F}, \qquad \bar{\mathbf{C}} = J^{-\frac{2}{3}}\mathbf{C} = \bar{\mathbf{F}}^T\bar{\mathbf{F}} \tag{4}$$

$$\mathbf{b} = \mathbf{F}\mathbf{F}^T, \qquad \bar{\mathbf{b}} = J^{-\frac{2}{3}}\mathbf{b} = \bar{\mathbf{F}}\bar{\mathbf{F}}^T, \tag{5}$$

where $J^{\frac{1}{3}}\mathbf{I}$ and $\bar{\mathbf{F}}$ represent the volumetric and deviatoric deformation gradients, respectively. $\mathbf{C}$ and $\mathbf{b}$ are the right and left Cauchy-Green strain tensors and $\bar{\mathbf{C}}$ and $\bar{\mathbf{b}}$ their modified counterparts.

Assume that the deformation associated to the muscle activity can be modelled as two fictitious processes[29] (see Figure 1): the first process is associated to the relative motion of the myosin with respect to actin, and the second process relates the elastic deformation of cross bridges. Mathematically, it can be expressed as a multiplicative decomposition of the deformation gradient $\bar{\mathbf{F}}$:

$$\bar{\mathbf{F}} = \bar{\mathbf{F}}_e \bar{\mathbf{F}}_a, \tag{6}$$

where $\bar{\mathbf{F}}_a$ defines the deformation associated with the contractile response provoked by the filament translation (actin and myosin), whereas $\bar{\mathbf{F}}_e$ represents a deformation due to cross bridges elasticity. It is important to note that the gradient $\bar{\mathbf{F}}_a$ represents the active contraction so it does not need to be integrable. Thus, infinitesimal parts of the tangent space Ω_0 are deformed independently and the configuration they form after the motion may not be compatible. The gradient $\bar{\mathbf{F}}_e$ guarantees the compatibility in the deformed configuration Ω_t. Accordingly, let $\bar{\mathbf{C}}_e = \bar{\mathbf{F}}_e^T \bar{\mathbf{F}}_e = \bar{\mathbf{F}}_a^{-T} \bar{\mathbf{C}} \bar{\mathbf{F}}_a^{-1}$ be a deformation measure due to the titin and cross bridges motion which is not a state variable since it depends on $\bar{\mathbf{C}}$ y $\bar{\mathbf{F}}_a$.

It is necessary to distinguish between collagen fibres, which are mainly responsible for the passive mechanical response, and muscular fibres, which are associated with the contractile muscle behaviour. Moreover, muscular and collagen fibres are frequently not aligned in the same direction[17,22]. The direction of collagen fibres is assumed to determine the direction of material anisotropy in order to study the passive behaviour of the tissue[1], whereas muscle fibres have to be considered in the modelling of the active behaviour. Thus, the anisotropy in a point $\mathbf{X} \in \Omega_0$ associated with the active and passive responses is described by unit vectors $\mathbf{m}_0(\mathbf{X})$ ($|\mathbf{m}_0| = 1$) and $\mathbf{n}_0(\mathbf{X})$ ($|\mathbf{n}_0| = 1$), respectively. Let $\mathbf{E}_i$ be a set of global orthogonal vectors and let $\mathbf{G}_i = (\mathbf{m}_0, \mathbf{r}_0, \mathbf{l}_0)$ be a set of local orthogonal base vectors in the tangent space Ω_0, where $\mathbf{r}_0$ is in the plane spanned by $\mathbf{m}_0$ and $\mathbf{n}_0$ such that $\mathbf{m}_0 \cdot \mathbf{r}_0 = 0$ and $\mathbf{l}_0 = \mathbf{m}_0 \times \mathbf{n}_0$ (see Figure 1).

Let us assume that muscle fibres contract along the direction $\mathbf{m}_0$ only, and let $\bar{\lambda}_a$ be the contraction. Thus, the active contractile tensor, $\bar{\mathbf{F}}'_a$, in the local coordinate system, $\mathbf{G}_i$, can be written as:

$$\bar{\mathbf{F}}'_a = \bar{\lambda}_a \mathbf{G}_1 \otimes \mathbf{G}_1 + \bar{\lambda}_a^{-1/2} \mathbf{G}_2 \otimes \mathbf{G}_2 + \bar{\lambda}_a^{-1/2} \mathbf{G}_3 \otimes \mathbf{G}_3, \tag{7}$$

where we have assumed the active contractile tensor $\bar{\mathbf{F}}'_a$ to be isochoric and $\bar{\lambda}_2 = \bar{\lambda}_3$, and a dual base is formed between $\mathbf{G}_i$ and $\mathbf{G}^i$, i.e. $\mathbf{G}^i$ is defined as $\mathbf{G}^i \cdot \mathbf{G}_j = \delta^i_j$ where δ^i_j is the Kronecker Delta.

The components of the contractile tensor in the global system of coordinates, $\bar{\mathbf{F}}_a$, are found as:

$$\bar{\mathbf{F}}_a = \mathbf{R} \bar{\mathbf{F}}'_a \mathbf{R}^T, \tag{8}$$

where $\mathbf{R}_{ij} = \mathbf{E}_i \cdot \mathbf{G}_j$ is the rotation tensor.

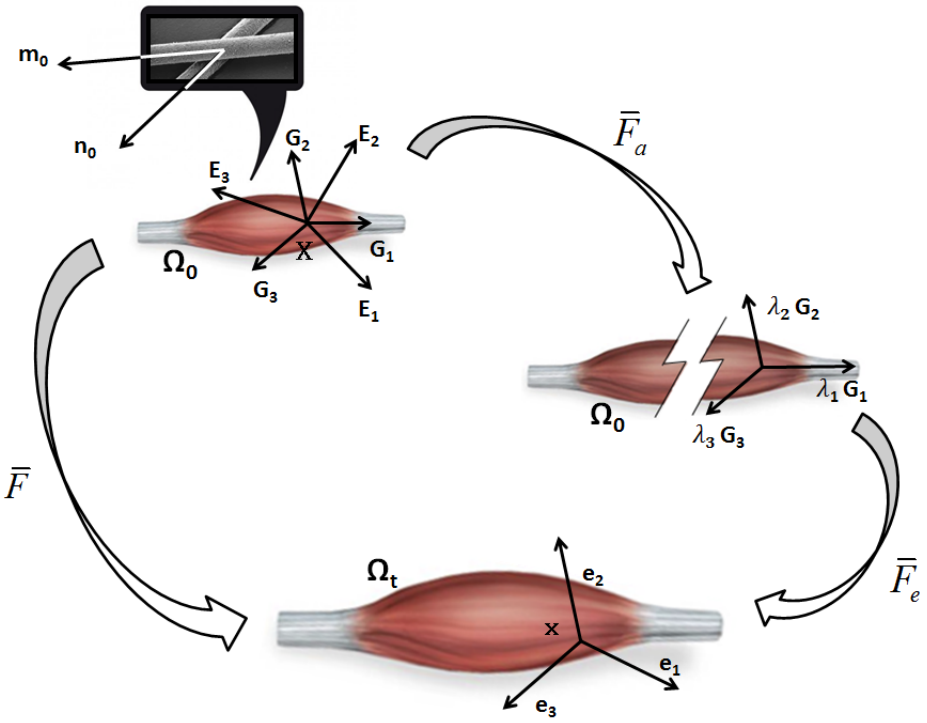

Figure 1: Scheme of the defined configurations. Vectors $\mathbf{G}_i$ at a point $\mathbf{X}$ in the reference configuration transform in new vectors $\lambda_i \mathbf{G}_i$ in their own directions by the active contraction $\mathbf{F}_a$. $\mathbf{F}_a$ is not associated to a real deformation since infinitesimal parts of the tangent space Ω_0 are deformed independently and the configuration they form after the motion may no be compatible. The compatibility is restored by $\mathbf{F}_e$ in the deformed configuration Ω_t.

2.2 Balance laws

The principle of virtual power in continuum mechanics [12] is applied to obtain the balance laws for the contracting skeletal muscles. This principle states the external and internal power production $\hat{P}_i$ and $\hat{P}_e$, respectively, must satisfy the following equality:

$$\hat{P}_i(\eta) + \hat{P}_e(\eta) = 0, \tag{9}$$

where η symbolizes the set of admissible velocities. Specifically, the internal and external power production are defined according to:

$$\hat{P}_i = -\int_{\varphi_o} \mathbf{P} : \nabla_X \eta \, \mathrm{d}V \quad \text{in} \quad \Omega_o \tag{10}$$

$$\hat{P}_e = \int_{\partial\varphi_o} \mathbf{T} \cdot \eta \, \mathrm{d}A \quad \text{in} \quad \partial\Omega_o, \tag{11}$$

where $\cdot$, : and ∇_X correspond to the dot product, the double contraction and the material gradient, respectively, $\mathbf{T}$ is the material traction vector and $\mathbf{P}$ is the first Piola-Kirchhoff stress tensor. Substituting Equation 10 and Equation 11 into Equation 9, and applying the divergence theorem, the equilibrium equations are obtained:

$$\nabla_X \cdot \mathbf{P} = 0 \quad \text{in} \quad \Omega_o, \ \mathbf{T} = \mathbf{P}^T \mathbf{\Gamma} \quad \text{in} \quad {\partial\Omega_o}^S \quad \text{and} \quad U = U_0 \quad \text{in} \quad {\partial\Omega_o}^U, \tag{12}$$

where $\partial\Omega_o = {\partial\Omega_o}^S \cup {\partial\Omega_o}^U$ and $\mathbf{\Gamma}$ corresponds to the unit normal to the boundary in the reference configuration $\partial\Omega_o$.

2.3 3D Hyperelastic constitutive laws

A frequently used methodology to formulate an elastic constitutive law for fibred soft tissues is to postulate the existence of a strain energy function [27]. Mathematically, the free energy is taken to be a function of the state variables $\mathbf{F}$ and λ_a, and the structural tensors $\mathbf{M}, \mathbf{N}$ defined as $\mathbf{M} = \mathbf{m}_0 \otimes \mathbf{m}_0$ and $\mathbf{N} = \mathbf{n}_0 \otimes \mathbf{n}_0$ consider the anisotropy of the muscles due to muscular and collagen fibres, respectively. Furthermore, the free energy is considered to be dependent on $\mathbf{C}_e$, despite not being a state variable, because it represents the elastic deformation of the cross-bridges. Therefore:

$$\Psi = \Psi(\mathbf{C}, \mathbf{C}_e, \lambda_a, \mathbf{N}, \mathbf{M}). \tag{13}$$

The strain energy function is usually expressed in a decoupled form into a volume-changing and a volume-preserving parts in order to handle the quasi-incompressibility constraint [10]. Furthermore, the deviatoric part is divided into a passive contribution, due to the collagen and elastin, $\bar{\Psi}_p$, and an active contribution associated with the muscular fibres, $\bar{\Psi}_a$. Thus, the total strain energy function Ψ can be expressed as follows:

$$\Psi = \Psi_{vol}(J) + \bar{\Psi}_p(\bar{\mathbf{C}}, \mathbf{N}) + \bar{\Psi}_a(\bar{\mathbf{C}}_e, \bar{\lambda}_a, \mathbf{M}). \tag{14}$$

The passive strain energy function, $\bar{\Psi}_p$, is defined as a function of the invariants:

$$\bar{I}_1 = tr\bar{\mathbf{C}}, \qquad \bar{I}_2 = \frac{1}{2}((tr\bar{\mathbf{C}})^2 - tr\bar{\mathbf{C}}^2), \quad \bar{I}_4 = \mathbf{n}_0.\bar{\mathbf{C}}\mathbf{n}_0 = \bar{\lambda}^2, \tag{15}$$

where $\bar{I}_1$ and $\bar{I}_2$ are the first and second modified strain invariants of the symmetric modified Cauchy-Green tensor $\bar{\mathbf{C}}$, and $\bar{I}_4$ is the pseudo-invariant related to the anisotropy of the passive response (collagen fibres). Similarly, the active contribution of the strain energy function, $\bar{\Psi}_a$, is expressed in term of the pseudo-invariant associated to $\bar{\mathbf{C}}_e$:

$$\bar{J}_4 = \mathbf{m}_0.\bar{\mathbf{C}}_e\mathbf{m}_0 = \lambda_e^2. \tag{16}$$

Hence:

$$\Psi = \Psi_{vol}(J) + \bar{\Psi}_p(\bar{I}_1, \bar{I}_2, \bar{I}_4) + \bar{\Psi}_a(\bar{J}_4, \bar{\lambda}_a). \tag{17}$$

During muscle contraction, the Clausius-Planck inequality reduces to:

$$\mathcal{D}_{int} = -\dot{\Psi} + \frac{1}{2}\mathbf{S} : \dot{\mathbf{C}} + \frac{1}{2}\mathbf{S}_a : \dot{\mathbf{C}}_a \geq 0. \tag{18}$$

In Equation 18, $\mathbf{S}_a$ represents active stress, and $\frac{1}{2}\mathbf{S}_a : \dot{\mathbf{C}}_a$ the muscle power stroke. Taking into account Equation 7, Equation 8 and Equation 13, Equation 18 reduces to:

$$\left(\frac{1}{2}\mathbf{S} - \frac{\partial \Psi}{\partial \mathbf{C}}\right) : \dot{\mathbf{C}} - \frac{\partial \Psi}{\partial \mathbf{C}_e} : \dot{\mathbf{C}}_e + \left(\frac{1}{2}\mathbf{S}_a - \frac{\partial \Psi}{\partial \mathbf{C}_a}\right) : \dot{\mathbf{C}}_a \geq 0. \tag{19}$$

Taking into account Equation 6 allows to eliminate the explicit dependance on $\dot{\mathbf{C}}_e$:

$$\left(\frac{1}{2}\mathbf{S} - \frac{\partial \Psi}{\partial \mathbf{C}} - \mathbf{F}_a^{-1}\frac{\partial \Psi}{\partial \mathbf{C}_e}\mathbf{F}_a^{-T}\right) : \dot{\mathbf{C}} + \left(\mathbf{F}_a\mathbf{S}_a - 2\mathbf{F}_a\frac{\partial \Psi}{\partial \mathbf{C}_a} + 2\mathbf{C}_e\frac{\partial \Psi}{\partial \mathbf{C}_e}\mathbf{F}_a^{-T}\right) : \dot{\mathbf{F}}_a \geq 0. \tag{20}$$

Hence, in order to satisfy Equation 20, the following constitutive relations are obtained:

$$\mathbf{S} = 2\frac{\partial \Psi}{\partial \mathbf{C}} + \mathbf{F}_a^{-1}(2\frac{\partial \Psi}{\partial \mathbf{C}_e})\mathbf{F}_a^{-T} \tag{21}$$

$$(\mathbf{P}_a - 2\mathbf{F}_a\frac{\partial \Psi}{\partial \mathbf{C}_a} + 2\mathbf{C}_e\frac{\partial \Psi}{\partial \mathbf{C}_e}\mathbf{F}_a^{-T}) : \dot{\mathbf{F}}_a \geq 0, \tag{22}$$

where $\mathbf{P}_a$ is the first Piola-Kirchoff active stress.

2.4 Stress tensors and elasticity tensor

Substituting Equation 14 into Equation 21, the second Piola Kirchhoff stress tensor is found to be:

$$\mathbf{S} = \mathbf{S}_{vol} + \bar{\mathbf{S}}_p + \bar{\mathbf{S}}_a, \tag{23}$$

with:

$$\mathbf{S}_{vol} = J\frac{d\Psi_{vol}}{dJ}\mathbf{C}^{-1} = Jp\mathbf{C}^{-1}, \tag{24}$$

$$\bar{\mathbf{S}}_p = J^{-\frac{2}{3}}DEV[2\frac{\partial \Psi}{\partial \bar{\mathbf{C}}}] = J^{-\frac{2}{3}}DEV[\bar{\mathbf{S}}_p], \tag{25}$$

$$\bar{\mathbf{S}}_a = J^{-\frac{2}{3}}\bar{\mathbf{F}}_a^{-1}DEV_{C_e}[2\frac{\partial \Psi}{\partial \bar{\mathbf{C}}_e}]\bar{\mathbf{F}}_a^{-T}, \tag{26}$$

where $p = \frac{d\Psi_{vol}(J)}{dJ}$ and:

$$DEV[\cdot] = (\cdot) - 1/3(\bar{\mathbf{C}} : (\cdot))\bar{\mathbf{C}}^{-1} \tag{27}$$

$$DEV_{C_e}[\cdot] = (\cdot) - 1/3(\bar{\mathbf{C}}_e : (\cdot))\bar{\mathbf{C}}_e^{-1} \tag{28}$$

are the deviator operators in the reference and fictitious material configurations.

The Cauchy stress tensor is obtained by means of a weighted the push-forward operation of $\mathbf{S}$, $\boldsymbol{\sigma} = J^{-1}\boldsymbol{\chi}_*(\mathbf{S}) = J^{-1}\mathbf{F}\mathbf{S}\mathbf{F}^{T}$ [23]. Hence:

$$\begin{aligned}\boldsymbol{\sigma} &= \boldsymbol{\sigma}_{vol} + \boldsymbol{\sigma}_p + \boldsymbol{\sigma}_a \\ &= p\mathbf{1} + \frac{1}{J}dev(\bar{\mathbf{F}}\frac{\partial\Psi}{\partial\bar{\mathbf{C}}}\bar{\mathbf{F}}^{\mathbf{T}}) + \frac{1}{J}dev(\bar{\mathbf{F}}_{\mathbf{e}}\frac{\partial\Psi}{\partial\bar{\mathbf{C}}_e}\bar{\mathbf{F}}_{\mathbf{e}}^{\mathbf{T}}),\end{aligned} \tag{29}$$

where:

$$dev[\bullet] = (\mathbb{I}) - \frac{1}{3}tr[\bullet]\mathbf{1} \tag{30}$$

is the deviatoric operator in the spatial configuration. The linearization of the constitutive equations is required for the numerical solution of the non linear problem by means of the Newton method. Differentiating Equation 23 with respect to $\mathbf{C}$ leads to the material elasticity tensor $\mathbb{C}$:

$$\mathbb{C} = 2\frac{\partial\mathbf{S}(\mathbf{C})}{\partial\mathbf{C}}. \tag{31}$$

According to Equation 23, the elastic tensor can be divided in a volumetric and a deviatoric parts associated to the passive and active responses as follows:

$$\mathbb{C} = \mathbb{C}_{vol} + \bar{\mathbb{C}}_p + \bar{\mathbb{C}}_a = 2\frac{\partial\mathbf{S}_{vol}}{\partial\mathbf{C}} + 2\frac{\partial\bar{\mathbf{S}}_p}{\partial\mathbf{C}} + 2\frac{\partial\bar{\mathbf{S}}_a}{\partial\mathbf{C}}, \tag{32}$$

where:

$$\mathbb{C}_{vol} = 2\mathbf{C}^{-1}\otimes\left(p\frac{\partial J}{\partial\mathbf{C}} + J\frac{\partial p}{\partial\mathbf{C}} + 2Jp\frac{\partial\mathbf{C}^{-1}}{\partial\mathbf{C}}\right) = J\tilde{p}\mathbf{C}^{-1}\otimes\mathbf{C}^{-1} - 2J\mathbb{I}_{C^{-1}}, \tag{33}$$

with:

$$(\mathbb{I}_{C^{-1}})_{IJKL} = -(\mathbf{C}^{-1}\odot\mathbf{C}^{-1})_{IJKL} = -\frac{1}{2}(C^{-1}_{IK}C^{-1}_{JL} + C^{-1}_{IL}C^{-1}_{JK}), \tag{34}$$

and:

$$\tilde{p} = p + J\frac{dp}{dJ}. \tag{35}$$

The term $\bar{\mathbb{C}}_p$ corresponding to the passive response is given by:

$$\begin{aligned}\bar{\mathbb{C}}_p = &-\frac{4}{3}J^{-\frac{4}{3}}\left(\frac{\partial\bar{\Psi}_p}{\partial\bar{\mathbf{C}}}\otimes\bar{\mathbf{C}}^{-1} + \bar{\mathbf{C}}^{-1}\otimes\frac{\partial\bar{\Psi}_p}{\partial\bar{\mathbf{C}}}\right) \\ &+ \frac{4}{3}J^{-\frac{4}{3}}\left(\frac{\partial\bar{\Psi}_p}{\partial\bar{\mathbf{C}}} : \bar{\mathbf{C}}\right)\left(\mathbb{I}_{\bar{C}^{-1}} - \frac{1}{3}\bar{\mathbf{C}}^{-1}\otimes\bar{\mathbf{C}}^{-1}\right) + J^{-\frac{4}{3}}\bar{\mathbb{C}}^{p}_{\bar{w}},\end{aligned} \tag{36}$$

where term $\bar{\mathbb{C}}^{p}_{\bar{w}}$ is defined as:

$$\bar{\mathbb{C}}^{p}_{\bar{w}} = 4\frac{\partial^2 \bar{\Psi}_p}{\partial \bar{\mathbf{C}} \partial \bar{\mathbf{C}}} - \frac{4}{3}\left[\left(\frac{\partial^2 \bar{\Psi}_p}{\partial \bar{\mathbf{C}} \partial \bar{\mathbf{C}}} : \bar{\mathbf{C}}\right) \otimes \bar{\mathbf{C}}^{-1} + \bar{\mathbf{C}}^{-1} \otimes \left(\frac{\partial^2 \bar{\Psi}_p}{\partial \bar{\mathbf{C}} \partial \bar{\mathbf{C}}} : \bar{\mathbf{C}}\right)\right] + \frac{4}{9}\left(\bar{\mathbf{C}} : \frac{\partial^2 \bar{\Psi}_p}{\partial \bar{\mathbf{C}} \partial \bar{\mathbf{C}}} : \bar{\mathbf{C}}\right) \bar{\mathbf{C}}^{-1} \otimes \bar{\mathbf{C}}^{-1}. \tag{37}$$

The last term in Equation 32, $\bar{\mathbb{C}}_a$, is given by:

$$\bar{\mathbb{C}}_a = \bar{\mathbf{F}}_a^{-1} \odot \bar{\mathbf{F}}_a^{-1}\left[-\frac{4}{3}J^{-\frac{4}{3}}\left(\frac{\partial \bar{\Psi}_a}{\partial \bar{\mathbf{C}}_e} \otimes \bar{\mathbf{C}}_e^{-1} + \bar{\mathbf{C}}_e^{-1} \otimes \frac{\partial \bar{\Psi}_a}{\partial \bar{\mathbf{C}}}_e\right) + \frac{4}{3}J^{-\frac{4}{3}}\left(\frac{\partial \bar{\Psi}_a}{\partial \bar{\mathbf{C}}_e} : \bar{\mathbf{C}}_e\right)\left(\mathbb{I}_{\bar{C}_e^{-1}} - \frac{1}{3}\bar{\mathbf{C}}_e^{-1} \otimes \bar{\mathbf{C}}_e^{-1}\right) + J^{-\frac{4}{3}}\bar{\mathbf{C}}^{a}_{\bar{w}}\right] \bar{\mathbf{F}}_a^{-T} \odot \bar{\mathbf{F}}_a^{-T}, \tag{38}$$

where:

$$\bar{\mathbb{C}}^{a}_{\bar{w}} = 4\frac{\partial^2 \bar{\Psi}_a}{\partial \bar{\mathbf{C}}_\mathbf{e} \partial \bar{\mathbf{C}}_e} - \frac{4}{3}\left[\left(\frac{\partial^2 \bar{\Psi}_a}{\partial \bar{\mathbf{C}}_e \partial \bar{\mathbf{C}}_e} : \bar{\mathbf{C}}_e\right) \otimes \bar{\mathbf{C}}_e^{-1} + \bar{\mathbf{C}}_e^{-1} \otimes \left(\frac{\partial^2 \bar{\Psi}_a}{\partial \bar{\mathbf{C}}_e \partial \bar{\mathbf{C}}_e} : \bar{\mathbf{C}}_e\right)\right] + \frac{4}{9}\left(\bar{\mathbf{C}}_e : \frac{\partial^2 \bar{\Psi}_a}{\partial \bar{\mathbf{C}}_e \partial \bar{\mathbf{C}}_e} : \bar{\mathbf{C}}_e\right) \bar{\mathbf{C}}_e^{-1} \otimes \bar{\mathbf{C}}_e^{-1}, \tag{39}$$

where we have assumed that $\bar{\lambda}_a$ updates are obtained explicitly at each increment so that $\bar{\mathbf{S}}_a$ does not depend on $\bar{\mathbf{F}}_a$ during the increment.

The elasticity tensor in the spatial configuration, $\mathbb{c}$, is obtained by a weighted push-forward operation of $\mathbb{C}$, $\mathbb{c} = J^{-1}\boldsymbol{\chi}_*(\mathbb{C})$. Hence:

$$\mathbb{c} = \mathbb{c}_{vol} + \bar{\mathbb{c}}_p + \bar{\mathbb{c}}_a, \tag{40}$$

where:

$$\mathbb{c}_{vol} = (\tilde{p}\mathbf{1} \otimes \mathbf{1} - 2p\mathbb{I}). \tag{41}$$

The passive term, $\mathbb{c}_p$, can be obtained using the expression:

$$\bar{\mathbb{c}}_p = \frac{2}{3}tr(\bar{\boldsymbol{\sigma}}_p)\mathbb{P} - \frac{2}{3}(\mathbf{1} \otimes dev(\bar{\boldsymbol{\sigma}}_p) + dev(\bar{\boldsymbol{\sigma}}_p) \otimes \mathbf{1}) + \bar{\mathbb{c}}^{p}_{\bar{w}}, \tag{42}$$

where $\mathbb{P}$ is defined as the projection tensor:

$$\mathbb{P} = \mathbb{I} - \frac{1}{3}\mathbf{1} \otimes \mathbf{1}. \tag{43}$$

The third term in Equation 40 relates to the active response, $\mathbb{c}_a$:

$$\bar{\mathbb{c}}_a = \frac{2}{3}tr(\bar{\boldsymbol{\sigma}}_a)\mathbb{P} - \frac{2}{3}(\mathbf{1} \otimes dev(\bar{\boldsymbol{\sigma}}_a) + dev(\bar{\boldsymbol{\sigma}}_a) \otimes \mathbf{1}) + \bar{\mathbb{c}}^{a}_{\bar{w}}. \tag{44}$$

$\bar{\mathbb{c}}^{i}_{\bar{w}}$, $i = p, a$ in Equation 42 and Equation 44 is the weighted push forward of $\bar{\mathbb{C}}^{i}_{\bar{w}}$:

$$\bar{\mathbb{c}}^{i}_{\bar{w}} = \mathbb{P} : \bar{\mathbb{C}}^{i}_{\bar{w}} : \mathbb{P}. \tag{45}$$

2.5 Contractile element

The time derivative of $\bar{\mathbf{F}}_a$, $\dot{\bar{\mathbf{F}}}_a$, is given by:

$$\dot{\bar{\mathbf{F}}}_a = \frac{\partial \bar{\mathbf{F}}_a}{\partial \bar{\lambda}_a} \dot{\bar{\lambda}}_a, \tag{46}$$

where $\dot{\bar{\lambda}}_a$ is the contraction speed along the muscle fibre and:

$$\frac{\partial \bar{\mathbf{F}}_a}{\partial \bar{\lambda}_a} = \mathbf{E}^1 \otimes \mathbf{E}_1 - \frac{1}{2}\bar{\lambda}_a^{-3/2}\mathbf{E}^2 \otimes \mathbf{E}_2 - \frac{1}{2}\bar{\lambda}_a^{-3/2}\mathbf{E}^3 \otimes \mathbf{E}_3. \tag{47}$$

Since contraction occurs along the muscle fibre only, Equation 22 reduces to:

$$\left[P_a - \frac{\partial \bar{\Psi}}{\partial \bar{\lambda}_a} + \left(2\bar{\mathbf{C}}_e \frac{\partial \bar{\Psi}}{\partial \bar{\mathbf{C}}_e} \bar{\mathbf{F}}_a^{-T} \right) : \frac{\partial \bar{\mathbf{F}}_a}{\partial \bar{\lambda}_a} \right] \dot{\bar{\lambda}}_a \geq 0. \tag{48}$$

This expression leads to the following constitutive relation for $\bar{\lambda}_a$:

$$P_a - \frac{\partial \bar{\Psi}}{\partial \bar{\lambda}_a} + \left(2\bar{\mathbf{C}}_e \frac{\partial \bar{\Psi}}{\partial \bar{\mathbf{C}}_e} \bar{\mathbf{F}}_a^{-T} \right) : \frac{\partial \bar{\mathbf{F}}_a}{\partial \bar{\lambda}_a} = C\dot{\bar{\lambda}}_a, \tag{49}$$

where $C = C(\bar{\lambda}_a) \geq 0$.

2.6 Particularization of the hyperelastic model

The general thermodynamic framework is particularized to model muscle skeletal contraction. According to the model proposed by Stålhand et al.[29], the free energy in Equation 14 is assumed to be:

$$\Psi = \Psi_{vol}(J) + \bar{\Psi}_p(\bar{I}_1, \bar{I}_2, \bar{I}_4) + P_0 f_1(\bar{\lambda}_a) f_2(f_r, t) \bar{\Psi}'_a(\bar{J}_4). \tag{50}$$

The third term in Equation 50, represents the strain energy associated to the active response and, consequently, with the actin-myosin interaction. This term is expressed as the product of a series of functions that scale the maximum isometric stress. P_0 is a proportionality factor related to the maximum active stress due to skeletal muscle contraction. The filament overlap is considered through the function $0 < f_1(\bar{\lambda}_a) < 1$ and the response to an electrical signal that stimulates the muscle is represented by the function $f_2(f_r, t)$, which relates the stress and the activation level generated by a stimulation frequency f_r. The function $f_1(\bar{\lambda}_a)$ has been formulated by different authors in the literature[3,4,26]. In this work, we assume the function proposed by Ramirez et al.[26]:

$$f_1(\bar{\lambda}_a) = e^{\frac{-(\bar{\lambda}_a - \lambda_{opt})^2}{2\xi^2}}, \tag{51}$$

where λ_{opt} is the optimum length of the muscle at which isometric contraction occurs and ξ determines the curvature of the function. In formulating $f_2(f_r, t)$ we assume that the electrical signal corresponds to the sum of pulses or train waves at a given frequency and amplitude.

Therefore, let us first assume that n pulses act in the muscle and that the time interval between stimulus is t_i so it corresponds to $1/f_r$. Following Ramirez et al.[26], the function $f_2(f_r, t)$ can be expressed as follows[26]:

$$f_2(f_r, t) = \sum_{i=1}^{n} \left[\left(1 - re^{(f_r T')/c} \right) \left(P' \frac{t - t_i}{T'} e^{1-(\frac{t-t_i}{T'})} \right) \right]. \tag{52}$$

After a pulse, the contraction takes place after an apparent contraction time $T' > 0$ and provokes a stress whose apparent amplitude equals $P' > 0$. The factor $r > 0$ determines the relation between the stress after a pulse and a tetanus, and $c > 0$ is the rate of force increment as the frequency increases. The parameters that fit Equation 51 and Equation 52 are given in Table 1[26].

λ_{opt} (-)	$\alpha(-)$	$T^{'}$ (s)	$P^{'}$ (N)	t_i (s)	r (-)	c (-)
1.0	0.83616	0.04	0.11	0.01667	1.0535	1.1245

Table 1: Material model parameters to characterize the active behaviour of the muscle obtained from the literature[26].

The free energy stored in the cross bridges is assumed to be:

$$\bar{\Psi}'_a = \frac{1}{2}(\bar{J}_4 - 1)^2. \tag{53}$$

In order to obtain the contraction velocity along the muscle fibre, $\dot{\bar{\lambda}}_a$, and to satisfy Equation 49, we assume:

$$C = \frac{1}{v_0} P_0 f_1(\bar{\lambda}_a) f_2(f_r, t), \tag{54}$$

where v_0 is associated with the initial contraction velocity. P_a is defined as a function of P_0, $f_1(\lambda_a)$, $f_2(f_r, t)$ and ν, that is a friction parameter that takes into account the relative sliding speed between actin and myosin:

$$P_a = -\nu P_0 f_1(\bar{\lambda}_a) f_2(f_r, t). \tag{55}$$

Substituting Equation 54, Equation 55 and the last term of Equation 50 into Equation 49, the expression of the contraction velocity is obtained as follows:

$$\dot{\bar{\lambda}}_a = v_0 \left[-\nu - \frac{1}{f_1(\bar{\lambda}_a)} \frac{\partial f_1(\bar{\lambda}_a)}{\partial \bar{\lambda}_a} \bar{\Psi}'_a(\bar{J}_4) + \left(2\bar{\mathbf{C}}_e \frac{\partial \bar{\Psi}'_a(\bar{J}_4)}{\partial \bar{\mathbf{C}}_e} \bar{\mathbf{F}}_a^{-T} \right) : \frac{\partial \bar{\mathbf{F}}_a}{\partial \bar{\lambda}_a} \right]. \tag{56}$$

Since $\bar{\Psi}'_a$ depends on $\bar{J}_4$ and considering Equation 16, Equation 56 reduces to:

$$\dot{\bar{\lambda}}_a = v_0 \left[-\nu - \frac{1}{f_1(\bar{\lambda}_a)} \frac{\partial f_1(\bar{\lambda}_a)}{\partial \bar{\lambda}_a} \bar{\Psi}'_a(\bar{J}_4) + 2\frac{\bar{\lambda}_e^2}{\bar{\lambda}_a} \frac{\partial \bar{\Psi}'_a(\bar{J}_4)}{\partial \bar{J}_4} \right]. \tag{57}$$

1D Particularization

Let us assume relative movement between actin and myosin at each muscular fibre takes place in 1D dimension. The free energy is assumed to be decomposed into the passive and active contributions according to:

$$\Psi_{1D} = \Psi_{1Dp} + \Psi_{1Da} = \Psi_{1Dp}(\bar{\lambda}) + P_0 f_1(\bar{\lambda}_a) f_2(f_r, t) \Psi'_{1Da}(\bar{\lambda}_e), \tag{58}$$

where Ψ_{1Dp} and Ψ_{1Da} are denoted by the deviatoric part associated to the passive and active responses, respectively. As for the 3D formulation, P_0 is a proportionality factor related to the maximum active stress due to skeletal muscle contraction and $f_1(\lambda_a)$ and $f_2(f_r, t)$ are given by Equations 51 and 52.

To model the active response in 1D problems, Equation 53 reduces to:

$$\Psi'_{1Da} = \frac{1}{2}(\bar{\lambda}_e^2 - 1)^2. \tag{59}$$

The second Piola Kirchhoff stress tensor in 1D is given by:

$$S = \frac{1}{\bar{\lambda}} \frac{\partial \Psi_{1D}}{\partial \bar{\lambda}}. \tag{60}$$

Hence, the contraction velocity along muscle fibre reduces to:

$$\dot{\bar{\lambda}}_a = v_0 \Big(-\nu - \frac{1}{f_1(\bar{\lambda}_a)} \frac{\partial f_1(\bar{\lambda}_a)}{\partial \bar{\lambda}_a} \Psi'_{1Da}(\bar{\lambda}_e) + \frac{\bar{\lambda}_e}{\bar{\lambda}_a} \frac{\partial \Psi'_{1Da}(\bar{\lambda}_e)}{\partial \bar{\lambda}_e} \Big). \tag{61}$$

3 Simulating skeletal muscle contraction

Skeletal muscle contraction is simulated using one and three dimensional models to prove the accuracy of the continuum model proposed. The passive response, $\bar{\Psi}_p$ in Equation 50, is assumed to be characterized by the Calvo's SEF[5]:

$$\begin{aligned} &\bar{\Psi}_p = c_1(\bar{I}_1 - 3) + \bar{\Psi}_{pf} \\ &\bar{\Psi}_{pf} = \begin{cases} 0 & \bar{I}_4 < \bar{I}_{4_0} \\ \frac{c_3}{c_4}(e^{c_4(\bar{I}_4 - \bar{I}_{4_0})} - c_4(\bar{I}_4 - \bar{I}_{4_0}) - 1) & \bar{I}_4 > \bar{I}_{4_0} \text{ and } \bar{I}_4 < \bar{I}_{4_{ref}} \\ c_5\sqrt{\bar{I}_4} + \frac{1}{2}c_6 \ln(\bar{I}_4) + c_7 & \bar{I}_4 > \bar{I}_{4_{ref}}, \end{cases} \end{aligned} \tag{62}$$

where c_1, c_3, c_5, c_6 and c_7 are positive material constants with units of stress, and c_4, $\bar{I}_{4_0}$ and $\bar{I}_{4_{ref}}$ are positive dimensionless parameters. $\bar{I}_{4_0} > 0$ characterizes the stretch at which collagen fibres begin to straighten and the transition from the linear to the exponential part of the function occurs at $\bar{I}_{4_{ref}}$. Note that the anisotropic response only appears when stretched ($\bar{I}_4 > \bar{I}_{4_0}$). Note that c_5, c_6 and c_7 are not independent parameters as they enforce continuity in the stress and the stress derivative. In one dimension, Equation 62 reduces to:

$$\Psi_{1Dp} = c_1(\bar{\lambda}^2 - 1) - 2c_1(\bar{\lambda} - 1) + \Psi_{1Dpf},$$
$$\Psi_{1Dpf} = \begin{cases} 0 & \bar{\lambda}^2 < \bar{\lambda}_0^2 \\ \frac{c_3}{c_4}(e^{c_4(\bar{\lambda}^2 - \bar{\lambda}_0^2)} - c_4(\bar{\lambda}^2 - \bar{\lambda}_0^2) - 1) & \bar{\lambda}^2 > \bar{\lambda}_0^2 \text{ and } \bar{\lambda}^2 < \bar{\lambda}_{ref}^2 \\ c_5\bar{\lambda} + \frac{1}{2}c_6\ln(\bar{\lambda}) + c_7 & \bar{\lambda}^2 > \bar{\lambda}_{ref}^2. \end{cases} \tag{63}$$

Material constants that fit Equations 62 and 63 are shown in Table 2. These constants correspond to tibialis anterior rat muscle[6].

Parameters v_0 and ν, in Equation 54 and Equation 55, are taken from other studies[2]. P_0 was determined to fit experimental data obtained during isometric contractions in the tibialis anterior rat muscle[26], Table 2 (see Figure 6.a). The proposed material model was implemented in a UMAT subroutine in the commercial finite element software ABAQUS.

Passive response[6]		Active response	
c_1 (MPa)	0.008837	P_0 (MPa)	11.0
c_3 (MPa)	0.009877	v_0 (-)[2]	7.0
c_4 (-)	2.237879	ν (-)[2]	0.5
$c_5(MPa)$	3.063670		
$c_6(MPa)$	-4.759628		
$c_7(MPa)$	-2.763531		
$\bar{I}_{4_0}(-)$	1.256385		
$\bar{I}_{4_{ref}}(-)$	2.472600		

Table 2: Material model parameters for the muscle passive and active responses taken from the literature[2,6]. Note that $\bar{I}_{4_0}$ and $\bar{I}_{4_{ref}}$ in Equation 62 are equivalent to $\bar{\lambda}_0^2$ and $\bar{\lambda}_{ref}^2$ in Equation 63, respectively. P_0 is determined so that the response fit experimental data obtained during isometric contractions in the tibialis anterior rat muscle[26].

3.1 Simulating contraction in 1D

A simplified FE model of a fusiform muscle composed of a bundle of muscular and collagen fibres was constructed to analyze the mechanics of the muscle contraction. The main purpose of this simulation was the understanding of the relationship between the different parameters involved in the formulation proposed. This model assumes collagen and muscular fibres to be oriented in the same direction, as usually found in fusiform muscles. Muscle contraction was analyzed after three different types of contraction: isometric, concentric and eccentric (see Figure 2). The length of the muscle was 10 mm and the FE model consisted of 101 nodes and 100 truss elements whose transversal section was established at 1 mm^2. Boundary conditions mimic the uniaxial contraction and are different depending on the type of contraction studied. The following subsections describe each of them.

3.1.1 Isometric contraction

In order to assure that muscle length remains constant, displacements are fixed in all directions at the ends and no external load is applied (see Figure 2.a). The electrical signal provokes a

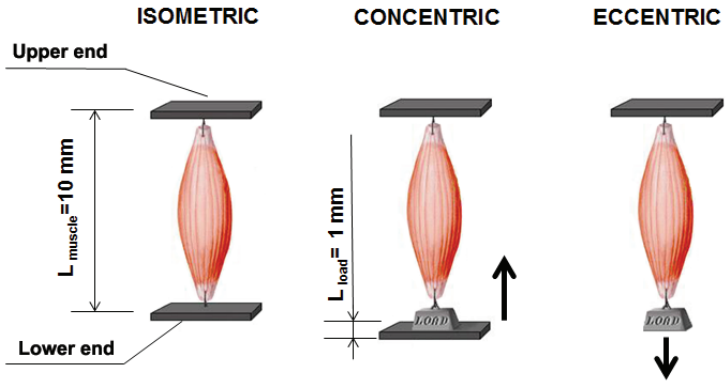

(a) (b) (c)

Figure 2: Scheme modelling the three different types of contraction: isometric (a), concentric (b) and eccentric (c).

response of the muscle which is modelled by $f_2(f_r, t)$ (see Figure 3.c). Results are analyzed in a central element of the model far enough from the boundaries.

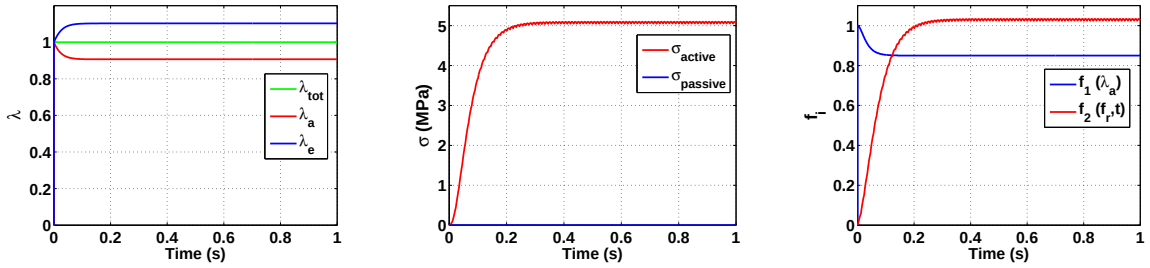

(a) (b) (c)

Figure 3: Results of the one dimensional FE simulation after an isometric contraction during 1 second. (a) Contractile and elastic stretch. (b) Active and passive stress (MPa). (c) $f_1(\lambda_a)$ and $f_2(f_r, t)$ at 90 Hz.

The stretch-time curve is represented in Figure 3.a. The total stretch remains constant whereas λ_a, associated to the contractile behaviour, decreases and λ_e increases due to the elastic response of the cross-bridges to assure the compatibility in the deformed configuration. The total stress generated after the given stimulus is purely an active stress since no passive contributions appears in the isometric contraction (see Figure 3.b). The function $f_1(\lambda_a)$ that considers the filament overlap decreases according to λ_a since the maximum active stress appears when $\lambda_a = 1.0$.

3.1.2 Concentric contraction

Concentric contraction occurs when the muscle lifts a load which is less than the maximum it can move and, consequently, the muscle begins to shorten (see Figure 2.b). To model the external weight applied to the muscle ten additional truss elements whose transversal section was established at 1 mm^2 and total length at 1 mm were added in the lower end of the simplified one dimensional FE model. The mechanical response of the weight was considered elastic and its Young's modulus was established at 10^4 MPa to assure its stiffness is higher than that of the muscle. The body force assigned to the weight was established to obtain a resultant force of 3 **N**. In addition, contact elements known as gap elements were added to model in the lower end of the muscle below the weight. These elements model the contact between the nodes belonging to the weight and those used to define the boundary conditions in displacements. Specifically, displacements are fixed in all directions in the last ones. These elements assure no displacement in the muscle until maximum tetanic tension is reached.

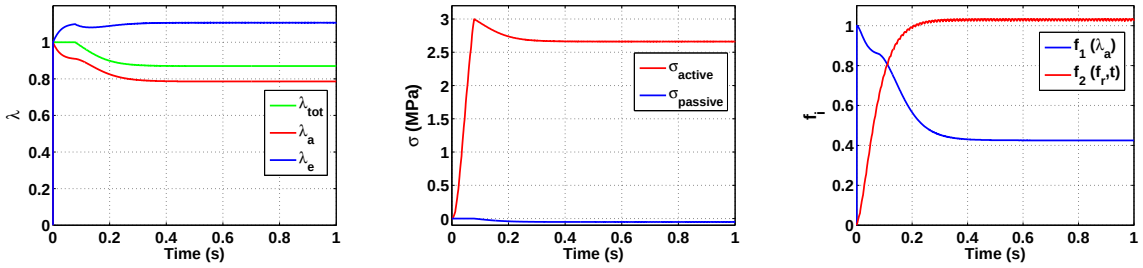

(a) (b) (c)

Figure 4: Results of the one dimensional FE simulation after a concentric contraction during 1 second. (a) Contractile and elastic stretch. (b) Active and passive stress (MPa). (c) $f_1(\lambda_a)$ and $f_2(f_r, t)$ at 90 Hz.

Results obtained after an external stimulus are shown in Figure 4. Active stress increases progressively until its value equals the external force applied at 0.08 seconds (see Figure 4.b). In this time interval until 0.08 seconds, total stretch remains constant since it corresponds to an isometric contraction (see Figure 4.a). The total stretch decreases indicating muscle shortens since external weight is lower that the maximal one the muscle could move. This shortening is due to the contraction of the contractile element, λ_a, whereas the length of the elastic element remains practically constant to assure the compatibility in the deformed configuration. $f_1(\lambda_a)$ acts as a penalty to the active stress and its value decreases as λ_a does (see Figure 4.c). Total stress is defined as the addition of both, active and passive stress. The modelling is defined within the large deformation hyperelasticity, so Cauchy stress was computed as $\sigma = \frac{F}{A_0}\lambda$, where F is the applied load and A_0 is the initial cross section. Since λ decreases, σ does not remains constant.

3.1.3 Excentric contraction

If the load applied to the muscle increases, it finally reaches a point where the external force on the muscle is greater than the force that the muscle can generate. Thus, even though the muscle is fully activated, it is forced to lengthen due to the high external load (see Figure 2.c). The FE model used in that simulation is that described for the concentric contraction. However, in this case, the simulation includes two load steps. In the first one, the muscle is fully activated due to an isometric contraction during 0.5 seconds and after that, the second load step release the boundary conditions in displacements in the lower end to allow the weight to descend during 0.2 seconds. In this simulation, the body force applied to the weight was established to obtain a resultant force of 5.3 **N**, lightly higher than the maximum active stress the muscle can generate (see Figure 3.b).

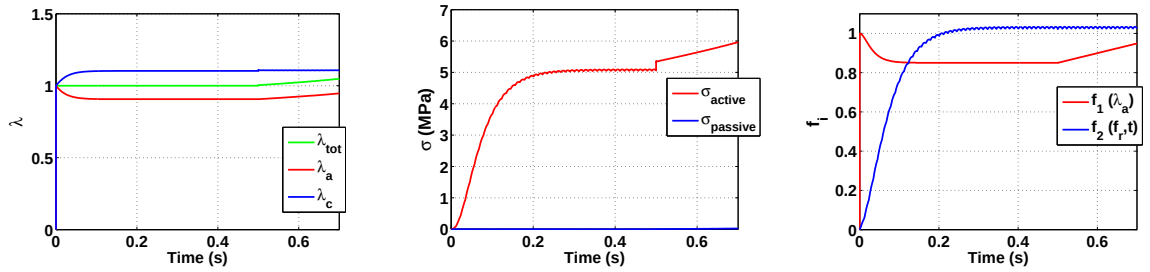

(a) (b) (c)

Figure 5: Results of the one dimensional FE simulation after an isometric (0.5 seconds)-eccentric (0.2 seconds) contraction. (a) Contractile and elastic stretch. (b) Active and passive stress (MPa). (c) $f_1(\lambda_a)$ and $f_2(f_r, t)$ at 90 Hz.

The eccentric contraction addressed the results shown in Figure 5. During isometric contractions, results are similar to those in Figure 3. After that, total stretch and λ_a increase since the weight provokes a stretching movement in the muscle (see Figure 5.a). λ_e practically remains constant and maintains the compatibility. Besides, since the muscle is elongated, there is an increase in active stress. Figure 5.c shows the response to the external stimulus, $f_2(f_r, t)$, until the contraction finishes. Red curve showing $f_1(\lambda_a)$ computed higher values after isometric contraction since λ_a starts increasing due to muscle elongation and becomes nearer to the optimal length.

3.2 Simulating contraction in 3D

Skeletal muscle contraction was analyzed in two different three dimensional FE models: the first one is the tibialis anterior rat muscle, a fusiform muscle, and was used to validate the model, and the other one is the human rectus abdominis muscle, a parallel muscle, and was modelled to present the applicability of the model proposed to other types of muscles. Only isometric and concentric contractions are simulated.

3.2.1 Tibial anterior muscle

The geometry of the tibialis anterior rat muscle was reconstructed from magnetic resonance imaging (MRI) of a female Wistar adult rat with a body mass of 215 ± 15 g[14]. The FE model includes a total 2376 hexahedral elements and 3060 nodes. The preferential direction of anisotropy given by collagen and muscular fibres is disposed in a fusiform form in the whole model. Boundary conditions reproduce the isometric and concentric contractions in each case and they are described in the following subsections.

Isometric contraction

Displacements of the nodes corresponding to both ends of the mesh were fixed to reproduce an isometric contraction. The external stimulus is applied at different frequencies: 10, 30, 60 and 90 Hz. Total reaction force in a node corresponding to an end is represented in Figure 6.a. The total force generated by the muscle increases at higher frequencies.

Figure 6.a shows the experimental results in a dotted line that corresponds to a previous work reported on the literature[26]. The experiment consists on an isometric contraction given by an external electrical stimulus at 90 Hz. It is observed that the fitted curve in Figure 6.a at 90 Hz shows a good agreement with the experimental data until maximum active stress is reached. After that, the computational results do not fit the experimental ones since fatigue effects are not taken into account in the model. Displacements computed in the tibialis anterior rat muscle after an stimulus at 90 Hz, during 1 second, are displayed in Figure 6.b. Note that displacements at muscle ends are null whereas muscle deforms according to the isometric contraction.

Concentric contraction

An external weight is applied to the muscle directly in the upper end of the FE model. For that purpose, 54 additional hexahedral elements were defined in that position of the model. The external weight was modelled with elastic properties and its Young's modulus was considered equal to 10^4 MPa. In addition, another 54 additional hexahedral elements, namely auxiliary elements, were defined in the upper end of the muscle next to the external load to define a normal contact with the weight and the initial boundary conditions in displacements. The material properties of these new elements were defined to achieve a stiffness much higher than that of the muscle. Its Young's modulus was considered equal to 10^8 MPa. Displacements were fixed in the auxiliary elements and the contact allows the muscle to shorten since the weight applied is less than the maximum weight the muscle can move.

To analyze the shortening of the muscle different loads were applied in the end of the tibialis anterior muscle. Specifically, the body force assigned to the weight was established to obtain resultant forces of 1, 2, 3, 4 and 5 N. Therefore, different lengths of shortening were obtained after muscle contraction given by an external stimulus at 90 Hz. Figure 7.a shows the maximum displacement of a node corresponding to the upper end in the muscle. The maximum displacement increases as the external weight is lower. The displacement decreases at the end of the curve since the external stimulus is applied during 1 second and after that no contrac-

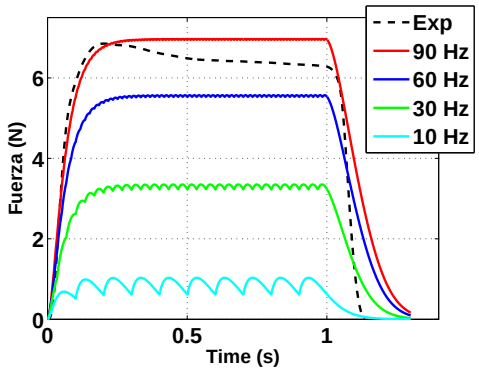

(a)

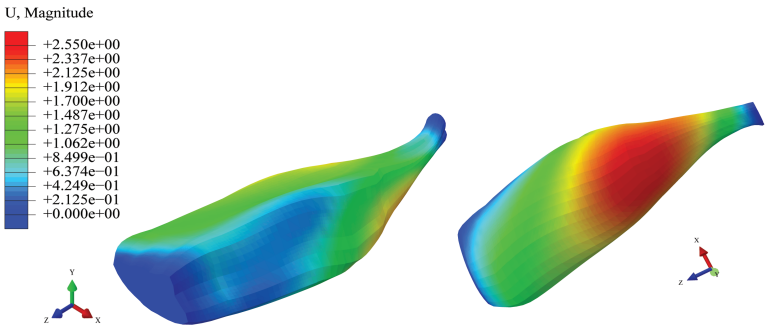

(b)

Figure 6: (a) Reaction force (N) in a node corresponding to the end of the tibialis anterior rat muscle after an isometric contraction due to an external electrical stimulus given at different frequencies: 10, 30, 60 and 90 Hz. The reaction force after the stimulus at 90 Hz is compared to the experimental results shown in a dotted line which corresponds to a previous work reported on the literature[26]. (b) Displacements computed in the tibialis anterior rat muscle in the isometric contraction (time=1 second) with an external stimulus at 90 Hz.

tion exists. Furthermore, the contraction velocity that corresponds to the slope of the curve is higher at lower weights. Figure 7.b represents the maximum contraction velocity obtained in each simulation by means of applying different external loads. The fitting of the points obtained shows that the contraction velocity increases as the external load is lower. When the maximal external load corresponds to the maximum isometric force, the contraction velocity is null. Therefore, the model proposed is capable of reproducing the fact that contraction velocity is different depending on the external load applied.

3.2.2 Rectus abdominis muscle

A three dimensional FE model of the human rectus abdominis muscle was constructed to simulate the muscle contraction using DICOM files generated by MRI of a healthy 38-year-old man[18].

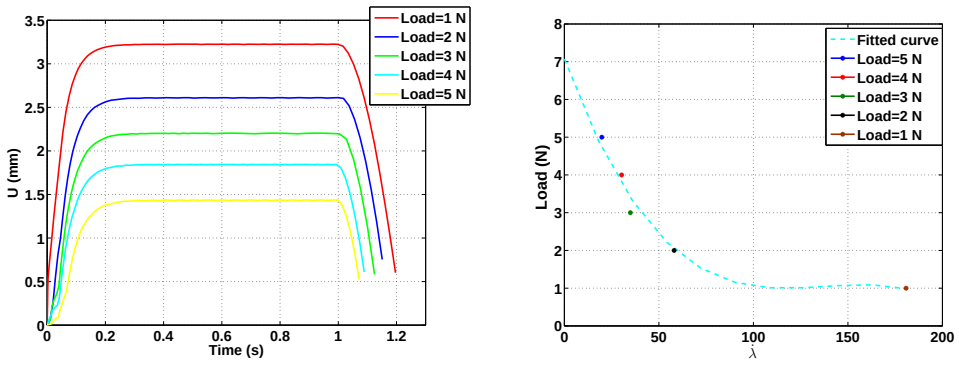

(a) (b)

Figure 7: (a) Displacements (mm) computed in a node corresponding to the non-fixed end during a concentric contraction while muscle lifts different external weights. (b) Force-velocity relationship obtained in concentric contractions from the different simulations.

In addition, the FE model includes the skeleton of the trunk including ribs, hip, sacrum, vertebrae bones and intervertebral disks. This geometry was obtained from a free model available on the net and was scaled to fit rectus abdominis dimensions. The part of the model corresponding to the rectus abdominis muscle includes a total of 22400 hexahedral elements and 26334 nodes, the skeleton of the trunk is composed of a total of 56527 shell elements, which were considered as totally rigid, and 28364 nodes and the intervertebral disks include a total of 94784 shell elements and 47438 nodes.

Due to the lack of experimental data on the characterization of the active response in the rectus abdominis, material properties were taken from the literature[2,6,26] and correspond to the mechanical characterization of the tibialis anterior muscle (Tables 1 and 2). The preferential direction of anisotropy given by the collagen and muscular fibres is disposed along the craneo-caudal direction of the body meaning that both contributions act in the same direction[32]. It is important to note that there are some tendinous insertions in the rectus abdominis muscle, as depicted in Figure 8[32]. These anatomical structures does not include muscular fibres so contraction does not occur in them. The external stimulus is given at 90 Hz in both, isometric and concentric contractions, and is applied simultaneously to the whole rectus muscle.

Isometric contraction

Boundary conditions in displacements restrict the movement of the whole skeleton and intervertebral disks. Furthermore, displacements of the nodes corresponding at the upper and lower ends of the rectus abdominis are fixed. Maximum displacements and principal stresses are shown in Figure 9. Maximum displacements appear in the lower half of the rectus abdominis and maximum principal stresses are reported in the higher half of it meaning that this is the stiffer area. Note that tendinous insertions are remarked after isometric contraction due to the non existing contraction, making displacements smaller in these areas.

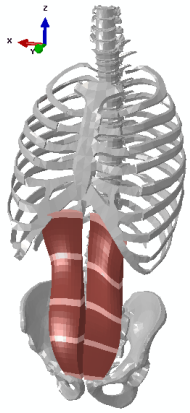

Figure 8: FE model of the human skeleton of the trunk including intervertebral disks and human rectus abdominis muscle showing their tendinous insertions in a lighter colour.

Concentric contraction

Contrary to the simulation of the isometric contraction, displacements of the upper end of the rectus abdominis muscle are allowed. In addition, the skeleton moves as a rigid body whereas the intervertebral disks have no restriction in displacements to permit the rotation of the spine. The rotation of the spine is visible in the perspective view (see Figure 10.a) and displacements after concentric contraction are presented frontally and laterally in Figures 10.b and 10.c.

4 Discussion

In this study, we have presented an thermodynamically consistent three-dimensional electromechanical continuum model for simulating skeletal muscle contraction within the framework of the large deformation hyperelasticity. Thus, the second law of the thermodynamics is satisfied for any thermodynamic process.

According to several studies in the literature [17,22], muscular and collagen fibres are frequently not aligned in the same direction. Furthermore, the direction of collagen fibres is assumed to determine the direction of material anisotropy in order to study the passive behaviour of the tissue [1], whereas muscle fibres have to be considered in the modelling of the active behaviour. This model proposes a decoupled strain energy function into the passive and active contributions [4,9,24,28], meaning that it can be also applied to muscles where collagen and muscle fibres are not aligned in the same direction.

The main concern of this study is the contractile response of the model. The active force is obtained as the maximum tetanic force the muscle can generate multiplied by two functions acting as penalties. The function $f_2(f_r, t)$ represents the response to the external stimulus that depends on the frequency of the electrical signal and the total time of the stimulus and $f_1(\lambda_a)$ considers the overlap between actin and myosin filaments [13,29]. Contrary to other studies in the

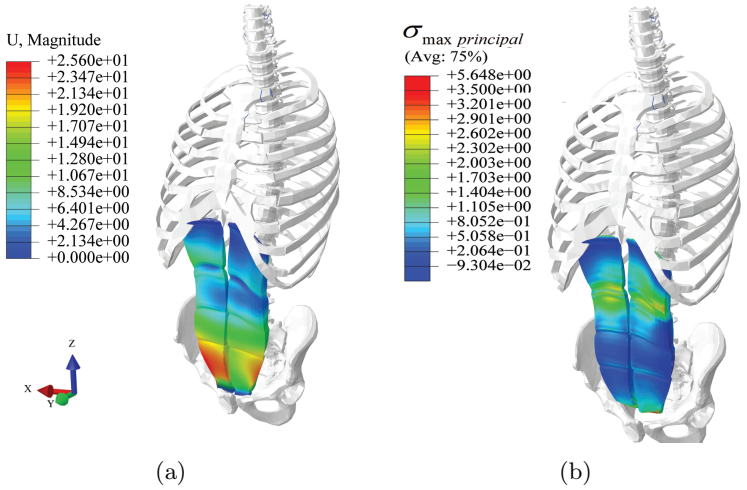

(a) (b)

Figure 9: Displacement distribution (mm) and maximum principal stresses (MPa) addressed along the rectus abdominis in the isometric contraction.

literature[4,13], this model does not considers any velocity function. However, the model proposed is capable of reproducing the effects of the velocity contraction depending on the external load applied (see Figure 7.b).

One dimensional FE simulations reproduce isometric, concentric and eccentric contractions in a muscle composed of a bundle of collagen and muscle fibres aligned along the same direction. The aim of these simulations is to validate the response of the proposed model. Furthermore, the three dimensional problem has been simulated using the FE method where more complex boundary conditions exist. Some studies in the literature reproduce the active response according to idealized geometries[4] or geometries from cadavers[7]. In this study, we defined two FE models obtained from MRI: one of the tibialis anterior rat muscle[14] and other one of the human rectus abdominis muscle[18]. Furthermore, real fibre disposition was taken into account to introduce the preferential direction of anisotropy.

Despite we are mainly concern about the qualitative response instead of about exact values, the model has been validated using experimental data obtained from the literature[26]. In these experiments, active force generated by isolated tibialis anterior rat muscles was measured. In our work, the chosen constants to simulate the active response were determined to fit experimental curves when the frequency of the activation signal was equal to 90 Hz and the results obtained are in good agreement with experimental data (see Figure 6.a).

The three dimensional simulation of the isometric contraction reports no displacements at the ends of the model since they are restricted. However, muscle fibres shorten until they reach an equilibrium along the direction where contraction occurs. The elastic element representing the behaviour of the cross bridges assure the compatibility in the deformed configuration. Regarding the concentric contraction, results are similar to those obtained previously in other studies in the literature that uses different geometries[4,31].

One of the limitations of the model is that we do not model chemical processes that generate

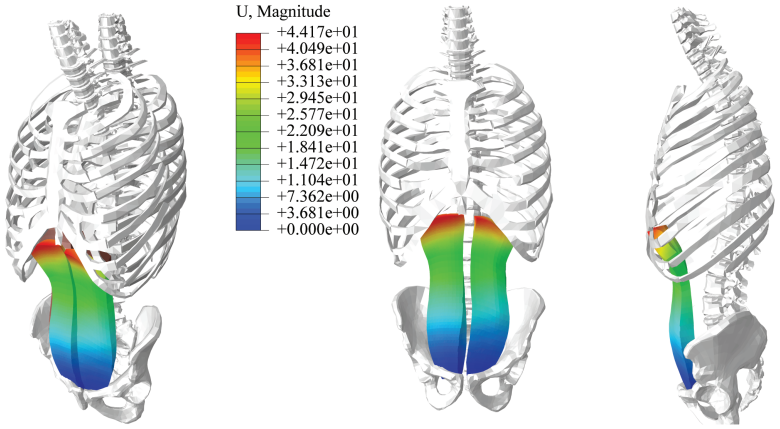

(a) (b) (c)

Figure 10: Displacement distribution (mm) computed along the rectus abdominis in the concentric contraction shown in perspective (a), frontal (b) and lateral (c) views.

the contraction movements. However, it is important to note that experimentally in the laboratory, an electrical stimulus is the preferable option when a isolated nerve exists[26]. When there is no access to a nerve, a $[Ca^{2+}]$ ionic fluid is used to stimulate the skeletal muscle. In our study, we considered the response to the stimulus through the function $f_2(f_r, t)$ where parameters are previously fitted according to the experimental protocol using an electrical stimulus[26]. Furthermore, the proposed model does not include fatigue effects and, consequently, the loss of active force due to damage reported in experimental data is not achieved in the FE simulation (see Figure 6.a). Thus, further three dimensional continuum models to simulate the active response of skeletal muscle should incorporate fatigue effects[30]. To the author' knowledge, there is no experimental data about the characterization of the active response of the abdominal muscles. Thus, the simulation of the active response of the rectus abdominis should be validated in further studies.

In summary, the proposed model is thermodynamically consistent and is capable of simulating the skeletal muscle contraction to obtain the evolution of active stresses and muscle length. Three dimensional approaches using the FE method provide realistic simulations of real geometries with complex boundary conditions and are capable to predict the physiological state after muscle contraction.

5 Acknowledgments

This study was supported by the Spanish Ministry of Economy and Competitiveness through research project DPI2011-27939-C02-01, the University of Zaragoza through the research project UZ2011-TEC02 and the Instituto de Salud Carlos III (ISCIII) through the CIBER initiative project ABDOMESH. B. Hernández-Gascón was also funded by a grant (BES-2009-021515) from the Spanish Ministry of Science and Technology.

References

[1] E. M. Arruda, K. Mundy, S. Calve, and K. Baar. Denervation does not change the ratio of collagen I and collagen II mRNA in extracellular matrix of muscle. *American Journal of Physiology* , 292:983–987, 2006.

[2] T. Arts, P. C. Veenstra, and R. S. Reneman. Epicardial deformation and left ventricular wall mechanics during ejection in the dog. *American Journal of Physiology*, 243:H379–H390, 1982.

[3] B. B. Blemker, P. M. Pinsky, and S. L. Delp. A 3D model of muscle reveals the causes of nonuniform strains in the biceps brachii. *Annals of Biomedical Engineering*, 38:657–665, 2005.

[4] M. Bol and S. Reese. Micromechanical modelling of skeletal muscles based on the finite element method. *Computer Methods in Biomechanics and Biomedical Engineering*, 11:489–504, 2008.

[5] B. Calvo, E. Peña, P. Martins, T. Mascarenhas, M. Doblaré, R. Natal, and A. Ferreira. On modelling damage process in vaginal tissue. *Journal of Biomechanics*, 42:642–651, 2009.

[6] B. Calvo, A. Ramírez, A. Alonso, J. Grasa, F. Soteras, R. Osta, and M. J. Muñoz. Passive non linear elastic behaviour of skeletal muscle: Experimental results and model formulation. *Journal of Biomechanics*, 43:318–325, 2010.

[7] D. d'Aulignac, J. A. C. Martins, E. B. Pires, T. Mascarenhas, and R. M. Jorge. A shell finite element model of the pelvic floor muscles. *Computer Methods in Biomechanics and Biomedical Engineering*, 8(5):339–347, 2005.

[8] F. Dong, G. J. Clapworthy, M. A. Krokos, and J. Yao. An anatomy-based approach to human muscle modeling and deformation. *IEEE Transactions on Visualization and Computer Graphics*, 8(2):154–170, 2002.

[9] J. W. Fernandez and M. G. Pandy. Integrating modelling and experiments to assess dynamic musculoskeletal function in humans. *Experimental Physiology*, 91(2):371–382, 2006.

[10] P. J. Flory. Thermodynamic relations for high elastic materials. *Transaction of the Faraday Society*, 57:829–838, 1961.

[11] M. Gatton, M. Pearcy, and G. Pettet. Modelling the line of action for the oblique abdominal muscles using an elliptical torso abdomen. *Journal of Biomechanics*, 34:1203–1207, 2001.

[12] P. Germain. The method of virtual power in continuum mechanics. Part 2. *SIAM Journal on Applied Mathematics*, 50:556–575, 2002.

[13] J. Grasa, B. Hernández-Gascón, A. Ramírez, J. F. Rodríguez, and B. Calvo. Numerical simulation of the behaviour of musculoskeletal tissue. *Revista Internacional de Métodos Numéricos para Cálculo y Diseño en Ingeniería*, 28(3), 2013.

[14] J. Grasa, A. Ramírez, R. Osta, M. J. Muñoz, F. Soteras, and B. Calvo. A 3D active-passive numerical skeletal muscle model incorporating initial tissue strains. Validation with experimental results on rat tibialis anterior muscle. *Biomechanics and Modeling in Mechanobiology*, 10:779–787, 2011.

[15] C. M. Hai and R. A. Murphy. Cross-bridge phosphorylation and regulation of latch state in smooth muscle. *American Journal of Physiology*, 254:C99–C106, 1988.

[16] H. Hatze. A myocybernetic control model of skeletal muscle. *Biological Cybernetics*, 25:103–119, 1977.

[17] B. Hernández, E. Peña, G. Pascual, M. Rodríguez, B. Calvo, M. Doblaré, and J. M. Bellón. Mechanical and histological characterization of the abdominal muscle. A previous step to model hernia surgery. *Journal of the Mechanical Behavior of Biomedical Materials*, 4:392–404, 2011.

[18] B. Hernández-Gascón, A. Mena, E. Peña, G. Pascual, J. M. Bellón, and B. Calvo. Understanding the passive mechanical behavior of the human abdominal wall. *Annals of Biomedical Engineering*, In Press:DOI: 10.1007/s10439–012–0672–7, 2012.

[19] A. V. Hill. The heat of shortening and the dynamic constans of muscle. *Proceedings of the Royal Society B*, 126:136–195, 1938.

[20] A. F. Huxley. Muscle structure and theories of contraction. *Progress in Biophysics and Biophysical Chemistry*, 173:257–318, 1957.

[21] R. R. Lemos, M. Epstein, W. Herzog, and B. Wyvill. A framework for structured modeling of skeletal muscle. *Computer Methods in Biomechanics and Biomedical Engineering*, 7(6):305–317, 2004.

[22] Van Der Linden. *Mechanical modeling of skeletal muscle functioning.* PhD thesis, University of Twente, The Netherlands, 1998.

[23] J. E. Marsden and T. J. R. Hughes. *Mathematical Foundations of Elasticity.* Dover, New York, 1994.

[24] J.A.C. Martins, E.B. Pires, R. Salvado, and P.B. Dinis. A numerical model of passive and active behavior of skeletal muscles. *Computer Methods in Applied Mechanics and Engineering*, 151:419–433, 1998.

[25] M. G. Pandy. Computer modelling and simulation of human movement. *Annual Review of Biomedical Engineering*, 3:245–273, 2004.

[26] A. Ramírez, J. Grasa, A. Alonso, F. Soteras, R. Osta, M. J. Muñoz, and B. Calvo. Active response of skeletal muscle: *in vivo* experimental results and model formualtion. *Journal of Theoretical Biology*, 267:546–553, 2010.

[27] J. C. Simo and R. L. Taylor. Quasi-incompresible finite elasticity in principal stretches. Continuum basis and numerical algorithms. *Computer Methods in Applied Mechanics and Engineering*, 85:273–310, 1991.

[28] J. Stålhand, A. Klarbring, and G. A. Holzapfel. Smooth muscle contraction: mechanochemical formulation for homogeneous finite strains. *Progress in Biophysics & Molecular Biology*, 96:465–481, 2008.

[29] J. Stålhand, A. Klarbring, and G. A. Holzapfel. A mechanochemical 3D continuum model for smooth muscle contraction under finite strains. *Journal of Theoretical Biology*, 268:120–130, 2011.

[30] C. Y. Tang, B. Stojanovic, C. P. Tsui, and M. Kojic. Modeling of muscle fatigue using hill's model. *Biomedical Materials and Engineering*, 15:341–348, 2005.

[31] C. P. Tsui, C. Y. Tang, C. P. Leung, K. w. Cheng, Y. F. Ng, D. H. K. Chow, and C. K. Li. Active finite element analysis of skeletal muscle-tendon complex during isometric, shortening and lengthening contraction. *Biomedical Materials and Engineering*, 14:271–279, 2004.

[32] W. Moore . *Gray's Anatomy celebrates 150th anniversary.* The Telegraph (Telegraph Media Group), 2008.

Work 9: The long term behavior of lightweight and heavyweight meshes used to repair abdominal wall defects is determined by the host tissue repair process provoked by the mesh

Journal: *Surgery*, **152**(5) (2012): 886-895.
Journal impact factor: 3.103

The long-term behavior of lightweight and heavyweight meshes used to repair abdominal wall defects is determined by the host tissue repair process provoked by the mesh

Gemma Pascual, PhD,[a] Belén Hernández-Gascón, PhD,[b] Marta Rodríguez, PhD,[a] Sandra Sotomayor, PhD,[a] Estefania Peña, PhD,[b] Begoña Calvo, PhD,[b] *and* **Juan M. Bellón, MD, PhD,[a]**
Madrid and Zaragoza, Spain

Background. *Although heavyweight (HW) or lightweight (LW) polypropylene (PP) meshes are widely used for hernia repair, other alternatives have recently appeared. They have the same large-pore structure yet are composed of polytetrafluoroethylene (PTFE). This study compares the long-term (3 and 6 months) behavior of meshes of different pore size (HW compared with LW) and composition (PP compared with PTFE).*
Methods. *Partial defects were created in the lateral wall of the abdomen in New Zealand White rabbits and then repaired by the use of a HW or LW PP mesh or a new monofilament, large-pore PTFE mesh (Infinit). At 90 and 180 days after implantation, tissue incorporation, gene and protein expression of neocollagens (reverse transcription-polymerase chain reaction/immunofluorescence), macrophage response (immunohistochemistry), and biomechanical strength were determined. Shrinkage was measured at 90 days.*
Results. *All three meshes induced good host tissue ingrowth, yet the macrophage response was significantly greater in the PTFE implants (*$P < .05$*). Collagen 1/3 mRNA levels failed to vary at 90 days yet in the longer term, the LW meshes showed the reduced genetic expression of both collagens (*$P < .05$*) accompanied by increased neocollagen deposition, indicating more efficient mRNA translation. After 90–180 days of implant, tensile strengths and elastic modulus values were similar for all 3 implants (*$P > .05$*).*
Conclusion. *Host collagen deposition is mesh pore size dependent whereas the macrophage response induced is composition dependent with a greater response shown by PTFE. In the long term, macroporous meshes show comparable biomechanical behavior regardless of their pore size or composition. (Surgery 2012;152:886-95.)*

From the Department of Surgery and Medical Specialities,[a] Faculty of Medicine, University of Alcalá, Networking Research Center on Bioengineering, Biomaterials and Nanomedicine (CIBER-BBN), Alcalá de Henares, Madrid, Spain; and Group of Structural Mechanics and Materials Modelling (GEMM),[b] Aragón Institute of Engineering Research (I3A), University of Zaragoza, Zaragoza, Spain

DESPITE THE APPEARANCE of many new prosthetic materials designed to repair abdominal wall defects, polypropylene (PP) continues to be used the most widely. This is because of the good cost/benefits and excellent biocompatibility of PP, along with an improved tolerance to infection compared with other materials.[1] However, because of certain adverse effects produced when it is placed at the

This study was supported by the Spanish Ministry of Science and Technology through research projects DPI2008-02335/DPI2010-20746-C03-01/DPI2011-27939 and the Instituto de Salud Carlos III (ISCIII) through the CIBER initiative project ABDOMESH. CIBER-BBN is an initiative funded by the VI National R&D&i Plan 2008-2011, Iniciativa Ingenio 2010, Consolider Program, CIBER Actions and financed by the Instituto de Salud Carlos III with assistance from the European Regional Development Fund.

Accepted for publication March 8, 2012.

Reprint requests: Juan M. Bellón, MD, PhD, Department of Surgery, Faculty of Medicine, Alcalá University, Ctra. Madrid-Barcelona, Km 33,600, 28871, Alcalá de Henares, Madrid, Spain. E-mail: juanm.bellon@uah.es.

0039-6060/$ - see front matter

doi:10.1016/j.surg.2012.03.009

peritoneal interface, namely adhesions to the intestinal loops and fistulas,[2,3] PP is not recommended for use in contact with the visceral peritoneum. Notwithstanding, when extraperitoneal placement is called for in hernia repair, this material continues to be used the most widely.[4]

Research and development in prosthetic materials has aimed to improve the wound repair process elicited by prosthetic mesh implant. Thus, rather than being relegated, macroporous meshes have been subjected to modifications to their structure, porosity, and composition. This has led to the construction of new large-pore meshes composed of other polymers such as polytetrafluoroethylene (PTFE)[5] and polyvinylidene fluoride.[6]

One of the main goals of surgery has been to assess the effects of varying the amount of implanted material. To this end, composite meshes have been designed[7,8] with both absorbable and nonabsorbable components. Pore size has also been considered an important factor in new mesh designs, along with other characteristics such as the diameter and spatial distribution of fibers.

These new designs have led to the classification of macroporous meshes[9] as heavy weight (HW), medium weight (MW), or low weight (LW), respectively, according to whether their density values are greater than 80 g/m^2, between 50 and 80 g/m^2, or less than 50 g/m^2. Some authors[10] have even defined an ultralightweight material whose density is less than 35 g/m^2.

Prosthetic mesh density is sometimes independent of pore size, and some designs, despite having a small pore size, are classified as LW because they are constructed from a loosely woven light monofilament conferring them an overall low density in g/m^2.

Despite this classification, in line with the concepts of the German authors,[11] we consider pore size to be the main factor that determines whether a material is HW or LW. Thus, it is generally considered that HW meshes have a small-pore design and LW meshes have large pores.[12]

Given that when a LW mesh is used, less material is implanted in the host, we would expect a reduced foreign body reaction and a repair process that generates less fibrosis in the host tissue, with the consequence of improved tissue compliance.[13] Although individual variation exists in terms of the repair process induced by the implant of a biomaterial,[14] it is clear that the sometimes excessive fibrosis induced by conventional HW materials could be minimized through the use of a LW implant.

In recent work,[15] we observed the excellent short-term collagenization of LW-PP implants. This prompted the design of the present study, in which we sought to determine whether during longer periods (3 and 6 months) the behavior of a LW mesh (tissue incorporation and tensile strength) remains the same regardless of pore size or its composing polymer (PP or PTFE). A further objective was to determine the effect of the implant material on the host tissue response produced in the long term.

MATERIAL AND METHODS

Experimental animals. The experimental animals were 36 male New Zealand White rabbits weighing approximately 2,200 g caged under conditions of constant light and temperature according to European Union animal care guidelines (European Directive 609/86/EEC and European Convention of the Council of Europe ETS123). All procedures were approved by our institutions Review Board.

Prosthetic materials. The biomaterials used were (Fig 1, *A–C*) as follows:

- Surgipro (Covidien, Mansfield, MA): HW PP (85 g/m^2); pore size 0.26 ± 0.03 mm^2;
- Optilene elastic (B/Braun, Berlin, Germany): LW PP (48 g/m^2); pore size 7.64 ± 0.32 mm^2; and
- Infinit mesh (Gore and Associates, Flagstaff, AZ): LW nonexpanded PTFE (70 g/m^2); pore size 4.05 ± 0.22 mm^2.

Surgical technique. To minimize pain, all animals were administered 0.05 mg/kg buprenorphine (Buprecare; Divasa Farmavic, Barcelona, Spain) 1 hour before and 3 days after the surgical procedure. Anesthesia was induced with a mixture of ketamine hydrochloride (Ketolar, 70 mg/kg; Parke-Davis, S.A., Spain), diazepam (Valium, 1.5 mg/kg; Roche, Madrid Spain), and chlorpromazine (Largactil, 1.5 mg/kg; Rhone-Poulenc, S.A., Spain), administered intramuscularly.

With the use of a sterile surgical technique, 4 × 4-cm defects were created in the lateral wall of the abdomen comprising the planes of the external and internal oblique muscles, sparing the transversalis muscle, parietal peritoneum, and skin. The defects were then repaired by fixing a mesh of the same size to the edges of the defect with a running 4-0 PP suture interrupted at the 4 corners (Fig 1, *D–F*). The skin was closed by 3-0 PP running suture.

Experimental design. A total of 36 animals were implanted with each of the materials to establish 3 groups of 12 animals each. In each of these

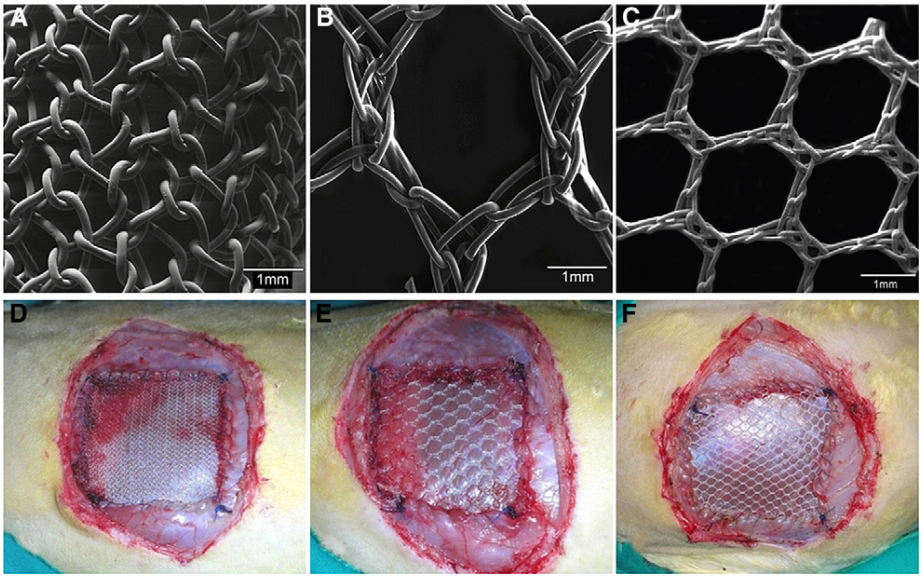

Fig 1. Biomaterials used in this experimental study. SEM images of the pore size detail: (*A*) Surgipro (15×); (*B*) Optilene (15×); (*C*) Infinit mesh (15×). Implanted biomaterials: (*D*) Surgipro; (*E*) Optilene; (*F*) Infinit mesh. (Color version of figure is available online.)

groups, 6 animals were euthanized in a CO_2 chamber after 90 days, and the remaining 6 were euthanized at 180 days post-implant.

Shrinkage. Shrinkage of the implanted meshes was determined by image analysis. For this purpose, we designed a set of transparent templates of the same dimensions as the original meshes (4 × 4 cm). At the end of the implant period, the outlines of the meshes were traced on the templates before their removal. The surface area of the templates could them be determined by computerized image analysis with the MIP program incorporated in the image analyzer (MICRON, Barcelona, Spain). Results are expressed as the percentage size reduction suffered by each implant. Shrinkage was assessed at 90 days after implant when the tissue repair process is practically complete.

Morphological analysis. *Light microscopy.* For light microscopy, specimens were collected from the mesh/host tissue interface. The samples were fixed in F13 solution (ethanol 60%, methanol 20%, polyethylene glycol 7%, water 13%), embedded in paraffin, and cut into 5-μm sections. Once cut, the sections were stained with Masson's trichrome (Goldner–Gabe) and examined under the light microscope (Zeiss Axiophot; Carl Zeiss, Oberkochen, Germany).

Gene expression of collagens. *Real-time reverse transcription polymerase chain reaction (RT-PCR).* Tissue fragments 1 cm^2 in size were obtained from the central mesh zone, and stored at −80°C until use. RNA was extracted by the use of guanidine-phenol-chloroform isothiocyanate procedures with trizol (Invitrogen, Carlsbad, CA). The RNA was recovered from the aqueous phase and precipitated by adding isopropanol and incubating overnight at −20°C. Complementary DNA was synthesized with 200 ng of the total RNA by RT with oligo dT primers (Amersham, Fairfield, CT) and the M-MLV RT enzyme (Invitrogen). RT reactions were run in the absence of M-MLV to confirm the RNA lacked genomic DNA.

cDNA was amplified using the following primers: collagen one (sense 5′-GAT GCG TTC CAG TTC GAG TA-3′ and antisense 5′-GGT CTT CCG GTG GTC TTG TA-3′); collagen three (sense 5′-TTA TAA ACC AAC CTC TTC CT-3′ and antisense 5′-TAT TAT AGC ACC ATT GAG AC-3′); GAPDH (sense 5′-TCA CCA TCT TCC AGG AGC GA-3′ and antisense 5′-CAC AAT GCC GAA GTG GTC GT-3′).

The RT-PCR mixture contained 5 μL of the inverse transcription product (cDNA) diluted 1:20, 10 μL of iQ SYBR Green Supermix (Bio-Rad, Laboratories, Hercules, CA), and 1 μL (6 μM) of each primer in a final reaction volume of 20 μL. RT-PCR was performed in a StepOnePlus Real-Time PCR System (Applied Biosystemx, Foster City, CA). Samples were subjected to an initial stage of 10 min at 95°C. The conditions for cDNA amplification were: 40 cycles of 95°C for 15 seconds, 60°C (collagens I and III) or 55°C (GAPDH) for 30 seconds, and 72°C for 1 minute. Negative controls containing ultraPureTM DNase, RNase-free distilled water

(Invitrogen) were run in each reaction. Products were subjected to 2% agarose gel electrophoresis, stained with SYBR Green II RNA gel stain (Invitrogen), and visualized with ultraviolet light. Gene expression was normalized against the expression recorded for the constitutive gene glyceraldehyde 3-phosphate-dehydrogenase.

Immunofluorescence. To detect the protein expression of collagens I and III, tissue fragments were fixed in F13 solution, embedded in paraffin, and cut into 5 μm-thick sections. Once cut, the sections were deparaffinated, hydrated, equilibrated in phosphate-buffered saline buffer and incubated with the monoclonal antibodies anti-collagen I (Sigma Chemical Co., St. Louis, MO) and anti-collagen III (Medicorp, Montreal, Canada). The secondary antibody used was conjugated with rhodamine. An immunofluorescence technique was used to detect the antigen–antibody reaction. Cell nuclei were counterstained with DAPI. Samples were examined under a confocal microscope Leica SP5 (Leica Microsystems, Wetzlar, Germany) to detect fluorescence.

Macrophage response. For immunohistochemistry, a specific monoclonal antibody to rabbit macrophages, RAM 11 (DAKO M-633, USA), was applied to paraffin-embedded sections. The alkaline phosphatase-labeled avidin-biotin method was performed as the following steps: incubation with the primary antibody (1:50 in Tris-buffered saline or TBS) for 30 minutes, incubation with immunoglobulin G and biotin (1:1,000 in TBS) for 45 minutes, and labeling with avidin (1:200 in TBS) for 30 minutes. These steps were conducted at room temperature. Images were developed with the use of a chromogenic substrate containing naphthol phosphate and fast red. Nuclei were counterstained for 5 minutes in acid hematoxylin. RAM-11–labeled macrophages were quantified according to a method described elsewhere.[16]

Biomechanical strength. To determine the biomechanical strength and modulus of elasticity of the meshes after implant, strips of the different biomaterials 1 cm wide and 5 cm long, with an effective gauge length of 3 cm, were analyzed with an INSTRON 3340 (static load 500 N; Instron Corp., High Wycombe, UK). The cross-head speed was 5 cm per minute and recording speed 2 cm per minute.

The strips obtained at 90 and 180 days after implantation included the mesh and infiltrated host tissue. All tests were conducted immediately after animal sacrifice.

Statistical analysis. Statistical analysis was performed by use of the Graph Pad Prism 5 package. Shrinkage percentages, collagen one and three mRNA expression, RAM-11–positive cells, biomechanical strength, and modulus of elasticity values were compared among the 3 study groups using the Mann-Whitney *U* test. The level of statistical significance was set at $P < .05$.

RESULTS

There were no cases of mortality or signs of infection and/or rejection of the implants in the animals operated on. Seroma was detected in 2 of the animals with PTFE implants at 14 days after implantation.

Shrinkage. Shrinkage values determined at 90 days after implantation were as follows: Surgipro (13.69 ± 3.52%), Optilene (10.11 ± 3.07%), and Infinit (10.42 ± 1.19%). These values failed to differ significantly ($P < .05$).

Morphological analysis. *Light microscopy.* At 90 days after implantation, the three biomaterials tested showed ingrowth by a disorganized, well-vascularized, loose connective scar tissue. This neoformed tissue occupied all the spaces between the PP (Surgipro and Optilene) and PTFE (Infinit) filaments and was interspersed with areas in which the infiltration of adipose tissue could be observed in all the implant types. After 6 months, there was a significant increase in adipose tissue ingrowth. Most neoformed connective tissue was observed around the prosthetic filaments. The preserved transversalis muscle in the lower zone of the partial defect showed no evident morphological alterations at any of the follow-up times or any of the study groups (data not shown).

Gene expression of collagens. *Real time RT-PCR.* The three mesh types induced similar collagen gene expression patterns reflected by the collagen one and three mRNA levels detected. At 90 days after implantation, the PP biomaterials (Surgipro and Optilene) induced the higher expression of mRNA for collagen three (immature) and one (mature) with significant differences with PTFE (Infinit) emerging at 180 days for collagen three when compared with the PP-HW mesh (Surgipro; $P < .05$; Fig 2, *A*) and for collagen one, compared with both PP-HW ($P < .01$) and PP-LW ($P < .05$; Fig 2, *B*). In the PTFE (Infinit) mesh group, the drop produced in collagen one mRNA expression from 90–180 days (Fig 2, *B*) was significant ($P < .01$).

Immunofluorescence. Both collagen types were immunodetected in the three implant groups at both study times. Collagen fibers ran parallel to the mesh surface in zones far from the filaments or were arranged concentrically to these filaments in areas closer to the implant edges. For Surgipro and Optilene, collagen III protein expression was

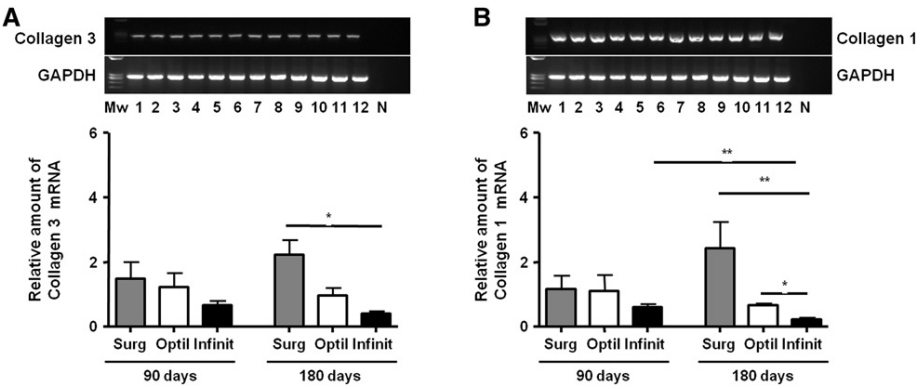

Fig 2. Relative amounts of collagen three (*A*) and one (*B*) mRNA in the implant of Surgipro, Optilene, and Infinit mesh determined by RT-PCR. Upper panels: RT-PCR products of both genes. Lanes: 1/2 Surgipro, 3/4 Optilene, and 5/6 Infinit mesh at 90 days, and 7/8 Surgipro, 9/10 Optilene, and 11/12 Infinit mesh at 180 days. *N*, Negative control; *Mw*, molecular weight markers. Results are the mean ± SEM of three experiments performed in duplicate. Gene expression was normalized to values recorded for the GAPDH gene. $*P < .05$; $**P < .01$.

homogeneously distributed throughout the newly formed tissue around the prosthetic filament at 90 and 180 days after implantation. In contrast, the Infinit mesh induced an intense pattern of collagen III expression confined to localized areas around the filaments.

Labeling for the mature form of collagen (collagen I) was more extensive and intense for the higher porosity implants (Optilene and Infinit) at both time points, but Optilene showed the greatest staining for this type of collagen. Surgipro showed moderate collagen I staining. In all the study groups, collagen I staining was confined to areas of new tissue formation adjacent to the prosthetic filaments (Fig 3).

Macrophage response. In all the study groups, macrophage cells were detected in the neoformed tissue between the mesh filaments. Most inflammatory cells were found to concentrate around the filaments where, besides macrophages, multinucleated foreign-body giant cells, typical of a wound repair response, could be seen. These cells appeared mostly around the filaments of PTFE (Infinit).

At both time points, macrophage numbers were significantly greater for the PTFE meshes compared to the PP implants ($P < .05$). The macrophage reaction gradually diminished from 90 to 180 days in all 3 groups (Fig 4).

Biomechanics. The tensile strengths, or breaking points, recorded for the different meshes implanted for 90 and 180 days were comparable ($P = .05$; Fig 5, *A*).

At 90 days, the postimplant elastic modulus was significantly greater for PTFE ($P < .05$) than the PP meshes, although by 180 days, this variable was similar across the 3 groups (Fig 5, *B*).

DISCUSSION

As standard permanent prosthetic materials, PP and expanded PTFE (ePTFE) have been constantly subjected to modifications to improve both their host tissue incorporation and complications of bowel injury and infection, in an effort to achieve the best functional repair of the abdominal wall possible.

The most recent modifications made to PP meshes have involved minimizing the material implanted in the host without compromising their mechanical resistance. This approach led to the development of composite[8] and large pore meshes.[17]

The modifications made to sheets of ePTFE prosthetics, such as introducing multiperforations[18] or creating a rough surface on one side,[19] have not improved their biomechanical strength. The only strategy that has served to improve tissue incorporation and tensile strength has been the construction of a largely porous ePTFE mesh.[5] Bioassays conducted on this mesh have revealed that rather than the chemical composition of the biomaterial, it is its loosely woven structure that determines its tissue behavior. Accordingly, the behavior of classic microporous-expanded PTFE, which induces little tissue ingrowth and instead becomes encapsulated by host tissue, may be manipulated to simulate that of a largely porous PP mesh.

In the present experimental study, we compared the postimplantation behavior of a conventional PP-HW mesh to that of 2 LW meshes, one composed of PP and the other of nonexpanded PTFE. The first prosthetic materials generated by our group[5] were composed of an expanded PTFE monofilament CV-4. The material examined here

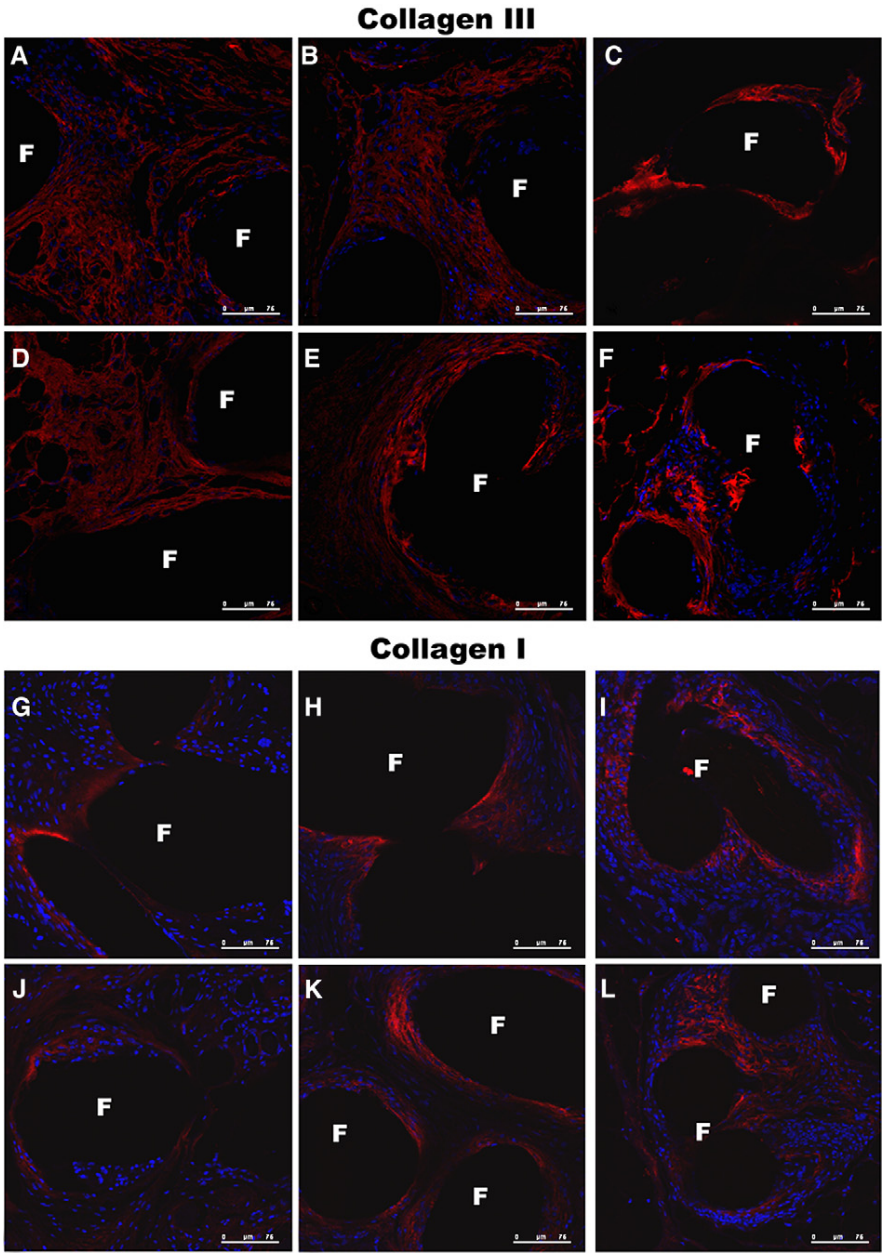

Fig 3. Tissue incorporation and collagen expression around the mesh filaments of the different biomaterials. Collagen appears as red fluorescence observed by laser scanning confocal microscopy. (*A–F*) Collagen III (immature): (*A*) Surgipro, 90 days (200×); (*B*) Optilene, 90 days (200×); (*C*) Infinit, 90 days (200×); (*D*) Surgipro, 180 days (200×); (*E*) Optilene, 180 days (200×); (*F*) Infinit, 180 days (200×). (*G–L*) Collagen I (mature): (*G*) Surgipro, 90 days (200×); (*H*) Optilene, 90 days (200×); (*I*) Infinit, 90 days (200×); (*J*) Surgipro, 180 days (200×); (*K*) Optilene, 180 days (200×); (*L*) Infinit, 180 days (200×). *F*, Prosthetic filaments. (Color version of figure is available online.)

is composed of a nonexpanded PTFE monofilament that is knitted to create a large pore size such that it is a MW mesh.

In our study, partial defects were created in the lateral wall of the abdomen to avoid involving the peritoneum in the repair process. When the animals were killed 90 days after implantation, seroma was detected in 2 of the animals who received a PTFE implant (similar to observations after the implant of laminar ePTFE meshes). This finding seems consistent with our immunohistochemistry results obtained with the anti- RAM-11 macrophage monoclonal antibody. Hence, at each time point, the PTFE implants showed a significantly

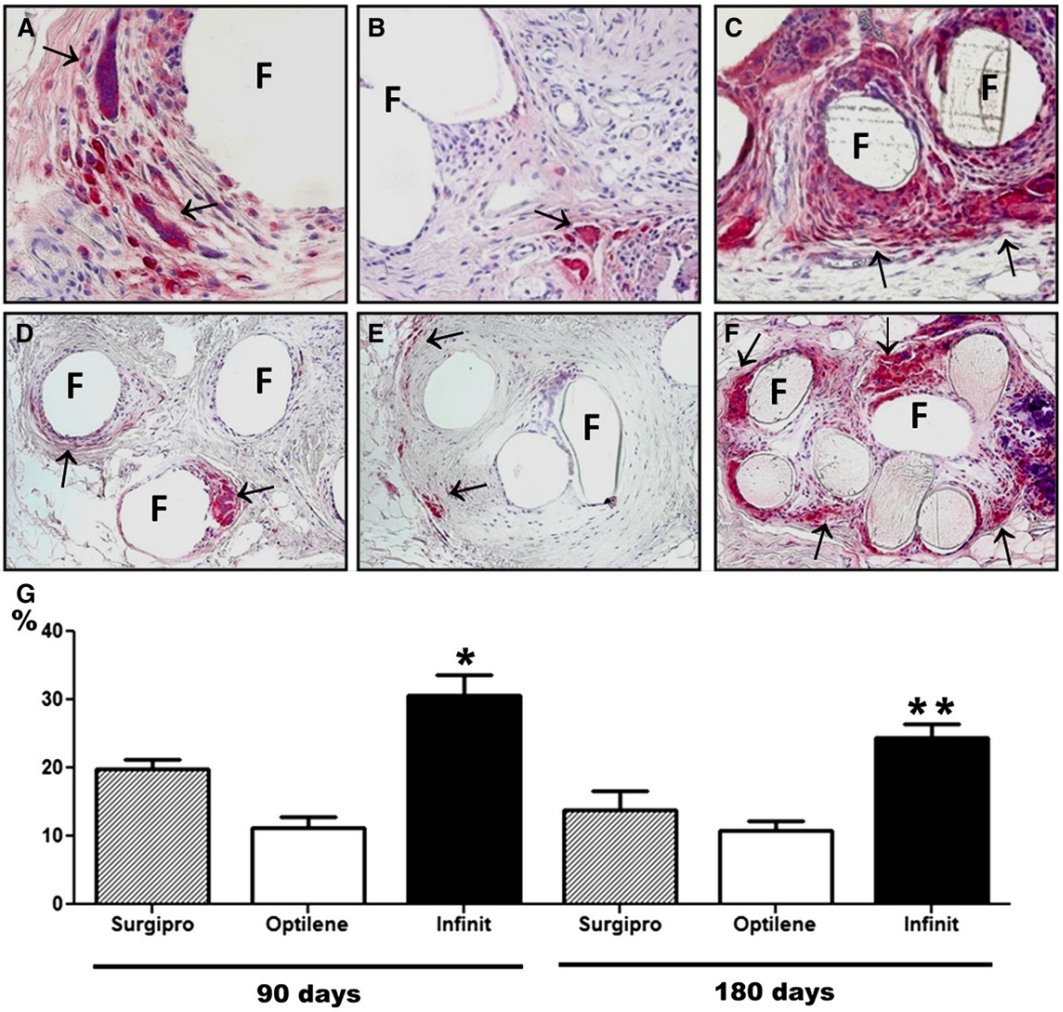

Fig 4. Immunohistochemical labeling of rabbit macrophages (*arrows*) using the RAM-11 monoclonal antibody. (*A*) Surgipro, 90 days (640×); (*B*) Optilene, 90 days (500×); (*C*) Infinit, 90 days (360×); (*D*) Surgipro, 180 days (200×); (*E*) Optilene, 180 days (200×); (*F*) Infinit, 180 days (200×); (*G*) mean numbers of RAM-11–positive cells recorded for each study group and follow-up time. Significant differences between Infinit vs Surgipro and Optilene were observed at 90 (*$P < .05$) and 180 days after implantation (**$P < .05$). *F*, Prosthetic filaments. (Color version of figure is available online.)

augmented macrophage reaction over that shown by the PP implants. This behavior would be comparable with that displayed by some absorbable materials in the early postimplant course,[7,20] possibly having clinical implications such as the presence of reactive seroma. For the PP meshes, macrophage counts gradually decreased during the study period as occurred, although at a slower pace, for the PTFE implants. The observed immune response to these implants requires further investigation.

With regard to shrinkage at 90 days, the lack of significant differences observed between the 3 meshes is in line with previous results from our laboratory.[21] After PP mesh placement in dogs, other authors[9] observed significant shrinkage of the implant area close to 30% at 90 days postimplantation. In our study, shrinkage at this time point was closer to 15% and probably attributable to interspecies differences.

We contemplate the phenomenon of prosthetic shrinkage as a physiological factor in the context of the wound repair process.[22] Possible variations among implants could be related to the implant site. Thus, some authors[23] have noted less shrinkage when the implant is placed in a retromuscular compared with a prefascial position.

In terms of host tissue incorporation, the 3 implant types showed good behavior. The PTFE meshes behaved differently than the classic microporous expanded PTFE, which becomes encapsulated by host tissue. Although collagen I (mature) could be observed both at 90 and 180 days in the

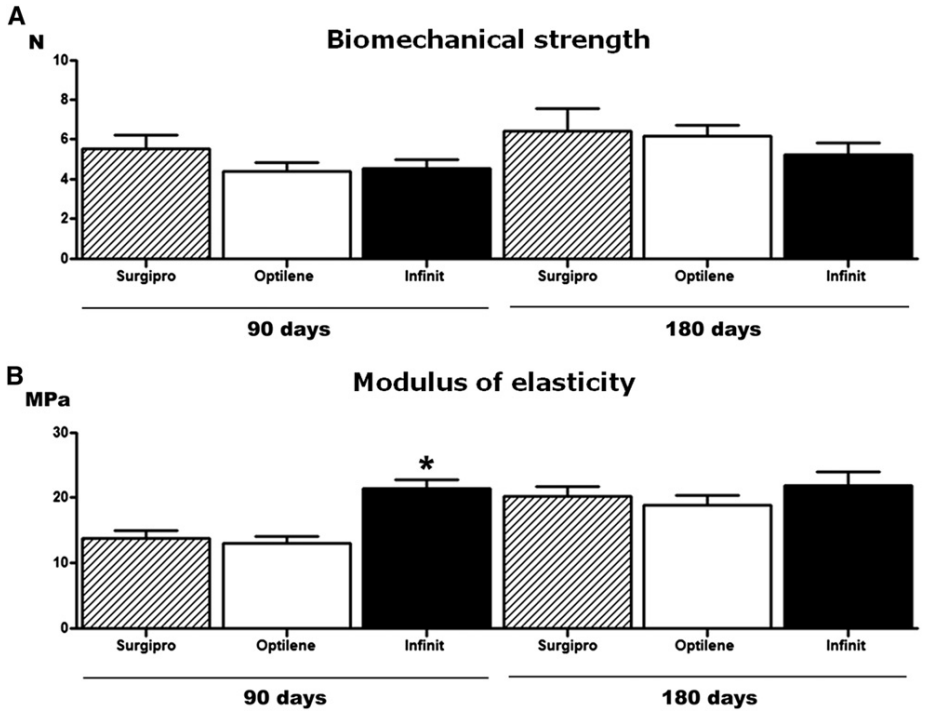

Fig 5. (*A*) Biomechanical resistance values (Newtons) for each type of prosthesis and study time. No statistically significant differences were observed; (*B*) modulus of elasticity for each type of prosthesis and study time. Significant differences were observed between Infinit vs Surgipro and Optilene at 90 days after implantation (*$P < .05$).

different mesh groups, the greater porosity meshes (Optilene and Infinit) induced the greater protein expression of mature collagen. This result is in agreement with the findings of Greca et al,[24,25] who observed greater type I collagen deposition after the implant of large-pore prosthetic materials. The greater expression of collagen I protein observed here in the high-porosity meshes was accompanied by reduced mRNA expression for this protein in the long term, indicating the efficient translation of all the mRNA into protein. In contrast, the response to the implant of the low-porosity HW mesh would in the long-term lead to the buildup of mRNA because of the reduced effectiveness of its protein translation.

In previous work[15] in a different defect model with complete excision of the abdominal wall, we noted significantly greater gene expression levels for collagens one and three in meshes with pores larger than 3 mm in the short term (14 days after implantation). This finding could be correlated with colonization of the mesh by the cellular contingency of fibroblasts. A possible explanation could be that these cells undergo stress depending on the pore area that is to be occupied by neoformed tissue. Thus, cells that colonize large pore meshes will need to rapidly synthesize collagen to create a cell substrate. Conversely, if pore size is small, the small amount of space between filaments will require minimal occupation by newly formed tissue.

Similar behavior to this was observed in the present study at this time point of 14 days (data not shown) in that the more porous implants showed greater gene expression for both types of collagen. This finding suggests that in the short term, messenger RNA transcription and translation reach their peak and that hereafter translation into the proteins diminishes over time.

Our biomechanical results indicated a greater tensile strength for Surgipro at the 2 time points, but differences were not significant compared with the other 2 implants. At 180 days after implantation, the tensile strengths of all three materials had increased, but again no significant differences were observed between the implants. A similar trend towards acquiring similar biomechanical resistance of different implants, including partially absorbable meshes, was observed at 90 days in a previous study.[26] It therefore seems that LW meshes regardless of their chemical composition show a similar response to breakage in the mid- and long term to that shown by HW meshes. This behavior correlates with the optimal

collagenization (collagen type I deposition) of LW implants. The deposition of collagen in the repair tissue around the filaments of the LW meshes causes an increase in stiffness that substantially modifies the original properties of the mesh. Thus in long term, the growth of collagen tends to unify the mechanical response shown by LW and HW meshes. The elastic modulus was significantly greater at 90 days ($P < .05$) for the PTFE meshes compared with the other implants, although similar values were attained at 180 days for the 3 implants.

According to the biomechanical data obtained, both the resistance to breakage and elasticity of the different implants was gradually modulated by the host tissue. Thus, besides offering the advantage of a reduced amount of implanted material, the mechanical properties of LW implants seem to be improved, especially in terms of tensile strength, by the newly formed tissue around the prosthetic filaments. In line with this observation, in a recent clinical study of incisional hernia repair,[27] surgical outcomes at three years were similar when small or large pore PP meshes were used. In view of these findings, larger pore meshes would need to be tested to determine how much further the amount of foreign material placed in the host could be reduced without mechanically compromising the implants.

Our study is not without its limitations. In our experience, although the rabbit model has provided excellent results in terms of tissue repair and immune response, its biomechanical behavior is less translatable to human clinical practice.

In conclusion, our findings indicate that the following:

- Compared with PP, the use of PTFE in a macroporous mesh induces an augmented macrophage response;
- In the long term, the collagen mRNA translation induced by a high-porosity mesh is more efficient, resulting in increased collagen deposition in the repair zone; and
- In the long-term postimplantation, the tensile strengths and elastic moduli of both HW and LW materials attain comparable values.

In general terms, it therefore seems that the long-term behavior of LW meshes used to repair an abdominal wall defect, whether composed of PP or PTFE, is conditioned by the host tissue repair process, with a correlation observed between collagen deposition and prosthetic pore size.

The authors are indebted to Gore and Associates, Flagstaff, AZ, for providing the meshes used in this study. This company played no role in the design of this study, data collection, or analysis.

REFERENCES

1. Alaedeen DI, Lipman J, Medalie D, Rosen MJ. The single-staged approach to the surgical management of abdominal wall hernias in contaminated fields. Hernia 2007;11:41-5.
2. Chuback JA, Sigh RS, Sill C, Dick LS. Small bowel obstruction resulting from mesh plug migration after open inguinal hernia repair. Surgery 2000;127:475-6.
3. Chew DK, Choi LH, Rogers AM. Enterocutaneous fistula 14 years after prosthetic mesh repair of a ventral incisional hernia. A life-long risk? Surgery 2000;125:109-11.
4. Bellón JM, Contreras LA, Buján J, Palomares D, Carrera-San Martin A. Tissue response to polypropylene meshes used in the repair of abdominal wall defects. Biomaterials 1998;19: 669-75.
5. Bellón JM, Jurado F, García-Honduvilla N, López R, Carrera-San Martín A, Buján J. The structure of a biomaterial rather than its chemical composition modulates the repair process at the peritoneal level. Am J Surg 2002;184:154-9.
6. Klinge U, Klosterhalfen B, Ottinger AP, Junge K, Schumpelick V. PVDF as a new polymer for the construction of surgical meshes. Biomaterials 2002;23:3487-93.
7. Rosch R, Junge K, Quester R, Klinge U, Klosterhalfen B, Schumpelick V. Vypro II mesh in hernia repair: impact of polyglactin on long-term incorporation in rats. Eur Surg Res 2003;35:445-50.
8. Junge K, Rosch R, Krones J, Klinge U, Martens PR, Lynen P, et al. Influence of polyglecaprone 25 (Monocryl) supplementation on the biocompatibility of a polypropylene mesh for hernia repair. Hernia 2005;9:212-7.
9. Cobb WS, Burns JM, Peindl RD, Carbonell AM, Matthews BD, Kercher KW, et al. Textile analysis of heavy weight, mid-weight, and light weight polypropylene mesh in a porcine ventral hernia model. J Surg Res 2006;136:1-7.
10. Earle DB, Mark LA. Prosthetic material in inguinal hernia repair: How do I choose? Surg Clin North Am 2008;88: 179-201.
11. Klinge U. Experimental comparison of monofile light and heavy polypropylene meshes: less weight does not mean less biological response. World J Surg 2007;31:867-8.
12. Deeken CR, Abdo MS, Frisella MM, Matthews BD. Physicomechanical evaluation of polypropylene, polyester, and polytetrafluoroethylene meshes for inguinal hernia repair. J Am Coll Surg 2011;212:68-79.
13. Klinge U, Klosterhalfen B, Birkenhauer V, Junge K, Conze J, Schumpelick V. Impact of polymer pore size on the interface scar formation in a rat model. J Surg Res 2002;103:208-14.
14. Schachtrupp A, Klinge U, Junge K, Rosch R, Bhardwaj RS, Schumpelick V. Individual inflammatory response of human blood monocyte to mesh biomaterials. Br J Surg 2003;90:114-20.
15. Pascual G, Rodriguez M, Gómez-Gil V, García-Honduvilla N, Buján J, Bellón JM. Early tissue incorporation and collagen deposition in lightweight polypropylene meshes: bioassay in an experimental model of ventral hernia. Surgery 2008;144:427-35.
16. Bellón JM, Bujan J, Contreras L, Hernando A, Jurado F. Macrophage response to experimental implantation of polypropylene prostheses. Eur Surg Res 1994;26:46-53.
17. Klosterhalfen B, Junge K, Klinge U. The lightweight and large porous mesh concept for hernia repair. Espert Rev Med Devices 2005;2:103-17.
18. Simmermacher RKJ, Van der Lei B, Schakenraad JM, Bleichrodt RP. Improved tissue ingrowth and anchorage of

expanded polytetrafluoroethylene by perforation: an experimental study in the rat. Biomaterials 1991;12:22-4.
19. Bellón JM, Contreras L, Buján J, Carrera-San Martín A. The use of biomaterials in the repair of abdominal wall defects: a comparative study between polypropylene meshes (Marlex) and a new polytetrafluoroethylene prosthesis (Dual Mesh). J Biomater Appl 1997;12:121-35.
20. Klinge U, Schumpelick V, Klosterhalfen B. Functional assessment and tissue response of short and long-term absorbable surgical meshes. Biomaterials 2001;22:1415-24.
21. Bellón JM, García-Honduvilla N, Rodriguez M, Pascual G, Gómez-Gil V, Buján J. Influence of the estructure of new generation prostheses on shrinkage alter implant in the abdominal wall. J Biomed Mar Res Part B: Appl Biomater 2006;78B:340-6.
22. Berry DP, Harding KG, Stanton MR, Jasani B, Ehrlich P. Human wound contraction: collagen organization, fibroblasts, and myofibroblasts. Plast Reconstr Surg 1998;102:124-31.
23. Garcia-Ureña MA, Vega V, Díaz A, Baez JM, Marín LM, Carnero FJ, et al. Differences in polypropylene shrinkage depending on mesh position in an experimental study. Am J Surg 2007;193:538-42.
24. Greca FH, De Paula JB, Biondo-Simoes MPL, Costa FD, Da Silva APG, Time S, et al. The influence of differing pore sizes on the biocompatibility of two polypropylene meshes in the repair of abdominal defect: experimental study in dogs. Hernia 2001;5:59-64.
25. Greca FH, Souza-Filho ZA, Giovanini A, Rubin MR, Kuenzer RF, Reese FB, et al. The influence of porosity on the integration histology of two polypropylene meshes for the treatment of abdominal wall defects in dogs. Hernia 2008; 12:45-9.
26. Bellón JM, Rodríguez M, García-Honduvilla N, Pascual G, Buján J. Partially absorbable meshes for hernia repair offer advantages over nonabsorbable meshes. Am J Surg 2007; 194:68-74.
27. Berrevoet F, Maes L, De Baerdemaeker L, Rogiers X, Troisi R, De Hemptinne B. Comparable results with 3 year follow-up for large-pore versus small-pore meshes in open incisional hernia repair. Surgery 2010;148:969-75.

Work 10: Short-term behaviour of different polymer structure lightweight meshes used to repair abdominal wall defects

Journal: *Histology and Histopathology*, **Accepted**, (2012)
Journal impact factor: 2.480

Short-term behavior of different polymer structure lightweight meshes used to repair abdominal wall defects

G. Pascual[a,d], B. Hernández-Gascón[c,d], S. Sotomayor[a,d], E. Peña[c,d], B. Calvo[c,d], J. Buján[a,d], J. M. Bellón[b,d]

[a] *Department of Medical Specialities. Faculty of Medicine. University of Alcalá. Spain*
[b] *Department of Surgery. Faculty of Medicine. University of Alcalá. Spain*
[c] *Aragón Institute of Engineering Research (I3A) University of Zaragoza. Spain*
[d] *Networking Research Center on Bioengineering, Biomaterials and Nanomedicine (CIBER-BBN), Spain*

Accepted in Histology and Histopathology

Abstract

Background. While lightweight (LW) polypropylene (PP) meshes are been used for hernia repair, new prosthetic meshes also of low-density and with largepores have recently been introduced composed of other polymer materials. This study compares the behavior in the short-term of two macroporous LW prosthetic materials, PP and non-expanded PTFE.
Methods. Partial defects were created in the lateral wall of the abdomen in New Zealand White rabbits and then repaired using a LW PP mesh or a new monofile, LW PTFE mesh. At 14 days postimplant, shrinkage and tissue incorporation, gene and protein expression of neocollagens (qRT-PCR/immunofluorescence), macrophage response (immunohistochemistry) and biomechanical strength were determined.
Results. Both meshes induced good host tissue ingrowth, yet the macrophage response was significantly greater for the PTFE implants ($p < 0.05$). Collagen 1/3 mRNA expression was greater for the PP mesh but differences lacked significance. Similar patterns of collagen I and III protein expression were observed in the neoformed tissue infiltrating the two meshes. After 14 days of implant, tensile strengths were also similar, while elastic modulus values were higher for the PTFE mesh ($p < 0.05$).
Conclusions. In the short term, host collagen deposition and biomechanical performance seemed unaffected by the polymer structure of the implanted mesh. In contrast, the inflammatory response to mesh implant produced at this early time point was more intense for the PTFE.

Keywords: abdominal wall repair, polymers, PP, PTFE, lightweight mesh.

1 Introduction

The use of a biomaterial in the form of a mesh to repair a large abdominal wall defect is today virtually standard practice. The prosthetic material of choice for this purpose is sometimes large-pore polypropylene (PP) because of its good cost/benefit, biocompatibility and tolerance to infection[1,3].

Research and development in the field of biomaterials has nevertheless yielded new polymer materials of larger pore size conferring these designs the benefits of a lighter-weight implant able to better adapt to the biomechanics of the abdominal wall, thus improving compliance post-surgery and reducing the amount of foreign material implanted in the host. These new designs have led to the classification of macroporous meshes[7] as heavy weight (HW) or light-weight (LW) respectively according to their density values.

The functional, morphological and histological properties of HW versus LW PP meshes have been addressed by several authors[5,14]. The conclusions of these studies are that the lower amount of foreign material implanted when a LW rather than a HW material is used improves abdominal wall compliance to the extent that physiological compliance is achieved in the long term after a LW mesh is used for hernia repair. In a molecular and histological study[19] examining the early host tissue incorporation of several meshes, it was observed that larger pore meshes induced the genetic overexpression of collagen types I and III, the greater deposition of collagen type III, its faster conversion to collagen I, and that these features conferred the meshes greater tensile strengths 14 days after implant.

At least in theory, low-density meshes should show an improved foreign body reaction in that the amount of material implanted is minimized, thus reducing its contact surface with host tissue[16]. Effectively, studies have shown that a LW mesh will elicit a less intense acute inflammatory response compared to its HW counterpart[17,24]. Hence, the development of reduced-material implants adapted to the physiological requirements of the anterior abdominal wall has served to improve both biocompatibility and patient comfort[13,22].

Given these benefits of macroporous meshes, LW PP implants are currently widely used for hernia repair. However, several alternative materials based on the same concept of low density have recently appeared. These prosthetic materials have a similar large-pore structure but are composed of other polymers such as the new non-expanded polytetrafluoroethylene (PTFE) mesh, a loosely woven solid monofilament of PTFE[4].

In this study, we compare the behavior of two LW meshes of similar pore size but of different polymer composition (PP versus PTFE) in the short term after implant. Having previously established the key role of mesh structure in host tissue regeneration[18], this study was designed to determine whether the chemical composition of a mesh conditions the behavior of host tissue towards the implant regardless of its density or porosity. The early host tissue incorporation process was examined in terms of mesh collagenization and the acute inflammatory reaction induced by the different polymer structures since both these processes are essential for good wound healing. Collagen deposition was also correlated with the biomechanical response of the implanted meshes. The time point of 14 days was selected since the initial acute phase reaction to mesh implantation is critical for the success or failure of the implant process.

2 Materials and methods

2.1 Experimental animals

The experimental animals were 16 male New Zealand White rabbits weighing approximately 2200 g caged under conditions of constant light and temperature according to European Union animal care guidelines (European Directive 609/86/EEC and European Convention of the Council of Europe ETS123). All procedures were approved by our institution's Review Board.

2.2 Prosthetic materials

The biomaterials used were (Fig. 1.a and 1.b):

- Optilene® mesh elastic (B/Braun, Germany): LW polypropylene ($48g/m^2$); pore size $7.64 \pm 0.32mm^2$.
- Infinit® mesh (Gore and Associates, Arizona, USA): LW non-expanded polytetrafluoroethylene (PTFE) ($70g/m^2$); pore size $4.05 \pm 0.22mm^2$.

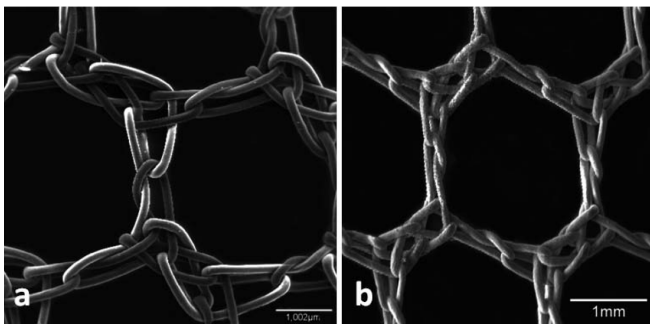

Figure 1: Scanning electron microscopy images of the different biomaterials used in this experimental study. a) Optilene® elastic (PP) (15x) and b) Infinit® mesh (PTFE) (15x).

2.3 Experimental design

The two different biomaterials were implanted in 16 animals to give two experimental groups of 8 animals each (PP and PTFE). Four animals of each group were used for the morphological and gene and protein expression studies and the other four for the shrinkage and biomechanical studies. Animals were euthanized in a CO_2 chamber after 14 days of implant.

2.4 Surgical technique

To minimize pain, all animals were given 0.05 mg/kg buprenorphine (Buprecare®, Divasa Farmavic, Barcelona, Spain) 1 hour before the surgical procedure. Anesthesia was induced with a

mixture of ketamine hydrochloride (Ketolar, Parke-Davis, Spain) (70 mg/kg), diazepam (Valium, Roche, Spain) (1.5 mg/kg), and chlorpromazine (Largactil, Rhone-Poulenc, Spain), (1.5 mg/kg) administered intramuscularly.
Using a sterile surgical technique, 4 x 4 cm defects were created in the lateral wall of the abdomen comprising the planes of the external and internal oblique muscles and sparing the transversalis muscle, parietal peritoneum and skin. The defects were then repaired by fixing a mesh of the same size to the edges of the defect using a running 4/0 polypropylene suture interrupted at the four corners. The skin was closed by 3/0 polypropylene running suture. Over the following three postoperative days, meloxidyl® (Esteve, Spain) (0.1 mg/kg) was administered orally by mixing with water for pain relief.

2.5 Shrinkage

Shrinkage of the implanted meshes was determined by image analysis. For this purpose, we designed a set of transparent templates of the same dimensions as the original meshes (4 x 4 cm). At the end of the implant period, the outlines of the meshes were traced on the templates before removing them from the animal. The surface areas of the templates could then be determined by computerized image analysis using the Image J software. Results were expressed as the percentage size reduction experienced by each implant. To examine the initial stage reaction, mesh shrinkage was determined 14 days after implant.

2.6 Morphological analysis

Light microscopy

For light microscopy, specimens were collected from the mesh/host tissue interface. The samples were fixed in F13 solution, embedded in paraffin and cut into $5 - \mu m$ sections. Once cut, the sections were stained with Masson's trichrome (Goldner-Gabe) and examined under a light microscope (Zeiss Axiophot, Carl Zeiss, Oberkochen, Germany).

2.7 Gene and protein expression of collagens

Real time RT-PCR

Tissue fragments 1 cm^2 in size were obtained from the central mesh zone and stored at -80^oC until use. RNA was extracted using guanidine-phenol-chloroform isothiocyanate procedures with trizol (Invitrogen, Carlsbad, CA, USA). The RNA was recovered from the aqueous phase and precipitated by adding isopropanol and incubating overnight at -20^oC. Complementary DNA was synthesized using 200 ng of total RNA by reverse transcription (RT) with oligo dT primers (Amersham, Fairfield, USA) and the M-MLV reverse transcriptase enzyme (Invitrogen). RT reactions were run in the absence of M-MLV to confirm the RNA lacked genomic DNA.
cDNA was amplified using the following primers: collagen 1 (sense 5'-GAT GCG TTC CAG TTC GAG TA-3' and antisense 5'-GGT CTT CCG GTG GTC TTG TA-3'; collagen 3 (sense 5'-TTA TAA ACC AAC CTC TTC CT-3' and antisense 5'-TAT TAT AGC ACC ATT GAG

AC-3'; and GAPDH (sense 5'-TCA CCA TCT TCC AGG AGC GA-3' and antisense 5'-CAC AAT GCC GAA GTG GTC GT-3').
The RT-PCR mixture contained: 5 μl of the inverse transcription product (cDNA) diluted 1:20, 10 μl of iQ SYBR Green Supermix (Bio-rad, Laboratories, Hercules, CA, USA) and 1 μl (6 μM) of each primer in a final reaction volume of 20 μl. RT-PCR was performed in a StepOnePlus Real-Time PCR system (Applied Biosystem, Foster City, California, USA). Samples were subjected to an initial stage of 10 min at 95^oC. The conditions for cDNA amplification were: 40 cycles of 95^oC for 15 s, 60^oC (collagens I and III) or 55^oC (GAPDH) for 30 s and 72^oC for 1 min. Negative controls containing ultraPureTM DNase, RNase free distilled water (Invitrogen) were run in each reaction. Products were electrophoresed on a 2% agarose gel, stained with SYBR Green II RNA gel stain (Invitrogen) and visualized with UV light.
Gene expression was normalized against the expression recorded for the constitutive gene glyceraldehyde 3-phosphate-dehydrogenase.

Immunofluorescence

To detect the protein expression of collagens I and III, tissue fragments were fixed in F13 fluid, embedded in paraffin and cut into 5 μm-thick sections. Once cut, the sections were deparaffinated, hydrated, equilibrated in PBS buffer and incubated with the monoclonal antibodies anti-collagen I (Sigma, St. Louis, MO, USA) and anti-collagen III (Medicorp, Montreal, Canada). The secondary antibody used was conjugated with rhodamine. An immunofluorescence technique was used to detect the antigen-antibody reaction. Cell nuclei were counterstained with DAPI. Samples were examined under a confocal microscope Leica SP5 (Leica Microsystems, Wetzlar, Germany) to detect fluorescence.

2.8 Macrophage response

For immunohistochemistry, a specific monoclonal antibody to rabbit macrophages, RAM 11 (DAKO M-633, USA) was applied to paraffin-embedded sections. The alkaline phosphatase-labeled avidin-biotin method was performed as the following steps: incubation with the primary antibody (1:50 in tris-buffered saline or TBS) for 30 minutes, incubation with immunoglobulin G (IgG) and biotin (1:1000 in TBS) for 45 minutes, and labeling with avidin (1:200 in TBS) for 30 minutes. These steps were conducted at room temperature. Images were developed using a chromogenic substrate containing naphthol phosphate and fast red. Nuclei were counterstained for 5 min in acid hematoxylin. RAM-11-labeled macrophages were quantified according to a method described elsewhere[2].

2.9 Biomechanical strength

To determine biomechanical properties, strips of the different biomaterials 1 cm wide and 5 cm long were tested in an INSTRON 3340 tensiometer (static load 500N) (Instron Corp., UK). The cross-head speed was 5 cm per min and recording speed 2 cm per min. The value of the thickness of the meshes cannot be defined due to its discontinuous cross sectional area including filaments

and interspersed empty areas. Therefore, Cauchy stress (MPa) could not be defined when testing the whole tissue-mesh. In its place, biomechanical strength and modulus of elasticity were determined in terms of force per unit width multiplied by stretch (λ), using the expression $\frac{Force[N]}{Width[mm]}\lambda$, where Force [N] is the load applied during the test[10].
The strips obtained at 14 days post-implant included the mesh and infiltrated host tissue. All tests were conducted immediately after animal sacrifice.

2.10 Statistical analysis

Statistical analysis was performed using the Graph Pad Prism 5 package. Shrinkage percentages, collagen 1 and 3 mRNA expression, RAM-11 positive cells, biomechanical strength and modulus of elasticity values were compared between the two study groups using the Mann-Whitney U test. The level of statistical significance was set at $p < 0.05$.

3 Results

There were no cases of mortality or signs of infection and/or rejection of the implants in the animals. Seroma was detected in two of the animals with PTFE implants at 14 days post-surgery.

3.1 Shrinkage

Shrinkage values determined at 14 days postimplant indicated a significantly greater ($p < 0.05$) percentage size reduction for Optilene® ($17.82 \pm 2.60\%$) compared to Infinit® ($9.33 \pm 2.35\%$). (Fig. 2).

3.2 Morphological analysis

Light microscopy

A similar wound healing process was observed in the animals implanted with both mesh types. Hence, after 14 days, the two biomaterials had become infiltrated by a disorganized, well-vascularized, loose connective scar tissue. This neoformed tissue surrounded the prosthetic filaments, filling all existing gaps (Fig. 3.a and 3.c). Collagen fibers ran parallel to the mesh surface in zones far from the filaments or were arranged concentrically to these filaments in areas closer to the implant edges. Around the prosthetic filaments, there was an evident yet moderate inflammatory reaction (Fig. 3.b and 3.d).

3.3 Gene and protein expression of collagens

Real time RT-PCR

After implant, the PP biomaterial (Optilene®) showed a more intense pattern of mRNA expression for collagen 3 (immature) and 1 (mature), than the PTFE mesh, whose expression of these mRNAs was low. Despite this difference in relative amounts of mRNAs, we detected no

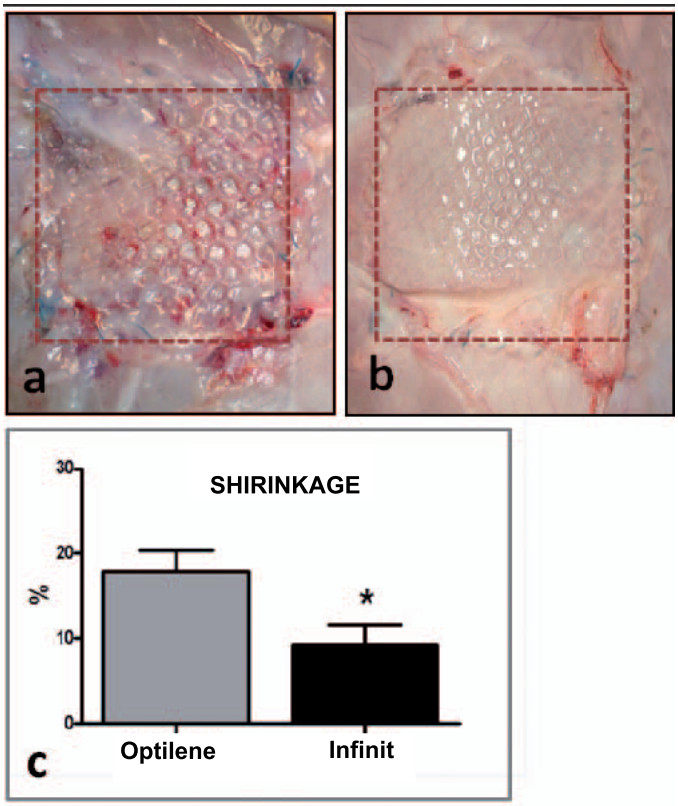

Figure 2: Macroscopic appearance of the implant site after 14 days: Optilene (a) and Infinit (b). Superimposed on the image is a template of the same dimensions as the originally implanted meshes (4 x 4 cm). c) % shrinkage of the implanted mesh.

significant differences in collagen 1 and 3 mRNA expression patterns between the PP and PTFE meshes ($p > 0.05$) or within each mesh group (Fig. 4).

Immunofluorescence

In the short term, collagen III protein was mostly expressed in the neoformed tissue surrounding the prosthetic filaments, regardless of their composition. Both groups showed a homogeneous distribution of the immature form of collagen (collagen III protein) throughout the newly formed tissue (Fig. 5.b and 5.d). However, a slightly more intense pattern of immunostaining for this collagen was observed in the Infinit mesh® (Fig. 5.b).
Compared with collagen III, immunostaining for the mature form of collagen (collagen I) was very weak (Fig. 5.a and 5.c). In the PP meshes labeling was virtually undetectable and in the PTFE implants it lacked a fibrillar appearance and was restricted to small areas of the neoformed tissue close to the prosthetic filaments (Fig. 5.a and 5.c).

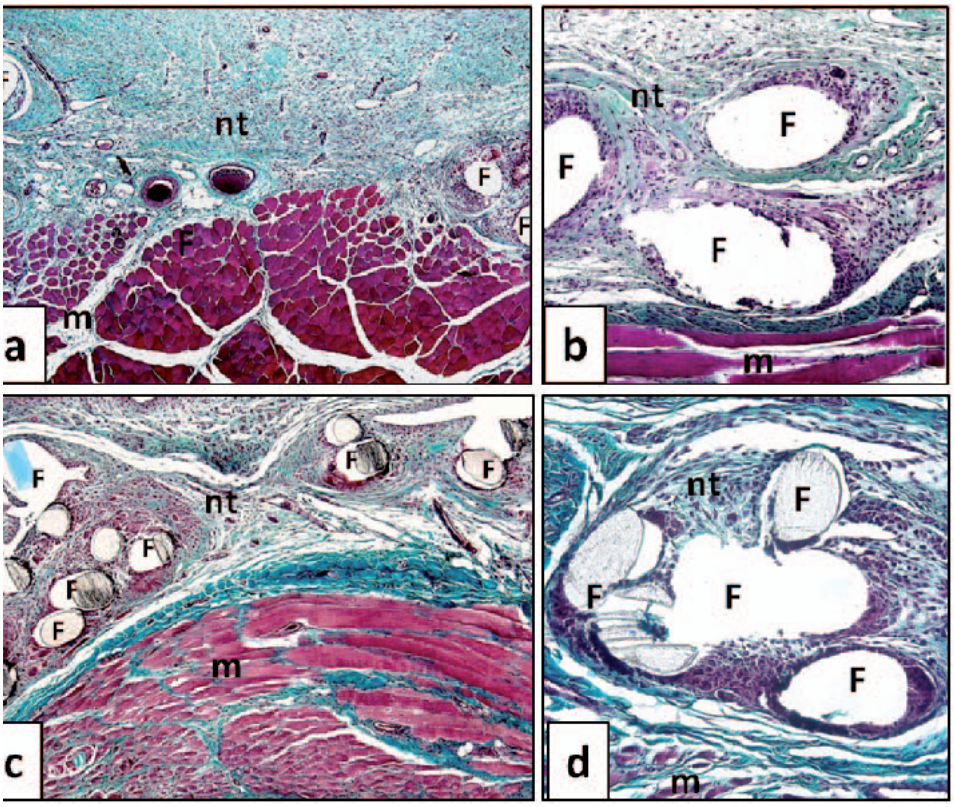

Figure 3: Histological findings on Masson's trichrome stained sections of the implanted meshes. Optilene (a/b) and Infinit (c/d) after 14 days of implant in the experimental animals (50X; 160X). (F: prosthetic filaments, m: muscle tissue, nt: neoformed tissue).

3.4 Macrophage response

In both study groups, macrophage cells were detected in the neoformed tissue between the mesh filaments (Fig. 6.a and 6.b). Most inflammatory cells concentrated around the filaments where, besides macrophages, multinucleated foreign-body giant cells, typical of a wound repair response, could be seen. These cells appeared mostly around the filaments of PTFE (Infinit®) (Fig. 6.c and 6.d).
Macrophage numbers were significantly higher for the PTFE meshes compared to the PP implants ($p < 0.05$) (Fig. 6.e).

3.5 Biomechanics

The tensile strengths, or breaking points (Fig. 7.a and 7.b), recorded for the two groups of meshes implanted for 14 days did not vary significantly (Optilene 3.026 ± 0.336 N/mm, Infinit 2.812 ± 0.223 N/mm) ($p > 0.05$) (Fig. 7.c). However, a significantly higher post-implant elastic modulus (N/mm) was recorded for the PTFE ($p < 0.05$) compared to the PP meshes (Fig. 7.d).

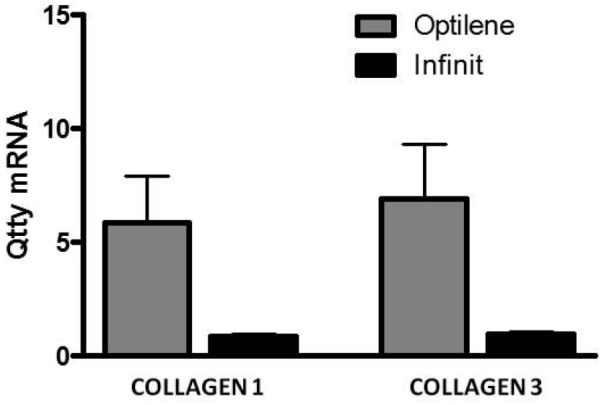

Figure 4: Relative amounts of collagen 1 and 3 mRNA in the Optilene® and Infinit® meshes determined by qRT-PCR. No significant differences were observed between the groups ($p > 0.05$). Results are the mean ± SEM of three experiments performed in duplicate. Gene expression was normalized to values recorded for the GAPDH gene.

4 Discussion

The most recent modifications made to PP meshes have pursued the idea of minimizing the material implanted in the host without compromising their mechanical resistance and this has led to the development of today's light-weight meshes[16]. Similarly, attempts to improve the tissue incorporation and tensile strength of conventional laminar PTFE prostheses have given rise to large pore meshes made by interweaving a solid monofilament of non-expanded PTFE[5]. Studies conducted on these new macroporous meshes have revealed that rather than the chemical composition of the biomaterial, it is their loosely woven structure that determines their tissue behavior. Some years ago, our group created a macroporous mesh[4] using CV-4, an expanded-PTFE suture thread. In contrast, the mesh examined here is composed of a non-expanded PTFE monofilament knitted to create a large pore size making it a LW mesh. Although this type of mesh in the meantime has been withdrawn from the European market, we believe it is very important to understand the behavior of this new abdominal prosthesis.
In our study, partial defects were created in the abdominal wall of the rabbit to avoid involving the peritoneum in the repair process. After sacrificing the animals, seroma was detected in two of the animals with PTFE implants. This means there was a more intense inflammatory reaction in these animals, in agreement with our immunohistochemistry results. Thus, using the anti-RAM-11 macrophage monoclonal antibody, the PTFE implants showed a significantly augmented macrophage reaction over that shown by the PP implants. This observation is in line with the findings of a recent study[11] in which the Infinit® mesh was compared with a mesh (Optilene LP) similar to the PP mesh used here but with a smaller pore size. The authors of this study also detected a significantly greater macrophage response for the PTFE meshes despite the fact that it was a long-term study (94 days post-implant) conducted a different experimental animal and model to ours.

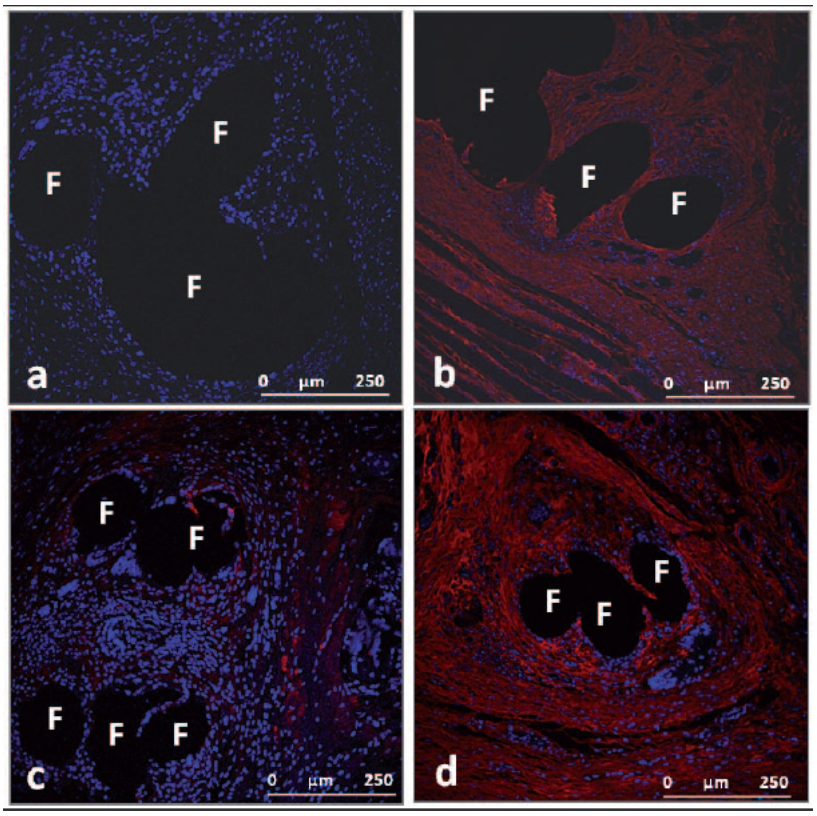

Figure 5: Collagen I and III protein expression around the mesh filaments of the biomaterials at 14 days post-implant. Collagen appears as red fluorescence upon laser scanning confocal microscopy. Cell nuclei appear blue (DAPI). a,c) Collagen I and b,d) Collagen III. a,b) Optilene® and c,d) Infinit®, 14 days (200x). (F=Prosthetic filaments).

This behavior is also similar to that exhibited by some absorbable materials in the early postimplant course[15,21] possibly with clinical implications like seroma. Several factors[12,20,23] influence the inflammatory response to an implanted prosthesis such as density, pore size, type of material, fiber structure, texture and mesh construction. However, a review[24] of the European medical literature on the outcome of hernia mesh repair concluded that mesh pore size and filament structure were the most important determinants of the foreign body reaction produced after mesh implantation.

In the present experimental study, we compared the short-term post-implant behavior of a conventional PP-LW mesh to that of a new LW mesh composed of non-expanded PTFE. In terms of host tissue incorporation, both LW mesh types showed good behavior. The behavior of the PTFE meshes showed little resemblance to that of the classic microporous ePTFE prosthetic materials, which gradually become encapsulated by host tissue.

Two weeks after implant, the immature form of collagen, collagen III, was the predominant collagen type present. Similar expression of the protein was observed for the two different

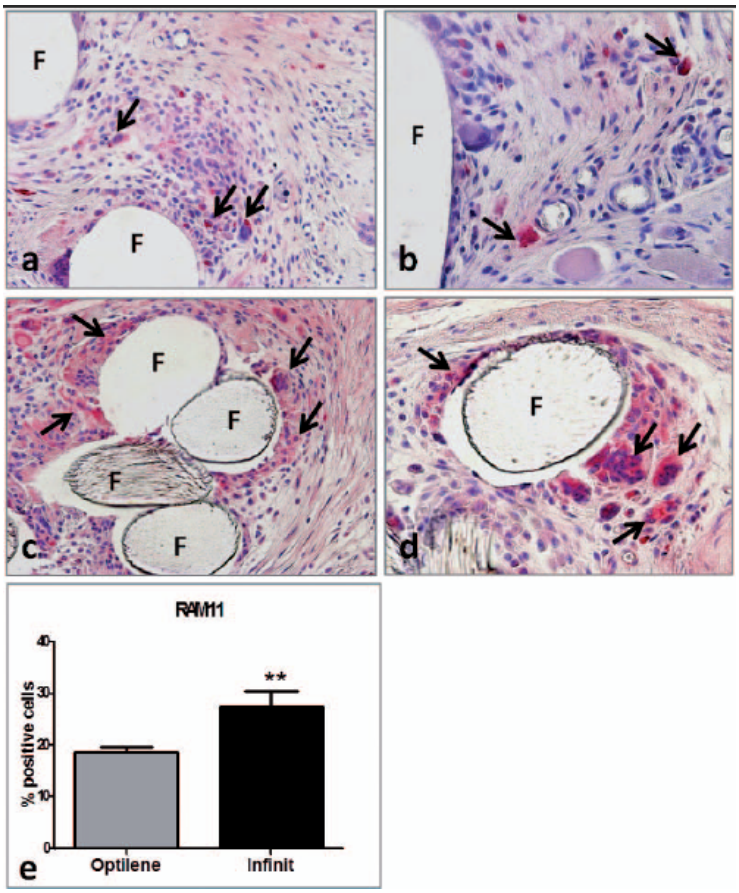

Figure 6: Immunohistochemical labeling of rabbit macrophages (arrows) using the RAM-11 monoclonal antibody. a,b) Optilene® and c,d) Infinit®, 14 days after implant. e) Mean RAM-11 positive cells recorded for each study group, indicating significant differences between the two meshes ($^{**}p < 0.05$). (F=Prosthetic filaments).

polymer structures. At this time point, collagen I expression was low. This is as expected, as the mature form of collagen is synthesized and secreted in the extracellular matrix later than the immature form. In prior work[18], we observed that in the mid to long term (3 and 6 months post-implant) these LW meshes (Optilene® and Infinit®) induced the greater protein expression of mature collagen. Other authors[8,9] have also reported greater type I collagen deposition following the implant of large-pore prosthetic materials.

In an earlier study[19], we also compared the influence of porosity on the behavior of different meshes, this time in a full-thickness abdominal wall defect model, and noted significantly higher collagen 1 and 3 gene expression levels for the larger pore meshes at 14 days post-implant. In the present study, we observed similar behavior at this time point; both LW implants showed higher gene expression levels for both collagen types than the levels recorded in another study in the long term[18]. This suggests that in the short term messenger RNA expression peaks,

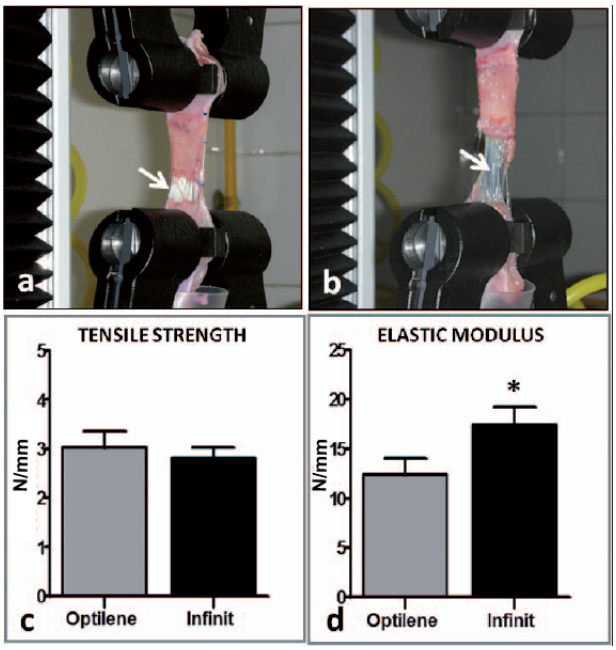

Figure 7: a,b) Tissue rupture points (arrows) during the development of the biomechanical study. c) Biomechanical resistance values (N/mm) obtained for Infinit® and Optilene® at 14 days post-implant indicating no significant differences. d) Modulus of elasticity (N/mm) recorded for the two mesh types. Significant differences were observed between Infinit® versus Optilene® ($^*p < 0.05$).

and consequently so does its transcription. The higher, though not significant, relative amount of mRNA observed in our PP meshes than PTFE meshes could point to less effective protein translation since similar protein levels were detected by immunofluorescence.
Our biomechanical results indicated similar tensile strengths at 14 days for the PP and PTFE meshes. Our previous studies have shown that this behavior persists in the long term, and that tensile strength increases over time[18]. In another study, we effectively observed that by 90 days post-implant, similar biomechanical strengths were attained by several different implants[6].
The elastic modulus recorded after implant was significantly higher ($p < 0.05$) for the PTFE than PP meshes, although as for their mechanical strength, similar values seem to be attained in the longer term for both implants as indicated in a previous study[18] in which both the resistance to breakage and elasticity of several implants were increasingly conditioned by the in-growing host tissue.
In conclusion, our findings suggest no effects of the chemical composition of LW meshes on the short-term collagenization of neoformed tissue and its consequent resistance to traction. Both these factors are crucial for the early failure or success of an implant. In contrast, the macrophage response does seem to depend on polymer structure and was appreciably more intense in response to PTFE than PP.

5 Acknowledgments

This study was supported by the Spanish Ministry of Science and Technology through research projects DPI2011-27939-C01-01 and C02-02 and the Instituto de Salud Carlos III (ISCIII) through the CIBER-BBN initiative project ABDOMESH. The authors are indebted to Gore and Associates, Flagstaff, Arizona, USA for providing the Infinit meshes used in this study. This company played no role in the design of this study, data collection or analysis. No conflicts of interest declared.

References

[1] D. I. Alaedeen, J. Lipman, D. Medalie, and M. J. Rosen. The single-staged approach to the surgical management of abdominal wall hernias in contaminated fields. *Hernia*, 11:41–45, 2007.

[2] J. M. Bellón, J. Buján, L. Contreras, A. Hernando, and F. Jurado. Macrophage response to experimental implantation of polypropylene prostheses. *European Surgical Research* , 26:46–53, 1994.

[3] J. M. Bellón, L. Contreras, J. Buján, D. Palomares, and A. Carrera-San-Martín. Tissue response to polypropylene meshes used in the repair of abdominal wall defects. *Biomaterials*, 19:669–675, 1998.

[4] J. M. Bellón, F. Jurado, N. García-Honduvilla, R. López, A. Carrera-San Martín, and J. Buján. The structure of a biomaterial rather than its chemical composition modulates the repair process at the peritoneal level. *American Journal of Surgery*, 184:154–159, 2002.

[5] J. M. Bellón, M. Rodríguez, N. García-Honduvilla, V. Gómez-Gil, G. Pascual, and J. Buján. Comparing the behavior of different polypropylene meshes (heavy and lightweight) in an experimental model of ventral hernia repair. *Journal of Biomedical Materials Research. Part B, Applied Biomaterials*, 89B(2):448–55, 2009.

[6] J. M. Bellón, M. Rodríguez, N. García-Honduvilla, G. Pascual, and J. Buján. Partially absorbable meshes for hernia repair offer advantages over nonabsorbable meshes. *The American Journal of Surgery*, 194:68–74, 2007.

[7] William S. Cobb, Justin M. Burns, Richard D. Peindl, Alfredo M. Carbonell, Brent D. Matthews, Kent W. Kercher, and B. Todd Heniford. Textile analysis of heavy-weight, mid-weight and light-weight polypropylene mesh in a porcine ventral hernia model. *Journal of Surgical Research*, 136:1–7, 2006.

[8] F. H. Greca, J. B. De Paula, M. P. L. Biondo-Simoes, F. D. Costa, A. P. G. Da Silva, S. Time, and A. Mansur. The influence of differing pore sizes on the biocompatibility of two polypropylene meshes in the repair of abdominal defect: experimental study in dogs. *Hernia*, 5:59–64, 2001.

[9] F. H. Greca, Z. A. Souza-Filho, a. Giovanini, M. R. Rubin, R. F. Kuenzer, F. B. Reese, and L. M. Araujo. The influence of porosity on the integration histology of two polypropylene meshes for the treatment of abdominal wall defects in dogs. *Hernia*, 12:45–49, 2008.

[10] B. Hernández-Gascón, E. Peña, G. Pascual, M. Rodríguez, J. M. Bellón, and B. Calvo. Long-term anisotropic mechanical response of surgical meshes used to repair abdominal wall defects. *Journal of the Mechanical Behavior of Biomedical Materials*, 5 (1):257–271, 2012.

[11] D. A. Jacob, C. Schug-Pass, F. Sommerer, A. Tannapfel, H. Lippert, and F. Köckerling. Comparison of a lightweight polypropylene mesh (Optilene® LP) and a large-pore knitted PTFE mesh (GORE® INFINIT® mesh)–Biocompatibility in a standardized endoscopic extraperitoneal hernia model. Langenbecks. *Langenbeck's Archives of Surgery*, 397:283–289, 2012.

[12] H. A. Kayaoglu, N. Ozkan, S. M. Hazinedaroglu, O. F. Ersoy, A. B. Erkek, and R. D. Koseoglu. Comparison of adhesive properties of five different prosthetic materials used in hernioplasty. *Journal of Investigative Surgery*, 18:89–95, 2005.

[13] U. Klinge. Experimental comparison of monofile light and heavy polypropylene meshes: less weight does not mean less biological response. *World Journal of Surgery*, 31:867–868, 2007.

[14] U. Klinge, B. Klosterhalfen, V. Birkenhauer, K. Junge, J. Conze, and V. Schumpelick. Impact of polymer pore size on the interface scar formation in a rat model. *Journal of Surgical Research*, 103:208–214, 2002.

[15] U. Klinge, V. Schumpelick, and B. Klosterhalfen. Functional assessment and tissue response of short and long-term absorbable surgical meshes. *Biomaterials*, 22:1415–1424, 2001.

[16] B. Klosterhalfen, K. Junge, and U. Klinge. The lightweight and large porous mesh concept for hernia repair. *Expert Review of Medical Devices*, 2:103–117, 2005.

[17] P. J. O'Dwyer, A. N. Kingsnorth, R. G. Mohillo, P. K. Small, B. Lammers, and G. Horeysee. Randomized clinical trial assessing impact of a lightweight or heavyweight on chronic pain after inguinal hernia repair. *British Journal of Surgery*, 92:166–70, 2005.

[18] G. Pascual, B. Hernández-Gascón, M. Rodríguez, S. Sotomayor, E. Peña, B. Calvo, and J. M. Bellón. The long term behavior of lightweight and heavyweight meshes used to repair abdominal wall defects is determined by the host tissue repair process provoked by the mesh. *Surgery*, 152(5):886–95, 2012.

[19] G. Pascual, M. Rodríguez, V. Gómez-Gil, N. García-Honduvilla, J. Buján, and J. M. Bellón. Early tissue incorporation and collagen deposition in lightweight polypropylene meshes: bioassay in an experimental model of ventral hernia. *Surgery*, 144:427–35, 2008.

[20] S. Post, B. Weiss, M. Willer, T. Neufang, and D. Lorenz. Randomized clinical trial of lightweight composite mesh for Lichtenstein inguinal hernia repair. *British Journal of Surgery*, 91:44–48, 2004.

[21] R. Rosch, K. Junge, R. Quester, U. Klinge, B. Klosterhalfen, and V. Schumpelick. Vypro II mesh in hernia repair: impact of polyglactin on long-term incorporation in rats. *European Surgical Research*, 35:445–50, 2003.

[22] V. Schumpelick, B. Klosterhalfen, M. Müller, and U. Klinge. Minimized polypropylene mesh for preperitoneal net plasty (PNP) of incisional hernias. *Chirurg*, 70:422–430, 1999.

[23] G. Vita, R. Patti, and M. Sparacello. Impact of different texture of polypropylene mesh on the inflammatory response. *International Journal of Immunopathology and Pharmacology*, 21:207–214, 2008.

[24] D. Weyhe, O. Delyaev, C. Müller, K. Meurer, K. h. Bauer, G. Papapostolou, and W. Uhl. Improving outcomes in hernia repair by the use of light meshes: a comparison of different implant constructions based on a critical appraisal of the literature. *World Journal of Surgery*, 31:234–244, 2007.

APPENDIX

APPENDIX 1

Characteristics of journals

Characteristics of journals

The works that comprise this thesis has been published in different journals whose characteristics are described below, except for those corresponding to the manuscripts submitted:

- Work 1: Published in *Journal of the Mechanical Behavior of Biomedical Materials* (Impact factor=2.814), which is ranked in 15th position (Q1) within the thematic area "Biomedical Engineering".
- Work 2: Published in *Acta Biomaterialia* (Impact factor=4.865), which is ranked in 3rd position (Q1) within the thematic area "Biomedical Engineering".
- Work 3: Published in *Journal of the Mechanical Behavior of Biomedical Materials* (Impact factor=2.814), which is ranked in 15th position (Q2) within the thematic area "Biomedical Engineering".
- Work 4: In Press in *Annals of Biomedical Engineering* (Impact factor=2.368), which is ranked in 20th position (Q2) within the thematic area "Biomedical Engineering".
- Work 5: In Press in *Computer Methods in Biomechanics and Biomedical Engineering* (Impact factor=1.169), which is ranked in 54th position (Q3) within the thematic area "Biomedical Engineering".
- Work 6: Published in *Revista Internacional de Métodos Numéricos para Cálculo y Diseño en Ingeniería* (Impact factor=0.167), which is ranked in 85th position (Q4) within the thematic area "Multidisciplinary Engineering".
- Work 7: Submitted.

- Work 8: Submitted.
- Work 9: Published in *Surgery* (Impact factor=3.103), which is ranked in 21st position (Q1) within the thematic area "Surgery".
- Work 10: Accepted in *Histology and Histopathology* (Impact factor=2.480), which is ranked in 120th position (Q3) within the thematic area "Cell Biology".

APPENDIX 2

Acceptance letter of work 10

Profs. F. Hernández and J.F. Madrid, Editors
School of Medicine
University of Murcia
30100 Espinardo – MURCIA
SPAIN Fax: 34-868887508 /34-868884150 e-mail: jfmadrid@um.es

Histology and Histopathology
http://www.hh.um.es

Our reference: B-4713
Mª Gemma Pascual González
Dept. of Medical Specialities
Faculty of Medicine
Alcalá University
Ctra. Madrid-Barcelona, Km 33,600
28871 Alcalá de Henares
Madrid
e-mail: gemma.pascual@uah.es

November 5, 2012

Dear Dr. Pascual,

I am pleased to inform you that your article entitled "SHORT-TERM BEHAVIOR OF DIFFERENT POLYMER STRUCTURE LIGHTWEIGHT MESHES USED TO REPAIR ABDOMINAL WALL DEFECTS (Pascual G., Hernández-Gascón B., Sotomayor S., Peña E., Calvo B., Buján J., Bellón J.M.) has been now formally accepted.

As soon as possible, you will receive the proofs.

Yours sincerely,

Prof. Juan F. Madrid, Editor

APPENDIX 3

Contribution of the Ph.D Student and resignation of the non Doctor coauthors

Contribution of the Ph.D Student and resignation of the non Doctor coauthors

Dr. Begoña Calvo Calzada and Dr. Estefanía Peña Baquedano, supervisors of the thesis presented by Belén Hernández Gascón to apply for the degree of International Doctor, certify that all coauthors of the works presented in this report are Doctors, except Andrés Mena Tobar and Natalia Espés Martín, who expressly renounce to present the works 4 and 5 of which they are coauthors, respectively, as part of another doctoral thesis, so they sign the present document. We also certify that the presented work has been completely developed by the author of this thesis, except for the histological studies which were developed by the Translational Research Group in Biomaterials and Tissue Engineering at the University of Alcalá de Henares (Madrid).

The Doctor coauthors in the presented articles are listed below:

- Juan Manuel Bellón
- Julia Buján
- Begoña Calvo
- Manuel Doblaré
- Jorge Grasa
- Hortensia Melero
- Gemma Pascual
- María Pau Ginebra

- Estefanía Peña
- Angélica María Ramírez
- José Félix Rodríguez
- Marta Rodríguez
- Sandra Sotomayor

Signed by the supervisors of the thesis, in Zaragoza, 10th of December 2012:

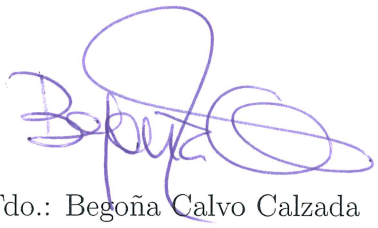

Fdo.: Begoña Calvo Calzada

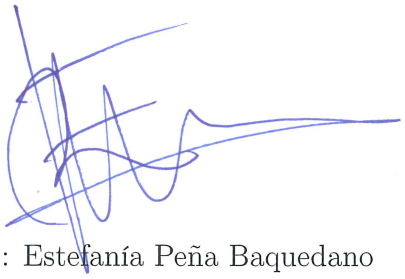

Fdo.: Estefanía Peña Baquedano

And the non Doctor coauthors:

Fdo.: Andrés Mena Tobar

Fdo.: Natalia Espés Martín